

STRUCTURAL, MINERALOGICAL, GEOCHEMICAL AND
GEOCHRONOLOGICAL INVESTIGATION OF THE BARRY GOLD
DEPOSIT, ABITIBI SUBPROVINCE, CANADA

by

Kathryn Elizabeth Kitney

A thesis submitted to the Department of Geological Sciences and Geological Engineering

In conformity with the requirements for
the degree of Master of Science (Engineering)

Queen's University

Kingston, Ontario, Canada

(May, 2009)

Copyright © Kathryn Elizabeth Kitney, 2009

Abstract

The Barry gold deposit is an example of an Archean greenstone-hosted lode gold deposit located in the Urban-Barry greenstone belt in the Abitibi subprovince of Québec, Canada. Auriferous zones are spatially associated with NE-trending ductile shear zones with moderate south-easterly dip. Gold mineralization occurs within albite-carbonate-quartz veins that are straight N64°E/64°SE and folded N20°E/60°SE and within the surrounding carbonate-quartz-pyrite and locally biotite-carbonate alteration zones of the host mafic volcanic rocks. The deposit has gold resources indicated at 52,300 oz (385,000 mt at 4.23 g/t Au) and inferred at 126,600 oz (966,000 mt at 4.07 g/t Au).

The host mafic volcanic rocks are part of the 2717 Ma Macho Formation that exhibit a geochemical signature transitional between mid-ocean and island arc. They are cut by pre-ore diorite, pre- and post-ore quartz-feldspar porphyry (QFP), and quartz monzonite dikes and plugs interpreted to have formed in a volcanic arc to syn-collisional setting.

The auriferous veins comprise 5-15% volume of the mafic volcanic rocks, are 1-5cm wide, and locally pinch and swell or are boudinaged. Although the volcanic units strike N55-60°E and dip 40°SE, the ore envelope (>2 g/t Au) is constrained from surface to a depth of 30m in an antiformal shape. Free gold is found in albite-carbonate-quartz veins, syn-mineralization altered host rocks, and locally within quartz veins cutting early QFP dikes.

The timing of gold mineralization at the Barry deposit is well constrained by U-Pb zircon dating of pre-mineralization diorite and post-mineralization QFP dikes. Analyses of single zircon grains by thermal ionization mass spectrometry (TIMS) give concordant and overlapping data with indistinguishable ages, yielding an average age of 2697 ± 0.6 Ma that is interpreted as the age of gold mineralization at the Barry deposit. This date indicates that gold mineralization was coeval with regional deformation and magmatism, and is, to our knowledge, the most precise age yet established for Archean lode gold mineralization. This finding confirms that the Barry lode gold deposit formed during an earlier, pre-2686, deformational period in the late Archean, similar to what was documented in the Kiena, Norlartic and Siscoe (Main Zone) mines in the Southern Abitibi greenstone belt.

Co-Authorship

Chapter 2 of this thesis was prepared as separate manuscript for journal publication as a co-authored paper, and will be submitted to *Economic Geology*. This chapter is co-authored with Dr. G.R. Olivo, who contributed to fieldwork, interpretations of the geochemical and structural data, and acted in a supervisory and review capacity throughout the entire project; Dr. D.W. Davis, who assisted with U-Pb zircon sample preparation and dating, and acted in a review capacity; Dr. J.-P. Desrochers, who was also involved with field work and acted in a review capacity; and A. Tessier, whose data collection in 1996 was built on in this project, and who acted in a review capacity.

Acknowledgements

K. E. Kitney gratefully acknowledges the Natural Sciences and Engineering Research Council (NSERC) and Murgor Resources Inc., for the generous funding of this project through an NSERC Industrial Scholarship. This research was also supported by the Society of Economic Geologists (SEG) and by an NSERC discovery grant to G. Olivo.

I wish to extend my thanks to my thesis advisor, Dr. Gema Olivo, for her guidance throughout this project. I would also like to thank her for her advice and assistance in the field, for always making time to discuss the various aspects of the research, and for carefully reviewing abstracts, the paper, and this thesis.

Thank you to the co-authors of the paper to be submitted to Economic Geology: Dr. G.R. Olivo, Dr. D.W. Davis, Dr. J.-P. Desrochers, and A. Tessier. I appreciate all of the help you have each given towards the interpretation and the reviews of this paper.

This project was made possible by the companies Murgor Resources Inc., and Metanor Resources Inc., who provided access to the deposit and were extremely helpful during fieldwork at the site. I would like to thank the Mr. Daniel Macameau of Metanor Resources, and the crew working at the site in August 2007, for being accommodating and looking out for me during field work. I would like to thank the following people from Murgor Resources: Dr. Jean-Philippe Desrochers and Chang Quang for assisting me during fieldwork with mapping and interpretations, André Tessier for his previous work

and insights on the deposit, Jaysen Johnson for assisting in the drill core logging, Christian Tessier, Marc Lavoie, and René De Carufel for their assistance in the preparation for mapping and the collection and cutting of samples, and Benjamin Batson for his assistance throughout the summer. I would especially like to thank Benoit and Kevin Boudreault, who arrived unannounced at the Barry deposit in 2007 and played a huge role in the collection of my 2007 surface samples, for all of their assistance and for looking out for me throughout my field work.

I would like to thank the many people in the Department of Geological Sciences and Geological Engineering at Queen's University that contributed to this study. Dr. P.L. Roeder is thanked for his assistance with microprobe analysis at Queen's, and his patience in answering my many microprobe-related questions. Mr. David Kempson is thanked for his assistance in the microprobe work. Mr. Alan Grant is thanked for his assistance with the use of the scanning electron microscope and x-ray diffraction. Mr. Roger Innes is thanked for his help with cutting rock samples, sample storage, and finding me numerous sample bags. Thanks are also extended to the personnel in the main office, Ms. Joan Charbonneau, Ms. Linda Brown, and Dianne Hyde, for their assistance and logistical support throughout my Master's project.

Thank you to Howard Poulsen for his assistance in discussions and access to information on the Abitibi; E.H. Chown, who took the time to discuss the intrusive rocks at the Barry

deposit and who spent time looking at intrusive samples in thin section; and Dr. Alan Gorman, who took time to look over my thesis.

I would like to thank the following people from the Jack Satterly Geochronology Laboratory in the Department of Geology at the University of Toronto. Dr. Donald W. Davis, Yim Ying (Kim) Kwok, and everyone else at the lab: thank you for taking the time to show me the whole U-Pb zircon dating process, from crushing of samples to zircon separation and sample preparation to U-Pb dating, during my various trips to the lab in Toronto.

Thank you to Mr. Lang Shi of the Electron Microprobe Microanalytical Facility in the Earth and Planetary Sciences Department of McGill University for helping me in my microprobe analysis of ore-minerals, and for answering my various questions related to the microprobe.

For all the good times, and interesting discussions, I would like to thank my fellow students and friends in the Geology Department at Queen's. A special thank you to Kyle Larson for his assistance and ideas with regards to the structural interpretation of the deposit. Thanks to all my friends who have always been there for me and who have shared in all the highs and lows of my project.

Finally, I would like to offer my heartfelt thanks to my parents, John and Karen Kitney, and my partner, Steve Garvin, for their love and for supporting me in any way they could throughout my time at Queen's. Thank you Steve for all of the time spent patiently listening to me and for offering your support and encouragement on this study since day one.

Table of Contents

Abstract.....	ii
Co-Authorship	iv
Acknowledgements.....	v
Table of Contents.....	ix
List of Figures.....	xii
List of Tables	xv
Chapter 1 Introduction.....	1
1.1 Archean Greenstone-hosted Gold Deposits	1
1.2 Gold Deposits in the Abitibi-Wawa Subprovince.....	7
1.3 Investigation of the Barry Gold Deposit.....	9
1.3.1 Objectives	11
1.3.2 Location and Access	11
1.3.3 Exploration and Production History	12
1.3.4 Previous Geological Studies and Research.....	18
1.3.5 Methodology	19
1.3.5.1 Mapping, Drill Core Logging, and Sampling	20
1.3.5.2 Analytical Procedures.....	22
1.4 Thesis Organization	22
References.....	24
Chapter 2 Structural, Mineralogical, Geochemical and Geochronological Investigation of the Barry Gold Deposit, Abitibi Subprovince, Canada: A Greenstone-hosted Gold Deposit Coeval with Late Archean Deformation and Magmatism.....	29
2.1 Introduction.....	29
2.2 Regional Geology	32
2.3 Analytical Methods.....	38
2.4 Geology of the Barry Gold Deposit.....	42
2.4.1 Mafic Volcanic Rocks.....	42
2.4.2 Intrusive Rocks	52
2.4.3 Structure.....	63
2.4.4 Gold Mineralization	68
2.4.4.1 Syn-ore Carbonate-quartz-pyrite Wall-rock Alteration.....	70

2.4.4.2 <i>Syn-ore Biotite-carbonate Alteration</i>	75
2.4.5 Post-ore Alteration.....	77
2.5 U-Pb Zircon Geochronology.....	79
2.6 Discussion.....	85
2.6.1 Tectonic Evolution of the Barry Property and Timing of Gold Mineralization.....	85
2.6.2 Mechanisms of Emplacement and Deformation of Auriferous Veins and Dikes	87
2.6.3 Implications for Regional Metallogeny and Exploration.....	91
2.7 Conclusion	95
References.....	97
Chapter 3 Discussion	103
3.1 Characteristics and Origin of Mineralizing Hydrothermal Fluids and Source of Metals ..	103
3.2 Temporal Relationship between Gold Mineralization and Metamorphism.....	106
References.....	109
Chapter 4 Conclusion.....	110
4.1 Conclusion	110
4.2 Implications for Exploration	111
Appendix A: GEOLOGIC MAPS AND CROSS SECTIONS OF THE BARRY DEPOSIT	114
A1. Mapping Methodology.....	115
Appendix B: SURFACE AND DRILL CORE SAMPLE LOCATIONS AND DESCRIPTIONS FROM THE BARRY DEPOSIT	125
B1. Sample Collection and Methodology.....	126
Appendix C: STRUCTURAL DATA AND FAULT PLANE RESOLUTION METHOD	152
C1. Structural Measurements.....	153
C2. Fault Plane Resolution Method	164
Appendix D: LITHOGEOCHEMISTRY.....	167
D1. Sample Preparation for Whole Rock Analysis.....	168
D2. Analytical Precision in Major and Trace Element Chemical Analysis	168
Appendix E: MICROPROBE ANALYSES OF SELECT MINERALS AT THE BARRY DEPOSIT	196
E1. Microprobe Results	197
Appendix F: DRILL CORE LOGGING FROM THE BARRY DEPOSIT	214
Appendix G: PETROGRAPHIC DESCRIPTIONS	294

G1. Mafic Volcanics: Pillowed.....	296
G2. Mafic Volcanics: Brecciated.....	300
G3. Mafic Volcanics: Amygdular.....	307
G4. Mafic Volcanics: Massive.....	317
G5. Mafic Volcanics: Feldspar-phyrlic.....	339
G6. Mafic Volcanics: Tuffaceous	347
G7. Syn-ore Carbonate-quartz-pyrite Alteration of the Mafic Volcanics.....	352
G8. Syn-ore Biotite-carbonate Alteration of the Mafic Volcanics	366
G9. Diorite 1	371
G10. Diorite 2	374
G11. Diorite 3	378
G12. Quartz-feldspar Porphyry (QFP).....	383
G13. Quartz Monzonite	408
Appendix H: XRD ANALYSES	417
H1. Purpose of XRD analyses.....	418

List of Figures

Fig. 1.1: Grade-tonnage diagram of Canadian and world greenstone-hosted quartz-carbonate vein gold deposits.	2
Fig. 1.2: Map showing the Archean Slave and Superior Provinces, and the locations of various Canadian gold deposits	4
Fig. 1.3: Simplified geologic map of the Superior craton, showing the main subprovinces and significant gold deposits and camps	5
Fig. 1.4: Tectonic setting of gold-rich epigenetic mineral deposits.....	6
Fig. 1.5: Tectonic and metallogenic evolution diagram for the Timmins-Val d'Or gold belt.....	8
Fig. 1.6: Compilation of age constraints on selected gold deposits of the Superior craton.	10
Fig. 1.7: Location map of the Barry property	13
Fig. 1.8: Aerial photograph of the trenched region of the Barry deposit prior to mining.....	15
Fig. 1.9: Aerial photograph of the Barry open pit in the first stages of mining.....	17
Fig. 2.1: Simplified geology of the Abitibi subprovince, Québec	33
Fig. 2.2: Simplified geological map of the Urban-Barry belt - Picquet and Mesplet Lakes.....	37
Fig. 2.3: Simplified geologic map of the Barry deposit showing the locations of drill holes and cross sections studied in detail.....	43
Fig. 2.4: Simplified NW-SE vertical cross section of the Barry deposit along grid line 1074.	44
Fig. 2.5: Photographs of mafic volcanic flows of the Barry main zone.....	46
Fig. 2.6: Photomicrographs of pre-ore alteration at the Barry deposit.....	48
Fig. 2.7: Paragenesis of the minerals in Types A, B, and C mafic volcanic rocks that have undergone pre-ore, syn-ore, and post-ore alteration at the Barry deposit.....	49
Fig. 2.8: Ti versus Zr discrimination diagram for the mafic volcanic rocks.....	50
Fig. 2.9: Y versus Zr geochemical affinity diagram of mafic volcanic types.....	51
Fig. 2.10: Chondrite-normalized REE plots for least altered mafic volcanic Types A and B	52
Fig. 2.11: Photographs and photomicrographs of the intrusive rocks at the Barry deposit	54
Fig. 2.12: Paragenesis of the minerals and alteration of pre-mineralization diorite (1-3) at the Barry deposit.....	55
Fig. 2.13: Paragenesis of the minerals and alteration of pre- and post-mineralization QFP and post-mineralization quartz monzonite at the Barry deposit.	56
Fig. 2.14: Nb versus Y discrimination diagram for the intrusive rocks of the Barry deposit.	62

Fig. 2.15: Stereographic representation of the structural features of the Barry deposit, surface trench.	64
Fig. 2.16: Straight (N64°E/64°SE) and folded (N20°E/60°SE) auriferous albite-carbonate-quartz veins at the Barry deposit and their associated carbonate-quartz-pyrite alteration.....	67
Fig. 2.17: Photomicrographs of syn-ore carbonate-quartz-pyrite alteration at the Barry deposit..	71
Fig. 2.18: Photomicrographs and backscatter electronic images of the mode of occurrence of gold at the Barry deposit.....	73
Fig. 2.19: Iscon diagrams with weighted elements in which the protolith (least altered Type B and Type A respectively) versus the altered samples are plotted	77
Fig. 2.20: Photomicrographs of post-ore alteration at the Barry deposit.....	78
Fig. 2.21: Photomicrographs of air abraded and chemically abraded zircon grains for TIMS U-Pb analyses.....	80
Fig. 2.22: Concordia diagram showing TIMS U-Pb analyses of zircon grains	83
Fig. 2.23: Concordia diagram showing the TIMS U-Pb analyses of pooled primary data from zircon grains.....	84
Fig. 2.24: Idealized NW-SE vertical cross section illustrating the evolution of the Barry deposit	86
Fig. 2.25: Block diagram and shear sense diagram for the mineralized albite-quartz-carbonate veins and deformed diorite and QFP dikes at the Barry deposit.....	90
Fig. A1: Simplified geologic map of the Barry deposit showing the locations of drill holes and cross sections studied in detail.....	129
Fig. A2: Geologic map of the northeast corner of the Barry deposit main trenched zone.....	130
Fig. A3: Geologic map of the 1074 block in middle of the Barry deposit main trenched zone...	131
Fig. A4: Vertical SE-NW geologic cross section of the Barry deposit along grid line 1037 E...	132
Fig. A5: Vertical SE-NW geologic cross section of the Barry deposit along grid line 1074 E...	133
Fig. A6: Vertical SE-NW geologic cross section of the Barry deposit along grid line 1088 E...	134
Fig. A7: Vertical SE-NW geologic cross section of the Barry deposit along grid line 1124 E...	135
Fig. A8: Vertical SE-NW geologic cross section of the Barry deposit along grid line 1166 E...	136
Fig. C1: Fault plane resolution on northern-most early fault.....	177
Fig. E1: Ternary Al-Mg-Fe diagram showing the composition of early and late chlorite.....	219
Fig. E2: Ternary Al-Mg-Fe Diagram showing the composition of early and late biotite.....	222
Fig. H1: Sample 118-16.70 - less altered Type A mafic volcanic.....	420
Fig. H2: Sample 91-1119 - least altered Type B mafic volcanics.....	421

Fig. H3: Sample 81-1119 - low gold grade carbonate alteration in Type B mafic volcanics.....	422
Fig. H4: Sample 59-1113 - pillow, low gold grade carbonate alteration in Type A mafic volcanics	423
Fig. H5: Sample 62-1088 - pillow, low gold grade carbonate alteration in Type A mafic volcanics	424
Fig. H6: Sample 31-12.00 - high gold grade carbonate alteration in Type B mafic volcanics....	425
Fig. H7: Sample 71-1099 - high gold grade carbonate alteration in Type B mafic volcanics.....	426
Fig. H8: Sample 69-1164 - Diorite 1.....	427
Fig. H9: Sample 70-1167 - Diorite 1.....	428
Fig. H10: Sample 69-1170 - Diorite 2.....	429
Fig. H11: Sample 17-1159 - Diorite 2.....	430
Fig. H12: Sample 59-1164 - Diorite 3.....	431
Fig. H13: Sample 85-1058 - Diorite 3.....	432
Fig. H14: Sample 58-1165 – QFP.....	433
Fig. H15: Sample 83-1038 – QFP.....	434
Fig. H16: Sample 210-4.33 - Quartz Monzonite.....	435
Fig. H17: Sample 443945 - Quartz Monzonite.....	436

List of Tables

Table 2.1: U-Pb isotope data from single-grain zircon TIMS analyses of pre-ore diorite and post-ore QFP dikes at the Barry deposit	82
Table 2.2: Summary of geologic characteristics of pre-2690 Ma deposits: Barry, Kiena, Norlartic, and Siscoe (main zone)	92
Table A1: UTM coordinates for the NE corner map and drill hole locations.....	128
Table A2: UTM coordinates for the 1074 block map and drill hole locations.....	128
Table B1: Location and description of surface samples.....	139
Table B2: Location and description of drill core samples.....	141
Table C1: Location and description of structural measurements.....	166
Table D1: Analytical precision in major and trace element chemical analysis.....	182
Table D2: Mafic volcanic rocks – whole rock analysis of major oxides, minor and trace elements	184
Table D3: Intrusive rocks – whole rock analysis of major oxides, minor and trace elements.....	199
Table E1: Microprobe analyses of magnetite.....	210
Table E2: Microprobe analyses of chalcopyrite.....	211
Table E3: Microprobe analyses of pyrite.....	212
Table E4: Microprobe analysis of gold.....	216
Table E5: Microprobe analysis of chlorite.....	217
Table E6: Microprobe analysis of biotite.....	220
Table E7: Microprobe analysis of plagioclase.....	223
Table F1: List of diamond drill holes logged at Barry.....	216
Table H2: Samples chosen for XRD analyses.....	418

Chapter 1

Introduction

1.1 Archean Greenstone-hosted Gold Deposits

Archean greenstone belts have been recognized as prospective regions for gold, and are host to a number of world class (>100 metric tonnes of Au) lode gold deposits, which account for approximately 13% of gold production in the world (Jenkins et al., 1997; Goldfarb et al., 2001) and comprise various types. The greenstone-hosted quartz-carbonate vein type deposits, as defined by Dubé and Gosselin (2007), contain the second largest total tonnage of gold globally: only the Witwatersrand paleo-placer deposits of South Africa have higher amounts of contained gold (Dubé and Gosselin, 2007). Some of the world's largest gold deposits, including the Golden Mile (1800 t Au) in Kalgoorlie, Australia, and the Hollinger-McIntyre (987 t Au) in Timmins, Canada, belong to this type (Dubé and Gosselin, 2007).

Greenstone-hosted quartz-carbonate vein deposits generally have an average grade of 5 to 15 g/t Au, but can range in tonnage from a few thousand tonnes to over 100 million tonnes of ore (Dubé and Gosselin, 2007; Fig. 1.1). These deposit are found globally in cratons of Canada, U.S.A., Australia (Yilgarn), India (Dharwar), South America (Sao Francisco), southern Africa (Kaaopvaal, Zimbabwe, and Tanzania), Russia, and China, although there are currently no known world class deposits in the latter two countries

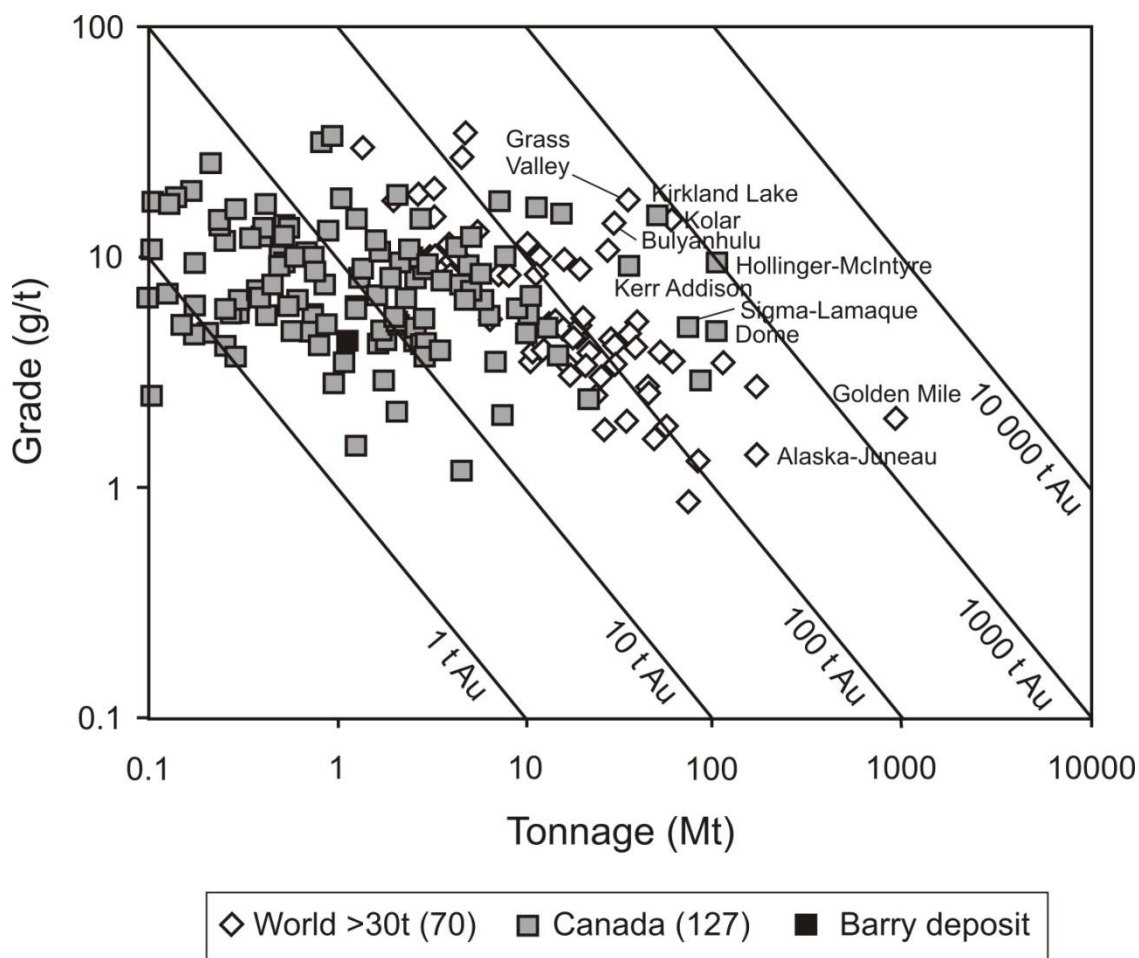


Fig. 1.1: Grade-tonnage diagram of Canadian and select world greenstone-hosted quartz-carbonate vein gold deposits. Selected world deposits contain at least 30 tonnes Au in combined production and reserves (modified after Dubé and Gosselin, 2007).

(Hagemann and Cassidy, 2000; Goldfarb et al., 2001; Dubé and Gosselin, 2007).

In Canada, the Superior and Slave Provinces are the main hosts of Archean lode gold deposits (Fig. 1.2). Fourteen deposits in Canada are considered world-class, with 12 of these occurring in the Superior Province (Robert and Poulsen, 1997; Fig. 1.2). Of these deposits, six are greenstone-hosted quartz-carbonate vein deposits: Red Lake (Campbell-

A.W. White), Dome, Hollinger-McIntyre, Kerr Addison, Kirkland Lake, and Sigma-Lamaque (Dubé and Gosselin, 2007; Figs. 1.2 and 1.3). This gold endowment in the Superior Province means that globally, in terms of historic gold production, it is second only to the Kaapvaal craton (Goldfarb et al., 2001). The Abitibi-Wawa subprovince of the Superior Province is host to all but one of the twelve world-class deposits in the Superior Province of Canada, and contains all five of the world class greenstone-hosted quartz-carbonate vein deposits (Robert and Poulsen, 1997; Dubé and Gosselin, 2007; Fig. 1.2).

Greenstone-hosted quartz-carbonate vein deposits can occur in belts of all ages, but are more common in Archean belts with variolitic tholeiitic basalts and ultramafic komatiitic flows metamorphosed to the greenschist facies that are intruded by felsic porphyry, albitite, or lamprophyre dikes (Dubé and Gosselin, 2007). The deposits form along major compressional or transtensional crustal-scale fault zones (Fig. 1.4), and are often spatially associated with fluvial-alluvial conglomerate, such as the Timiskaming conglomerate (Dubé and Gosselin, 2007). Gold mineralization occurs within laminated quartz-carbonate veins hosted by moderately to steeply dipping compressional brittle ductile shear zones and faults and within the associated shallow-dipping extensional veins and/or hydrothermal breccias (Dubé and Gosselin, 2007). Iron-carbonate alteration is generally associated with this type of deposit, with significant amounts of gold present

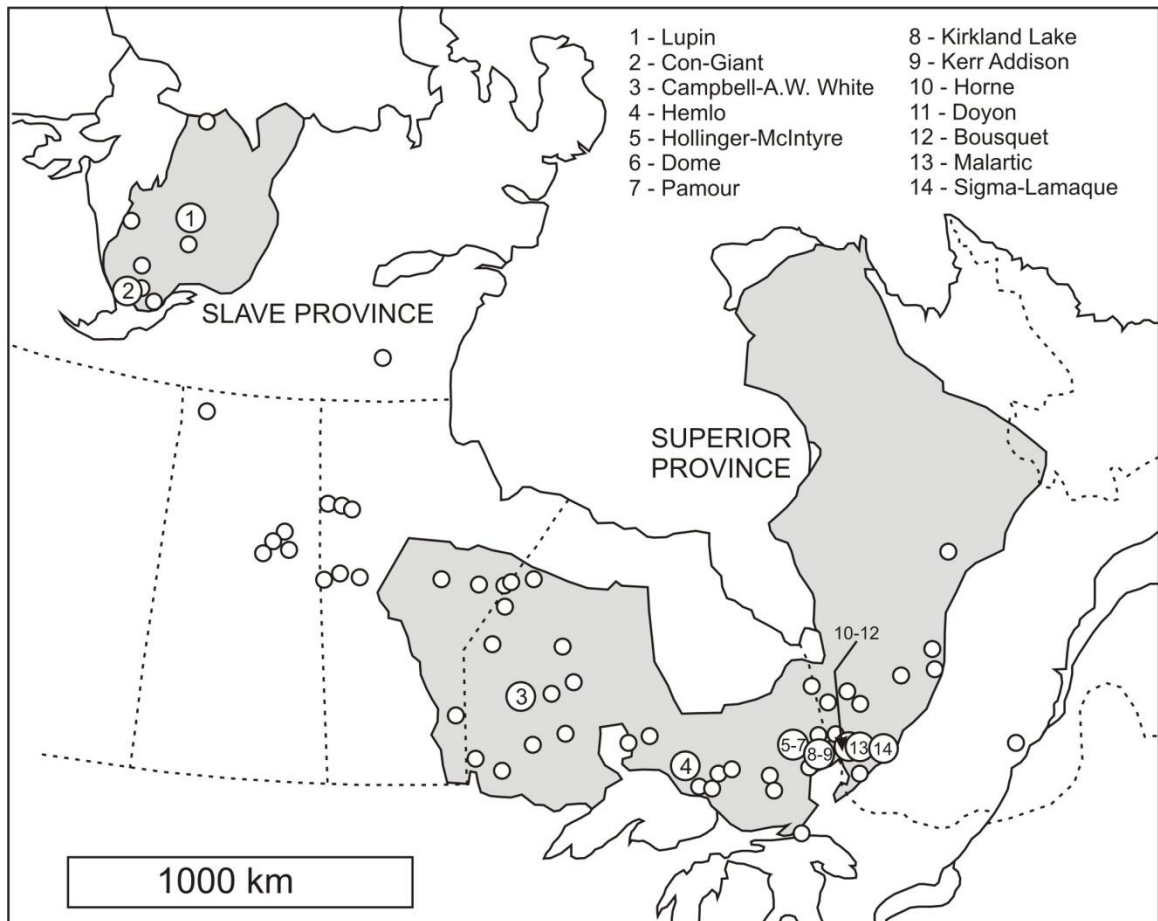


Fig. 1.2: Map showing the Archean Slave and Superior Provinces, and the locations of various Canadian gold deposits, including the 14 world class deposits (modified after Robert and Poulsen, 1997).

within iron-rich sulfidized wall-rock selvages or silicified and arsenopyrite-rich replacement zones (Dubé and Gosselin, 2007).

Archean greenstone-hosted quartz-carbonate vein deposits are thought to form at paleocrustal levels from 5 to 20 km deep during active deformation and metamorphism (Groves et al., 1998; Hagemann and Cassidy, 2000; Dubé and Gosselin, 2007). The

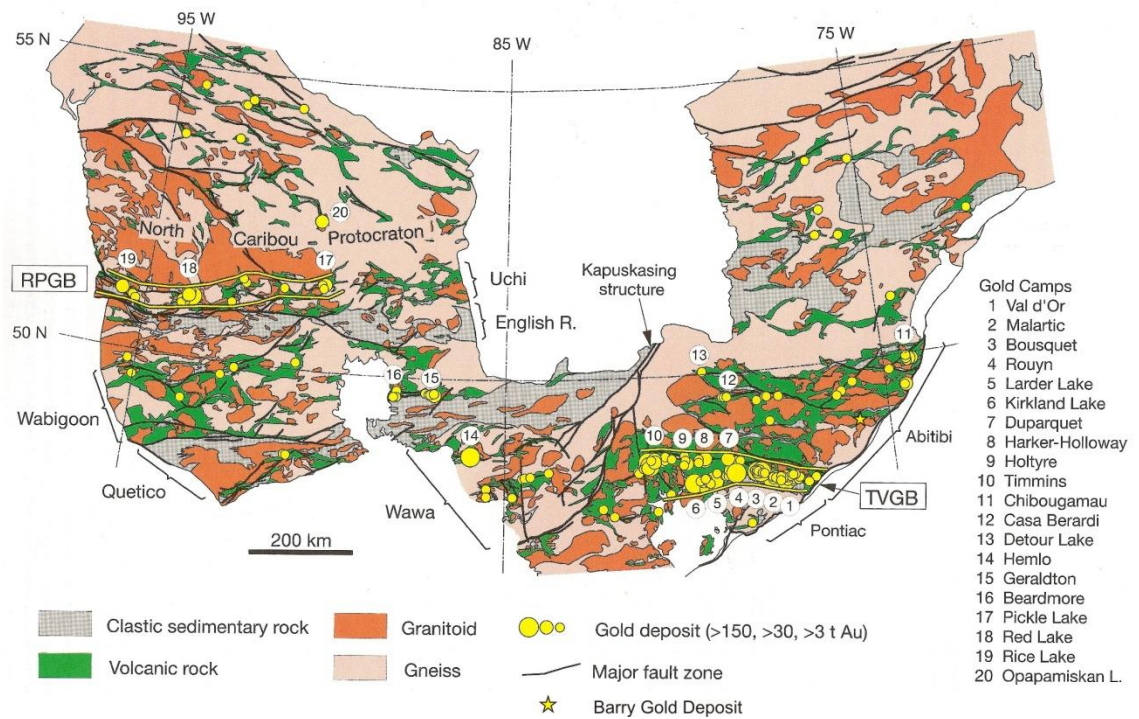


Fig. 1.3: Simplified geologic map of the Superior craton, showing the main subprovinces and significant gold deposits and camps (modified after Robert et al., 2005). RPGGB = Rice Lake-Pickle Lake gold belt, TVGB = Timmins-Val d'Or gold belt.

hydrothermal fluids forming these deposits are considered to be broadly uniform, low salinity, and aqueous-carbonic (Hagemann and Cassidy, 2000). The source of the fluids is largely unknown, although fluids may potentially be derived from a variety of sources including metamorphic devolatilization, felsic magmas, and mantle sources (Hagemann and Cassidy, 2000; Dubé and Gosselin, 2007). Differences in mineralogical and chemical characteristics are common for lode gold deposits, and are often attributed to variations at the deposition site (Hagemann and Cassidy, 2000) such as host rock and P-T conditions of emplacement (Colvine et al., 1988; Cassidy et al., 1998; Groves et al., 1998; McCuaig and Kerrich, 1998).

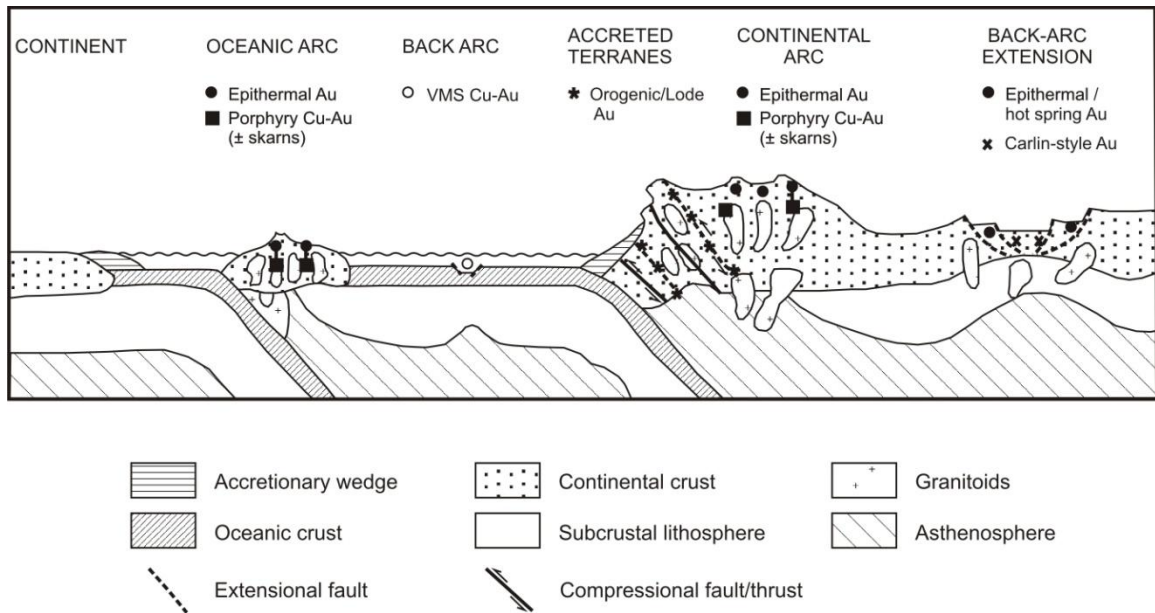


Fig: 1.4: Tectonic setting of gold-rich epigenetic mineral deposits (modified after Groves et al., 1998). Note that both the lateral and vertical scale of the arcs and accreted terrane have been exaggerated in order to show the spatial position and relative depth of the deposits.

Although many of these deposits are spatially associated with intrusive rocks, and some of the deposits are interpreted to be contemporaneous with magmatism (Hodgson and MacGeehan, 1982; Hodgson and Troop, 1988; Sauvé et al., 1993; Morasse et al., 1995; Goldfarb et al. 2001, 2005; Dubé and Gosselin, 2007), most deposits lack features that could accurately constrain the temporal relationship between magmatism and mineralization (Robert et al., 2005). In a similar manner, the temporal relationship between mineralization and metamorphism is very well constrained (Fig. 1.5). For instance, in the southern Abitibi subprovince gold mineralization is proposed to form coeval with (e.g., Claoué-Long et al., 1990; Kerrich and King, 1993) and post-peak metamorphism (e.g., Jemielita et al., 1990; Corfu and Davis, 1991; Wong et al., 1991;

Hagemann and Cassidy, 2000; Olivo and William-Jones, 2002; Goldfarb et al., 2005; Olivo et al., 2006; Dubé and Gosselin, 2007; Fig. 1.5).

1.2 Gold Deposits in the Abitibi-Wawa Subprovince

Several types of lode gold mineralization occur in the Abitibi-Wawa subprovince. These include disseminated/pyritic and quartz-carbonate vein type gold deposits (Robert, 1990; Robert and Poulsen, 1997; Robert et al., 2005; Dubé and Gosselin, 2007) and intrusion-related deposits (Morasse et al., 1995) in the Timmins and Val-d'Or mining district, as well as Cu-Au (generally having a high sulfide and copper content) deposits in the Chibougamau mining district (Robert, 1990; Robert et al., 2005; Fig. 1.3).

In the Timmins-Val d'Or gold belt (Fig. 1.3), gold deposits are hosted in mafic-ultramafic volcanic or intermediate to felsic volcanic rocks of the older (2750-2710 Ma) and younger (2710-2695 Ma) volcanic cycles (Robert et al., 2005; Fig. 1.5). Locally, narrow belts of clastic sedimentary rocks along the Porcupine-Destor and Larder Lake-Cadillac fault zones are also associated with mineralization (Robert et al., 2005; Fig. 1.3).

Plutonism in the belt occurred during volcanism and sedimentation and continued until ca. 2650 Ma (Robert et al., 2005; Fig. 1.5). The rocks of the Timmins-Val d'Or districts are metamorphosed to prehnite-pumpellyite to amphibolite facies during dynamothermal metamorphism ca. 2660 Ma (Powell et al., 1995; Robert et al., 2005; Fig. 1.5).

Timmins-Val d'Or Gold Belt

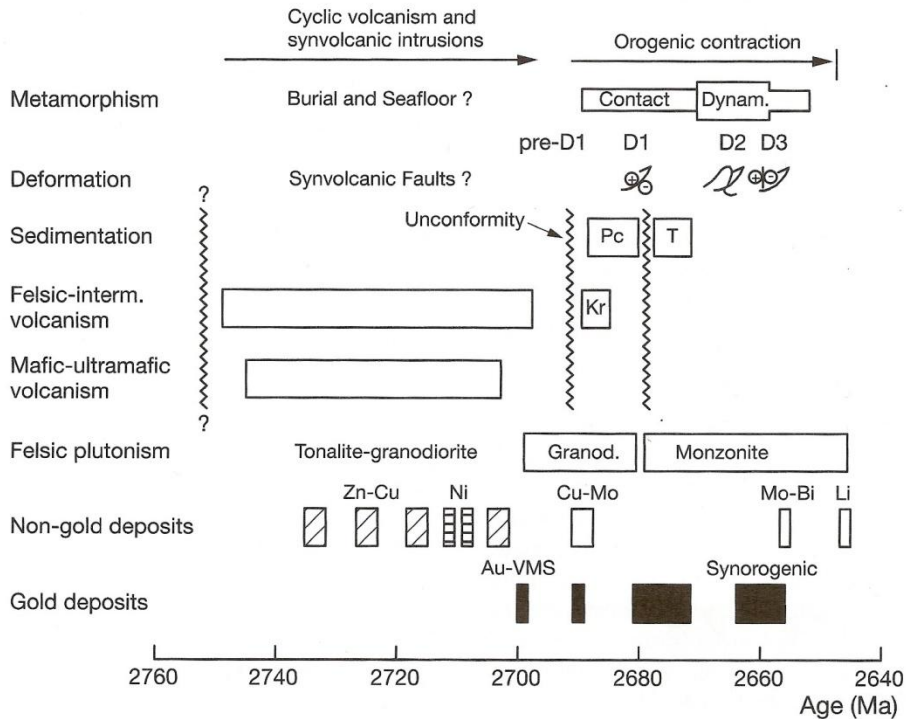


Fig. 1.5: Tectonic and metallogenic evolution diagram for the Timmins-Val d'Or gold belt (after Robert et al., 2005). Data from Corfu (1993), Robert (2001), and Ayer et al., (2002, 2003). Dynam = dynamothermal metamorphism, Pc = Porcupine Group, Kr = Krist Formation, T = Timiskaming Group.

In the Val d'Or-Malartic mining district two major events of lode (quartz-carbonate vein) gold mineralization (Fig. 1.5 and 1.6) have been identified based on vein geometry, mineralogy, wall-rock alteration, and cross-cutting relationships with intrusive rocks (Robert, 1990; Kerrich and Cassidy, 1994; Couture et al., 1994; Olivo and William-Jones, 2002; Robert et al., 2005). An earlier event, pre-2686 Ma, is recorded in the Kiena, Norlartic, and Siscoe Main ore zone (Couture et al., 1994; Morasse et al., 1995; Olivo and Hughes, 2004), which are commonly folded or boudinaged and cut by 2886 Ma-old dikes. The later, post-2680 Ma, auriferous veins (e.g., Sigma-Lamaque, Siscoe late

quartz-tourmaline veins: Jemielita et al., 1990; Wong et al., 1991; Olivo and William-Jones, 2002; Robert et al., 2005; Olivo et al., 2007) cross-cut the dikes and are interpreted to have formed after D₁ deformation and syn to late D₂ deformation (Robert et al., 2005: Figs. 1.5 and 1.6).

One of the most interesting questions about the evolution of greenstone belt hosted gold mineralization is the absolute timing of mineralization. This is due to the fact that, in most deposits, the hydrothermal phases coeval with gold mineralization are not suitable for dating using robust geochronological methods (e.g., Wong et al., 1991; Couture et al., 1994; Kerrich and Cassidy, 1994; Morasse et al., 1995; Hagemann and Cassidy, 2000; Kerrich and Ludden, 2000; Groves et al., 2003; Robert et al., 2005). In most of the deposits, the intrusive rocks that can be dated using robust geochronological methods (e.g. U-Pb zircon dating) either cut or are overprinted by gold mineralization, therefore dating the intrusive rocks can only give a minimum or maximum age for gold mineralization, respectively.

1.3 Investigation of the Barry Gold Deposit

The Barry gold deposit is an example of an Archean greenstone-hosted gold deposit in the Abitibi subprovince. The deposit is hosted in the Urban-Barry volcanic belt, which lies approximately 100km east of Lebel-sur-Quévillon and 200 km northeast of the Val

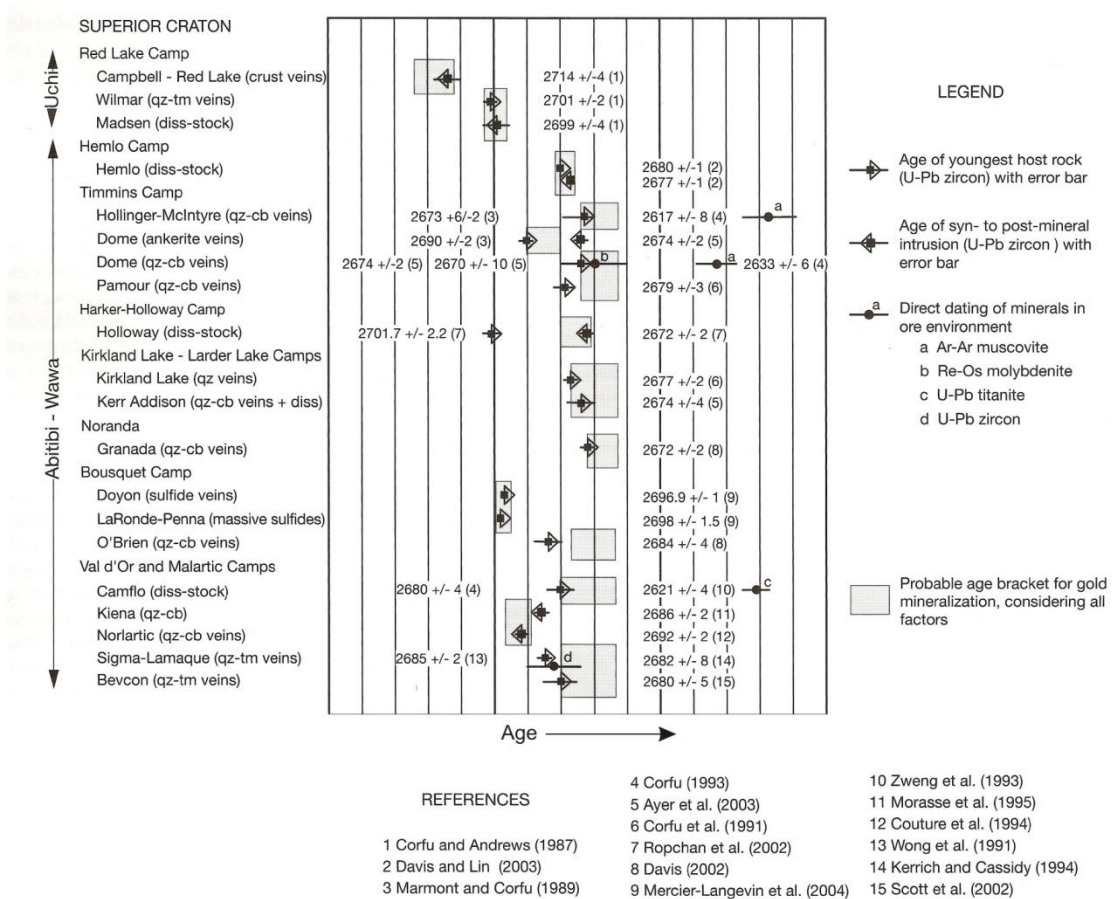


Fig. 1.6: Compilation of age constraints on selected gold deposits of the Superior craton (modified after Robert et al., 2005).

d'Or district (Fig. 1.7). In the Barry deposit, gold mineralization is spatially associated with NE-trending shear zones with moderate dip. Gold is found within contemporaneous straight and folded albite-carbonate-quartz veins and their surrounding carbonate-quartz-pyrite, and locally biotite-carbonate, alteration of the mafic volcanic rocks. Auriferous veins cut dioritic and early quartz-feldspar porphyry (QFP) dikes, but locally the mineralized zone is cut by late QFP dikes. The presence of both the pre-ore dioritic and post-ore QFP dikes provides a unique opportunity to determine the maximum and

minimum age of mineralization in this sector of the Abitibi greenstone belt using U-Pb zircon geochronological methods.

1.3.1 Objectives

Greenstone-hosted lode gold deposits are an important source of gold in Canada and around the world (Goldfarb et al., 2001). Although these types of deposits have been studied in detail in various locations and a variety of genetic models have been proposed, the source of fluids and metals, mechanisms for metal transport and deposition, and the absolute age of gold mineralization are still poorly understood.

The objective of this MScE thesis on the Barry deposit main zone is to contribute to the understanding of the formation of gold deposits during the evolution of Archean greenstone belts by studying the evolution of the Barry deposit in order to design exploration models. This is accomplished through the investigation of: (1) the nature and composition of the host rocks; (2) the styles of alteration and mineralization; (3) the structural controls on gold mineralization; and (4) the age of intrusive phases using U-Pb zircon geochronology.

1.3.2 Location and Access

The Barry gold deposit is hosted in the Abitibi subprovince of the Superior Province, Canada (Fig. 1.5). The deposit lies in the Urban-Barry volcanic belt of the Abitibi

subprovince (Figs. 2.1 and 2.2) and approximately 100 km east of Lebel-sur-Quévillon and 200 km northeast of the Val d'Or district.

The Barry deposit is located in Barry Township, approximately 95 km east of Lebel-sur-Quévillon, Québec. The property is accessible year round by Domtar Inc.'s logging roads (Fig. 1.7), which begin just outside of Quévillon towards the Domtar pulp and paper mill. From Boulevard Quévillon (the main route through Quévillon), take Chemin du Moulin southeast toward the Domtar plant. Before the plant, turn left (east) onto logging road 1000. Take road 1000 east to road 5000 (at approximately kilometre 11.5). Turn right (southeast) onto road 5000, and follow 5000 until approximately kilometre 69 before turning left (northeast) onto road 6000. Follow 6000 to approximately kilometre 97.5 and turn right (southeast) onto road 6600. Follow road 6600 for approximately 8 kilometres to the Barry deposit and camp. The Barry deposit is located to the right (east) of the road, and the camp is located to the left (west) of the road.

1.3.3 Exploration and Production History

As with many other mines in the region, the exploration history leading to the discovery and subsequent mining of the Barry deposit spans several decades with alternating periods of activity and inactivity (Systèmes Géostat International Inc., 2007). For many years the Barry deposit was explored to extend the known mineralized zones and

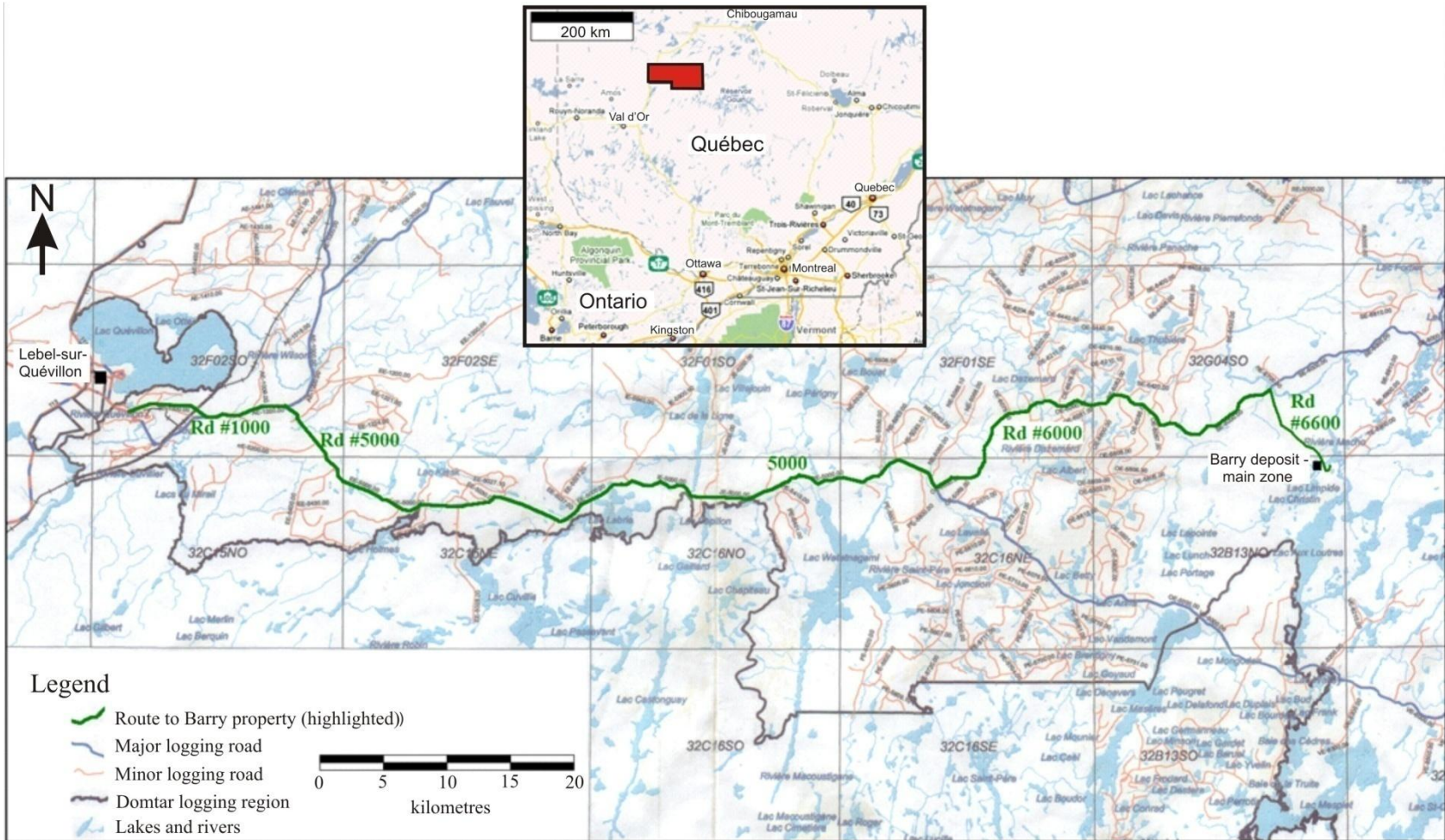


Fig. 1.7: Location map of the Barry property (modified after Domtar, 1994)

understand the deposit geometry in an attempt to make the deposit economic, but due to low gold prices, the small size, and the location of the Barry deposit, the deposit remained undeveloped. Fortunately in 2006 a combination of rising gold prices and the circumstances of Metanor Resources Inc., (current owner) transformed the Barry deposit into an economic gold deposit. With the higher gold prices, Metanor Resources Inc. had purchased the Bachelor Lake Mine and mill facility, 65 km northwest of the Barry deposit, with the intent to re-open the mine and mill. The Barry deposit, connected by logging roads to the Bachelor Mine, became a local source of mill feed for Metanor Resources Inc. while the Bachelor Lake Mine came back online.

Exploration of the Barry property began in ca. 1958 with local mapping by the Geologic Survey of Canada (GSC), and airborne MAG-EM performed in 1961 by Claims Ostiguy (Systèmes Géostat International Inc., 2007). From 1962-1990, various companies conducted geophysical surveys (MAG and EM), drilled 18 diamond drill holes (ddh), and conducted an evaluation of the property (Systèmes Géostat International Inc., 2007).

In 1994 Murgor Resources Inc. began an option to acquire 100% of the 14 claim properties (which include the Barry deposit) from Le Société de Développement de la Baie James (Systèmes Géostat International Inc., 2006). In 1995, the main zone was stripped (Fig. 1.8), allowing for extensive channel sampling, detailed mapping, geophysical surveys, and drilling of an additional 56 diamond drill holes from 1995-1996 (Systèmes Géostat International Inc., 2007). Further work, including IP survey, mapping,



Fig. 1.8: Aerial photograph of the trenched region of the Barry deposit prior to mining (after Metanor Resources Inc., 2008a). The trenched region in this picture measures approximately 200 m (east-west) and 75 m (north-south).

lithochemical sampling, and drilling of 4,456 m of core was conducted in 1997 by Teck Exploration as a joint venture with Murgor Resources Inc. (Systèmes Géostat International Inc., 2007). From 2005-2007, 96 new diamond drill holes were drilled and preliminary assessment studies were conducted on the main zone by Murgor Resources Inc. (Systèmes Géostat International Inc., 2007).

As of the end of August 2006, 248 holes had been drilled on the Barry property (this includes holes drilled to intersect several deeper shear zones). Over 55 of these were drilled on the trenched region of the main zone. The majority of the holes in the main zone have

been drilled at near vertical angles at NNW azimuths to an average depth of 30m. As of the summer of 2006, drill sections on the main zone were spaced approximately every eight to fifteen metres (northeast to southwest), with an average of two holes per section drilled within the trenched region.

The property was under 100% ownership by Murgor until December 2006, when it sold six claims of the Barry I property, including the Barry deposit, to Metanor Resources Inc. (Murgor, 2009). In September 2007 Metanor Resources Inc. signed an agreement to acquire the remaining interest of Murgor in the 8 additional claims of the Barry I property (Metanor Resources Inc., 2007a).

In the spring of 2007 the gold resources at the Barry deposit were re-evaluated by Systèmes Géostat International Inc. in compliance with National Instrument (NI) 43-101. The company outlined a near surface gold resource (with a 2 g/t cut-off) indicated at 1.48 t Au (52,300 oz Au; 385,000 t of ore at 4.23 g/t Au) and inferred at 3.58 t Au (126,000 oz Au; 966,000 t of ore at 4.07 g/t Au) (Systèmes Géostat International Inc., 2007).

Metanor Resources Inc. began clearing trees (for waste rock pads), further trenching of the main zone, and set-up on a site office and camp in the fall of 2007 in preparation for open pit mining at the site (Fig. 1.9). Bulk sampling of the Barry deposit by Metanor Resources Inc. began in October 2007, with two blasts releasing 5,100 t of material, of which 2,950 t was evaluated as mill feed. (Metanor Resources Inc., 2007b). Metanor

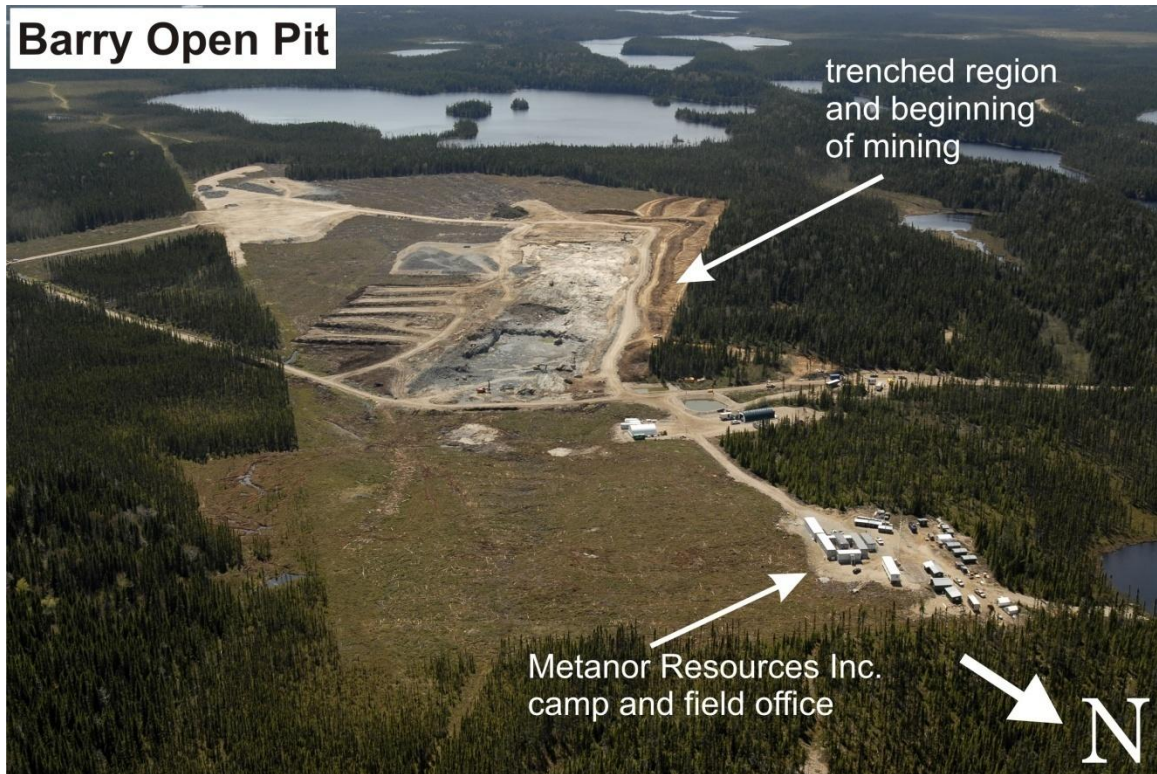


Fig. 1.9: Aerial photograph of the Barry open pit in the first stages of mining (after Metanor Resources Inc., 2008a)

Resources Inc. (2007b) calculated from channel samples that the grade of the mill-feed material was 4.33 g/t Au. Ore from the Barry deposit is crushed on site and is transported to the Bachelor Mine (owned and operated by Metanor Resources Inc.), which is located approximately 65 km northwest of the Barry deposit and is connected by forestry roads. In December 2007, the Bachelor Lake mill was given permission to begin the treatment of a bulk sampling of approximately 50,000 t of mill feed from the Barry deposit (Metanor Resources Inc., 2007c), and in October 2008 Metanor Resources Inc. began formal commercial production of gold from the Barry deposit (Metanor Resources Inc., 2008b). During the bulk sampling and pre-production phases at the Barry deposit between December 2007 and October 2008, Metanor Resources Inc. poured approximately 13,000 oz (368.5 kg) of gold bars with a production cost of approximately

\$375 CDN/oz (Metanor Resources Inc., 2008b). As of May 2009, Metanor Resources Inc. is still extracting ore from the Barry deposit.

1.3.4 Previous Geological Studies and Research

The main zone of the Barry deposit was trenched by Murgor Resources Inc. in 1995 to the dimensions of approximately 75m (NNW-SSE) by 200m (ENE-WSW; Fig. 1.8). Detailed mapping of the trench at a scale of 1:100 was conducted by André Tessier for Murgor Resources Inc. in the fall of 1995. Surface channel and grab samples were assayed for gold mineralization along the trenched region of the main zone.

Two petrographic reports were completed on the main zone: one as an internal report for Murgor Resources Inc. conducted by Clark Damer in 1996, and the second by James M. Lariviere, as a MinEx Master's thesis project at Queen's University, in 1997. Lariviere (1997) identified and described the volcanic facies (massive, feldspar-phyric, amygdular, pillowed, and flow breccia) and intrusive (quartz-feldspar porphyry) rocks, as well as the alteration assemblages ('inner biotite-ankerite-albite' and 'outer chloritic') present at the Barry deposit. Lariviere (1997) also identifies the quartz-ankerite-albite veins as the main host to gold, and describes gold as occurring as (1) free grains (<1-200 µm in diameter) in quartz-ankerite-albite veins, altered vein selvages, and gangue; and (2) within pyrite as inclusions, along microfractures, and along the edge of pyrite grains.

1.3.5 Methodology

The description of the Barry deposit geology is based on data collected during our fieldwork conducted from June to August 2006 and during August 2007, lithogeochemical and petrographic investigations, and data collected in the field by Tessier in 1996.

The goals of this MScE project are achieved through an integration of the field and laboratory studies outlined below:

1. Detailed mapping, core logging, and sampling of the Barry deposit main zone, focusing on:
 - a. the geometry of rock units, mineralized veins, and host rock alteration;
 - b. the relative ages of events (intrusive units, mineralization, and alteration);
and
 - c. the structural controls on mineralization;
2. Detailed petrological, mineralogical, and geochemical investigation in order to:
 - a. characterize the host mafic volcanic and intrusive rocks;
 - b. determine relative timing and composition of the various alteration types in the mafic volcanic and intrusive rocks;
 - c. evaluate the elements enriched and depleted in alteration zones associated with gold mineralization; and
 - d. determine the mode of occurrence and composition of gold and minerals associated with gold mineralization and alteration

3. U-Pb zircon dating of pre-ore and post-ore intrusive dikes in order to constrain the age of mineralization.

1.3.5.1 Mapping, Drill Core Logging, and Sampling

Mapping and sampling at the Barry deposit was conducted from June to August 2006 and during August 2007. Two areas of the trenched surface were selected to be mapped in detail at 1:50 scale to complement the map that was done by at a scale of 1:100 by Tessier in 1996. Mapping at a scale of 1:50 was conducted in two regions of the trenched main zone during the 2006 field season. The two mapped zones consist of the northeast corner (Barry deposit main grid 1050E to 1080E and 55S to 75S) and the 1074 block (Barry deposit main grid 070E to 1090E and 55S to 100S; Appendix A). These regions were chosen to add detail to the 1:100 trench map as they contain various important structural features (e.g. faults, foliation, mineralized veins, boudinaged veins) and intrusive dikes that were not previously identified. Surface channel samples (43) were collected throughout the main zone at this time for petrographic and geochemical investigations.

A total of 23 drill holes were logged throughout the main trenched zone (Appendix F), with 13 holes selected to be studied in detail. Mafic volcanic units, intrusive rocks, and zones of various types of alteration were sampled in the trenched region and in 13 drill holes that were selected to be studied in detail. Both surface and drill core samples were taken in order to petrographically and geochemically characterize the various rock units

and their alteration. Descriptions and locations of drill core and surface samples are summarized in Appendix B.

Drill core samples (309) were taken from holes 127, 135, 210 (cross section 1037); 31, 117, 118 (cross section 1074); 142, 143, 151 (cross section 1088); 27, 136, 201 (cross section 1124); 101 and 182 (cross section 1166; Appendix B). Drill hole samples consist of one quarter to one half of the core, which were used for lithochemical analysis and polished thin sections.

Surface samples were taken using a diamond saw. Samples were cut from various lithologies across the main zone (including rusty carbonatized zones) to provide enough samples for comparison of petrographic and geochemical information of rock types (Appendix B). The orientation of some samples has been taken so that detailed work on microstructures could be conducted in the future. Large samples (approximately 10 cm³) of the quartz-feldspar porphyries and diorite dikes in the main trench were taken for geochronological investigation in order to constrain the age of mineralization.

Structural measurements were taken across the main zone, with a focus on obtaining data on the two structural blocks mapped in detail. Measurements of foliation, faults, lithologic contacts, orientations of intrusive dikes, and vein orientations, with special attention paid to measuring fold axis of folded veins were taken. Structural measurements from the 2007 field season are summarized in Appendix C.

Several GPS points were taken on each of the 2006 mapping grids (Appendix A) in order to georeference the grids for future digitizing of the detailed maps (Map 1: 1070E to 1090E and 55S to 100S; Map 2 - northeast corner: 1050E to 1080E and 55S to 75S).

1.3.5.2 Analytical Procedures

Samples were investigated using transmitted and reflected light microscopy (detailed description of individual samples are in Appendix G), scanning electron microscopy (SEM), litho-geochemistry (Appendix D), electron microprobe analysis (EMPA) (Appendix E), X-ray diffraction (Appendix H), and were dated using U-Pb isotope systematics on zircon grains. The summary of operating conditions for the laboratory work outlined above and the U-Pb methodology are described in Chapter 2: ‘Analytical Methods’.

1.4 Thesis Organization

This thesis has been written in manuscript format. The first chapter of this thesis focuses on the current state of knowledge of Archean greenstone-hosted lode gold deposits in the world, and in the Abitibi greenstone belt in particular, and outlines the thesis scope.

Chapter 2 is a manuscript titled ‘Structural, Mineralogical, Geochemical and Geochronological Investigation of the Barry Gold Deposit, Abitibi Subprovince, Canada: Greenstone-hosted Gold Coeval with Late Archean Deformation and Magmatism’, to be submitted to *Economic Geology*. This chapter outlines the geology, structure,

mineralogy, geochemistry, and geochronology conducted at the Barry deposit and discusses the evolution of the deposit and the implications of the Barry deposit's unique geological features in a regional context. Chapter 3 briefly summarizes the main findings, discusses some relevant questions about the genesis of this type of deposit that were not covered during this investigation, and proposes future work to address these questions. A synopsis of the conclusions and the main contributions of this research, as well as some guidelines for exploration of this type of deposit are included in Chapter 4. Appendices comprise: A) Geologic maps and vertical cross sections of the Barry gold deposit; B) Sample locations and descriptions; C) Structural data and fault plane resolution method; D) Lithochemical results; E) Microprobe results; F) Drill core logging from the Barry deposit; G) Petrographic descriptions; and H) XRD analyses.

References

- Ayer, J., Amelin, Y., Corfu, F., Kamo, S., Ketchum, L., Kwok, K., and Trowell, N.F., 2002, Evolution of the southern Abitibi greenstone belt based on U-Pb geochronology: Autochthonous volcanic construction followed by plutonism, regional deformation and sedimentation: *Precambrian Research*, v. 115, p. 63-95.
- Ayer, J., Barr, E., Bleeker, W., Creaser, R.A., Hall, G., Ketchum, J.W.F., Powers, D., Salier, B., Still, A., and Trowell, N.F., 2003, Discover Abitibi. New geochronological results from the Timmins area: Implications for the timing of late tectonic stratigraphy, magmatism, and gold mineralization: Ontario Geological Survey Open File Report 6120, p. 33-1 to 33-11.
- Cassidy, K.F., Groves, D.I., and McNaughton, N.J., 1998, Late-Archean granitoid-hosted lode-gold deposits, Yilgarn Craton, Western Australia: Deposit characteristics, crustal architecture and implications for ore genesis: *Ore Geology Reviews*, v. 13, p. 65-102.
- Claoué-Long, J.C., King, R.W., and Kerrich, R., 1990, Archean hydrothermal zircon in the Abitibi greenstone belt: constraints on the timing of gold mineralization: *Earth and Planetary Science Letters*, v. 98, p. 109-128.
- Colvine, A.C., Fyon, J.A., Heather, K.B., Marmont, S., Smith, P.M., and Troop, D. G., 1988, Archean lode gold deposits in Ontario: Ontario Geological Survey, Miscellaneous Paper 139, 136 p.
- Corfu, F., 1993, The evolution of the southern Abitibi greenstone belt in light of precise U-Pb geochronology: *Economic Geology*, v. 88, p. 1323-1340.
- Corfu, F., and Andrews, A.J., 1987, Geochronological constraints on the timing of magmatism, deformation, and gold mineralization in the Red Lake greenstone belt, northwestern Ontario: *Canadian Journal of Earth Sciences*, v. 24, p. 1302-1320.
- Corfu, F., and Davis, D.W., 1991, Comment on "Archean hydrothermal zircon in the Abitibi greenstone belt: constraints on the timing of gold mineralization" by J.C. Claoué-Long, R.W. King, and R. Kerrich: *Earth and Planetary Science Letters*, v. 104, p. 545-552.
- Corfu, F., Jackson, S.L., and Sutcliffe, R.H., 1991, U-Pb ages and tectonic significance of late Archean alkali magmatism and non-marine sedimentation: Timiskaming Group, southern Abitibi belt, Ontario: *Canadian Journal of Earth Sciences*, v. 28, p. 489-503.
- Couture, J.-F., Pilote, P., Machado, N., and Desrocher, J.-P., 1994, Timing of gold mineralization in the Val d'Or district, southern Abitibi belt: Evidence for two distinct mineralizing events: *Economic Geology*, v. 89, p. 1542-1551.

- Davis, D.W., 2002, U-Pb geochronology of Archean metasedimentary rocks in the Pontiac and Abitibi subprovinces, Quebec: Constraints on timing, provenance and regional tectonics: *Precambrian Research*, v. 115, p. 97-118.
- Davis, D.W., and Lin, S., 2003, Unraveling the geologic history of the Hemlo Archean gold deposit, Superior province, Canada: A U-Pb geochronological study: *Economic Geology*, v. 98, p. 51-67.
- Domtar, 1994, Forestry map, <www.Domtar.com>, August 2007.
- Dubé, B., and Gosselin, P., 2007, Greenstone-hosted quartz-carbonate vein deposits, *in* Goodfellow, W.D., ed., *Mineral Deposits of Canada: A synthesis of major deposit-types, district metallogeny, the evolution of geological provinces, and exploration methods*: Geological Association of Canada, Mineral Deposits Division, Special Publication No. 5, p. 49-73.
- Goldfarb, R.J., Baker, T., Dubé, B., Groves, D.I., Hart, C.J.R., and Gosselin, P., 2005, Distribution, character, and genesis of gold deposits in metamorphic terranes: *Economic Geology 100th Anniversary Volume*, p. 407-450.
- Goldfarb, R.J., Groves, D.I., and Gardoll, S., 2001, Orogenic gold and geologic time: A global synthesis: *Ore Geology Reviews*, v. 18, p. 1-75.
- Groves, D.I., Goldfarb, R.J., Gebre-Mariam, M., Hagemann, S.G., and Robert, F., 1998, Orogenic gold deposits: A proposed classification in the context of their crustal distribution and relationship to other gold deposit types: *Ore Geology Reviews*, v. 13, p. 7-27.
- Groves, D.I., Goldfarb, R.J., Robert, F., and Hart, C.J.R., 2003, Gold deposits in metamorphic belts: Overview of current understanding, outstanding problems, future research, and exploration significance: *Economic Geology*, v. 98, p. 1-29.
- Hagemann, S.G., and Cassidy, K.F., 2000, Archean orogenic lode gold deposits: *SEG Reviews*, v. 13, p. 9-68.
- Hodgson, C.J., and MacGeehan, P.J., 1982, Geologic characteristics of old deposits in the Superior Province of the Canadian Shield: *In* *Geology of Canadian Gold Deposits*, Edited by R.W. Hodder and W. Petruk, Canadian Institute of Mining and Metallurgy, Special Volume 24, p. 211-229.
- Hodgson, C.J., and Troop, D.G., 1988, A new computer-aided methodology for area selection in gold exploration: A case study from the Abitibi greenstone belt: *Economic Geology*, v. 83, p. 952-977.

- Jemielita, R.A., Davis, D.W., Krogh, T.E., 1990, U-Pb evidence for Abitibi gold mineralization postdating greenstone magmatism and metamorphism: *Nature*, v. 345, p. 831-834.
- Jenkins, C.L., Vincent, R., Robert, F., Poulsen, K.H., Garson, D.F., and Blondé, J.A., 1997, Index-level database for lode gold deposits of the world: Geological Survey of Canada Open File 3490, 18 p. (with map and CD).
- Kerrick, R., and Cassidy, K.F., 1994, Temporal relationships of lode gold mineralization to accretion, magmatism, metamorphism, and deformation – Archean to present: A review: *Ore Geology Reviews*, v. 9, p. 263-310.
- Kerrick, R., and King, R., 1993, Characteristics of hydrothermal zircon and baddeleyite in Val d'Or mesothermal gold deposits: Age of primary gold mineralization (ca. 2680 Ma) versus secondary fluid resetting events (2630-2579 Ma) [abs.]: *Geological Association of Canada Program with Abstracts*, v. 346, p. A-52.
- Kerrick, R., and Ludden, J., 2000, The role of fluids during formation and evolution of the southern Superior Province lithosphere: an overview: *Canadian Journal of Earth Sciences*, v. 37, p. 135-164.
- Lariviere, J.M., 1997, Petrographic Analysis of Alteration and Gold Mineralization at the Barry Gold Property, Barry Township, Québec, MinEx Master's Thesis, Queen's University, Kingston, 52 p.
- Marmont S., and Corfu, F., 1989, Timing of gold introduction in the Late Archean tectonic framework of the Canadian Shield: Evidence from U-Pb zircon geochronology of the Abitibi subprovince: *Economic Geology Monograph* 6, p. 101-111.
- McCuaig, T.C., and Kerrich, R., 1998, P-T-t-deformation-fluid characteristics of lode gold deposits: evidence from alteration systematic: *Ore Geology Reviews*, v. 12, p. 381-453.
- Mercier-Langevin, P., Dubé, B., Hannington, M.D., Davis, D., and Lafrance, B., 2004, Contexte géologique et structural des sulfures massifs volcanogènes aurifères du gisement LaRonde, Abitibi: *Ministères des Ressources naturelles de la faune et des parcs*, ET 2003-03, 60 p.
- Metanor Resources Inc., 2007a, Metanor acquires more properties, <http://www.metanor.ca/exploration-miniére/investisseurs_communiqueDePresseDetails_ang.cfm?noCommuniquePresseMetanor=105>, September, 2007.
- Metanor Resources Inc., 2007b, Bulk sampling has begun at the Barry open pit, <[26](http://www.metanor.ca/exploration-</p>
</div>
<div data-bbox=)

- miniere/investisseurs_communiqueDePresseDetails_ang.cfm?noCommuniquePresseMetanor=108>, October, 2007.
- Metanor Resources Inc., 2007c, Metanor restarts the Bachelor mill, <http://www.metanor.ca/exploration-mini%C3%A9rie/investisseurs_communiqueDePresseDetails_ang.cfm?noCommuniquePresseMetanor=117>, December, 2007.
- Metanor Resources Inc., 2008a, Barry, <http://www.metanor.ca/exploration-mini%C3%A9rie/trousseMedia_images-hautes-resolutions_ang.cfm>, December, 2008.
- Metanor Resources Inc., 2008b, Commercial production begins, <http://www.metanor.ca/exploration-mini%C3%A9rie/investisseurs_communiqueDePresseDetails_ang.cfm?noCommuniquePresseMetanor=135>, October, 2008.
- Morasse, S., Wasteneys, H.A., Cormier, M., Helmstaedt, H., and Mason, R., 1995, A pre-2686 Ma intrusion-related gold deposit at the Kienna mine, Val d'Or, Québec, southern Abitibi subprovince: *Economic Geology*, v. 90, p. 1310-1321.
- Murgor, 2009, The Barry gold deposit and project, Quebec, Canada, <<http://www.murgor.com/index.php?module=CMS&id=58>>, April, 2009.
- Olivo, G.R., Chang, F., and Kyser, T.K., 2006, Formation of the auriferous and barren north dipper veins in the Sigma mine, Val d'Or, Canada: Constraints from structural, mineralogical, fluid inclusion, and isotopic data: *Economic Geology*, v. 101, p. 607-631.
- Olivo, G.R. and Hughes, K.A., 2004, The two distinct types of auriferous veins in the Val d'Or district, Southern Abitibi, Canada: structural, alteration, mineralogical and fluid constraints [abs.]: 32th International Geological Congress, Florence, August 20-28, 2004, Conference Abstract cd-rom.
- Olivo, G.R., Isnard, H., William-Jones, A.E., and Gariépy, C., 2007, Pb isotope compositions of pyrite from the C quartz-tourmaline vein of the Siscoe gold deposit, Val d'Or, Quebec: Constraints on the origin and age of the gold mineralization: *Economic Geology*, v. 102, p. 137-146.
- Olivo, G.R., and William-Jones, A.E., 2002, Genesis of the auriferous C quartz-tourmaline vein of the Siscoe mine, Val d'Or district, Abitibi subprovince, Canada: Structural, mineralogical and fluid inclusion constraints: *Economic Geology*, v. 97, p. 929-947.
- Powell, W.G., Carmichael, D.M., and Hodgson, C.J., 1995, Conditions and timing of metamorphism in the southern Abitibi greenstone belt, Quebec: *Canadian Journal of Earth Sciences*, v. 32, p. 787-805.

- Robert, F., 1990, An Overview of gold deposits in the eastern Abitibi subprovince: The Canadian Institute of Mining and Metallurgy Special Volume 43, p. 93-105.
- Robert, F., 2001, Syenite-associated disseminated gold deposits in the Abitibi greenstone belt, Canada: *Mineralium Deposita*, v. 36, p. 503-516.
- Robert, F., and Poulsen, K.H., 1997, World-class Archaean gold deposits in Canada: and overview: *Australian Journal of Earth Sciences*, v. 44, p. 329-351.
- Robert, F., Poulsen, K.H., Cassidy, K.F., and Hodgson, J., 2005, Gold metallogeny of the Superior and Yilgarn Cratons: *Economic Geology 100th Anniversary Volume*, p. 1001-1033.
- Ropchan, J.R., Luinstra, B., Fowler, A.D., Benn, K., Ayer, J., Berger, B., Dahn, R., Labine, R., and Hamelin, Y., 2002, Host-rock and structural controls on the nature and timing of gold mineralization at the Holloway mine, Abitibi subprovince, Ontario: *Economic Geology*, v. 97, p. 291-309.
- Sauvé, P., Imreh, L., and Trudel, P., 1993, Description des gîtes d'or de la région de Val d'Or: Ministère de l'Énergie et des Ressources, Québec, MM 91-03, 178 p.
- Scott, C.R., Mueller, W.U., and Pilote, P., 2002, Physical volcanology, stratigraphy, and litho-geochemistry of an Archean volcanic arc: Evolution from plume-related volcanism to arc rifting of SE Abitibi greenstone belt, Val d'Or, Canada: *Precambrian Research*, v. 115, p. 223-260.
- Systemes Géostat International Inc., 2006, Technical Report: Resources Evaluation of March 2006 on the Barry I Project, Barry township, Murgor Resources Inc.: SEDAR <www.sedar.com>, date of filing: July 14, 2006, 246 p.
- Systemes Géostat International Inc., 2007, NI 43-101 Technical Report of the Preliminary Assessment on Barry-1 and Bachelor Properties of Metanor Resources Inc.: SEDAR <www.sedar.com>, date of filing: Oct. 16, 2007, 370 p.
- Wong, L., Davis, D.W., Krogh, T.E., and Robert, F., 1991, U-Pb zircon and rutile chronology of Archean greenstone formation and gold mineralization in the Val d'Or region, Québec: *Earth and Planetary Science Letters*, v. 104, p. 325-336.
- Zweng, P.L., Mortensen, J.K., and Dalrymple, G.B., 1993, Thermochronology of the Camflo gold deposit, Malartic, Quebec: Implications for magmatic underplating and the formation of gold-bearing quartz veins: *Economic Geology*, v. 88, p. 1700-1721.

Chapter 2

Structural, Mineralogical, Geochemical and Geochronological Investigation of the Barry Gold Deposit, Abitibi Subprovince, Canada: A Greenstone-hosted Gold Deposit Coeval with Late Archean Deformation and Magmatism

2.1 Introduction

Archean greenstone-hosted lode gold deposits provide about thirteen percent of the world's gold resources (Jenkins et al., 1997; Goldfarb et al., 2001; Dubé and Gosselin, 2007), hosting some of the world's largest gold deposits, including the Golden Mile (>2,000 t Au) in Kalgoorlie, Australia, and the Hollinger-McIntyre (>1,000 t Au) in Timmins, Canada (Hagemann and Cassidy, 2000). They are second in total tonnage of gold only to paleoplacer deposits of the Witwatersrand-type. In Canada, the Archean Superior and Slave provinces contain more than 220 gold deposits with reserves exceeding 1 t Au at a grade varying between 4 and 12 g/t (Robert and Poulsen, 1997; Hagemann and Cassidy, 2000), totaling 5972 tonnes of Au in combined production and reserves (Dubé and Gosselin, 2007).

The Abitibi-Wawa subprovince of the Superior Province is host to eleven 'world-class' (> 100 t Au) gold deposits and represents one of the best gold-endowed regions in the world (Robert and Poulsen, 1997). Archean gold mineralization in this region ranges from quartz-vein, to disseminated sulfides, to massive sulfides (Robert and Poulsen, 1997), with the first two types generically referred to as "Archean orogenic gold

deposits” by Groves et al. (1998). The Archean orogenic deposits are thought to form at a range of paleocrustal levels from shallow (<5km) to deep (20km) during active deformation and metamorphism (Hagemann and Cassidy, 2000). These deposits are considered to have formed from broadly uniform, low salinity, aqueous-carbonic hydrothermal fluids that transported Au and other metals, with the fluids potentially derived from a variety of sources including metamorphic devolatilization, felsic magmas, and mantle sources (Hagemann and Cassidy, 2000).

Different styles of mineralization that formed at distinct stages have been documented in gold camps such as the Val d’Or-Malartic district. There, two major events of lode gold mineralization have been recognized on the basis of vein geometry, mineralogy, wall-rock alteration, and cross-cut relationships with intrusive rocks (Robert, 1990; Kerrich and Cassidy, 1994; Couture et al., 1994; Olivo and William-Jones, 2002; Robert et al., 2005). The early, pre-2692 Ma, deposits (eg. Kiena, Norlartic, and Siscoe Main ore zone: Couture et al., 1994; Olivo and Hughes, 2004; Morasse et al., 1995) are commonly folded or boudinaged and cut by 2692 Ma-old dikes. Whereas the later, post-2630 Ma auriferous veins (e.g., Sigma-Lamaque, Siscoe late quartz-tourmaline veins: Jemielita et al., 1990; Wong et al., 1991; Robert et al, 2005; Olivo and William-Jones, 2002; Olivo et al., 2007), cross-cut the dikes and are interpreted to be formed during to late in the main stage of regional deformation (syn-orogenic).

Many orogenic gold deposits hosted in Archean terranes are spatially associated with mafic to intermediate dikes and plugs, and some of the deposits are interpreted to be

contemporaneous with magmatism according to crosscutting relationships (Hodgson and MacGeehan, 1982; Hodgson and Troop, 1988; Sauvé et al., 1993; Morasse et al., 1995; Goldfarb et al. 2001, 2005). However, in most of the deposits the temporal relationship between mineralization and magmatic events is not well constrained (Robert et al., 2005) and the difference in age between mineralized intrusive rocks and cross-cutting, post-mineralization dikes are in the order of several tens of millions of years. Determination of the absolute ages of mineralization has been proven difficult, as most of the hydrothermal minerals coeval with gold mineralization are not suitable for dating using robust geochronological methods (e.g., Wong et al., 1991; Couture et al., 1994; Kerrich and Cassidy, 1994; Morasse et al., 1995; Hagemann and Cassidy, 2000; Kerrich and Ludden, 2000; Groves et al., 2003; Robert et al., 2005). Similarly, the temporal relationship between mineralization and metamorphism is highly debated, having been proposed as coeval with (e.g., Claoué-Long et al., 1990; Kerrich and King, 1993) or post-peak metamorphism (e.g., Jemielita et al., 1990; Corfu and Davis, 1991; Wong et al., 1991; Hagemann and Cassidy, 2000; Olivo and William-Jones, 2002; Goldfarb et al., 2005; Olivo et al., 2006).

The Barry gold deposit is hosted by the Urban-Barry volcanic belt of the Abitibi subprovince and lies approximately 100km east of the town of Lebel-sur-Quévillon and 200 km northeast of the Val d'Or gold district (Fig. 2.1). In the Barry deposit, gold mineralization is mainly present within sheeted albite-carbonate-quartz veins and their surrounding mafic volcanic rocks, which are altered to carbonate-quartz-pyrite and locally biotite-carbonate assemblages, spatially associated with NE-trending shear zones

of moderate dip. The auriferous veins cut dioritic and early quartz-feldspar porphyry (QFP) dikes, and are cut by late QFP dikes, which provides a good opportunity to constrain the age of the gold mineralization in this sector of the Abitibi greenstone belt.

In this study we characterized the host rocks, the geometry and compositions of mineralized veins and alteration zones, and determined the age of the pre- and post-mineralization dikes using U-Pb dating of zircon in order to further our understanding of the timing and processes related to formation of gold deposits during the evolution of late Archean greenstone belts. This study reveals that gold mineralization at the Barry deposit is coeval with deformation, as well as with arc-related syn-collisional intermediate to felsic magmatism emplaced ca. 2697 Ma.

2.2 Regional Geology

The Urban-Barry belt is a narrow E-W belt comprising mafic volcanic rock units in the Northern Volcanic Zone (NVZ) of the Abitibi greenstone belt (Fig. 2.1; Chown et al., 1992). This 6.5-20 km wide volcano-sedimentary belt extends from the Grenville front in the east to Lebel-sur-Quévillon to the west (Fig. 2.1). The Barry deposit is located in a southwest trending limb of the Urban-Barry belt, and is approximately 25 km north of Lac aux Loutres. The geology of the Urban-Barry belt and Lac aux Loutres region has been described by Milner (1939), Milner (1943), Joly (1990), Bandyayera et al. (2002, 2003, 2004a, 2004b),

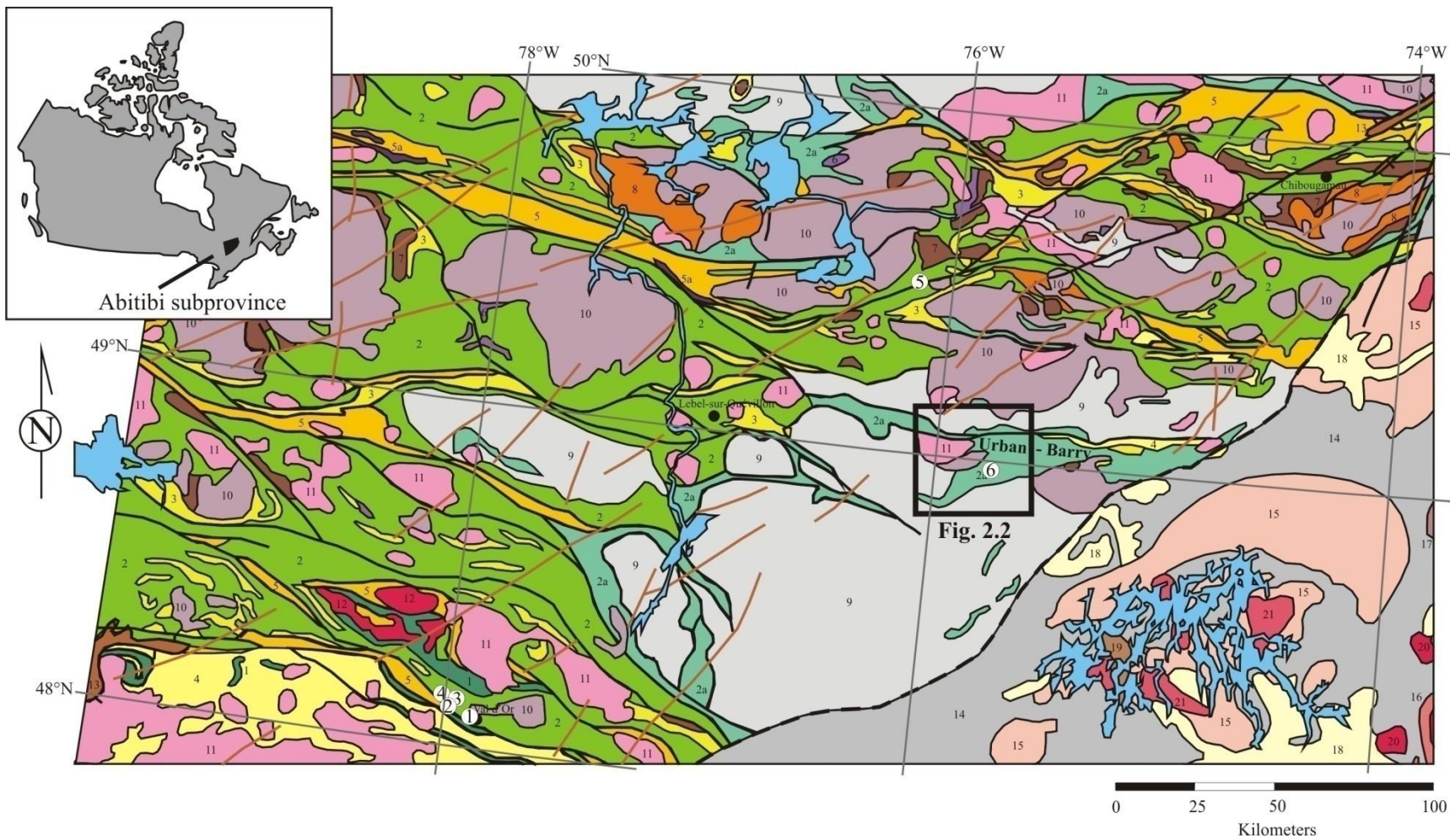


Fig. 2.1: Simplified geology of the Abitibi subprovince, Québec (modified after MRN, 2002), locating selected gold deposits, including the Barry deposit (at 6).

Grenville Province

PROTEROZOIC

GRANITOIDS

- 21 Granite and pegmatite
- 20 Orthopyroxene bearing granitoids: charnockite, mangerite, jotunite and hypersthene syenite

MAFIC TO ULTRAMAFIC ROCKS

- 19 Gabbro, pyroxenite, troctolite and amphibolite

SEDIMENTARY ROCKS

- 18 Paragneiss, quartzite and amphibolite

ARCHEAN AND/OR PROTEROZOIC

- 17 Migmatite
- 16 Charnockitic gneiss and orthopyroxene bearing granitoids
- 15 Granodioritic and granitic gneisses; foliated or migmatized granitoids

ARCHEAN

- 14 Grey gneiss with quartz, plagioclase, biotite and/or hornblende, mafic gneiss with hornblende and/or biotite, and amphibolite

Superior Province

PROTEROZOIC

- Diabase and gabbro dykes
- 13 Argillite, wacke, conglomerate and tillite (Cobalt Group and Chibougamau Formation)

ARCHEAN

GRANITOIDS

- 12 Post-tectonic granitic rocks: alkalic granite with fluorite, and monzogranite
- 11 Syn- to late-tectonic granitic rocks: granite, granodiorite, monzonite and syenite; minor diatexite

- 10 Syn- to late-tectonic tonalitic rocks: tonalite, trondhjemite and granodiorite; minor diorite and monzodiorite

- 9 Pre- to syn-tectonic granitoids: tonalitic and trondhjemitic gneisses; undivided gneiss; minor diorite

MAFIC TO ULTRAMAFIC INTRUSIONS

- 8 Stratiform complexes: anorthosite, gabbro and pyroxenite
- 7 Mafic intrusive rocks: gabbro, gabbronorite, diorite, and carbonatite complex; minor intrusive and extrusive ultramafic rocks
- 6 Ultramafic intrusive rocks: pyroxenite, peridotite, hornblende, serpentinite, and ultramafic and mafic sills

SEDIMENTARY ROCKS

- 5 Sedimentary rocks: wacke, mudrock, conglomerate and iron formation
- 5a Iron formation

- 4 Metasedimentary rocks: paragneiss and schist with biotite, garnet, orthopyroxene, sillimanite, andalusite, cordierite, staurolite and/or kyanite; iron formation, marble and white anatectic granite associated with the metasedimentary rocks; common presence of intrusive and volcanic rocks

VOLCANIC ROCKS

- 3 Felsic volcanic rocks: rhyolite, rhyodacite, dacite, pyroclastic rocks, and felsic porphyry intrusions; minor intermediate to mafic volcanic rocks and sedimentary rocks
- 2 Mafic and intermediate volcanic rocks: basalt, andesite and pyroclastic rocks; minor amphibolite, felsic and ultramafic volcanic rocks, mafic intrusions and sedimentary rocks
- 2a Amphibolite, metabasalt and mafic gneiss
- 1 Ultramafic volcanic rocks: komatiite, magnesian basalt and ultramafic rocks of indeterminate origin; minor mafic volcanic rocks and sedimentary rocks

SYMBOLS

-  Indeterminate fault
-  Boundary of major geological divisions
-  Water

- ① Sigma-Lamaque
- ② Kiena
- ③ Siscoe
- ④ Norlartic
- ⑤ Bachelor Lake
- ⑥ Barry

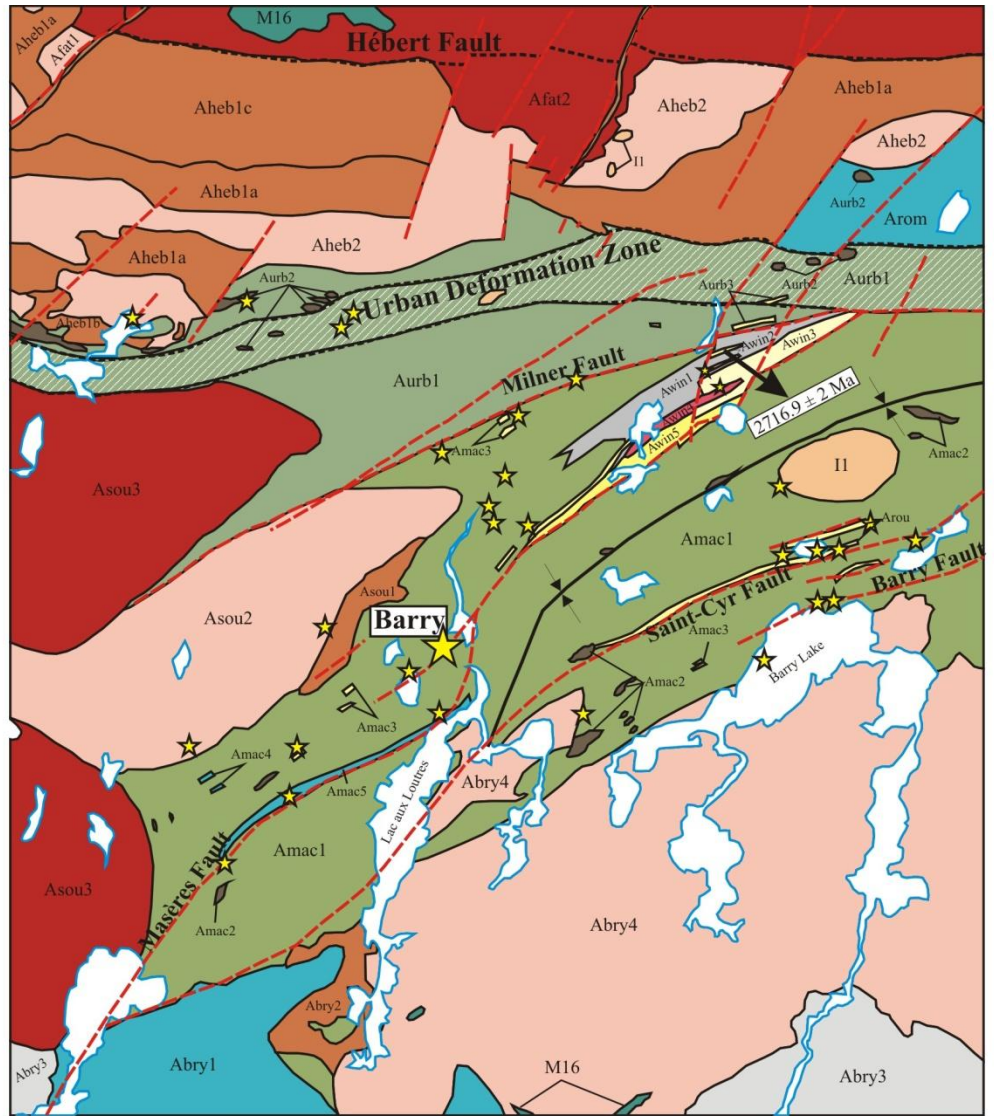
Rhéaume et al. (2004), Fallara et al. (2004), and Rhéaume and Bandyayera (2006).

Information from these sources is summarized below.

The Urban-Barry belt comprises mainly mafic volcanic rocks and isolated felsic volcanic rocks with ages ranging from 2791 Ma to 2707 Ma (dating by D.W. Davis in Rhéaume and Bandyayera, 2006) interbedded with, or overlain by, volcanoclastic sedimentary rocks (Fig. 2.2). The Lac aux Loutres region, containing the Barry deposit, is comprised of mafic volcanic flows, co-magmatic gabbro sills, local felsic flows, lapilli and welded tuffs, and sedimentary rocks intruded by tonalite to granodiorite plutons, diorite dikes, and feldspar and/or quartz porphyry dikes (Fig. 2.2, Joly, 1990). The mafic volcanic rocks are basaltic to andesitic, and form part of the Urban, Macho (which hosts the Barry deposit), and Roméo formations (Fig. 2.2, Bandyayera et al., 2002). Mafic volcanic rocks consist of massive and pillowed flows that are commonly vesicular, porphyritic, brecciated, and locally contain phenocrysts of plagioclase (Joly, 1990). Co-magmatic gabbro sills can form bodies measuring 100-600 metres wide and 400-3000 metres long (Joly, 1990). Felsic flows are dacitic to rhyolitic in composition, equigranular and locally porphyritic. They form thin horizons that vary over 50-200 metres in width and 300-1000 metres in length (Joly, 1990). Felsic volcanic rocks from the Windfall member of the Macho Formation (*Awin2*: Fig. 2.2) yield a U-Pb zircon age of 2716.9 ± 2 Ma (dating by D.W. Davis in Bandyayera et al., 2002). Sedimentary rocks in the region include conglomerates composed of volcanic and intrusive rock fragments, and locally siltstone, argillite, and wacke. Intrusive rocks consist of the Archean Father, Hébert, and Souart

plutons, and the Barry complex (Fig. 2.2, Bandyayera et al., 2002), which are locally cut by Proterozoic diabase dikes.

Rocks in the region were deformed during the 2.71-2.66 Ga Kenoran orogeny (Card, 1990; Goldfarb et al., 2001), giving them a dominant east-west trend (Chown et al., 1992). The regional foliation generally strikes NE to ENE with a variable dip from 30 to 85° SE (Hocq, 1989; Joly, 1990). Associated regional folds are generally isoclinal with steeply plunging axes (Chown et al., 1992). The three main fault sets present in the region are oriented NE-SW, E-W, NNE-SSW. The NE- trending faults, are characterized by an intense, and locally mylonitic, foliation with associated minor brecciated and silicified wall-rocks (Joly, 1990) and contain subvertical stretching lineations (Bandyayera et al., 2002). This set of structures is cross-cut by E-trending shear zones. The NNE-trending faults are generally brittle structures cross-cutting the other two fault sets and they are interpreted as late features by Bandyayera et al. (2002). These faults have a sinistral sense of offset (from several centimetres to metres), with lineations plunging 45° to the NE (Joly, 1990). Rocks are generally metamorphosed to the greenschist facies, but locally conditions reached the amphibolite facies in zones of intense deformation or adjacent to intrusions (Joly, 1990).



0 2.5 5 Kilometers 10

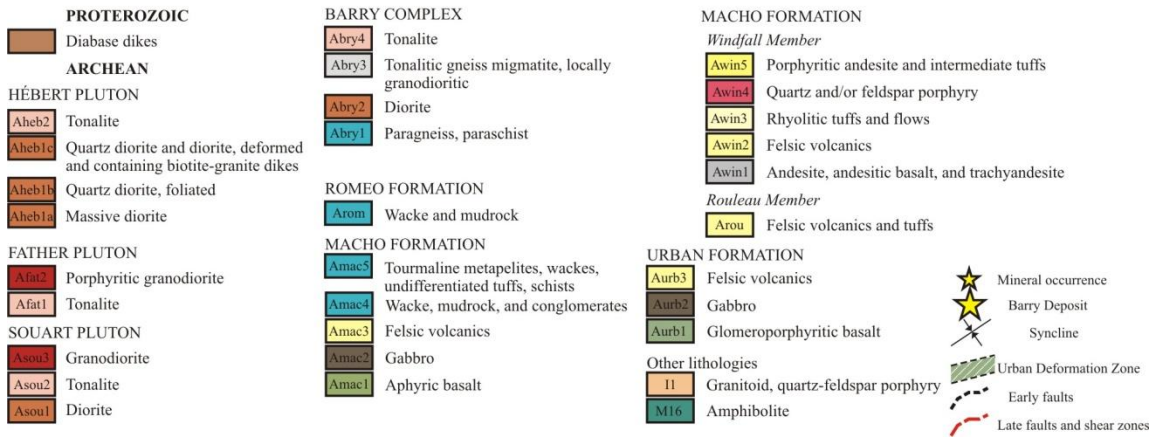


Fig. 2.2: Simplified geological map of the Urban-Barry belt - Picquet and Mesplet Lakes (SNRC 32G/04 and 32B/13; modified after Bandyayera et al., 2002), locating the Barry property.

2.3 Analytical Methods

At the Barry deposit, two areas of the trenched surface were mapped in detail at 1:50 scale and a total of 23 drill holes were logged throughout the main trenched zone to document critical relationships and compare with the data collected by Tessier in 1996, who mapped the area at 1:100 scale. Mafic volcanic units, intrusive rocks, and zones of various types of alteration were sampled in the trenched region and in 13 drill holes that were selected to be studied in detail. Samples were investigated using transmitted and reflected light microscopy, scanning electron microscopy (SEM), lithochemistry, electron microprobe analysis (EMPA), X-ray diffraction (XRD), and U-Pb zircon geochronology.

Whole rock major oxides and trace elements were determined in 59 selected drill core and 37 surface samples using a lithium metaborate / tetraborate fusion and nitric acid digestion followed by Inductively Coupled Emission Spectrometry and Inductively Coupled Mass Spectrometry (ICP-MS). A split of each sample was digested in aqua regia and analyzed by ICP-MS for precious and base metals in all samples, as well as tellurium for select samples. All samples were analyzed for precise determinations of gold using lead collection fire assay, and selected samples were also analyzed for silver, platinum and palladium using fire assay. A subset of intrusive rock samples was analyzed for fluorine by specific ion electrode following NaOH fusion. Geochemical analyses were performed at Acme Labs in Vancouver, British Columbia.

Electron microprobe analyses were performed on 12 samples. Gold, pyrite, and magnetite from six samples were analyzed at the Earth and Planetary Sciences Department at McGill University, Québec. Silicates including feldspars, chlorite, and biotite from another subset of six samples were analyzed at the Department of Geological Sciences and Geological Engineering at Queen's University, Ontario.

At McGill University, spot analyses were conducted using wavelength-dispersion spectrometry (WDS) and a JEOL JXA-8900L instrument. Quantitative EMPA were conducted at 20 kV with a beam current of 50 nA. The following standards and x-ray lines were employed for pyrite and gold analyses: Au₆₀ Ag₄₀ (AgLa, AuMa), metal (SeLa, WLa), pyrite (FeKa, SKa), Stibnite (SbLa), AgBiSe₂ (BiMb), CoNiAs (AsLb), HgS (HgLa), CdTe (TeLa), ZnS (ZnLa), Tl₂S (TlLa), TiO₂ (TiKa), PbS (PbMa), Pentlandite (NiKa, CoKa), SnO₂ (SnLa), and chalcopyrite (CuKa). Peaks for pyrite and gold were counted as follows: Ag (50s for pyrite, 20s for gold), Se (60s), Fe (10s), Sb (270s), S (10s), Bi (300s), As (40s), Hg (340s), Te (270s), Au (540s for pyrite, 20s for gold), Zn (40s), Tl (340s), Ti (60s), Pb (150s), Ni (80s), Sn (40s), Co (40s), Cu (50s), and W (20s). The standards and analytical lines used for magnetite are the same as those outlined above for pyrite and gold except for the following: hematite (FeKa), chromite (AlKa, MgKa, CrKa) and spessartine (MnKa). Peaks for magnetite are the same as those outlined for pyrite (above) and include the following: Al (20s), Mg (20s), Cr (20s), and Mn (20s).

At Queen's University, electron-microprobe analyses were conducted using the Applied Research Lab's scanning electron microscope quantometer (SEM-Q). Quantitative microprobe analyses of plagioclase, chlorite, and biotite were made using energy-dispersion spectrometry (EDS) at 15 kV with a beam current of 40 nA. A scanned area of at least 12 x 12 μm was used for all plagioclase analyses. Standards included kaersutite listed by Smithsonian Contributions to the Earth Sciences v. 22, 1976, pg. 53-72 (USNM 143965) and glass from the U.S. National Bureau of Standards (NBS 470 K-412).

Seventeen powdered whole rock samples were analyzed for mineralogical composition using XRD at the Department of Geological Sciences and Geological Engineering at Queen's University (Appendix H). Samples were ground into powder and mounted as thin smears of fine powder on glass disks. Samples were scanned with a Philips X'Pert Pro Multi-purpose X-ray Diffractometer fitted with an X'Celerator high speed strip detector under CoK α radiation between 6° and 70° with a count time of 10 sec per 0.2° increment. Peak positions were identified using PanAlytical HighScore software that compares peak intensities from the unknown samples to those in a database of known phases.

U-Pb sample preparation and dating was conducted at the Jack Satterly Geochronology Laboratory in the Department of Geology at the University of Toronto, Ontario. Samples were crushed using a jaw crusher and disk mill. Heavy minerals were initially separated using one pass on a Wilfley table. Samples were sieved and coarse materials (+70 mesh) were rejected. Ferromagnetic material was removed by free fall in front of a Frantz

magnet, followed by paramagnetic separations with a Frantz isodynamic separator. Light materials (s.g. <3.3) were removed using methylene iodide. Pyrite was dissolved in 4N nitric acid.

A population of zircon grains from each sample was hand-picked from the remaining heavy minerals. Several intact zircon grains were physically abraded using compressed air (Krogh, 1982), whereas the remainder of the sample underwent chemical abrasion by annealing grains at 1000°C for three days to remove radiation damage induced by decay of U and Th contained in the mineral (Mattinson, 2005). This renders the unaltered zircon more inert to chemical attack. After cooling, grains were leached in HF at 200°C for several hours. Zircon for U-Pb analysis was hand-picked under a microscope choosing the freshest, least fractured grains from both air abraded and chemically abraded zircons. Weights of single grains were estimated from digital photomicrographs using the method of Matthews and Davis (1999). Estimated weights affect only the U and Pb concentrations, not age information, which depends only on isotope ratio measurements. Single zircon grains were washed in 7N HNO₃ prior to dissolution, and a ²⁰⁵Pb–²³⁵U spike was added to the dissolution capsules during loading into Teflon bombs. Zircon grains were dissolved using concentrated HF at 200°C for five days, then redissolved in 3N HCl to ensure equilibrium with the spike. Samples were loaded onto 50 microlitre anion exchange columns to separate out Zr and REE in 3.5N HCl. Uranium and lead were loaded together onto Re filaments using silica gel. Pb and U were analyzed on a VG354 mass spectrometer using a Daly collector in pulse counting mode for small samples. The mass discrimination correction for this detector is constant at 0.07%

/AMU. Larger samples were analyzed in multidynamic mode using 3 high mass Faraday collectors and the axial Daly detector. The Daly gain was continually monitored by measuring the ^{205}Pb signal in the Daly and adjacent Faraday collectors. Thermal mass discrimination corrections are 0.10% /AMU. Dead time of the Daly system (about 20 nsec) and multi-collector Faraday cup efficiencies were monitored using the SRM982 Pb standard. Faraday amplifier gains were monitored daily using a constant current source.

2.4 Geology of the Barry Gold Deposit

Gold mineralization in the Barry deposit occurs in albite-carbonate-quartz veins and in altered host rocks, which are exposed in a trenched surface 50 m (NW to SE) by 200m (NE to SW). The mineralized veins are hosted mainly in volcanic rocks of the Macho Formation (Fig. 2.2, Bandyayera et al., 2002), which have been locally pervasively altered to carbonate. The generally N60°E-striking, 45°SE dipping volcanic units are folded, foliated, and cut by intermediate to felsic intrusions of various geometries and ages (Figs. 2.3 and 2.4, Appendix A). The main ore zone is bound by an early N55-60°E-striking, 58°SE-dipping shear zone to the north and by a quartz monzonite intrusion to the south and is truncated and offset by various late brittle faults (Fig. 2.3, Appendix A).

2.4.1 Mafic Volcanic Rocks

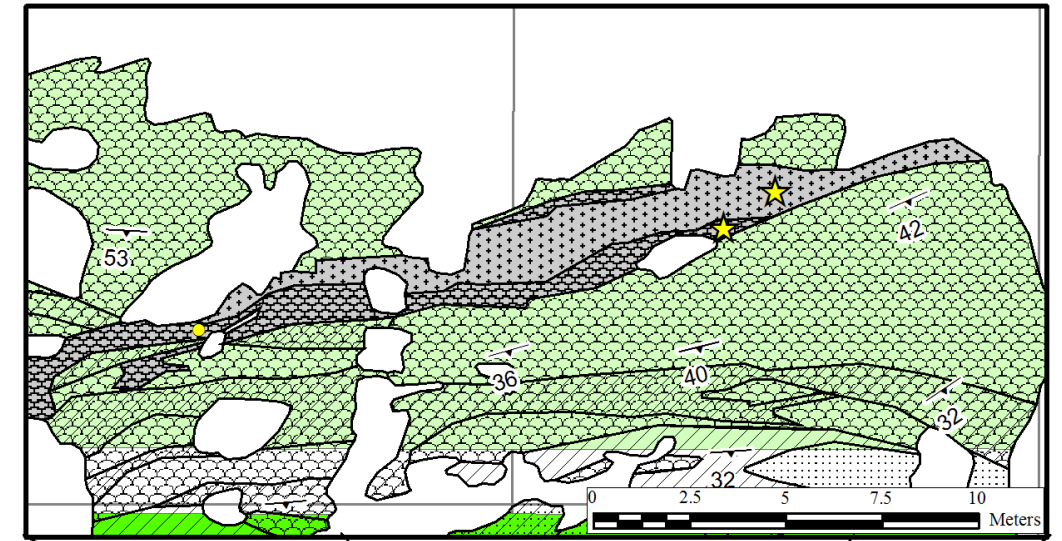
The mafic volcanic rocks exhibit various volcanic structures including pillows, breccias, amygdules, as well as being massive (Figs. 2.3-2.5A-D; Appendix A). Locally, feldspar-phyric and tuffaceous units were observed (Fig. 2.5E-F). The pillows are weakly flattened and range in size from 30 cm to 3 m along their long axes (Fig. 2.5A).

Legend

- Foliation
- Linciation
- ⊗ Drill Hole
- Vertical Section
- Contact (observed)
- Fault (observed)
- - - Fault (inferred)
- ★ Geochron sample
- Visible gold

- Volcanic Facies**
- ⊘ Amygdular
 - ⊘ Breccia
 - ⊘ Feldspar-phyric
 - ⊘ Massive
 - ⊘ Pillow
- Volcanic Types**
- A
 - B

- Intrusive Rocks**
- ⊘ QFP
 - Diorite 1
 - Diorite 2
 - Diorite (type unknown)
- Alteration**
- ▨ Carbonate



Barry Trench

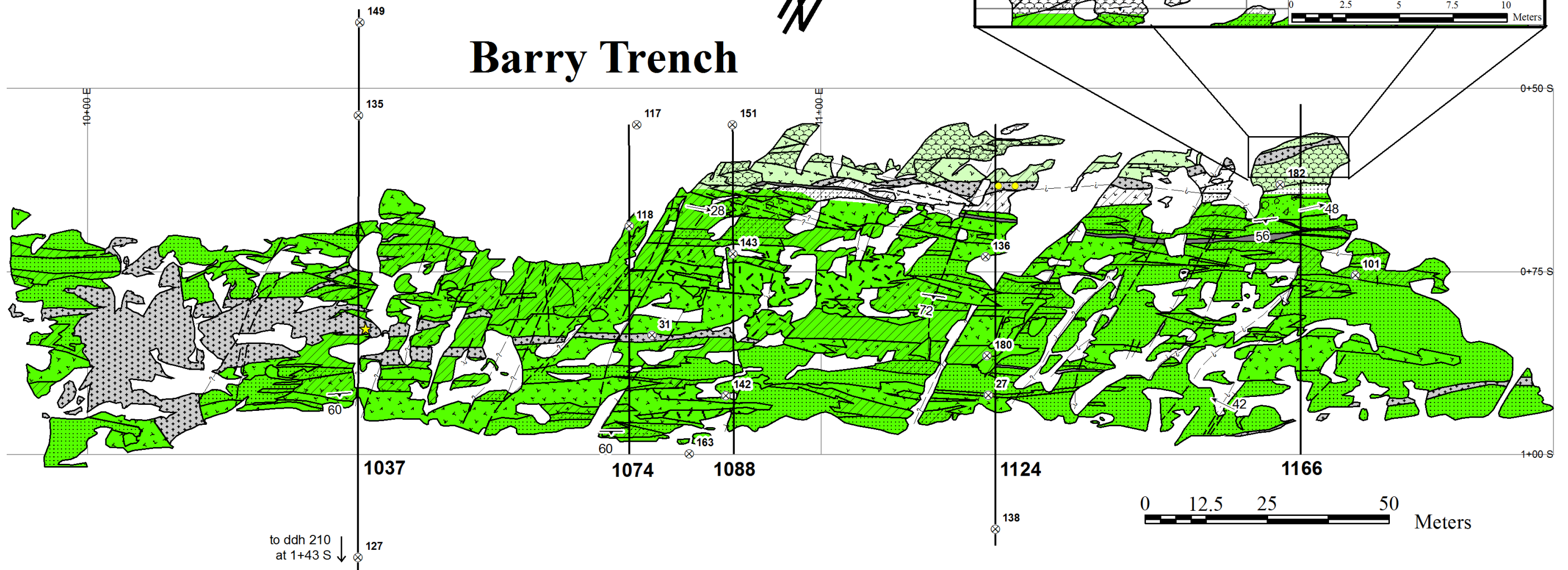


Fig. 2.3: Simplified geologic plan map of the Barry deposit showing the locations of drill holes and cross sections studied in detail.

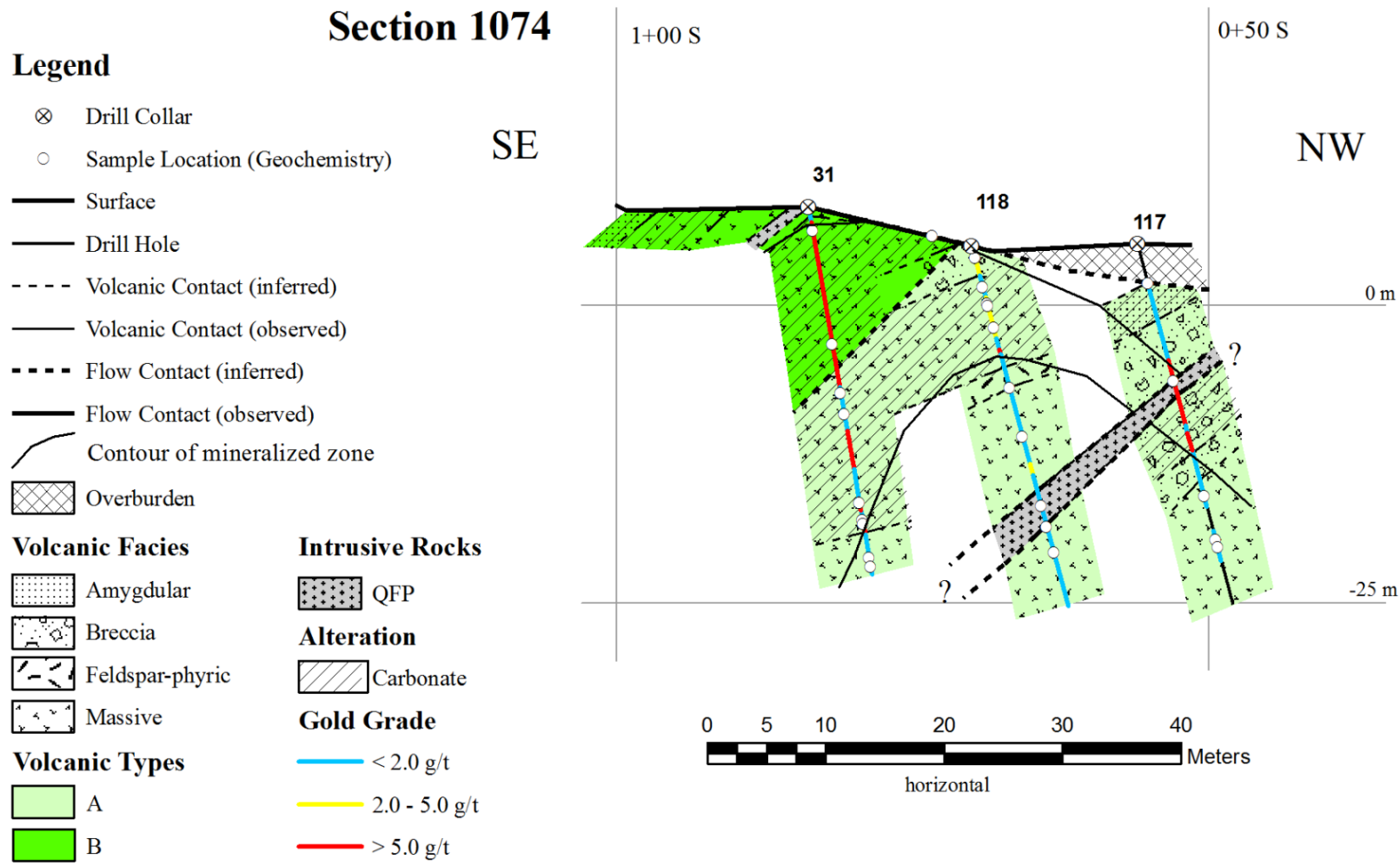


Fig. 2.4: Simplified NW-SE vertical cross section of the Barry deposit along grid line 1074.

The brecciated units comprise sub-rounded fragments (1-30 cm long) of massive volcanic rocks and minor amygdular rocks (Fig. 2.5B). The amygdules (1-3mm in diameter) are round to slightly elongated and are commonly filled with carbonate and quartz (Fig. 2.5C). Massive flows (Fig. 2.5D) and locally amygdular units are enriched in disseminated magnetite. The feldspar-phyric units contain up to 30% subhedral plagioclase phenocrysts up to 3mm in length (Fig. 2.5E). Tuffaceous units are up to 1m thick with graded bedding. These contain crystal fragments of plagioclase up to 2 mm in length and are found only in core samples at depths greater than 30m, with graded bedding indicating an upward younging direction (Fig 2.5F). Primary contacts between these facies are generally gradational to sharp and the sequence forms a coherent volcanic succession. These rocks have been deformed, hydrothermally altered (locally pervasively), and metamorphosed, which makes it difficult to identify the composition of their protoliths.

Based on geochemical composition of volcanic units and on the mineralogical composition of the least altered samples (i.e, with < 7ppb Au and minimal hydrothermal alteration associated with the auriferous event), two distinct types of volcanic flows were indentified and will be further referred to as types A and B. The least altered Type A rock is composed mainly of plagioclase (70%), chlorite (15%), epidote (10%), quartz (2-5%), carbonate (1-2%), biotite (1-2%), pyrrhotite (1-2%), ilmenite (trace-1%), muscovite (trace), pyrite (trace), and chalcopyrite (trace) (e.g. sample 210-74.00). The least altered Type B volcanic rock has similar amounts of plagioclase (64%), quartz (2%), carbonate (1-3%), biotite (5%), ilmenite (1%), and pyrite (trace-1%), but higher abundance of

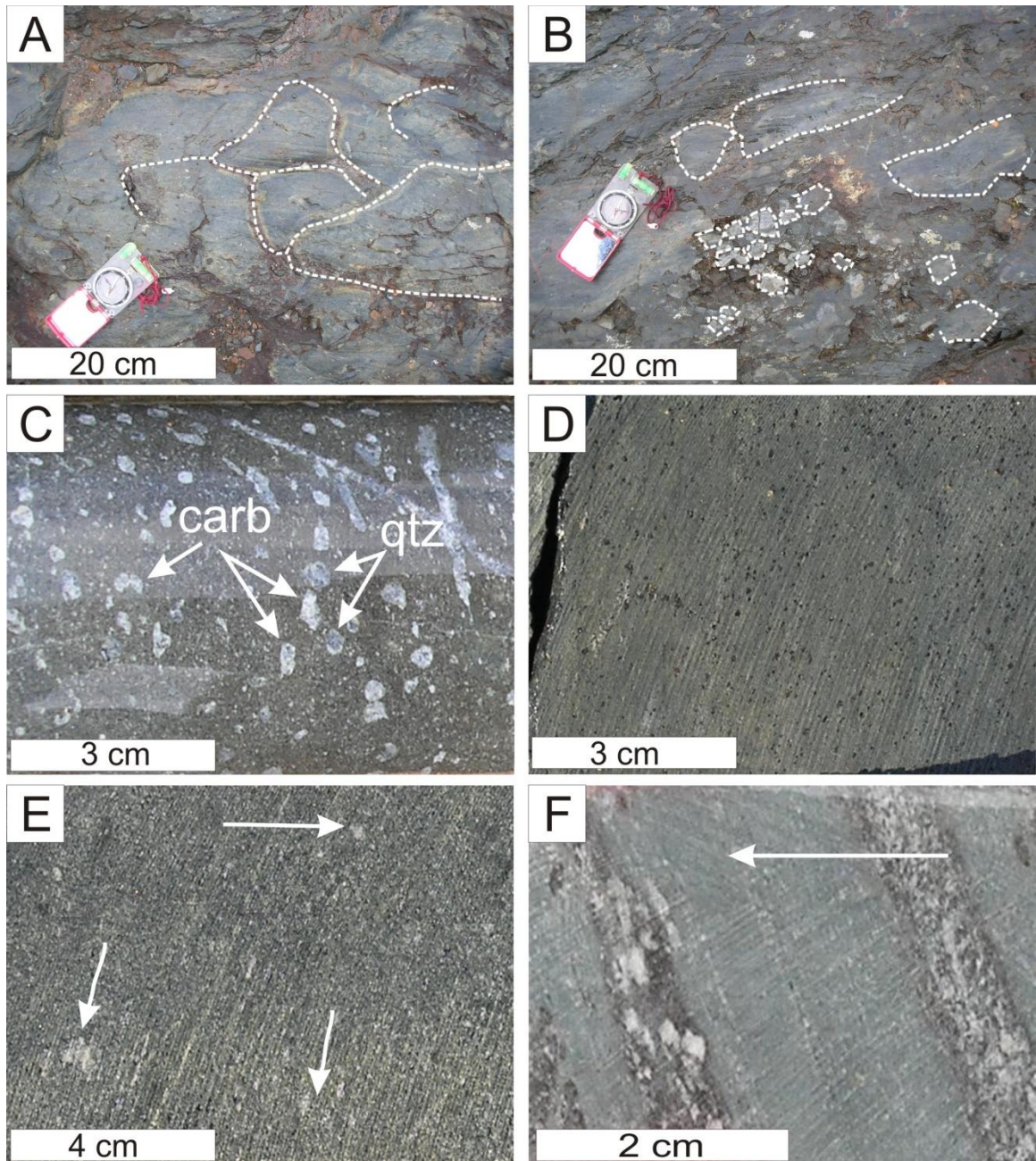


Fig. 2.5: Photographs of mafic volcanic flows of the Barry main zone: A) Pillowed flow with some of the pillows outlined in white (Type A volcanic rock at grid location 1162E/62S); B) Brecciated flow with angular fragments outlined in white (Type B volcanic rock a grid location 1163.5E/67S); C) Amygdular flow with quartz and calcite round to slightly elongated amygdules (volcanic type unknown, drill core sample 136-33.30); D) Massive flow with disseminated cubic magnetite (volcanic type unknown, drill core sample 151-13.57); E) Feldspar-phyric flow with subhedral plagioclase phenocrysts indicated with arrows (Type A drill core sample 151-4.91); F) Tuffaceous unit displaying graded bedding with beds grading from coarse to fine in the direction of the arrow (Type A drill core sample 135-24.35). carb = carbonate; qtz = quartz

epidote (15%), muscovite (4%), and magnetite (trace), and lower abundance of chlorite (3%) (e.g. sample 91-1119).

Although the proportions of minerals vary in types A and B volcanic rocks, their textural relationships are similar and are summarized below. Type A and B volcanic rocks that have undergone more extensive pre-ore alteration have higher proportions of the following minerals: 5 to 30% chlorite, trace to 10% biotite, trace to 4% magnetite, and trace ilmenite and rutile in addition to the magmatic phases (Fig. 2.6). Chlorite₁ and biotite₁ form flakey crystals (on average 44µm in size) that appear to be replacing of each other, fill corroded zones of plagioclase, and locally fill veinlets in the host.

Microprobe and XRD analyses of pre-ore chlorite₁ indicate that chlorite is an Fe-rich clinocllore ($\text{Mg}_{5.0}\text{Fe}_{4.1}\text{Al}_{2.7}(\text{Si}_{5.5}\text{Al}_{2.5})\text{O}_{12}(\text{OH})_{16}$; Appendix E). Optical identification of biotite-phlogopite series was confirmed by microprobe analyses, and will be further referred to as biotite in the text ($\text{K}_{1.8}\text{Mg}_{2.4}\text{Fe}_{2.5}\text{Al}_{1.6}\text{Ti}_{0.2}(\text{Si}_{5.7}\text{Al}_{1.3}\text{O}_{20})(\text{OH})_4$; Appendix E, Fig. E2). Ilmenite forms euhedral laths and locally crystal aggregates that fill embayments in plagioclase, chlorite₁, and biotite₁. It is also found as inclusions in magnetite or filling its corroded edges. Magnetite occurs as euhedral cubic to anhedral crystals ($\leq 1\text{mm}$ in size) and commonly occupies embayments in plagioclase, chlorite₁, and biotite₁. Acicular crystals of rutile fill corroded zones in biotite₁ and ilmenite. Based on these relationships, as well as those observed in ore samples and described in ‘Gold Mineralization’ section, an interpreted paragenetic sequence is proposed for the mafic volcanic rocks, and is summarized in Figure 2.7.

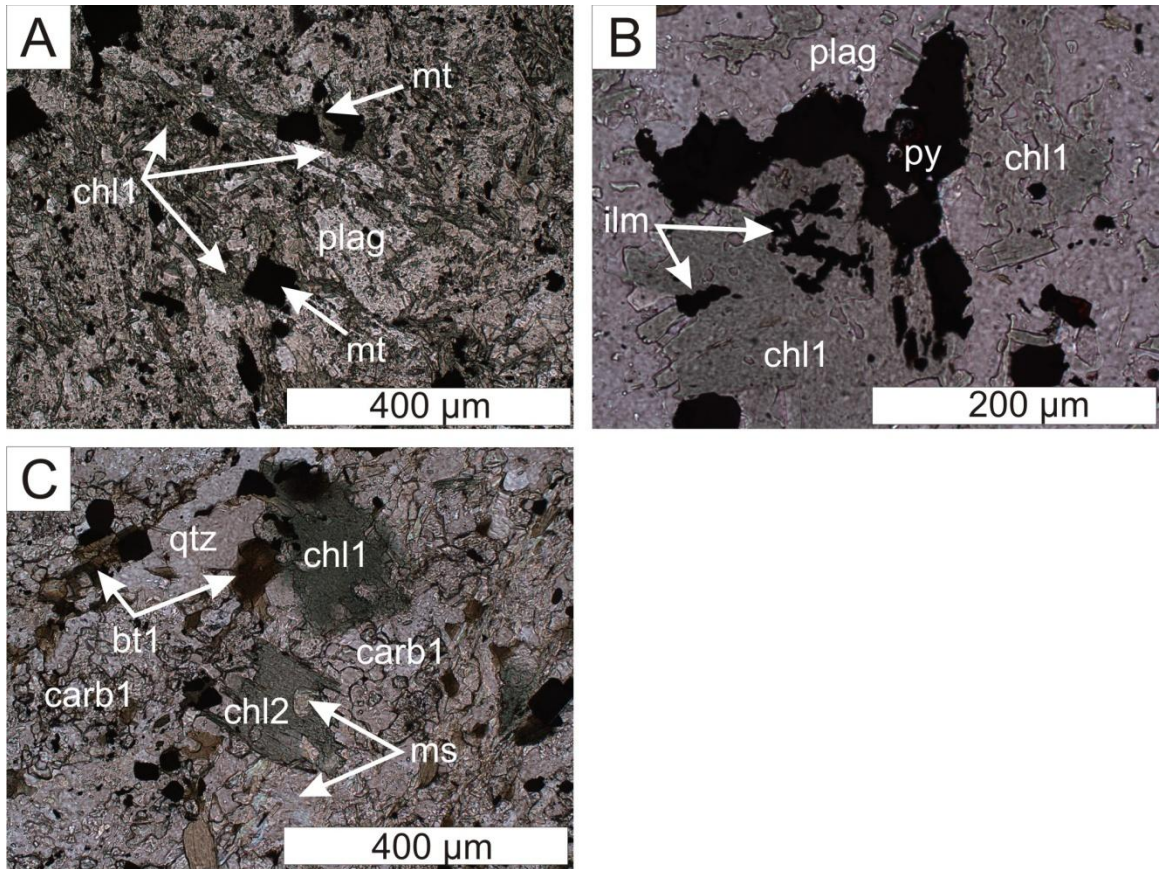


Fig. 2.6: Photomicrographs of pre-ore alteration at the Barry deposit in plane-polarized transmitted light. A) Type B drill core sample 31-0.31. Chlorite1 laths replace plagioclase and are partially replaced by cubic magnetite. B) Type B surface sample 76-1090. Chlorite1 replaces plagioclase, and embayments in chlorite1 are filled with crystal aggregates of ilmenite and pyrite. C) Type B surface sample 81-1119. Chlorite1 and biotite1 are partially replaced by quartz and carbonate1. Chlorite2 fills corroded zones of carbonate, and embayments in chlorite2 are filled with muscovite. bt1 = biotite 1; carb1 = carbonate 1; chl1 = chlorite 1; chl2 = chlorite 2; ilm = ilmenite; ms = muscovite; mt = magnetite; plag = plagioclase; py = pyrite; qtz = quartz.

In order to identify the possible protoliths of the Barry deposit volcanic rocks we used fields based on binary relationships among relatively immobile Ti, Zr, and Y (Pearce and Cann, 1973; Pearce, 1982; Barrett and MacLean, 1997).

On a Ti versus Zr diagram, samples that belong to Type A mafic volcanic rocks define a linear trend passing through the origin, indicating that indeed Ti and Zr were relatively immobile during the alteration of these rocks (Fig. 2.8). Their Ti/Zr ratios (73-94) are

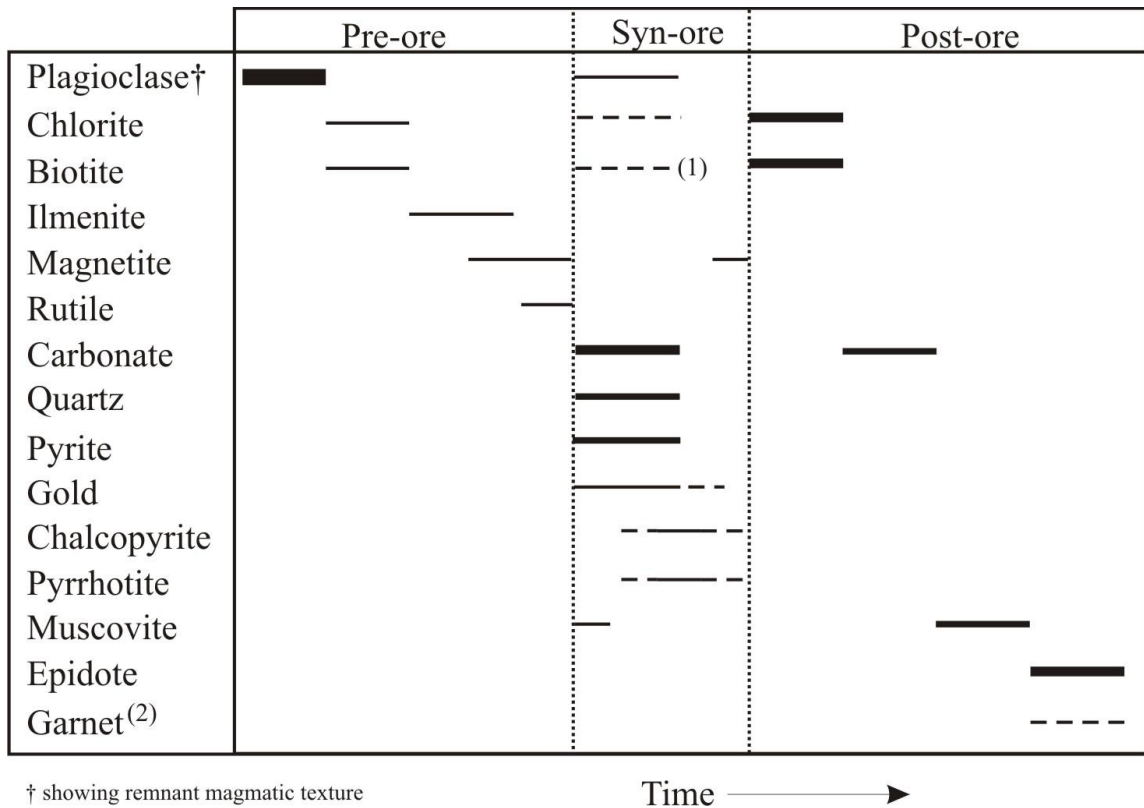


Fig. 2.7: Paragenesis of the minerals in Types A, B, and C mafic volcanic rocks that have undergone pre-ore, syn-ore, and post-ore alteration at the Barry deposit. Lines indicate the relative timing of formation of each mineral, while the thickness of the line indicates the relative abundance of each mineral phase. Dashed lines indicate local mineral occurrence, (1) abundant in zones of high strain, (2) at depth greater than 30m.

similar to those reported from mid-ocean ridge basalt (MORB) and volcanic-arc tholeiite (Pearce and Cann, 1973; Appendix D). The samples of Type B volcanic rocks have lower Ti/Zr ratios (50-71) than Type A and form a cluster with the samples that underwent pervasive carbonate alteration. Type B Ti/Zr ratios are transitional between tholeiitic and calc-alkaline fields (Pearce and Cann, 1973) and they have Ti/Zr values similar to those of the aphyric basalt of the Macho Formation reported by Bandyayera et al. (2002). Samples from the tuffaceous unit have Ti/Zr ratios ranging from 70-103. A small subset of samples with lower Ti and Zr contents plots away from A and B types in a field more typical of calc-alkaline basalts and island arc tholeiites. This subset is referred to as Type

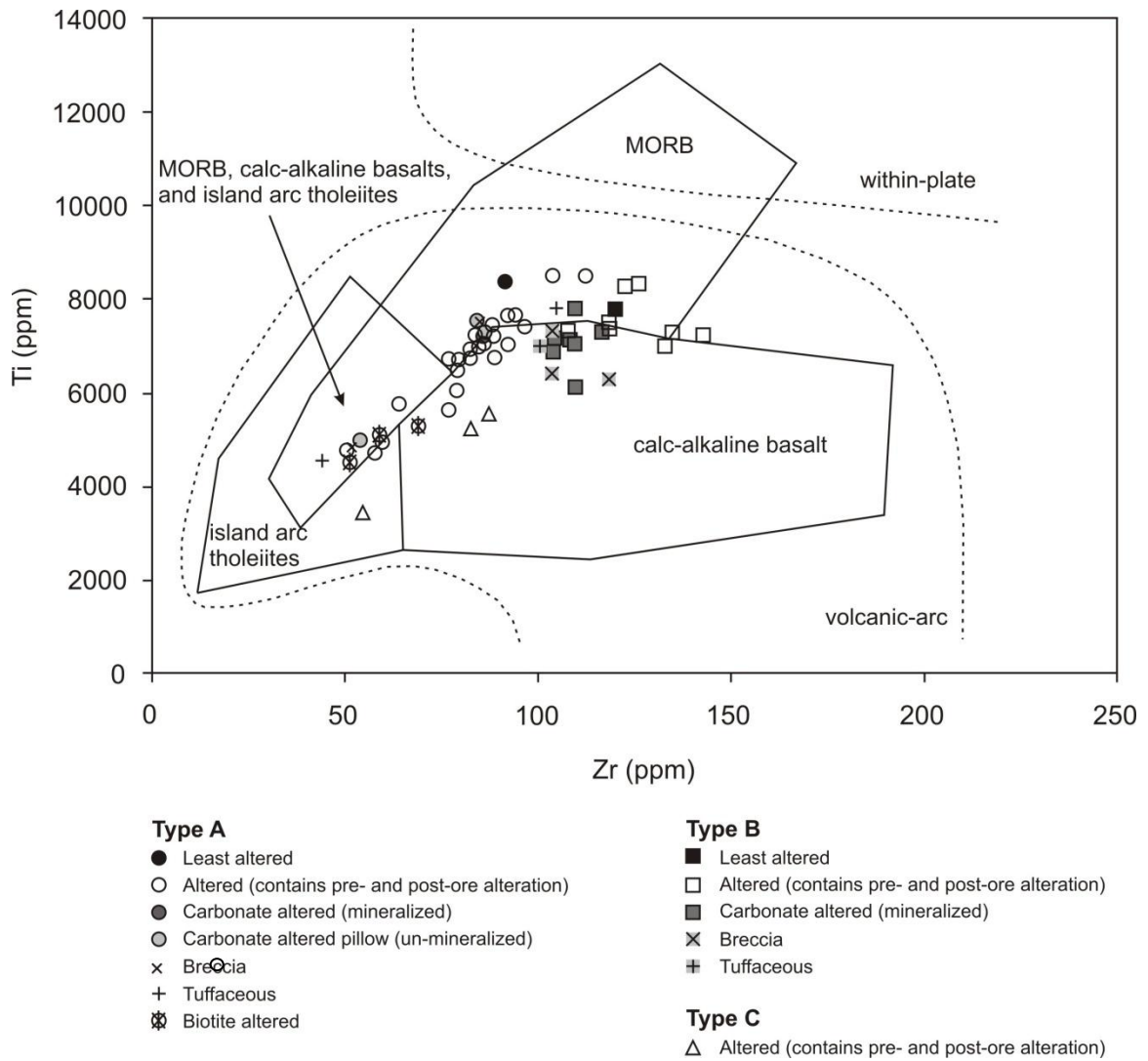


Fig. 2.8: Ti versus Zr discrimination diagram for the mafic volcanic rocks after Pearce and Cann (1973) and Pearce (1982).

C. All samples have Ti/Zr ratios typical of the volcanic arc field (Fig. 2.8), as defined by Pearce (1982). On a Y versus Zr diagram (Fig. 2.9), samples that belong to Types A and C mafic volcanic rocks, with Zr/Y ratios (4.29-5.36 and 2.99-5.15 respectively), fall on the interface between tholeiitic and transitional basalts according to Barrett and MacLean (1997). Samples from Type B define a roughly linear trend passing through the origin (Fig. 2.9), with Zr/Y ratios (4.42-6.62) similar to transitional basalts. The Zr/Y ratios

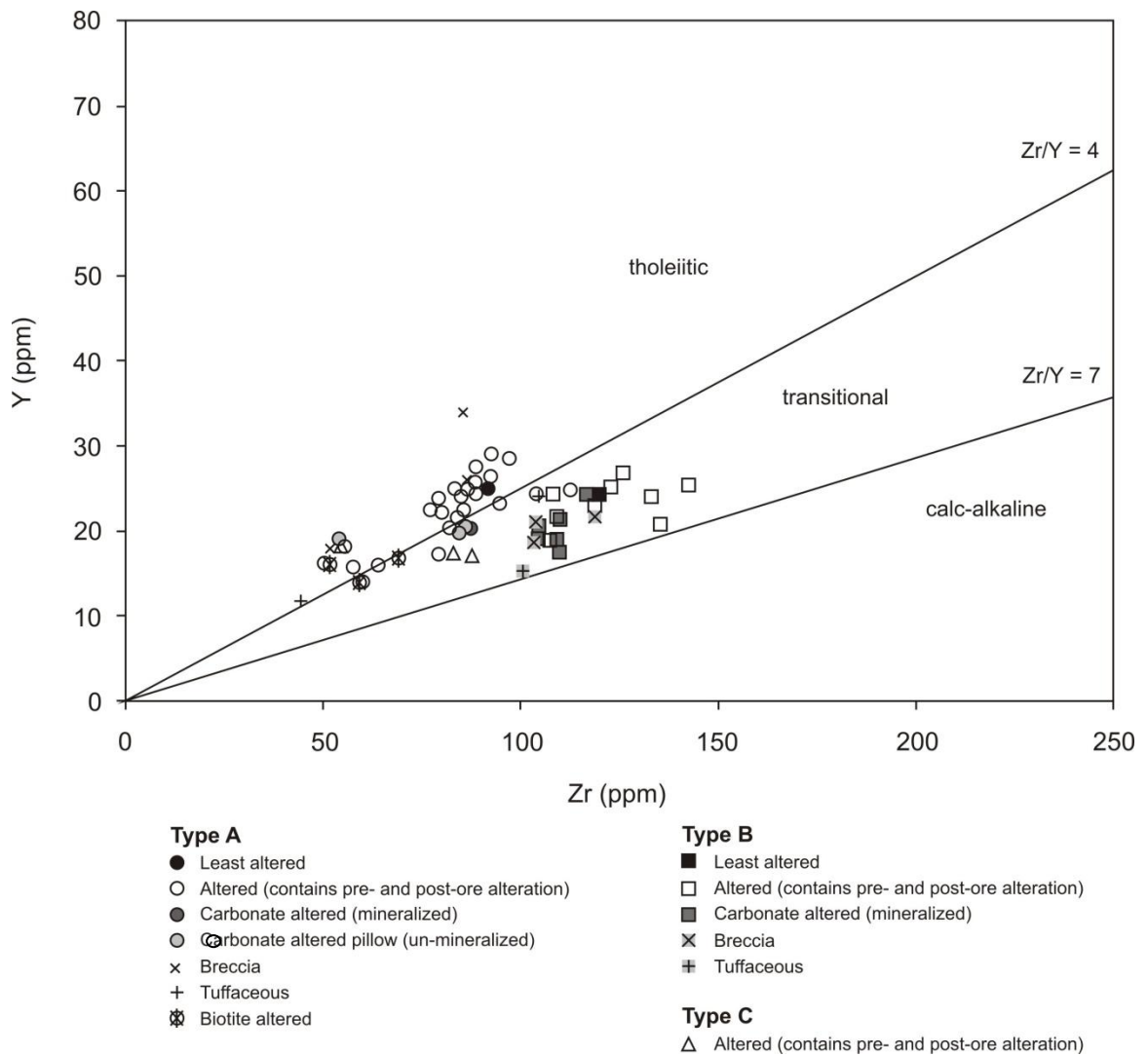


Fig. 2.9: Y versus Zr geochemical affinity diagram of mafic volcanic types from the Barry deposit. Tholeiitic and calc-alkaline boundaries are from Barrett and MacLean (1997).

of these rocks are similar to those of the Macho Formation reported by Bandyayera et al. (2002).

Normalized rare earth elements (REE) from the least altered samples of Type A and Type B are plotted on Figure 2.10. Values are normalized using chondrite data from McDonough and Sun (1995). The light rare earth elements (LREE) are enriched

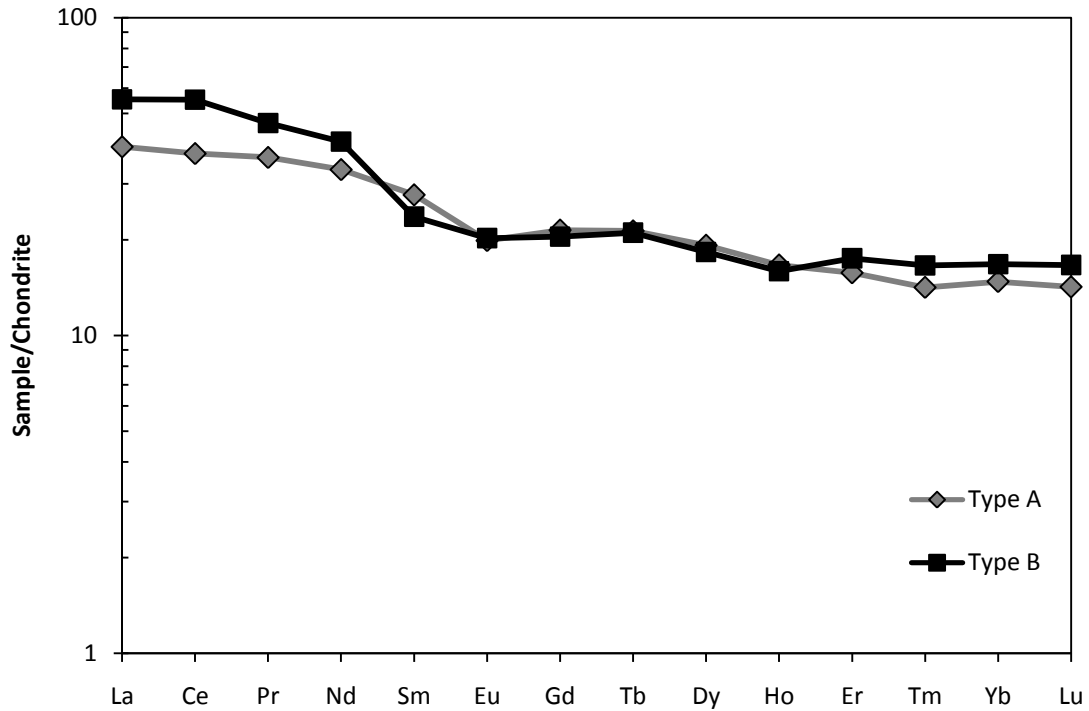
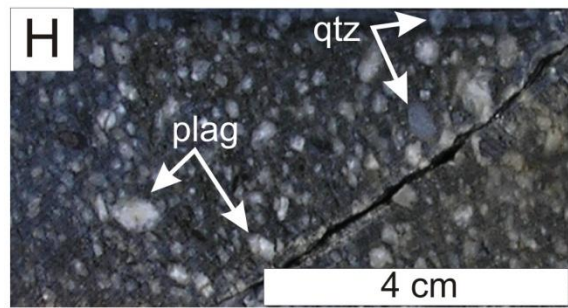
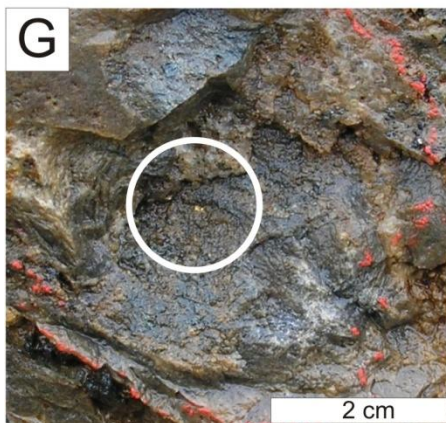
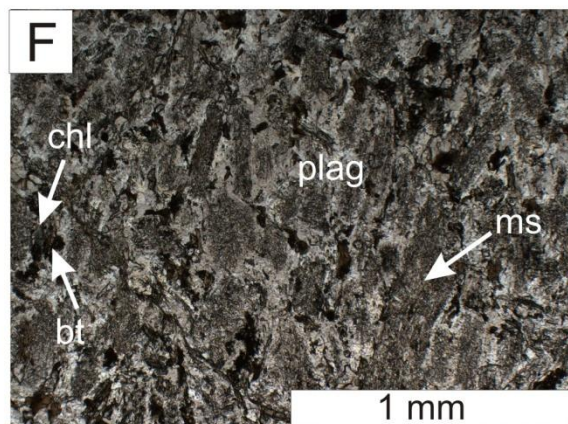
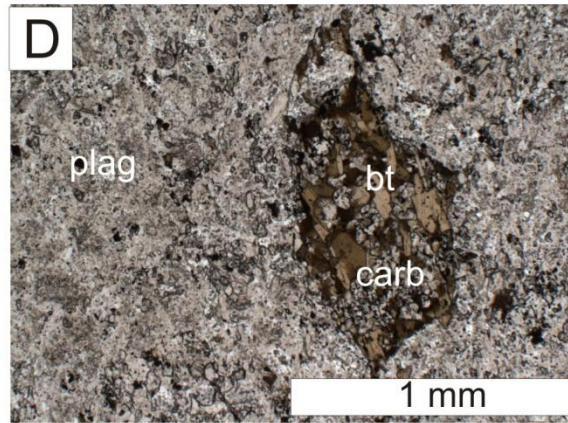
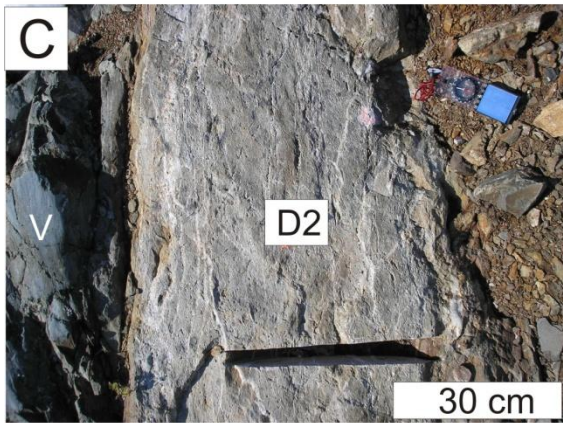
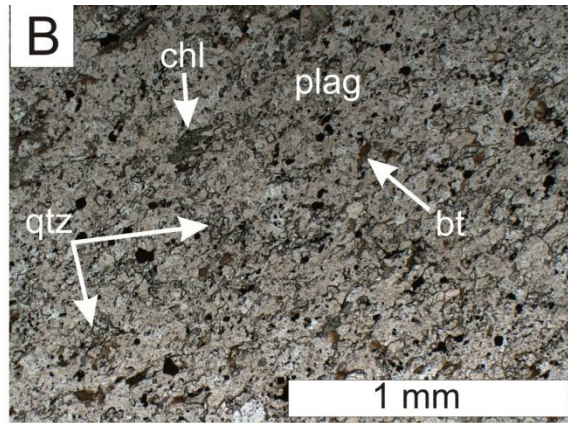


Fig. 2.10: Chondrite-normalized REE plots for least altered mafic volcanic Types A and B. Chondrite normalization values taken from McDonough and Sun (1995).

between 39 times to 55 times chondrite values, and the La_N/Yb_N ratios for least altered Type A and Type B volcanic rocks are respectively 3.9 and 4.9. These values are typical of basaltic-andesitic volcanic rocks transitional between tholeiitic and calc-alkaline (Wilson, 1989; Pearce and Peate, 1995), which is consistent with the results obtained using ratios of Ti, Zr and Y.

2.4.2 Intrusive Rocks

Three distinct major types of intrusive rocks were identified at the Barry Property, based on their mineral composition and igneous textures: (a) diorite, (b) quartz feldspar porphyry (QFP), and (3) quartz monzonite (Fig. 2.11). These rocks have been variably



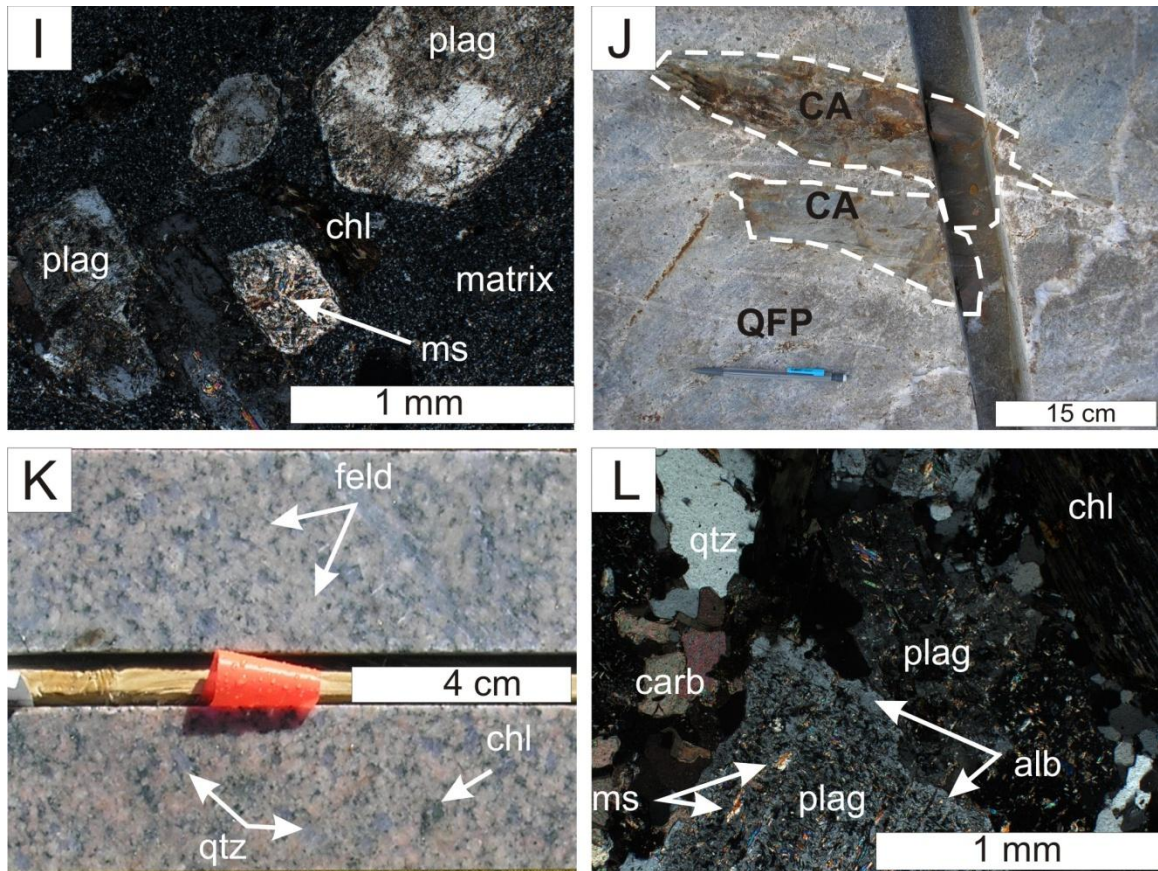


Fig. 2.11: Photographs and photomicrographs of the intrusive rocks at the Barry deposit. A) Photograph of the diorite 1 dike at grid location 1164 E/69 S cutting brecciated mafic volcanic rock; B) Photomicrograph of the diorite 1 dike surface sample 70-1167 in plane polarized light.; C) Photograph of the diorite 2 dike cutting mafic volcanic rocks at grid location 1159 E/71 S. D) Photomicrograph of the diorite 2 dike drill core sample 101-05.50 in plane polarized light. Plagioclase laths are replaced by crystal aggregates of biotite laths. Carbonate replaces portions of biotite crystal aggregates. E) Photograph of a diorite 3 dike along a QFP margin cutting mafic volcanic rocks at grid location 1083 E/84.5 S); F) Photomicrograph of a diorite 3 dike along QFP margin surface sample 85-1058 in plane polarized light. Plagioclase laths are replaced by flakey and tabular chlorite and biotite. The centres of plagioclase laths are replaced by fine-grained muscovite, giving the laths a mottled look in this picture; G) Photograph of visible gold grain (center of white circle) within diorite 3 dike at surface grid location 1161 E/70.5 S (near U-Pb sample 59-1164); H) Photograph of QFP drill core sample 27-22.95 containing plagioclase and quartz phenocrysts in a fine-grained (dark) groundmass; I) Photomicrograph of QFP drill core sample 118-22.78 in cross-polarized transmitted light. Plagioclase and chlorite phenocrysts are present in a fine-grained groundmass. Muscovite laths replace portions of the plagioclase phenocrysts; J) Photograph of QFP containing xenoliths of pervasive carbonate altered mafic volcanic rock at surface grid location 10+37 E/0+80 S (near U-Pb sample 83-1038). Carbonate alteration and albite-carbonate-quartz veins are restricted to the mafic volcanic fragments; K) Photograph of quartz monzonite drill core sample 210-5.97. Light pink K-feldspar, quartz, and chlorite crystals are coarse-grained with little to no groundmass in between; L) Photomicrograph of quartz monzonite drill core sample 210-5.97 in crossed-polarized light. Quartz, chlorite, and plagioclase have sharp contacts, with little to no groundmass between crystals. Carbonate replaces portions of and fills corroded zone of coarse-grained quartz, chlorite, and plagioclase. Muscovite replaces portions of plagioclase crystals as fine-grained flakey and acicular, radiating crystals, but does not replace albite overgrowth along the rim of the plagioclase as extensively. alb = albite; CA = carbonate altered mafic volcanic rock; bt = biotite; carb = carbonate; chl = chlorite; D1 = diorite 1; D2 = diorite 2; D3 = diorite 3; feld = K-feldspar; ms = muscovite; plag = plagioclase; qtz = quartz; V = mafic volcanic rock.

Diorite 1-3

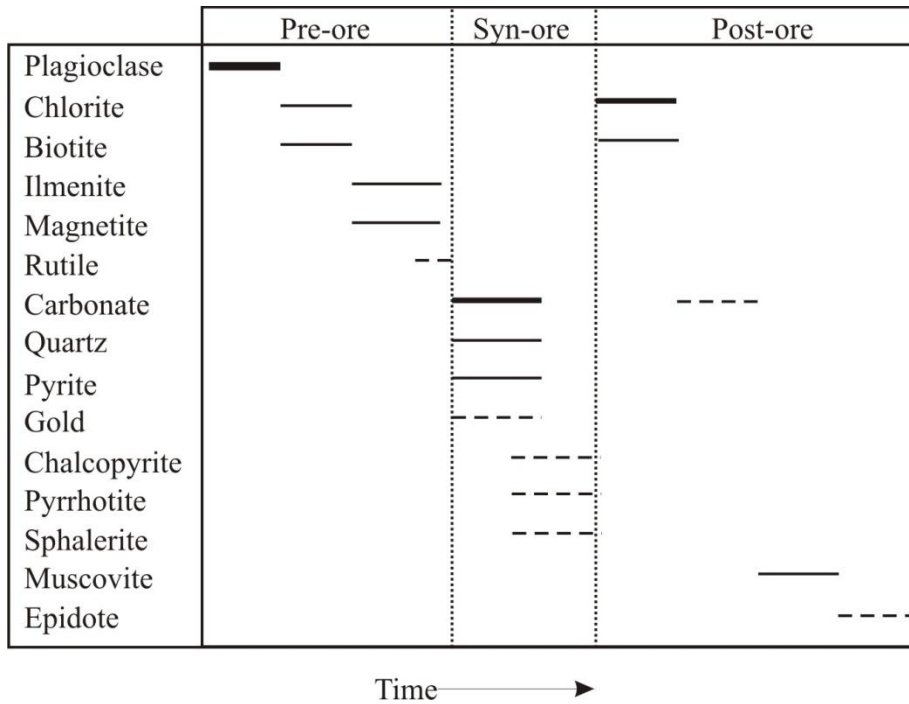


Fig. 2.12: Paragenesis of the minerals and alteration of pre-mineralization diorite (1-3) at the Barry deposit. Lines indicate the relative timing of formation of each mineral, while the thickness of the line indicates the relative abundance of each mineral phase. Dashed lines indicate local mineral occurrence

deformed, hydrothermally altered, and metamorphosed, but generally the identification of the protoliths is straightforward. Their mineralogical composition and paragenetic sequence are summarized in Figures 2.12 and 2.13, and described below.

Three distinct types of diorite dikes cut the mafic volcanic rocks in the trenched surface (Fig. 2.3): a 10cm-wide fine-grained dike that strikes approximately N70°E and dips 70° S (diorite 1); a 30cm-wide fine-grained dike containing mafic laths >1mm in size that strikes N60-70°E and dips approximately 50° S (diorite 2); and fine-grained dikes (up to 55cm wide) along the margin between QFP dikes and the mafic volcanic rocks in the surface trench (diorite 3). In the eastern portion of the trenched zone, the diorite 1 and 2

QFP and Quartz Monzonite

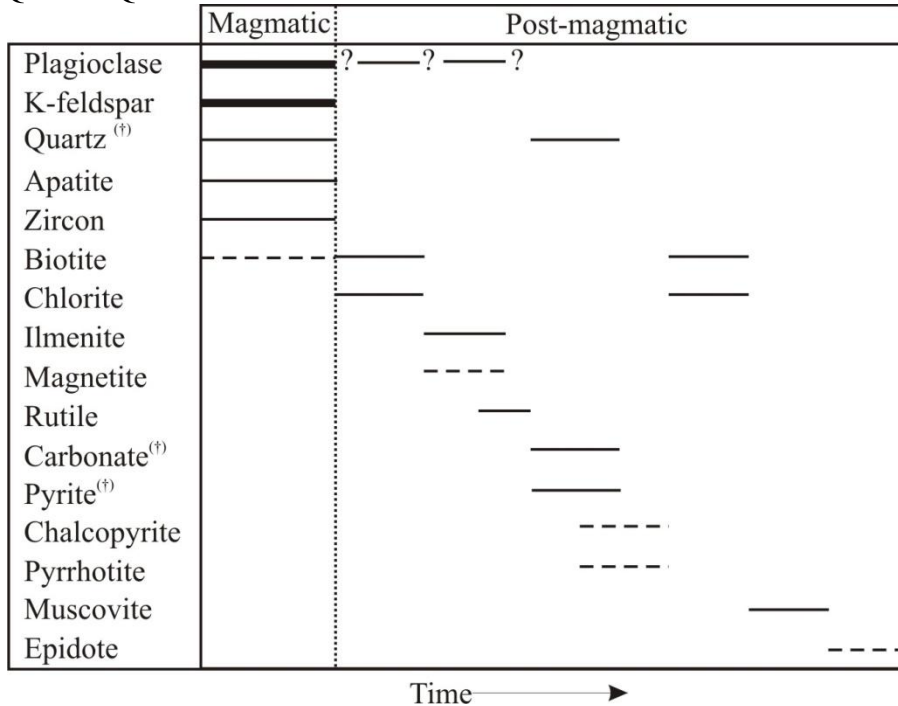


Fig. 2.13: Paragenesis of the minerals and alteration of pre- and post-mineralization QFP and post-mineralization quartz monzonite at the Barry deposit. Lines indicate the relative timing of formation of each mineral, while the thickness of the line indicates the relative abundance of each mineral phase. Dashed lines indicate local mineral occurrence. (†) carbonate, pyrite, and late quartz are more abundant in the early QFP.

dikes crosscut one another and are offset by an early fault (Fig. 2.3; Appendix A), and locally contain carbonate alteration typical of the mineralized zones. Diorite 3 dikes in the margin of the QFP are cut by albite-carbonate-quartz veinlets and veins (associated with gold mineralization) ranging in width from 0.2mm wide to 2cm, contain carbonate alteration typical of the mineralized zones (carbonate-quartz-pyrite), and locally contain free gold (Fig. 2.3 and 2.11G). The presence of the carbonate alteration, free gold, and albite-carbonate-quartz veins that cut the diorite 3 indicate that these dikes pre-date the gold mineralizing event. A pre-ore diorite 3 dike in the north-eastern section of the trench was selected for dating to constrain the maximum age of gold mineralization (Fig. 2.3;

Appendix A). All diorite dikes are weakly foliated, as seen in the elongation and alignment of plagioclase, carbonate, and biotite laths.

The diorite 1 dike (Fig. 2.11A-B) comprises 30-60% plagioclase laths (0.1mm by 0.05mm in size, identified as albite using XRD), whose cores are locally replaced by trace fine-grained muscovite and sinuous crystal aggregates of chlorite (5-30%) and biotite (trace-8%). Magnetite (trace-1%) is present as subhedral to euhedral cubic crystals (30-55 μ m in size) and trace ilmenite forms laths (60 μ m by 7 μ m in size) disseminated throughout the rock. Corroded zones of magnetite and ilmenite are filled with chlorite. Embayment in plagioclase, chlorite, biotite, and muscovite are filled with carbonate (25-30%) and quartz (trace-3%, up to 0.1mm in size). Pyrite (1-3%) occurs as euhedral cubic to subhedral crystals approximately 20 μ m in diameter that are spatially associated with carbonate crystals, and fill the embayments in plagioclase, chlorite, and biotite. Locally ilmenite is present as inclusions and filling fractures in pyrite. Trace rutile and sphalerite fill corroded zones in pyrite. Epidote (trace-3%) occupies embayments in plagioclase, chlorite, biotite and carbonate.

The diorite 2 dike (Fig. 2.11C-D) is composed mainly of plagioclase laths (55-75%; approximately 0.2 mm in size, identified as albite using XRD and microprobe analysis) and minor euhedral crystals quartz (trace to 2%; approximately 30 μ m in size). Chlorite (trace-5%) and biotite (trace-15%) laths (0.08- 0.24mm in size) fill cleavage planes of one another, and embayments in plagioclase laths. Corroded zones of plagioclase and quartz are filled with muscovite laths (trace-2%), and carbonate (10-20%). Sub-rounded

crystals of magnetite, and aggregates and isolated prismatic grains of ilmenite (trace-1%; approximately 0.02 mm in size) occur disseminated in the host, and the latter is spatially associated with biotite. Ilmenite and trace sphalerite fill corroded zones along the rims and fractures in early pyrite. Late pyrite (trace-2%; 0.27 mm in size) is generally cubic, contains trace inclusions of ilmenite, magnetite, chalcopyrite, and locally sphalerite, and fills embayments in plagioclase, biotite, and chlorite.

Diorite 3 dikes (11E-G) comprise plagioclase laths (60-85%; 0.22mm by 0.33mm in size; identified as albite using XRD and microprobe analysis) with corroded zones filled by elongated flakey chlorite1 (1-10%, 0.27mm in size) and biotite (trace-5%). Cubic to sub-rounded crystals of magnetite (trace-1%; 88µm in size) occur disseminated in the groundmass or as inclusions in pyrite, and its corroded zones are filled with biotite and chlorite2. Trace ilmenite is present as laths disseminated in the groundmass and as coarser crystal aggregates. Rare rutile fills corroded zones of ilmenite. Carbonate (3-20%) and trace quartz (locally lacking) fills embayments in plagioclase, chlorite1, and biotite, and shows sharp contacts with euhedral pyrite (1-2%; 0.11-0.44mm in size) and free gold. Locally pyrite contains trace inclusions of chalcopyrite and pyrrhotite. Chlorite2 is in sharp contact with pyrite and fills corroded zones in chlorite1 and plagioclase. Muscovite (5-8%) occurs as laths (20-550 µm in size) that fill embayments in plagioclase, carbonate, chlorite, and biotite. Epidote (up to 1%; 70µm in size) occupies embayment in chlorite1, chlorite 2, and muscovite.

Two generations of QFP dikes were documented. Both generations (Fig. 2.11H-I) occur as thin dikes (up to 1m wide) striking approximately N55°E and dipping from 60° to 80° SE in the northeast, southeast, and central sectors of the trench (Fig. 2.3; Appendix A), whereas dikes from the late generation of QFP are also found as an irregularly shaped body in the western portion of the trenched main zone. Some QFP dikes intercepted in the drill holes attain up to 18 m in thickness (drill hole 127: 25.35-43.37m in Appendix A - Section 1037). Locally earlier QFP dikes have undulating margins, are boudinaged, and are offset by early NE-trending and SE dipping faults and late N-trending E and W dipping brittle faults E (Fig. 2.3; Appendix A). The QFP dikes can vary greatly in colour and texture due to alteration and deformation. The earlier generation of QFP dikes are crosscut by white quartz veins that locally contain free gold (Fig. 2.3) and are locally crosscut by quartz-carbonate-albite veins. Locally, these dikes are weakly foliated, with elongated crystals aligned in a weak fabric. However, the late generation of QFP dike in the north-eastern sector of the trench cuts the mineralized and altered mafic volcanic rocks and diorite 3 dike (Fig. 2.3; Appendix A), does not contain mineralization, and was selected for further geochronological study to constrain the minimum age of mineralization. In the western sector, a QFP dike contains xenoliths of mafic volcanic rock with gold and pervasive carbonate alteration (Fig. 2.11J), and was also selected for geochronological study.

The textural relationships of magmatic phases in post-mineralization and least altered pre-mineralization QFP dikes are similar, however, within the pre-mineralization QFP dikes plagioclase has locally been replaced by the carbonate-quartz-pyrite alteration

assemblage associated with gold mineralization. The interpreted paragenetic sequence for both types of QFP is shown in Figure 2.13, where two major events are distinguished: magmatic (phenocrysts and fine-grained groundmass) and post-magmatic (referring to any alteration of the phenocrysts and fine-grained groundmass). In the QFP, the phenocrysts (1-3 mm in size) comprise K-feldspar (15-30%), quartz (2-10%), plagioclase (4-8%), and biotite (2-5%) in a groundmass (with crystals averaging 0.1 mm in size) of plagioclase (23-56%), quartz (4-11%), muscovite (1-4%), carbonate (trace-7%), biotite (trace-7%), chlorite (trace-2%), epidote (trace-2%), apatite (trace-2%), pyrite (trace-1%), magnetite (trace), rutile (trace), ilmenite (trace), chalcopyrite (trace), pyrrhotite (trace), and zircon (trace). Carbonate, pyrite, and late quartz are more abundant in the early QFP. K-feldspar and plagioclase phenocrysts exhibit oscillatory zoning and albite twinning, and locally plagioclase phenocrysts contain zones of albite overgrowth along the margin of the crystals. Fine-grained muscovite replaces the cores of feldspar and plagioclase phenocrysts and preferentially replaces phenocrysts along oscillatory zoning. Quartz phenocrysts are fractured and locally contain quartz sub-grains. Early biotite (and locally early chlorite) occurs as large flaky crystals or sinuous crystal aggregates that are pseudomorphs after mafic magmatic crystals. Late biotite locally replaces plagioclase and feldspar. Late chlorite pseudomorphs replace and fill corroded zones of K-feldspar, plagioclase, quartz, and biotite. Carbonate occurs as anhedral crystals generally 0.2 mm across and fills corroded zones and fractures in plagioclase, k-feldspar, and quartz phenocrysts. Apatite forms euhedral prismatic crystals in the groundmass and epidote occurs as sub-rounded and euhedral crystals replacing the groundmass minerals. Magnetite forms anhedral and euhedral crystals disseminated in the groundmass and is

locally associated with biotite. Pyrite occurs as anhedral crystals disseminated in the groundmass and contains minor inclusions of ilmenite, pyrrhotite and chalcopyrite.

Ilmenite forms euhedral lath-like grains in the groundmass, while rutile is present as needle-shaped euhedral crystals. Zircon forms doubly terminating crystals and prismatic crystal sections included within feldspar phenocrysts, quartz phenocrysts, and disseminated in the groundmass.

Quartz monzonite is found to the south of the main trenched zone from surface to a depth of approximately 19 metres (Fig. 2.11K-L) and cross-cuts some auriferous veins. It comprises coarse grained (1.3-3mm) plagioclase (30-50%, identified as albite using XRD and microprobe analysis), K-feldspar (20-35%), quartz (6-15%), as well as muscovite (5-10%), chlorite (7-9%), carbonate (5-8%), pyrite (up to 2%), apatite (trace), zircon (trace), and rutile (trace). A few samples contain up to 4% epidote, and traces of biotite, pyrrhotite, and chalcopyrite.

Equigranular quartz, albite, K-feldspar, and mafic minerals are in sharp contact with each other (no groundmass in between) and their embayments are filled with aggregates of chlorite (chlorite1). Plagioclase and K-feldspar crystals are locally overgrown by albite. Chlorite1 contains inclusions of quartz and feldspar grains. A second generation of chlorite (chlorite2) forms flaky crystals replacing the finer-grained plagioclase, quartz, feldspar, carbonate, and chlorite1 crystals. Pyrite forms euhedral to subhedral crystals between coarse-grained plagioclase, feldspar, and quartz and fills embayments in plagioclase and feldspar crystals. Muscovite replaces plagioclase and feldspar as flaky

and acicular, radiating crystals, and replaces chlorite1 and chlorite2 as laths. Carbonate fills corroded zones of plagioclase, K-feldspar, quartz, and chlorite1. Apatite crystals are found included in the coarse-grained plagioclase and K-feldspar, and between the finer-grained quartz, plagioclase, feldspar, and chlorite crystals. Zircon forms doubly terminating crystals and cubic crystal sections included in plagioclase and quartz crystals.

In order to establish the tectonic setting of these magmas, we plot the composition of the least altered intrusions on Nb versus Y diagram of Pearce et al. (1984) in Figure 2.14.

This method assumes that Nb and Y are immobile elements in this type of system where

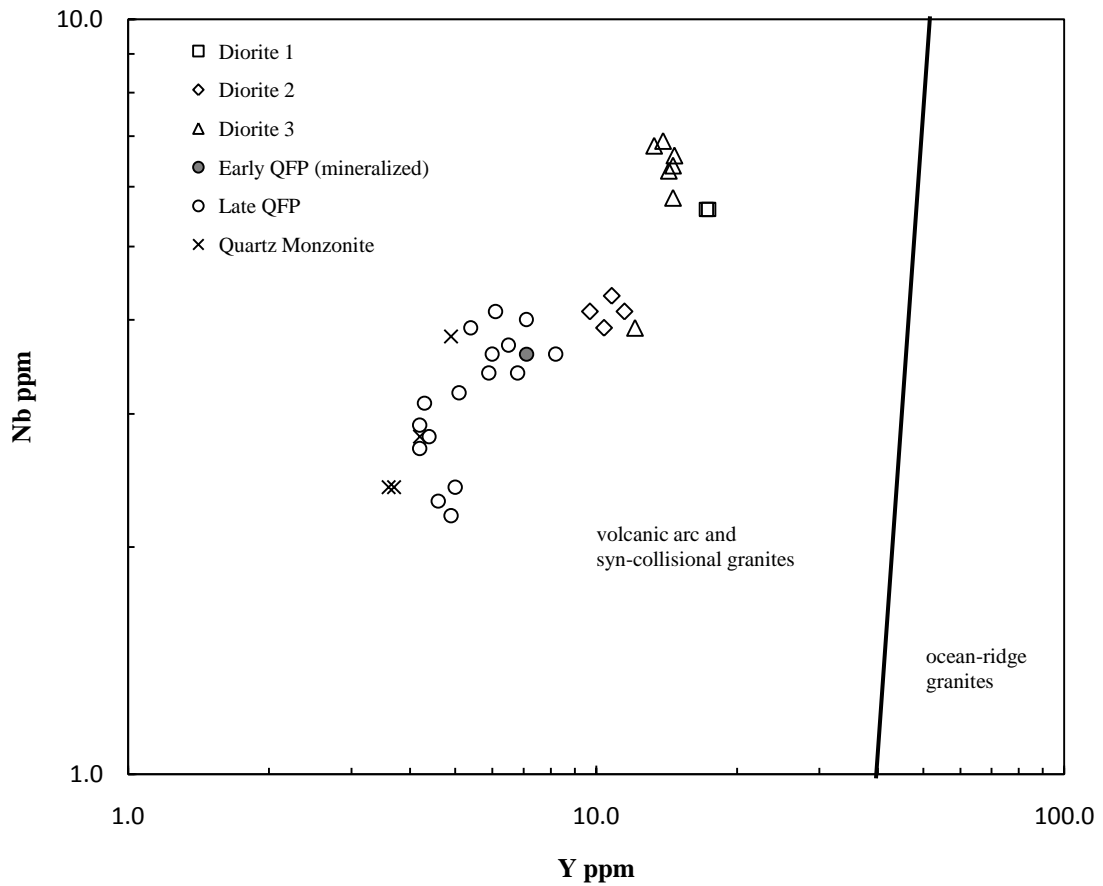


Fig. 2.14: Nb versus Y discrimination diagram (after Pearce et al., 1984) for the intrusive rocks of the Barry deposit.

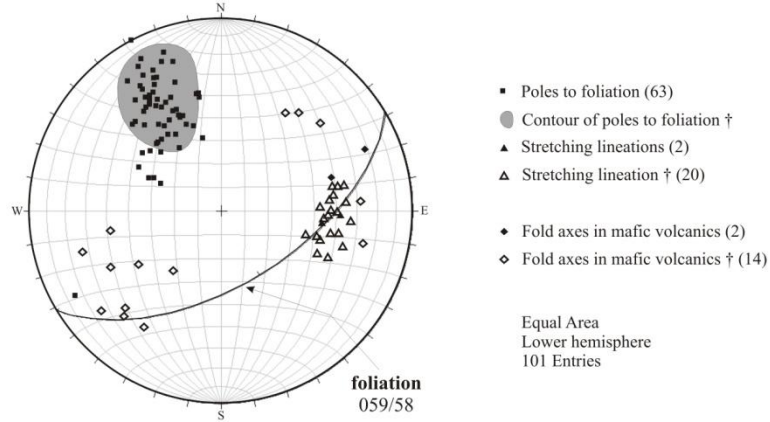
granite is defined as any plutonic igneous rock containing >5 per cent modal quartz (Pearce et al., 1984). As shown in Figure 2.14, the intrusive units at the Barry deposit have distinct Nb/Y ratios, with the quartz monzonite (0.65-0.78), both generations of QFP (0.44-0.72), diorite 3 (0.32-0.57), diorite 2 (0.36-0.42) and diorite 1 (0.32-0.33) plotting in the field of volcanic arc and syn-collisional granites.

2.4.3 Structure

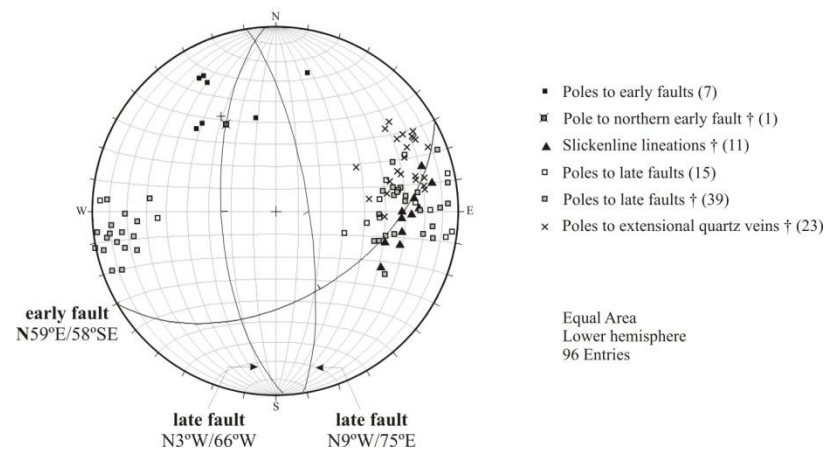
The mafic volcanics at the Barry deposit are locally folded along the S_0 planes between volcanic facies. The folds are open, symmetrical, and 50cm to 1m in size. Their fold axes commonly trend N60-75°E and plunge 20°-40° to the NE. Limbs of folds are cut by minor shear zones, shear fractures, and veinlets (Figs. 2.3 and 2.15A; Appendix A). This observation, and the fact that the fold axes are not confined to the foliation plane (Fig. 2.15A), suggest that folding is associated with a D_1 deformation that preceded the development of the foliation and shear zones.

The volcanic rock units of the Barry gold deposit are cross-cut by a well-defined N59°E-striking and 58°SE dipping D_2 tectonic foliation (Fig. 2.3 and 2.15A; Appendix A and C). This is sub-parallel to several ductile shear zones on the property, and is consistent with the attitude of the regional foliation (Hocq, 1989; Joly, 1990). The foliation is characterized by the planar orientation of phyllosilicates on sub-millimetre schistosity planes and flattening of amygdules and breccia fragments. Stretching lineations, which trend at 095→42 S and rake approximately 52° from the northeast in the foliation plane (Fig. 2.15A), are defined by elongated chlorite, pyrite, amygdules, vesicles, and breccia

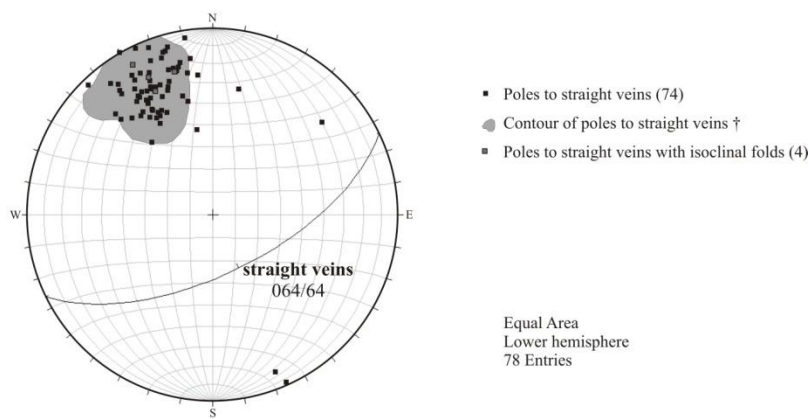
A: POLES AND CONTOUR PLOT OF POLES TO FOLIATION, STRETCHING LINEATIONS, AND FOLD AXES IN THE MAFIC VOLCANIC ROCKS



B: POLES TO EARLY AND LATE FAULTS AND SLICKENLINE LINEATIONS ON EARLY FAULTS



C: POLES AND CONTOUR PLOT OF POLES TO STRAIGHT ALBITE-CARBONATE-QUARTZ VEINS



D: POLES AND CONTOUR PLOT OF POLES TO FOLDED ALBITE-CARBONATE-QUARTZ VEINS

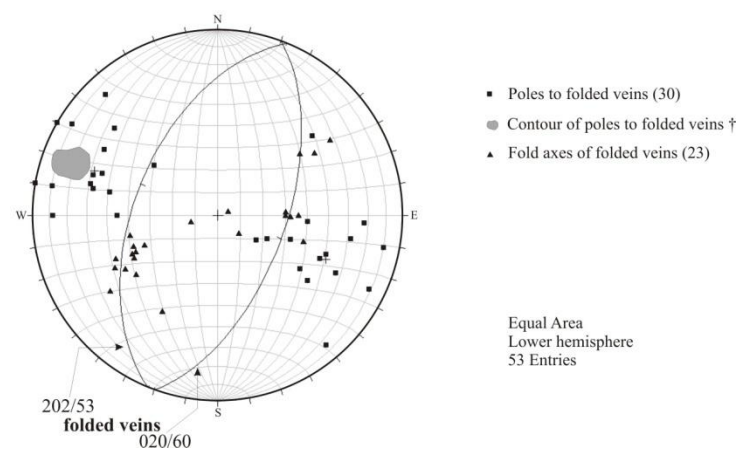


Fig. 2.15: Stereographic representation of the structural features of the Barry deposit, surface trench. A) Poles and contour plot of poles to foliation, stretching lineations, and fold axes in the mafic volcanic rocks. B) Poles to early and late faults and slickenline lineations on early faults. C) Poles and contour plot of poles to straight albite-carbonate-quartz veins. D) Poles and contour plot of poles to folded albite-carbonate-quartz veins. † indicates data collected by Tessier during mapping in 1996.

fragments. Cleavages are commonly observed along contacts of flow units. Boudinage of both early and late QFP dikes along N055°E strike is subparallel to the main foliation trend.

Two fault systems are observed at the Barry deposit: an earlier one oriented at N55-60°E, dipping 40°-58° SE (Fig. 2.15B), and a later one with two fault orientations: N3°W strike with moderate to steep dip (66°-90° W); and N9°W strike with moderate to steep dip (70°-90° E) (Fig. 2.15B). The majority of the earlier faults occur in the north portion of the main zone where they anastomose parallel to foliation, extend approximately 20 m along strike, and terminate where they are bounded on the east and west by the later faults. Slickenlines on the earlier faults trend and plunge 105°→33°, and rake on the fault plane approximately 55° from the northeast (Fig. 2.15B). Generally these faults have an apparent dextral offset of up to 3.5m, and they locally contain mineralized albite-carbonate-quartz veins. An early brittle-ductile fault, 1 to 5m wide, observed at surface from line 10+45E to line 11+75E between stations 0+65S and 0+70S marks the northern boundary of the mineralized zone (Fig. 2.3, Appendix A). Intense (locally mylonitic) S and L fabrics and boudinaged albite-carbonate-quartz veins are present where the fault is narrow. The presence of deformed albite-carbonate-quartz veins (associated with gold mineralization) within the early fault indicates that gold mineralization occurred pre- to syn-ductile deformation (D_2) of this fault. The northern-most early fault has most recently offset mafic volcanic facies, intrusive dikes, and the mineralized zone to the north, indicating that it has undergone brittle deformation post-mineralization. Based on the offsets of a QFP marker unit and attitude of the slickenlines on the fault, the brittle

movement along this fault is interpreted as oblique reverse dextral, the SE block having moved up and towards the SW relative to the NW block, according to the fault plane resolution method of Davis (1984; Appendix C).

The second fault system (Fig. 2.3 and 2.15B; Appendix A) comprises brittle structures, ranges in width from <10cm to 1m, and is continuous for at least 50m along strike. The offsets caused by their displacement controls the topography of the trenched region with differences of 0.5 to 3m in elevation across a fault. These late faults offset lithologic units and mineralization, with faults dipping to the west appearing to have a sinistral sense of offset, while faults dipping to the east appear to have dextral offset (Fig. 2.3).

Slickenlines observed on two fault planes have shallow rakes from 10° to 30°N.

Throughout the trenched zone, veins comprise 1-3% of the volume of the mafic volcanic rock package and 5-15% of the volume in mineralized zones. Four main vein types have been identified in the Barry deposit main zone based on their mineralogical composition: (a) auriferous albite-carbonate-quartz, (b) barren quartz-carbonate, (c) barren carbonate, and (d) locally extensional quartz veins (the latter locally auriferous). The auriferous albite-carbonate-quartz veins exhibit four main geometries: a) straight, planar veins at N64°E/64°SE (Figs. 2.15C and 2.16); b) straight (N64°E/64°SE) veins with rootless isoclinal folding and/or transposition along the isoclinal fold hinge (Fig. 2.15C); c) folded veins at N20°E/60°SE (Figs. 2.15D, 2.16); and d) locally shallow veins. Their mode of occurrence and mineralogy will be described in detail in the “Gold Mineralization” section.

Barren quartz-carbonate and carbonate veins are observed at surface and throughout drill core. These veins are composed primarily of calcite and/or quartz, and locally contain traces of biotite and chlorite. At depths greater than 30 m epidote and garnet are locally present in veinlets. Calcite veins comprise approximately 1% of the rock volume, whereas from surface to 30m depth quartz-calcite veins comprise approximately 1%, and at depths greater than 30m they comprise 3% of the rock volume. Both quartz-carbonate and carbonate veins can be straight, folded, or sinuous, with irregular orientations as

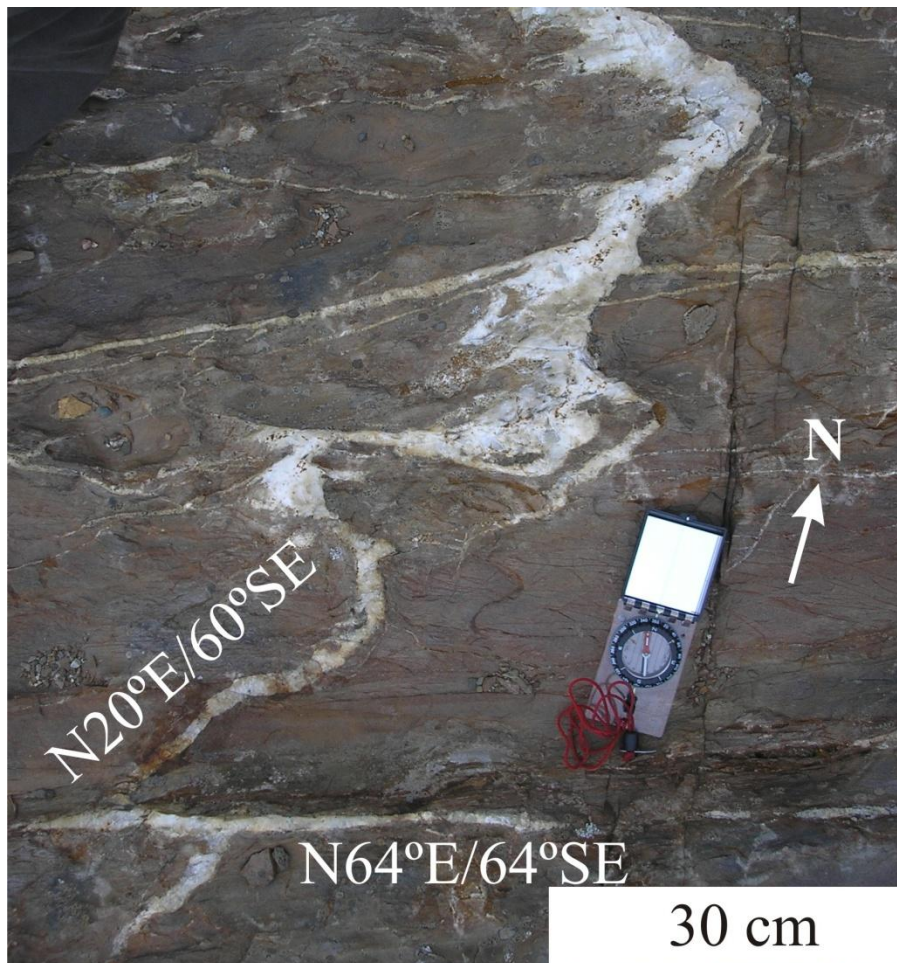


Fig. 2.16: Straight ($N64^{\circ}E/64^{\circ}SE$) and folded ($N20^{\circ}E/60^{\circ}SE$) auriferous albite-carbonate-quartz veins at the Barry deposit and their associated carbonate-quartz-pyrite alteration of the Type B mafic volcanic rock (rusty colour) [surface location 1068 E/76 S].

shown by variable core intersections of 30-90° from the core axis in vertical drill holes.

Extensional white quartz veins locally crosscut the mafic volcanic rocks and the mineralized albite-carbonate-quartz veins but are generally found within the more competent early QFP dikes. These 3-5 cm wide, mainly vitreous quartz veins cut the dikes perpendicular to their strike at N20-40°W/64-66° SW. Veins contain up to 12% chlorite in their selvages or growing inwards from the vein wall to the centre, 3% sericite, and locally free gold. These veins appear to be syn-kinematic with early faults, as their approximately coincide with stretching lineations and slickenlines observed on the early faults (Fig. 2.15B).

2.4.4 Gold Mineralization

Although the volcanic units generally strike northeast and dip to the southeast (approximately N55-60°E/40°SE), the envelope containing economic gold grades (>2 g/t) is constrained from surface to a depth of 30m. In northwest-southeast vertical cross sections, the outline of the mineralized zone has an antiformal/domal shape (Fig. 2.4; Appendix A) and both Types A and B volcanic rock types are hosts for the mineralization.

The gold mineralization is constrained to zones containing 5-15% albite-carbonate-quartz veins and their associated hydrothermally altered wall rocks. Albite-carbonate-quartz veins are typically 1-5cm wide (1-2cm wide on average), and comprise euhedral albite

(20-50%), carbonate (30-40%), and quartz (20-40%). Albite identification was confirmed using XRD and microprobe analysis. In addition to albite, carbonate, and quartz, these veins locally contain trace biotite +/- sericite, chlorite (fine-grained anhedral), pyrite (fine-grained anhedral, or coarse-grained euhedral), pyrrhotite, rare euhedral magnetite, and fine-grained visible gold as inclusions or fracture infill in pyrite, or in sharp contact with carbonate crystals in the vein. Biotite and chlorite are present along vein selvages. Veins locally pinch and swell or are boudinaged with biotite generally filling the cusps.

Gold grades in mineralized veins and altered mafic volcanic rocks range from <2 g/t to >100 g/t, and gold resources for the deposit (with a 2 g/t cut-off) are indicated at 52,300 oz gold (385,000 metric tonnes at 4.23 g/t Au) and inferred at 126,600 oz gold (966,000 metric tonnes at 4.07 g/t Au, Systèmes Géostat International Inc., 2007).

In addition to the pre-ore alteration described for the least altered samples in the previous sections, the following alteration types were identified at the Barry deposit main ore zone based on the mineralogical composition and textural relationships: (a) syn-ore carbonate-quartz-pyrite alteration associated with the mineralized albite-carbonate-quartz veins (Figs. 2.7 and 2.17); (b) syn-ore biotite-calcite alteration associated with mineralized albite-carbonate-quartz veins in areas of intense foliation (Fig. 2.19); and c) post-ore biotite-chlorite, carbonate, muscovite, and epidote alteration (Figs. 2.7 and 2.20). Post-ore epidote alteration is generally found at depths greater than 25 m, where it is commonly associated with epidote-garnet veinlets, or in non-mineralized zones at shallower depths.

2.4.4.1 Syn-ore Carbonate-quartz-pyrite Wall-rock Alteration

Volcanic rocks that have undergone carbonate-quartz-pyrite alteration are comprised of carbonate 1 (5-45%), quartz (2-8%), pyrite (2-8%), albite (trace-3%: identified using XRD and microprobe analysis), pyrrhotite (trace-3%), muscovite 1 (trace), chalcopyrite (trace), biotite (locally trace) and locally native gold, which pseudomorphously replace and fill corroded zones of pre-ore alteration minerals (Fig. 2.17). In mineralized zones the carbonate is ferroan dolomite to ankerite in composition, as determined by XRD.

Carbonate1, quartz, and albite (6-10 μ m in size) replace plagioclase laths and fill corroded portions of chlorite1, biotite1, and rare crystals of magnetite. Rare magnetite contains inclusions of chalcopyrite and pyrrhotite, and mantles cubic pyrite. Locally biotite has sharp contacts with quartz, albite, carbonate, and pyrite. Pyrite forms euhedral cubic to subhedral crystals (11-50 μ m in size) and crystal aggregates, has sharp contacts with carbonate1 and quartz, contains inclusions of ilmenite, magnetite, rutile, chalcopyrite, pyrrhotite, native gold (Fig. 2.17 and 2.18), and gold tellurides, and locally pyrite mantles muscovite 1 (Fig. 2.17C).

Trace element composition of pyrite is variable and does not relate to the composition of inclusions or amount of corrosion of pyrite grains. Pyrite locally contains variable Ni, Co, W, Ti, Te, and Se, Hg, and Zn were near detection limits of 0.0085 wt%, 0.0331 wt%, and 0.0196 wt%, respectively (Appendix E). Gold is near or below detection limit in pyrite, with the exception of one sample that contains Au over three times the detection limit of 0.0067 wt% (sample 31-21.80C2a.2-2: 0.025 wt% Au). Arsenic is above

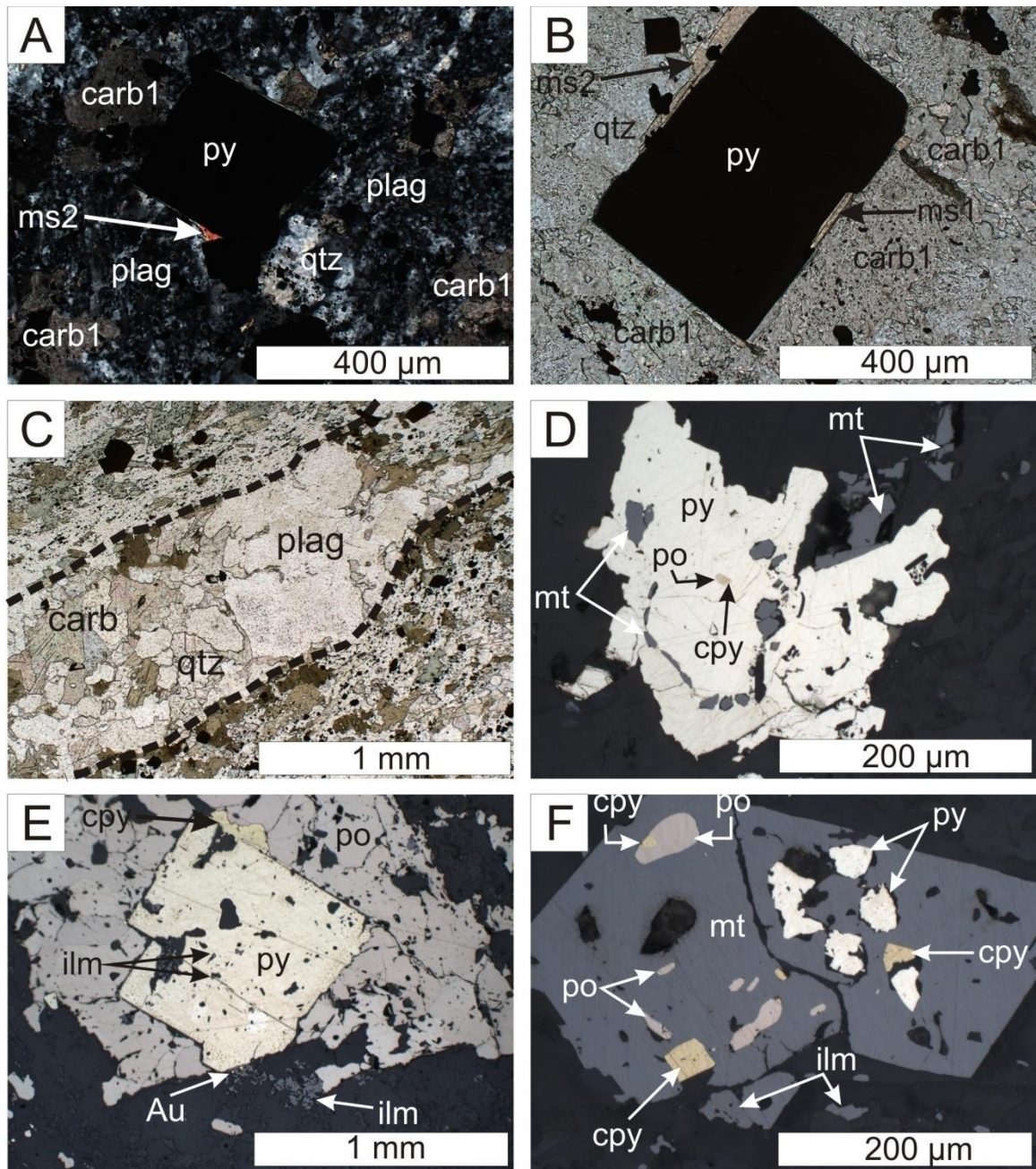


Fig. 2.17: Photomicrographs of syn-ore carbonate-quartz-pyrite alteration at the Barry deposit. A) Type B volcanic rock (drill core sample 31-10.27 in cross-polarized transmitted light). Plagioclase replaced by carbonate1, quartz, and pyrite. Pyrite has sharp contacts with carbonate1 and quartz. Muscovite 2 mantles the pyrite euhedral rim. B) Type B volcanic rock (surface sample 71-1099 in plane-polarized transmitted light). Cubic pyrite has sharp contacts with quartz and carbonate1. Pyrite mantles muscovite 1 lath. Muscovite 2 replaces carbonate1 and quartz, and has sharp contacts with pyrite. C) Type A volcanic rock (drill core sample 210-25.12 in plane-polarized transmitted light). Albite-carbonate-quartz vein cuts biotite and chlorite altered mafic volcanic rock. Biotite 2 and local chlorite 2 fill embayments in plagioclase, carbonate, and quartz crystals in the vein. D) Type B volcanic rock (surface sample 90-1040 in plane-polarized reflected light). Pyrite with inclusions of magnetite, chalcopyrite, and pyrrhotite. E) Type A volcanic rock (drill core sample 31-26.43 in plane-polarized reflected light). Cubic pyrite is pitted and contains inclusions of ilmenite. Pyrite is partially encompassed by pyrrhotite, which is locally replaced by chalcopyrite along the rim of the pyrite grain. Ilmenite also forms crystal aggregates in the host, and gold is locally found filling the spaces between ilmenite grains adjacent to the pyrite crystal. F) Type B volcanic rock (drill core sample 31-2.26 in plane-polarized reflected light). Magnetite with inclusions of pyrrhotite and chalcopyrite, and corroded zones of magnetite are filled with pyrite.

Magnetite partially encompasses cubic chalcopyrite (likely pseudomorphously replacing pyrite). Ilmenite forms laths and crystal aggregates in the host. Au = gold-silver alloys; carb1 = carbonate 1; cpy = chalcopyrite; ilm = ilmenite; ms1 = muscovite 1; ms2 = muscovite 2; mt = magnetite; plag = plagioclase; po = pyrrhotite; py = pyrite; qtz = quartz.

detection limit in one sample (sample 74-1175C4-2: 0.059 wt% As). Locally carbonate 1, pyrrhotite, chalcopyrite, and gold (Figs. 2.17 and 2.18) fill embayments and fractures in pyrite grains. Rare pyrrhotite and chalcopyrite replace euhedral cubic pyrite. Chalcopyrite locally contains variable amounts of Ti, Zn, Au, and Se (Appendix E). Gold is spatially associated with pyrite (or pyrrhotite after pyrite), and although gold grade can vary in samples containing trace pyrite and/or pyrrhotite, in samples containing >3% pyrite and/or pyrrhotite, the gold grade is generally >2 g/t Au.

Gold grains are visible at a microscopic scale (2-8 μ m in size) (Fig. 2.18 A-D) and are locally visible at hand sample scale (up to 1mm in size). Energy dispersive X-ray spectroscopy (EDS) analysis indicates that locally gold is also present as micro-inclusions (generally <1 μ m in diameter) of native gold and gold tellurides within pyrite crystals (Fig. 2.18E-F). Electron microprobe analyses indicate that the composition of gold is variable within the mineralized zone. Gold included in pyrite has a lower Ag content (3.6-5.12 wt%) than gold grains filling cracks in, or in contact with pyrite grains have an intermediate Ag content (5.72-8.07 wt%), and gold grains included in carbonate grains contain higher Ag amounts (8.2-9.04 wt%). In general, gold grains contained low levels of Te (0.01-0.07 wt%), whereas most other elements identified are at concentrations near detection limits.

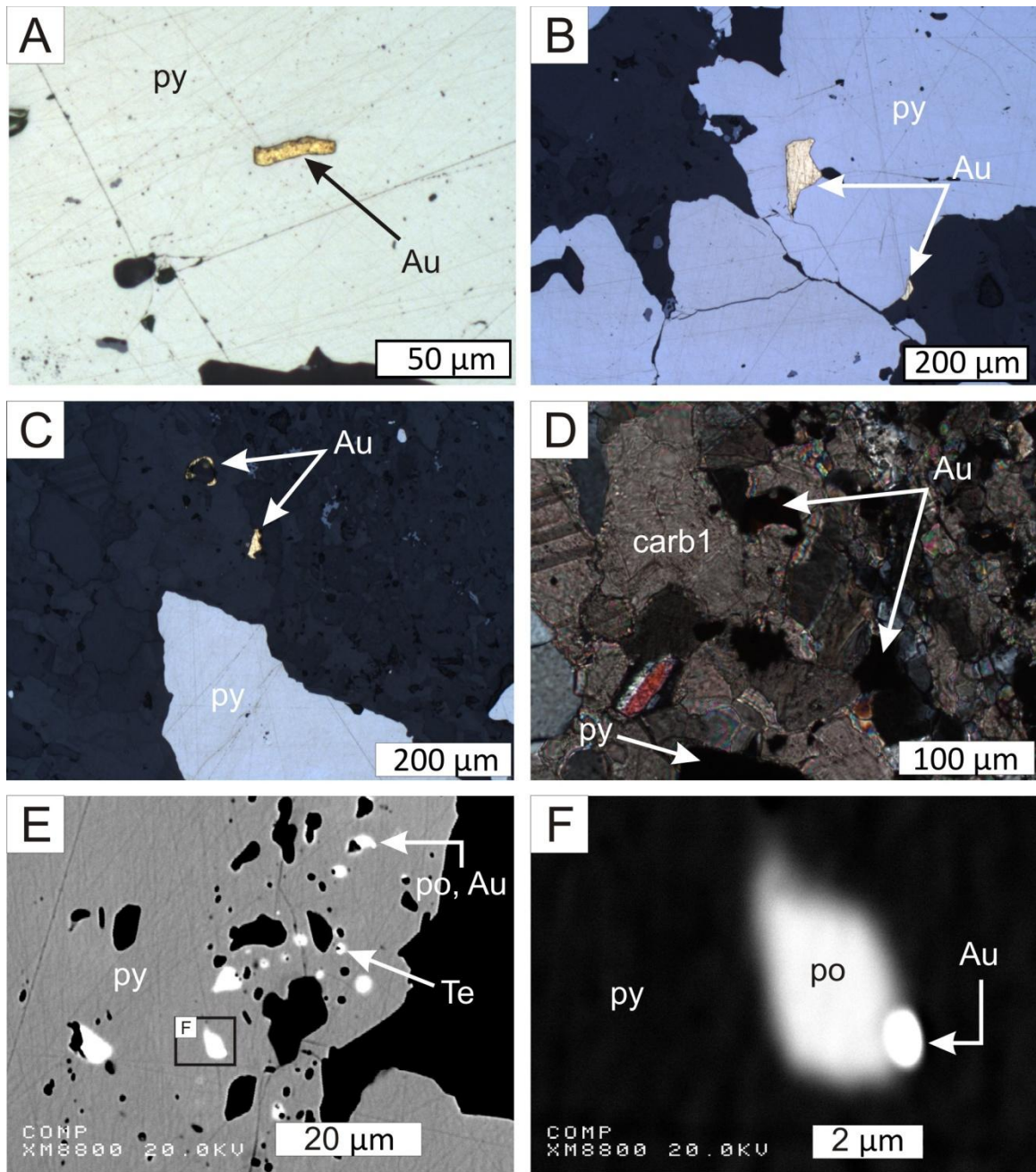


Fig. 2.18: Photomicrographs and backscatter electronic images of the mode of occurrence of gold at the Barry deposit. A) Photomicrograph of Type A volcanic rock (drill core sample 210-42.75 taken in reflected light). Gold is included in pyrite. B) Photomicrograph of Type B volcanic rock (drill core sample 31-12.00 taken in reflected light). Gold fills fractures in pyrite, and is present along the rim of pyrite grain. C) Photomicrograph of Type B volcanic rock (drill core sample 31-12.00 taken in reflected light). Gold grains have sharp contact with syn-ore carbonate-quartz alteration adjacent to pyrite grain. D) Photomicrograph of Type B volcanic rock (drill core sample 31-12.00 under increased magnification in cross-polarized transmitted light). Gold has sharp contacts with carbonate grains that have replaced plagioclase in the mafic volcanic rock. E) Backscatter electron image of Type C volcanic rock (drill core sample 136-26.26). Pyrite grain is corroded/pitted and contains inclusions of pyrrhotite, gold-silver alloys, and tellurium. F) Backscatter electron image of portion of pyrite grain shown in E. Gold and silver is included in pyrrhotite, which is included in pyrite. Au = gold-silver alloys; carb1 = carbonate1; po = pyrrhotite; py = pyrite; Te = telluride.

In order to identify the elements that are enriched and depleted in mafic volcanic rocks that have undergone carbonate-quartz-pyrite alteration we used the methods of Grant (1986, 2005) to create an isocon diagram. Ti, Zr, and Y define the isocon as they are the least mobile elements in these rocks, as shown in the binary diagrams in Figures 2.8 and 2.9.

Three samples of Type B volcanic rock (samples 31-12.00; 71-1099; 74-1175) with an average gold grade of 8.1 g/t and containing pervasive carbonate-quartz-pyrite alteration with trace amounts of biotite and epidote ($\leq 2\%$) alteration, are plotted against the least altered sample of Type B (sample 91-1119) (Fig. 2.19). Elements above the solid line are enriched in the altered samples compared to the least altered sample, whereas elements below the line are depleted in comparison to the least altered sample.

The elements significantly added ($>100\%$ increase) to the Type B volcanic rocks that underwent carbonate-quartz-pyrite alteration are: Au, S, Mo, Ag, Bi, W, Se, Pb, Cu, and Na, as well as LOI (Fig. 2.20A). Mg, Ca, Mn, Sr, U, As, and Sb were added in considerable amounts (20-100% increase), and Ba, Ga, Sm, and Si show a modest gain (6.7-20% increase). Whereas P, Zn, Ni, and Sc are considerably depleted (20-100% decrease) and Cs, Dy, Er, Fe, Lu, Rb, Ta, Tb, Tm, and Yb show modest decreases (6.7-20% decrease).

2.4.4.2 Syn-ore Biotite-carbonate Alteration

The syn-ore biotite-carbonate (carbonate₁) alteration is found locally within the deposit and is associated with areas of intense foliation and shear zones in drill core (e.g. drill core sample 31-27.20). Where present, it is impossible to determine the primary volcanic textures and structures, as they have been destroyed by deformation and alteration.

However, biotite-carbonate altered samples have Ti/Zr and Zr/Y ratios (77-89 and 3.2-4.3 respectively; Appendix D) similar to Type A volcanic rocks, suggesting that their protoliths belong to this volcanic unit. Volcanic rocks that have undergone syn-ore biotite-carbonate alteration are comprised of biotite (10-55%), carbonate (20-30%), pyrite (trace-2%), and rare pyrrhotite, which replace the pre-ore alteration assemblage.

Biotite₂ forms flakey and lath-like crystals (10-30µm in size) that generally have sharp contacts with carbonate₁, and locally fill embayments in carbonate₁ and pyrrhotite.

Pyrite forms cubic crystals (11-30µm in size) that are mantled by pyrrhotite. Pyrrhotite has sharp contacts with carbonate₁ and flakey biotite₂, and is locally replaced by chalcopyrite.

Using the methods of Grant (1986, 2005), one sample of biotite-carbonate alteration (sample 31-27.20) belonging to Type A volcanic rocks, with an average gold grade of 65.5 g/t and containing pervasive biotite-carbonate alteration with no post-ore epidote alteration, is plotted against the least altered sample of Type A (sample 210-74.00) (Fig. 2.19B).

Fig. 2.19: Isocon diagrams with weighted elements in which the protolith (least altered Type B and Type A, respectively) versus the altered samples are plotted. A) Syn-ore carbonate-quartz-pyrite alteration; and B) syn-ore biotite-carbonate alteration. Various elements are multiplied or divided by a constant to fit a common scale of the diagram. The black line (isocon) is defined by the elements Ti, Y, and Zr, which are the most immobile elements in the volcanic rocks at the Barry deposit. Elements above the line are enriched in the altered rock, whereas elements below the line are depleted during alteration. Element concentrations are in ppm, oxide is in weight percent. In order to estimate the minimum gain or loss of some elements that were below detection limit in samples 91-1119, 210-74.00, 71-1099, and 31-27.20, the isocons were calculated using the detection limit value (i.e. for samples 91-1119 and 210-74.00: Ag=0.1 ppm, Se=0.5 ppm; for sample 71-1099: Cr₂O₃=0.001 ppm, Cs=0.2 ppm, Sb=0.1 ppm; and for sample 31-27.20: As=0.5 ppm). Elements below detection limit, and excluded from isocon diagrams, are: Be, Cd, Hg, Pd, Pt, Sn, Te, Tl (below detection in carbonate-quartz-pyrite altered samples), and Sb (below detection in biotite-carbonate altered sample).

The elements significantly added (>100% increase) to the biotite-carbonate altered rock are: Au, Ag, Mo, S, Se, Bi, W, Cu, K, Rb, Pb, Ba, Cs, Tl, Na, Ga, Fe, and Ca. Si, Al, Mg, Mn, Co, U, Zn, Ni, and As were added in considerable amounts (20-100% increases), and Cr, Hf, Ta, Th, and Sc show a modest gain, whereas P and Sm are considerably depleted (20-100% decreases) and Sr, V, Dy, and Ho show modest decreases.

2.4.5 Post-ore Alteration

Post-ore biotite 3, chlorite 3, carbonate 2, muscovite 2, and epidote are present throughout the main zone within the mafic volcanic and intrusive units. Volcanic rocks that have undergone post-ore alteration are comprised of epidote (5-30%), carbonate (5-25%), chlorite (5-20%), muscovite (trace-15%), and biotite (trace-10%), which replace or fill embayments in pre-ore and syn-ore alteration minerals (Fig. 2.20).

Biotite 3 and chlorite 3 comprise 2-10% of the rock and pseudomorphously replace and fill embayments in one another and quartz-carbonate-albite crystals in veins. In post-ore QFP, chlorite forms coarse grains that replace the mafic phenocrysts. Microprobe analysis of post-ore chlorite₃ indicates that it is Fe-rich clinocllore (Appendix E), and is

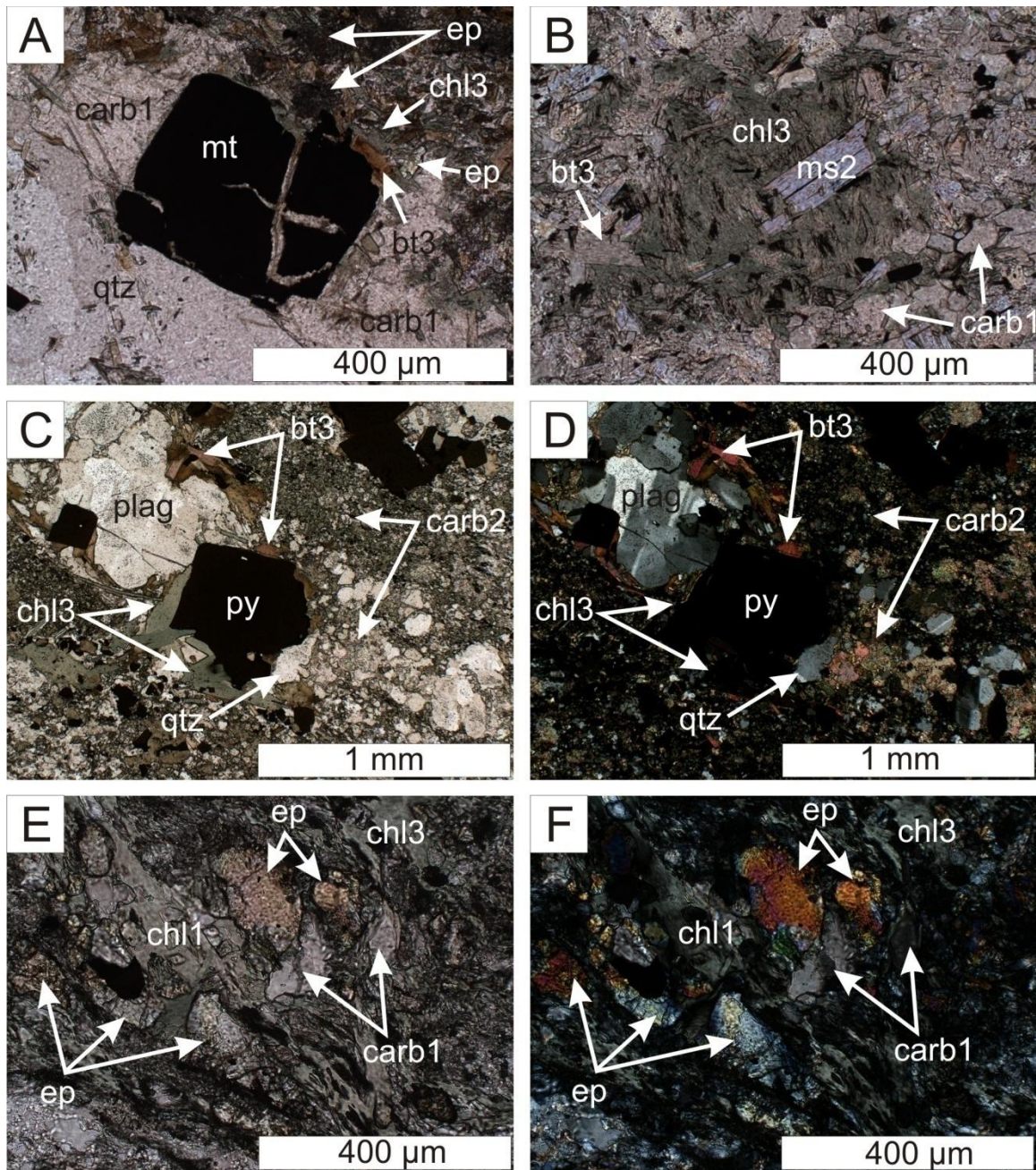


Fig. 2.20: Photomicrographs of post-ore alteration at the Barry deposit. A) Type A volcanic rock (drill core sample 31-25.48 in plane-polarized transmitted light). Corroded zones of and cracks in magnetite are filled with quartz, carbonate1, biotite2, and chlorite2. Epidote replaces chlorite 2, biotite 2, and carbonate 1 as granular aggregates. B) Type A drill core sample 31-17.89 in plane-polarized transmitted light. Chlorite2 and biotite2 replace carbonate1 crystals. Muscovite 2 replaces chlorite 2 as laths. C) Type A drill core sample 118-5.98 in plane-polarized transmitted light. Pyrite has sharp contacts with plagioclase and quartz in the veinlet. Carbonate 2 is present as fine-grained crystals replacing plagioclase in the host, and replacing portions of plagioclase and quartz crystals in the veinlet. Chlorite 2 and biotite 2 replace portions of plagioclase, carbonate 2, and quartz crystals in the vein, and fill corroded zones of pyrite. D) Type A drill core sample 118-5.98 from C, now in cross-polarized transmitted light. Note the high birefringence of the biotite2 and the extensive replacement of plagioclase and quartz in the veinlet by carbonate2. E) Type A drill core sample 117-26.26 in plane-polarized transmitted light. Chlorite1 forms flakey crystals that are replaced by euhedral carbonate1. Epidote replaces portions of flakey chlorite and carbonate1 as euhedral crystals. F) Type A drill core sample 117-26.26 as in E, now in cross-polarized transmitted light. Note the low birefringence of the chlorite1 flakes

and the pervasive euhedral epidote. bt2 = biotite 2; carb1 = carbonate 1; carb2 = carbonate 2; chl2 = chlorite 1; chl2 = chlorite 2; ep = epidote; ms2 = muscovite 2; mt = magnetite; plag = plagioclase; py = pyrite; qtz = quartz.

similar chemically to pre-ore chlorite. Post-ore biotite has a similar composition (Fe, Mg, and Al values) to pre-ore biotite (Appendix E). Carbonate 2 is fine grained and fills corroded zones of biotite 3, chlorite 3, and quartz-carbonate 1-albite crystals in veins as fine-grained granular aggregates and anhedral crystals. Muscovite 2 occurs as fine-grained laths that fill embayments in biotite 3, chlorite 3, and carbonate 2. Epidote occurs as euhedral crystals (2-10 μm in size) and fine-grained crystal aggregates that fill embayments in all other alteration minerals, including quartz, carbonate, and albite in the veins. Garnet is locally present at depths greater than 25 m, and is spatially associated with epidote alteration.

2.5 U-Pb Zircon Geochronology

Three samples were chosen for U-Pb dating: one pre-mineralization diorite 3 (59-1164) along the margin of a QFP dike, and two post-mineralization QFP samples (83-1038 and 58-1165, Fig. 2.3). Kilogram size samples of these dikes yielded a small amount of zircon. Zircon crystals proved to be abundant in the QFP samples, but rare in diorite 3 sample. Zircon grains range in size from 50 microns (diorite 3) to 350 microns in length (QFP), and are generally doubly terminated crystals or tips of broken zircon grains (Fig. 2.21). The length to width ratio of separated zircon crystals is approximately 3:1 for all samples. Grains for U-Pb analysis were handpicked under a microscope to choose the freshest, least cracked grains from both air abraded and chemically abraded zircon. U-Pb analysis was conducted on one air abraded and three chemically abraded zircon grains for

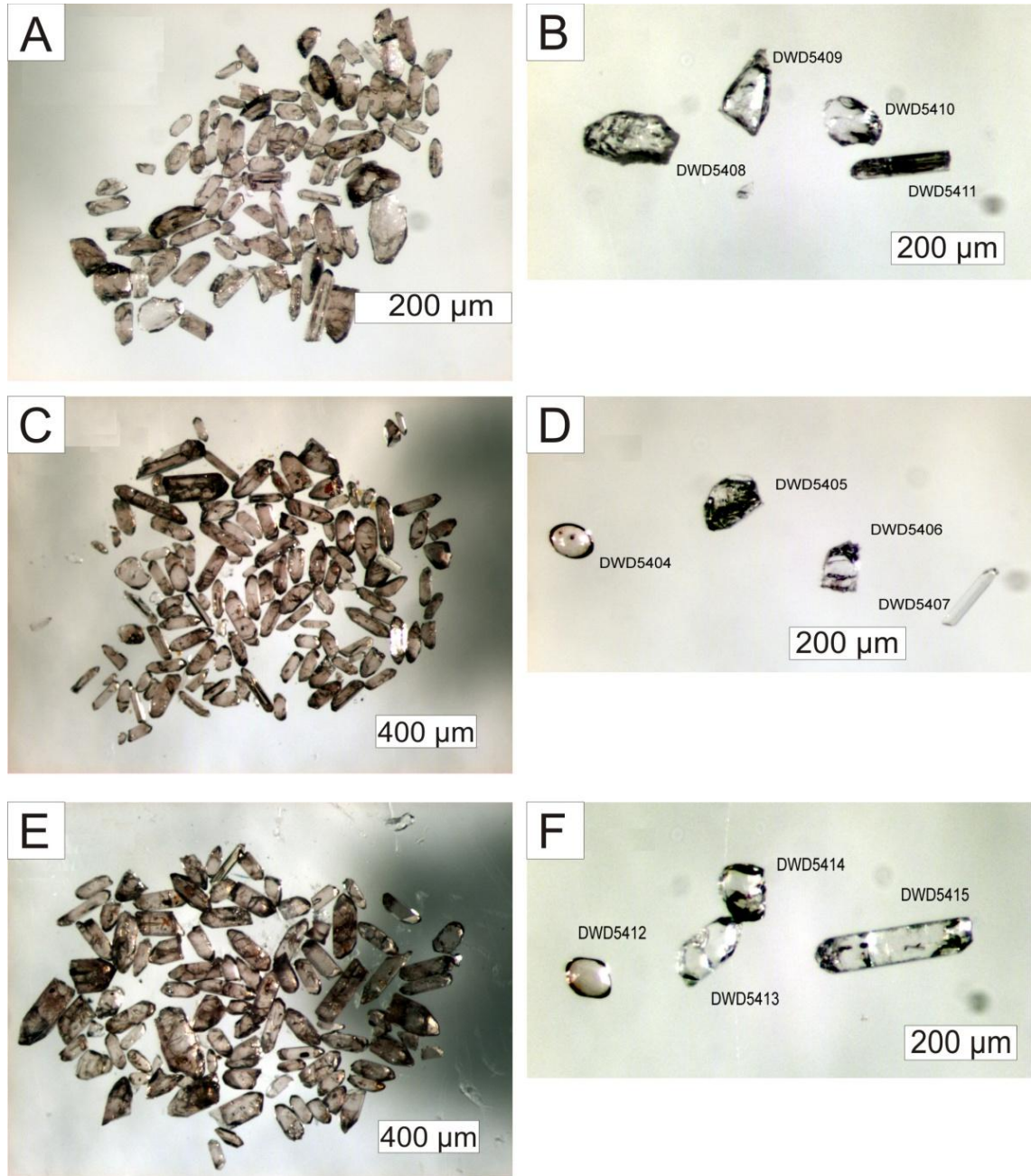


Fig. 2.21: Photomicrographs of air abraded and chemically abraded zircon grains for TIMS U-Pb analyses. A) Pre-ore diorite 3 sample 59-1164 example of zircon population prior to annealing. B) Pre-ore diorite 3 sample 59-1164 zircon grains chosen for U-Pb dating: chemically abraded zircon (DWD5408-5411); C) Post-ore QFP sample 58-1165 example of zircon population prior to annealing. D) Post-ore QFP sample 58-1165 zircon grains chosen for U-Pb dating: air abraded (DWD5404) and chemically abraded (DWD5405-5407) zircon; E) Post-ore QFP sample 83-1038 example of zircon population prior to annealing. F) Post-ore QFP sample 83-1038 zircon grains chosen for U-Pb dating: air abraded (DWD5412) and chemically abraded (DWD5413-5415) zircon.

each of the QFP samples (58-1165 and 83-1038; Fig. 2.22), and four chemically abraded zircons for the diorite 3 sample (59-1164, Fig. 2.22).

Ages were calculated by regressing the data to a line forced through 0 Ma using the Isoplot program (Ludwig, 2003). This gives the average $^{207}\text{Pb}/^{206}\text{Pb}$ ages. Analytical errors are given at 2σ (Table 2.1, Figs. 2.22 and 2.23). Average age errors and error ellipses are given at 95% confidence levels.

The pre-mineralization diorite 3 sample, 59-1164, yielded the smallest zircon population, consisting of only a few grains and fragments. An average of all four data gives a $^{207}\text{Pb}/^{206}\text{Pb}$ age of 2696.8 +/- 0.9 Ma with a 19% probability of fit (Fig. 2.22A). The two most concordant data give an age of 2697.9 +/- 1.5 Ma (Fig. 2.22B), which may be a more accurate age for the diorite 3 dike. Even if these grains are xenocrysts, their age is still an older limit on emplacement and, considering the ages of the post-mineralization dikes, must be within error of the true emplacement age.

Two grains from QFP sample 58-1165 appear to contain slight amounts of inheritance, and have been omitted from final average ages. The two youngest grains from 58-1165 yield a $^{207}\text{Pb}/^{206}\text{Pb}$ age of 2696.7 +/- 1.2 Ma (Fig. 2.22C). The second QFP sample, 83-1083, which had the largest zircon population, yields a tight cluster with an average $^{207}\text{Pb}/^{206}\text{Pb}$ age of 2697.7 +/- 1.1 Ma from all four data (Fig. 2.22D).

Table 2.1: U-Pb isotope data from single-grain zircon TIMS analyses of pre-ore diorite and post-ore QFP dikes at the Barry deposit

Site/Analysis	Weight (mg)	U (ppm)	Th/U	Pbtot (pg)	Pbcom (pg)	²⁰⁷ Pb/ ²⁰⁴ Pb measured	²⁰⁶ Pb/ ²³⁸ U	2σ	²⁰⁷ Pb/ ²³⁵ U	2σ	²⁰⁷ Pb/ ²⁰⁶ Pb Age (Ma)	2σ	% Disc	Rho
59-1164 (Diorite 3)														
dwd5409 CA	0.0008	186	0.15	81.4	1.7	555.6	0.5198	0.0016	13.260	0.045	2698.3	2.4	0.0	0.9088
dwd5410 CA	0.0009	63	0.39	32.8	0.3	1092.1	0.5190	0.0018	13.235	0.049	2697.6	2.1	0.1	0.9405
dwd5408 CA	0.0018	133	0.15	130.4	0.7	2130.1	0.5184	0.0012	13.210	0.035	2696.6	1.6	0.2	0.9312
dwd5411 CA	0.001	135	0.43	78.7	0.4	1909.6	0.5180	0.0017	13.192	0.045	2695.5	1.7	0.2	0.9523
58-1165 (QFP)														
dwd5404 Ab	0.0008	104	0.37	47.7	0.5	1021.5	0.5196	0.0014	13.320	0.039	2706.4	2.4	0.4	0.8770
dwd5407 CA	0.0002	725	0.12	78.4	0.3	2891.9	0.5156	0.0014	13.161	0.040	2699.3	1.5	0.8	0.9525
dwd5405 CA	0.0028	198	0.21	307.0	0.6	5888.4	0.5188	0.0012	13.222	0.035	2696.8	1.6	0.1	0.9318
dwd5406 CA	0.0011	144	0.20	87.7	0.9	1072.5	0.5175	0.0014	13.186	0.038	2696.5	2.0	0.4	0.9117
83-1038 (QFP)														
dwd5412 Ab	0.0005	182	0.27	51.1	0.3	1830.5	0.5172	0.0015	13.192	0.041	2698.2	1.7	0.5	0.9430
dwd5414 CA	0.002	64	0.13	69.1	1.0	815.8	0.5183	0.0013	13.216	0.038	2697.6	1.9	0.2	0.9176
dwd5415 CA	0.0042	95	0.23	221.9	19.3	142.6	0.5184	0.0014	13.217	0.074	2697.4	6.6	0.2	0.7666
dwd5413 CA	0.002	35	0.22	38.9	0.3	1466.2	0.5188	0.0014	13.226	0.039	2697.1	2.0	0.1	0.9136

Fractions are ordered from highest to lowest ²⁰⁷Pb/²⁰⁶Pb age

CA - chemical abrasion; Ab - air abrasion

Pbcom - common Pb assuming the isotopic composition of laboratory blank: ²⁰⁶Pb/²⁰⁴Pb - 18.221; ²⁰⁷Pb/²⁰⁴Pb - 15.612; ²⁰⁸Pb/²⁰⁴Pb - 39.360 (errors of 2%).

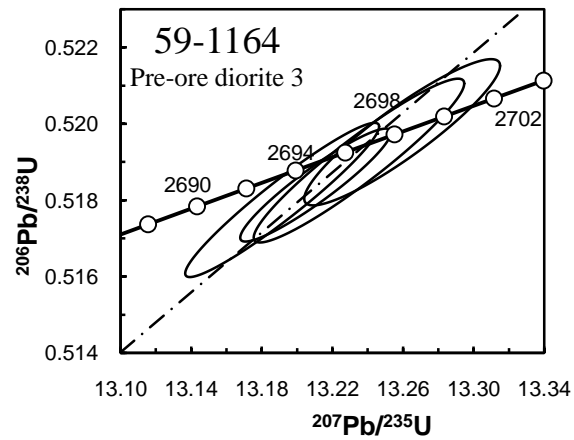
Th/U calculated from radiogenic ²⁰⁸Pb/²⁰⁶Pb ratio and ²⁰⁷Pb/²⁰⁶Pb age assuming concordance

Disc - per cent discordance for the given ²⁰⁷Pb/²⁰⁶Pb age

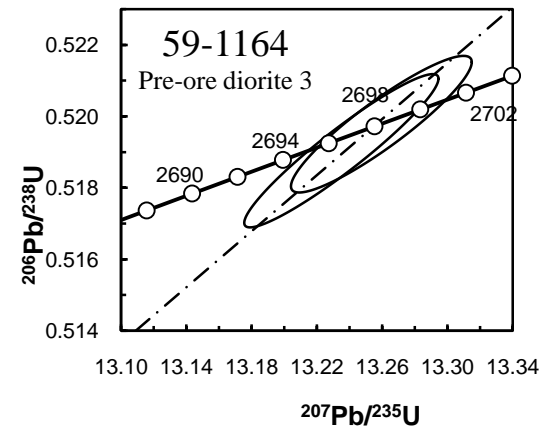
Rho - Error correlation coefficient

Uranium decay constants are from Jaffey et al. (1971).

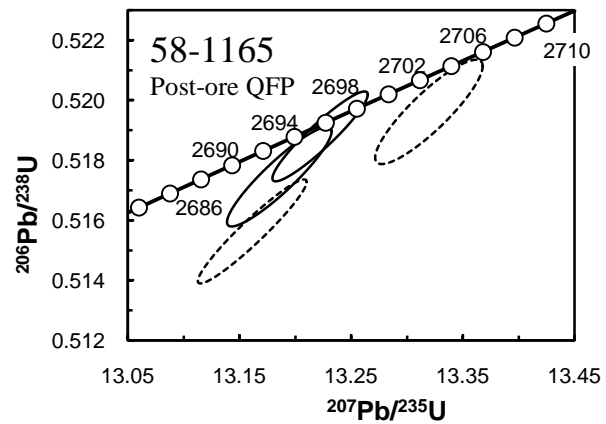
A



B



C



D

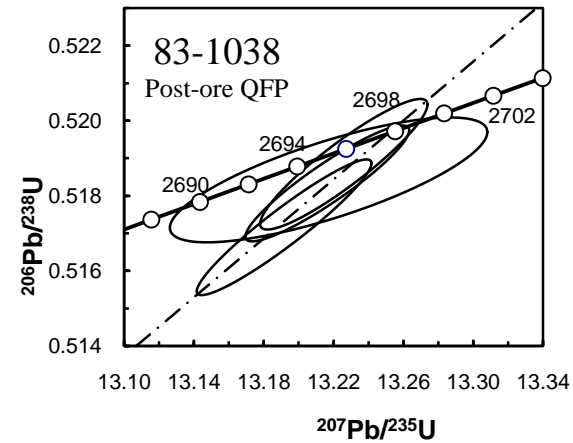


Fig. 2.22: Concordia diagram showing TIMS U-Pb analyses of zircon grains. Regression lines are forced through 0 Ma. A) Diorite 3 sample 59-1164 – four data; B) Diorite 3 sample 59-1164 – two oldest data.; C) QFP sample 58-1165 – four data, two youngest ellipses in solid line; D) QFP sample 83-1038 – four data).

The three samples analyzed (pre- and post-mineralization) are indistinguishable in age, indicating a close temporal relationship between the magmatism and mineralization.

Pooling ten data points (leaving out only the two inherited analyses) gives a best estimate for the age of mineralization at 2697.1 +/- 0.6 Ma (Fig. 2.23).

The age and orientations (parallel to sub-parallel to foliation and early faults) of the dikes at the Barry deposit are similar to those of widespread small- to medium-sized plutons of the Abitibi belt that are syn-tectonic and emplaced during the late phases of regional folding and faulting from 2700-2692 Ma (Chown et al., 2002).

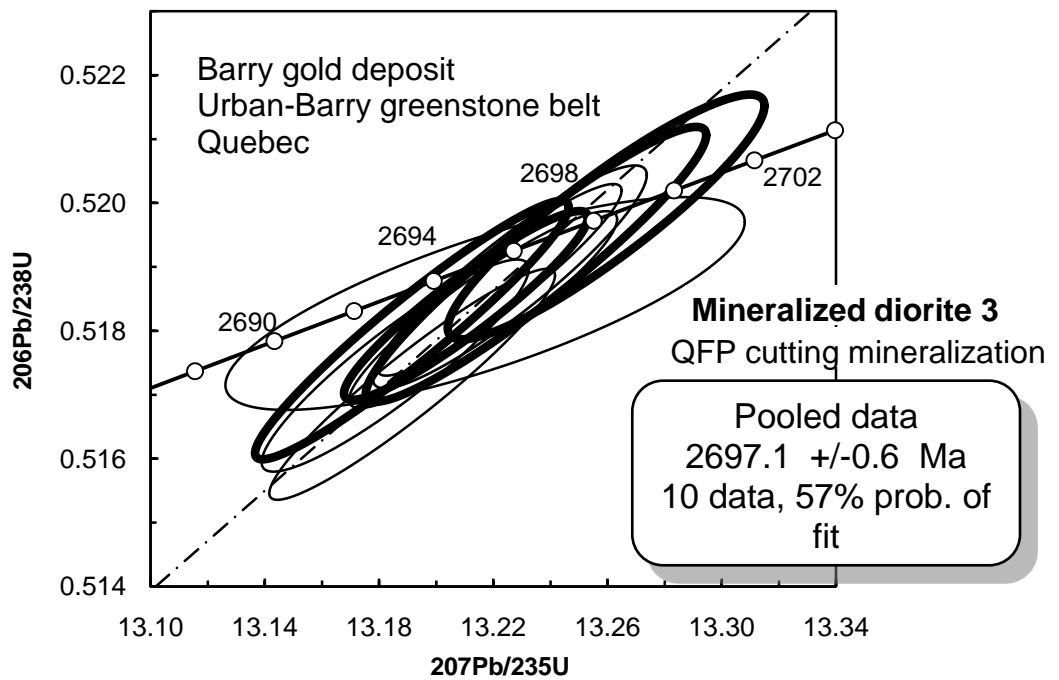


Fig. 2.23: Concordia diagram showing the TIMS U-Pb analyses of pooled primary data from zircon grains – Samples 58-1165 (two youngest data), 83-1038 (four data), and 59-1164 (diorite 3, four data, ellipses in bold). The regression line is forced through 0 Ma.

2.6 Discussion

2.6.1 Tectonic Evolution of the Barry Property and Timing of Gold Mineralization

The data obtained during this study of the Barry property allowed for the interpretation of the tectonic history, the age of gold mineralization, and the mechanisms of vein emplacement, as summarized below.

At the Barry deposit, the three distinct types of mafic volcanic flows (A, B, C), which are part of the ca. 2717 Ma-old Macho Formation (Fig. 2.2; Bandyayera et al., 2002), formed in a tectonic setting transitional from mid-ocean ridge to island arcs (Figs. 2.8 and 2.9). These volcanic rocks were accreted to form a portion of the Superior Province. The rocks were folded (D_1), foliated (D_2), faulted (D_2) (Fig. 2.15), and intruded at ca. 2697 Ma by arc-related, syn-deformational intermediate to felsic dikes (diorite dikes 1-3 and early QFP dikes; Fig. 2.24A). The dikes were emplaced preferentially sub-parallel to the main foliation trend ($N59^\circ E/58^\circ SE$), which is oriented parallel to the early faults that cut the volcanic rocks (Fig. 2.3 and 2.15B). Auriferous albite-carbonate-quartz veins formed pre-to syn- D_2 deformation and cut the volcanic rocks sub-parallel and oblique to foliation (Figs. 2.3, 2.15 C-D, and 2.16) and locally fill early faults (Fig. 2.24B). The carbonate-quartz-pyrite alteration (Figs. 2.3 and 2.16) associated with these veins mineralized the surrounding volcanic rocks and diorite dikes (Fig. 2.24B). Locally extensional quartz veins with free gold cut the pre-mineralization QFP dikes (Fig. 2.3) and auriferous albite-carbonate-quartz veins in the volcanic rocks. Ductile movement along the early faults/shear zones deformed the veins and dikes, causing veins in the $N20^\circ E/60^\circ SE$

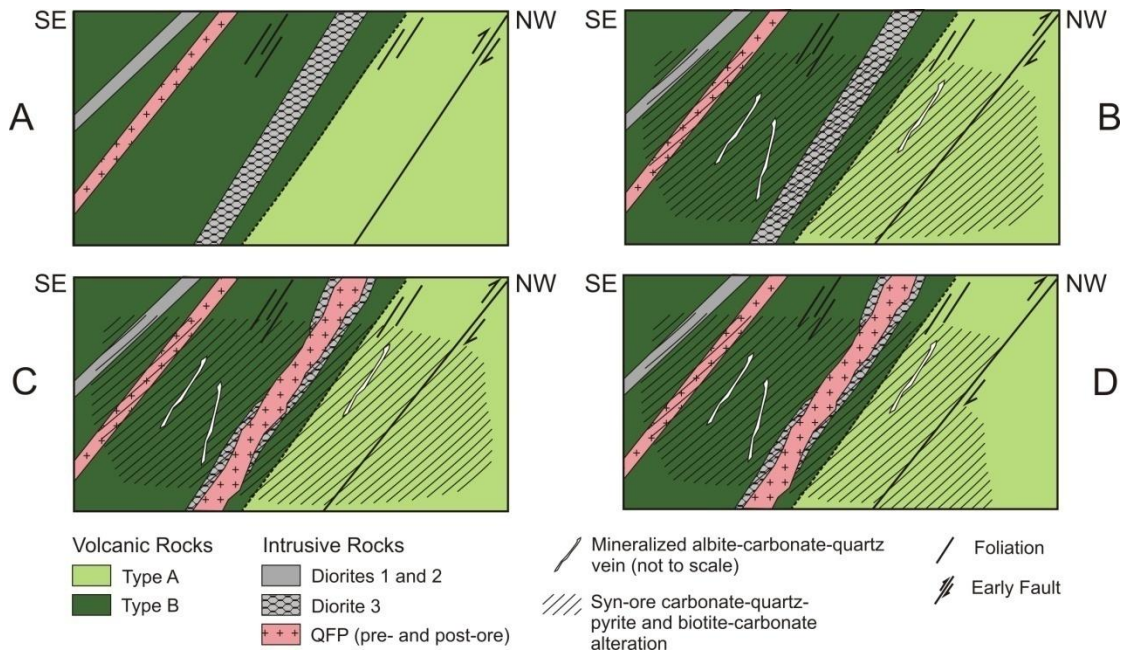


Fig. 2.24: Idealized NW-SE vertical cross section illustrating the evolution of the Barry deposit. A) Mafic volcanic rocks have formed and are cut by early NE-trending faults (D_2), are foliated (D_2), and are intruded by diorites 1 and 2 and early QFP dikes. B) Auriferous albite-carbonate-quartz veins cut the mafic volcanic rocks and the mafic volcanic rocks undergo syn-ore carbonate-quartz-pyrite and biotite-carbonate alteration. Gold is hosted in veins, in carbonate altered mafic volcanic rocks and diorite dikes, and locally in quartz veins cutting early QFP dikes. Ductile movement along the early faults deforms the veins and early intrusive rocks. C) Late QFP dikes intrude the mafic volcanic rocks and locally intrude the diorite 3 dikes. Continued ductile deformation along the early faults deforms dikes and veins. D) Brittle deformation along the early faults cut and offset mineralization in the north of the trenched zone.

orientation to fold, and the veins and dikes sub-parallel to foliation ($N59^\circ E/58^\circ SE$) to be elongated (pinch and swell or locally boudinaged, Fig. 2.24 and 2.25, discussed in detail below). Late arc-related, syn-collisional QFP dikes, also dated at ca. 2697 Ma, cut the mineralized volcanic rocks (Fig. 2.24C) and incorporated rare xenoliths of mineralized mafic volcanic rock (Fig. 2.11C). At the northern boundary of the property, late brittle movement along the early fault offset the mineralized volcanic rocks and QFP with an oblique reverse dextral sense of movement (Figs. 2.3 and 2.24D; Appendix C). Late brittle faults oriented at $N3^\circ W$ with moderate to steep dip ($66^\circ-90^\circ W$) and striking $N9^\circ W$ with moderate to steep dip ($70^\circ-90^\circ E$) cut the volcanic and intrusives offsetting rock

units and mineralization (Fig. 2.3 and 2.15). The faults dipping to the west have a sinistral sense of offset, while faults dipping to the east show dextral offset (Fig. 2.3).

The timing of gold mineralization at the Barry deposit is therefore well constrained by cross-cutting relationships between the various dikes and the gold-bearing veins and U-Pb zircon dating of pre-mineralization diorite 3 (containing free gold) and post-mineralization QFP dikes (containing xenoliths of mafic volcanic rock with pervasive gold-related carbonate-quartz-pyrite alteration). The ages of single grains from these two intrusions are concordant and overlapping, with indistinguishable ages of 2697.9 ± 1.4 – 1.5 for the pre-mineralization diorite 3, and 2696.7 ± 1.2 – 1.2 and 2697.7 ± 0.98 – 1.1 for the post-mineralization QFP dikes. Taking into consideration all overlapping ages (excluding those of inherited zircon) and their associated errors for the pre- and post-mineralization intrusions, the absolute age of the gold mineralization is attributed to be 2697.1 ± 0.6 Ma. To our knowledge, this is the most precise age yet available for Archean greenstone-belt hosted lode gold mineralization. It shows that gold mineralization at the Barry deposit is both spatially and temporally related to arc-type, intermediate to felsic intrusions, as well as pre- to syn- local deformation (D_2) and, according to Chown et al. (2002), is coeval with regional deformation.

2.6.2 Mechanisms of Emplacement and Deformation of Auriferous Veins and Dikes

According to the field relationships, vein mineralogy, and wall-rock alteration reported in this study, the straight ($N64^\circ E/64^\circ SE$) and folded ($N20^\circ E/60^\circ SE$) auriferous albite-quartz-carbonate veins are interpreted to be contemporaneous with ductile movement in the

early fault/shear zone. The evidence is (1) the concentration of albite-quartz-carbonate veins in the fault/shear zone, (2) the fact that the two vein sets cross-cut each other and have similar composition and wall-rock alteration, and (3) the indication of shortening (folding) and elongation (pinch and swell of both straight and folded veins and boudinage of straight veins) with directions of the veins that correspond to zones of shortening and elongation in the fault/shear zone (Fig. 2.25). The veins and mineralized host rocks were later cut and offset by the brittle oblique reverse dextral movement on the northernmost fault (Fig. 2.3). The formation of straight and folded veins coeval with the shear zone can be explained if the shear zone underwent oblique reverse dextral movement in both ductile and brittle stages, with veins forming in the ductile stage at oblique angles to one another. The 'straight' veins would have formed sub-parallel to the shear zone and foliation along the zone of weakness created by these structures, and the 'folded' veins possibly formed as extensional veins in the shear zone, roughly perpendicular to the zone of elongation (Fig. 2.25B). 'Folded' veins would have lain in the zone of shortening in the strain ellipse and became folded, while the 'straight veins' became elongated (Fig. 2.25B) with progressive deformation. As shearing continued, both vein sets would have rotated towards the orientation of the shear zone, with the folded veins rotating at a faster rate, and getting into the zone of elongation, causing them to pinch and swell (Figs. 2.16 and 2.25). The straight veins remained in the zone of elongation and further pinched and swelled and locally boudinaged. Isoclinal folding, rootless isoclinal folds, and transposition of straight 064/64 veins are explained in the above model if the veins formed sub-parallel to the shear zone and underwent minor deformation (folding) and then elongation as they rotated to become parallel with the shear zone (Fig. 2.25B). This

model also applies to the formation and deformation of the diorite and the majority of pre- and post-ore QFP dikes at the Barry deposit, as they are all roughly parallel to the shear zone and straight veins (diorite 1: N70°E/70°S; diorite 2: N60°E/70°SE; diorite 3 and QFP dikes: N55-60°E/80°SE), and have deformed in a similar manner as the straight veins. Evidence for this is seen in the pinch and swell of the diorite 3 and QFP dikes, and the local boudinage of the QFP dikes (Fig. 2.3). In the western portion of the trench, the QFP dike orientation is more irregular, which could be a result in the change of the strain axis due to the competent behaviour of the stock relative to the surrounding mafic volcanic rocks.

Although gold mineralization at the Barry deposit is coeval with both regional deformation and local magmatism, the source of the mineralizing fluids at the Barry deposit is unknown. Possible sources for the mineralizing fluids include: deep-seated fluids transported along the regional and local shear zones and fractures, or hydrothermal magmatic fluids from the felsic to intermediate intrusions. The fact that the ore zone has an antiformal shape within the mafic volcanic rocks, which is not controlled by the spatial distribution of the dikes (Fig. 2.4), suggests that the mineralizing fluids at the Barry deposit are not derived from the local intrusions and are most likely deep-seated. However, we cannot exclude the possibility that part of the fluids and metals have a deeper magmatic source that is cogenetic with the local dikes.

Mass balance results indicate that Au, Ag, Mo, W, Pb, Cu, and Bi were significantly added to the host-rocks exhibiting syn-ore alteration. These elements are also commonly

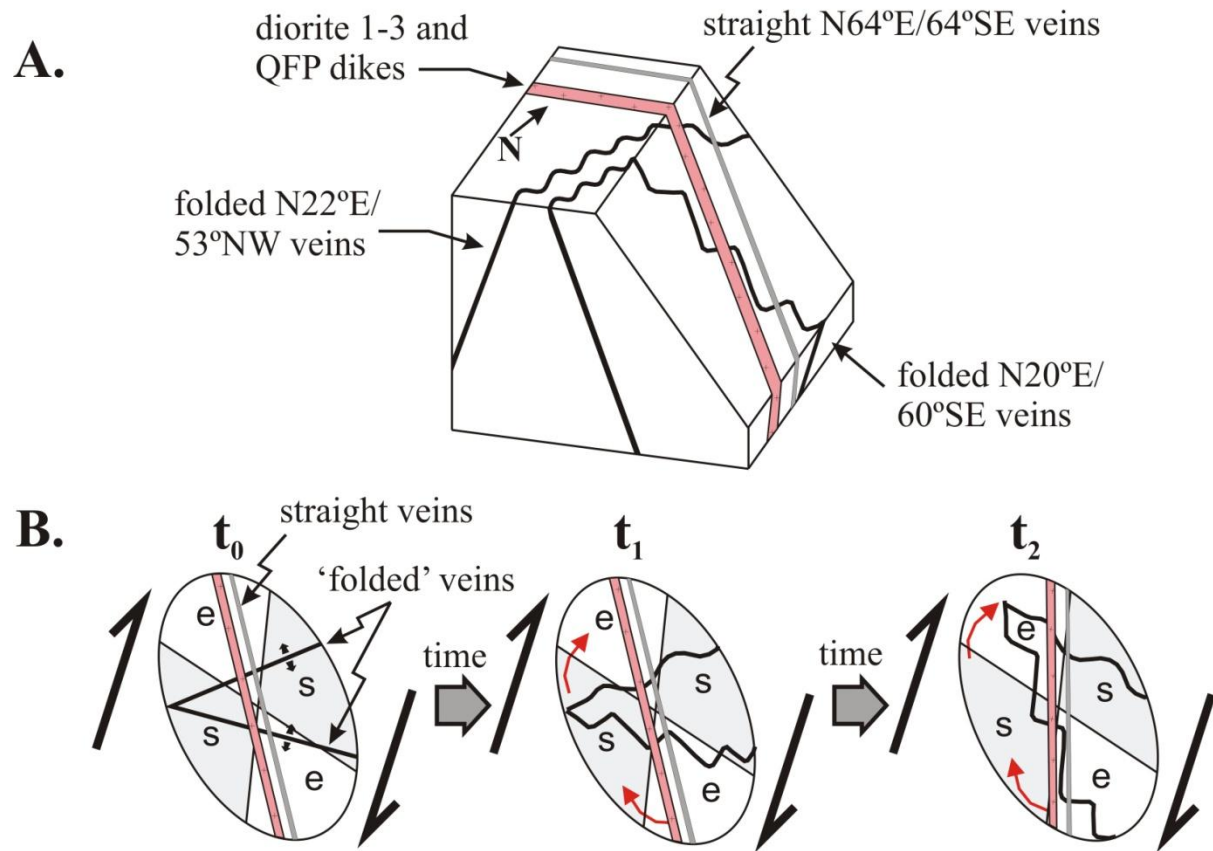


Fig. 2.25: Block diagram and shear sense diagram for the mineralized albite-quartz-carbonate veins and deformed diorite and QFP dikes at the Barry deposit. A) Block diagram showing the straight (N64°E/64°SE) and folded (N20°E/60°SE) albite-quartz-carbonate veins and dikes at the Barry deposit. Cut surface is perpendicular to shear zone and parallel to slickenline lineations on the northernmost fault in order to view the plane containing shear sense. B) View of cut plane from A with superimposed strain ellipse and oblique reverse dextral shear sense indicated. Black 'folded' veins form in the zone of shortening and 'straight' veins and dikes form in the zone of elongation (t_0). 'Folded' veins are folded in the zone of shortening (t_1), then become elongated (pinch and swell) as they rotate into the zone of elongation (t_2). Straight veins and dikes rotate a small amount toward the orientation of the shear zone (t_2) and become pinch and swell and boudinaged.

reported to be associated with “intrusion-related” gold deposits (Goldfarb et al., 2005), which suggests that there may have been magmatic input into the ore system.

2.6.3 Implications for Regional Metallogeny and Exploration

The characterization of the vein geometry, mineralogy and wall-rock alteration, and the determination of the absolute age of mineralization for the Barry deposit provide further evidence that some lode gold deposits formed during regional deformation of the northern Abitibi greenstone-belt at circa 2697 Ma. The Barry deposit has an age consistent with, and similar features to, those documented at the Kiena, Norlartic, and Siscoe (Main Zone) mines in the southern Abitibi (Pilote et al., 1993; Couture et al., 1994; Morasse et al., 1995; Olivo and William-Jones, 2002; Table 2.2). However, in contrast to the Barry deposit, where the majority of gold mineralization occurs within albite-carbonate-quartz veins and their surrounding carbonate-quartz-pyrite alteration in the mafic volcanic rocks, at the Kiena, Norlartic, and Siscoe deposits, gold is mainly hosted within felsic to intermediate dikes and stocks (Table 2.2). At Kiena, the majority of gold is hosted in an albitite dike swarm, with gold mineralization occurring within fine carbonate-quartz-albite stringer to stockwork veinlets with disseminated pyrite ± pyrrhotite, and gold (Morasse et al., 1995; Table 2.2). The remainder of the gold is hosted by iron tholeiites and basaltic komatiites along the margins of, or between, the albitite dikes, and locally these dikes are cut by high-grade mineralization (Morasse et al., 1995). The close spatial association and crosscutting relationship between gold mineralization and albitite dikes led Morasse et al. (1995) to propose that gold mineralization at Kiena is intrusion-related. There, the mineralized dikes are cut by later granodiorite and feldspar

Table 2.2: Summary of geologic characteristics of pre-2690 Ma deposits: Barry, Kiena, Norlartic, and Siscoe (main zone)

	Size (Au)	Summary Description	Host Rocks	Structure	Metamorphic Grade	Age Constraints	Alteration	Composition of ore	References
Barry deposit	5.07 t	Albite-carbonate-quartz veins and their surrounding carbonate-quartz-pyrite alteration of the host rocks	Mafic volcanic rocks, diorite dikes, and quartz veins in early QFP dikes	Coeval folded (N20°E/60° E and W) and straight (N64°E/64°SE) veins. Veins and alteration form an antiformal/ domal shape	Greenschist	Gold mineralization constrained at 2697.1 ±0.6 Ma	Syn-ore carbonate-quartz-pyrite +/- pyrrhotite and chalcopyrite Pre/post ore biotite-chlorite and post-ore epidote	Gold associated with pyrite in veins and altered host rock	
Kiena	minimum 52 t	'Intrusion-related' carbonate-quartz-albite stringer to stockwork veinlets	Albitite dike swarm and iron tholeiites and basaltic komatiites along the margins of, or in between, albitite dikes	Stockwork veins and alteration are mainly confined to or centered on the albitite dikes	Greenschist	Mineralization is ≥2686 Ma. (cut by granodiorite and feldspar porphyry dikes dated at 2686 ± 2 Ma)	Early pervasive albite and late stage sericite, biotite, magnetite, and chlorite	Gold associated with disseminated pyrite ± pyrrhotite	Morasse et al., 1995
Norlartic	6.3 t	Stockwork quartz-carbonate-pyrite-gold stringers, veinlets, and disseminated pyrite	5-15m wide microdiorite dike	Veins and alteration mainly confined within the microdiorite dike	Greenschist	≥ 2692± 2 Ma	Strongly chloritized, carbonatized, and albitized	Gold associated with carbonate-pyrite-gold stringers, veinlets, and disseminated pyrite	Couture et al., 1994; Morasse, 1998
Siscoe (main zone)	27 t (for all of deposit)	Gold-quartz veins hosted by the Siscoe stock	Gabbroic intrusion	Folded extensional veins striking N35°E and dipping 60°-70°SE-E	Greenschist	>2690 Ma	Extensive carbonitization, pyrite and minor muscovite and chlorite	Au, Ag associated with pyrite± chalcopyrite± pyrrhotite±sphalerite± galena	Couture et al., 1994; Morasse et al., 1995; Morasse, 1998; Olivo and Hughes, 2004

porphyry dikes dated at 2686 ± 2 Ma, indicating that gold mineralization at Kiena is older than 2686 Ma (Morasse et al., 1995). Alteration at Kiena dominantly consists of a pervasive albite (early and intermediate stages), and late stage sericite, biotite, magnetite, and chlorite, both of which are centred around the abite dike swarms (Morasse, 1998), further supporting the genetic link between mineralization and intrusions. Although the Barry deposit has similar mineral assemblages as Kiena, the albite wall-rock alteration is not as pervasive as that documented at Kiena, and magnetite formed prior to mineralization.

At Norlartic, the main mineralized zone consists of stockwork quartz-carbonate-pyrite-gold stringers and veinlets, and disseminated pyrite along fractures within a 5-15m wide microdiorite dike (Couture et al., 1994; Table 2.2). Near the ore zone, the host rocks are strongly chloritized, carbonatized, and albitized, which is similar to the alteration seen at the Barry deposit, although at the Barry deposit chlorite alteration of the mafic volcanic rocks is both pre- and post-mineralization (Fig. 2.7).

The main zone of the Siscoe deposit is hosted in a dioritic stock, and mineralization is found in older quartz-carbonate veins that are cut by younger tourmaline veins and by mafic and felsic dikes (Tessier et al., 1990; Sauvé et al., 1993; Morasse, 1998; Olivo and Hughes, 2004; Olivo and William-Jones, 2002). Trudel (1985), Sauvé et al. (1993), and Morasse (1998) suggest that the albitite and diorite dikes are coeval with gold mineralization based on descriptions of mutual crosscutting relationships between the dikes and the main ore zone by Backman (1936), Moss (1939), and Auger (1947). The

early quartz-carbonate veins in the Main zone occur as folded extensional veins striking N35°E to NS and dipping 60°-70° SE-E, and comprise minor amounts of chlorite, albite, pyrite, chalcopyrite, pyrrhotite and gold (Olivo and Hughes, 2004). The wall-rock alteration is characterized by extensive distal and proximal carbonatization, with pyrite abundance increasing in the proximal zone (up to 10%), where minor muscovite and chlorite are locally found (Olivo and Hughes, 2004; Table 2.2).

Although the Barry deposit has some distinct characteristics when compared with the deposits in the southern Abitibi that formed pre-2686 Ma and are coeval with magmatism, overall they share many common features and may have formed by similar processes. Further research on these deposits is required in order to evaluate the possibility of the auriferous mineralization being formed mainly by fluid derived from the coeval intrusive rocks.

This type of deposit has been overlooked when exploring in the eastern part of the Southern Abitibi belt, where late quartz-tourmaline veins (similar to the Sigma-Lamaque system) have been the main exploration target. Based on the results obtained here, and the fact that gold mineralization at the Barry deposit is similar and contemporaneous with the Kiena, Malartic and Siscoe (Main Zone) mines, we suggest that the early albite-carbonate-quartz sheeted veins and/or stringer and stockwork zones associated with shear zones (pre- to syn-deformation of the shear zones) and syn-tectonic diorite and quartz-feldspar porphyry should be included in exploration models for the region. In addition to Au, Ag, Mo, W, Pb, Cu, and Bi are suggested as pathfinder elements associated with this

type of system as they are significantly enriched in the wall-rock alteration zones proximal to, and containing, auriferous mineralization.

2.7 Conclusion

The Barry deposit has many similarities to other Archean lode gold deposits in the southern Abitibi subprovince, including vein mineralogy, wall rock alteration, host rock, and association with shear zones. Gold mineralization is hosted in rocks that formed in a tectonic setting transitional from mid-ocean ridge to island-arc and are intruded by diorite, QFP, and quartz monzonite dikes and stocks interpreted to be volcanic arc to syn-collisional. The mineralized zone is associated with NE-trending and southeasterly dipping brittle-ductile shear zones that localized gold mineralization and deformed intrusive rocks and mineralized veins at the Barry deposit. Gold is hosted within albite-carbonate-quartz veins and the surrounding carbonate-quartz-pyrite and biotite-carbonate alteration of the mafic volcanic rocks.

The timing of mineralization at the Barry deposit is interpreted to be 2697 +/- 1 Ma, well constrained by U-Pb zircon dating of pre-mineralization diorite and post-mineralization QFP dikes. This age shows that gold mineralization formed pre- to syn deformation (foliation and faulting), as well as coeval with arc-related, syn-collisional intermediate to felsic magmatism. This finding confirms that in the northern Abitibi belt some gold mineralization occurred during a pre-2686, deformational period in the late Archean, and

is, to our knowledge, the most precise age yet established for Archean lode gold mineralization.

References

- Auger, P.E., 1947, Région de la mine Siscoe, Cantons de Dubuisson et de Vassan, Comté d'Abitibi-Est, Ministère des Mines, Province de Québec, Rapport géologique 17, 45 p.
- Backman, O.L., 1936, Geology of the Siscoe gold mine: Canadian Mining Journal, v. 57, p. 467-475.
- Bandyayera, D., Daigneault, R., and Sharma, K., 2003, Géologie de la région du lac de la Ligne (32F/01): Ministère des Ressources Naturelles, de la Faune et des Parcs, Québec, RG 2004-02, 31 p., 4 maps.
- Bandyayera, D., Rhéaume, P., Cadéron, S., Giguère, E., and Sharma, K., 2004b, Géologie de la région du Lac Lagacé (32B/14): Ministère des Ressources Naturelles, de la Faune et des Parcs, Québec, RG 2004-02, 32 p., 4 maps.
- Bandyayera, D., Rhéaume, P., Doyon, J., and Sharma, K., 2004a, Géologie de la région du lac Hébert (32G/03): Ministère des Ressources Naturelles, de la Faune et des Parcs, Québec, RG 2003-07, 57 p., 4 maps.
- Bandyayera, D., Théberge, L., and Fallara, F., 2002, Géologie de la région des lacs Piquet et Mesplet (32G/04 et 32B/13): Ministère des Ressources Naturelles, Québec, RG 2001-14, 56 p., 8 maps.
- Barrett, T.J., and MacLean, W.H., 1997, Volcanic sequences, lithochemistry and hydrothermal alteration in some bimodal volcanic-associated massive sulphide systems, Reviews in Economic Geology, v. 8, p. 101-131.
- Card, K.D., 1990, A review of the Superior Province of the Canadian Shield, a product of Archean accretion: Precambrian Research, v. 48, p. 99-156.
- Chown, E.H., Daigneault, R., Mueller, W., and Mortensen, J.K., 1992, Tectonic evolution of the Northern Volcanic Zone, Abitibi belt, Québec: Canadian Journal of Earth Sciences, v. 29, p. 2211-2225.
- Chown, E.H., Harrap, R., and Moukhsil, Abdelali, 2002, The role of granitic intrusions in the evolution of the Abitibi belt, Canada: Precambrian Research, v. 115, p. 291-310.
- Claoué-Long, J.C., King, R.W., and Kerrich, R., 1990, Archean hydrothermal zircon in the Abitibi greenstone belt: constraints on the timing of gold mineralization: Earth and Planetary Science Letters, v. 98, p. 109-128.
- Corfu, F., and Davis, D.W., 1991, Comment on "Archean hydrothermal zircon in the Abitibi greenstone belt: constraints on the timing of gold mineralization" by J.C.

- Claoué-Long, R.W. King, and R. Kerrich: *Earth and Planetary Science Letters*, v. 104, p. 545-552.
- Couture, J.-F., Pilote, P., Machado, N., and Desrocher, J.-P., 1994, Timing of gold mineralization in the Val d'Or district, southern Abitibi belt: Evidence for two distinct mineralizing events: *Economic Geology*, v. 89, p. 1542-1551.
- Davis, G.H., 1984, *Structural geology of rocks and regions*: New York, John Wiley and Sons, Inc., p. 91-96, 268-269.
- Dubé, B. and Gosselin, P., 2007, Greenstone-hosted quart-carbonate vein deposits, *in* Goodfellow, W.D., ed., *Mineral Deposits of Canada: A synthesis of major deposit-types, district metallogeny, the evolution of geological provinces, and exploration methods*: Geological Association of Canada, Mineral Deposits Division, Special Publication No. 5, p. 49-73.
- Fallara, F., Rhéaume, P., Cheng, L. Z., Boudrias, G., Bandyayera, D., 2004, Modèle 3D géo-intégré du secteur du Lac aux Loutres, synthèse métallogénique d'Urban-Barry (phase 1 de 2): Ministère des Ressources Naturelles, de la Faune et des Parcs, Québec, RP 2004-06, 12 p.
- Goldfarb, R.J., Baker, T., Dubé, B., Groves, D.I., Hart, C.J.R., and Gosselin, P., 2005, Distribution, character, and genesis of gold deposits in metamorphic terranes: *Economic Geology 100th Anniversary Volume*, p. 407-450.
- Goldfarb, R.J., Groves, D.I., and Gardoll, S., 2001, Orogenic gold and geologic time: A global synthesis: *Ore Geology Reviews*, v. 18, p. 1-75.
- Grant, J.A., 1986, The isocon diagram – a simple solution to Gresen's equation for metasomatic alteration: *Economic Geology*, v. 81, p. 1976-1982.
- Grant, J.A., 2005, Isocon analysis: A brief review of the method and applications: *Physics and Chemistry of the Earth*, v. 30, p. 997-1004.
- Groves, D.I., Goldfarb, R.J., Gebre-Mariam, M., Hagemann, S.G., and Robert, F., 1998, Orogenic gold deposits: A proposed classification in the context of their crustal distribution and relationship to other gold deposit types: *Ore Geology Reviews*, v. 13, p. 7-27.
- Groves, D.I., Goldfarb, R.J., Robert, F., and Hart, C.J.R., 2003, Gold deposits in metamorphic belts: Overview of current understanding, outstanding problems, future research, and exploration significance: *Economic Geology*, v. 98, p. 1-29.
- Hagemann, S.G., and Cassidy, K.F., 2000, Archean orogenic lode gold deposits: *SEG Reviews*, v. 13, p. 9-68.

- Hocq, M., 1989, Carte Lithotectonique des sous-provinces de l'Abitibi et du Pontiac, 1:500,000: Ministère de l'Énergie et des Ressources (Mines), Gouvernement du Québec, DV 89-04.
- Hodgson, C.J., and MacGeehan, P.J., 1982, Geologic characteristics of old deposits in the Superior Province of the Canadian Shield: *In Geology of Canadian Gold Deposits, Edited by R.W. Hodder and W. Petruk, Canadian Institute of Mining and Metallurgy, Special Volume 24, p. 211-229.*
- Hodgson, C.J., and Troop, D.G., 1988, A new computer-aided methodology for area selection in gold exploration: A case study from the Abitibi greenstone belt: *Economic Geology, v. 83, p. 952-977.*
- Jaffey, A.H., Flynn, K.F., Glendenin, L.E., Bentley, W.C. and Essling, A.M. 1971. Precision measurement of half-lives and specific activities of ²³⁵U and ²³⁸U. *Physical Review* 4: 1889-1906.
- Jemielita, R.A., Davis, D.W., Krogh, T.E., 1990, U-Pb evidence for Abitibi gold mineralization postdating greenstone magmatism and metamorphism: *Nature, v. 345, p. 831-834.*
- Jenkins, C.L., Vincent, R., Robert, F., Poulsen, K.H., Garson, D.F., and Blondé, J.A., 1997, Index-level database for lode gold deposits of the world: Geological Survey of Canada Open File 3490, 18 p. (with map and CD).
- Joly, M., 1990, Géologie de la région du lac aux Loutres et du lac Lacroix: Ministère de l'Énergie et des Ressources, Gouvernement du Québec, MB 90-42, 55 p.
- Kerrich, R., and Cassidy, K.F., 1994, Temporal relationships of lode gold mineralization to accretion, magmatism, metamorphism, and deformation – Archean to present: A review: *Ore Geology Reviews, v. 9, p. 263-310.*
- Kerrich, R., and King, R., 1993, Characteristics of hydrothermal zircon and baddeleyite in Val d'Or mesothermal gold deposits: Age of primary gold mineralization (ca. 2680 Ma) versus secondary fluid resetting events (2630-2579 Ma) [abs.]: *Geological Association of Canada Program with Abstracts, v. 346, p. A-52.*
- Kerrich, R., and Ludden, J., 2000, The role of fluids during formation and evolution of the southern Superior Province lithosphere: an overview: *Canadian Journal of Earth Sciences, v. 37, p. 135-164.*
- Krogh, T.E., 1982, Improved accuracy of U-Pb zircon ages by the creation of more confident systems using an air abrasion technique: *Geochimica et Cosmochimica Acta, v. 46, p. 637-649.*

- Ludwig, K.R., 2003, User's manual for Isoplot 3.00 a geochronological toolkit for Excel: Berkeley Geochronological Center Special Publication 4, 71 p.
- Matthews, W., Davis, W.J., 1999. A practical image analysis technique for estimating the weight of abraded mineral fractions used in U–Pb dating: Radiogenic Age and Isotopic Studies, Geological Survey of Canada, Current Research 1999-F, Report 12, p. 1–7.
- Mattinson, J.M., 2005, Zircon U–Pb chemical abrasion (CA-TIMS) method: Combined annealing and multi-step partial dissolution analysis for improved precision and accuracy of zircon ages: *Chemical Geology*, v. 220, p. 47-66.
- McDonough, W.F., and Sun, S.-s., 1995, The Composition of the Earth: *Chemical Geology*, v.120, p. 223-253.
- Milner, R., L., 1939, Barry Lake area, Abitibi County and Abitibi Territory: Department of Mines, Québec, RP 143, 9 p.
- Milner, R.L., 1943, Barry Lake area, Abitibi County and Abitibi Territory: Department of Mines, Québec, RG 014, 28 p.
- Morasse, S., 1998, Geology, structure, and timing of gold mineralization at the Kienna deposit, Val d'Or, Québec: Unpublished Ph.D. thesis, Ontario, Canada, Queen's University, 362 p.
- Morasse, S., Wasteneys, H.A., Cormier, M., Helmstaedt, H., and Mason, R., 1995, A pre-2686 Ma intrusion-related gold deposit at the Kienna mine, Val d'Or, Québec, southern Abitibi subprovince: *Economic Geology*, v. 90, p. 1310-1321.
- Moss, A. E., 1939, The geology of the Siscoe gold mine, province of Quebec: Unpublished Ph.D. thesis, Quebec, Canada, McGill University, 159 p.
- MRN, 2002, Geological map of Québec, Edition 2002, 1:2,000,000: Ministère des Ressources Naturelles, DV 2002-07.
- Olivo, G.R. and Hughes, K.A., 2004, The two distinct types of auriferous veins in the Val d'Or district, Southern Abitibi, Canada: structural, alteration, mineralogical and fluid constraints [abs.]: 32th International Geological Congress, Florence, August 20-28, 2004, Conference Abstract cd-rom.
- Olivo, G.R., Chang, F., and Kyser, T.K., 2006, Formation of the auriferous and barren north dipper veins in the Sigma mine, Val d'Or, Canada: Constraints from structural, mineralogical, fluid inclusion, and isotopic data: *Economic Geology*, v. 101, p. 607-631.

- Olivo, G.R., Isnard, H., William-Jones, A.E., and Gariépy, C., 2007, Pb isotope compositions of pyrite from the C quartz-tourmaline vein of the Siscoe gold deposit, Val d'Or, Quebec: Constraints on the origin and age of the gold mineralization: *Economic Geology*, v. 102, p. 137-146.
- Olivo, G.R., and William-Jones, A.E., 2002, Genesis of the auriferous C quartz-tourmaline vein of the Siscoe mine, Val d'Or district, Abitibi subprovince, Canada: Structural, mineralogical and fluid inclusion constraints: *Economic Geology*, v. 97, p. 929-947.
- Pearce, J.A., 1982, Trace element characteristics of lavas from destructive plate boundaries: Thorpe, R.S. (ed), *Andesites*, Wiley, Chichester, p. 525-548.
- Pearce, J.A., and Cann, J.R., 1973, Tectonic setting of basic volcanic rocks determined using trace element analysis: *Earth Planet. Sci. Lett.*, v. 19, p. 290-300.
- Pearce, J.A., Harris, N.B.W., and Tindle, A.G., 1984, Trace element discrimination diagrams for the tectonic interpretation of granitic rocks: *Journal of Petrology*, v. 25, p. 956-983.
- Pearce, J.A., Peate, D.W., 1995. Tectonic implications of the composition of volcanic arc magmas: *Annu. Rev. Earth Planet. Sci.*, v. 23, p. 251–285.
- Pilote, P., Couture, J.-F., Desrochers, J.-P., Machado, N., and Peltz, P., 1993, Minéralisations aurifères multiphasées dans la région de Val d'Or: l'exemple de la mine Norlartic, *in* L'exceptionnel potentiel minéral du Québec, une réalité à découvrir: Résumé des conférences, séminaire d'information 1993: Ministère de l'Énergie et des Ressources du Québec, DV 93-03, p. 61-66.
- Rhéaume, P. and Bandyayera, D., 2006, Révision stratigraphique de la Ceinture d'Urban-Barry: Ministère des Ressources naturelles et de la Faune, Québec, RP 2006-08, 11p.
- Rhéaume, P., Bandyayera, D., Fallara, F., Boudrias, G., and Cheng, L.Z., 2004, Géologie et métallogénie du secteur du lac aux Loutres, synthèse métallogénique d'Urban-Barry (phase 1 de 2): Ministère de Ressources naturelles et de la Faune et des Parcs, Québec, RP 2004-05, 10 p.
- Robert, F., 1990, An Overview of gold deposits in the eastern Abitibi subprovince: *The Canadian Institute of Mining and Metallurgy Special Volume 43*, p. 93-105.
- Robert, F., and Poulsen, K.H., 1997, World-class Archaean gold deposits in Canada: and overview: *Australian Journal of Earth Sciences*, v. 44, p. 329-351.

- Robert, F., Poulsen, K.H., Cassidy, K.F., and Hodgson, J., 2005, Gold metallogeny of the Superior and Yilgarn Cratons: Economic Geology 100th Anniversary Volume, p. 1001-1033.
- Sauvé, P., Imreh, L., and Trudel, P., 1993, Description des gîtes d'or de la région de Val d'Or: Ministère de l'Énergie et des Ressources, Québec, MM 91-03, 178 p.
- Systèmes Géostat International Inc., 2007, NI 43-101 Technical Report of the Preliminary Assessment on Barry-1 and Bachelor Properties of Metanor Resources Inc.: SEDAR <www.sedar.ca>, date of filing: Oct. 16, 2007, 370 p.
- Tessier, A., Trudel, P., and Imreh, L., 1990, Petrology and alteration of the Siscoe stock at the Siscoe gold mine, Val d'Or, Quebec, *in* Rive, M., Verpaelst, P., Gagnon, Y., Lulin, J.-M., Riverin, G., and Simard, A., eds., The Northwestern Quebec Polymetallic Belt: a summary of 60 years of mining exploration: Rouyn-Noranda, Canadian Institute of Mining and Metallurgy Special Volume 43, p. 285-298.
- Trudel, P., 1985, Géologie de la mine Siscoe, Val d'Or, Québec, Ministère de l'Énergie et des Ressources du Québec, MB 85-16, 33 p.
- Wilson, Marjorie, 1989, Igneous Petrogenesis: London, United Kingdom, Unwin Hyman, 466 p.
- Wong, L., Davis, D.W., Krogh, T.E., and Robert, F., 1991, U-Pb zircon and rutile chronology of Archean greenstone formation and gold mineralization in the Val d'Or region, Québec: Earth and Planetary Science Letters, v. 104, p. 325-336.

Chapter 3

Discussion

The evolution of the Barry deposit, including the petrogenesis of the host rocks, the deformation, the age of intermediate to felsic magmatism, timing of gold mineralization, and mechanisms of vein emplacement and deformation, was well constrained during this study, as presented in Chapter 2 and summarized in section 2.6.1 and in Figure 2.24.

However, there are still some relevant questions that were not fully addressed in the scope of this study. They include:

- (1) the composition and origin of the mineralizing hydrothermal fluids, source of metals, and the mechanisms of metal transport and deposition; and
- (2) the metamorphic events and their relationship with gold mineralization and magmatism

3.1 Characteristics and Origin of Mineralizing Hydrothermal Fluids and Source of Metals

Although gold mineralization at the Barry deposit is coeval with both regional deformation and local magmatism, the source of the mineralizing fluids at the Barry deposit is unknown. Several sources of fluids are possible, including: (1) deep-seated (metamorphic? magmatic?) fluids transported along the regional and local shear zones and fractures; or (2) hydrothermal magmatic fluids from the intermediate to felsic

intrusions. The mineralized zone at the Barry deposit has an antiformal shape (possibly controlled by the D₁ folding event in the mafic volcanics) and is not controlled by the spatial distribution of the dikes (Fig. 2.4). It is therefore unlikely that the mineralizing fluids at the Barry deposit were derived mainly from the local intrusions. This means that the fluids were most likely derived from a deep-seated source.

The syn-ore carbonate-quartz-pyrite alteration assemblage in the mafic volcanic rocks at the Barry deposit is similar to other well-studied lode gold deposits, and specifically greenstone-hosted quartz-carbonate vein deposits, in Archean greenstone belts. This suggests that the ore-forming fluids at the Barry deposit may have been similar in composition to the low salinity, aqueous-carbonic fluids that formed those lode gold deposits (Hagemann and Cassidy, 2000; Ridley and Diamond, 2000).

However, we cannot exclude the possibility that part of the fluids and metals have a deeper magmatic source cogenetic with the local intrusive dikes. The mass balance results for the syn-ore carbonate-quartz-pyrite and biotite-carbonate altered mafic volcanic rocks at the Barry deposit indicate that Au, Ag, Mo, W, Pb, Cu, and Bi were significantly added to the host-rocks exhibiting syn-ore alteration. Goldfarb et al. (2005) propose that these elements are commonly associated with “intrusion-related” gold deposits, which suggests that there was some magmatic input into the ore system.

In order to address this question we suggest the following for future work:

1. A fluid inclusion study looking at inclusions in the least deformed mineralized veins in order to determine the composition of fluids and the temperature/pressure of fluid trapping.
2. A stable isotope investigation involving:
 - a. the measurement of $\delta^{18}\text{O}$ and δD of syn-ore minerals such as biotite and chlorite in order to determine the conditions under which gold precipitated and constrain the reservoir for H_2O .
 - b. the determination of the C isotopic composition of syn-ore carbonate alteration to determine the possible sources for CO_2 .
 - c. the determination of the O isotopic composition of syn-ore quartz and carbonate veins and alteration in order to estimate the thermal composition during vein formation and gold mineralization.
 - d. the determination of the Pb isotopic composition of pyrite, carbonate, and other phases coeval with gold mineralization in order to determine the source(s) for Pb (and possibly the sources for gold and other metals).
 - e. the determination of the S isotopic composition in the sulfides associated with mineralization (i.e. pyrite, chalcopyrite, and pyrrhotite) in order to determine the possible sources for S. In combination with C

isotopic composition, S isotope determination can be used to establish the pH and oxygen fugacity of the ore-bearing fluid.

The determination of the composition of the fluids and the sources of fluids and metals associated with the mineralizing event would enable us to provide further insights to understand the genesis of Archean greenstone belt gold mineralization and better understand the conditions of metal transport and deposition in this system.

3.2 Temporal Relationship between Gold Mineralization and Metamorphism

The temporal relationship between gold mineralization and metamorphism at the Barry deposit is currently unknown. The regional metamorphic grade is greenschist (Joly, 1990; Bandyayera et al., 2002), however, the age of metamorphism in the Urban-Barry greenstone belt, and within the Abitibi greenstone belt as a whole, is not very well constrained (Robert et al., 2005). For example, in the Timmins-Val d'Or gold belt of the southern Abitibi subprovince metamorphism is thought to span about 40 Ma, with contact metamorphism occurring from ~2690-2670 Ma, and dynamothermal metamorphism occurring from ~2670-2650 (Kerrick and Cassidy, 1994; Robert et al., 2005; Fig. 1.5). In the central portion of the Abitibi greenstone belt, in particular the Urban-Barry belt, very little is known about the timing of metamorphism as less mapping and research have been conducted in the area.

The petrography and paragenesis of mafic volcanic rocks at the Barry deposit indicate that there are albite and chlorite present in the pre-ore alteration assemblage, whereas chlorite and epidote are present in the post-mineralization alteration assemblage. Garnet is locally observed at the Barry deposit and is associated with epidote in the post-mineralization assemblage at depths greater than 30m. This mineral assemblage is reported to be stable at temperatures greater than 400°C and pressures of 1-4 kbar (Liou, 1971) and is the highest temperature assemblage at the Barry deposit. This mineral assemblage needs to be investigated in order to determine if it is associated with dynamothermal metamorphism or local contact metamorphism. If this assemblage was formed in the deepest areas in the deposit during regional dynamothermal metamorphism, then the gold mineralization pre-dates peak metamorphic conditions. However, if this assemblage represents contact metamorphism with dikes, the relationship between peak-metamorphism and mineralization is still to be determined.

In order to better constrain the relationship between magmatism/metamorphism and gold mineralization at the Barry deposit, we suggest the following for future work:

1. Regional mapping of metamorphic isograds (outside of the mineralized zone) to determine the relationship between metamorphism, deformation, and intrusions.
 - a. dating of minerals suitable for robust geochronological studies that may have formed during metamorphism (i.e. monazite)

- b. detailed study, including petrology and U-Pb dating, of the various generations of intrusive rocks, and investigation of their relationships with regional metamorphism and deformation
- 2. Integration of the findings of the regional studies (1) with the tectonic evolution of the Barry deposit and the age of mineralization established in our investigation.

References

- Bandyayera, D., Théberge, L., and Fallara, F., 2002, Géologie de la région des lacs Piquet et Mesplet (32G/04 et 32B/13): Ministère des Ressources Naturelles, Québec, RG 2001-14, 56 p., 8 maps.
- Goldfarb, R.J., Baker, T., Dubé, B., Groves, D.I., Hart, C.J.R., and Gosselin, P., 2005, Distribution, character, and genesis of gold deposits in metamorphic terranes: Economic Geology 100th Anniversary Volume, p. 407-450.
- Hagemann, S.G., and Cassidy, K.F., 2000, Archean orogenic lode gold deposits: SEG Reviews, v. 13, p. 9-68.
- Joly, M., 1990, Géologie de la région du lac aux Loutres et du lac Lacroix: Ministère de l'Énergie et des Ressources, Gouvernement du Québec, MB 90-42, 55 p.
- Kerrich, R., and Cassidy, K.F., 1994, Temporal relationships of lode gold mineralization to accretion, magmatism, metamorphism, and deformation – Archean to present: A review: Ore Geology Reviews, v. 9, p. 263-310.
- Liou, J.G., 1971, Synthesis and stability relations of prehnite, $\text{Ca}_2\text{Al}_2\text{Si}_3\text{O}_{10}(\text{OH})_2$. American Mineralogist, v. 56, p. 507-531.
- Ridley, J.R., and Diamond, L.W., 2000, Fluid chemistry of orogenic lode gold deposits and implications for genetic models: SEG Reviews, v. 13, p. 141-162.
- Robert, F., Poulsen, K.H., Cassidy, K.F., and Hodgson, J., 2005, Gold metallogeny of the Superior and Yilgarn Cratons: Economic Geology 100th Anniversary Volume, p. 1001-1033.

Chapter 4

Conclusion

4.1 Conclusion

The evolution of the Barry deposit, based on existing data and data obtained in this study, can be summarized as follows (see also Fig. 2.24):

ca. 2717 Ma

→ extrusion of the mafic volcanic rocks of the Macho Formation, which have a geochemical signature similar to basalts formed in a tectonic setting transitional from mid-ocean ridge (Type A) to island arc (Types B and C).

? → folding of the mafic volcanics (D₁)

ca. 2697 Ma (Fig. 2.24 A-C)

→ ductile deformation along early shear zones (D₂)

→ development of foliation in the mafic volcanic rocks (D₂)

→ intrusion of pre-ore diorites and QFP in the mafic volcanic rocks

→ **formation of gold mineralization**

- albite-carbonate-quartz veins
- carbonate-quartz-pyrite alteration of mafic volcanic rocks and pre-ore dikes, and locally biotite-carbonate alteration

→ intrusion of late QFP in the mafic volcanic rocks and mineralized zone

→ ductile deformation along early faults leading to folding and pinch and swell in N20°E veins and pinch and swell and local boudinage of ~N60°E veins and dikes

Post 2697 Ma (Fig. 2.24D)

→ brittle oblique reverse dextral deformation of early faults along the northern boundary of the deposit, offsetting the mineralized zone

→ brittle deformation of late faults

This study on the Barry gold deposit provides further evidence of an ‘early’, pre-2686 Ma, gold mineralizing event in the Abitibi greenstone belt. This mineralizing event is coeval with intermediate to felsic magmatism and a regional D₂-deformation in the northern Abitibi, and is prior to the main D₂ deformation event of the southern Abitibi (Fig. 1.5) that is associated with the many quartz-carbonate-(tourmaline) vein-type gold deposits (i.e. Sigma-Lamaque).

4.2 Implications for Exploration

This type of deposit is often overlooked when exploring in the eastern part of the Southern Abitibi belt, where late quartz-tourmaline veins (similar to the Sigma-Lamaque system) have been the main exploration target. Based on the results obtained here, and the fact that Barry deposit gold mineralization is similar and contemporaneous with the

Kiena, Malartic and Siscoe (Main Zone) mines, it is suggested that the ‘older’, pre-2686 Ma, albite-carbonate-quartz sheeted veins and/or stringer and stockwork zones associated with syn-tectonic diorite and quartz-feldspar porphyry should be included in the exploration model for the region.

Based on the findings of this research, and the previous work in “early” greenstone gold deposits summarized in this thesis, the following features are proposed to be relevant for exploration of gold that formed during the pre-2686 deformation of the Abitibi Archean greenstone belt:

- first order structures at a district scale that are connected to second and third order faults and shear zones, the latter being relevant at the local scale, as gold mineralization is hosted proximal to these structures
- host rocks with favourable physical and/or chemical properties to allow for interaction with mineralizing fluids (e.g. fractured, deformed, or dilated rock increases permeability; iron-rich host rocks which provide a chemical trap)
- syn-tectonic felsic to intermediate intrusive rocks (ca. 2697 Ma in age) and locally intermineral dikes, which may have provided fluids and/or metals or may have served as sources of heat to promote hydrothermal fluid flow
- sheeted and stockwork carbonate-quartz±albite veins in mafic volcanic and intrusive dikes, which contain a large proportion of gold

- wall-rock alteration containing carbonate, albite, quartz, and pyrite (as well as minor chlorite±biotite±magnetite±muscovite±pyrrhotite ±chalcopyrite), which is commonly mineralized
- enrichment in the pathfinder elements Au, Ag, Mo, W, Pb, Cu, and Bi. In contrast to many Archean lode gold deposits, large increases in As are not present in the syn-ore altered mafic volcanic rocks at the Barry deposit and therefore may not be crucial pathfinder element for this type of mineralization.

Appendix A
GEOLOGIC MAPS AND CROSS SECTIONS OF THE BARRY
DEPOSIT

A1. Mapping Methodology

The geologic map of the Barry deposit main zone trench is modified after André Tessier's 1:100 scale map from 1996. The map has been altered to reflect the observations made during our 2006 and 2007 field seasons when selected sectors were mapped at 1:50 scale (Fig. A1). The two mapped zones consist of the northeast corner (Barry deposit main grid 1050E to 1080E and 55S to 75S: Fig. A2) and the 1074 block (Barry deposit main grid 070E to 1090E and 55S to 100S: Fig. A3). These regions were chosen to allow for better correlation between units identified on the surface and in drill core, to clarify the relationships between the various types of alteration and vein types, and to assist in the selection of samples for petrographic and geochemical investigations. During mapping, locations were identified for surface channel sampling of the various units for petrographic and geochemical analysis.

Vertical cross sections were compiled to determine the geometry of the deposit up to ~30 m deep. These include five detailed vertical NW-SE sections were created of the deposit using information from the logging of 17 drill holes during the 2006 and 2007 field seasons (Figs. A4-A8). Drill core was also extensively sampled for petrographic and geochemical analysis.

UTM coordinates for the corners of the two mapped regions and drill holes on these maps were collected during the 2007 field season using a handheld GPS unit (Tables A1 and A2). This information was collected so that the maps could be properly georeferenced.

The grid locations, drill holes, and their associated UTM coordinates are summarized below.

Table A1: UTM coordinates for the NE corner map and drill hole locations

NE Corner				
Description	Grid E	Grid S	Easting	Northing
	1150	75	443931	5426591
DDH BA-04 101	1173.5	75.5	443951	5426603
DDH MB-21-95	1073	75.5	443951	5426604
	1177	75	443954	5426609
	1160	65	443936	5426607
	1150	57	443923	5426608
DDH MB-06 182	1163.5	65	443936	5426610
	1169	60	443939	5426616

Table A2: UTM coordinates for the 1074 block map and drill hole locations

1074 Block				
Description	Grid E	Grid S	Easting	Northing
	1075	95	443876	5426542
	1075	80	443869	5426552
	1090	85	443884	5426550
	1090	70	443878	5426565
DDH BA 04-143	1089	72	443876	5426562
	1085	64	443869	5426568
DDH BA 04-103	1078.5	84	443873	5426550
DDH MB-31	1078	84	443873	5426550

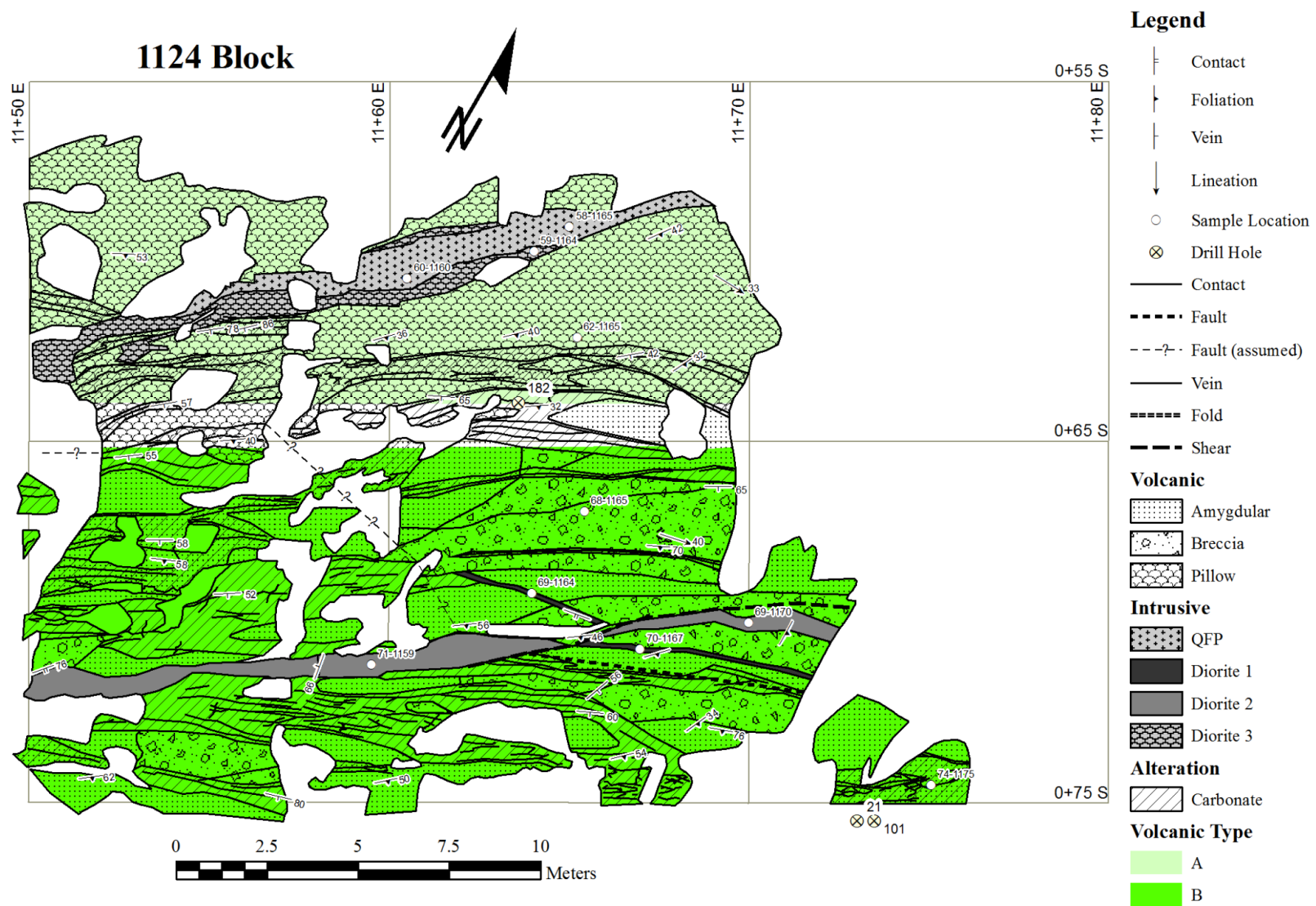


Fig. A2: Geologic map of the northeast corner of the Barry deposit main trench zone.

1074 Block

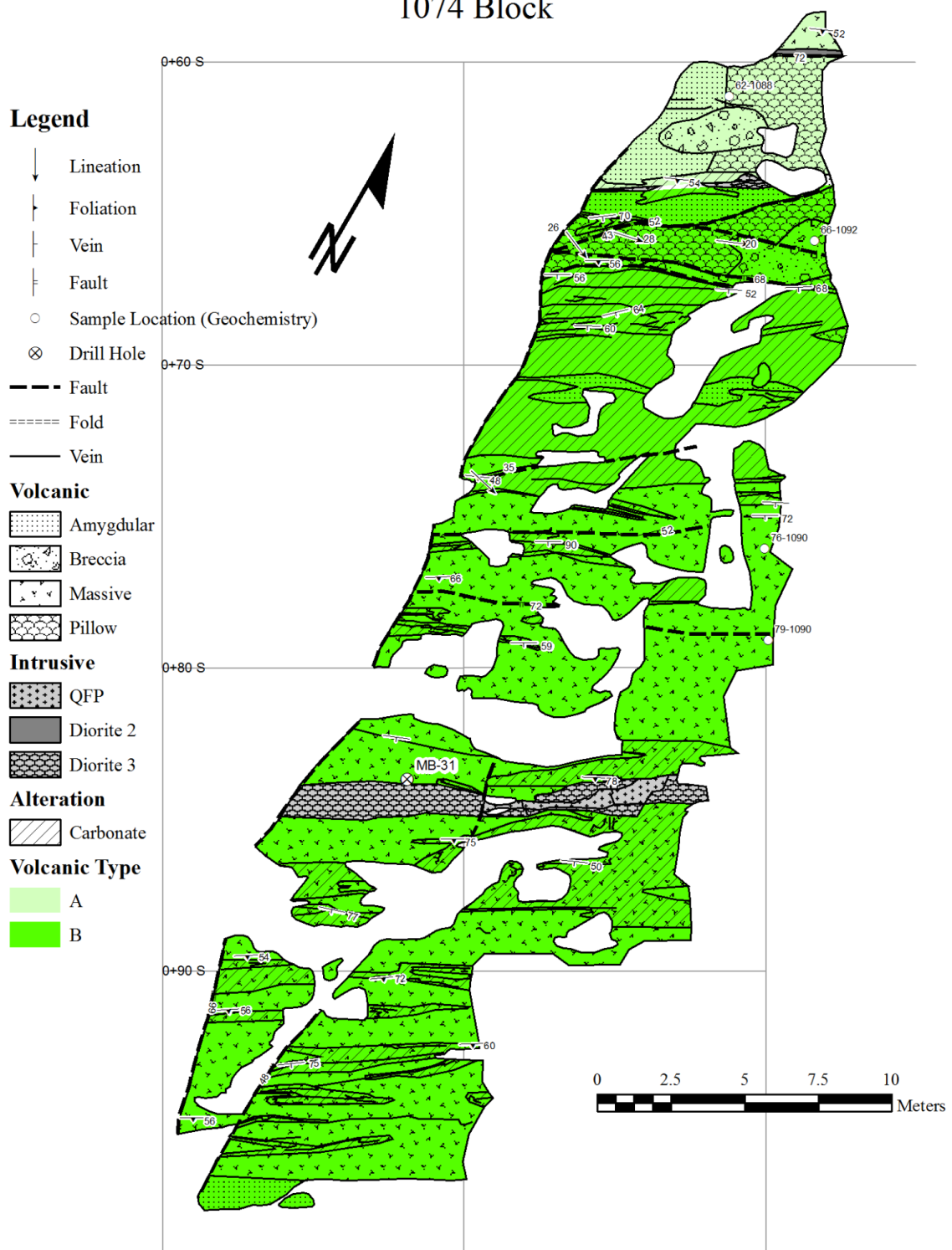


Fig. A3: Geologic map of the 1074 block in middle of the Barry deposit main trenched zone.

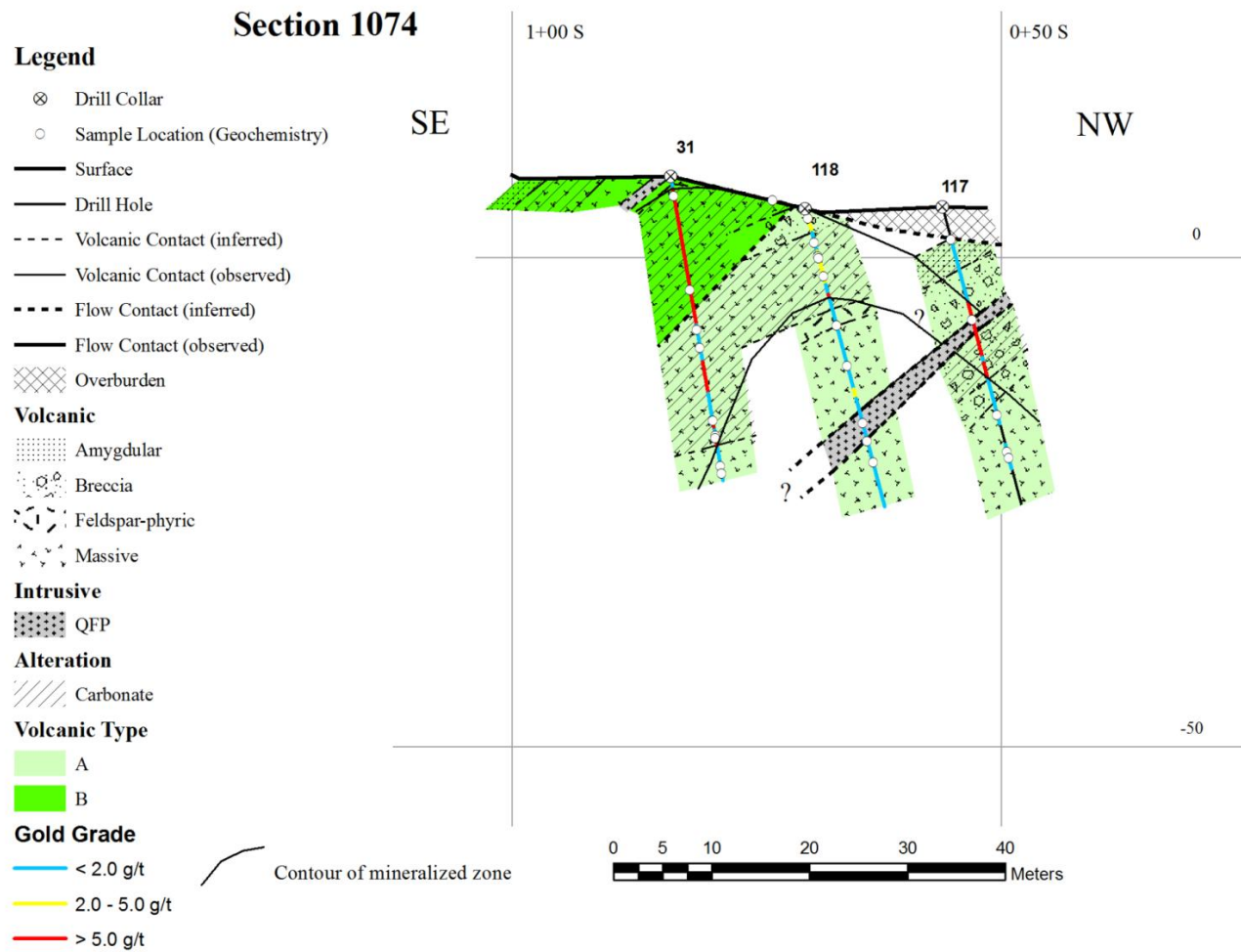


Fig. A5: Vertical SE-NW geologic cross section of the Barry deposit along grid line 1074 E.

Legend

- ⊗ Drill Collar
- Sample Location (Geochemistry)
- Surface
- Drill Hole
- - - Volcanic Contact (inferred)
- Volcanic Contact (observed)
- - - Flow Contact (inferred)
- Flow Contact (observed)
- ⊗ Overburden
- Volcanic**
- ⊗ Amygdular
- ⊗ Breccia
- ⊗ Feldspar-phyric
- ⊗ Massive
- ⊗ Pillow
- ⊗ Tuff
- Intrusive**
- ⊗ QFP
- Alteration**
- ⊗ Carbonate
- Volcanic Type**
- A
- B
- C
- Gold Grade**
- < 2.0 g/t
- 2.0 - 5.0 g/t
- > 5.0 g/t

Section 1088

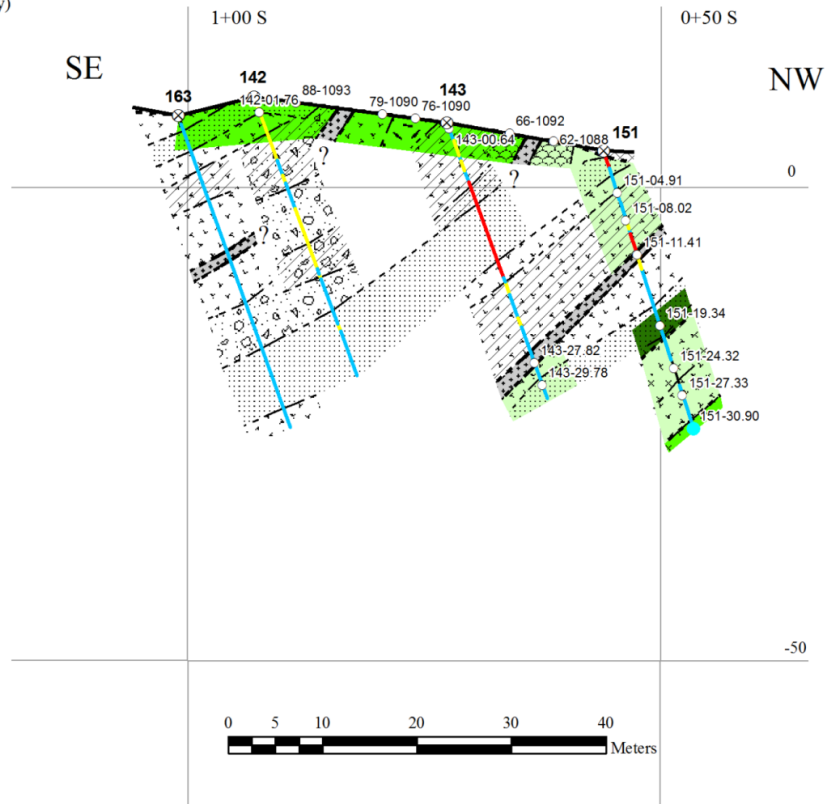


Fig. A6: Vertical SE-NW geologic cross section of the Barry deposit along grid line 1088 E.

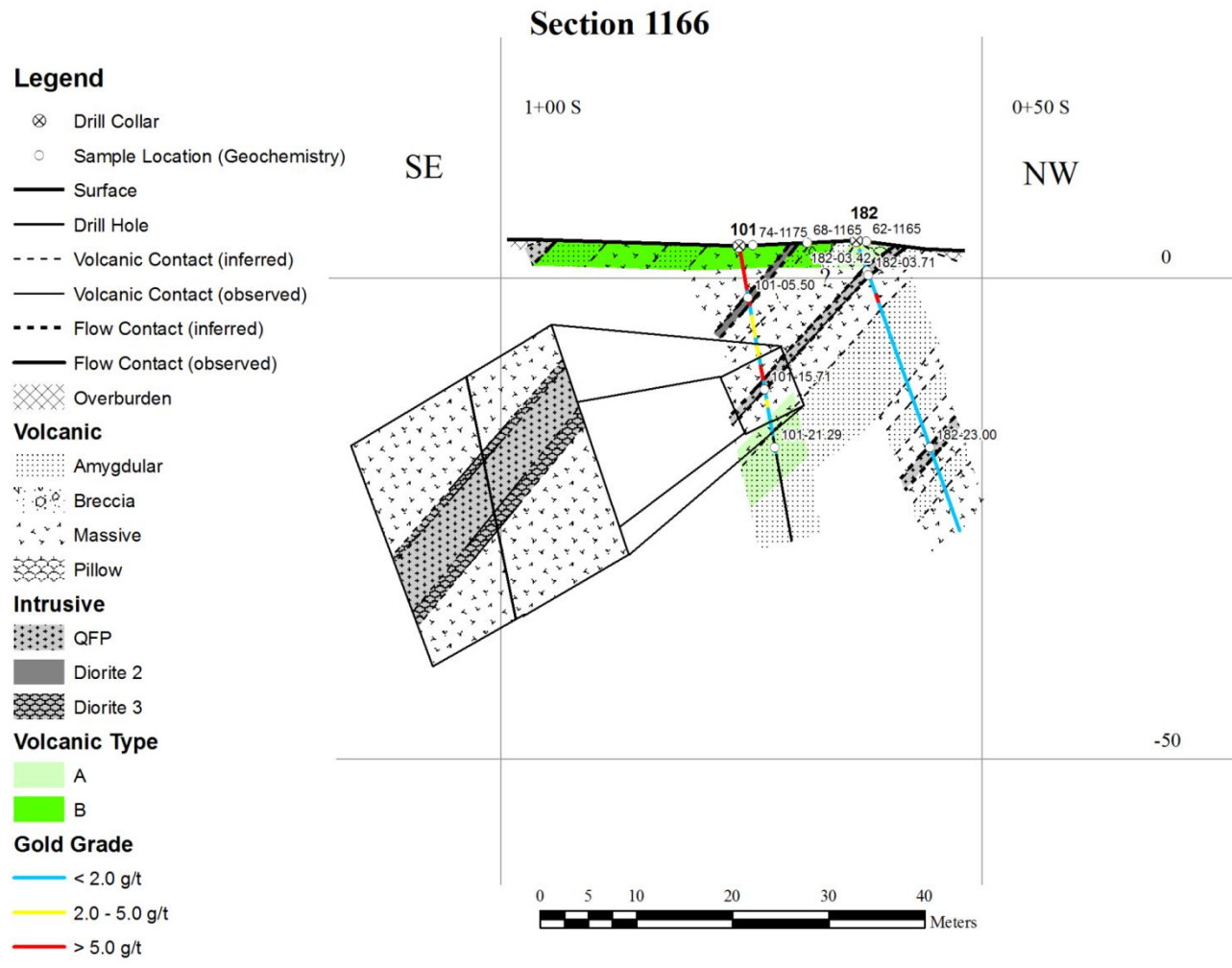


Fig. A8: Vertical SE-NW geologic cross section of the Barry deposit along grid line 1166 E.

Appendix B
SURFACE AND DRILL CORE SAMPLE LOCATIONS AND
DESCRIPTIONS FROM THE BARRY DEPOSIT

B1. Sample Collection and Methodology

Surface samples were taken using a diamond saw. Samples were cut from various rock types across the main zone (including rusty carbonatized zones) to provide representative samples for petrographic and geochemical investigation. The orientation of some samples has been taken so that detailed work on microstructures could be conducted in the future. Large samples of the quartz-feldspar porphyries and diorite dikes in the main trench were taken for geochronological investigation in order to constrain the age of mineralization. A list of surface samples and descriptions are included in Table B1.

Drill core samples were taken from holes 127, 135, 210 (Appendix A: cross section 1037); 31, 117, 118 (Appendix A: cross section 1074); 142, 143, 151 (Appendix A: cross section 1088); 27, 136, 201 (Appendix A: cross section 1124); 101 and 182 (Appendix A: cross section 1166). Drill hole samples consist of $\frac{1}{4}$ to $\frac{1}{2}$ of the core, which were used for lithochemical analysis and polished thin sections. A list of drill core samples and descriptions is summarized in Table B2.

Samples that were studied for petrography, lithochemical, and geochronology are indicated in tables B1 and B2 using superscript 1, 2, and 3, respectively.

Table B1: Location and description of surface samples

Sample ID	Grid East	Grid South	Sample Description
443846 ^{1,2}	443846	5426446	Quartz Monzonite +/- 3m
443945 ^{1,2}	443945	5426525	Quartz Monzonite +/- 6m
58-1165 ^{1,2,3}	1165	58	QFP
59-1113 ^{1,2}	1113.5	59.5	V3 Pillow
59-1164 ^{1,2,3}	1164	59	Diorite 3 (along margin of QFP)
60-1160 ^{1,2}	1160.5	60.5	QFP
61-1168	1168	61	V3 Pillow
62-1088 ^{1,2}	1088.5	62	V3 Pillow
62-1119 ^{1,2}	1118.8	63	QFP
62-1165 ^{1,2}	1165.5	62	V3 Pillow
66-1092 ^{1,2}	1092	66	V3 Breccia
68-1165 ²	1165.5	68	V3 Breccia
69-1164 ^{1,2}	1164	69	Diorite 1: 10cm wide, very fine-grained mafic dike
69-1170 ^{1,2}	1170.5	69	Diorite 2: 20-30 cm wide, fine- to medium-grained, contains "lath-like" mafic crystals (possibly biotite)
70-1159	1159	70.5	Diorite 2: 20-30 cm wide, fine- to medium-grained, contains "lath-like" mafic crystals (possibly biotite)
70-1167 ^{1,2}	1167.5	70	Diorite 1: 10cm wide, very fine-grained mafic dike
71-1075	1074.8	71	V3 Carbonate Alteration
71-1099 ^{1,2}	1099.5	71	V3 Carbonate Alteration
71-1144 ^{1,2}	1144	71	Diorite 2: 20-30 cm wide, fine- to medium-grained, contains "lath-like" mafic crystals (possibly biotite)
71-1159 ^{1,2}	1159.5	71	Diorite 2: 20-30 cm wide, fine- to medium-grained, contains "lath-like" mafic crystals (possibly biotite)
71-1168	1168	71	V3 Amygdular
74-1074 ²	1074	74	V3 Carbonate Alteration
74-1123 ^{1,2}	1123	74	V3 Massive
74-1175 ^{1,2}	1175	74.5	V3 Carbonate Alteration
76-1028 ^{1,2}	1029.9	76.4	V3 Amygdular
76-1090 ^{1,2}	1089.8	76.2	V3 Feldspar-phyric
77-1101 ^{1,2}	1101	77	V3 Feldspar-phyric

Sample ID	Grid East	Grid South	Sample Description
79-1057 ^{1,2}	1057	79	V3 Carbonate Alteration
79-1090 ²	1090	79.5	V3 Mass
80-1025 ^{1,2}	1025	80	QFP
81-1119 ^{1,2}	1119	81	V3 Carbonate Alteration
83-1038 ^{1,2,3}	1038	83	QFP
84-1059 ^{1,2}	1059	84	QFP
84-1077 ²	1077	84	QFP
85-1058 ^{1,2}	1058.5	85	Diorite 3 (along margin of QFP)
85-1108	1108.5	85	V3 Breccia
86-1103	1103.5	86	V3 Carbonate Alteration
87-1163	1163.5	87.5	V3 Massive
88-1093 ^{1,2}	1092.5	88.7	V3 Amygdular
88-1124 ^{1,2}	1124.5	88	Diorite 3
90-1040 ^{1,2}	1040.8	88.8	V3 Massive
91-1119 ^{1,2}	1119.5	91	V3 Amygdular
94-1015 ^{1,2}	1015	94.3	QFP
97-1158 ^{1,2}	1158	97	QFP

Table B2: Location and description of drill core samples

Section	Hole	From	To	Rock Unit	Description	Sample #	Au Assay
1037	127	3.83	4	V3 massive/feldspar-phryic	quartz-carbonate-epidote + pink (garnet?) in vein at 15dca	250001	
1037	127	4.24	4.3	V3 massive/feldspar-phryic	quartz-carbonate-epidote vein offset by small fractures	250002	
1037	127	6.36	6.61	V3 amygdular/breccia	weak brown (biotite) alteration	30041	0.29 g/t
1037	127	6.93	7.04	V3 amygdular/breccia	quartz-carbonate-chlorite-pyrite vein folded, 1-2% pyrite	30042	6.97 g/t
1037	127	7.04	7.17	V3 amygdular/breccia	quartz-carbonate vein, 1-2% pyrite, light tabular crystals	30042	6.97 g/t
1037	127	8.42	8.69	V3 breccia	minor carbonate veins (stockwork, 1mm)	30044	0.03 g/t
1037	127	9.95	10.2	Shear in V3	weak to mod shear at ~55dca, 2-3% pyrite (blebs and cubic) up to 2mm disseminated	30046	4.28 g/t
1037	127	11.4	11.59	V3 breccia	high angle folded quartz vein, fold axis perpendicular to core axis	30048	7.73 g/t
1037	127	12.09	12.32	V3 breccia	mottled texture	30049	0.32 g/t
1037	127	12.4	12.67	V3 amygdular	mottled texture, 5% dark amygdules (1-2mm), 5-10% white amygdules (3-4mm)	30049	0.32 g/t
1037	127	16.02	16.23	V3 breccia	1% visible disseminated magnetite (<1mm)	30053	0.54 g/t
1037	127	17.48	17.59	Shear in V3	shear at 70dca with quartz-carbonate veins	30055	4.23 g/t
1037	127	18.68	18.94	Shear in V3	shear at ~70dca with quartz-carbonate veins, 1-2% pyrite (<=2mm)	30057	3.69 g/t
1037	127	19.3	19.5	V3 breccia	fine grained disseminated pyrite, small quartz-carbonate veins	30058	1.23 g/t
1037	127	20.13	20.27	QFP 1?	altered (smeared crystal boundaries) with quartz vein and large pyrite bleb (5mm) and fine grained pyrite along the quartz vein	30059	0.43 g/t
1037	127 ^{1,2}	21.35	21.64	QFP 1?		250003	
1037	127	22.3	22.5	QFP 2?		30062	0.75 g/t
1037	127	23.05	23.26	V3 massive?	quartz-carbonate-epidote vein with pink colour (garnet?)	250004	
1037	127	25.3	25.48	V3 massive?/QFP 2	contact between V3 and large QFP 2	250006	
1037	127	35.21	35.42	QFP 2	faint pink staining	250015	

Section	Hole	From	To	Rock Unit	Description	Sample #	Au Assay
1037	127	41.7	41.8	QFP 2	hot pink stained feldspar crystals along fracture	250020	
1037	127	43.3	43.46	QFP 2/V3	lower contact between QFP 2 and V3 with texture destructive alteration, folded white quartz vn, trace pyrite, 1% pyrrhotite (2-3mm)	30066	1.73 g/t
1037	127	43.86	44.03	V3 texture destructive	folded quartz vein, 1% pyrite, texture destructive alteration	30066	1.73 g/t
1037	127	44.19	44.4	V3 amygdular		250022	
1037	127	45.6	45.83	V3 amygdular/breccia		250023	
1037	135	4.22	4.5	V3 carbonatized - rusty	quartz-albite vein, light foliation ~70dca, 1% pyrite in and near veins, trace white tabular crystals, trace fine grained disseminated magnetite	30098	6.71 g/t
1037	135	6.27	6.55	V3 carbonatized - rusty	quartz-albite veins (70dca), light foliation (70dca), 5cm band of 20% pyrite (1-3mm)	30101	10.45 g/t
1037	135	6.6	6.86	V3 carbonatized/breccia	contact between rusty alteration and unaltered bre	30102	0.43 g/t
1037	135	7.06	7.2	V3 carbonatized/QFP 1?	contact between rusty alteration and pink smeared QFP1(?) at ~70dca	30103	0.12 g/t
1037	135	7.36	7.5	QFP 1?	pink alteration, crystal boundaries smeared, QFP becomes white with less smeared crystal boundaries on either side of a quartz vein	30103	0.12 g/t
1037	135	7.5	7.67	QFP 1?	white colour, trace cubic disseminated pyrite	30104	1.02 g/t
1037	135	8.5	8.73	V3 breccia	VG, late brittle movement (volcanic+tectonic breccia), white tabular crystals (<1mm), pyrite	30105	3.09 g/t
1037	135	8.93	9.07	V3 texture destructive alt	quartz-albite veins, some with rusty or pink discolouration, visible fine grained disseminated magnetite, 1-2% pyrite (cubic and blebs <=1mm), white tabular crystals	30107	18.2 g/t
1037	135	9.83	10	V3 texture destructive alt	vuggy quartz-albite veins with infilling texture, 2% pyrite (cubic and blebs, <1mm-4mm), visible fine grained disseminated magnetite, white tabular crystals (<=1mm)	30108	12.3 g/t

Section	Hole	From	To	Rock Unit	Description	Sample #	Au Assay
1037	135	10.28	10.5	V3 texture destructive alt	vuggy quartz-albite veins with infilling texture, 2% pyrite (cubic and blebs, 2mm), visible fine grained disseminated magnetite, white tabular crystals (<=1mm)	30109	15.6 g/t
1037	135 ^{1,2}	10.8	11.1	V3 texture destructive alt	vuggy quartz-albite veins, beige/pink alteration, 5-10% pyrite (blebs and cubic, <1mm-2mm) in and along vns, visible fine grained disseminated magnetite, white tabular crystals	30110	25.2 g/t
1037	135	11.58	11.76	Shear in V3	shear at 70dca, dark grey colour, trace-1% pyrite (blebs and cubic, <=1mm), 1.5cm boudined quartz-albite vein with dark (biotite?) selvage, quartz-carbonate veins (2mm)	30112	0.81 g/t
1037	135	12.8	12.9	V3 texture destructive alt	folded quartz-carbonate-pyrite veins, dark (biotite?) selvage, vuggy quartz-carbonate or quartz-albite vein, 1% pyrite	30113	3.04 g/t
1037	135	15.39	15.66	V3 amygdular	1-2% white amygdules (1mm), 5-10% dark amygdules	30117	0.01 g/t
1037	135	16.16	16.32	V3 amygdular/breccia	1% pyrite blebs (1-2mm), trace-1% pyrrhotite blebs (<1mm)	30118	0.02 g/t
1037	135	19.5	19.68	V3 breccia	quartz-carbonate vein with light green alteration	30121	0.01 g/t
1037	135	19.68	19.81	V3 breccia/T3	fairly sharp V3 breccia and T3 contact at 70dca	30121	0.01 g/t
1037	135	19.81	20.04	T3	brown and green bands with some minor feldspar crystals	30121/22	0.01 g/t
1037	135	20.94	21.14	T3	quartz vein with silvery metallic mineral (non-magnetic, blebs up to 4mm in vn), vein is 5mm-1.5cm wide and runs at ~65dca	30122/23	0.01 g/t
1037	135 ^{1,2}	24.35	24.63	T3	green and brown/dark grey bands, looks as if green may be an alteration overprinting the tuff, general foliation at 65-70dca, white crystals (feldspar?) in tuff up to 1mm in size	129267	
1037	135	25.35	25.5	T3	alteration green looks "netted" and looks to possibly be overprinting dark grey/brown	129268	

Section	Hole	From	To	Rock Unit	Description	Sample #	Au Assay
1037	135	26.63	26.73	T3	2-5mm quartz-carbonate vein containing host, beige-green strange alt pattern ("netted")	129269	
1037	135 ^{1,2}	26.96	27.12	V3 massive	medium to turquoise green	129270	
1037	135	29.85	30.1	V3 breccia	green and brown shapes and "swirls", trace silvery metallic mineral in very fine stringers along green band	129272	
1037	135	31.16	31.46	V3 breccia	brown and green coloured, last 5-10cm has a pale green-beige alteration colour	129274	
1037	210 ^{1,2}	4.33	4.59	Crowded porphyry	white coloured	249532	0.17 g/t
1037	210 ^{1,2}	5.97	6.23	Crowded porphyry	pink coloured	249535	0.22 g/t
1037	210 ¹	14	14.25	Crowded porphyry	white with white quartz veins with white alteration along selvage	249543	0.79 g/t
1037	210 ²	20.07	20.26	V3 amygdular	1-2% dark amygdules (calcite + biotite?)	249551	0.25 g/t
1037	210 ²	24.16	24.38	V3 massive	foliation at 45-50dca, 5-10% q-c veins, trace fine grained cubic pyrite	249555	2.05 g/t
1037	210	25.12	25.3	Shear in V3	50dca, veins follow this orientation, 3-5% veins (1mm), trace to 1% sulphides	249556	2.88 g/t
1037	210	28.42	28.52	V3 amygdular	localized garnet + epidote in vein	249559	0.60 g/t
1037	210	40.35	40.47	V3 breccia?	4cm epidote + calcite + quartz + garnet vein, low angle (~80dca?)	249572	0.05 g/t
1037	210 ^{1,2}	40.69	40.91	V3 breccia?	array of 2mm folded epidote + calcite + sulphide veins cut by quartz-carbonate vein	249573	0.06 g/t
1037	210 ¹	42.75	42.97	V3 texture destructive alteration	quartz-carbonate and carbonate veins, fine grained cubic pyrite in wall rock and within veins	249576	6.37 g/t
1037	210 ^{1,2}	48.38	48.6	QFP 2	pink coloured, crystal boundaries smeared, trace sulphides	249582	0.76 g/t
1037	210 ^{1,2}	55.21	55.43	QFP 2	near contact with V3	249588	-0.01 g/t
1037	210	60.85	61.01	V3 breccia/amygdular	quartz-carbonate veins with dark selvage and sulphides: likely pyrite and pyrrhotite	249593	0.26 g/t
1037	210 ^{1,2}	65.11	65.29	V3 amygdular	q-c vn with light green alteration along the side of the vn, very fine grained sulfides (py?, po? Can't tell) in selvage	263302	0.00 g/t

Section	Hole	From	To	Rock Unit	Description	Sample #	Au Assay
1037	210	70.07	70.24	Shear in V3	bt alt, folded q-c+cl vn, various deformed vns	249599	0.16 g/t
1037	210 ²	71.1	71.36	V3 amygdular	15% calcite amy (1x2 and larger) in chloritized background	249601	0.05 g/t
1037	210 ^{1,2}	74	74.22	V3 breccia	q-car-ep-po at low angle (25dca) slightly folded and cut by carb band with dark alteration around it (bt?)	263309	0.00 g/t
1037	210	75.48	75.69	V3 breccia	q-c-ep-po vn at 55dca	263311	0.00 g/t
1074	31 ^{1,2}	0.31	0.66	V3 massive	5% carbonate vns (rusted, 2mm), fine grained disseminated pyrite	585759/60	0.03 - 0.75 g/t
1074	31 ^{1,2}	2.26	2.68	V3 massive	chlorite veins, fine grained disseminated pyrite, quartz-carbonate veins some with chlorite selvage	585763	2.18 g/t
1074	31	6.1	6.38	V3 carbonitized - rusty	15-10% stockwork quartz-albite veins, 1-2% fine grained pyrite in selvage, rusty surface alteration, non-magnetic host	585772/73	6.95 - 6.39 g/t
1074	31 ¹	10.03	10.27	V3 carbonitized - rusty	1.5cm quartz-carbonate vein at 85-90dca with dark (biotite?) selvage, carbonate alteration, trace-1% fine grained disseminated pyrite, rusty ankerite weathering	585779	4.35 g/t
1074	31 ¹	10.27	10.48	V3 carbonitized - rusty	6cm brittle quartz-albite vein at 50dca, 2-3% disseminated pyrite (blebs <=1mm)	585779/80	4.35 - 4.66 g/t
1074	31	10.7	10.93	V3 carbonitized - rusty	20-30% quartz-albite stockwork, 10-15% pyrite (blebs 1-3mm)	585780	4.66 g/t
1074	31 ¹	11.1	11.26	V3 carbonitized - rusty	quartz-albite veins at 50-55dca, 5-10% pyrite (blebs 2-3mm), biotite/magnetite selvage	585780	4.66 g/t
1074	31 ^{1,2}	12	12.22	V3 carbonitized - rusty	10% quartz-albite veins with carbonate selvage at 45dca	585782	4.6 g/t
1074	31	12.22	12.39	V3 carbonitized - rusty	10% quartz-albite veins with carbonate selvage at 45dca	585782	4.6 g/t
1074	31	12.5	12.65	V3 breccia	4cm quartz-albite vein with carbonate selvage at 45dca, 5mm quartz-albite veins at 65dca, 5-10% pyrite	585783	6.48 g/t
1074	31	14.02	14.18	V3 breccia	7mm-3cm pinching and swelling quartz-albite vein at 45dca with thin biotite-pyrite selvage	585787	0.41 g/t

Section	Hole	From	To	Rock Unit	Additional description	Sample #	Au Assay
1074	31	15.53	15.76	V3 breccia	boudined/deformed quartz-albite vein with pink (calcite?), 1mm selvage of biotite and fine grained pyrite, fine grained pyrite disseminated in wall rock, several quartz-albite veins at 60dca	585790/91	0.17 - 1.74 g/t
1074	31	16.17	16.28	V3 breccia	-60dca quartz-carbonate vein cuts/cut by boudined quartz-albite vein at 50-55dca, chlorite and ankerite selvage	585791/92	1.74 - 0.33 g/t
1074	31 ^{1,2}	16.28	16.4	Shear in V3	quartz-albite veins in shear at 55dca with strong biotite, chlorite, ankerite alteration	585792/93	0.33 - 0.99 g/t
1074	31 ^{1,2}	17.89	18.12	V3 massive	visible disseminated magnetite	585795	0.98 g/t
1074	31	18.31	18.46	V3 massive	chlorite bands at 75-80dca, 3% pyrite (cubic <1mm-2+ mm) along/near quartz-carn\bonate veins, visible disseminated magnetite	585796	0.07 g/t
1074	31	18.7	18.83	V3 massive	2cm quartz-albite vein at 50dca, biotite+carbonate (some moderately rusty ankerite) alteration	585796/97	0.07 - 0.57 g/t
1074	31 ¹	20.02	20.25	Shear in V3	VG, chlorite vein/band, strong biotite alteration along 3mm boudined quartz-carbonate vein at 50dca, strong calcite alteration Why is the assay value low?	585800	0.17 g/t
1074	31	21.43	21.63	Shear in V3	green V3 then strong biotite in shear at 40dca, folded quartz-carbonate-chlorite vein, straight quartz-carbonate-biotite-pyrite vein with VG, 5% fine grained pyrite	585803	0.07 g/t
1074	31	21.8	21.88	V3 breccia	quartz-carbonate+pyrite+pyrrhotite vein at 45-50dca, biotite and chlorite alteration surrounding vein	585804	21.96 g/t
1074	31	22.44	22.55		Quartz-carbonate vein cut and offset by smaller quartz veins		
1074	31	22.71	22.93	V3 breccia	quartz vein +biotite+sulfide (pyrrhotite?) in 2cm band at 40dca	585805	0.48 g/t
1074	31 ^{1,2}	25.48	25.67	V3 amygdular	dark amygdules with light rims	585809	6.88 g/t
1074	31	26.43	26.58	V3 breccia+amygdular	2-3mm quartz vein along core axis (0dca), 1% pyrrhotite, 1% pyrite	585810	0.1 g/t

Section	Hole	From	To	Rock Unit	Additional description	Sample #	Au Assay
1074	31 ^{1,2}	27.03	27.2	V3 amygdular	visible magnetite, contact with shear zone at 80dca	585811	12.1 g/t
1074	31 ^{1,2}	27.2	27.4	Shear in V3	possible VG, folded quartz-carbonate veins, shear at 50-55dca, strong biotite and calcite alteration, pyrrhotite, Au Assay possibly mixed with 585813 below	585812	0.57 g/t
1074	31	27.65	27.88	V3 amygdular	chlorite and biotite bands at 35dca, increase in magnetite at end, Au Assay possibly mixed with 585812 above	585813	52.77 g/t
1074	31 ^{1,2}	30.23	30.35	V3 feldspar-phyric	small white/silver tabular crystals	585816	0.03 g/t
1074	31 ^{1,2}	31.06	31.25	V3 feldspar-phyric		585817	0.17 g/t
1074	117 ^{1,2}	3.48	3.76	V3 amygdular	2% white and 2% dark amygsules, with 2-5% visible disseminated magnetite, so few amygdules that it looks almost massive	30313	0.00 g/t
1074	117	5.75	5.94	V3 amygdular	green chlorite alteration bands, less visible magnetite, trace pyrite in chlorite band	30315	0.09 g/t
1074	117	9.33	9.65	V3 breccia	1% py near quartz-carbonate veins, trace disseminated magnetite	30321	0.03 g/t
1074	117	10.14	10.28	V3 breccia	quartz-carbonate vn (mostly calcite, 60-70dca), trace py, dark biotite/magnetite selvage	29690	7.76 g/t
1074	117	10.64	10.9	V3 breccia	quartz-carbonate veins with fine grained pyrite and biotite selvages, larger pyrite blebs in V3 breccia host	29691	1.89 g/t
1074	117	11.09	11.3	V3 breccia	boudined quartz veins with dark (biotite) selvage, increased brown biotite throughout this region, pyrite (blebs) and near veins	29692	1.62 g/t
1074	117	11.6	11.85	V3 breccia	boudined quartz-carbonate vein with dark (biotite?) selvage, pyrite bands, rusty alteration and magnetite in boudins	29693	7.88 g/t
1074	117 ^{1,2}	11.95	12.15	QFP 2	altered - beige colour and smeared crystal boundaries, rusty upper contact at 60-65dca, foliation 60-70dca	29694	2.49 g/t

Section	Hole	From	To	Rock Unit	Additional description	Sample #	Au Assay
1074	117	12.79	12.98	V3 breccia	boudined quartz-albite vein with dark (biotite?) selvage, very magnetic between veins, disseminated fine grained pyrite in and near veins	29695	5.7 g/t
1074	117	14.04	14.21	V3 breccia	VG near vein, boudined quartz-albite vein at 60dca with dark (biotite?) selvage, pyrite-rich band (1mm cubes)	29697	6.15 g/t
1074	117	14.9	15.03	V3 breccia	boudined quartz vein, pyrite (2mm cubic)	29698	2.02 g/t
1074	117	15.75	15.89	V3 breccia	VG in 2-3mm pyrite bleb, 50%pyrite <1mm to 4mm, chlorite bands, calcite-pyrite vein,	29699	12.5 g/t
1074	117	16.16	16.36	V3 amygdular	quartz vein with trace-1% pyrite and trace pyrrhotite, disseminated pyrite and 1% visible disseminated magnetite in volcanic host	29700	0.18 g/t
1074	117	16.72	16.86	V3 breccia	strong biotite alteration, boudined quartz-albite vein, fine grained disseminated pyrite	29701	1.87 g/t
1074	117	17.07	17.27	V3 breccia	"stockwork" quartz-carbonate veins from 30-60dca, strong biotite alteration, pyrite in 60-70dca vein, <1mm to 5mm cubic and blebs in volcanic host	29702	4.92 g/t
1074	117	17.47	17.65	V3 amygdular	VG in or beside pyrite, bands of cubic pyrite (1mm-2mm) in and near "stockwork" quartz veins with beige-brown alteration, strong bt alteration	29704	19.55 g/t
1074	117	18.04	18.21	V3 amygdular	contact between calcite-pyrite-biotite zone and V3 breccia, 30% fine grained disseminated pyrite, strong biotite and calcite alteration, sharp contact at 80-85dca	29705	0.25 g/t
1074	117	18.21	18.4	V3 breccia	green/brown colour	29705	0.25 g/t
1074	117	18.72	18.98	V3 breccia/amygdular	1-2% white and 1-2% dark amygdules, trace-1% pyrrhotite in blebs disseminated in host	29706	0.1 g/t
1074	117	19.69	19.9	V3 breccia	trace-1% pyrite and pyrrhotite, weak to moderate biotite and calcite alteartion, calcite veinlets (<=1mm) with various orientations, quartz-carbonate veinlts (2mm) at 35dca	29707	0.05 g/t

Section	Hole	From	To	Rock Unit	Additional description	Sample #	Au Assay
1074	117	21.13	21.48	V3 amygdular	medium grey-green, trace disseminated pyrite/pyrrhotite/magnetite, 1-2% white amygdules (1mm-3mm)	29709	0.01 g/t
1074	117 ^{1,2}	22.07	22.32	V3 massive	no visible mineralization/veins in this sample	30322	0.01 g/t
1074	117	23.36	23.66	V3 breccia?	pale green colour with biotite-rich zones, trace disseminated pyrrhotite	129275	
1074	117	24.84	25.03	V3 breccia/amygdular	pale green colour + biotite in long stretched strands and small dark blebs (amygdules?) was this once a V3 amygdular before pale green alt?	129276	
1074	117 ^{1,2}	25.95	26.11	Shear in V3	biotite-calcite shear at 70dca, contains folded and boudined quartz-carbonate-chlorite-pyrrhotite-pyrite veins at 65-70dca	129278	
1074	117 ^{1,2}	26.66	26.88	V3 breccia	pale coloured alteration	129279	
1074	117	29.32	29.63	V3 breccia	pale coloured alteration, some biotite-rich bands at 55dca, sharp contact with surrounding V3 breccia	129282	
1074	117	29.81	30.11	V3 breccia?	trace pyrite and pyrrhotite mostly in carbonate vein with chlorite selvages	129283	
1074	117	30.47	30.74	V3 breccia	medium grey-green, 1mm stockwork carboante veins, trace visible magnetite, similar to pale altered unit above	129283	
1074	118	0	0.23	V3 breccia		30406	0.53 g/t
1074	118 ^{1,2}	1.01	1.31	V3 breccia		30407	0.08 g/t
1074	118	1.87	2.1	V3 breccia	quartz-albite vein, pink-red alteration, carbonate alteration, dark selvages (biotite?) on veins, trace pyrite	29388	3.36 g/t
1074	118 ^{1,2}	3.62	3.81	V3 breccia or massive	2-3% disseminated magnetite (<1mm)	30408	0.04 g/t
1074	118 ^{1,2}	5.16	5.33	V3 breccia	quartz-albite veins (pinch and swell at 60dca) with dark (biotite?) selvage	29390	3.02 g/t
1074	118	5.33	5.5	V3 breccia	quartz-carbonate veins	29391	2.47 g/t
1074	118 ^{1,2}	5.98	6.17	V3 breccia	quartz-albite vein at 80-90dca cut by 1mm quartz-calcite(?) vein at 35dca	29391	2.28 g/t

Section	Hole	From	To	Rock Unit	Additional description	Sample #	Au Assay
1074	118	7.03	7.19	V3 breccia	quartz-carbonate?albite? Vein, orange alteration along side	29393	1.08 g/t
1074	118 ²	7.19	7.34	V3 massive or breccia	fine grained disseminated magnetite	29393	1.08 g/t
1074	118	7.5	7.62	V3 breccia	pinch and swell quartz-albite (with biotite or chlorite-magnetite) and orange alteration	29394	8.47 g/t
1074	118	7.84	8.07	V3 breccia	quartz-albite vein with dark (biotite?) selvage, 5-10% pyrite	29394	8.47 g/t
1074	118	9.14	9.34	V3 breccia	3cm quartz-albite vein, biotite and carbonate In shear at 70dca	29396	11.7 g/t
1074	118 ²	12.39	12.59	V3 feldspar-phyric	carbonate vein and amygdule?	30413	0.01 g/t
1074	118	15.45	15.54	V3 breccia	quartz-carbonate veins, disseminated pyrite	30417	0.02 g/t
1074	118 ^{1,2}	16.7	16.9	V3 breccia	calcite veins	29399	0.01 g/t
1074	118	18.63	16.8	V3 breccia	quartz-carbonate vein	29401	0.01 g/t
1074	118	19.2	19.34	V3 breccia	quartz-carbonate vein with dark (biotite?) selvage	29402	3.37 g/t
1074	118	19.4	19.5	V3 breccia	quartz-carbonate vein along core axis, dark (biotite?) and pyrite selvage	29402	3.37 g/t
1074	118 ^{1,2}	22.78	23.07	QFP 2	possibly contact with lower V3 unit	30421	0.01 g/t
1074	118 ^{1,2}	24.56	24.79	V3 amygdular	10% quartz? amy (1-2mm), 5% beige-brown amygdules (calcite?), hairline fractures/veins	29407	0.01 g/t
1074	118 ²	26.87	27.17	V3 amygdular	5% quartz?, 5% calcite? amygdules, hairline fractures/veins	29408	0.01 g/t
1088	142	0.57	0.76	V3 breccia/amygdular	rusty alteration, 3-4cm quartz vein with minor beige-yellow carbonate crystals at 40dca	42115	0.81 g/t
1088	142	1.2	1.38	V3 breccia/amygdular	weak biotite alteration in bands, visible disseminated magnetite, trace pyrite	42116	1.64 g/t
1088	142 ^{1,2}	1.76	2.08	V3 breccia	green and grey coloured, unaltered	42116/17	1.64 - 1.15 g/t
1088	142	2.37	2.51	V3 breccia/amygdular	minor amygdules, stockwork veinlets with green (epidote? or chlorite?)	42117	1.15 g/t
1088	142	2.69	2.8	V3 breccia	5cm quartz+/-carbonate vein with rusty alteration	42117	1.15 g/t

Section	Hole	From	To	Rock Unit	Additional description	Sample #	Au Assay
1088	142	2.93	3.06	V3 breccia	weak rusty alteration, folded quartz-carbonate vein, trace-1% visible disseminated magnetite, trace pyrite	42117	1.15 g/t
1088	142	4.2	4.32	V3 breccia/amygdular	carbonate veins offset by microveins/fractures in rusty background alteration	42120	6.32 g/t
1088	142	4.32	4.53	V3 breccia/amygdular	1-2cm quartz vein with beige/orange carbonate crystals at 40dca cuts/cut by (can't tell) 4-5mm irregular quartz vein ~0dca, trace fine grained disseminated pyrite near vn, rusty alteration, small rusty weathered microveins/fractures	42120	6.32 g/t
1088	142	4.65	4.79	V3 breccia/amygdular	quartz-albite vein at 50dca with thin dark (biotite?) selvage and rusty alteration around it, pyrite (<1mm near vein to 3mm in vein)	42121	2.69 g/t
1088	142	4.96	5.22	V3 breccia/amygdular	quartz veins at 45-50dca, minor carbonate veins, rusty alteration, trace pyrite near and in quartz veins, trace visible disseminated magnetite	42122	5.53 g/t
1088	142	5.45	5.65	V3 breccia	1cm quartz vein at 50dca, rusty alteration, 1-2% pyrite (blebs 2-3mm) in host and veins	42122/23	5.53 -
1088	142	5.65	5.8	V3 breccia	quartz-carbonate (orange stained) vein at 60dca, 2cm quartz+/-carbonate vein at 35-40dca, quartz vein at 40-45dca, rusty alteration, 2-3% pyrite (cubic and blebs <2mm)	42123	17.65 g/t
1088	142	6.19	6.4	V3 breccia	quartz-carbonate veins at 40-50dca, one with dark (biotite?) selvage, rusty alteration, 1% pyrite (blebs and cubic <1mm-2mm), dark orange rusty colour (fine grained disseminated pyrite?), possible chalcopyrite in small adjacent broken piece?	42124	3.74 g/t
1088	142	6.96	7.1	V3 breccia	folded quartz+/-albite veins, biotite stringers, some biotite/chlorite growing into some of the smaller veins, pink alteration near veins, host is medium/dark grey colour, no rusty alt, trace-1% fine grained disseminated pyrite	42125	4.37 g/t

Section	Hole	From	To	Rock Unit	Additional description	Sample #	Au Assay
1088	142	7.57	7.72	V3 breccia	homogeneous, small chlorite veinlets	42126	0.84 g/t
1088	142	8.65	8.78	V3 breccia	chlorite bands/veins, foliation at 45dca, 8.63-8.65m is broken up rock (pieces <5mm) possibly brittle fault zone?, visible fine grained disseminated magnetite	42127	0.18 g/t
1088	142	9.02	9.16	V3 breccia	16cm wide quartz+/-albite vein at 25-30dca with chlorite/host rock inside vein, fine grained pyrite along edges of vein, stockwork of thin rusty orange folded veins	42128	2.18 g/t
1088	142	10.55	10.77	V3 breccia	unaltered, possibly V3 massive at beginning of this piece?	42130	1.22 g/t
1088	142	10.77	10.98	V3 breccia	quartz-carbonate veins, trace disseminated pyrite (<1mm), chlorite veins	42130	1.22 g/t
1088	142	11.97	12	V3 breccia	folded quartz-carbonate vein with epidote, fine grained disseminated magnetite, no visible sulfides. What is causing the increased Au grade?	42132	0.89g/t
1088	142	12.44	12.58	V3 breccia	deformed quartz-albite+biotite+carbonate (rusty orange crystals) vein at 40-50dca, rusty alteration along one side, dark (biotite?) selvage on other side, trace-1% fine grained disseminated pyrite near vein, rusty stockwork veinlets in dark grey side	42132/33	0.89g/t - 5.19g/t
1088	142	13.94	14.19	V3 breccia	quartz-carbonate+pyrite+VG(in pyrite) veins at 40-45dca, veins cut by veins/fracture fills of dark mineral (biotite?) at 20dca	42135	3.73 g/t
1088	142	15.07	15.22	V3 breccia	deformed quartz-carbonate veins, pink alteration around veins, pyrite (cubic and blebs <=2mm)	42137	5.76 g/t
1088	142	15.48	15.58	V3 breccia	"swirled" texture of alteration, biotite+chlorite+rusty alteration, 1% pyrite (blebs and cubic <=2mm)	42138	5.99 g/t
1088	142	16.47	16.64	V3 breccia	chlorite-rich zone, rusty orange zone, quartz vein at 55dca	42139	4.54 g/t

Section	Hole	From	To	Rock Unit	Additional description	Sample #	Au Assay
1088	142	17.63	17.9	V3 breccia	quartz vein with dark (biotite?) selvage, 2 vein directions: larger at 45dca, smaller at 55dca, rusty alteration, 1-2% pyrite (cubic and blebs <=1mm)	42142	6.83 g/t
1088	142	18.21	18.34	V3 breccia	blocky boudined quartz vein, medium grey and some small rusty alteration in host	42143	1.32 g/t
1088	142	18.74	18.96	V3 breccia	quartz-carbonate+pyrite vein with pyrite selvage at 55dca, one is boudined with biotite selvage, 1-2% py (cubic and blebs <1mm-3mm) in and near vn	42144	1.09 g/t
1088	142	20.14	20.33	V3 breccia	boudined quartz veins with dark (biotite?) selvage at 80dca, biotite banding in host, trace-1% pyrite (cubic and blebs <=1mm)	42146	2.35 g/t
1088	142	20.76	20.86	V3 breccia	boudined quartz-carbonate and quartz-albite veins at 85-90dca with dark (biotite?) selvage, weak biotite alteration throughout, trace pyrite in veins and host (<=1mm)	42147	0.67 g/t
1088	142	22.2	22.47	V3 breccia	bleb of quartz-carbonate+biotite/chlorite+magnetite 2-3% pyrite, quartz-carbonate vein at 50dca	42150	0.46 g/t
1088	142	23.51	23.71	V3 breccia	"swirled" texture of chlorite+/-biotite alteration	42152	0.01 g/t
1088	142	25.04	25.33	V3 amygdular	dark amygdules rimmed by biotite, white amygdules	42154	0.01 g/t
1088	142	25.76	25.91	V3 amygdular	several generations of carbonate at 35-40dca and quartz-carbonate veins at -75to-80dca, 3cm band of biotite and calcite alteration with pyrite (50% cubic pyrite <3mm in band)	42155	4 g/t
1088	142	27.82	28.09	V3 breccia		42157	0.01 g/t
1088	142	29.3	29.42	V3 breccia/amygdular	boudined quartz-carbonate vein at 70dca, trace pyrrhotite+pyrite	42159	0.18 g/t
1088	142	31.04	31.26	V3 breccia/amygdular	irregular shaped alteration blob of green surrounding dark (biotite? or chlorite+magnetite?) alteration. Not known which alt is replacing whicg.	42161	0.27 g/t

Section	Hole	From	To	Rock Unit	Additional description	Sample #	Au Assay
1088	143	0.09	0.21	V3 breccia	thin carbonate and larger quartz/quartz-albite veins with rusty/dark (chlorite/biotite?) selvage, similar to 7.07-8m in hole 142	42376	13.6 g/t
1088	143	0.21	0.36	V3 breccia	folded quartz-albite vein with yellow-beige alteration along the sides (carbonate alteration)	42376	13.6 g/t
1088	143 ^{1,2}	0.64	0.85	V3 breccia		42377	0.39 g/t
1088	143	1.88	2.1	V3 breccia	quartz-albite vein at 35-40dca with pyrite-biotite selvage, rusty orange alteration around vein, 5-10% pyrite (cubic and blebs 1mm-4mm)	42379	5.8 g/t
1088	143	3.38	3.49	V3 breccia	dark orange-red rusty alteration - could be fine grained disseminated pyrite?	42381	1.11 g/t
1088	143	4.43	4.58	V3 breccia	quartz-albite vein at 50dca, dark (biotite?) selvage, trace-1% pyrite (cubic and blebs <=1mm) surrounding vn, rusty orange alteration around vn	42383	1.24 g/t
1088	143	4.78	4.88	V3 breccia	quartz-carbonate veins at 60-70dca, one vein is folded, rusty alteration around veins	42384	2.5 g/t
1088	143	5.36	5.6	V3 breccia	quartz-carbonate veins at 60dca	42384/85	2.5 - 0.22 g/t
1088	143	6.79	6.89	V3 breccia	quartz-carbonate-albite vein at 70-80dca with rusty alteration, 1% py (cubic and blebs <=1mm) in vein and host	42387	2.61 g/t
1088	143	6.89	7.1	V3 breccia	blocky/brittle (tectonic) deformation of V3 breccia	42387	2.61 g/t
1088	143	7.56	7.7	V3 breccia/amygdular	quartz-albite vein at 55-60dca, py-biotite selvage, light rusty alteration around vein, 1% pyrite in rusty alteration (1-2mm)	42388	7.92 g/t
1088	143	8.3	8.42	V3 breccia/amygdular	quartz-albite vein with dark (chlorite-biotite?) selvage at 45dca cuts quartz-carbonate vein at 30-35dca, rusty alteration around quartz-carbonate and along one side of quartz-albite vein, 1-2% disseminated pyrite (cubic, 1mm) in rusty zones, pink coloured alteration in dark grey host	42389	8.42 g/t

Section	Hole	From	To	Rock Unit	Additional description	Sample #	Au Assay
1088	143	8.9	9.1	V3 massive?	quartz-albite vein with dark (biotite?) selvage at 70dca cut by quartz vein at -60dca (opposite direction), 1-2% pyrite (cubic and blebs <=1mm), rusty alteration around veins	42390	13.35 g/t
1088	143	9.15	9.34	V3 massive?	quartz-albite vein at 85dca, quartz-carbonate veins (no general direction), rusty weathering throughout, trace-1% pyrite (<1mm-2mm) in quartz-carbonate vein, trace magnetite?	42391	10.65 g/t
1088	143	10.3	10.51	V3 breccia	1% visible disseminated magnetite	42394	1.6 g/t
1088	143	11.31	11.57	V3 breccia	chlorite bands, rusty alteration with quartz-carbonate at 45 and -45dca and quartz-albite veins at 50-60dca, biotite stringers near veins, fine grained pyrite near veins, 2-3mm pyrite blebs in bands of rusty alteration	42395	31.9 g/t
1088	143	12.43	12.67	V3 breccia	quartz-albite-biotite-chlorite vein at 45dca with dark (biotite?) selvage, rusty alteration in and near vein, trace-1% pyrite (cubic <=1mm)	42397	4.26 g/t
1088	143	14.09	14.25	V3 breccia	Green and grey colour, quartz-carbonate vein at 60dca which contains pyrite	42400	0.95 g/t
1088	143	14.31	14.4	V3 breccia	boudined quartz-albite vein at 60dca with dark (biotite?) selvage, trace pyrite+chlorite? in vn, orange-beige crystals in and near vein	42401	9.59 g/t
1088	143	15.01	15.17	V3 breccia/amygdular	quartz-albite vein at 65dca with orange rusty crystals (ankerite?) and dark (biotite?) selvage, 1% pyrite (blebs <1m-3mm)	42402	10.35 g/t
1088	143	15.62	15.82	V3 massive	quartz-albite veins at 70-90dca with dark (biotite?) selvage, rusty alteration around vein, trace-1% pyrite (blebs <=1mm) in and near veins	42403	1.64 g/t
1088	143	16.31	16.5	V3 massive	weak to moderate biotite and calcite alteration, weak foliation at 65dca, quartz-albite vein with light orange (ankerite?) crystals and dark (biotite?) selvage, trace pyrite (blebs <1mm) in vein	42404	0.53 g/t

Section	Hole	From	To	Rock Unit	Additional description	Sample #	Au Assay
1088	143	16.51	16.78	V3 breccia/amygdular	1% disseminated pyrite blebs, trace white tabular crystals, visible disseminated magnetite, 10% white amygdules (1-3mm)	42404	0.53 g/t
1088	143	18.18	18.37	V3 breccia	3mm quartz-carbonate vein at 50-55dca, 1mm carbonate vn at 50-55dca, trace fine grained disseminated magnetite+pyrite	42407	1.7 g/t
1088	143	19.1	19.33	V3 breccia	deformed quartz-carbonate veins at 70-75dca, some with biotite selvages, local increase in pyrite (cubic, 1mm) near and in veins	42408	2.45 g/t
1088	143	19.55	19.69	V3 breccia	boudined quartz-albite vein at 75dca, dark (biotite?) selvage, trace pyrite along vein	42409	0.42 g/t
1088	143	24.16	24.35	V3 breccia	fractured in places, stockwork carbonate veins (1mm)	42414	0.04 g/t
1088	143	26.5	26.64	V3 breccia/QFP 2	contact between V3 breccia and QFP 2	42416/17	0.03 - 0.2 g/t
1088	143	26.82	27.04	QFP 2		42417	0.2 g/t
1088	143 ^{1,2}	27.82	27.96	QFP 2/V3 breccia	QFP 2 lower contact with V3 breccia	42418	0.44 g/t
1088	143	28.1	28.26	V3 breccia	quartz-carbonate vein at 25dca with green inside cuts 1mm stockwork carbonate vns, trace fine grained pyrite+pyrrhotite, moderate biotite alteration	42419	0.14 g/t
1088	143	28.68	28.82	V3 breccia	<1mm quartz-ccarbonate-pyrite-pyrrhotite vein at 30dca with green alteration halo appears to cut and offset <=1mm carbonate veins at -60dca	42420	0.02 g/t
1088	143	29.58	29.78	V3 amygdular	deformed quartz-carbonate vein, starts into V3 amygdular	42421	0.01 g/t
1088	143 ^{1,2}	29.78	29.99	V3 amygdular	possibly with V3 breccia, 10-15% white amygdules (1-2mm)	42421	0.01 g/t
1088	143	30.1	30.23	V3 amygdular	deformed quartz-carbonate vein with some pyrrhotite at 70dca appears to cut vein at -30dca, green chlorite banding	42422	

Section	Hole	From	To	Rock Unit	Additional description	Sample #	Au Assay
1088	143	30.44	30.66	V3 amygdular	grey/green coloured with quartz-carbonate vein at 55dca	42422	
1088	151	1.15	1.34	V3 carbonitized - rusty	quartz-carbonate-pyrite vein with white elongated crystals, some carbonate is beige-brown in vein + chlorite, 8% pyrite (blebs <=2mm)	42336	11.95 g/t
1088	151	1.55	1.7	V3 amygdular	quartz-carbonate vein with chlorite+/-biotite selvage, 5% pyrite blebs (<1mm) in/along vns, white tabular crystals	42337	5.02 g/t
1088	151	2.04	2.21	V3 amygdular	5% calcite amygdules (<=1mm)	42338	0.34 g/t
1088	151	2.49	2.72	V3 massive	quartz-carbonate-epidote vein at 50dca	42338	0.34 g/t
1088	151	3.1	3.27	V3 amygdular	quartz vein (1mm) at 50dca cuts epidote vn (1-2mm+halo in places) at 20dca	42339	1.83 g/t
1088	151	4.34	4.46	V3 massive/feldspar-phyric	2 quartz-carbonate-pyrite (<2mm) veins at 40dca, white tabular crystals, looks slightly brecciated	42341	0.03 g/t
1088	151 ^{1,2}	4.91	5.14	V3 mass/feldspar-phyric	trace fine grained disseminated pyrite, trace of white tabular crystals	42342	0.03 g/t
1088	151	5.7	5.83	V3 mass/feldspar-phyric	biotite and calcite shear at 65dca, with quartz-carbonate-chlorite-pyrite (3-5mm) vein	42343	0.43 g/t
1088	151	5.97	6.19	V3 mass/feldspar-phyric	quartz-carbonate-pyrite-chlorite veins with dark (biotite?) selvage	42343	0.43 g/t
1088	151	7.04	7.2	V3 breccia	rusted quartz-carbonate-pyrite vein with infilling texture at 20dca +/- epidote, cut by white quartz-carbonate vein at 40dca	42344	0.02 g/t
1088	151 ^{1,2}	8.02	8.29	V3 breccia		42346	2.91 g/t
1088	151	8.42	8.65	V3 breccia	white quartz bleb with beige alteration halo	42346	2.91 g/t
1088	151	9.57	9.77	V3 breccia	flow and tectonic breccia, 7mm boudined quartz-albite vein at 50dca cut by 5cm brittle carbonate/quartz-carbonate vein at 40dca	42349	2.86 g/t
1088	151	10.08	10.2	V3 breccia	boudined quartz-carbonate vein at 60-65dca, 1-2% fine grained disseminated pyrite blebs	42350	2.28 g/t
1088	151	10.92	11.19	V3 breccia	near QFP contact, quartz-carbonate-albite +/-biotite vein with rusty surface alteration at 40dca, this vein cuts into adjacent QFP	42351	12.95 g/t

Section	Hole	From	To	Rock Unit	Additional description	Sample #	Au Assay
1088	151 ^{1,2}	11.41	11.61	QFP cro? / QFP 1?	bt selvages along the q-alb vns (q-alb unusual to begin with in QFP), cl replacemnt of mafics	42352	0.49 g/t
1088	151	11.76	12.02	QFP/V3 breccia / amygdular	quartz-albite veins (these veins unusual in QFP - often are white quartz) with dark (biotite?) selvages, chlorite replacement of mafics in QFP	42352	0.49 g/t
1088	151	12.52	12.67	V3 breccia/amygdular	quartz-carbonate-pyrite veins at 60-70dca with dark (biotite?) selvage, pyrite blebs (<=5mm)	42354	3.96 g/t
1088	151	13.39	13.57	V3 breccia/amygdular	quartz-carbonate +/-chlorite veins, trace pyrrhotite in veins, beginning of visible disseminated magnetite	42355	0.75 g/t
1088	151	13.57	13.72	V3 massive?	visible disseminated magnetite (~1mm)	42355	0.75 g/t
1088	151	13.85	14.05	V3 breccia		42356	0.52 g/t
1088	151	14.8	14.93	V3 breccia/amygdular	carbonate-chlorite-biotite veins at 50-55dca	42357	0.21 g/t
1088	151	16.24	16.45	V3 breccia	grey/green "swirled" texture	42359	0.02 g/t
1088	151 ^{1,2}	19.34	19.52	Shear in V3	biotite and calcite shear at 30dca, 5-7cm quartz (with minor calcite) vein at 30dca, fine grained disseminated pyrite throughout	42363	0.63 g/t
1088	151	19.94	20.08	V3 breccia/amygdular	1cm 'blocky boudined' quartz vein at ~10ca	42364	0.12 g/t
1088	151	20.69	20.92	V3 breccia/amygdular	deformed amygdules - end is likely fault zone, blobs likely quartz veins boudined and rotated?, biotite and calcite alteration throughout, foliation at 45dca	42365	0.04 g/t
1088	151	21.07	21.29	V3 breccia	light beige coloured alteration - hard, possibly fine grained carbonate alteration (calcite or dolomite)	42366	0.01 g/t
1088	151	22.65	22.83	V3 mass? / breccia?		42368	0.01 g/t
1088	151	23.61	23.75	T3	fine and medium grained, becoming coarser grained downhole, to bottom of hole	NO SAMPLE	
1088	151	23.84	24.06	T3		NO SAMPLE	
1088	151 ^{1,2}	24.32	24.43	T3	medium grained	NO SAMPLE	
1088	151	24.82	25.03	V3 breccia		NO SAMPLE	

Section	Hole	From	To	Rock Unit	Additional description	Sample #	Au Assay
1088	151	25.64	25.84	V3 breccia? / T3?		NO SAMPLE	
1088	151	26.2	26.52	V3 breccia		42369	0.01 g/t
1088	151 ^{1,2}	27.33	27.49	V3 amygdular	quartz-carbonate-epidote vein at 75dca cut by micro vn at -15dca (opposite direction to previous vein)	42371	0.01 g/t
1088	151	29.54	29.71	V3 breccia		42373	0.01 g/t
1088	151 ^{1,2}	30.9	31.1	T3	fine to medium grained, fining uphole, from no vis crystals to 1-2mm crystals near bottom of hole	NO SAMPLE	
1124	27 ^{1,2}	2.63	2.78	V3 massive/breccia	possibly some amygdules (3+mm) or inclusions, trace fine grained disseminated pyrite and magnetite	585531	0.42 g/t
1124	27 ^{1,2}	3.24	3.53	V3 massive/breccia	quartz-albite veins stained pink/red at 20-25dca, dark rusty orange alteration, 1-3% fine grained disseminated pyrite (<=3mm)	585532	13.23 g/t
1124	27	7.2	7.4	V3 massive/breccia	possibly some amygdules (1-2mm), quartz or quartz-carbonate vein + pyrite, no rusty alteration	595540	2.12 g/t
1124	27	10.12	10.25	V3 massive/breccia	pinch and swell quartz-albite vein at 40dca, pyrite blebs <1mm-3mm, rusty orange alteration	585545	12.61 g/t
1124	27	10.77	11.03	V3 massive/breccia	folded quartz-albite vein, fine grained disseminated magnetite+pyrite, rusty orange alteration	585547	2.79 g/t
1124	27	11.33	11.6	V3 massive/breccia	sharp contact of rusty orange alteration and green-grey coloured V3	585548	3.34 g/t
1124	27	12.77	12.94	V3 massive/breccia	quartz-albite veins (somewhat folded) at 40dca with dark (biotite?) selvage, rusty orange alteration, pyrite (<1mm in host to 5mm in vein)	585552	14.64 g/t
1124	27	14.85	14.96	V3 breccia	quartz-carbonate vein with pyrite+pyrrhotite, grey/green coloured host	585556	4.05 g/t
1124	27	16.87	17.01	V3 breccia	"swirled" texture	585558	0.03 g/t
1124	27	17.72	18	V3 breccia	green and grey coloured, weak foliation at 70dca	585559	0.21 g/t
1124	27	18.79	18.98	V3 breccia	dark green and brown coloured	585561	0.03 g/t
1124	27	20.67	20.9	V3 breccia/amygdular	5% dark amygdules	585563	0.03 g/t

Section	Hole	From	To	Rock Unit	Additional description	Sample #	Au Assay
1124	27	22.34	22.54	V3 breccia/amygdular	medium to light grey, green and brown coloured, 2-3% amygdules	585565	0.03 g/t
1124	27	22.93	23.21	QFP 2	50-60% feldspar, 3-5% quartz, 10% mafics (some elongated to <1mmx3mm), other crystals ~1x1-3x3mm	585566	0.17 g/t
1124	27	25.55	25.73	V3 breccia/amygdular	<=5% amygdules, rusty coloured alteration	585569	0.03 g/t
1124	27	28	28.2	V3 breccia/amygdular	quartz-carbonate vein at 50dca, 1-2cm rusty band at 70dca, dark grey host, 1% disseminated pyrite	585572	5.9 g/t
1124	27	28.64	28.83	V3 breccia/amygdular	more veins here - carbonate veins at 50dca with orange coloured staining	585573	0.07 g/t
1124	136	0.14	0.4	V3 breccia	pinch and swell quartz+albite veins at 45-50dca, medium to light grey	42423	2.45 g/t
1124	136	0.77	0.94	V3 breccia	background with weak rusty orange alteration quartz-albite vein with biotite in fractures vein, folded small rusty vns, trace-1% fine grained disseminated pyrite, weak rusty alteration	42424	4.55 g/t
1124	136	1.85	2.09	V3 breccia	green and grey coloured, unaltered, fine grained disseminated magnetite	42426	0.2 g/t
1124	136	2.09	2.24	V3 breccia	quartz or quartz-carbonate vein with dark (biotite?) selvage, rusty alteration bands and fine grained disseminated pyrite near veins, medium grey background colour	42427	6.99 g/t
1124	136	2.55	2.78	QFP?	upper contact at ~65dca, crystal boundaries are "smeared" and one cannot tell for sure if it was a QFP, foliation follows upper contact, 15% elongated mafic crystals	42427/28	6.99 - 0.61 g/t
1124	136	5.87	6.03	V3 massive/breccia	quartz-albite vein with dark (biotite?) selvage at 65dca, rusty alteration bands, visible disseminated magnetite and pyrite	42432	6.64 g/t
1124	136	7.26	7.45	V3 massive/breccia	Green and grey coloured, 1% visible disseminated magnetite	42435	2.59 g/t

Section	Hole	From	To	Rock Unit	Additional description	Sample #	Au Assay
1124	136	7.58	7.8	V3 massive/breccia	boudined quartz-albite veins with dark (biotite?) selvage at 65-70dca, 1% pyrite in and near veins, rusty orange colour	42436	16.85 g/t
1124	136	8.1	8.32	V3 massive/breccia	quartz-albite vein at 70dca, rusty orange and brown (biotite?) alteration, dark rusty orange at 8.32m for 2 cm on either side of a natural fracture, 1% disseminated pyrite within rusty zones	42437	22.7 g/t
1124	136	8.43	8.63	V3 massive/breccia	quartz-albite veins, 80-90% pyrite in large blebs	42437	22.7 g/t
1124	136	9.7	9.89	V3 breccia/massive	medium grey and green contact here, 1% visible disseminated magnetite	42439	0.82 g/t
1124	136	10.23	10.57	V3 breccia/massive	"mottled" look in places, not normal look of breccia	42440	0.56 g/t
1124	136	13.83	14	V3 breccia/amygdular	quartz-albite veins with dark (biotite?) selvage at 45dca, rusty orange alteration, 1-3% pyrite (cubic <=2mm)	42445	6.95 g/t
1124	136	14.11	14.42	V3 breccia/amygdular	green and grey	42445	6.95 g/t
1124	136 ^{1,2}	16.26	16.46	V3 breccia/amygdular	boudined quartz-albite vein at 55 dca cuts/cut by white quartz vein at 70dca, rusty orange and brown alteration, fine grained disseminated pyrite	42449	24.8 g/t
1124	136	16.46	16.62	V3 amygdular	contact between rusty alteration and green-grey coloured V3 at 70dca, fine grained disseminated pyrite in rusty alteartion, 1% disseminated magnetite (<=1mm) in grey-green, 5% white amygdules (2mm)	42449	24.8 g/t
1124	136	17.93	18.18	V3 breccia	quartz-albite veins at 70dca, rusty orange and brown (biotite?) alteration, "swirled" texture in places, fine grained disseminated pyrite	42455	15.6 g/t
1124	136	18.18	18.35	V3 breccia/amygdular	quartz-albite veins at 70dca, rusty orange and brown (biotite?) alteration, "swirled" texture in places, disseminated pyrite (<=5mm)	42455	15.6 g/t

Section	Hole	From	To	Rock Unit	Additional description	Sample #	Au Assay
1124	136	19	19.23	V3 breccia	green and grey coloured, bands of weak biotite alteration, few to no veins, very weak rusty alteration (if any), trace fine grained disseminated magnetite	42457	4.68 g/t
1124	136	23.66	23.88	V3 breccia/amygdular	green and grey coloured, up to 5% amygdules (clustered), 2mm quartz-carbonate vein at 60dca	NOT SAMPLED	
1124	136	25.04	25.22	V3 bre? or pillow?	discolouration is larger in this area, possible pyrrhotite in quartz-carbonate vein	NOT SAMPLED	
1124	136	26.67	26.86	V3 breccia	unaltered, green and grey colour, one area of chlorite/biotite bands	NOT SAMPLED	
1124	136	29.23	29.59	QFP 1	upper contact with V3 breccia at 55dca, 50% quartz, 10% feldspar, 10% mafics, 30% aphanitic matrix	NOT SAMPLED	
1124	136	30.08	30.3	V3 amygdular	amygdules <=1mm, slight foliation at 55dca	NOT SAMPLED	
1124	136	32.43	32.62	V3 breccia/amygdular	biotite or magnetite around blebs in the medium grey background	NOT SAMPLED	
1124	136	33.3	33.49	V3 breccia/amygdular	amygdules 2-3mm, band of lighter grey colour, stockwork of 2mm quartz-carbonate veins (1-2%)	NOT SAMPLED	
1124	136	35.15	35.39	V3 breccia	white quartz vein with dark metallic looking mineral (biotite?), beige to brown colour, trace-1% amygdules, no pyrite visible	NOT SAMPLED	
1124	201	20.88	21.07	Qtz Monzonite	background crystals look "smeared" with some well formed feldspar crystals, quartz veins with strong red staining throughout, QFP is pink/beige colour, some feldspar crystals have pink colour, (hematite/kspar alteration?)	249054	0.131g/t

Section	Hole	From	To	Rock Unit	Additional description	Sample #	Au Assay
1166	101 ^{1,2}	5.5	5.67	Diorite 2	fine-grained dyke: with 8-10% elongated mafics (biotite?) 0.5mmx2mm		
1166	101	15.35	15.45	QFP	QFP 2 ? Crystal boundaries smeared/blurred, 50% fine-grained dark grey matrix, 40% white feld/quartz crystals (2-3mm), 10% mafic (2-3mm)		
1166	101 ^{1,2}	15.71	15.92	Diorite 3	Fine-grained mafic dyke (associated with QFP) and contact with V3 Massive		
1166	101 ^{1,2}	21.29	21.4	V3 Massive/feldspar-phyric			
1166	182 ^{1,2}	3.42	3.53	QFP	QFP: 50% matrix, 5% quartz, 40% feldspar, 3% chlorite, 2% other mafics (biotite?) This dyke has fine-grained mafic dykes along the margin (see 182-3.71)		
1166	182 ^{1,2}	3.71	3.81	Diorite 3	Fine-grained mafic dyke along QFP 2 margin		
1166	182 ^{1,2}	23	23.14	QFP	QFP: 50% matrix, 40% feldspar/quartz, 10% mafic (5% biotite, 5%chlorite)		

Appendix C
STRUCTURAL DATA AND FAULT PLANE RESOLUTION
METHOD

C1. Structural Measurements

Structural measurements were taken during detailed mapping of the Barry deposit main zone in the 2006 field season, and during sampling/general mapping during the 2007 field season, including foliation, faults, lithologic contacts, orientations of intrusive dikes, vein orientations, and fold axis of folded veins and volcanic rocks (Table C1). Structural measurements were plotted on stereonet (Fig. 2.15) in order to determine the general orientation of structures and the relationships between key structures.

Table C1: Location and description of structural measurements

Measurement Type	Grid E	Grid S	Strike	Dip	Trend	Plunge	Description
fold axis in mafic volcanics	1167.5	68.5			48	48	folded mafic volcanic
fold axis in mafic volcanics	1167.5	69			61	48	folded mafic volcanic
fold axis in mafic volcanics	1160	96			254	40	folded amygdular basalt
fold axis in mafic volcanics	1160	96			266	42	folded amygdular basalt
fold axis in mafic volcanics	1089	66			70	25	folded mafic volcanic
fold axis in mafic volcanics	1167.5	67.5			73	40	gently dipping folded bedding?
fold axis in mafic volcanics	1085.4	65.8			78	28	gently dipping folded bedding?
fold axis in mafic volcanics	1088.8	66			68	20	fold of contact between pillow and breccia units
contact	1160	71.5	56	68			south contact between diorite 2 dike and mafic volcanics
contact	1167	60	56	80			south contact between QFP dike and pillow basalt
contact	1157	59.5	54	62			south contact between QFP dike and mafic volcanic
contact	1160	94	70	60			south contact between QFP dike and mafic volcanic
contact	1160	94	48	60			estimated south contact between QFP and mafic volcanic
contact	1075.5	84	57	64			north contact of QFP/diorite 3 dike and mafic volcanics
contact	1089.5	64	65	40			south contact of QFP/diorite 3 dike and mafic volcanics
contact	1150.3	71.4	40	76			QFP dike and breccia contact
contact	1165	69.75	80	70			diorite 1 dike and amygdular/breccia contact
foliation	1173.5	73	62	90			
foliation	1167	73	70	60			
foliation	1161.5	74.5	78	52			
foliation	1158	70	47	40			
foliation	1151	70	60	45			
foliation	1151.5	64.5	28	40			
foliation	1161	68	40	40			
foliation	1164.5	65	72	38			rusty alteration

Measurement Type	Grid E	Grid S	Strike	Dip	Trend	Plunge	Description
foliation	1169	64	24	28			
foliation	1169	67	68	40			
foliation	1157	62	50	40			
foliation	1154	58	68	40			
foliation	1119	78.5	68	72			rusty alteration
foliation	1070.5	95	60	60			
foliation	1077	97.5	76	32			
foliation	1075.5	91	64	66			
foliation	1070	85	68	44			
foliation	1083	89	62	63			
foliation	1088.5	80	79	50			
foliation	1075.5	84	57	64			
foliation	1077	71.5	64	48			
foliation	1080.5	75.5	79	52			
foliation	1087.5	71	58	60			
foliation	1085	71	63	66			
foliation	1085	67	66	45			
foliation	1085	65.5	59	38			
foliation	1086	64	56	44			
foliation	1089	62	66	44			
foliation	1034	84	56	60			rusty alteration
foliation	1167.5	59.25	36	42			
foliation	1168	63	26	32			
foliation	1164	64	56	32			
foliation	1163.5	62	46	40			
foliation	1152.5	60	63	53			
foliation	1155.5	65	55	40			

Measurement Type	Grid E	Grid S	Strike	Dip	Trend	Plunge	Description
foliation	1159.75	62.25	44	36			
foliation	1151.6	74.4	52	62			
foliation	1153.9	68.4	57	58			
foliation	1155.1	65.1	55	40			
foliation	1162	70.25	54	56			
foliation	1159.75	74.5	48	50			
foliation	1167.25	68	64	70			
foliation	1164.75	70.5	54	46			foliation at contact of large QFP dike and V3
foliation	1167.4	71	44	54			
foliation	1166.25	73.75	46	54			
foliation	1168.5	73	24	34			
foliation	1169	73	70	76			
foliation	1070.75	95	60	56			
foliation	1072	91.4	56	56			
foliation	1072.5	89.7	58	54			
foliation	1072	90	52	55			with lineation raking 60 from NE
foliation	1077	90.4	54	72			
foliation	1080	92.6	58	60			
foliation	1079.5	85.75	60	75			
foliation	1080.5	87.9	60	70			
foliation	1084.25	83.8	62	78			
foliation	1087.25	82.5	72	70			
foliation	1080.25	73.75	66	48			
foliation	1079	78.25	57	66			intense foliation
foliation	1084.25	66.75	60	56			
foliation	1087	64	66	54			
foliation	1091.1	60	330	77			

Measurement Type	Grid E	Grid S	Strike	Dip	Trend	Plunge	Description
foliation	1091.75	59	60	52			
stretching lineation	1170	62			92	38	stretching lineation on foliation plane
stretching lineation	1072	90			97	46	stretching lineation on foliation plane
fault plane	1080.5	73.9	55				early brittle/ductile fault
fault plane	1086	75.75	46	52			early brittle/ductile fault
fault plane	1081.5	78	62	72			early brittle/ductile fault
fault plane	1084	66	78	43			early brittle/ductile fault
fault plane	1085.75	65.4	50	52			early brittle/ductile fault
fault plane	1089.5	67.25	62	68			early brittle/ductile fault
fault plane	1090.75	59.75	60	72			early brittle/ductile fault
fault plane	1070	92	174	48			late brittle fault
fault plane	1072	90.5	168	86			late brittle fault
fault plane	1075	83	282	82			late brittle fault
fault plane	1085	82	165	53			late brittle fault
fault plane	1078	78	177	66			late brittle fault
fault plane	1075	76	3	85			late brittle fault
fault plane	1078	70	187	87			late brittle fault
fault plane	1080	75	180	74			late brittle fault
fault plane	1083	68	189	84			late brittle fault
fault plane	1085	63	348	90			late brittle fault
fault plane	1087.5	65	103	66			late brittle fault
fault plane	1091	62.5	188	42			late brittle fault
fault plane	1071.75	90.5	157	66			late brittle fault (separating blocks)
fault plane	1073.5	93.4	184	48			late brittle fault (separating blocks)
fault plane	1080.75	84	356	54			late brittle fault (separating blocks)
slickenline lineation	1080.5	73.9			103	38	slickenline lineation on early fault
slickenline lineation	1084	66			108	27	slickenline lineation on early fault

Measurement Type	Grid E	Grid S	Strike	Dip	Trend	Plunge	Description
vein, straight	1174	75	60	54			straight sugary quartz vein
vein, straight	1170	72	56	62			straight 5cm wide sugary quartz vein + pyrite
vein, straight	1160	74	58	64			straight sugary quartz vein
vein, straight	1156	68	60	60			straight sugary quartz vein with biotite/chlorite selvage
vein, straight	1152	74	75	70			straight pinch and swell quartz vein
vein, straight	1153	65	62	50			straight quartz vein with dark biotite/chlorite selvage
vein, straight	1167	68	102	58			straight quartz vein - short, appears to pinch out
vein, straight	1166.5	68.5	72	64			straight pinch and swell quartz vein
vein, straight	1150	61	62	64			straight quartz vein + pyrite with biotite/chlorite selvage
vein, straight	1153	59	60	55			straight quartz vein + pyrite with biotite/chlorite selvage
vein, straight	1160.5	63	60	50			straight 2cm wide sugary quartz vein with chlorite in vein
vein, straight	1140	61	70	60			straight quartz vein cuts the folded vein at the same location
vein, straight	1109	83	78	52			straight vein which cuts and is cut by the above folded vein
vein, straight	1158	91	76	68			straight sugary quartz vein, cuts folded vein at 000/45
vein, straight	1154	90	77	70			straight sugary quartz vein
vein, straight	1137	84	78	72			straight sugary quartz vein + pyrite with biotite/chlorite selvage
vein, straight	1125	76	66	72			straight sugary quartz vein
vein, straight	1121	81	46	60			straight sugary quartz vein with pyrite selvage
vein, straight	1119	78.5	67	58			straight quartz vein
vein, straight	1091	83	74	80			straight quartz vein
vein, straight	1100	71	65	68			straight quartz vein
vein, straight	1074	93.5	60	72			straight quartz vein
vein, straight	1070	96	70	60			straight quartz vein
vein, straight	1074	90	53	72			straight quartz vein
vein, straight	1075	87	62	52			straight quartz vein
vein, straight	1085	86.5	72	64			straight quartz vein
vein, straight	1089.5	84.5	64	64			straight quartz vein

Measurement Type	Grid E	Grid S	Strike	Dip	Trend	Plunge	Description
vein, straight	1090	74	58	63			straight quartz vein
vein, straight	1090	74.5	82	73			straight quartz vein
vein, straight	1082	80.5	80	66			straight quartz vein
vein, straight	1075	78	65	70			straight quartz vein
vein, straight	1075	72	66	64			straight quartz vein
vein, straight	1075	70	68	64			straight quartz vein
vein, straight	1082	76	69	85			straight quartz vein
vein, straight	1085.5	75	246	88			straight quartz vein
vein, straight	1087	77	81	85			straight quartz vein
vein, straight	1085	69	71	62			straight quartz vein
vein, straight	1087	68	56	56			straight quartz vein with dark biotite/chlorite selvage
vein, straight	1087	67	84	64			straight quartz vein
vein, straight	1091	64.5	80	38			straight quartz vein + pyrite with biotite/chlorite selvage
vein, straight	1089.5	60.5	60	50			straight quartz vein
vein, straight	1068	76	75	82			straight quartz vein cuts folded vein at 205/24
vein, straight	1068	76	248	80			straight quartz vein cut by folded vein at 205/24
vein, straight	1157.5	76.5	73	70			straight quartz vein
vein, straight	1051.5	85	65	88			straight quartz vein cut by folded vein at 183/68
vein, straight	1033.5	87	76	55			straight quartz vein
vein, straight	1153.75	64	50	57			straight vein in rusty alteration
vein, straight	1155	62	52	78			straight vein in rusty alteration
vein, straight	1155.75	61.75	46	86			straight vein in rusty alteration
vein, straight	1152.75	65.5	54	55			straight vein in rusty alteration
vein, straight	1161.75	64.75	64	65			straight vein in rusty alteration
vein, straight	1153.6	67.75	60	58			straight vein in rusty alteration

Measurement Type	Grid E	Grid S	Strike	Dip	Trend	Plunge	Description
vein, straight	1156.9	74.9	73	80			straight vein in rusty alteration
vein, straight	1155.5	69.25	57	52			straight vein in rusty alteration
vein, straight	1158	71.25	140	66			extensional vein in QFP
vein, straight	1169.5	66.25	60	65			straight vein in breccia/amygdular basalt
vein, straight	1165.5	72.5	65	68			straight vein in rusty alteration
vein, straight	1166.5	62.5	50	42			straight vein in rusty alteration
vein, straight	1074.25	93.25	54	75			straight vein in rusty alteration
vein, straight	1075.5	88.1	72	77			straight vein in rusty alteration
vein, straight	1077.75	82.4	68	78			straight vein in rusty alteration
vein, straight	1080.7	88.1	60	75			straight vein in rusty alteration
vein, straight	1083.5	86.6	66	50			straight vein in rusty alteration
vein, straight	1082.75	76	60	90			straight vein in rusty alteration
vein, straight	1082	79.25	60	59			straight vein in rusty alteration
vein, straight	1090.25	74.75	63	74			straight vein in rusty alteration
vein, straight	1090	75.1	60	72			straight vein in massive basalt
vein, straight	1084	68.9	62	60			straight vein in rusty alteration
vein, straight	1085.2	68.4	46	64			straight vein in rusty alteration
vein, straight	1083	67.25	60	65			straight vein in rusty alteration
vein, straight	84.25	65.1	53	70			straight vein in rusty alteration
vein, straight	1085	64.3	60	47			straight vein in rusty alteration
vein, straight	1089	67.75	64	52			straight vein in rusty alteration
vein, straight	1091.25	67.6	58	68			straight vein in rusty alteration
vein, straight with isoclinal fold	1076.5	96	62	80			straight vein with isoclinal folds
vein, straight with isoclinal fold	1077.5	93.5	65	62			straight vein with isoclinal folds
vein, straight with isoclinal fold	1080	95	65	70			straight vein with isoclinal folds (fold axis not measured)

Measurement Type	Grid E	Grid S	Strike	Dip	Trend	Plunge	Description
vein, straight with isoclinal fold	1077	91	75	68			straight vein with isoclinal folds (fold axis not measured)
fold axis of isoclinally folded vein	1076.5	96			56	28	isoclinal fold axis of straight vein 062/80
fold axis of isoclinally folded vein	1074.5	93.5			57	38	isoclinal fold axis of straight vein 065/62
vein, folded	1176	75	213	44			folded sugary quartz vein
vein, folded	1156	69	30	90			folded sugary quartz vein
vein, folded	1150	73	10	80			folded sugary quartz vein
vein, folded	1168	68	32	82			folded sugary quartz vein
vein, folded	1160.5	62	38	36			folded quartz vein
vein, folded	1148	70	0	78			folded quartz vein
vein, folded	1146	68	12	50			folded quartz vein
vein, folded	1140	61	40	62			folded quartz vein
vein, folded	1104	64	14	60			folded quartz vein
vein, folded	1110	72.5	203	50			folded quartz vein
vein, folded	1110	72.5	47	78			folded quartz vein
vein, folded	1109	83	198	34			folded vein
vein, folded	1106	82	10	90			folded vein
vein, folded	1158	91	0	45			folded quartz vein
vein, folded	1155	90	12	58			folded sugary quartz vein
vein, folded	1160	96	140	56			folded sugary quartz vein
vein, folded	1119	78.5	190	62			folded sugary quartz vein
vein, folded	1091	83	206	80			folded sugary quartz vein
vein, folded	1100	71	184	40			folded quartz vein cuts two straight veins and is cut by a third
vein, folded	1076	87	18	60			folded quartz vein - ambiguous relationships with straight veins

Measurement Type	Grid E	Grid S	Strike	Dip	Trend	Plunge	Description
vein, folded	1085	85.5	206	60			folded quartz vein
vein, folded	1089.5	86.5	30	60			folded quartz vein
vein, folded	1084	72	191	80			folded quartz vein
vein, folded	1068	76	205	24			folded quartz vein
vein, folded	1158.5	77	213	20			folded quartz vein
vein, folded	1054.5	73	230	80			folded quartz vein
vein, folded	1053.5	82	200	52			folded quartz vein
vein, folded	1051.5	85	183	68			folded quartz vein
vein, folded	1033.5	87	216	50			folded quartz vein
vein, folded	1165.75	71.75	20	56			folded vein in breccia/amygdule basalt
fold axis of folded vein	1150	73			130	78	fold axis of folded vein 010/80
fold axis of folded vein	1148	70			240	42	fold axis of folded vein 000/78
fold axis of folded vein	1148	70			257	78	fold axis of folded vein 000/78
fold axis of folded vein	1146	68			90	54	fold axis of folded vein 012/50
fold axis of folded vein	1140	61			90	60	fold axis of folded vein 040/62
fold axis of folded vein	1104	64			87	60	fold axis of folded vein 014/60
fold axis of folded vein	1110	72.5			246	50	fold axis of folded vein 246/50
fold axis of folded vein	1109	83			210	40	fold axis of folded vein 198/34
fold axis of folded vein	1106	82			68	85	fold axis of folded vein 010/90
fold axis of folded vein	1158	91			248	55	fold axis of folded vein 000/45
fold axis of folded vein	1155	90			107	50	fold axis of folded vein 012/58
fold axis of folded vein	1160	96			234	45	fold axis of folded vein 140/56
fold axis of folded vein	1119	78.5			257	50	fold axis of folded vein 190/62
fold axis of folded vein	1091	83			53	44	fold axis of folded vein 206/80
fold axis of folded vein	1100	71			243	48	fold axis of folded vein 184/40
fold axis of folded vein	1085	85.5			243	38	fold axis of folded vein 206/60
fold axis of folded vein	1089.5	86.5			91	58	fold axis of folded vein 030/60

Measurement Type	Grid E	Grid S	Strike	Dip	Trend	Plunge	Description
fold axis of folded vein	1068	76			247	40	fold axis of folded vein 205/24
fold axis of folded vein	1158.5	77			235	30	fold axis of folded vein 213/20
fold axis of folded vein	1053.5	82			250	50	fold axis of folded vein 200/52
fold axis of folded vein	1033.5	87			246	48	fold axis of folded vein 216/50

C2. Fault Plane Resolution Method

An early brittle-ductile fault, 1 to 5m wide, observed at surface from line 10+45E to line 11+75E between stations 0+65S and 0+70S marks the northern boundary of the mineralized zone (Fig. 3). Slickenlines on the early faults trend and plunge $105^{\circ}\rightarrow 33^{\circ}$, and rake on the fault plane approximately 55° from the northeast (Fig. 16B). Based on the off-sets of a QFP marker unit and attitude of the slickenlines, the northern-most early fault is interpreted to be brittle-ductile anastomosing shear zone with the latest brittle movement along the fault interpreted as oblique reverse dextral, with the SE block having moved up and towards the SW relative to the NW block, as shown from the fault plane resolution method (Davis, 1984) conducted in the northeast corner of the trenched region (below). For this method the fault is taken to strike 060° and dip 45° SE and the marker QFP is taken to strike 045° and dip 45° SE, with an intersection lineation between the fault and QFP of raking 87° from the NE in the fault plane (Fig. C1).

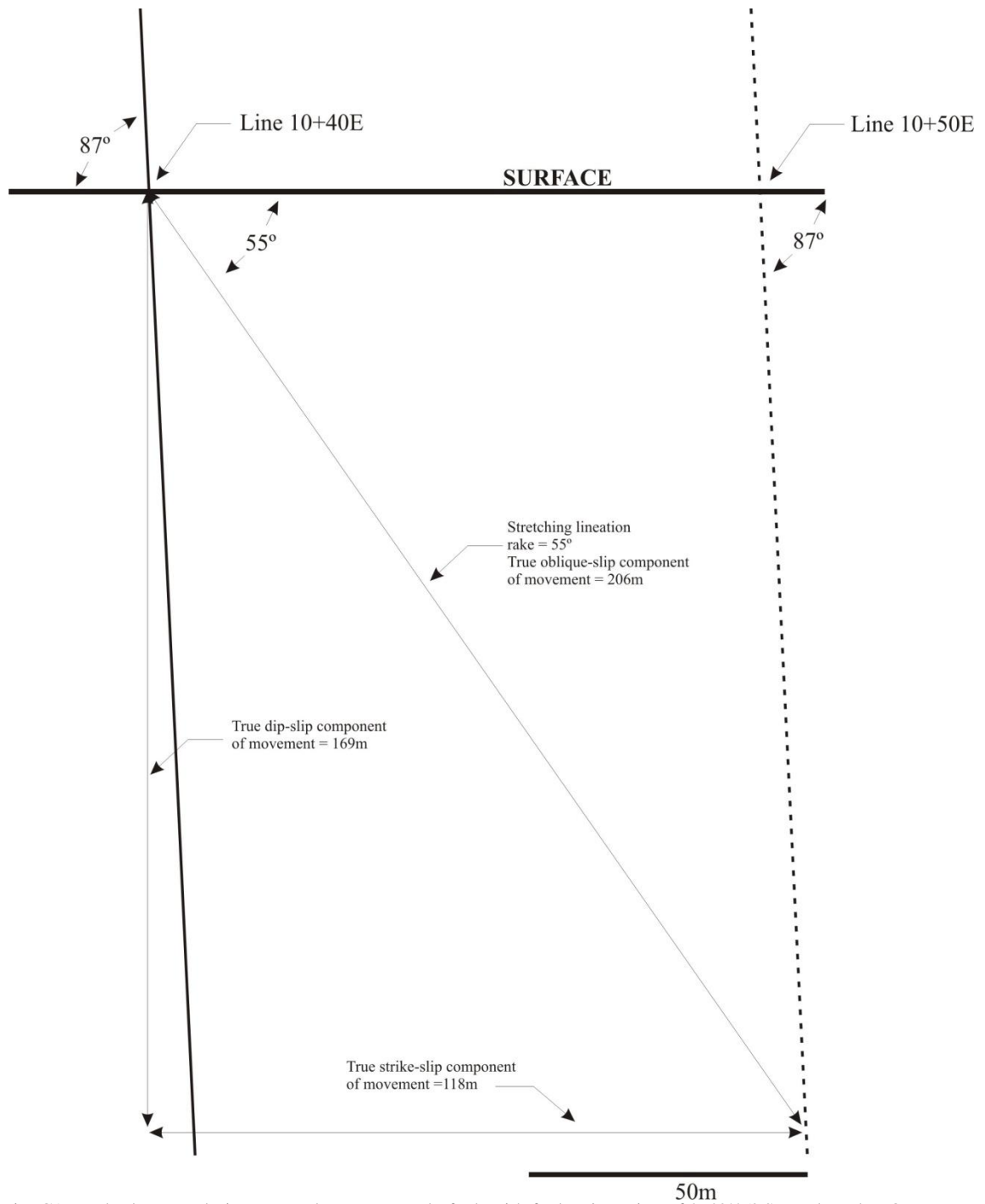


Fig. C1: Fault plane resolution on northern-most early fault with fault orientation of $060^{\circ}/45^{\circ}$ SE and marker QFP orientation of $045^{\circ}/45^{\circ}$ SE showing the true components of movement on the fault. The view is perpendicular to the plane of the fault, looking at 330° and plunging 45° , so that the offset on the fault is seen in true length. Solid lines represent features on the hanging wall (south side) and the dotted line represents a feature on the footwall (north side)

of the fault. The true oblique offset calculated in this model is 206m, with a reverse-dextral sense of movement (ie. the south block moved up and towards the west relative to the north block).

Appendix D
LITHOGEOCHEMISTRY

Lithogeochemical data were applied to discriminate between the tectonic settings in which mafic volcanics (Fig. 2.8-2.10) and intrusive rocks (Fig. 2.14) formed. These data were also used to construct isocon diagrams (Fig. 2.20) of syn-ore carbonate-quartz-pyrite and biotite-carbonate alteration to determine the elements enriched and depleted in mafic volcanic rocks that have undergone these types of alteration.

D1. Sample Preparation for Whole Rock Analysis

Surface and drill core samples were taken from various lithologies across the main zone (including rusty carbonatized zones: Appendix B). Samples collected in the field were cut to fist-size (for surface samples) and smaller fragments (for drill core ¼ core) using a rock saw at Queen's University. All samples were greater than 30g in size (minimum required for whole rock analysis conducted at Acme Labs). Samples were sent to Acme Labs in Vancouver, British Columbia, and were prepared using the code R150: crush, split and pulverize rock to 150 mesh (106 µm).

D2. Analytical Precision in Major and Trace Element Chemical Analysis

Selected drill core and surface samples (97 samples) were analyzed using a Lithium metaborate / tetraborate fusion and nitric acid digestion followed by ICP-emission spectrometry and ICP mass spectrometry (ICPMS) respectively for whole rock and selected trace element determination. A split of each sample was digested in aqua regia and analyzed by ICPMS for precious and base metals, including tellurium for all samples. All samples were analyzed for precise determinations of gold using the classical lead collection fire assay, and selected samples were also analyzed for silver, platinum and

palladium. A subset of intrusive rock samples were analyzed for fluorine. Geochemical analyses were conducted at Acme Labs.

Table D1 summarizes the elements analyzed, the method used, and the upper and lower detection limits for each element.

Table D1: Analytical precision in major and trace element chemical analysis

Analysis Type	Method	Element	Detection Limit	Upper Limit	
Whole Rock Group 4A (<i>SiO₂, Al₂O₃, Fe₂O₃, CaO, MgO, Na₂O, K₂O, MnO, TiO₂, P₂O₅, Cr₂O₃, LOI, C, S</i>)	0.1 g sample dissolved using Lithium metaborate/tetraborate fusion and dilute nitric digestion, then analysed by ICP-emission spectrometry. Loss on ignition (LOI) is by weigh difference after ignition at 1000°C. Total C and S by Leco.	SiO ₂ , Al ₂ O ₃ ,	0.01%	100%	
		CaO, MgO,			
		Na ₂ O, K ₂ O,			
		MnO, TiO ₂ ,			
		P ₂ O ₅ , C, S	0.04%		
		Fe ₂ O ₃	0.002%		
		Cr ₂ O ₃	0.1%		
Whole Rock Group 4B (<i>Au, Ag, As, Ba, Be, Bi, Cd, Co, Cs, Cu, Ga, Hf, Hg, Mo, Nb, Ni, Pb, Rb, Sb, Sc, Se, Sn, Sr, Ta, Th, Tl, U, V, W, Y, Zn, Zr, La, Ce, Pr, Nd, Sm, Eu, Gd, Tb, Dy, Ho, Er, Tm, Yb, Lu</i>)	Rare earth and refractory elements are determined by ICP mass spectrometry following a Lithium metaborate/tetraborate fusion and nitric acid digestion of a 0.1 g sample. Precious and base metals (highlighted) are tested using a separate 0.5 g split digested in Aqua Regia and analysed by ICP mass spectrometry.	Au	0.5 ppb	100 ppm	
		Ag	0.1 ppm	100 ppm	
		As	1 ppm	10000 ppm	
		Ba		50000 ppm	
		Be		10000 ppm	
		Bi	0.1 ppm	2000 ppm	
		Cd	0.1 ppm	10000 ppm	
		Co			0.2 ppm
		Cs			0.1 ppm
		Cu			0.5 ppm
		Ga			0.1 ppm
		Hf			100 ppm
		Hg			2000 ppm
		Mo			50000 ppm
		Nb			10000 ppm
		Ni			
		Pb			
		Rb	2000 ppm		
		Sb			
		Sc	--	10000 ppm	
		Se	0.5 ppm	100 ppm	
		Sn	1 ppm	10000 ppm	
		Sr	0.5 ppm	50000 ppm	
		Ta	0.1 ppm		
		Th	0.2 ppm	10000 ppm	
		Tl	0.1 ppm	1000 ppm	
		U			
		V		8 ppm	
		W	0.5 ppm	10000 ppm	

Analysis Type	Method	Element	Detection Limit	Upper Limit
Whole Rock 4B <i>Continued...</i>		Y	0.1 ppm	50000 ppm
		Zn	1 ppm	10000 ppm
		Zr	0.1 ppm	50000 ppm
		La		
		Ce		
		Pr	0.02 ppm	10000 ppm
		Nd	0.3 ppm	
		Sm	0.05 ppm	
		Eu	0.02 ppm	
		Gd	0.05 ppm	
		Tb	0.01 ppm	
		Dy	0.05 ppm	
		Ho	0.02 ppm	
		Er	0.03 ppm	
		Tm	0.01 ppm	
		Yb	0.05 ppm	
		Lu	0.01 ppm	
Fire Assay (Au)	Fire assay on 30g sample, analysis by ICP-ES.	Au	0.01 g/t	
Fire Assay (Au, Ag*, Pt, Pd)	Fire assay on 30g sample. * Hot Aqua Regia digestion on a 1 g split for base-metal sulphide and precious metal ores. ICP-ES analysis.	Au, Pt, Pd	0.01 g/t	
		Ag*	0.2 g/t	
Tellurium	0.50 g sample leached with 3 mL 2-2-2 HCl-HNO ₃ -H ₂ O at 95°C for one hour, diluted to 10 mL, analysed by ICP-MS.	Te	1 ppm	
Flourine	Minimum 1g of pulp. Analysis by specific ion electrode following NaOH fusion.	F		

Table D2: Mafic volcanic rocks – whole rock analysis of major oxides, minor and trace elements

Type	A												
Lithology	Amygdular									Breccia			Carbonate Alteration
Sample	31-25.48	31-27.03	117-03.48	118-24.55	118-26.87	143-29.78	151-27.33	210-20.07	210-71.10	118-01.01	118-05.16	118-16.70	135-10.80
SiO ₂ (wt%)	51.38	52.46	45.14	53.96	54.48	50.97	53.55	47.49	48.80	38.41	42.47	47.64	48.56
TiO ₂	1.42	1.16	1.13	1.17	1.21	1.17	1.21	0.94	1.18	0.81	1.20	1.25	1.21
Al ₂ O ₃	17.32	14.83	14.17	14.80	15.06	15.19	15.13	14.11	15.38	14.33	15.61	16.34	12.73
Fe ₂ O ₃	11.17	10.20	11.28	12.05	13.76	11.02	12.98	14.08	13.78	9.66	10.79	13.02	11.84
MnO	0.20	0.23	0.19	0.21	0.23	0.24	0.18	0.16	0.29	0.18	0.21	0.29	0.17
MgO	2.44	2.26	2.62	2.42	2.52	2.17	2.18	3.42	2.82	4.13	2.16	2.98	1.73
CaO	7.72	9.81	10.51	8.78	7.97	10.28	6.51	9.60	11.47	13.70	10.81	11.58	8.83
Na ₂ O	4.11	3.01	3.96	1.69	2.12	2.93	6.28	2.94	2.88	2.75	3.56	1.32	6.53
K ₂ O	0.93	0.21	1.04	1.70	0.73	0.76	0.27	0.45	0.36	2.18	2.58	0.70	0.71
P ₂ O ₅	0.190	0.180	0.187	0.200	0.210	0.244	0.134	0.170	0.220	0.100	0.180	0.260	0.159
Cr ₂ O ₃	0.004	0.002	nd	0.002	0.003	0.003	0.002	0.005	0.004	0.006	0.003	0.002	0.004
LOI	3.1	5.6	9.7	3	1.7	5.0	1.6	6.6	2.8	13.7	10.4	4.6	7.5
Sum (%)	99.99	99.97	99.93	99.99	99.98	99.99	100.03	99.98	99.99	99.97	99.98	99.99	99.97
TOTAL S (%)	0.13	0.02	0.05	0.63	0.17	0.95	1.05	0.16	nd	0.16	0.16	0.11	4.22
Au (ppb)	15.2	16.4	0.0	2.5	11.7	110.9	26.4	2.6	3.1	27.0	1040.2	3.0	83009.8
V (ppm)	262	216	229	217	233	215	278	213	246	178	265	234	211
Sc	33	25	27	27	28	24	33	27	27	24	28	32	21
Co	50.2	35.4	41.3	40.9	41.7	37.0	35.1	46.3	48.1	46.2	37.7	35.5	46.5
Ni	39.7	30	36.8	30.5	31.7	31.7	12.8	60.6	19.1	77.5	40	34.5	46.1
Cu	13	3.7	7.4	44.7	25.7	92.1	122.3	47.1	5.7	58.2	25.7	11.5	80.6
Zn	90	73	97	97	77	84	61	89	47	82	76	94	59
As	1.1	0.8	0.7	0.8	1.1	1.3	1.0	0.5	0.9	1.1	0.8	0.9	2.0

Type	A												
Lithology	Amygdular									Breccia			Carbonate Alteration
Sample	31-25.48	31-27.03	117-03.48	118-24.55	118-26.87	143-29.78	151-27.33	210-20.07	210-71.10	118-01.01	118-05.16	118-16.70	135-10.80
Rb	27.5	5.7	22.9	56.1	20.8	22.3	5.7	14.3	5	59.3	51	20.2	25.0
Sr	318.2	299.6	185.4	176.2	174.1	190.9	158.6	349.1	260.6	222.1	299.4	233.6	240.1
Y	24.3	25	20.3	22.4	27.5	24.4	21.6	22.5	29.1	17.8	25.8	33.8	20.4
Zr	103.9	83.1	82.4	85.2	88.4	84.4	84.0	77.1	92.3	52	86.5	85.3	86.5
Nb	5.3	4.5	4.6	4.5	4.3	4.7	3.9	3.9	4.8	3	4.5	4.9	4.8
Mo	0.4	1.2	1.3	0.5	0.3	2.2	0.2	1	0.8	0.6	2	3.4	4.7
Ag	nd	nd	nd	nd	nd	0.1	0.1	nd	nd	nd	0.1	nd	7.2
Sn	1	1	nd	1	1	nd	nd	1	1	nd	1	1	nd
Sb	nd	nd	nd	nd	nd	nd	0.2	nd	nd	nd	0.1	0.1	nd
Cs	1.6	0.4	0.6	4.7	1.6	1.4	0.6	1.4	0.4	2.3	1.7	1.3	2.6
Ba	198.2	63.6	308	301.8	150.2	166	47	187.3	85.5	355	395.3	113.8	44
La	7.6	7.7	8.1	8.3	9.2	9.9	6.4	10.2	9.7	6.4	8.1	10	12.0
Ce	22.2	20.9	20.7	20.8	23.3	23.5	16.2	25.3	23.1	17.5	21.1	26.2	28.0
Pr	3.1	2.85	3.01	2.96	3.18	3.37	2.50	3.52	3.41	2.34	3	3.76	3.90
Nd	14.1	12.5	12.9	12.9	14.5	14.6	11.4	15.1	15.1	10.2	13	16.7	16.7
Sm	3.5	3.1	2.85	3.3	3.5	3.10	2.66	3.6	4	2	3.5	4.2	3.35
Eu	1.06	0.99	1.03	1.02	1.14	1.20	1.05	1.05	1.11	0.74	0.95	1.38	1.20
Gd	4.04	3.73	3.69	3.88	4.11	4.18	3.87	3.67	4.41	2.55	3.95	5.03	4.05
Tb	0.73	0.71	0.57	0.66	0.74	0.61	0.59	0.65	0.77	0.47	0.71	0.95	0.59
Dy	4.43	4.02	4.04	4.18	4.48	4.34	4.35	3.94	5.07	2.8	4.28	5.75	4.21
Ho	0.86	0.85	0.87	0.85	0.94	1.01	0.95	0.79	1	0.61	0.89	1.09	0.84
Er	2.75	2.46	2.54	2.39	2.66	2.95	2.96	2.39	2.92	1.81	2.59	3.35	2.49
Tm	0.42	0.34	0.37	0.35	0.43	0.44	0.43	0.33	0.42	0.27	0.42	0.49	0.37
Yb	2.79	2.32	2.23	2.36	2.78	2.73	2.80	2.17	2.85	1.73	2.57	3.19	2.26

Type	A												
Lithology	Amygdular						Breccia						Carbonate Alteration
Sample	31-25.48	31-27.03	117-03.48	118-24.55	118-26.87	143-29.78	151-27.33	210-20.07	210-71.10	118-01.01	118-05.16	118-16.70	135-10.80
Lu	0.42	0.36	0.35	0.39	0.42	0.42	0.41	0.34	0.42	0.29	0.39	0.47	0.35
Hf	2.7	2.3	2.2	2.3	2.4	2.3	2.4	2.2	2.6	1.4	2.3	2.1	2.5
Ta	0.3	0.3	0.2	0.3	0.3	0.2	0.2	0.2	0.3	0.2	0.3	0.3	0.3
W	1	1.1	1.7	0.7	0.9	0.7	nd	1.1	1.2	2	2.7	1.2	13.4
Pb	1.3	1	2.4	1.4	0.7	1.8	2.1	2.2	1.4	3.1	4.1	1.3	39.9
Bi	0.1	nd	nd	0.1	nd	0.1	0.2	nd	nd	nd	0.1	nd	13.3
Th	0.7	0.6	1.1	1	1.2	0.7	0.8	0.8	0.9	nd	1	1.2	0.6
U	0.2	0.2	0.3	0.2	0.3	0.3	0.2	0.3	0.3	0.1	0.2	0.3	0.7
Be	1	nd	nd	nd	nd	nd	nd	1	1	nd	1	nd	nd
Ga	19.2	16.5	16.8	17.2	16.4	17.9	16.0	14.8	17.7	13.1	16.9	17.8	19.9
Cd	nd	nd	0.1	nd	nd	nd	nd	nd	0.1	0.1	0.1	nd	nd
Hg	nd	0.01	nd	nd	nd	nd	nd	0.01	nd	0.01	0.01	nd	0.05
Tl	0.1	nd	nd	0.2	0.1	nd	nd	0.1	nd	0.1	0.1	0.1	0.1
Se	nd	nd	nd	nd	nd	nd	nd	nd	nd	nd	nd	nd	4.2
Te													
Pt		nd									nd		
Pd		nd									nd		
Ti (ppm)	8519.1	6959.2	6774.5	7017.1	7247.6	7010.8	7254.1	5639.4	7070.0	4857.5	7196.3	7499.2	7271.6
Ti/Zr	81.99	83.75	82.21	82.36	81.99	83.07	86.36	73.14	76.60	93.41	83.19	87.92	84.06
Zr/Y	4.28	3.32	4.06	3.80	3.21	3.46	3.89	3.43	3.17	2.92	3.35	2.52	4.24
La _N /Yb _N	2.72	3.32	3.63	3.52	3.31	3.63	2.29	4.70	3.40	3.70	3.15	3.13	5.31
% py+po	trace-1	2	trace	2-3		trace-1	5						10

Type	A												
Lithology	Feldspar-phyrlic						Massive						
Sample	31-30.23	31-31.06	118-12.39	31-17.89	101-21.29	117-22.07	117-26.66	118-03.62	118-05.98	118-07.19	151-04.91	151-08.02	210-24.16
SiO ₂ (wt%)	54.35	50.70	46.93	44.06	44.62	47.22	43.89	48.84	38.32	47.28	44.10	45.17	43.71
TiO ₂	1.08	1.13	1.18	0.79	1.28	0.79	0.96	1.24	1.42	1.12	1.28	0.83	1.01
Al ₂ O ₃	14.97	16.53	16.25	15.06	15.54	15.47	14.33	15.57	17.63	14.72	16.24	14.55	14.03
Fe ₂ O ₃	9.98	11.91	13.17	11.64	14.02	10.26	10.71	11.52	14.54	8.94	13.18	9.87	8.81
MnO	0.21	0.21	0.22	0.15	0.20	0.15	0.15	0.19	0.21	0.17	0.20	0.16	0.16
MgO	2.17	2.36	2.69	3.53	3.43	6.22	7.48	2.54	3.13	1.87	3.95	4.26	2.25
CaO	10.25	11.43	12.11	9.50	11.67	8.87	10.09	7.29	8.50	10.18	11.19	10.33	13.31
Na ₂ O	2.72	2.29	1.91	2.68	2.38	2.33	1.99	1.15	3.13	4.21	2.31	5.12	4.84
K ₂ O	0.37	0.34	0.34	1.93	0.30	1.39	0.11	3.24	3.39	1.82	0.92	0.11	1.07
P ₂ O ₅	0.180	0.160	0.170	0.130	0.187	0.107	0.127	0.200	0.110	0.170	0.184	0.121	0.160
Cr ₂ O ₃	0.003	0.003	0.002	0.012	0.003	0.034	0.027	0.002	0.003	0.002	0.003	0.011	0.006
LOI	3.7	2.9	5	10.5	6.4	7.1	10.1	8.2	9.6	9.5	6.4	9.5	10.6
Sum (%)	100.00	99.98	99.98	99.99	100.02	99.95	99.97	99.98	99.98	99.98	99.96	100.04	99.97
TOTAL S (%)	0.06	0.13	0.2	0.08	nd	nd	nd	0.07	0.26	0.19	0.05	0.18	0.36
Au (ppb)	234.7	645.0	23.0	137.4	0.0	0.0	5.2	52.0	124.0	16.0	8.1	30.1	97.0
V (ppm)	206	227	242	224	262	248	225	234	368	220	259	242	237
Sc	26	28	29	30	34	36	32	27	39	26	31	31	27
Co	42.6	40.1	45.8	33.2	46.6	42.7	41.0	37.6	49.8	31.4	51.0	37.5	38.6
Ni	30.8	29.2	45	50.8	36.5	80.0	84.9	38.4	49.6	30.3	42.0	48.4	54.5
Cu	8.1	23.1	50	25.4	2.7	1.2	16.3	20.8	55.8	35.8	10.8	7.2	58.4
Zn	75	71	104	91	108	94	88	92	94	73	124	106	77
As	1.1	1.1	2.9	0.5	0.7	1.1	0.6	0.5	2	nd	1.0	0.6	0.7
Rb	8.7	7.2	11.1	35.8	16.8	46.3	2.9	53.7	77.7	36.2	15.5	2.7	29.1
Sr	211.6	254.7	275.6	332.9	300.3	276.4	222.5	220.7	241.8	253.3	345.2	219.2	236
Y	23.7	24.5	24.9	15.8	23.3	16.2	15.9	25.7	25	22.3	26.5	14.0	17.3

Type	A												
Lithology	Feldspar-phyric						Massive						
Sample	31-30.23	31-31.06	118-12.39	31-17.89	101-21.29	117-22.07	117-26.66	118-03.62	118-05.98	118-07.19	151-04.91	151-08.02	210-24.16
Zr	79	88.8	86.3	57.7	94.2	50.6	63.8	88.2	112.3	79.6	92.3	59.5	79
Nb	4.4	4.4	4.5	2.4	5.2	3.0	3.8	4.7	5.4	4.1	5.0	2.7	4
Mo	1.9	1.2	0.6	0.6	0.4	10.7	0.4	0.8	6.6	4.6	0.3	0.3	1.5
Ag	nd	nd	nd	nd	nd	nd	nd	nd	nd	nd	nd	nd	nd
Sn	1	1	1	nd	nd	nd	nd	1	1	1	nd	nd	1
Sb	nd	nd	0.1	nd	nd	nd	nd	nd	nd	nd	nd	nd	0.1
Cs	0.5	0.4	0.8	0.8	1.1	4.0	0.3	1	2.9	1	0.5	0.3	1.9
Ba	170.9	143.2	81.3	421.5	38	379	36	482.9	997.6	460.9	182	25	521.4
La	7.8	7.9	7.6	9.5	9.6	6.1	5.7	7.8	8.2	7.2	8.9	12.1	7.9
Ce	20	21.7	20.6	25.3	23.6	15.1	15.1	20.7	20.7	19.6	21.6	28.3	18.9
Pr	2.79	2.9	2.91	3.21	3.38	2.23	2.18	2.88	2.83	2.7	3.10	4.01	2.65
Nd	12.1	11.9	12	14.4	14.8	9.8	9.6	12.5	13.5	11.8	14.9	16.8	10.9
Sm	3.2	3.2	3.1	3	3.22	2.00	2.21	3.1	3	2.9	3.32	2.80	2.4
Eu	0.96	1.02	1.13	0.82	1.16	0.80	0.78	1.02	0.97	0.89	1.13	0.95	0.76
Gd	3.76	4.02	3.85	2.69	4.30	2.84	2.90	3.96	3.62	3.62	3.99	3.06	2.57
Tb	0.66	0.7	0.72	0.43	0.66	0.43	0.45	0.7	0.65	0.62	0.73	0.42	0.45
Dy	4.13	4.12	4.27	2.78	4.33	3.09	3.18	4.28	4.06	3.82	4.42	2.77	2.88
Ho	0.81	0.87	0.95	0.52	0.99	0.66	0.66	0.87	0.87	0.78	0.95	0.63	0.61
Er	2.49	2.52	2.56	1.75	2.89	1.97	2.04	2.68	2.65	2.42	2.93	1.85	2.05
Tm	0.37	0.41	0.39	0.24	0.46	0.31	0.33	0.38	0.42	0.37	0.47	0.27	0.27
Yb	2.33	2.49	2.58	1.65	2.73	1.85	1.95	2.51	2.7	2.37	2.82	1.68	2.12
Lu	0.34	0.4	0.41	0.26	0.44	0.27	0.29	0.42	0.45	0.38	0.43	0.26	0.34
Hf	2.2	2.2	2.5	1.5	2.6	1.5	1.9	2.2	2.7	2	2.8	1.6	2.3
Ta	0.3	0.2	0.3	0.2	0.3	0.1	0.2	0.3	0.3	0.2	0.3	0.1	0.3
W	1	1.1	1	1.5	0.7	1.2	0.7	1.5	6.2	2.4	2.0	1.1	2.3

Type	A												
Lithology	Feldspar-phyric						Massive						
Sample	31-30.23	31-31.06	118-12.39	31-17.89	101-21.29	117-22.07	117-26.66	118-03.62	118-05.98	118-07.19	151-04.91	151-08.02	210-24.16
Pb	0.8	0.9	1.1	5	1.1	0.8	0.9	10.3	2.7	2.4	2.0	3.4	5.9
Bi	nd	nd	nd	0.1	nd	nd	nd	nd	0.1	nd	nd	0.1	nd
Th	0.7	0.6	0.5	0.8	0.7	0.5	0.6	0.5	0.7	0.5	0.7	0.9	0.6
U	0.2	0.2	0.2	0.2	0.4	0.3	0.2	0.2	0.2	0.2	0.3	0.3	0.3
Be	nd	1	nd	1	nd	nd	nd	nd	1	nd	1	nd	1
Ga	16.1	19	18.4	15.3	18.5	16.2	14.8	17.4	21.2	16.4	18.8	15.4	16
Cd	0.1	nd	nd	nd	nd	nd	nd	nd	nd	0.1	nd	nd	0.1
Hg	nd	0.01	0.01	nd	nd	nd	nd	nd	0.01	nd	nd	nd	0.01
Tl	nd	nd	0.1	nd	nd	0.1	nd	nd	0.2	nd	nd	nd	0.1
Se	nd	nd	nd	nd	nd	nd	nd	nd	nd	nd	nd	nd	nd
Te													
Pt	0.01												0.01
Pd	0.01												nd
Ti (ppm)	6479.9	6777.9	7079.9	4733.3	7663.0	4746.1	5770.3	7436.2	8520.8	6717.9	7665.3	4963.5	6060.5
Ti/Zr	82.02	76.33	82.04	82.03	81.35	93.80	90.44	84.31	75.88	84.40	83.05	83.42	76.72
Zr/Y	3.33	3.62	3.47	3.65	4.04	3.12	4.01	3.43	4.49	3.57	3.48	4.25	4.57
La _N /Yb _N	3.35	3.17	2.95	5.76	3.52	3.30	2.92	3.11	3.04	3.04	3.16	7.20	3.73
% py+po	trace	trace-1		trace	trace	0	trace	trace			trace-1	trace-1	

Type	A										B		
Lithology	Massive		Pillow			Biotite-calcite Alteration			Tuff		Amygdular		
Sample	210-65.11	210-74.00	59-1113	62-1088	62-1165	31-16.28	31-27.2	117-25.95	135-24.35	151-24.32	76-1028	88-1093	91-1119
SiO ₂ (wt%)	46.40	52.48	52.17	52.27	46.80	43.82	45.92	47.30	50.71	44.35	53.73	49.09	53.95
TiO ₂	1.24	1.40	1.26	1.22	0.83	0.76	0.85	0.89	1.30	0.76	1.21	1.25	1.30
Al ₂ O ₃	16.63	17.98	15.89	16.75	15.30	14.50	13.73	11.61	15.78	15.72	16.44	15.27	15.95
Fe ₂ O ₃	13.76	12.05	10.62	7.05	8.98	9.23	16.39	8.81	11.42	11.30	11.43	10.36	12.31
MnO	0.25	0.24	0.13	0.15	0.14	0.14	0.24	0.18	0.13	0.14	0.16	0.14	0.11
MgO	2.82	2.75	2.53	1.74	2.61	5.61	2.47	4.48	5.16	7.66	2.35	1.94	2.34
CaO	11.39	7.04	5.84	6.76	9.95	8.13	8.92	11.38	9.01	10.44	7.91	8.68	6.38
Na ₂ O	2.79	3.52	2.78	6.09	2.69	5.31	5.64	3.28	0.83	1.08	2.72	2.16	3.76
K ₂ O	0.80	0.53	2.16	1.07	2.60	1.51	1.84	2.47	1.53	1.46	0.60	2.48	0.35
P ₂ O ₅	0.200	0.180	0.200	0.170	0.170	0.150	0.080	0.208	0.201	0.099	0.240	0.190	0.220
Cr ₂ O ₃	0.003	0.003	0.004	0.002	0.008	0.005	0.002	0.018	0.011	0.020	nd	0.002	0.002
LOI	3.7	1.8	6.4	6.7	9.9	10.8	3.9	9.3	3.9	7.0	3.2	8.4	3.3
Sum (%)	99.99	99.99	99.99	99.98	99.97	99.97	99.99	99.92	99.99	100.03	100.00	99.97	99.99
TOTAL S (%)	0.04	0.29	0.35	0.05	0.23	0.54	4.02	0.51	0.05	nd	0.1	0.09	0.1
Au (ppb)	1.6	5.0	11.6	13.9	8.9	868.8	65518.1	253.2	55.0	2.2	39.8	31.9	6.3
V (ppm)	260	246	251	215	197	180	123	216	262	192	179	259	259
Sc	31	29	29	21	27	25	19	28	35	27	19	21	26
Co	49	38.5	35.3	32	33.8	40.4	37.6	26.6	30.1	54.9	26.5	35	35
Ni	32.6	39.8	36.2	32.2	59.1	63.7	36.6	57.1	36.9	190.9	7.1	32.5	43
Cu	13.2	46.4	31.1	12.5	37.4	60.6	207.9	135.5	23.1	0.8	75.2	47.7	39.3
Zn	79	79	72	59	46	69	73	87	100	74	88	83	102
As	0.8	0.6	0.5	nd	1.4	1	nd	1.0	0.7	0.7	1	nd	1.1
Rb	20.2	15.3	50.9	25.8	59.3	44.2	49.1	83.1	52.7	44.6	21.9	68.4	8.5
Sr	234.8	200.7	150.2	192	280.4	336.7	99.2	113.1	176.4	244.7	305.2	380.8	391.2

Type	A										B		
Lithology	Massive		Pillow			Biotite-calcite Alteration			Tuff		Amygdular		
Sample	210-65.11	210-74.00	59-1113	62-1088	62-1165	31- 31-16.28	27.2	117-25.95	135-24.35	151-24.32	76-1028	88-1093	91-1119
Y	28.5	25	19.9	20.4	19	16	13.7	16.9	24.1	11.8	25.4	23.3	24.2
Zr	96.6	91.5	84.3	86.4	54	51.3	59.3	69.1	104.8	44.2	142.8	118.6	120.2
Nb	4.9	5.6	4.6	4.8	3.1	3	3.3	4.5	5.7	2.6	6.2	5.7	5.6
Mo	0.2	0.4	0.8	0.5	1.2	1.6	11.4	1.6	0.5	1.5	1.7	0.5	0.3
Ag	nd	nd	nd	nd	nd	0.1	4.1	0.1	nd	nd	0.1	0.1	nd
Sn	1	1	1	1	1	1	1	nd	nd	nd	1	1	1
Sb	nd	nd	nd	nd	nd	nd	nd	nd	nd	nd	0.1	0.1	0.1
Cs	1	1.1	1.2	0.5	1.4	2.5	2.9	6.3	3.6	2.8	0.8	1.3	0.3
Ba	246.1	123.8	192.9	320.7	668	503.6	373.4	432	290	249	154.1	596.5	156.6
La	10.8	9.3	7.3	7.3	8.9	7.2	4.9	6.3	11.9	5.5	15.2	13.1	13.1
Ce	25.9	22.9	18.3	18.9	22.4	20.1	13.6	16.6	28.9	13.7	35.4	33	33.8
Pr	3.67	3.37	2.6	2.59	3.05	2.74	1.8	2.39	4.06	2.04	4.5	4.23	4.32
Nd	15.9	15.2	11.7	11.5	13.7	12.5	8.5	10.6	17.9	9.0	19.5	18.7	18.6
Sm	3.5	4.1	2.7	2.6	2.4	2.4	1.9	2.28	3.52	1.70	3.8	3.7	3.5
Eu	1.12	1.12	0.93	0.85	0.9	0.86	0.61	0.72	1.21	0.77	1.13	1.13	1.14
Gd	4.59	4.27	3.16	2.94	2.71	2.71	2.49	2.78	4.33	2.17	4.02	3.94	4.07
Tb	0.82	0.77	0.62	0.59	0.53	0.44	0.44	0.42	0.65	0.33	0.74	0.72	0.76
Dy	5	4.73	3.44	3.3	3.08	2.69	2.48	3.18	4.59	2.30	4.14	4.11	4.5
Ho	1.05	0.91	0.74	0.71	0.65	0.55	0.46	0.71	0.99	0.50	0.81	0.79	0.87
Er	2.98	2.52	2.18	2.21	2.02	1.61	1.48	2.17	2.99	1.50	2.5	2.36	2.8
Tm	0.41	0.35	0.33	0.36	0.32	0.24	0.21	0.34	0.45	0.23	0.41	0.38	0.41
Yb	2.96	2.38	2.2	2.24	2.03	1.59	1.35	2.07	2.87	1.38	2.53	2.26	2.7
Lu	0.46	0.35	0.34	0.33	0.3	0.25	0.22	0.32	0.43	0.21	0.38	0.35	0.41

Type	A									B			
Lithology	Massive		Pillow			Biotite-calcite Alteration			Tuff		Amygdular		
Sample	210-65.11	210-74.00	59-1113	62-1088	62-1165	31-16.28	31-27.2	117-25.95	135-24.35	151-24.32	76-1028	88-1093	91-1119
Hf	2.5	2.5	2.3	2.5	1.6	1.5	1.7	1.8	3.1	1.3	4	3.5	3.4
Ta	0.3	0.3	0.3	0.3	0.2	0.2	0.2	0.2	0.3	0.1	0.4	0.4	0.4
W	0.8	0.8	2	1.5	2.1	1.7	4.1	1.1	5.2	0.8	0.5	1.6	1.1
Pb	1	0.7	2.6	2.1	3	2.4	2.2	3.4	0.6	0.4	1.6	4.1	1.9
Bi	nd	0.1	0.1	nd	0.1	0.1	0.6	1.0	nd	nd	nd	0.1	0.1
Th	1	1	0.5	0.8	0.5	0.6	0.7	0.9	1.6	0.5	1.4	1.6	1.5
U	0.2	0.2	0.2	0.3	0.1	0.2	0.2	0.5	0.6	0.2	0.5	0.4	0.4
Be	nd	1	1	1	1	nd	1	nd	nd	nd	1	1	nd
Ga	18.7	19.8	18.5	17.6	14.1	12.4	27.1	16.2	18.0	13.9	20.3	20.9	20.9
Cd	nd	nd	nd	nd	nd	0.1	0.1	0.1	nd	nd	nd	0.1	nd
Hg	nd	nd	nd	0.01	nd	0.01	0.03	nd	nd	nd	nd	nd	nd
Tl	0.1	0.1	nd	nd	nd	0.2	0.2	0.3	0.2	0.1	nd	nd	nd
Se	nd	nd	nd	nd	nd	nd	4.2	nd	nd	nd	nd	nd	nd
Te			nd	nd	nd						nd	nd	nd
Pt	nd						nd						
Pd	0.01						0.01						
Ti (ppm)	7430.2	8397.4	7550.1	7321.4	4982.9	4560.0	5098.9	5305.5	7800.7	4553.1	7251.9	7505.9	7803.0
Ti/Zr	76.92	91.77	89.56	84.74	92.28	88.89	85.99	76.78	74.43	103.01	50.78	63.29	64.92
Zr/Y	3.39	3.66	4.24	4.24	2.84	3.21	4.33	4.09	4.35	3.75	5.62	5.09	4.97
La _N /Yb _N	3.65	3.91	3.32	3.26	4.38	4.53	3.63	3.04	4.15	3.99	6.01	5.80	4.85
% py+po	trace-1	2	trace-1	trace	trace-1	trace	trace		0	trace	trace	1-2	trace-1

Type	B											
Lithology	Breccia			Carbonate Alteration							Feldspar-phyric	
Sample	66-1092	68-1165	142-01.76	71-1099	74-1074	74-1175	79-1057	81-1119	31-12.00	143-00.64	76-1090	77-1101
SiO ₂ (wt%)	47.57	41.39	50.76	46.05	43.37	50.41	50.98	45.44	51.04	48.11	45.86	54.61
TiO ₂	1.05	1.07	1.22	1.19	1.18	1.15	1.30	1.22	1.02	1.19	1.23	1.38
Al ₂ O ₃	14.58	13.20	14.60	13.61	14.44	13.65	15.51	14.70	12.92	14.02	14.43	16.14
Fe ₂ O ₃	11.96	14.99	10.73	8.95	13.46	10.53	11.30	11.17	8.89	12.47	12.15	12.26
MnO	0.18	0.23	0.17	0.18	0.18	0.12	0.14	0.14	0.12	0.16	0.16	0.14
MgO	4.27	5.34	2.07	2.29	3.29	2.05	3.06	2.60	2.87	2.10	3.49	2.63
CaO	9.25	10.14	10.92	9.11	7.31	6.63	7.89	7.20	6.85	8.43	8.51	6.98
Na ₂ O	2.53	0.78	3.16	7.33	5.37	7.22	7.78	6.31	7.47	1.96	5.12	4.00
K ₂ O	0.33	1.01	0.69	0.34	1.42	0.38	0.88	1.31	0.16	2.99	0.26	0.66
P ₂ O ₅	0.150	0.150	0.217	0.172	0.170	0.120	0.204	0.170	0.140	0.191	0.170	0.226
Cr ₂ O ₃	0.003	0.003	0.003	nd	0.002	0.002	0.003	nd	0.002	nd	nd	nd
LOI	8.1	11.7	5.5	10.8	9.8	7.7	1.0	9.7	8.5	8.4	8.6	1.0
Sum (%)	99.98	100.00	100.03	100.01	99.99	99.98	100.03	99.97	99.99	100.03	99.99	100.03
TOTAL S (%)	0.04		0.17	1.18	0.34	2.12	1.05	0.51	1.01	0.74	0.16	0.05
Au (ppb)	7.3	0.0	243.2	3240.8	6.8	10494.2	5819.9	95.4	10541.5	5011.4	660.9	55.2
V (ppm)	161	238	236	217	270	280	219	344	187	252	275	257
Sc	19	23	21	18	20	19	21	22	15	22	21	24
Co	32.2	43.3	37.9	30.0	36.5	31.5	34.0	40	24.4	33.8	33.8	37.4
Ni	24	19.1	30.3	23.6	32.4	30.4	30.3	29	9.1	31.8	32.5	30.1
Cu	20.3	3	57.1	122.1	93.9	62.5	53.8	77.2	51.5	53.2	55.3	72.5
Zn	94	123	90	48	82	87	163	44	55	85	103	95
As	nd	nd	0.9	1.4	nd	1	0.7	1.2	1.1	0.6	0.7	0.6
Rb	8.1	26.3	15.4	6.9	43.4	8	20.6	34.9	3.6	76.4	12.6	12.9
Sr	351	254.9	396.6	439.4	201.5	448.4	414.1	350.4	422.5	217.6	236.8	458.2
Y	21.7	21.1	18.6	20.2	21.7	18.9	21.4	24.3	17.5	19.0	24.4	25.2

Type	B											
Lithology	Breccia			Carbonate Alteration							Feldspar-phyrlic	
Sample	66-1092	68-1165	142-01.76	71-1099	74-1074	74-1175	79-1057	81-1119	31-12.00	143-00.64	76-1090	77-1101
Zr	118.4	103.8	103.7	104.4	109.7	104.2	109.9	116.6	110	109.0	118.9	122.8
Nb	5.2	4.9	5.3	5.2	5	4.7	5.6	5.5	5	5.2	5.5	6.2
Mo	2	1.2	0.8	5.3	1.3	1.8	2.0	0.8	3.9	0.9	0.4	0.9
Ag	nd	nd	0.1	0.4	nd	1.1	0.7	nd	1	0.4	0.2	0.1
Sn	1	1	nd	nd	1	1	nd	1	nd	nd	1	nd
Sb	nd	nd	0.1	nd	0.1	0.1	nd	nd	0.2	nd	nd	0.1
Cs	0.3	0.6	0.5		1.6	0.2	0.7	1	0.3	2.2	1.1	0.2
Ba	81.8	280.7	259	143	207.5	171.2	169	191.9	146.2	427	77.7	144
La	12.1	10.9	11.7	13.7	12.3	10	10.2	12.6	10.2	12.2	13.1	13.5
Ce	28.8	24.8	27.8	30.1	29.4	24.5	23.8	31	25.9	28.2	30.9	30.7
Pr	3.68	3.38	3.79	3.98	3.77	3.24	3.24	4.06	3.26	3.83	4.04	4.14
Nd	16.1	15.2	15.6	17.5	16.1	14.1	14.3	17.6	13.5	15.4	17.6	18.5
Sm	3.1	3.3	2.95	3.57	3.2	2.9	3.07	3.5	3.1	3.09	3.3	3.98
Eu	0.97	1	1.04	1.10	1.02	0.89	0.95	1.16	0.86	1.10	1.08	1.29
Gd	3.39	3.43	3.78	3.68	3.43	2.99	3.28	3.98	2.94	3.79	3.85	4.14
Tb	0.66	0.63	0.54	0.59	0.65	0.57	0.55	0.72	0.52	0.54	0.69	0.69
Dy	3.7	3.56	3.85	3.38	3.78	3.12	3.56	4.18	2.95	3.73	4.12	4.32
Ho	0.77	0.75	0.79	0.73	0.74	0.64	0.76	0.82	0.62	0.82	0.84	0.90
Er	2.31	2.1	2.34	2.04	2.29	2.01	2.33	2.64	1.78	2.47	2.42	2.64
Tm	0.35	0.37	0.37	0.31	0.37	0.31	0.34	0.38	0.27	0.39	0.37	0.39
Yb	2.39	2.27	2.25	1.96	2.29	2.01	2.21	2.48	1.83	2.28	2.52	2.60
Lu	0.36	0.34	0.35	0.28	0.34	0.29	0.33	0.37	0.29	0.37	0.38	0.38
Hf	3.4	3.1	2.9	3.0	3.1	2.9	3.0	3.4	2.7	2.9	3.4	3.4
Ta	0.3	0.3	0.3	0.3	0.3	0.3	0.3	0.4	0.3	0.3	0.3	0.3
W	0.9	1.4	1.3	5.9	1.2	5.6	4.2	3.3	5	2.1	1.2	0.6

Type	B											
Lithology	Breccia			Carbonate Alteration						Feldspar-phyrlic		
Sample	66-1092	68-1165	142-01.76	71-1099	74-1074	74-1175	79-1057	81-1119	31-12.00	143-00.64	76-1090	77-1101
Pb	2.2	3.1	2.0	3.4	3.7	5.4	5.5	3.1	6.6	6.1	2.9	2.0
Bi	nd	0.1	0.1	0.3	0.1	0.7	0.3	0.3	0.6	0.4	0.1	nd
Th	1.4	1	1.3	1.6	1.3	1.1	1.0	1.4	0.9	1.2	1.4	1.2
U	0.4	0.3	0.4	0.5	0.4	0.5	0.4	0.3	0.4	0.4	0.4	0.4
Be	1	1	nd	nd	1	1	nd	1	nd	nd	nd	1
Ga	17.2	18.4	18.0	20.3	19.1	19.1	18.9	21.6	17.9	18.1	19.2	18.6
Cd	nd	0.1	nd	0.1	0.1	0.1	0.2	0.1	0.1	nd	0.1	nd
Hg	nd	nd	nd	nd	nd	0.01	nd	nd	0.01	nd	nd	nd
Tl	nd	nd	nd	nd	0.1	nd	nd	nd	nd	nd	0.1	nd
Se	nd	nd	nd	1.6	0.5	2.7	0.9	nd	0.6	0.9	nd	0.7
Te	nd	nd			nd	nd		nd			nd	
Pt						nd			0.02			
Pd						0.01			0.01			
Ti (ppm)	6300.6	6412.9	7307.5	7116.4	7072.1	6902.0	7806.2	7320.7	6121.8	7138.5	7379.2	8281.6
Ti/Zr	53.21	61.78	70.47	68.16	64.47	66.24	71.03	62.78	55.65	65.49	62.06	67.44
Zr/Y	5.46	4.92	5.58	5.17	5.06	5.51	5.14	4.80	6.29	5.74	4.87	4.87
La _N /Yb _N	5.06	4.80	5.20	6.99	5.37	4.98	4.62	5.08	5.57	5.35	5.20	5.19
% py+po	trace			3		3-4	2-5	trace	10	1	1	

Type	B							C			
Lithology	Massive						Tuff	Massive	Biotite-calcite alteration	Carbonate Alteration	
Sample	74-1123	79-1090	90-1040	27-02.63	31-00.31	31-02.26	210-40.69	151-30.90	135-26.96	151-19.34	136-16.26
SiO ₂ (wt%)	54.27	51.86	47.40	51.61	49.30	47.26	53.18	52.60	42.59	49.29	15.01
TiO ₂	1.17	1.19	1.22	1.22	1.24	1.15	1.39	1.17	0.88	0.93	0.58
Al ₂ O ₃	15.64	14.92	16.46	14.98	15.02	14.67	16.30	15.32	12.20	14.39	4.15
Fe ₂ O ₃	9.50	9.62	12.69	10.73	10.92	10.53	12.21	11.40	11.61	12.09	38.72
MnO	0.14	0.13	0.16	0.16	0.14	0.13	0.13	0.10	0.27	0.15	0.63
MgO	2.02	2.59	2.76	2.81	2.85	3.05	3.29	5.91	8.12	3.14	5.31
CaO	6.81	7.17	6.28	6.14	6.97	6.76	4.01	6.12	16.37	6.42	19.08
Na ₂ O	3.28	2.51	3.89	3.95	6.02	6.28	5.60	2.53	0.40	5.71	1.76
K ₂ O	1.35	2.10	1.82	1.70	0.54	1.46	0.37	0.91	0.29	2.26	0.21
P ₂ O ₅	0.200	0.190	0.200	0.188	0.180	0.180	0.210	0.175	0.167	0.135	0.135
Cr ₂ O ₃	nd	nd	nd	nd	nd	nd	nd	0.009	0.008	0.007	0.007
LOI	5.6	7.7	7.1	6.5	6.8	8.5	3.3	3.8	7.1	5.5	12.5
Sum (%)	99.99	99.97	99.99	100.00	99.98	99.98	99.99	100.05	100.00	100.01	98.08
TOTAL S (%)	0.16	0.13	0.15	0.30	0.39	0.06	0.16	nd	0.04	2.18	15.94
Au (ppb)	8.2	4.0	10.8	8.9	478.4	26.6	20.4	0.0	1771.9	1692.6	100000.0
V (ppm)	183	250	181	249	255	244	271	255	183	208	201
Sc	18	21	18	22	22	20	24	30	24	22	20
Co	20.4	29.8	27.5	37.6	34.5	33.2	33.4	33.2	34.2	33.0	94.3
Ni	5.3	29.5	7.5	32.5	31.2	29.7	33.3	45.6	20.2	45.6	49.1
Cu	39.6	50.1	58	75.3	61.4	43.1	46	4.6	4.1	43.3	228.0
Zn	98	74	102	101	89	72	89	86	55	79	101
As	nd	0.5	0.5	1.3	1	0.5	1.2	0.7	0.6	1.5	11.9
Rb	35.7	40	46.9	37.2	19	45.9	11.4	33.3	7.9	69.5	4.6
Sr	318.8	267.9	208.5	291.2	335.1	329.9	339.1	214.7	159.6	113.0	637.8

Type	B							C			
Lithology	Massive							Tuff	Massive	Biotite-calcite alteration	Carbonate Alteration
Sample	74-1123	79-1090	90-1040	27-02.63	31-00.31	31-02.26	210-40.69	151-30.90	135-26.96	151-19.34	136-16.26
Y	24.1	21.7	20.8	18.8	24.4	20.9	26.8	15.2	17.3	17.0	18.2
Zr	133.1	108.6	134.9	107.8	107.9	104.2	126.1	100.6	82.8	87.4	54.5
Nb	6	5.2	6.2	5.7	5.2	4.8	6.1	5.4	4.3	4.6	2.5
Mo	3.4	2	2.1	3.9	2.4	0.5	5.5	0.3	0.8	0.3	4.7
Ag	nd	nd	nd	nd	0.2	nd	nd	nd	0.2	0.3	12.5
Sn	1	1	1	1	1	1	1	nd	nd	nd	nd
Sb	0.1	0.1	0.1	nd	0.2	nd	nd	nd	0.1	nd	0.6
Cs	0.7	1	1.2	1.2	2.3	3.3	1	2.9	0.6	7.3	0.4
Ba	253.8	534.1	326.6	683	211.6	413	108.6	206	38	229	83
La	14.2	11.8	14.7	11.6	13	12.3	13.4	9.5	9.3	10.9	8.3
Ce	34	29.2	36.2	27.1	32	30.6	31	22.9	21.8	22.9	17.5
Pr	4.42	3.71	4.56	3.68	4.06	3.88	4.26	3.25	3.14	3.21	2.53
Nd	18.4	15.3	18.7	15.4	16.6	15.4	17.3	14.5	14.0	15.0	12.3
Sm	3.5	3.3	3.6	2.97	3.8	4	4	2.66	2.53	3.10	2.64
Eu	1.14	1.02	1.06	0.98	1.07	1.05	1.23	1.00	0.93	0.86	0.97
Gd	3.84	3.51	3.84	3.59	4.29	3.67	4.31	3.10	3.28	2.95	3.17
Tb	0.72	0.64	0.69	0.53	0.74	0.64	0.79	0.45	0.45	0.52	0.53
Dy	4.06	3.87	3.91	3.54	4.42	3.81	4.73	3.42	3.40	2.74	2.89
Ho	0.8	0.74	0.73	0.79	0.84	0.74	0.93	0.74	0.69	0.61	0.60
Er	2.44	2.34	2.26	2.41	2.64	2.2	2.77	2.20	2.09	1.88	1.72
Tm	0.39	0.37	0.35	0.39	0.39	0.32	0.42	0.34	0.32	0.32	0.28
Yb	2.48	2.25	2.28	2.31	2.3	2.1	2.77	2.29	1.98	1.84	1.63
Lu	0.35	0.33	0.34	0.36	0.35	0.32	0.42	0.34	0.32	0.28	0.25
Hf	3.7	3.1	4	2.9	2.9	2.8	3.6	2.9	2.3	2.3	1.4

Type	B							C			
Lithology	Massive							Tuff	Massive	Biotite-calcite alteration	Carbonate Alteration
Sample	74-1123	79-1090	90-1040	27-02.63	31-00.31	31-02.26	210-40.69	151-30.90	135-26.96	151-19.34	136-16.26
Ta	0.4	0.3	0.4	0.3	0.3	0.3	0.4	0.3	0.2	0.3	nd
W	0.6	1.3	1.6	1.9	1.1	1.9	0.9	0.7	1.4	1.1	6.4
Pb	3.5	2.3	3.6	3.0	4.6	2.9	1	0.7	1.6	3.4	24.7
Bi	0.1	nd	0.1	0.1	0.3	nd	0.1	nd	0.2	1.3	5.6
Th	1.7	1.5	1.6	1.5	1.5	1	1.8	1.0	0.7	0.6	0.6
U	0.4	0.3	0.5	0.6	0.5	0.3	0.6	0.3	0.3	0.2	0.3
Be	1	1	1	1	nd	1	1	nd	nd	nd	nd
Ga	20.3	19.4	20.8	17.9	18.6	17.1	19	17.5	14.7	18.9	8.2
Cd	0.1	0.1	0.1	nd	0.1	0.1	nd	nd	nd	nd	0.2
Hg	nd	nd	nd	nd	0.01	nd	nd	nd	nd	nd	0.05
Tl	nd	nd	nd	nd	0.1	0.3	0.1	0.1	nd	0.3	nd
Se	nd	nd	nd	nd	nd	nd	nd	nd	nd	1.0	17.1
Te	nd	nd	nd								
Pt											
Pd											
Ti	0.0	0.0	0.0	0.0	0.0	0.0	0.0	0.0	0.0	0.0	0.0
Ti/Zr	52.69	65.78	54.28	67.96	68.95	66.22	66.04	69.70	63.77	63.70	63.31
Zr/Y	5.52	5.00	6.49	5.73	4.42	4.99	4.71	6.62	4.79	5.14	2.99
La _N /Yb _N	5.73	5.24	6.45	5.02	5.65	5.86	4.84	4.15	4.70	5.92	5.09
% py+po	trace-1		trace	trace-1	trace	trace-1	2	trace	trace	23	20

Table D3: Intrusive rocks - whole rock analyses of major oxides, minor and trace elements

Lithology	Diorite 1		Diorite 2				Diorite 3						
	Sample	69-1164*	70-1167	101-05.50	69-1170	71-1144*	71-1159	27-03.24	101-15.71	182-03.71	59-1164*	84-1077	85-1058*
SiO ₂ (wt%)	52.96	51.13	56.37	58.46	52.44	56.59	58.38	59.03	49.52	59.47	59.39	60.87	58.15
TiO ₂	0.84	0.82	0.52	0.52	0.51	0.53	0.29	0.31	0.85	0.30	0.35	0.29	0.33
Al ₂ O ₃	16.33	15.60	15.09	15.65	15.34	14.83	17.09	18.33	14.03	18.33	18.45	17.97	17.92
Fe ₂ O ₃	7.49	7.12	4.79	4.70	4.77	5.10	3.77	3.74	11.06	4.42	4.60	4.15	4.62
MnO	0.15	0.10	0.07	0.07	0.10	0.09	0.08	0.07	0.13	0.06	0.08	0.06	0.08
MgO	3.24	3.15	2.22	2.29	2.35	2.27	0.98	1.25	3.14	1.11	1.23	1.04	1.13
CaO	6.42	5.76	4.84	4.96	6.63	5.45	5.02	3.96	7.57	4.02	4.18	3.93	4.16
Na ₂ O	6.16	7.81	7.92	7.00	8.41	7.71	8.32	8.53	5.62	6.19	5.71	6.17	7.27
K ₂ O	0.04	0.65	0.65	1.69	0.22	0.33	0.98	1.20	2.28	1.93	2.02	2.14	1.85
P ₂ O ₅	0.443	0.417	0.254	0.236	0.191	0.170	0.315	0.278	0.133	0.282	0.271	0.255	0.280
Cr ₂ O ₃	0.004	0.003	0.008	0.009	0.008	0.007	0.006	nd	0.008	nd	nd	nd	nd
LOI	5.9	7.4	7.3	4.4	9.1	6.9	5.0	3.3	5.7	3.9	3.7	3.1	4.2
Sum (%)	99.99	99.97	100.05	99.99	100.05	99.99	100.25	100.03	100.02	100.02	100.00	99.99	100.00
TOTAL S (%)	0.16	0.23	0.15	0.15	0.32	0.38	0.39	0.12	1.28	0.20	0.27	0.08	0.05
Au (ppb)	1.4	148	280.3	198	566.5	472.4	1.4601	266.1	3682.3	5.4	6.1	5.9	17.4
V (ppm)	130	142	108	111	79	106	91	79	301	53	54	41	70
Sc	9	10	8	7	8	9	5	5	27	2	3	2	3
Co	20.6	20.8	12.7	11.4	12.6	14.1	5.2	4.5	47.0	5.2	6.9	5.4	6.5
Ni	20.9	26.7	34.7	34.6	23.5	24	2.9	3.6	93.9	0.4	1.2	0.3	0.8
Cu	17.4	40.2	23.9	14.1	20.7	10.6	13.7	26.6	57.6	1.8	14.7	3.8	6.1
Zn	90	131	65	67	44	41	41	62	78	61	57	42	53
As	1.7	0.8	1	1.3	0.8	0.6	0.7	0.6	3.3	5.1	0.7	0.5	0.5
Rb	0.8	26.5	16.0	92.4	4.4	8.7	20.9	37.6	84.6	46.6	52.5	50.9	58.2
Sr	457.3	533.6	690.6	467.8	489.3	565.0	505.0	773.1	332.0	1565.3	1952.1	1392.4	501.3
Y	17.2	17.4	9.7	10.8	11.5	10.4	14.6	14.3	12.1	13.9	14.6	13.3	14.7

	Diorite 1		Diorite 2				Diorite 3						
	69-1164*	70-1167	101-05.50	69-1170	71-1144*	71-1159	27-03.24	101-15.71	182-03.71	59-1164*	84-1077	85-1058*	88-1124
Zr	126.8	122.6	114.9	116.9	115.1	110.1	179.6	205.9	51.7	195.5	194.5	199.3	197.1
Nb	5.6	5.6	4.1	4.3	4.1	3.9	5.8	6.3	3.9	6.9	6.4	6.8	6.6
Mo	0.9	1.5	0.8	0.8	7.4	0.7	0.7	0.4	1.2	0.2	0.1	0.1	0.1
Ag	nd	nd	nd	0.4	0.1	0.1	0.2	nd	1.0	nd	nd	nd	nd
Sn	nd	nd	nd	nd	nd	1	nd	nd	nd	nd	1	nd	1
Sb	nd	0.1	nd	nd	nd	nd	0.1	nd	nd	nd	0.1	nd	0.1
Cs	nd	1.6	0.8	6.7	nd	0.4	0.5	2.7	7.6	1.3	1.7	2.1	3.4
Ba	18	313	561	414	208	227	592	915	537	1411	1450	1289	887
La	46.3	43.9	31.8	30.0	30.7	27.0	85.9	98.5	10.2	91.3	93.6	84.4	88.8
Ce	103.1	96.9	69.5	64.6	67.9	63.2	191.7	219.5	24.8	199.9	235.5	189.8	225.6
Pr	13.33	12.45	8.75	7.98	8.41	7.68	23.66	26.79	3.54	24.08	25.86	22.58	24.58
Nd	55.0	50.3	34.6	33.2	34.5	30.8	88.2	99.9	14.5	92.6	99.3	85.7	92.2
Sm (ppm)	8.21	8.01	4.67	4.81	5.20	4.40	10.62	11.43	2.30	11.67	12.20	11.09	11.50
Eu	2.14	1.99	1.32	1.21	1.35	1.16	2.70	2.87	0.78	2.57	2.55	2.49	2.43
Gd	5.97	5.79	3.79	3.37	3.67	2.85	6.87	7.33	2.43	6.68	6.07	6.45	5.63
Tb	0.65	0.67	0.41	0.41	0.44	0.44	0.65	0.66	0.34	0.61	0.70	0.61	0.71
Dy	3.10	3.46	2.11	2.02	2.07	1.88	3.22	3.24	2.41	2.83	2.96	2.60	2.93
Ho	0.52	0.56	0.39	0.34	0.37	0.34	0.53	0.49	0.53	0.40	0.42	0.38	0.41
Er	1.36	1.48	1.01	0.94	1.03	0.93	1.42	1.30	1.69	0.98	1.21	1.12	1.27
Tm	0.21	0.20	0.17	0.13	0.17	0.15	0.22	0.24	0.25	0.17	0.20	0.15	0.20
Yb	1.27	1.30	0.95	0.90	1.04	0.90	1.30	1.32	1.64	1.11	1.23	1.13	1.23
Lu	0.18	0.19	0.14	0.12	0.14	0.13	0.20	0.21	0.25	0.18	0.20	0.15	0.19
Hf	2.7	3.1	2.9	3.0	2.8	3.1	4.3	4.8	1.5	4.5	5.1	4.7	4.4
Ta	0.2	0.2	0.2	0.2	0.2	0.3	0.3	0.3	0.2	0.3	0.4	0.3	0.4
W	nd	2.3	2.2	1.7	3.2	2.8	4.3	1.8	1.7	1.8	3.0	1.2	1.2
Pb	4.6	4.3	3.3	2.1	3	2.6	4.1	4.7	4.2	2.9	4.3	4.6	2.9
Bi	0.2	0.1	0.2	0.2	0.3	0.3	0.3	nd	1.3	0.1	0.1	nd	0.1

	Diorite 1		Diorite 2				Diorite 3						
	69-1164*	70-1167	101-05.50	69-1170	71-1144*	71-1159	27-03.24	101-15.71	182-03.71	59-1164*	84-1077	85-1058*	88-1124
Th	4.60	4.9	4.2	4.20	3.70	2.80	12.3	13.30	0.60	11.70	11.20	11.8	12
U	1.40	1.2	1.3	1.10	1.10	0.80	2.5	3.20	0.40	2.40	3.20	2.8	2.4
Be	nd	1	nd	nd	nd	nd	1	2	nd	2	2	1	1
Ga	19.0	18.7	19.6	19.4	22.7	20.1	24.0	22.2	16.3	18.7	20.8	18.8	20.8
Cd	nd	0.2	nd	nd	nd	0.1	nd	nd	nd	nd	nd	nd	nd
Hg	nd	nd	nd	nd	nd	nd	nd	nd	nd	nd	nd	nd	nd
Tl	nd	0.2	nd	0.7	nd	nd	nd	0.2	0.5	nd	0.1	0.1	0.2
Se	nd	nd	nd	nd	0.7	0.6	nd	nd	1.4	nd	nd	nd	nd
Te						nd					nd		nd
F						120							
Nb/Y	0.33	0.32	0.42	0.40	0.36	0.38	0.40	0.44	0.32	0.50	0.44	0.51	0.45
Zr/Y	7.37	7.05	11.85	10.82	10.01	10.59	12.30	14.40	4.27	14.06	13.32	14.98	13.41
La _N /Yb _N	36.46	33.77	33.47	33.33	29.52	30.00	66.08	74.62	6.22	82.25	76.10	74.69	72.20

	QFP												
	117-11.95	118-22.78*	127-21.35	143-27.82	151-11.41	182-03.42	182-23.00	210-48.38	210-55.21	58-1165	60-1160	62-1119	80-1025
SiO2 (wt%)	64.11	64.28	65.81	64.31	64.19	61.44	62.21	65.40	66.94	62.11	64.94	64.78	66.68
TiO2	0.32	0.35	0.30	0.37	0.30	0.30	0.33	0.32	0.33	0.32	0.31	0.32	0.30
Al2O3	15.52	16.38	15.78	15.81	15.41	17.66	15.95	15.72	15.89	16.25	16.23	16.37	15.54
Fe2O3	2.71	3.07	2.30	3.33	2.74	2.74	3.13	2.50	2.58	3.11	3.00	3.07	2.34
MnO	0.05	0.05	0.03	0.06	0.05	0.06	0.05	0.03	0.03	0.06	0.06	0.06	0.03
MgO	1.08	1.26	0.87	1.44	1.15	0.78	1.40	1.28	1.31	1.10	1.12	0.95	0.92
CaO	3.72	4.07	3.86	4.58	3.94	3.86	3.85	3.46	3.59	4.23	3.69	2.68	3.33
Na2O	7.36	5.99	6.55	5.89	7.35	9.50	7.41	6.15	5.75	7.32	6.14	7.31	6.35
K2O	0.86	1.26	1.27	1.49	0.79	0.36	1.04	1.57	1.43	1.03	1.29	1.05	1.28
P2O5	0.164	0.190	0.138	0.194	0.173	0.197	0.185	0.150	0.150	0.169	0.181	0.191	0.142
Cr2O3	nd	0.002	0.002	0.003	nd	nd	0.003	0.002	0.003	0.002	nd	0.002	nd
LOI	4.1	3.1	3.1	2.5	3.9	3.1	4.4	3.4	2.0	4.3	3.0	3.2	3.1
Sum (%)	100.00	100.01	100.01	99.99	99.98	100.00	99.98	100.00	100.00	100.01	99.99	100.00	100.02
TOTAL S (%)	0.31	0.13	0.15	0.15	0.32	0.54	0.31	0.10	0.09	0.48	0.30	0.49	0.08
Au (ppb)	176.8	18	260.8	100.7	181.5	281.8	263.9	11.2	7	411.1	143.3	189.5	96.2
V (ppm)	53	48	47	47	44	28	64	44	45	49	41	44	38
Sc	5	5	3	5	4	3	5	4	4	4	4	4	3
Co	6.9	7.7	5.3	8.2	7.2	5.9	8.7	8	6.9	7.1	6.6	8.5	5.1
Ni	8.3	9.6	8.3	11.3	9.6	5.8	12.9	13.2	13.9	8.4	7.2	7.9	5.2
Cu	9.3	4.2	14.8	6.8	5.8	4.8	8.4	10	8	3	5.1	11.2	18.7
Zn	38	52	54	54	63	31	55	40	50	49	62	44	45
As	0.7	0.9	nd	0.9	nd	1	0.8	nd	0.7	1.3	0.6	nd	nd
Rb	17.3	30.7	30.0	34.9	15.6	10.1	25.8	36.7	38.3	27.2	39.4	26.5	31.8
Sr	508.8	871.5	604.9	745.9	507.9	308.5	531.4	694.1	911.8	755.6	1056.1	716.9	458.3
Y	5.9	6.8	4.2	6.0	5.1	5.4	8.2	4.9	5.0	7.1	6.1	7.1	4.2
Zr	106.5	110.2	108.2	115.8	109.4	113.7	108.4	99.8	100.9	119.3	123.7	125.7	101.2
Nb	3.4	3.4	2.9	3.6	3.2	3.9	3.6	2.2	2.4	4.0	4.1	3.6	2.7

QFP													
	117-11.95	118-22.78*	127-21.35	143-27.82	151-11.41	182-03.42	182-23.00	210-48.38	210-55.21	58-1165	60-1160	62-1119	80-1025
Mo	0.4	0.1	0.3	0.3	3.1	0.3	0.3	0.1	0.3	0.3	0.1	0.4	0.2
Ag	0.1	nd	0.1	nd	nd	nd	nd	nd	nd	nd	nd	nd	nd
Sn	nd	nd	nd	nd	nd	nd	nd	nd	nd	nd	1	1	nd
Sb	nd	nd	nd	nd	nd	nd	nd	0.1	nd	0.1	nd	nd	nd
Cs	0.7	1.3	1.1	1.9	0.5	0.7	1.8	1.3	1.9	1.3	3.0	1.3	0.8
Ba	738	607	1022	692	723	115	802	782	764	695	831	664	777
La	36.8	21.8	23.6	30.5	31.3	27.4	26.0	19.0	20.0	52.5	36.9	39.3	15.4
Ce	82.1	50.7	51.7	68.3	68.7	59.3	57.3	41.7	43.2	110.5	83.1	89.9	33.4
Pr	10.14	6.37	6.52	8.61	8.65	7.60	7.54	5.42	5.50	13.26	9.69	10.63	4.17
Nd	38.8	23.2	23.4	32.0	32.3	27.9	28.9	20.5	20.6	49.0	36.9	40.8	16.5
Sm (ppm)	4.52	3.90	2.92	3.78	3.79	3.30	4.42	3.10	3.40	6.10	4.70	4.90	2.51
Eu	1.17	1.05	0.83	1.04	1.03	0.87	1.20	0.80	0.86	1.36	1.18	1.28	0.65
Gd	3.00	2.18	2.15	2.63	2.64	2.27	2.94	2.04	2.07	3.72	2.67	2.87	1.68
Tb	0.27	0.26	0.20	0.25	0.24	0.22	0.36	0.22	0.22	0.36	0.32	0.34	0.19
Dy	1.36	1.34	1.03	1.31	1.17	1.18	1.69	1.04	0.94	1.45	1.26	1.37	0.90
Ho	0.21	0.23	0.16	0.23	0.17	0.20	0.24	0.14	0.17	0.22	0.20	0.24	0.13
Er	0.55	0.58	0.40	0.60	0.49	0.52	0.58	0.39	0.44	0.57	0.56	0.59	0.32
Tm	0.09	0.07	0.07	0.09	0.07	0.09	0.10	nd	nd	0.10	0.08	0.10	0.05
Yb	0.57	0.53	0.35	0.54	0.47	0.51	0.58	0.42	0.39	0.54	0.51	0.56	0.29
Lu	0.08	0.08	0.05	0.08	0.07	0.08	0.08	0.06	0.05	0.08	0.09	0.09	0.04
Hf	3.1	3.0	2.9	3.1	3.0	3.2	2.8	2.4	2.7	3.1	3.3	3.4	2.8
Ta	0.2	0.2	0.2	0.2	0.1	0.2	0.3	0.1	0.1	0.2	0.2	0.2	0.1
W	4.8	0.5	3.5	0.6	4.3	1.2	3.1	2.1	0.5	4.8	1.0	4.4	4.1
Pb	2.3	2.2	1.9	4.2	2.6	2	2.3	2	2.2	2.7	4.2	5.3	1.3
Bi	0.1	0.1	nd	nd	0.2	0.2	0.1	nd	0.1	0.1	0.1	0.2	nd
Th	4.90	3.50	3.2	4.80	4.30	3.00	3.50	3.1	2.80	7.10	4.40	4.90	2.1
U	1.30	1.40	1	1.20	1.20	1.00	1.40	1.1	1.00	1.20	1.10	1.10	0.7

QFP													
	117-11.95	118-22.78*	127-21.35	143-27.82	151-11.41	182-03.42	182-23.00	210-48.38	210-55.21	58-1165	60-1160	62-1119	80-1025
Be	2	1	1	1	1	nd	1	1	1	nd	2	1	nd
Ga	22.2	18.7	19.3	18.5	20.1	27.6	22.0	20.4	20.3	21.9	20.2	20.5	18.5
Cd	nd	nd	nd	nd	nd	nd	nd	nd	nd	nd	nd	nd	nd
Hg	nd	nd	nd	nd	nd	nd	nd	0.01	nd	nd	nd	nd	nd
Tl	nd	0.1	nd	0.1	nd	nd	nd	nd	0.1	nd	0.2	0.1	nd
Se	nd	nd	nd	nd	nd	nd	nd	nd	nd	0.6	nd	nd	nd
Te		nd						nd	nd		nd	nd	
F		520						500	650		730		
Nb/Y	0.58	0.50	0.69	0.60	0.63	0.72	0.44	0.45	0.48	0.56	0.67	0.51	0.64
Zr/Y	18.05	16.21	25.76	19.30	21.45	21.06	13.22	20.37	20.18	16.80	20.28	17.70	24.10
La _N /Yb _N	64.56	41.13	67.43	56.48	66.60	53.73	44.83	45.24	51.28	97.22	72.35	70.18	53.10

	QFP				Quartz Monzonite			
	83-1038	84-1059*	94-1015	97-1158	210-04.33	210-05.97*	443846*	443945
SiO2 (wt%)	65.04	63.44	64.61	65.83	66.56	66.82	65.47	64.67
TiO2	0.31	0.31	0.30	0.33	0.32	0.30	0.31	0.29
Al2O3	15.94	16.73	15.63	15.95	15.50	16.34	16.06	15.87
Fe2O3	2.34	2.92	2.28	2.40	2.42	2.33	2.15	2.21
MnO	0.03	0.05	0.04	0.03	0.03	0.03	0.03	0.04
MgO	0.84	1.16	1.17	1.00	0.95	0.91	0.92	0.72
CaO	3.54	3.74	3.50	3.64	3.66	3.43	3.68	4.27
Na2O	6.50	6.49	6.64	6.22	5.67	6.16	5.89	6.91
K2O	1.30	1.59	1.39	1.42	1.36	1.03	1.55	0.96
P2O5	0.140	0.189	0.130	0.162	0.120	0.160	0.130	0.150
Cr2O3	nd	0.002	0.002	nd	nd	nd	nd	nd
LOI	4.0	3.4	4.3	3.0	3.4	2.5	3.8	3.9
Sum (%)	100.00	100.03	100.00	100.00	100.00	100.01	100.00	99.99
TOTAL S (%)	0.15	0.13	0.09	0.02	0.33	0.58	0.08	0.24
Au (ppb)	21.9	33.5	9.9	25.2	373.4	43.6	62.6	357.8
V (ppm)	41	41	38	40	38	32	35	33
Sc	3	3	4	3	3	3	2	2
Co	5.3	6	6.4	5.5	6.1	5.4	5.1	5.5
Ni	5.5	8.8	8.4	6.3	6	6	5.6	4.8
Cu	24	3.7	12.7	27.8	9.3	9.3	7.7	25.4
Zn	43	52	22	50	39	42	45	43
As	nd	nd	nd	0.6	nd	0.5	nd	nd
Rb	31.8	41.9	34.1	31.6	29.5	22.6	43.5	24.8
Sr	616.7	823.6	647.5	666.1	723.5	703.0	718.3	811.7
Y	4.4	6.5	4.6	4.3	3.6	3.7	4.2	4.9
Zr	102.2	132.7	99.6	115.2	97.8	105.1	100.1	144.7
Nb	2.8	3.7	2.3	3.1	2.4	2.4	2.8	3.8

	QFP				Quartz Monzonite			
	83-1038	84-1059*	94-1015	97-1158	210-04.33	210-05.97*	443846*	443945
Mo	0.1	0.2	0.1	0.1	0.1	0.1	nd	0.3
Ag	nd	nd	nd	nd	0.2	nd	nd	0.2
Sn	nd	nd	nd	nd	nd	nd	nd	nd
Sb	nd	nd	nd	nd	nd	nd	nd	nd
Cs	1.2	1.5	0.9	1.2	1.0	0.8	1.4	0.8
Ba	949	911	794	768	693	654	880	581
La	19.3	32.3	20.6	33.5	21.2	21.9	19.8	23.3
Ce	47.8	70.5	49.5	71.4	47.0	47.2	47.8	60.3
Pr	5.69	8.84	5.81	8.71	5.61	5.89	5.43	6.94
Nd	20.9	35.7	21.5	33.3	21.1	20.5	19.9	25.9
Sm (ppm)	2.90	4.82	2.90	4.07	2.80	3.20	2.80	3.80
Eu	0.69	1.21	0.76	0.98	0.77	0.73	0.74	0.91
Gd	1.66	2.80	1.93	2.53	1.60	1.73	1.70	2.02
Tb	0.21	0.28	0.25	0.22	0.19	0.19	0.21	0.25
Dy	0.93	1.25	0.98	0.89	0.85	0.64	0.91	0.97
Ho	0.13	0.19	0.13	0.12	0.13	0.11	0.13	0.11
Er	0.38	0.54	0.34	0.29	0.28	0.29	0.38	0.33
Tm	0.06	0.07	0.06	0.03	nd	nd	nd	0.07
Yb	0.34	0.47	0.36	0.30	0.30	0.25	0.33	0.36
Lu	0.05	0.07	0.05	0.04	0.04	0.04	0.05	0.05
Hf	2.9	3.3	2.9	3.0	2.4	2.7	3.0	3.8
Ta	0.2	0.2	0.2	0.1	0.1	0.2	0.2	0.2
W	1.7	2.3	2.2	1.5	2.9	1.6	2.9	3.5
Pb	1.9	2.9	1.6	1.5	16	1.4	1.5	8.2
Bi	0.1	nd	nd	nd	0.1	0.1	0.1	0.1
Th	2.40	4.2	3.4	4.2	2.8	3.2	2.90	4
U	0.70	1.1	0.9	0.8	0.6	0.7	0.80	0.9

	QFP				Quartz Monzonite			
	83-1038	84-1059*	94-1015	97-1158	210-04.33	210-05.97*	443846*	443945
Be	1	nd	1	1	1	1	1	1
Ga	20.1	18.7	19.5	19.7	18.5	19.1	20.9	18.7
Cd	nd	nd	nd	nd	nd	nd	nd	nd
Hg	nd	nd	0.01	nd	nd	nd	nd	nd
Tl	nd	nd	nd	nd	nd	nd	nd	nd
Se	nd	nd	nd	nd	nd	nd	nd	nd
Te	nd		nd		nd	nd	nd	nd
F					540	410		
Nb/Y	0.64	0.57	0.50	0.72	0.67	0.65	0.67	0.78
Zr/Y	23.23	20.42	21.65	26.79	27.17	28.41	23.83	29.53
La _N /Yb _N	56.76	68.72	57.22	111.67	70.67	87.60	60.00	64.72

Appendix E
MICROPROBE ANALYSES OF SELECT MINERALS AT THE
BARRY DEPOSIT

E1. Microprobe Results

The analytical methods for microprobe analyses are summarized in Chapter 2, section 2.4, titled 'Analytical Methods', and the complete set of results are presented in tables E1-E7. Ternary diagrams for classification of chlorite and biotite are shown in Figures E1 and E2 respectively.

Table E1: Microprobe analyses of magnetite

Sample no.	pre-ore				syn-ore	
	included in pyrite	pyrite mantle	adjacent to pyrite		pyrite inclusion	pyrite inclusion?
	31-21.80 C5bb.2-1MT	136-26.26 C11a-3MT	74-1175 C4-4MT	74-1175 C10-1MT	135-10.80 C10b-1MT	135-10.80 C10a-1MT
FeO ⁺ _i (wt %)	92.44	92.03	92.77	92.42	92.59	92.88
SO ₃	0.16	0.09	0.07	0.04	nd	nd
Al ₂ O ₃	0.08	0.10	0.07	0.04	0.04	0.04
Cr ₂ O ₃	0.06	0.30	0.15	0.10	nd	nd
TiO ₂	0.05	0.06	0.04	0.05	0.02	nd
PbO	0.04	0.04	0.03	0.05	0.05	0.04
NiO	nd	nd	nd	nd	nd	0.02
SeO ₂	nd	nd	nd	0.02	nd	nd
HgO	nd	0.02	nd	nd	nd	nd
Total	92.89	92.71	93.20	92.80	92.81	93.12
Fe (atm %)	71.86	71.54	72.11	71.84	71.97	72.20
S	0.06	0.04	0.03	0.02	nd	nd
Al	0.04	0.05	0.04	0.02	0.02	0.02
Cr	0.04	0.20	0.10	0.07	nd	nd
Ti	0.03	0.04	0.03	0.03	0.01	nd
Pb	0.04	0.04	0.03	0.04	0.04	0.04
Ni	nd	nd	nd	nd	nd	0.02
Se	nd	nd	nd	0.01	nd	nd
Hg	nd	0.01	nd	nd	nd	nd

Ag₂O, As₂O₅, Au₂O, Bi₂O₃, CoO, CuO, MgO, MnO, Sb₂O₅, SnO₂, TeO₂, Ti₂O₃, WO₃, and ZnO are below detection limit
nd = not detected

Table E2: Microprobe analyses of chalcopyrite

Sample no.	filling corroded zones of pyrite			filling corroded zones of pyrrhotite		adjacent to pyrite
	31-21.80C2a.2-1	135-10.80C62-2	136-26.26C72-1	31-21.80C2a.2-3	136-26.26C11-1	74-1175C12-1
Cu (wt %)	33.87	33.10	34.11	34.58	34.39	34.51
Fe	30.52	30.02	30.61	30.53	30.30	30.32
Zn	0.02	nd	nd	nd	nd	nd
Au	nd	0.01	nd	nd	nd	nd
Ti	nd	0.04	nd	0.01	0.02	nd
S	34.82	33.14	34.65	34.82	34.71	35.04
Se	0.01	nd	nd	nd	0.01	nd
Total	99.24	96.31	99.36	99.94	99.43	99.87

Ag, As, Bi, Co, Hg, Ni, Pb, Sb, Sn, Te, Tl, and W are below detection limit

nd = not detected

Table E3: Microprobe analyses of pyrite

not corroded														
Sample no.	core					rim								
	31-12.00 C1a-2	31-12.00 C2-2	31-21.80 C1.3-1	210-42.75 C8.2-2	210-42.75 C8.2-3	31-12.00 C3-2	31-21.80 C1.3-6	74-1175 C1b-3	74-1175 C4-2	135-10.80 C1-1	135-10.80 C2c2-2	136-26.26 C2a-1	136-26.26 C4a-1	136-26.26 C92-1
Inclusion										Au	Au in fracture			
Fe (wt %)	46.72	46.88	45.80	46.53	46.63	46.65	46.23	46.68	46.13	46.90	46.76	46.68	46.89	46.59
Zn	nd	nd	nd	nd	nd	nd	nd	nd	nd	nd	nd	nd	nd	0.02
Ti	nd	nd	nd	nd	nd	nd	nd	nd	nd	nd	nd	nd	nd	nd
Ni	nd	nd	nd	nd	0.02	nd	nd	nd	nd	nd	0.09	nd	nd	0.04
Au	nd	nd	nd	nd	nd	nd	nd	nd	nd	nd	nd	nd	nd	nd
Te	nd	nd	nd	nd	nd	nd	nd	nd	nd	nd	nd	nd	nd	nd
Hg	nd	nd	nd	nd	0.04	nd	nd	nd	nd	nd	nd	nd	nd	0.04
Co	nd	0.05	0.61	nd	nd	nd	nd	nd	0.47	nd	nd	nd	0.02	nd
S	53.04	53.10	52.86	53.04	52.93	52.92	53.07	53.26	52.94	53.17	53.28	53.18	53.11	53.34
Se	nd	nd	nd	nd	nd	0.01	0.01	0.02	nd	nd	nd	nd	nd	nd
As	nd	nd	nd	nd	nd	nd	nd	nd	0.06	nd	nd	nd	nd	nd
Total	99.75	100.03	99.27	99.57	99.61	99.58	99.31	99.95	99.60	100.07	100.12	99.86	100.02	100.03

Ag, Bi, Cu, Pb, Sb, Sn, Tl, and W are lower than the detection limits

nd = not detected

not corroded														
Sample no.	rim			internal zoning in pyrite	included in pyrite	adjacent to magnetite	adjacent to chalcopyrite	adjacent to pyrrhotite and magnetite	mantled by pyrrhotite		31-12.00 C1b-1	31-21.80 C2a.2-2	74-1175 C1b-1	74-1175 C1b-2
	136-26.26 C102-1	136-26.26 C102-2	210-42.75 C8.2-1	31-21.80 C1.3-3	136-26.26 C1c-1	74-1175 C4-1	74-1175 C12-2	136-26.26 C11-2	31-21.80 C4a.2-1					
Inclusion									ccp	ccp				
Fe (wt %)	46.57	46.58	46.46	46.12	46.60	46.25	46.08	46.57	44.33	46.31	46.25	46.95	46.67	
Zn	nd	nd	nd	0.02	nd	nd	nd	nd	nd	nd	nd	nd	0.03	
Ti	nd	nd	nd	nd	nd	nd	nd	0.03	nd	0.04	nd	nd	nd	
Ni	0.26	nd	0.02	nd	0.05	nd	nd	nd	nd	0.01	0.02	nd	0.02	
Au	nd	0.01	nd	nd	0.01	nd	nd	nd	nd	nd	0.03	nd	nd	
Te	nd	nd	nd	nd	nd	nd	nd	nd	nd	nd	0.03	nd	nd	
Hg	nd	nd	nd	0.03	nd	nd	nd	nd	nd	nd	nd	nd	nd	
Co	nd	nd	0.06	0.31	0.09	0.53	0.47	nd	2.37	0.19	nd	nd	nd	
S	53.22	53.14	52.88	53.06	53.23	53.27	53.27	53.10	52.91	53.14	52.84	53.00	53.01	
Se	nd	nd	nd	nd	nd	nd	nd	nd	nd	nd	nd	0.01	0.02	
As	nd	nd	nd	nd	nd	nd	nd	nd	nd	nd	nd	nd	nd	
Total	100.06	99.73	99.42	99.54	99.97	100.05	99.82	99.70	99.60	99.69	99.17	99.96	99.73	

Ag, Bi, Cu, Pb, Sb, Sn, Tl, and W are lower than the detection limits
nd = not detected

Sample no.	not corroded						corroded						
	74-1175 C4-3	74-1175 C5b-2	135-10.80 C72-2	136-26.26 C4c-1	210-42.75 C4.2-2	210-42.75 C7.2-2	internal zoning in pyrite			included in pyrite			corroded zones filled by chalcopyrite
							31-21.80 C1.3-2	31-21.80 C1.3-4	31-21.80 C1.3-5	136-26.26 C52-1	136-26.26 C11b-1	136-26.26 C11b-2	135-10.80 C62-1
Inclusion			Au		Au	Au							
Fe (wt %)	46.59	45.53	46.90	46.81	46.73	46.51	46.49	46.35	46.47	46.99	46.84	46.66	46.72
Zn	nd	nd	nd	nd	nd	nd	nd	nd	nd	nd	nd	nd	nd
Ti	nd	nd	nd	nd	nd	nd	nd	nd	nd	nd	0.04	0.04	nd
Ni	0.02	nd	nd	nd	nd	nd	nd	0.02	0.05	nd	nd	nd	nd
Au	nd	0.01	nd	0.01	nd	nd	nd	nd	nd	nd	nd	nd	nd
Te	nd	nd	nd	nd	nd	nd	nd	nd	0.03	nd	nd	nd	nd
Hg	nd	nd	nd	nd	0.04	nd	nd	nd	nd	nd	nd	nd	nd
Co	nd	1.05	nd	0.04	nd	nd	nd	0.03	nd	nd	nd	0.16	nd
S	52.96	53.81	53.28	52.91	53.02	52.96	53.03	53.16	53.08	53.16	53.33	52.92	53.14
Se	nd	nd	nd	nd	nd	nd	nd	0.01	0.01	nd	0.01	nd	nd
As	nd	nd	nd	nd	nd	nd	nd	nd	nd	nd	nd	nd	nd
Total	99.57	100.40	100.18	99.75	99.78	99.47	99.52	99.58	99.64	100.15	100.22	99.77	99.85

Ag, Bi, Cu, Pb, Sb, Sn, Tl, and W are lower than the detection limits
nd = not detected

corroded

Sample no.	pyrite mantles magnetite		74-1175 C5b-1	135-10.80 C1-2	135-10.80 C72-1	136-26.26 C1a-1	136-26.26 C2a-2	136-26.26 C4c2-1	136-26.26 C6-1	136-26.26 C6-2	136-26.26 C92-2	136-26.26 C102-3	136-26.26 C11b3-3	
	31-21.80 C5bb.2-2	135-10.80 C10a-2												
Inclusion														Au, po, Te
Fe (wt %)	43.45	46.21	46.55	46.32	46.68	46.50	46.38	59.10	46.37	46.56	46.70	46.58	46.19	
Zn	nd	nd	nd	nd	nd	nd	0.03	nd	nd	nd	nd	0.02	nd	
Ti	nd	nd	nd	nd	nd	nd	0.01	0.02	nd	nd	nd	nd	nd	
Ni	nd	0.08	nd	0.04	0.02	nd	0.03	0.03	0.02	nd	0.02	0.02	0.08	
Au	nd	nd	nd	nd	nd	nd	nd	nd	nd	nd	nd	nd	nd	
Te	nd	nd	nd	nd	nd	nd	nd	nd	nd	nd	nd	nd	nd	
Hg	nd	nd	nd	nd	nd	nd	nd	nd	nd	nd	nd	0.03	nd	
Co	3.21	0.18	nd	nd	nd	0.55	0.29	0.05	nd	nd	nd	nd	nd	
S	53.00	53.50	53.04	53.05	53.11	52.88	52.92	40.33	53.07	53.39	53.43	53.15	53.16	
Se	0.02	nd	0.01	nd	nd	nd	0.01	0.01	nd	nd	nd	nd	nd	
As	nd	nd	nd	nd	nd	nd	nd	nd	nd	nd	nd	nd	nd	
Total	99.67	99.97	99.60	99.41	99.81	99.93	99.67	99.54	99.46	99.96	100.15	99.81	99.44	

Ag, Bi, Cu, Pb, Sb, Sn, Tl, and W are lower than the detection limits
 nd = not detected

Table E4: Microprobe analysis of gold

Sample no.	included in pyrite					included/filling fracture in pyrite		filling fracture in pyrite		included in carbonate-quartz alteration				
	135-10.80 C72-3	135-10.80 C12-1	210-42.75 C4.2-1	210-42.75 C7.2-1	210-42.75 C9a.2-1	31-12.00 C2-1	31-12.00 C3-1	135-10.80 C2e2-1	210-42.75 C3.2-1	31-12.00 C4.2-1	210-42.75 C1.2-1	210-42.75 C1.2-2	210-42.75 C1.3-1	210-42.75 C2.2-1
Au (wt %)	94.45	93.21	91.06	93.20	94.11	92.09	93.79	92.22	90.19	89.96	85.39	89.03	89.20	89.54
Ag	3.76	4.75	3.60	5.12	4.44	8.07	5.72	6.06	7.91	8.69	8.20	8.62	9.01	9.04
Bi	nd	nd	nd	nd	nd	0.03	0.04	nd	nd	nd	0.37	nd	nd	nd
Hg	nd	nd	nd	nd	nd	nd	nd	nd	nd	nd	nd	nd	nd	0.04
Te	0.02	nd	nd	nd	0.01	0.01	nd	nd	0.01	nd	0.07	0.02	0.01	nd
Ti	nd	nd	0.01	nd	nd	nd	nd	nd	nd	nd	nd	nd	nd	nd
Co	nd	nd	nd	nd	nd	nd	nd	nd	nd	nd	nd	0.02	nd	nd
Cu	0.07	0.05	0.08	0.07	0.11	0.04	0.04	0.05	0.03	0.03	0.05	nd	0.03	nd
S	0.19	0.19	0.46	0.18	0.12	0.13	2.55	0.11	0.13	0.36	0.13	0.07	0.12	0.13
Fe	1.41	0.90	2.08	0.33	0.58	0.18	2.67	0.10	0.47	0.25	0.14	0.03	0.24	0.12
Total	99.89	99.10	97.30	98.90	99.37	100.56	104.81	98.53	98.74	99.29	94.35	97.78	98.60	98.87

Ni, Pb, Sb, Se, Sn, W, and Zn are below detection limit
nd = not detected

Table E5: Microprobe analyses of chlorite. * denotes analyses of non-chlorite remnant magmatic phenocrysts

Sample no.	Pre-ore									
	CH 3	CH 6	* CH 7	CH 7	* CH1 7	* CH 7	CH 1	CH 2	CH 6	CH PY 7
	58-1165 1290-472	58-1165 1201- 2540	58-1165 1103-3095	58-1165 1200-3093	58-1165 1126-3024	58-1165 1156-3082	69-1170 1197-2806	69-1170 1060-2526	210-433 1068-600	83-1038 518-1743
SiO ₂ (wt%)	25.97	26.32	31.30	25.53	33.48	34.00	25.23	25.61	25.80	25.84
TiO ₂	0.00	0.00	0.00	0.00	0.00	0.15	0.06	0.06	0.10	0.00
Al ₂ O ₃	20.54	21.00	25.01	21.48	26.95	27.48	21.31	21.09	21.26	21.59
Fe ₂ O ₃	0.00	0.00	0.00	0.00	0.00	0.00	0.00	0.00	0.00	0.00
Cr ₂ O ₃	0.00	0.00	0.00	0.00	0.00	0.00	0.37	0.17	0.00	0.00
FeO	24.40	23.92	22.48	25.12	18.37	19.58	23.04	22.83	24.34	22.10
MnO	0.11	0.16	0.11	0.30	0.00	0.00	0.18	0.19	0.00	0.19
MgO	15.92	16.28	2.53	15.15	1.92	2.08	15.76	16.12	15.86	17.33
CaO	0.05	0.00	0.10	0.08	0.19	0.09	0.11	0.06	0.06	0.00
Na ₂ O	0.00	0.00	3.50	0.00	3.28	2.17	0.00	0.00	0.09	0.11
K ₂ O	0.08	0.00	0.19	0.00	0.18	0.23	0.00	0.06	0.00	0.00
H ₂ O	11.36	11.50	11.40	11.39	11.68	11.88	11.28	11.32	11.44	11.52
SUM	98.43	99.18	96.62	99.05	96.05	97.66	97.34	97.51	98.95	98.68
Si (atm%)	12.14	12.30	14.63	11.93	15.65	15.89	11.79	11.97	12.06	12.08
Ti	0.00	0.00	0.00	0.00	0.00	0.09	0.04	0.04	0.06	0.00
Al	10.87	11.11	13.24	11.37	14.26	14.54	11.28	11.16	11.25	11.43
Fe	0.00	0.00	0.00	0.00	0.00	0.00	0.00	0.00	0.00	0.00
Cr	0.00	0.00	0.00	0.00	0.00	0.00	0.04	0.02	0.00	0.00
Fe	18.97	18.59	17.47	19.53	14.28	15.22	17.91	17.75	18.92	17.18
Mn	0.09	0.12	0.09	0.23	0.00	0.00	0.14	0.15	0.00	0.15
Mg	9.60	9.82	1.53	9.14	1.16	1.25	9.50	9.72	9.56	10.45
Ca	0.04	0.00	0.07	0.06	0.14	0.06	0.08	0.04	0.04	0.00
Na	0.00	0.00	2.60	0.00	2.43	1.61	0.00	0.00	0.07	0.08
K	0.07	0.00	0.16	0.00	0.15	0.19	0.00	0.05	0.00	0.00
H	1.27	1.29	1.28	1.27	1.31	1.33	1.26	1.27	1.28	1.29

Sample no.	Post-ore							Relative age is ambiguous					
	CH 10	CH 2	CH 2	CH 3	CH 4	CH 5	CH 7	CH 7	CH 1	CH 4	CH 6	CH 7	CH near 3
	83-1038	210-433	69-1170	210-433	58-1165	83-1038	69-1170	83-1038	59-1164	83-1038	58-1165	210-433	83-1038
	83-1038	669-1970	1055-2596	840-1900	1336-856	83-1038	1290-268	532-1712	1917-395	83-1038	1125-2512	652-415	1860-2560
SiO ₂ (wt%)	26.03	26.35	26.02	26.16	25.51	26.04	27.94	25.19	26.23	25.40	26.54	26.70	25.75
TiO ₂	0.13	0.00	0.00	0.13	0.00	0.00	0.07	0.16	0.00	0.00	0.00	0.10	0.00
Al ₂ O ₃	21.09	21.40	20.68	20.50	21.46	21.78	20.33	22.20	19.71	21.69	20.90	20.90	21.71
Fe ₂ O ₃	0.00	0.00	0.00	0.00	0.00	0.00	0.00	0.00	0.00	0.00	0.00	0.00	0.00
Cr ₂ O ₃	0.00	0.00	0.11	0.00	0.18	0.11	0.08	0.08	0.07	0.00	0.14	0.07	0.24
FeO	22.29	24.58	22.81	23.57	24.75	21.52	22.63	23.08	25.06	22.11	23.68	24.33	21.75
MnO	0.12	0.00	0.22	0.00	0.23	0.09	0.17	0.00	0.27	0.21	0.14	0.21	0.14
MgO	17.00	15.79	15.20	15.62	15.81	17.29	15.74	16.24	15.44	16.47	16.07	16.10	16.93
CaO	0.00	0.06	0.12	0.05	0.04	0.08	0.05	0.00	0.10	0.26	0.00	0.07	0.07
Na ₂ O	0.00	0.00	0.09	0.00	0.00	0.00	0.00	0.00	0.00	0.00	0.09	0.00	0.00
K ₂ O	0.03	0.00	0.08	0.36	0.06	0.05	0.11	0.00	0.00	0.00	0.00	0.15	0.06
H ₂ O	11.45	11.54	11.22	11.31	11.46	11.54	11.54	11.44	11.28	11.36	11.49	11.59	11.47
SUM	98.14	99.72	96.55	97.70	99.50	98.50	98.66	98.39	98.16	97.50	99.05	100.22	98.12
Si (atm%)	12.17	12.32	12.16	12.23	11.92	12.17	13.06	11.77	12.26	11.87	12.41	12.48	12.04
Ti	0.08	0.00	0.00	0.08	0.00	0.00	0.04	0.10	0.00	0.00	0.00	0.06	0.00
Al	11.16	11.33	10.95	10.85	11.36	11.53	10.76	11.75	10.43	11.48	11.06	11.06	11.49
Fe	0.00	0.00	0.00	0.00	0.00	0.00	0.00	0.00	0.00	0.00	0.00	0.00	0.00
Cr	0.00	0.00	0.08	0.00	0.12	0.08	0.05	0.05	0.05	0.00	0.10	0.05	0.16
Fe	17.33	19.11	17.73	18.32	19.24	16.73	17.59	17.94	19.48	17.19	18.41	18.91	16.91
Mn	0.09	0.00	0.17	0.00	0.18	0.07	0.13	0.00	0.21	0.16	0.11	0.16	0.11
Mg	10.25	9.52	9.17	9.42	9.53	10.43	9.49	9.79	9.31	9.93	9.69	9.71	10.21
Ca	0.00	0.04	0.09	0.04	0.03	0.06	0.04	0.00	0.07	0.19	0.00	0.05	0.05
Na	0.00	0.00	0.07	0.00	0.00	0.00	0.00	0.00	0.00	0.00	0.07	0.00	0.00
K	0.02	0.00	0.07	0.30	0.05	0.04	0.09	0.00	0.00	0.00	0.00	0.12	0.05
H	1.28	1.29	1.26	1.27	1.28	1.29	1.29	1.28	1.26	1.27	1.29	1.30	1.28

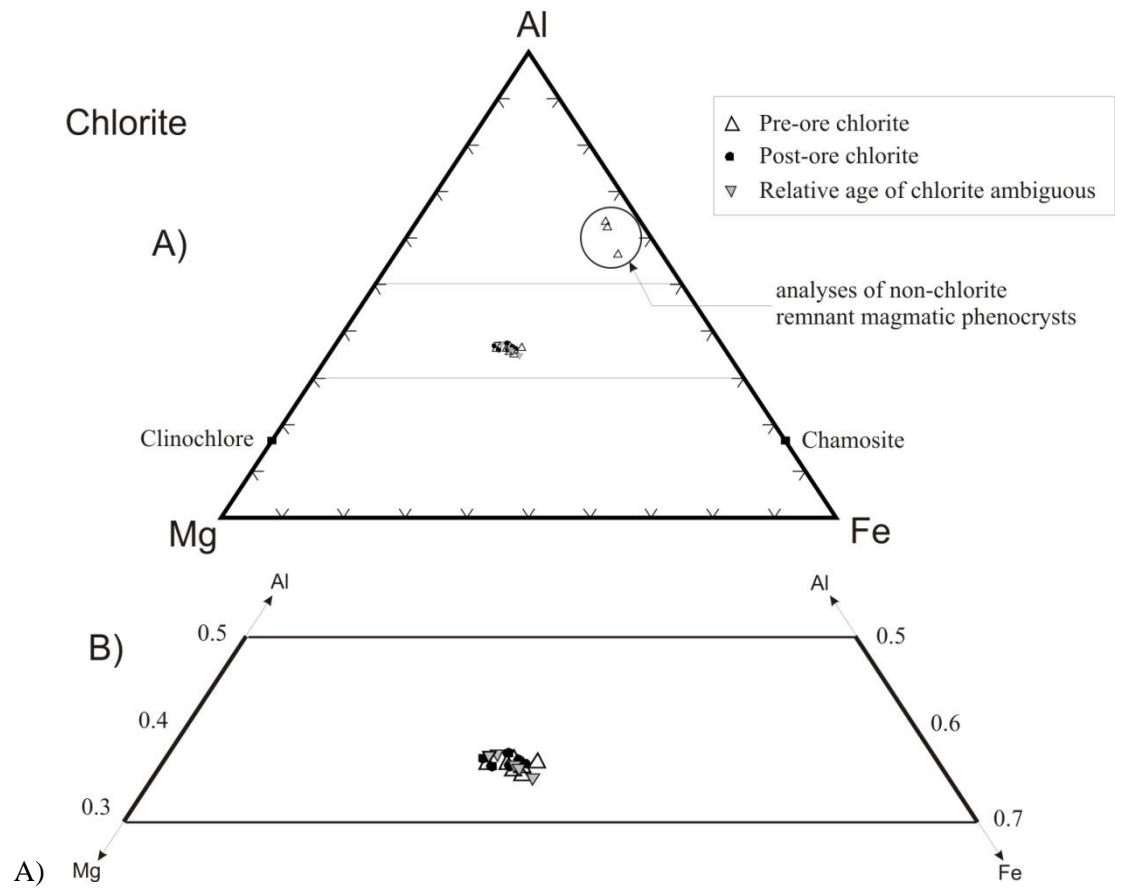


Fig. E1: A) Ternary Al-Mg-Fe diagram showing the composition of early and late chlorite; B) Blow-up of the mid-section of the ternary diagram.

Table E6: Microprobe analyses of biotite

Sample no.	Pre-ore					Post-ore				
	BI 3	BI 6	BI 1	BI 2	BI 4	BI 3	BI 6	BI 1	BI 2	BI 4
	58-1165	58-1165	69-1170	69-1170	69-1170	58-1185	58-1165	69-1170	69-1170	69-1170
	1323-468	1239-2539	1171-2769	1006-2572	1157-1298	1294-502	1227-2552	1106-2821	1008-2588	1201-1283
SiO ₂ (wt%)	36.65	47.17	35.79	36.54	36.56	36.73	38.30	36.47	37.20	37.10
TiO ₂	2.13	2.07	1.68	2.04	1.86	2.24	2.05	1.74	1.96	1.97
Al ₂ O ₃	17.08	14.65	15.87	15.60	16.06	16.82	15.31	15.68	15.96	15.88
Fe ₂ O ₃	0.00	0.00	0.00	0.00	0.00	0.00	0.00	0.00	0.00	0.00
Cr ₂ O ₃	0.07	0.00	0.22	0.00	0.07	0.00	0.00	0.13	0.00	0.10
FeO	18.69	16.46	18.04	17.48	17.86	18.88	19.44	19.58	19.01	18.44
MnO	0.00	0.15	0.11	0.19	0.25	0.21	0.00	0.16	0.00	0.11
MgO	11.06	9.68	11.34	11.60	11.46	11.07	11.48	12.00	11.95	11.65
CaO	0.13	0.09	0.06	0.08	0.07	0.00	0.12	0.15	0.00	0.08
Na ₂ O	0.00	0.00	0.00	0.00	0.00	0.00	0.00	0.00	0.00	0.15
K ₂ O	9.76	8.59	9.15	9.22	9.51	9.98	8.54	9.35	9.63	9.73
H ₂ O	3.96	4.29	3.83	3.86	3.89	3.96	3.97	3.92	3.96	3.94
SUM	99.53	103.15	96.09	96.61	97.59	99.89	99.21	99.18	99.67	99.15
Si (atm%)	17.13	22.05	16.73	17.08	17.09	17.17	17.90	17.05	17.39	17.34
Ti	1.28	1.24	1.01	1.22	1.11	1.34	1.23	1.04	1.17	1.18
Al	9.04	7.75	8.40	8.26	8.50	8.90	8.10	8.30	8.45	8.40
Fe	0.00	0.00	0.00	0.00	0.00	0.00	0.00	0.00	0.00	0.00
Cr	0.05	0.00	0.15	0.00	0.05	0.00	0.00	0.09	0.00	0.07
Fe	14.53	12.79	14.02	13.59	13.88	14.68	15.11	15.22	14.78	14.33
Mn	0.00	0.12	0.09	0.15	0.19	0.16	0.00	0.12	0.00	0.09
Mg	6.67	5.84	6.84	7.00	6.91	6.68	6.92	7.24	7.21	7.03
Ca	0.09	0.06	0.04	0.06	0.05	0.00	0.09	0.11	0.00	0.06
Na	0.00	0.00	0.00	0.00	0.00	0.00	0.00	0.00	0.00	0.11
K	8.10	7.13	7.60	7.65	7.89	8.28	7.09	7.76	7.99	8.08
H	0.44	0.48	0.43	0.43	0.44	0.44	0.44	0.44	0.44	0.44

Sample no.	Relative age is ambiguous					
	BI 4	BI 5	BI 7	BI 2	BI 3	BI 6
	58-1165 1381-905	69-1170 1076-912	69-1170 1298-358	136-1626 2148-1683	136-1626 2053-1921	136-1626 484-2754
SiO ₂ (wt%)	36.71	37.15	39.42	33.77	35.34	35.20
TiO ₂	2.15	1.85	1.61	1.09	1.87	1.67
Al ₂ O ₃	16.39	16.00	15.07	16.21	16.07	16.47
Fe ₂ O ₃	0.00	0.00	0.00	0.00	0.00	0.00
Cr ₂ O ₃	0.15	0.12	0.09	0.10	0.00	0.00
FeO	19.81	18.49	17.16	26.85	24.29	23.55
MnO	0.00	0.00	0.13	0.08	0.00	0.17
MgO	11.35	11.77	10.94	6.84	7.87	8.22
CaO	0.00	0.00	0.18	0.08	0.14	0.11
Na ₂ O	0.11	0.00	0.19	0.00	0.00	0.00
K ₂ O	9.45	9.70	8.48	8.78	9.33	9.25
H ₂ O	3.96	3.94	3.94	3.72	3.82	3.82
SUM	100.08	99.02	97.21	97.52	98.73	98.46
Si (atm%)	17.16	17.37	18.43	15.79	16.52	16.45
Ti	1.29	1.11	0.96	0.65	1.12	1.00
Al	8.67	8.47	7.98	8.58	8.51	8.72
Fe	0.00	0.00	0.00	0.00	0.00	0.00
Cr	0.10	0.08	0.06	0.07	0.00	0.00
Fe	15.40	14.37	13.34	20.87	18.88	18.31
Mn	0.00	0.00	0.10	0.06	0.00	0.13
Mg	6.84	7.10	6.60	4.12	4.75	4.96
Ca	0.00	0.00	0.13	0.06	0.10	0.08
Na	0.08	0.00	0.14	0.00	0.00	0.00
K	7.84	8.05	7.04	7.29	7.75	7.68
H	0.44	0.44	0.44	0.42	0.43	0.43

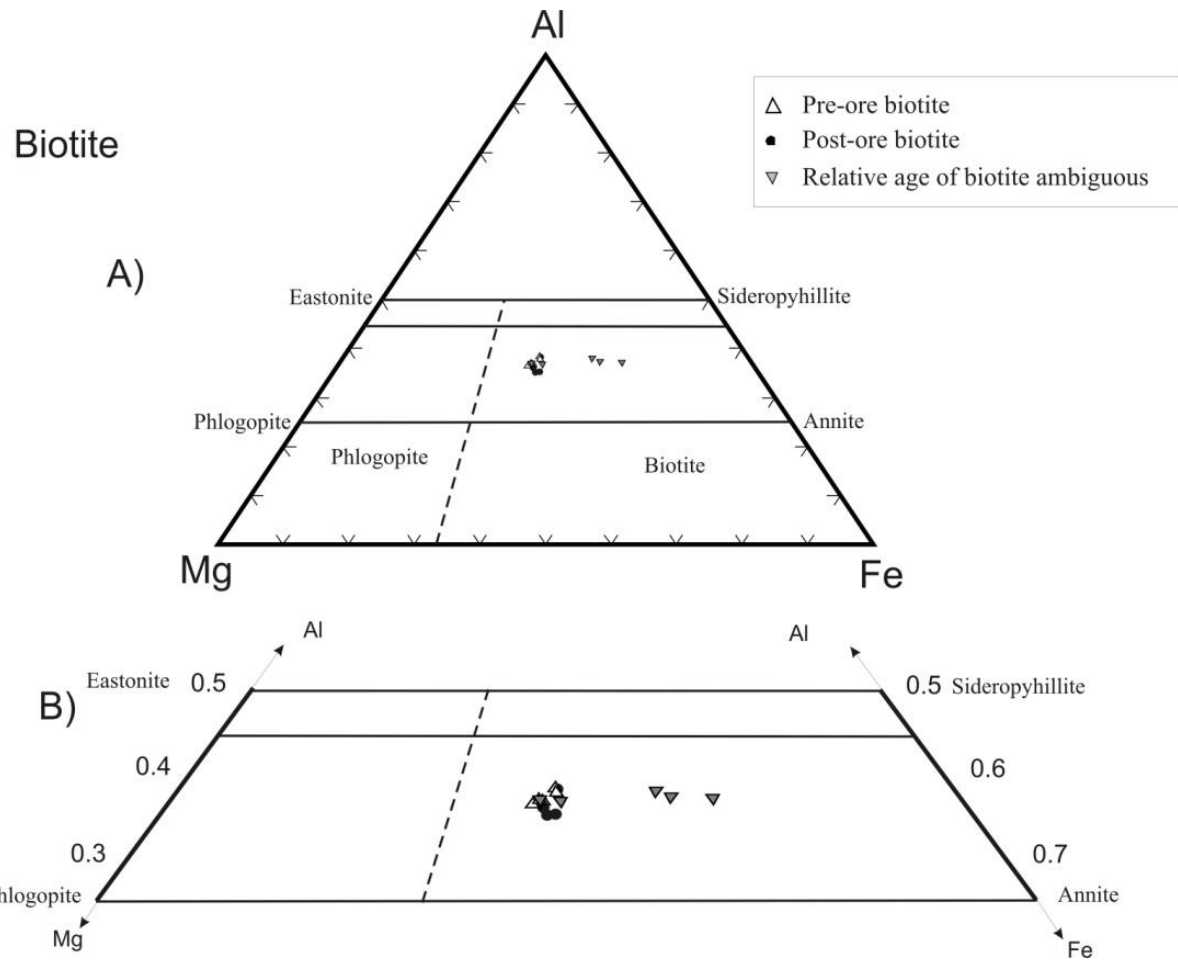


Fig. E2: A) Ternary Al-Mg-Fe Diagram showing the composition of early and late biotite; B) Blow-up of the mid-section of the ternary diagram.

Table E7: Microprobe analyses of plagioclase

Sample no.	QFP											
	rim		core						unknown			
	PL 6 58-1165	PL 6 58-1165	PL 5 58-1165	PL 6 58-1165	PL 6 58-1165	PL 6 58-1165	PL 6 58-1165	PL 6 83-1038	PL 8 83-1038	PL 9 83-1038	PL 1 58-1165	PL 1 83-1038
SiO ₂ (wt%)	69.66	66.56	69.32	67.67	62.77	64.18	68.98	67.25	65.96	69.27	69.73	63.02
TiO ₂	0.00	0.00	0.00	0.09	0.16	0.10	0.00	0.00	0.00	0.00	0.00	0.00
Al ₂ O ₃	20.03	21.41	19.87	21.14	22.64	22.13	20.07	20.87	21.98	19.82	19.84	21.67
Fe ₂ O ₃	0.00	0.00	0.00	0.00	0.00	0.00	0.00	0.00	0.00	0.00	0.00	0.00
Cr ₂ O ₃	0.00	0.00	0.00	0.00	0.00	0.11	0.00	0.00	0.14	0.16	0.00	0.00
FeO	0.14	0.00	0.13	0.14	0.96	0.68	0.27	0.00	0.56	0.00	0.00	0.83
MnO	0.00	0.00	0.00	0.00	0.15	0.00	0.00	0.00	0.00	0.00	0.07	0.00
MgO	0.00	0.08	0.00	0.14	0.54	0.44	0.00	0.20	0.12	0.00	0.00	0.28
CaO	0.42	1.65	0.39	1.66	1.18	0.71	0.54	0.97	0.28	0.39	0.08	0.71
Na ₂ O	11.39	10.28	11.29	10.77	7.89	8.83	11.43	10.36	9.98	11.33	11.43	8.56
K ₂ O	0.04	0.42	0.09	0.00	2.91	2.24	0.04	0.80	1.65	0.06	0.00	2.25
SUM	101.68	100.40	101.09	101.61	99.20	99.42	101.33	100.45	100.67	101.03	101.15	97.32
Si (atm%)	32.56	31.11	32.40	31.63	29.34	30.00	32.24	31.44	30.83	32.38	32.59	29.46
Ti	0.00	0.00	0.00	0.05	0.10	0.06	0.00	0.00	0.00	0.00	0.00	0.00
Al	10.60	11.33	10.52	11.19	11.98	11.71	10.62	11.05	11.63	10.49	10.50	11.47
Fe	0.00	0.00	0.00	0.00	0.00	0.00	0.00	0.00	0.00	0.00	0.00	0.00
Cr	0.00	0.00	0.00	0.00	0.00	0.08	0.00	0.00	0.10	0.11	0.00	0.00
Fe	0.11	0.00	0.10	0.11	0.75	0.53	0.21	0.00	0.44	0.00	0.00	0.65
Mn	0.00	0.00	0.00	0.00	0.12	0.00	0.00	0.00	0.00	0.00	0.05	0.00
Mg	0.00	0.05	0.00	0.08	0.33	0.27	0.00	0.12	0.07	0.00	0.00	0.17
Ca	0.30	1.18	0.28	1.19	0.84	0.51	0.39	0.69	0.20	0.28	0.06	0.51
Na	8.45	7.63	8.38	7.99	5.85	6.55	8.48	7.69	7.40	8.41	8.48	6.35
K	0.03	0.35	0.07	0.00	2.42	1.86	0.03	0.66	1.37	0.05	0.00	1.87

Sample no.	Diorite 2		Diorite 3					Quartz Monzonite				
	PL 5	PL 2	PL 3	PL 3	PL 5	PL 5	PL 6	rim		core	unknown	
	69-1170	59-1164	59-1164	59-1164	59-1164	59-1164	59-1164	PL 1	PL 4	PL 5	PL 4	PL 1 MID
	1086-939?	820-327	1242-1237	1318-1092	489-2049	497-2035	1141-2459?	440-2310	1917-2047	1241-1305	1888-2015	210-433
SiO ₂ (wt%)	68.80	68.89	65.80	68.08	68.26	65.20	67.70	66.36	70.13	68.44	65.92	69.68
TiO ₂	0.00	0.00	0.10	0.05	0.11	0.12	0.00	0.00	0.12	0.10	0.10	0.00
Al ₂ O ₃	19.78	20.10	21.45	20.42	19.37	22.04	21.01	21.79	19.25	20.23	22.57	19.31
Fe ₂ O ₃	0.00	0.00	0.00	0.00	0.00	0.00	0.00	0.00	0.00	0.00	0.00	0.00
Cr ₂ O ₃	0.00	0.00	0.00	0.11	0.10	0.00	0.00	0.00	0.00	0.00	0.08	0.00
FeO	0.08	0.00	0.51	0.29	0.11	0.77	0.00	0.10	0.10	0.00	0.34	0.00
MnO	0.00	0.00	0.00	0.00	0.00	0.00	0.09	0.00	0.00	0.10	0.08	0.00
MgO	0.06	0.00	0.13	0.13	0.00	0.24	0.00	0.07	0.00	0.00	0.06	0.00
CaO	0.44	0.72	0.53	0.61	1.69	0.50	1.49	2.68	0.00	0.76	0.68	0.28
Na ₂ O	11.18	11.14	10.01	10.67	10.26	9.11	10.60	10.08	11.60	11.02	9.79	11.39
K ₂ O	0.00	0.00	1.64	0.65	0.31	2.21	0.35	0.11	0.06	0.22	1.66	0.00
SUM	100.34	100.85	100.17	101.01	100.21	100.19	101.24	101.19	101.26	100.87	101.28	100.66
Si (atm%)	32.16	32.20	30.76	31.82	31.91	30.48	31.65	31.02	32.78	31.99	30.81	32.57
Ti	0.00	0.00	0.06	0.03	0.07	0.07	0.00	0.00	0.07	0.06	0.06	0.00
Al	10.47	10.64	11.35	10.81	10.25	11.66	11.12	11.53	10.19	10.71	11.95	10.22
Fe	0.00	0.00	0.00	0.00	0.00	0.00	0.00	0.00	0.00	0.00	0.00	0.00
Cr	0.00	0.00	0.00	0.08	0.07	0.00	0.00	0.00	0.00	0.00	0.05	0.00
Fe	0.06	0.00	0.40	0.23	0.09	0.60	0.00	0.08	0.08	0.00	0.26	0.00
Mn	0.00	0.00	0.00	0.00	0.00	0.00	0.07	0.00	0.00	0.08	0.06	0.00
Mg	0.04	0.00	0.08	0.08	0.00	0.14	0.00	0.04	0.00	0.00	0.04	0.00
Ca	0.31	0.51	0.38	0.44	1.21	0.36	1.06	1.92	0.00	0.54	0.49	0.20
Na	8.29	8.26	7.43	7.92	7.61	6.76	7.86	7.48	8.61	8.18	7.26	8.45
K	0.00	0.00	1.36	0.54	0.26	1.83	0.29	0.09	0.05	0.18	1.38	0.00

Plagioclase in carbonate-quartz-pyrite alteration				
	PL 3	PL 3	PL 5	PL 5
	136-1626	136-1626	136-1626	136-1626
Sample no.	2061-1930	2024-1910	2132-2543	2065-2505
SiO ₂ (wt%)	69.32	69.27	67.44	68.55
TiO ₂	0.00	0.22	0.00	0.00
Al ₂ O ₃	19.19	19.19	18.63	19.36
Fe ₂ O ₃	0.00	0.00	0.00	0.00
Cr ₂ O ₃	0.00	0.08	0.00	0.00
FeO	0.08	0.24	0.53	0.12
MnO	0.00	0.00	0.14	0.00
MgO	0.00	0.00	0.19	0.00
CaO	0.14	0.08	0.61	0.35
Na ₂ O	11.50	11.55	11.22	11.27
K ₂ O	0.06	0.00	0.08	0.03
SUM	100.29	100.63	98.84	99.68
Si (atm%)	32.40	32.38	31.52	32.04
Ti	0.00	0.13	0.00	0.00
Al	10.16	10.16	9.86	10.25
Fe	0.00	0.00	0.00	0.00
Cr	0.00	0.05	0.00	0.00
Fe	0.06	0.19	0.41	0.09
Mn	0.00	0.00	0.11	0.00
Mg	0.00	0.00	0.11	0.00
Ca	0.10	0.06	0.44	0.25
Na	8.53	8.57	8.32	8.36
K	0.05	0.00	0.07	0.02

Appendix F
DRILL CORE LOGGING FROM THE BARRY DEPOSIT

A total of 23 drill holes were logged throughout the main trenched zone, with 13 holes selected to be studied in detail. ‘Unaltered’ mafic volcanic units, zones of pervasive carbonate alteration, biotite-carbonate alteration, and intrusive units were sampled in the trenched region and in these 13 drill holes.

Table F1: List of diamond drill holes logged at Barry

Section	DDH Number	Section	DDH Number
1037	127*	1104	162
	135*	1111	28
	210*		140
1074	31*	1124	27*
	118*		136*
	117*		138
1088	142*	1158	180
	143*		182*
	151*		101*
	163		
1096	29		
	30		
	40		
	116		

* denotes drill holes logged and sampled in great detail

Murgor Resources

BARRY - MAIN ZONE - Drill Core Logging

Logged by Kathryn Kitney

V3=mafic volcanic
T3=mafic tuff
QFP=quartz-feldspar porphyry

q=quartz
alb=albite
c=carbonate
bt=biotite
ep=epidote
chl=chlorite

VG=visible gold
py=pyrite
po=pyrrhotite
TR=trace
vis=visible
fg=fine grained (<1mm)
diss=disseminated

DDH: 127 Section: 1037

Major Unit		Minor Unit												Veins				Mineralization			
From	To	From	To	Rock Name	Colour	Composition	Texture/Primary Structures	Foliation Angle	Alteration	% , Type	Size	Selvage	Angle to CA	min1	min2	Magnetite	Other				
0	3.57			OB																	
3.57	5.6			V3 massive / feldspar-phyric	dark green-grey	V3 + small white crystals <<1mm, possibly feldspar?	massive / feldspar-phyric	none	none	1% c, 1% q-c-ep	all 1mm	light beige /green alteration	40-45dca, some stockwork	TR fg diss py blebs		not magnetic					
5.6	7.3			Altered V3 amygdular	medium green	3-4% white amygdules, 2-3mm, 2-3% dark amyg (2-3mm)	amygdular	faint at 60dca	none	1% q-c-ep, 3% c, 1-2% q(+/-alb)	q-c-ep= 1-2mm, q-c=2mm-1cm, q+/- alb=5mm-2cm	light green halo, biotite selvage	40dca q veins, some stockwork	TR-1% fg py blebs	TR fg light tabular cryatals	moderate magnetic	q veins have red colour				
		6.8	7.3	dark grey colour																	
7.3	12.42			V3 massive	medium green and grey	V3	breccia	none	none-weak carbonate in light grey regions	1% c, 1%q-c, 30-50% q	q-c (5mm)	biotite-pyrite	deformed/stockwork	TR fg py in along veins							
		7.38	7.5	possibly breccia - stockwork of carbonate and chlorite veins give the core a brecciated appearance																	
		7.83	7.86	dark orange rusty alteration along fracture plane and within q-c vein. TR fg vis py blebs																	
		9.95	10.3	moderate biotite alteration and pyrite stringers, 3.5cm white quartz vein at 40dca, foliation at 40dca, cubic diss py (2mm)																	
		10.3	11.37	light green, medium grey, brown and white mottled, 1% c vns (<1mm), weak biotite alteration, weak to mod magnetism																	
		11.37	11.9	dark green with folded quartz vein (with minor carbonate +/- chl, py; 37cm long, 1-2.5cm wide), fold axis perpendicular to core axis, weak biotite alteration, 2% fg py in blebs in/near vn																	
		11.9	12.42	mottled texture (as above)																	

Major Unit		Minor Unit		DDH: 127 Section: 1037 CONTINUED						Veins				Mineralization			
From	To	From	To	Rock Name	Colour	Composition	Texture/Primary Structures	Foliation Angle	Alteration	%, Type	Size	Selvage	Angle to CA	min1	min2	Magnetite	Other
12.42	13.09			V3 amygdular	medium green and brown mottled	10% dark amygdules (2-4mm), 5-8% white amygdules (1-4mm)	amygdular	faint 60dca	none	3% q-c (+/-cl, py), 1% q	q-c=2mm -1.5cm, q=2mm	none	q-c~65, q~70dca	TR fg py blebs in veins		no to weakly magnetic	
13.09	20.07			V3 massive +/- breccia? Pillow?	medium green and grey	V3	massive +/- breccia? Pillow?		none-weak carbonate in light grey regions	2-3% q-c-cl, 1% c, 2% q-alb-cl-py (in sheared zones)	q-c=1mm -1.5cm, c=1-2mm, q-alb=2mm-1.5cm	biotite	q-c at 60-70dca, some stockwork	TR fg py in veins	TR po (in q-c vn at 14.09m)	moderately magnetic	
		14.57	14.84	possibly breccia - possible fragments of grey within green unit													
		14.84	15.04	possibly pillow - 10cm portion of dark grey within green. Brown/black colouration around the grey "fragment"													
		16.3	16.6	faint foliation at 70dca													
		17.49	17.61	shear at 75-80dca, weak to moderate biotite alteration													
		18.55	18.86	shear at 70dca, q-alb (+chl, py) vein, weak biotite and moderate to strong carbonate alteration, 1% fg cubic py													
		19.19	19.51	shear at 70dca, slightly darker green and grey, q and q-carb-cl-py veins													
20.07	21.73			QFP 1?	beige-pink	8-10% quartz (3-4mm), 50-60% beige feldspar (1-2mm; pink near microfractures), 1-2% mafics (1mm), 28-30% medium to dark grey aphanitic matrix	porphyry	none	none	5% q	~6mm	albite?	stockwork	TR fg py diss		not magnetic	upper contact: 50dca, lower contact: ~90dca
		20.78	21.24	"smeared" look, dark pink background with a few visible crystals of feldspar and quartz													
		21.24	21.27	light pink band at 60dca													

Major Unit		Minor Unit		DDH: 127 Section: 1037 CONTINUED						Veins				Mineralization			
From	To	From	To	Rock Name	Colour	Composition	Texture/Primary Structures	Foliation Angle	Alteration	%, Type	Size	Selvage	Angle to CA	min1	min2	Magnetite	Other
21.73	22.07			V3	dark green-grey	V3	?	faint at 60dca	moderate biotite and carbonate, chl in bands	<1% c	1mm	biotite?	60dca	1-2% py cubic/ blebs (4mm, 1mm in veins)		weakly magnetic	
22.07	22.15			swirled QFP (perhaps QFP 1???), contains swirled q vn, no contacts vis - perhaps occurred along fractures? Sides perhaps slightly blended into the surrounding V3													
22.15	22.34			V3 (as above 21.73-22.07m)													
22.34	22.85			QFP 2?	dark grey with white/beige feldspar	1-2% quartz, 30-50% feldspar? 5-10% mafics (elongated < 1mm x 2-3mm?), 30+% matrix? smeared - difficult to tell composition	porphyry	none	none	10-15% q (+/- bt, feldspar/alb?, cal?)	3-7mm	none	straight at ~60dca; folded/deformed	TR fg diss py cubic		not magnetic	upper contact: 55-60dca, smeared lower contact
22.85	25.35			V3 massive	dark green-grey	V3	massive?	none	none	2% q-c-ep, 1% q, 1% c	q-c-ep= 1mm-1.5cm, q-c=2mm, c=1mm	none	q-c-ep= deformed, c= stockwork, q=folded	TR fg py diss, 1mm cubic in veins		weakly magnetic	
		24.84	25.35	dark grey colour near QFP, faint foliation at 50-55dca													
25.35	43.37			QFP 2	dark grey with white/beige feldspar, light pink feldspar in places	1-2% quartz (1-2mm), 50-60% feldspar (beige to pink, 1-5mm), 5-10% mafics (1-2mm), 30% dark grey aphanitic matrix	porphyry	none	none	1% q	13cm wide	none	~30dca	TR fg cubic py		not magnetic	upper contact: folded, lower contact: ~70dca
		32.4	34	smeared and pink coloured feldspar													

Major Unit		Minor Unit		DDH: 127 Section: 1037 CONTINUED						Veins				Mineralization			
From	To	From	To	Rock Name	Colour	Composition	Texture/Primary Structures	Foliation Angle	Alteration	%, Type	Size	Selvage	Angle to CA	min1	min2	Magnetite	Other
		35.94	37	smeared and pink colour of feldspar													
		40.2	40.6	smeared and grey coloured													
		40.6	42.07	occasional feldspar crystals are hot pink coloured													
		42.07	42.24	majority of feldspar crystals are stained hot pink, remaining crystals have bright white/yellow colour													
43.37	44.19			V3 biotite shear	grey	V3	shear	shear (43.37- 43.81m) at 70dca	moderate biotite and carbonate	5-10% q-alb-chl	4mm	bt	veins in shear at 70dca, others are folded	TR-1% py fg along veins	TR-1% fg po along veins	not- weakly magnetic (from po?)	
44.19	46.3			V3 amygdular	medium green - grey	5-10% white amygdules (1- 2mm), 5% dark amygdules (1- 2mm)	amygdular, mottled texture	none	weak biotite	2% q-c (+/-ep), 1% c	q-c= 3-5mm, c=1mm	chl	stockwork	TR fg py +/- po in/near veins		not magnetic	
EOH																	

Murgor Resources

BARRY - MAIN ZONE - Drill Core Logging

Logged by Kathryn Kitney

V3=mafic volcanic
T3=mafic tuff
QFP=quartz-feldspar porphyry

q=quartz
alb=albite
c=carbonate
bt=biotite
ep=epidote
chl=chlorite

VG=visible gold
py=pyrite
po=pyrrhotite
TR=trace
vis=visible
fg=fine grained (<1mm)
diss=disseminated

DDH: 135 Section: 1037

Major Unit		Minor Unit												Veins				Mineralization			
From	To	From	To	Rock Name	Colour	Composition	Texture/Primary Structures	Foliation Angle	Alteration	% , Type	Size	Selvage	Angle to CA	min1	min2	Magnetite	Other				
0	3.72			overburden																	
3.72	7.04			V3 massive? Breccia?	orange rusty to green and grey	V3	massive? Breccia? Colour banding in core appear to pinch and swell	faint - 70-75dca	weak carbonate	none				TR-1% fg cubic py diss		1% fg diss					
		3.72	4.95	rusty orange alt				faint - 75dca	rusty on weathered surfaces	10-15% qtz- alb	1mm-3cm (larger is brittle host rock within vn), pinched and swell/boudin	thin bt on small veins	along weak foliation at 70-75dca	1-2% py blebs up to 2mm	TR fg white tabular crystals within/ near py	TR fg vis mt					
		5.09	5.36	rusty orange alt(as above)																	
		5.57	6.63	rusty orange alt (as above)																	
		6.53	6.63	rusty orange alt (as above) - band of 20-30% pyrite (cubic and blebs <=5mm)																	
		6.97	7.04	rusty orange alt (as above)																	
7.04	8.21			QFP 1?		5% qtz (2-3mm), 50-60% feld (2-3mm), 10-15% mafic (1mm - 2mm), smeared: no grey matrix	smeared QFP1 or QFPcro?	none	pink colour	6% qtz	2mm-2cm	white crystals +/- cl	45-60dca	TR-1% fg cubic py diss	TR white tabular crystals <1mm	not mag	upper contact ~70dca, lower not visible				

Major Unit		Minor Unit		DDH: 135 Section: 1037 CONTINUED						Veins				Mineralization			
From	To	From	To	Rock Name	Colour	Composition	Texture/Primary Structures	Foliation Angle	Alteration	%, Type	Size	Selvage	Angle to CA	min1	min2	Magnetite	Other
		7.04	7.42	pink coloured, smeared looking for most part													
		7.42	8.21	beige-white coloured, separated from above by qtz vn ~1cm thick at 45dca													
8.21	8.91			V3 massive with local tectonic breccia	medium green and grey	V3	massive with tectonic breccia	none	cl along fractures	1-2% q with yellow-orange colour, pink discolouration	1.5cm	none	50dca	2% py cubic/blebs up to 2mm diss	TR-1% fg white tabular crystals in/near py	TR fg diss vis mt	
		8.46	8.8	tectonic breccia - 3mm-3cm angular fragments													
		8.56	VG	small fleck of VG in py?													
8.91	11.09			V3	dark grey	V3	none	none	beige/pink	10-15% q-alb (vuggy/infilling texture), 5-10% c	q-alb= 1mm-1.5cm, c=~1cm blebs	thin bt	c=deformed and mostly just blebs, q-alb deformed or at 55-60dca	5% cubic py fg-4mm	1% fg white tabular crystals	strong magnetic, not vis	beige/pink alteration around vuggy veins
		9.95	10.33	strong beige/pink alteration, most vuggy q-alb vns are here with infilling texture, large cubic pyrite													
		10.88	10.94	mod beige/pink/yellow alteration around veins, vuggy vein texture													
11.09	13.34			V3 +/- amygdular	dark grey	V3 +/- amygdular		faint at 60dca	bands of weak bt	5%q-alb, 2-3% q-c, q-alb(+/-c)	q-alb= 5mm to 2cm pinch and swell, q-c=2-5mm	bt on q-alb	q-alb at 60dca, q-c at 60dca	1% py fg blebs and cubic in/along veins	TR fg white tabular crystals within/near py	strong magnetic, no vis mt	
		12.88	13.34	vuggy q-alb (+/-c) veins with infilling texture, rock broken up into cm long pieces													
13.34	13.69			V3 amygdular	dark grey with white amygdular	5-10% white amygdular (1mm round to 1x2mm)	amygdular										

Major Unit		Minor Unit		DDH: 135 Section: 1037 CONTINUED						Veins				Mineralization			
From	To	From	To	Rock Name	Colour	Composition	Texture/Primary Structures	Foliation Angle	Alteration	%, Type	Size	Selvage	Angle to CA	min1	min2	Magnetite	Other
13.69	18.04			V3 amygdular	medium grey-green	5-10% dark amyg (1-2mm)	amygdular+ breccia	none	green and grey wavy patterns	1% q-c (+/-ep)	1mm-1.5cm	chlorite	stockwork, deformed	TR py in fg blebs near/along veins	TR po in fg blebs in/along veins	no to weak mt	
		13.9	14.7	possibly pillow? - grey and green region 10cm in diameter with brown colour surrounding													
18.04	19.73			V3 massive	pale green	V3	massive	none	none	2% q-c (c>q)+/-ep	1mm-3.5cm	chlorite	stockwork	TR fg py+po			
19.73	26.83			T3	medium green to dark grey	T3- 3%-10% feldspar crystals ~1mm	graded bedding- finer up hole	faint at 60dca	brown and green banding	<1% q, 2% q-c, 1% c	q=1.5cm, q-c=2mm-1.5cm, c=1-3mm		stockwork, folded, q vn is at ~60dca	TR silver metallic blebs-large (3-4mm) in q vn			
26.83	28.5			V3 massive	turquoise green	V3	mass	none	weak carbonate		1mm in fractures		stockwork				
28.5	31.46			V3 breccia? Pillow?	dark brown/ grey and light green	V3	breccia and mottled/swirled texture	none	no carb alt	1% q-c	3mm-1cm		deformed	TR silver metallic mineral in/along q-c veins			epidote green colour, 31.36-31.46m is pale grey and green near q-c veins
EOH																	

Murgor Resources

BARRY - MAIN ZONE - Drill Core Logging

Logged by Kathryn Kitney

V3=mafic volcanic
T3=mafic tuff
QFP=quartz-feldspar porphyry

q=quartz
alb=albite
c=carbonate
bt=biotite
ep=epidote
chl=chlorite
gt = garnet

VG=visible gold
py=pyrite
po=pyrrhotite
TR=trace
vis=visible
fg=fine grained (<1mm)
diss=disseminated

DDH: 210 Section: 1037

Major Unit		Minor Unit												Veins			Mineralization			
From	To	From	To	Rock Name	Colour	Composition	Texture/Primary Structures	Foliation Angle	Alteration	% , Type	Size	Selvage	Angle to CA	min2	min1	Magnetite	Other			
0	3.2			overburden																
3.2	19.16			QFP Crowded	beige-pink	50 feldspar, 10-15% mafics (now chlorite), 20-30% quartz, 2% pyrite	"granitic"	none	potassium feldspar? (pink colour) near micro-fractures	20% q	1.5-3cm	white (albite?)	stockwork	1-2% fg py						
19.6	21.8			V3 amygdular	green to dark green/grey	1-2% dark amygdules	amygdular	none	weak carbonate	5% q-c	3mm-2.5cm	bt	moderate to high angles	TR fg py		weakly magnetic	increased Au grade with increased py			
		19.22	19.23	small pink quartz (+/- carb) vein at 75dca																
		20.61	20.68	ep+garnet vein, no specific direction																
21.8	28.9			V3 massive	dark grey-green	V3	massive	none	weak chl, bt, carbonate	1% c, 2% qtz- alb, 3% q-c	2mm-4cm	c= cl, q- c=bt+py, q= beige-brown (car+silic?)	moderate to high angles	TR fg py near veins		TR fg vis mt diss				
		23.1	23.34	minor shear at 60dca, veins follow this orientation																
		23.97	25.4	shear at 45dca, veins follow this orientation																
		27.7	28.9	shear at 75dca, veins follow this orientation																
		28.43	28.45	localized gt+/-ep																

Major Unit		Minor Unit		DDH: 210 Section: 1037 CONTINUED						Veins				Mineralization			
From	To	From	To	Rock Name	Colour	Composition	Texture/Primary Structures	Foliation Angle	Alteration	%, Type	Size	Selvage	Angle to CA	min2	min1	Magnetite	Other
28.9	29.5			V3 breccia?	green and grey	V3	deformed (elongated) volcanic breccia?	55dca in places	weak chl	1-2% q-c+py, 1% ep (folded)	1mm	none	stockwork	TR-1% fg py		weakly magnetic	
29.5	32.31			V3 amygdular	green-grey colour	1-2% dark amygdules, 1% white calcite amygdules (<=1mm)	amygdular	none	weak chl	2% q-alb-c+py, 2% c	q-c-alb-py=2-5cm, c=1-2mm	bt	70dca	TR-1% fg py		weakly magnetic	
		29.5	30.1	weak-moderate shear at 55dca, dark grey colour, moderate-strong bt, 5cm q-c-alb-py vein at 55dca, fg diss py near veins													
		30.9	31.1	minor weak shear, bands of bt, cl, q-c veins at 65-70dca													
		31.6	32.31	shear at 55dca, green grey to dark grey													
32.31	41.2			V3 massive +/- breccia	green-grey colour	V3	massive +/- breccia	weak 55-60dca	moderate to strong bt bands, moderate carbonate	1% q, 2% q-c, 3% c (=/- bt,cl), locally ep (2mm)	q=3-4cm, q-c=1-2cm, c=2mm-5cm	q=bt+fg py, all=bt	q=high, q-c and q=mod-low	TR fg py in/near veins		weakly magnetic	
		32.31	32.65	continuation of above shear at 60-70dca													
		35.45	35.7	minor shear at 45dca, increase in bt bands, q-c veins (2mm), py stringer													
		36.65	37.05	possibly breccia - dark grey portions have smeared contact with surrounding chlorite-rich rock													
		37.6	37.95	highly deformed carbonate veins, strong bt alteration, 0.75cm py+mt band, TR light/white tabular crystals, possibly tectonic breccia - 1cm fragments of grey material with brown/black (biotite?) matrix													
		39.2	39.5	deformed calcite vein + ep (+/- gt) within vein													
		40.4	40.9	several veins of ep+cal+/-qtz+/-gt+/-py (folded/deformed, 2-3mm)													

Major Unit		Minor Unit		DDH: 210 Section: 1037 CONTINUED						Veins				Mineralization			
From	To	From	To	Rock Name	Colour	Composition	Texture/Primary Structures	Foliation Angle	Alteration	% , Type	Size	Selvage	Angle to CA	min2	min1	Magnetite	Other
41.2	41.46			QFP 2	medium grey-pink	60%feld?, 3%qtz?, 5-10% mafics (now chl), 27% dark grey aphanitic matrix	crystal boundaries smeared	none	weak carbonate alteration	none				none			difficult to determine % feldspar. Named QFP2 based on % quartz
41.46	41.5			V3	green between QFPs												
41.5	41.98			QFP 2	medium grey-pink	60%feld?, 3%qtz?, 5-10% mafics (now chl), 27% dark grey aphanitic matrix	crystal boundaries smeared	none	weak carbonate alteration	1% q	5mm	none	stockwork	none			difficult to determine % feldspar. Named QFP2 based on % quartz
41.98	43.16			V3	green between QFPs	V3	none	weak, ~60dca	moderate to strong bt	1% q-c+py, 2% c	q-c=3-4mm, c<=1mm	q-c: bt+py	~60dca	TR-1% fg py diss, 1-2mm py cubic in veins			weakly magnetic
43.16	55.45			QFP 2	medium grey-pink	60%feld?, 3%qtz?, 5-10% mafics (now chl), 27% dark grey aphanitic matrix	porphyry		weak carbonate	3-5% q	5mm-1.5cm	none	stockwork	TR-1% fg py			
		43.16	50.43	pink QFP 2, crystal boundaries smeared, difficult to tell composition, weak to moderate carbonate alteration													
		50.43	50.5	unaltered QFP 2 - dark grey aphanitic groundmass, approx same composition													
		50.5	52.1	foliation in unaltered QFP 2 at 70dca, bt and mafic crystals intensely smeared (<0.5mmx2-3mm)													
		52.1	55.45	ep+garnet vein, no specific direction													

Major Unit		Minor Unit		DDH: 210 Section: 1037 CONTINUED						Veins				Mineralization			
From	To	From	To	Rock Name	Colour	Composition	Texture/Primary Structures	Foliation Angle	Alteration	%, Type	Size	Selvage	Angle to CA	min2	min1	Magnetite	Other
55.45	56.2			unaltered QFP 2 and V3													
56.2	61			V3 amygdular	green-grey	V3	mottled, white and dark amygdules (locally up to 10%)	60-90 dca	none	1% q-c+/- cl, 3% c	q-c=2.5cm, c=2mm	q-c=bt+py	folded q-c+cl at 25dca	TR fg py	TR fg po		
61	68.4			V3 massive	green-grey	V3	minor amouts of white amygdules (<1%)	none	none	1% q-c+/- cl, 3% c	q-c=2.5cm, c=2mm	q-c=bt+py, c=bt in shear		TR fg py	TR fg po		
		61.35	61.85	possibly breccia - indication of possible dark grey fragments within chlorite-rich rock													
		62	62.8	banding of dark grey and green within unit - could be indication of elongated clasts													
		63.22	63.75	shear at 65dca with bt, cl and carbonate alteration													
68.4	73.26			V3 amygdular	medium green-grey	5% dark amygdules, 5% light amygdules (1-2mm)	amygdular	none	bt bands, moderate chl	1% q-c, 1% c	1-2mm	bt	35-40 and -50dca				
		70.07	70.87	moderate shear at ~30dca, strong bt alteration, deformed c and q-c veins, stretched white amygdules (4x1mm), TR-1% py													
73.26	77			V3 massive +/- breccia	green and grey	V3	massive +/- breccia	none	cl	2% q-c-ep-po, carb+cl	3mm-1.5cm	bt along c+cl	stockwork	TR-1% po mostly with veins			
EOH																	

Murgor Resources

BARRY - MAIN ZONE - Drill Core Logging

Logged by Kathryn Kitney

V3=mafic volcanic
T3=mafic tuff
QFP=quartz-feldspar porphyry

q=quartz
alb=albite
c=carbonate
bt=biotite
ep=epidote
chl=chlorite

VG=visible gold
py=pyrite
po=pyrrhotite
TR=trace
vis=visible
fg=fine grained (<1mm)
diss=disseminated

DDH: 31 Section: 1074

Major Unit		Minor Unit												Veins				Mineralization			
From	To	From	To	Rock Name	Colour	Composition	Texture/Primary Structures	Foliation Angle	Alteration	% Type	Size	Selvage	Angle to CA	min1	min2	Magnetite	Other				
0	1.5			V3 massive	dark green	V3	none	none		1% cl, 2% q-c, 2% carb	cl=1mm, q-c=4mm, c=1-2mm	bt	q-c=45-50dca	TR-1% py fg diss		weakly magnetic					
1.5	2.26			V3	medium grey with orange-brown weathered surface	V3	none	none	weak rusty colour	8% q, 1% c	q=1-2cm, c=1mm	py on q veins	stockwork	1% fg py		TR vis mt diss					
2.26	2.9			V3	dark brown and green, dark red weathered surface	V3	none	none	red from weathered py	1% q-c, 1% cl	1mm	none	stockwork	5%?	fg diss py	TR vis mt diss					
2.9	14.03			V3	medium grey with orange-brown weathered surface	V3	none	none	weak to moderate carbonate	15-10% q-alb	5mm-3cm	carb/ank +/- py	stockwork	2% fg diss py (locally 10%)		TR vis mt diss					
		13.33	VG	VG grain																	
14.03	17.75			V3 massive/+/- breccia?	medium green and grey	V3	masive with possible volcanic breccia and shear	55dca in shear	strong carbonate	1% q-alb, 1% c	q-alb=2mm-2.5cm boudined, c=2-3mm	bt (1-2mm)	stockwork	Tr py fg diss		TR vis mt diss					
		14.95	15.20	appears brecciated - dark grey "fragments" surrounded by chlorite																	

Major Unit		Minor Unit		DDH: 31 Section: 1074 CONTINUED						Veins				Mineralization			
From	To	From	To	Rock Name	Colour	Composition	Texture/Primary Structures	Foliation Angle	Alteration	%, Type	Size	Selvage	Angle to CA	min1	min2	Magnetite	Other
		15.03	17.75	shear at 55dca - veins here are parallel to shear foliation													
		16.83	17.66	rusty orange-brown to red-brown alteration on weathered surface - combination of carb alteration (weak-moderate) and increase fg diss py													
17.75	19.7			V3 massive	medium grey-green	V3	none	none	strong carbonate	1% carb, 10% q-alb-c with cl+py, TR mt vnlt	c=1mm, q-alb-c=2cm, mt=<1mm	q-alb-c=bt	q-alb-c=50-55dca	TR py diss		TR vis mt diss	
		18.9	19.18	missing core													
19.7	28.28			V3 massive +/- local amygdules	medium green and grey	V3	"mottled" texture			1% q, 1% q-c	1cm	bt on q-c		TR-1% fg py		TR vis mt diss	
		20.16	20.33	moderate to strong shear with bt alteration, strong carbonate alteration													
		20.20	VG	grain in quartz vein													
		21.54	VG	grain													
		21.54	21.67	shear at 45-50dca, folded q-alb-c vein, strong bt and carbonate alteration, 8% py in large blebs (1-2mm)													
		21.74	22.04	locally contains 1-3% carbonate amygdules (1-2mm)													
		22.20	22.30	moderate to strong shear with increased biotite													
		22.40	22.60	quartz-calcite vein is cut and offset by 1mm quartz-calcite veins with brown weathered selvages													
		24.43	25.02	weak to moderate shear at 35dca, mod to strong bt and carbonate													
		27.20	28.18	weak to moderate shear at 50dca, mod to strong bt and calcite, folded q-alb vein													
28.28	29.21			V3 massive	medium green-grey	V3	none	none	strong carbonate	1% q-c, 2% c, 1% cl	1-2mm	none	~20dca	TR fg py	1% po blebs up to 1mm		
29.21	31.28			V3 feldspar-phyric	green-grey with small white crystals	V3 - 1-2% feldspar crystals (~0.5mm)	feldspar-phyric	none	none	1% c+/-cl, <1% q-c	c=1mm-1.5cm, q-c=2mm	none	c+cl=40 dca	TR sulfides	TR bright white crystals		
31.28	31.5			V3 amygdular	medium green	5% calcite amygdules (1mm)	amygdular	none	none	TR c	<1mm	none			none	weakly magnetic	
EOH																	

Murgor Resources

BARRY - MAIN ZONE - Drill Core Logging

Logged by Kathryn Kitney

V3=mafic volcanic
T3=mafic tuff
QFP=quartz-feldspar porphyry

q=quartz
alb=albite
c=carbonate
bt=biotite
ep=epidote
chl=chlorite

VG=visible gold
py=pyrite
po=pyrrhotite
TR=trace
vis=visible
fg=fine grained (<1mm)
diss=disseminated

DDH: 117 Section: 1074

Major Unit		Minor Unit												Veins			Mineralization			
From	To	From	To	Rock Name	Colour	Composition	Texture/Primary Structures	Foliation Angle	Alteration	% , Type	Size	Selvage	Angle to CA	min1	min2	Magnetite	Other			
0	3.48			Overburden																
3.48	6.67			V3 amygdular	dark grey-green	15% cal cite amygdules, 5-10% dark/clear amygdules (quartz?)	amygdular, "blotchy" look, rusty "pitted" look from weathering in places	none	moderate carbonate	q-alb=2%, q-c=5%, c=2%, q-ep=1%, cl=1-2%	q-alb=4mm-1.5cm, q-c=5-6cm, c=2-4mm, q-ep=1.5cm, cl=2mm	chl	c=none, q-alb=40-60dca	1-2% py (1-2mm) near veins		5% fg vis, diss mt				
		6.28	6.3	pitted rusty region, possible that the calcite amygdules have prefferentially weathered here to ankerite																
		6.39	6.52	broken up rock, average size 2-5cm "slices", rusty colour - brittle fault?																
6.67	12.03			V3 breccia +/- amygdular	medium green and grey	V3	breccia, "swirled" look	70dca	weak chl and carbonate	c=2-3%, c-q=1%, q-c=2%, q-alb=2%	c=3mm, q-c=pinch and swell 4mm-2cm, q-alb=folded/pinched, 1cm	bt and chl, increase in py with increased bt	q-c:45-50dca vein (3mm) cuts 50-55dca vein (3mm), q-alb=40-45dca	1% fg py		1% vis mt diss				
		7.03	7.15	broken up rock, average size 2mm-2cm "slices", rusty colour, brittle fault?																
		7.5	7.55	broken rock right at 7.5 marker, very small pieces (less then 1cmx 1cm), possible fault																
		7.55	8	V3 amygdular (as above from 3.48-6.67), local increase in mt																

Major Unit		Minor Unit		DDH: 117 Section: 1074 CONTINUED						Veins				Mineralization			
From	To	From	To	Rock Name	Colour	Composition	Texture/Primary Structures	Foliation Angle	Alteration	% , Type	Size	Selvage	Angle to CA	min1	min2	Magnetite	Other
12.03	12.66			QFP 2	beige/medium grey	3% quartz (3mm), 20% mafics (chloritized), 77% feldspar and matrix ("smeared")		60-65dca to 70-80dca near lower contact	chl of mafics								upper contact at 60-65dca, lower=70-80dca
12.66	17.47			V3 breccia +/- amygdular	medium green and grey	V3	breccia, "swirled" look	65dca	weak chl and carbonate	1% q-c, 5-10% q-alb	q-c=3m, q-alb=folded: 2mm-1cm	bt and py	folded, ~30-60dca	1% py diss		1% mt diss in chl altered zones	
		14.12	VG	VG grain in q-alb vein and wall rock, boudined, increased bt around vein													
		15.53	15.83	strong bt alteration with 40-50% fg py (1-3mm blebs)													
		15.71	VG	VG grain within large py bleb													
		15.83	16	cl-rich bands/vns (2-3mm), moderate bt alteration, 1-2% po (1-2mm blebs), 1% py (2mm blebs)													
		16	16.5	V3 amygdular (as above from 3.48-6.67), local increase in mt													
		16.79	17.47	strong bt alteration, bt and py selvages, py (3-4mm) blebs and cubeic in veins, veins folded at 30-60dca, upper contact at ~60dca, lower contact at 18.12m at 75-80dca													
17.47	18.12			V3 amygdular	dark grey/brown	10% calcite amygdules	amygdular	none	strong bt, moderate-strong carbonate	rusty orange/brown feathered veinlet (<1mm), possibly c vein +/- ep	<=1mm, feathery	none	none	2% fg py in bands, blebs and cubic		weakly magnetic, no vis mt	lower contact with V3 breccia at 75-80dca
		17.76	VG	3 grains of VG, in fg py													
18.12	20.17			V3 breccia	dark green/brown	V3	breccia - fragments of dark grey rock within green and brown speckled matix	none	weak carbonate, moderate chl	c=3%, q-c=1%	c=1-3mm, q-c =3mm	bt and chl	none	TR-1% py, diss blebs (1mm)	1-2% po blebs (1-3mm)		po and py replacing one another

Major Unit		Minor Unit		DDH: 117 Section: 1074 CONTINUED						Veins				Mineralization			
From	To	From	To	Rock Name	Colour	Composition	Texture/Primary Structures	Foliation Angle	Alteration	% , Type	Size	Selvage	Angle to CA	min1	min2	Magnetite	Other
20.17	22			V3 amygdular	medium grey/green	1-2% calcite amygdules (1mm)	amygdular	none		2% c	c=1-5mm	none	50dca and 35dca	1% py (1mm blebs)	2% po (1-2mm blebs)		
22	22.7			V3 massive	medium grey/green	V3	none	none	none	c=1%, q-c=1% (+cl)	c=1mm-4mm, q-c=4mm	q-c=bt?	c=20-25dca, q-c=35dca	1% py (1mm blebs)	2% po (1-2mm blebs)		
22.7	24.4			V3 breccia? Pillow?	pale green and brown	V3	breccia? Pillows?	none	weak to moderate bt	c=1%, q-c=1%, q=1%	c=2mm, q-c=3-4mm, q=1cm	bt +/- mt?	q-c at 40-50dca			fg diss mt starts at 26.9m	
		24.3	25	mottled look - possibly V3 amygdular with altered background? dark blebs (1mm)													
		25.9	26.12	strong bt-calcite shear at 70dca, with q-c+cl+po+py veins at 65-70dca (folded and boudined)													
24.4	30.41			V3 massive	pale green with small black crystals within the light bands	V3	mottled with very pale green/grey banding		pale green/grey colour								
30.41	31			V3 breccia	medium grey and green	V3	breccia, "swirled" texture in places	none	moderate carbonate and chl	1% c, 1% q-c+po	c=1mm, q-c=2mm			TR fg po within q veins		TR fg vis mt	
EOH																	

Murgor Resources

BARRY - MAIN ZONE - Drill Core Logging

Logged by Kathryn Kitney

V3=mafic volcanic
T3=mafic tuff
QFP=quartz-feldspar porphyry

q=quartz
alb=albite
c=carbonate
bt=biotite
ep=epidote
chl=chlorite

VG=visible gold
py=pyrite
po=pyrrhotite
TR=trace
vis=visible
fg=fine grained (<1mm)
diss=disseminated

DDH: 118 Section: 1074

Major Unit		Minor Unit												Veins			Mineralization			
From	To	From	To	Rock Name	Colour	Composition	Texture/Primary Structures	Foliation Angle	Alteration	% , Type	Size	Selvage	Angle to CA	min1	min2	Magnetite	Other			
0	2.4			V3 breccia	green and grey	V3	volcanic breccia	none	strong carbonate, rusty	8% q-alb-c	3mm-4cm pinch and swell			TR-1% py		weakly magnetic				
		1.82	1.85	dark red/orange rusty alteration band with bt at 35dca																
		1.91	2.2	increase in q veins with bt selvages, rusty alteration, bt selvages, red-pink colour between veins																
2.4	4.57			V3 massive	medium green	V3	none	none	weak carbonate	1% q-c	1-2mm	bt?.mt?	high-35-45dca	2% mt diss (<=1mm)	TR py, near veins	2% diss-vis (<=1mm)				
4.57	10.55			V3 massive	green and grey	V3	none	none	moderate-strong carbonate	3-5% q-alb	1-2cm, pinch and swell	often bt? 1mm thick	60-65dca, folded	TR fg diss py		TR fg vis mt				
		4.9	5.25	possibly breccia - gradational contacts between green and grey colours within unit																
		9.27	9.9	possibly breccia - gradational contacts between green and grey colours within unit																
10.55	12.45			V3 feldspar-phyric	medium green	2% feldspar crystals (~1mm)	feldspar-phyric	none	weak to moderate carbonate	2% q-c+cl	2mm-1cm		60-65dca	TR fg diss py						
12.45	21.51			V3 massive +/- breccia	green and grey	V3	massive +/- breccia: possible fragments seen, "swirled" texture	none	strong bt	1% q-c, 2% c	c=2-3mm, q-c=2mm	bt on q-c	veins measured at 50 and 80dca	TR fg po and py						
		14	14.5	- appears to contain fragments																
		16.7	17.2	- appears to contain fragments																

Major Unit		Minor Unit		DDH: 118 Section: 1074 CONTINUED						Veins				Mineralization					
From	To	From	To	Rock Name	Colour	Composition	Texture/Primary Structures	Foliation Angle	Alteration	%, Type	Size	Selvage	Angle to CA	min1	min2	Magnetite	Other		
21.51	24.56			QFP 2	3% quartz, 50% feldspar, 10-15% mafics, 32% dark grey aphanitic matrix		porphyry xenoliths of dark grey/fine grained unit (1x3cm and larger)	none	none	none									
24.56	25.5			V3 amygdular	medium green-grey	5-10% calcite amygdules (1mm)	amygdular	none	bt and chl bands	2% q-alb, 2% c	c=1-5mm, q-alb= 1cm	bt and chl	q-alb=50-55, c=deformed	TR fg sulfides					
25.5	26.09	V3 massive (see 2.4-4.7m)																	
26.09	27.64	V3 amygdular (see 24.56-25.5m)																	
27.64	28.5	V3 massive (see 2.4-4.7m)																	
28.5	31.5			V3 amygdular + massive	green-grey	5% white calcite amygdules (1mm)	volcanic breccia + amygdular	none	none	1% q-c, 5-8% c	q-c=1cm, c=1mm-2cm	Chl, bt +/- mt	low and high angles	TR fg sulfides			dark vein selvages are magnetic		
		30.7	31.5	massive, appears banded with some "swirled" texture															
EOH																			

Murgor Resources

BARRY - MAIN ZONE - Drill Core Logging

Logged by Kathryn Kitney

V3=mafic volcanic
T3=mafic tuff
QFP=quartz-feldspar porphyry

q=quartz
alb=albite
c=carbonate
bt=biotite
ep=epidote
chl=chlorite

VG=visible gold
py=pyrite
po=pyrrhotite
TR=trace
vis=visible
fg=fine grained (<1mm)
diss=disseminated

DDH: 142 Section: 1088

Major Unit		Minor Unit												Veins				Mineralization			
From	To	From	To	Rock Name	Colour	Composition	Texture/Primary Structures	Foliation Angle	Alteration	% , Type	Size	Selvage	Angle to CA	min1	min2	Magnetite	Other				
0	1.37			V3 amygdular	medium grey and green	3-5% calcite amygdules (1-3mm)	amygdular	55-60dca	moderate to strong carbonate, orange near large q vein	q-c=2%, q+/-alb=3%	q+/-alb=3cm, q-c=5mm-1cm pinch and swell	none	q+/-alb=deformed, q-c vn folded isoclinally ~40-60dca	Tr-1% py near folded q-c vein		moderately - strongly magnetic					
1.37	4.2			V3 massive? Breccia?	medium grey and green	TR dark amygdules	massive? Breccia?	50dca	moderate carbonate	q-c(+py)=1%, q+/-alb=3, c<=1%	q-c=3mm, q+/-alb=5mm-5cm, c=1mm	biotite and rusty	q-c=folded/deformed, q-alb=40dca, large q+/-alb=50dca	TR fg py diss		tr fg diss mt					
		1.86	2	possible breccia - possible grey fragments in green host here																	
		2.71	2.83	5cm q+/-alb with rusty alteration, 4-5 cm before this is broken rock in 2x2cm chunks																	
		2.83	4.2	2% small rusty ank? veins/bands																	
		3.08	3.2	possible breccia - possible grey fragments in green host here																	
4.2	5.55			V3 amygdular	medium grey and green	1-2% calcite amygdules (2-5mm) with rusty colour	amygdular	none	weak rusty colour	q-c+/-alb=1-2%, c=TR-1%	q-c=3mm-1.2cm, c<=3mm	rusty	q-c=40dca, some stockwork, c<1mm	TR py in q-c and q-alb+/-c veins		TR vis mt vis					

Major Unit		Minor Unit		DDH: 142 Section: 1088 CONTINUED						Veins				Mineralization			
From	To	From	To	Rock Name	Colour	Composition	Texture/Primary Structures	Foliation Angle	Alteration	%, Type	Size	Selvage	Angle to CA	min1	min2	Magnetite	Other
5.55	10.34			V3 breccia?	medium-dark grey	V3	breccia?	none	rusty orange, TR pink near some q veins	q-c=1% (boudined); c=1% :: In rusty orange breccia: q-c=3%, c=1%	q-c=3-4mm, c=1mm	biotite	q-c=35-40dca, c=stockwork	TR fg py in veins :: rusty= TR-1% fg py diss		TR-1% vis diss mt	
		5.55	6.71	weak rusty orange and grey alteration, 6.13-6.18m=strong orange-red rusty alteration and very hard (carbonate alt?)													
		6.71	7.07	medium to dark grey colour, 10% q veins with beige-orange carbonate crystals (40dca), folded, TR-1% fg diss py													
		7.07	7.2	weak rusty orange and grey alteration as above													
		8.82	8.91	medium green and grey (unaltered V3 breccia)													
		8.91	9.07	large quartz vein + bt/mt? and chl, pink/beige alteration at edge of vein, TR py fg diss													
		9.65	10.2	possible breccia - possible grey fragments in green host here													
10.34	10.69			V3 massive	Medium grey/green	V3	none	none	weak to moderate carbonate	none				TR fg diss py		TR-1% vis mt	
10.69	24.4			V3 breccia? +/- pillow?	medium grey and green with rusty orange colour	V3	breccia? Swirled texture in places	none	none-weak carbonate	1% q-c, 1% c, <1% q-alb	q-c=3-4mm (boudined), c=1-2mm, q-alb=5mm+	biotite	generally 80-90dca	1% fg cubic py diss, increased in areas of chl		<=1% viss diss mt (<=1mm)	
		11	11.2	possible breccia - possible grey fragments in green host													
		15.07	15.96	orange rusty alt around q-c vns, py (up to 1% diss), 2-3% q-c+/-alb veins													
		16	16.3	possible breccia - possible grey fragments in green host													

Major Unit		Minor Unit		DDH: 142 Section: 1088 CONTINUED						Veins				Mineralization				
From	To	From	To	Rock Name	Colour	Composition	Texture/Primary Structures	Foliation Angle	Alteration	%, Type	Size	Selvage	Angle to CA	min1	min2	Magnetite	Other	
		16.54	19.55	medium grey-brown with weak orange rusty alteration				80-90 dca	rusty	3-4% q-alb with orange-beige crystals	boudined, 4mm-1.3cm	dark grey	boudined and blocky boudined at 45dca	1-2% fg diss py, 1-4mm blebs/cubic near/in the veins			TR fg vis mt	
		21.8	22.3	possible breccia - possible grey fragments in green host														
		23.3	23.5	possible pillow - 10-15cm dark grey "fragment" with black/dark brown surrounding it in the host														
24.4	27.53			V3 amygdular	medium grey-green	5% calcite amyg (3-5mm), 5% dark amygdules (1-2mm)	amygdular	none	none	1% q-c and c (+/-cl)	~1mm	none	stockwork or folded	TR py fg diss, band of cl+py (2mm)		TR-1% vis mt		
		25.9	26.15	white amygdules														
		26.69	26.79	small broken pieces of rock mostly <=5mm thick, possibly location of brittle fault?														
		26.6	27	white rimmed amygdules														
27.53	28.45			V3 massive	medium grey	V3	massive	none	none	<1% q-c, TR dark (q?) in microfractures	q-c=3mm, q?=micro	white	stockwork or folded	TR fg py blebs		TR-1% fg vis mt diss		
28.45	31.41			V3 amygdular (as in 24.4-27.53 above)			amygdular	none	weak biotite	1% q-c and c (+/-cl)	~1mm	none	stockwork or folded	Trace fg py+po		TR-1% vis mt		
		28.45	28.6	white amygdules														
		29.75		1-2mm q-c vein with biotite bands, TR fg py+po in vein														
		30.04	30.18	chl and dark (bt? or cl+mt?) alteration in V3 amygdular + breccia														
EOH																		

Murgor Resources

BARRY - MAIN ZONE - Drill Core Logging

Logged by Kathryn Kitney

V3=mafic volcanic
T3=mafic tuff
QFP=quartz-feldspar porphyry

q=quartz
alb=albite
c=carbonate
bt=biotite
ep=epidote
chl=chlorite

VG=visible gold
py=pyrite
po=pyrrhotite
TR=trace
vis=visible
fg=fine grained (<1mm)
diss=disseminated

DDH: 143 Section: 1088

Major Unit		Minor Unit									Veins				Mineralization			
From	To	From	To	Rock Name	Colour	Composition	Texture/Primary Structures	Foliation Angle	Alteration	%, Type	Size	Selvage	Angle to CA	min1	min2	Magnetite	Other	
0	7.31			V3 massive	green and grey to rusty alt/ank discolouration	V3	massive with weak banding	none	weak carbonate	c=1%, q-c(+/-py)=1%	c=1mm, q-c=1-3mm	none	c=folded/deformed, q-c~60dca	TR fg py blebs		TR fg vis diss mt		
		0	0.65	rusty ankerite alteration (1)							q-alb(+/-py)=10-20%, c=5%	q-alb=4mm-3cm, c=1mm (folded/wavy)	q-alb=rusty (ank?) and in places cal (beige-yellow)	q-alb=40dca, c=folded	1% py (2-3mm)		TR fg vis diss mt	
		1.37	1.6	possibly breccia - grey portion of unit looks like it is possibly "fragments"														
		1.72	2.31	rusty weathered surface (2)							q-alb(+/-py, bt)=15%, c=1%	q-alb=4mm-5cm, c=1mm (folded/wavy)	q-alb=cal? (beige-yellow), and in some places thin bt	q-alb=50dca	5% py (1-3mm)		TR fg vis diss mt	
		3.06	3.49	see (1), near 3.49 several cm of dark orange rusty (ank? Or diss py?)														
		4.1	4.4	possibly breccia - grey portion of unit looks like it is possibly "fragments"														
		4.44	4.89	see (2), 1% py cubic diss and near vns (1mm)														
		6.64	6.8	see (1)														

Major Unit		Minor Unit		DDH: 143 Section: 1088 CONTINUED						Veins				Mineralization			
From	To	From	To	Rock Name	Colour	Composition	Texture/Primary Structures	Foliation Angle	Alteration	%, Type	Size	Selvage	Angle to CA	min1	min2	Magnetite	Other
7.31	8.73			V3 amygdular	medium to dark grey	5% calcite amygdules (~1mm)	amygdular	none	weak carbonate, rusty in places	q-c=1%, q-alb(+/-bt)=3%, 1% chl	q-c=1-2mm, q-alb (+/-bt)=2cm, chl=1mm	biotite	q-alb=60dca, folded q-c=40dca	1-2% fg py, 1-2mm blebs and cubic in vns		TR-1% vis diss mt	up to 5% py along q-alb veins (1-3mm)
8.73	9.94			V3 masssive/ altered	medium to dark grey and rusty weathering	V3	massive?	none	rusty (ank? fg py?)	q-alb=15%, q-c or c=1-2%	q-alb=3mm-2.5cm, c=1cm folded	q-alb=bt in places, boudined in places with bt in gaps	q-alb=70-80dca	2% fg py diss blebs and cubic, 3-4mm blebs in larger q-alb veins		TR vis fg diss mt	
9.94	15.74			V3 massive + amygdules+/- breccia	medium to dark green	V3	massive + amygdular	none	weak carbonate	q-alb=2%, q-c=3%, c=1%, q=1%	q-alb=1-2cm, q-c=3mm-1.5cm, c=1mm, q=3-4mm)	biotite +/- py	q=50dca, q-alb=boudined 70-80dca	1-2% fg py		moderately magnetic	
		11	11.2	possibly breccia - grey portion of unit looks like it is possibly "fragments"													
		13.45	13.8	possibly breccia - grey portion of unit looks like it is possibly "fragments"													
		14.36	14.7	up to 10% calcite amygdules (1-3mm) and 1-2% quartz amygdules (1-2mm)													
		15	15.4	up to 10% calcite amygdules (1-3mm) and 1-2% quartz amygdules (1-2mm)													
15.74	16.5			V3 massive	dark grey	V3	none	none	weak carbonate	q-alb=1%, q-c=2%, c=1%	q-alb=1-1.5cm, q-c=5mm-2cm, c=1mm	none	q-alb=55dca, q-c=folded, c=stockwork	TR fg py		TR fg diss mt	

Major Unit		Minor Unit		DDH: 143 Section: 1088 CONTINUED						Veins				Mineralization			
From	To	From	To	Rock Name	Colour	Composition	Texture/Primary Structures	Foliation Angle	Alteration	%, Type	Size	Selvage	Angle to CA	min1	min2	Magnetite	Other
16.5	17.22			V3 amygdular	grey and green	10% calcite amygdules (1-3mm), 1% quartz amygdules (1-2mm)	amygdular	~65dca in elongated amygdules	weak carbonate	1% c	1mm	none	stockwork	1% fg py diss cubic		1% vis mt diss	
17.22	26.48			V3 massive +/- breccia	medium grey and green	V3	massive	weak at 60dca	moderate carbonate	c-q=2%, q-c(+/-cl)=1%, c=1%	c-q=5mm-2cm, q-c=boudined 3-4mm, c=2-3mm	none	c-q=blebs/no direction, c=stockwork, q-c=50dca	Tr fg py, increased in chl alteration		TR vis mt	
		21.5	21.8	possibly breccia - grey portion of unit looks like it is possibly "fragments"													
		22.1	22.72	broken up - between 3mm-3cm in size. brittle fault?													
		25.2	25.6	possibly breccia - grey portion of unit looks like it is possibly "fragments"													
26.48	27.92			QFP 2	dark grey aphanitic groundmass, feldspar beige and pink	60% feldspar (1-5mm), 3%-5% quartz (3-4mm), 35% dark grey aphanitic matrix, 2-5% mafics (bt?)	porphyry	faint at 55dca	kspar alt in pink feldspar crystals	<1% c	c in microfractures	none	stockwork	TR-1% fg py in blebs diss			upper contact: 20-25dca, lower contact: irregular
27.92	28.82			V3 massive +/- breccia	medium grey and green	V3	massive +/- breccia	none	biotite, chlorite	c=2%, q-c-ep-py=1%	c=1-2mm, q-c-ep-py=3mm	biotite	c=stockwork, q-c-ep-py=20-30dca	TR fg po in q-c vn	TR fg py in q-c vein	weakly magnetic	
		28.1	28.2	1mm q-ep+po+py+/-cpy vein cuts c veins													
		28.25	28.35	possibly breccia - grey portion of unit looks like it is possibly "fragments"													
28.82	32.08			V3 amygdular	medium grey/green	V3	amygdular	none	chlorite	q-c (+/-po, py)=2-3%, c=1%	q-c=2-7mm, c=1mm	q-c=chl and grey selvage in places	irregular, one at 55-60dca	TR py fg	TR po fg in q-c vn	locally magnetic	
EOH																	

Murgor Resources

BARRY - MAIN ZONE - Drill Core Logging

Logged by Kathryn Kitney

V3=mafic volcanic
T3=mafic tuff
QFP=quartz-feldspar porphyry

q=quartz
alb=albite
c=carbonate
bt=biotite
ep=epidote
chl=chlorite

VG=visible gold
py=pyrite
po=pyrrhotite
TR=trace
vis=visible
fg=fine grained (<1mm)
diss=disseminated

DDH: 151 Section: 1088

Major Unit		Minor Unit												Veins			Mineralization			
From	To	From	To	Rock Name	Colour	Composition	Texture/Primary Structures	Foliation Angle	Alteration	% , Type	Size	Selvage	Angle to CA	min1	min2	Magnetite	Other			
0	0.7			Overburden																
0.7	2.15			V3 amygdular	dark to medium grey-green	5-10% calcite amygdules	amygdular	none	weak-mod carbonate, weak chl	c=2%, q-c=3%, q-alb=1%	c=2-5mm, q-c=5mm-7mm, q-alb=4mm	fg py	q-c=60-70dca	5% py (1-3mm blebs)		TR vis fg mt	chevron folds in c veinlets (<=1mm)			
2.15	2.84			V3 massive	medium grey/green	V3	none	none	weak-mod carbonate, weak chl	q-c=1%, q-c-ep (green tinge)=1%	q-c=3mm, q-c-ep=5mm	none	55-60dca			2-3% fg vis mt diss				
2.84	3.35	V3 amygdular (as above), py cubic and blebs within/near q-c and q-alb vns																		
3.35	4	V3 massive (as above), increased mt as seen in unit above																		
4	4.25	V3 amygdular (as above), whole region is dark grey/brown, moderate-strong bt alteration throughout																		
4.25	6.88			V3 massive/feldspar-phyric flow? + locally amygdules	grey/green	V3, locally 2% calcite amygdules ~1mm	none	none	moderate carbonate	1% pinched/boudined q-c	1mm-4mm	chl (1-2mm)	~55dca	TR fg py diss	TR fg white elongated crystal diss	TR vis fg mt				
		4.91	5	amygdules																
		5.81	6.25	shear zone, strong bt and carbonate alteration, 2-5cm q-c+chl+py(py=3mm-1cm blebs) vein, boudined q-c veins																
		6.25	6.88	shear zone at 55-60dca, bands of chl-rich and grey rock, 1% fg diss py, TR fg diss mt																

Major Unit		Minor Unit		DDH: 151 Section: 1088 CONTINUED						Veins				Mineralization			
From	To	From	To	Rock Name	Colour	Composition	Texture/Primary Structures	Foliation Angle	Alteration	%, Type	Size	Selvage	Angle to CA	min1	min2	Magnetite	Other
6.88	11.16			V3 massive	green and grey	V3	massive	weak 70dca	moderate-strong carbonate	c=2%, q-c=1%, q-alb=1%	c=2-7cm, q-c=1cm, q-alb=1-10cm	none	c=high angle, seen cutting q-alb vein	TR fg py diss		TR vis fg mt	
		7.2	7.32	TR po+mt+py													
		8.6	9.2	1-2% fg vis mt, 1% py in blebs													
		10.59	11.16	rusty orange alteration at contact with QFP - fg diss py?													
11.16	11.89			QFP 1? QFP cro?	beige-grey	5-10% quartz (2-4mm), 20-30% mafics (chloritized), 60% feldspars + matrix ("smeared")	none	none	chl/rusting of mafics	q-alb= 10-15%	0.5-2cm	bt	stockwork	TR-1% py (1mm-3mm)			upper contact: 60dca lower contact :irregular
11.89	13.1			V3 massive	dark grey brown to medium grey-green	1-10% calcite amygdules (2mm)	amygdular	none	weak bt, chl and carbonate	1% q-alb, 1/2-1% q-c, <=1% py stringers	q-alb= 4mm-7mm, q-c=2mm	bt, rusty +/- py	60-65dca	1% fg diss py, blebs 3-5mm near/in q-alb vns, stringers ~1mm thick		TR vis fg mt	
		11.89	11.97	rusty alteration near the contact with the QFP above													
		11.97	13	weak to moderate bt alteration throughout, py stringers and the fg diss py.													
		12.5	VG	1mm grain in py blebs within q-alb vein													

Major Unit		Minor Unit		DDH: 151 Section: 1088 CONTINUED						Veins				Mineralization			
From	To	From	To	Rock Name	Colour	Composition	Texture/Primary Structures	Foliation Angle	Alteration	%, Type	Size	Selvage	Angle to CA	min1	min2	Magnetite	Other
13.1	13.55			V3 amygdular	dark grey brown to medium grey-green	1-10% calcite amygdules (2mm)	amygdular	none	weak bt, chl and carbonate	1% q-alb, 1/2-1% q-c, <=1% py stringers	q-alb=4mm-7mm, q-c=2mm	bt, rusty +/- py	60-65dca	1% fg diss py, blebs 3-5mm near/in q-alb vns, stringers ~1mm thick		TR vis fg mt	
		13.1	13.55	+/- fg po in q-c vein, cl selvages on veins													
13.55	13.81			V3 massive	medium grey/green	V3	none	none	moderate carbonate	none				TR fg py diss	TR fg po diss	1% fg mt diss	
13.81	17.9			V3 massive +/- breccia	green and grey	V3	massive +/- breccia	none	weak carbonate and chl	c=2%, q-c (+bt, cl, py, po +/- mt)=1%	c=2-5mm, q-c=3mm	chl and bt	40dca and stockwork		TR fg po in/along q-c veins	TR vis fg mt	
		15.3	16.7	possibly breccia - possible fragments locally, or could be the result of chlorite veinlets													
17.9	20.97			V3 massive + amygdular	green and grey	<1% amygdules overall, but locally 2-3% calcite and quartz amygdules (1-2mm)	massive + amygdular	none	none	c=1%, q-c=2%, q-alb=1%	c=1mm, q-c=3mm-1cm, q-alb=5mm-2cm	q-c=cl+bt, q-alb=bt	q-alb=30dca, q-c=10-55dca, c=no general direction	TR-1% fg py diss	TR po fg in veins	none	q vein stretched and "block faulted", not just boudined
		19.18	19.7	strong bt alteration, q-alb veins only at 45-50dca, fg diss py, py up to 3mm in q-alb vein													
		19.7	20.82	weak to moderate bt alteration, amygdules elongated at 40-45dca (~1x3mm)													
		20.82	20.97	sheared at 45-50dca, bt and cl alteration, q and q-c vns are boudined/stretched, 1% fg cubic py and blebs													
20.97	21.5			V3 massive	medium green and pale green	V3	massive with lighter bands of pale green/grey	~45dca	pale colour - carbonate?					TR fg py cubic and blebs		no	

Major Unit		Minor Unit		DDH: 151 Section: 1088 CONTINUED						Veins				Mineralization			
From	To	From	To	Rock Name	Colour	Composition	Texture/Primary Structures	Foliation Angle	Alteration	%, Type	Size	Selvage	Angle to CA	min1	min2	Magnetite	Other
21.5	22			V3 massive	green and grey	V3	massive, pale green bands/swirls	45-50dca	none	3% c, 1% c-q (+/-py)	c=1-7mm, c-q=1-2mm	none	c-q at 60dca, c=various directions	TR py fg		no	
22	22.9			V3 massive	medium grey/green	V3	none	none	none	c=2%, q-c=1%	1-2mm	none	55-65dca	TR po in q-c vein			
22.9	24.62			T3 Tuff	medium green with brown and light grey flecks	T3 - "crystals" range from fg to 1mm	banded from coarse to fine uphole	faint at 50dca	cl and bt	c=1%, q-c=1%, 1% cl	1-3mm	none	50dca			no	upper contact: ~15 dca, lower contact: ~70dca
24.62	25.4			T3 Tuff	medium green and brown	T3	finer grained	70-75dca	pale colour - carbonate?	<=1% c	<=1mm	none	stockwork			no	
25.4	25.83			T3 Tuff	medium green and brown	T3	"swirled", mottled	55dca	none	5% c	2-5mm	none	55dca			no	
25.83	31			V3 massive + amygdules	medium - dark green and grey	V3	massive + amygdules	none	none	c=1%, q-c=2% (+/-py, po), cl=1-2%, q-c-ep=<1%	c=1-3mm, q-c=2mm, cl=2-5mm, q-c-ep=8mm	none	small are stockwork, large ~80dca		1% fg py diss		
		26.36	26.4	broken crumbled pieces ~1cm each, rest of surrounding rock is intact - possibly brittle fault?													
		27.5	27.8	3-5% calcite amygdules (2mm)													
		29.5	29.79	10-15% calcite amygdules (~1mm) in breccia													

Major Unit		Minor Unit		DDH: 151 Section: 1088 CONTINUED			Veins				Mineralization						
From	To	From	To	Rock Name	Colour	Composition	Texture/Primary Structures	Foliation Angle	Alteration	%, Type	Size	Selvage	Angle to CA	min1	min2	Magnetite	Other
30.9	31.1			T3 Tuff	medium to pale green, 5-8mm dark grey bands	T3 - crystals are fg to 2mm	tuff with very fine grained dark grey layers - possibly interflow sediments? Or saw marks?	90dca	none	1% c	c=1mm	none	60-65dca				
		36	36.15	Broken up pieces, <1cm to 2cm - fault?													
EOH																	

DDH: 163
Section: 1088
Logged by: Jaysen Johnson

August 10, 2006

Depth (m)	Description	DDH: 163	Section: 1088
0 – 0.9	Overburden		
0.9 – 1.5	V3 Massive Dark green 5% c veins, 1-2mm, various directions		
1.5 – 1.8	Fault? Broken up rock Moderately magnetic		
1.8 – 3.5	V3 Amygdular Dark green Strong chlorite alteration around amygdules 15% dark amygdules, 5-7mm 5% bands of chlorite +/- epidote 1% pyrite, ≤1mm		
3.5 – 6.0	V3 Massive Dark green 5% c veins, 5mm, various orientations 1% q veins, 4mm, folded 4.9-5.1m: Fault? broken rock		
6.0 – 6.7	Shear at 50 dca Dark grey colour 30-40% biotite, 30% carbonate 10% q veins, 1-3cm, py and bt selvages, parallel to shear 5% pyrite, 1-3mm		
6.7 – 9.1	V3 Massive Dark green 5% c veins, 1-3mm, various directions 1% q veins, 5mm, 60 dca, cut by c vein 5% fine-grained disseminated magnetite 8.5-8.7m: 25% c veins at 45 dca		

Depth (m)	Description	DDH: 163 CONTINUED Section: 1088
9.1 – 9.4	Shear at 45 dca Strong carbonate/biotite alteration 7% c veins, 1-2 mm, various directions 5% q veins, 5-12mm, py/chl/bt selvage, folded	
9.4 – 11.0	V3 Dark green 5% c veins, 1-10mm, various directions 3% mt, fine-grained, disseminated	
11.0 – 15.7	Weak to moderate shear at 50dca Medium to dark grey 10% biotite alteration, strong carbonate alteration 10% c veins, 1-5mm, bt selvage, parallel to shear 1-2% py, ≤1mm 2% po, ≤1mm Moderately to strongly magnetic	
15.7 – 22.1	V3 Massive Dark green 10% c veins, 2-3mm, various directions 2% chl, 2-3mm, 45dca 1% q veins, 1cm, irregular orientations 1-2% py, ≤1mm 1-2% po, ≤1mm 5% mt fine-grained, disseminated 15.95-16.15m: QFP – unknown type, almost like QFP ‘veins’ in V3 21.1-21.15m: small shear at 70dca	
22.1 – 26.7	Weak to moderate shear at 65dca 10% biotite, moderate chl alteration 5% q veins, 1cm, bt/chl/py selvage, parallel to shear 15% c veins, 2-3mm, irregular 2% py, up to 2mm 1% po, ≤1mm 2% mt, fine-grained 26.2-26.5m: minor ep alteration	

Depth (m)	Description	DDH: 163 CONTINUED Section: 1088
26.7 – 31.75	<p>V3 amygdular? Weak to moderate ep alteration Mottled texture</p> <p>1% q veins, 5mm, 75dca 2% q-c veins, 1cm, various directions</p> <p>2-3% py, ≤1mm 1-2% po, ≤1mm 2-3% mt</p> <p>27.3-27.5m and 28-28.4m: light green colour, bedded unit? 20% bt, 2% ep, local strong chlorite, this unit is strongly foliated – possible bedding defined by alteration?</p>	
31.75 – 32.9	<p>Shear at 40dca Strong bt an carb alteration</p> <p>10% q veins, 4-10mm, bt/py selvage, parallel to shear 7-10% c veins, 1-2mm, various orientations</p> <p>5% py, ≤1mm – 2mm, disseminate and in stringers 2% po, ≤1mm</p>	
32.9 – 34.2	<p>V3 Massive Greenish grey Foliation at 70dca, bands of more intense chl alteration</p> <p>10% c veins, 1-4mm, various orientations</p> <p>2% mt</p>	
34.2 – 35	<p>V3 Amygdular Dark green 20% calcite amygdules, 5-10mm</p> <p>10% c veins, 2-3mm</p>	
EOH	1-2% mt, fine-grained, disseminated	

DDH: 29
Section: 1096
Logged by: Jaysen Johnson

August 11/2006

Depth (m)	Description	DDH: 29 Section: 1096
0 – 2.8	V3 Medium to dark grey, reddish-brown colour Moderate carbonate alteration 10% q-a veins, 1-2cm, bt/ankerite selvage, straight at 45dca and folded 4-5% py, 1-5mm 3% mt, fine-grained, visible 0.18, 0.4, 0.8m: 2cm wide dark red/brown rusty alteration	
2.8 – 8.1	Shear at 55dca Medium green/grey colour Moderate carbonate alteration 10% q-a veins, 1cm, 45-55dca, locally pinch and swell 3% py, ≤1mm 2.8-3.3m: strong shear 5.7-6m: light brown/orange colour	
8.1 – 11.1	Missing core	
11.1 – 15.87	Shear at 70dca Dark grey and dark reddish brown Contains some amygdules Weak to moderate carbonate alteration 10% q-a veins, 5-10mm, bt/ankerite selvage, 45dca 5-7% py, ≤1mm	
15.87 – 16.47	V3 Amygdular Medium grey 20% white (carbonate?) amygdules, 5mm Moderate carbonate and weak biotite alteration 5% c veins, 1mm, various orientations 1% py, ≤1mm	

Depth (m)	Description	DDH: 29 CONTINUED Section: 1096
16.47 – 20	Shear at 60dca Medium grey colour with local reddish brown Weak to moderate carbonate and biotite alteration 10% q-a veins, 5-12mm, bt/ankerite selvage, 45-60dca 5-7% py, ≤1mm 17.95-18.15m: strong chlorite alteration	
20 – 30	V3 amygdular/breccia? Dark green to grey 10% carbonate amygdules, 5-10mm, Strong chlorite alteration near c veins 10-15% c veins, 5-15mm, various orientations 20-21.8m: apparent foliation at 60dca 29-30m: 1% po, ≤1mm	
EOH		

DDH: 30
 Section: 1096
 Logged by: Kathryn Kitney

August 11/2006

Depth (m)	Description Section: 1096 DDH: 30
0.00 – 1.60	<p>V3 Massive Medium grey Moderate carbonate alteration</p> <p>8% q-c veins, 2mm – 2cm, +/- bt/chl selvage, at 45-60dca</p> <p>TR py fine-grained disseminated TR mt fine-grained, visible</p> <p>0.00-0.18m: rusty alteration on fracture planes of broken rock 0.19m: rusty vuggy quartz vein 0.57-0.60m: rusty vuggy quartz vein</p>
1.60 – 4.05	<p>V3 Massive/locally amygdular Weak carbonate alteration</p> <p>3% q+/-c-alb veins, 2-7mm, pyrite on selvage, folded at 35 dca <=1% c veins, 1mm, stockwork</p> <p>TR-1% py fine-grained near veins Moderately to strongly magnetic</p> <p>1.60-1.92m: moderate rusty alteration 2.32-2.42m: strong rusty alteration 2.42-2.5m: cubic pyrite up to 3mm between rusty alteration and q+/-c-alb vein 2.59m: 10-20% white amygdules 3.00-4.05m: weak rusty alteration in bands</p>
4.05 – 5.90	<p>V3 Massive +/- breccia Dark green Weak carbonate alteration</p> <p>Locally 10% sugary q-c veins, 2mm-2cm, deformed, generally at 55dca</p> <p>TR py fine-grained disseminated blebs Moderately magnetic</p> <p>5.03-5.55m: sugary q-c veins 5.80-5.90m: sugary q-c veins</p>

Depth (m)	Description DDH: 30 CONTINUED Section: 1096
5.90 – 9.70	<p>V3 Massive Medium to dark green and grey Weak carbonate alteration Weak foliation at ~55dca</p> <p>1% q-c veins, 2mm-1cm, deformed <1% c veins, 1-2mm, deformed <1% chl veins, 1mm, anastomosing</p> <p>TR py fine-grained disseminated No-weakly magnetic</p>
9.70 – 10.56	<p>V3 Massive +/- breccia Dark grey No carbonate alteration</p> <p>3% q-alb veins, 4mm-1.3cm, bt +/- chl selvages, at 20dca <=1% q-c veins, <=1mm, deformed <1% c veins, 1-3mm, deformed</p> <p>1-2% py <1mm-2mm VG at 9.72m within q-alb vein near pyrite grain Not magnetic</p>
10.56 – 14.10	<p>V3 Massive +/- breccia No-weak carbonate alteration</p> <p>1% q-c veins, 1mm, stockwork <1% c veins, <=1mm, stockwork <1% q-alb veins, <5mm, boudinaged, at 45dca, in sheared zones</p> <p>TR-1% py fine-grained to 2mm cubic near q-alb veins Weakly to moderately magnetic</p> <p>10.82m: green alteration halo around q veins 12.28-12.51m, 13.60-13.87m: weak shear at 45dca</p>

Depth (m)	Description DDH: 30 CONTINUED Section: 1096
14.10 – 16.27	<p>V3 Massive Medium green-grey Weak rusty alteration</p> <p>2% q-c (rusty) veins, 2mm-1.5cm, folded TR q +/- alb veins, 2-5mm, +/- bt selvage, folded 2% rusty c veins, 1-5mm, deformed/folded</p> <p>TR-1% py fine-grained near veins, up to 2mm blebs and cubic in veins TR mt fine-grained visible NOT rusty: 14.77-14.99m; 15.35-15.78m; 15.95-16.27m;</p>
16.27 – 17.75	<p>V3 Massive Dark grey Moderate to strong orange rusty alteration throughout</p> <p>10% q+/-alb veins, 2mm-7cm, +/- bt selvage, folded/stockwork 2% rusty c veins, 1-3mm, stockwork</p> <p>TR-1% py fine-grained VG at 16.54m TR mt fine-grained disseminated visible</p>
17.75 – 20.85	<p>V3 Massive Moderate carbonate alteration</p> <p>8% q veins, 14cm, 40-45dca 1% q-c veins, 1-3mm, deformed <=1% c veins, <=1mm, stockwork/deformed</p> <p>TR py fine-grained disseminated blebs TR mt fine-grained disseminated visible</p> <p>18.76-18.90m: 14cm white quartz vein, py along edges cubic <=1mm 19.25-19.40m: weak rusty alteration bands</p>
20.85 – 22.85	<p>Shear Weak-moderate at 55dca Dark grey Weak-moderate rusty orange alteration, weak-moderate biotite alteration Moderate to strong carbonate alteration</p> <p>2% q-alb veins, pinch and swell, +/- biotite selvage, at 55dca <=1% q-c veins, 1-3mm, at 55dca</p> <p>TR-1% py fine-grained disseminated TR mt fine-grained disseminated</p> <p>21.10-22.60m: weak rusty alteration</p>

Depth (m)	Description DDH: 30 CONTINUED Section: 1096
22.85 – 24.26	<p>V3 Massive Medium green-grey Moderate-strong carbonate alteration, pink/purple alteration along veins</p> <p>1% q-alb+/-c veins, 2-7mm, +/- biotite selvage, at 25dca 2% q-c veins, 2-5mm, deformed 1% q-c-ep-gt, 5mm, at 60dca</p> <p>TR py fine-grained TR mt disseminated visible</p> <p>23.05-23.14m: purple/pink staining in/around q-c vein 23.29m: purple crystal in q-c vein 24.21-24.25m: epidote + garnet</p>
24.26 – 27.36	<p>V3 Amygdular/massive 1-2% dark amygdules (quartz?) and white (calcite) amygdules ~1mm Medium green to grey-green host</p> <p>1% q veins, 3-4mm, folded, at 30dca 2% q-c veins, 1-3mm, deformed, some at 60dca</p> <p>1% py fine-grained disseminated cubic and blebs TR mt fine-grained disseminated visible</p>
27.36 – 31.50 EOH	<p>V3 Amygdular +/- breccia 3-5% calcite and quartz amygdules ~1mm Weak biotite alteration in bands No-weak carbonate alteration</p> <p>1% q-c veins, 1-5mm, +/- biotite selvage, stockwork <=1% c veins, <=1mm, stockwork</p> <p>TR py fine-grained cubic and blebs TR-1% mt fine-grained disseminated visible</p> <p>30.41-30.61m: moderate-strong biotite-calcite shear at 40-45dca, locally increased veins 1% q-c veins, 2-4mm, +/- biotite selvage, 40-45dca; 3-5% c veins, 1-3mm, +/- biotite selvage, 40-45dca; TR po+py (<1mm blebs)</p>

DDH: 40
 Section: 1096
 Logged by: Kathryn Kitney

August 11/2006

Depth (m)	Description	DDH: 40 Section: 1096
0.00 – 6.00	<p>V3 Massive Green/grey Rusty alteration locally</p> <p>2-3% q-alb veins + rusty c, 2mm-1cm, +/- biotite selvage, 30-40dca 1-2% q veins, 4cm, 50-60dca? 1-2% rusty c veins, <=1mm, stockwork</p> <p>TR-1% py 1-2mm blebs and cubic in q-alb veins TR mt fine-grained disseminated visible</p> <p>0.00-0.13m; -0.71-079m, 1.29-1.50m, 2.78-2.82m: broken rock 0.00-0.71m, 1.07-1.21m, 2.07-2.29m: no rusty alteration, no veins 0.79-0.80m, 0.93-0.97m, 1.05-1.07m, 2.77-2.80m, 3.72-3.77m: strong rusty alteration</p>	
6.00 – 9.53	<p>V3 Altered Dark grey Rusty orange alteration</p> <p>3% q-alb veins, 2m-1.5cm, biotite selvage, larger veins folded, at 40dca 1% rusty c veins, <=1mm, stockwork</p> <p>TR-1% py <1mm disseminated and 2mm in veins TR mt fine-grained disseminated visible</p> <p>6.00-6.28m, 6.84-6.85m, 7.26-7.51m, 7.73-7.76m, 8.14-8.42m, 9.19-9.21m: q-alb veins</p>	
9.53 – 12.48	<p>V3 Massive +/- breccia Medium green-grey No-weak carbonate alteration, beige/brown staining</p> <p>1% c veins, 2mm-1cm, folded 1% q-c veins, 1-2mm</p> <p>TR py fine-grained disseminated blebs TR mt fine-grained disseminated</p>	

Depth (m)	Description DDH: 40 CONTINUED Section: 1096
12.48 – 12.86	<p>QFP 2? + possible fine-grained mafic dyke Dark grey colour, crystals smeared, 20% white feldspar crystals, no qtz? Faint foliation at 40dca</p> <p>5% q+/-feldspar veins, pinch and swell, 4mm, deformed</p> <p>TR py fine-grained Not magnetic</p> <p>12.69-12.86m: smeared, dark grey. Possible fine-grained mafic dyke</p>
12.86 – 15.00	<p>V3 Massive Medium green-grey Weak-moderate carbonate alteration</p> <p>1-2% q-c veins, 2mm-1.5cm, at 40-60dca TR c veins, <1mm, stockwork</p> <p>TR py fine-grained disseminated and within veins Weak-moderately magnetic</p> <p>14.50-15.00m: faint foliation at 60dca 13.96-14.02m: q-c vein with beige alteration, increased py locally 14.02m: broken rock</p>
15.00 – 17.80	<p>V3 Altered Medium to dark grey Weak rusty alteration</p> <p>1% q-alb veins, 2-5mm, +/- biotite selvage, at ~60dca 2-3% q-c veins, 2-5mm, +/- biotite/chlorite selvage, at ~60dca <1% rusty c veins, 1-2mm, deformed</p> <p>1-2% py fine-grained near veins Weakly-moderately magnetic</p>
17.80 – 19.50	<p>V3 Massive Dark green and dark grey No carbonate alteration, weak biotite alteration</p> <p>1% q veins, 2-5mm, +/- biotite, deformed 1% q-c veins, 1-3mm, +/- biotite, deformed</p> <p>1% py fine-grained cubic and blebs Moderately to strongly magnetic</p> <p>18.19-18.27m: q+/-c vein with cubic py (<=5mm) 19.00-19.15m: folded q vein, 1-2% py fine-grained cubic</p>

Depth (m)	Description	DDH: 40 CONTINUED	Section: 1096
19.50 – 25.82	<p>V3 Amygdular +/- breccia 5% dark amygdules (calcite and quartz), 1-2mm, rusty alteration around them No-weak carbonate alteration</p> <p><=1% q veins, 1-3mm, +/- biotite selvage, at ~55dca <=1% q-c veins, 2-5mm, +/- biotite selvage, at ~55dca</p> <p>TR py fine-grained blebs TR po (past 24.4m depth) fine-grained blebs Not magnetic</p> <p>22.59-22.82m: strong biotite band, magnetic, vuggy q-c vein, foliation at ~50dca >24.4m: po begins</p>		
25.82 – 26.74	<p>V3 Massive Medium green and grey Weak biotite alteration, “Swirled” look</p> <p>8% c veins, 1mm-1cm, deformed, at 60dca 1% q+/-c veins, 3mm, at 70dca</p> <p>TR py fine-grained TR po fine-grained Weakly magnetic near pyrrhotite</p>		
26.74 – 28.50	<p>V3 Feldspar-phyric Medium to dark green, feldspars <=1mm No carbonate alteration</p> <p>TR q-c+po-py veins, 1mm, stockwork, 1 vein along core axis TR c veins, 1mm, stockwork TR chl veins, <=1mm, anastomosing</p> <p>TR py fine-grained blebs TR po fine-grained blebs Not magnetic</p>		
28.50 – 30.00 EOH	<p>V3 Massive +/- amygdular/feldspar-phyric Feldspar/amygdules <4mm, possible vesicles (3x6 or 7mm)</p> <p>TR q-c veins, <=1mm, stockwork TR rusty c veins, <1mm, stockwork</p> <p>TR py fine-grained blebs TR po fine-grained blebs Not magnetic</p>		

DDH: 116
 Section: 1096
 Logged by: Kathryn Kitney

August 9/2006

Depth (m)	Description	DDH: 116	Section: 1096
0 – 0.22	Overburden		
0.22 – 10.46	<p>V3 Amygdular Medium green-grey 1-2% calcite amygdules, 1-2mm 1-2% dark (quartz?) amygdules, ≤1mm. Amygdules decrease with depth</p> <p>1-2% c, 1-2mm, +/-bt selvage, 60dca 1-2% q-c, 2-3cm, 60dca</p> <p>TR py, ≤1mm Not magnetic</p> <p>0.88-1.05; 4.46-5.60; 6.22-6.4; 9.98-10.46m: dark grey colour, rusty brown alteration, or pink/beige alteration 2-3% q-c +/-py veins, 2mm-1.5cm, +/-bt selvage, 45-50dca 1% q+/-py veins, 2-4mm, +/-bt selvage, 45-50dca TR-1% py near veins</p> <p>10-10.05m: broken rock – fault?</p>		
10.46 – 11.92	<p>V3 Dark grey and rusty colour with veins mostly in rusty sections (except q-c veins)</p> <p>3-4% q-a veins, 5mm-1.5cm, 65dca 1% q veins, 3mm-1cm, 65dca 1% q-c veins, 1-2mm, ~65dca</p> <p>TR-1% py, ≤1mm up to 2-3mm near veins</p>		
11.92 – 12.71	<p>QFP – unknown type 10-15% white feldspar crystals, 2-3mm, background is ‘smeared’ Upper contact: 90dca Lower contact: 20-65dca</p> <p>40% q-feld veins, 1.5cm-20cm</p>		
12.71 – 14.48	<p>V3 Dark grey and rusty colour with veins mostly in rusty sections (except q-c veins)</p> <p>14.08-14.2m: 10% white amygdules, 1-2mm 13.96-14.08 and 14.4-14.48m: broken rock</p>		

Depth (m)	Description	DDH: 116 CONTINUED Section: 1096
14.48 – 16.91	<p>V3 amygdular/breccia? Green-grey colour 2% dark and 3% white amygdules, 1-2mm Weak carbonate alteration</p> <p>1% c veins, ≤1mm, +/-chl selvage, stockwork TR py, <1mm TR po, <1mm TR-1% mt, ≤1mm</p> <p>15.8-16.15m: dark band – bt alt, increase py to 1%, foliation at 45dca</p>	
16.91 – 19.0	<p>V3 Grey colour Moderate bt alteration +/- 1% amygdules, 2mm Foliation 30-40dca</p> <p>1% q veins, 2-3mm, +/-bt selvage, 50-70dca 2% q-c veins, 2-5mm, +/-bt selvage, 50-70dca 1% c veins, ≤1mm, 30-40dca</p> <p>1% py, ≤2mm No to weak magnetism</p>	
19.0 – 20.24	<p>Shear at 45dca Dark grey-brown to black Strong biotite and calcite alteration</p> <p>3% c veins, ≤1mm, +/- bt selvage, 45dca 1% q-c veins, 2mm, +/- bt selvage, 45dca</p> <p>TR-1% py, ≤1mm Locally magnetic</p>	
20.24 – 25.04	<p>V3 Massive Medium-pale green, locally lighter coloured bands</p> <p>1% q veins, 2-5mm, boudinaged at 45dca 2% q-c veins, 2-5mm, deformed at 55dca</p>	
25.04 – 25.28	<p>V3 Massive? Medium to dark green, sharp contacts with other units – upper: 45-50dca, lower: ~60dca and undulating</p> <p>10% q-c-ep veins, 1mm-1cm, 45-50dca</p>	

Depth (m)	Description	DDH: 116 CONTINUED Section: 1096
25.28 – 26.61	<p>V3 Massive? Medium to pale green + brown alteration, fades to dark green with depth TR white amygdules, 1-2mm</p> <p>1% q-c+/-ep veins, 1-2mm, stockwork 1% c veins, 1mm, stockwork</p> <p>1% py, blebs 1-2mm 1% po, blebs 1-2mm Weakly magnetic (po?)</p>	
26.61 – 29.1	<p>V3 Massive? Dark green colour, many veins</p> <p>2-3% q-c-ep veins, 2mm-5cm, stockwork 1% q-c, 1mm-3mm, stockwork 1% c veins, ≤1mm, stockwork</p> <p>TR py, ≤1mm TR po, ≤1mm Both py and po are found in veins that do not contain epidote</p>	
29.1 – 31.0	<p>V3 Massive? Medium/pale green</p> <p>2-3% q-c-ep veins, 2mm-4cm, stockwork 1% q-c, 2mm-4mm, stockwork 1% c veins, ≤1mm, stockwork</p> <p>TR py+po, <1mm blebs</p>	
EOH	30.5-30.6m: Local white amygdules (not calcite – does not fizz)	

DDH: 162
 Section: 1104
 Logged by: Kathryn Kitney

August 9/2006

Depth (m)	Description	DDH: 162	Section: 1104
0.00 – 1.70	Overburden		
1.70 – 5.50	<p>V3 Altered Medium grey-green Locally rusty orange alteration (30-40% of this unit) Weak foliation at 55-60dca</p> <p>1% q+/-alb veins, 1-2mm, at 55-60dca 1% q-c veins, 1-2mm, at 55-60dca TR-1% c veins, <1mm, at 55-60dca</p> <p>TR py fine-grained blebs in and along veins</p> <p>2.24-2.29m, 5.10-5.18m, 5.33-5.36m: strong rusty alteration 4.32-4.40m: broken rocks – brittle fault?</p>		
5.50 – 16.17	<p>V3 Altered Medium grey colour Weak rusty alteration (~50% of this unit), locally pink/beige alteration or staining in veins</p> <p>8% q-alb veins, 2mm-1.2cm, pinch and swell, +/- biotite selvage, at 70dca 1% c veins, <=1mm, stockwork</p> <p>2% py fine-grained disseminated cubic and blebs up to 3mm TR mt fine-grained visible</p> <p>10.00-10.15m, 10.83-10.96m: moderate rusty alteration 11.76-11.80m, 11.99-12.04m: strong rusty alteration</p>		
16.17 – 20.92	<p>V3 Massive +/- mafic dyke Medium green and grey No-weak carbonate alteration Weak foliation at 70dca</p> <p>1% q-c veins, 3mm-1.2cm, +/- chlorite selvage, locally folded, at 75dca 1% c veins, 1-2mm, at ~75dca</p> <p>TR py fine-grained blebs 1% mt fine-grained disseminated</p> <p>17.25-17.6m: dark grey colour – possible mafic dyke</p>		

Depth (m)	Description DDH: 162 CONTINUED Section: 1104
20.92 – 26.44	<p>V3 amygdular +/- breccia 2-3% white amygdules (calcite – 2mm), 2% dark (quartz – 1-2mm) Medium green-grey host Moderate-strong carbonate alteration</p> <p>1% c veins, 1-5mm, stockwork</p> <p>TR py fine-grained blebs and cubic TR po fine-grained blebs TR mt fine-grained disseminated visible</p> <p>23.14-23.41m: dark grey/black and grey/blue bands 26.20-26.34m: locally increase in veins (5% q-c+py), 2-3% py fine-grained stringers and cubic to 3mm</p>
26.44 – 28.23	<p>V3 Feldspar-phyric 2-3% fine-grained disseminated white crystals Green-grey and brown host No carbonate alteration, weak to moderate biotite alteration Mottled / “swirled” texture</p> <p>1% q-c+/-ep veins, ~1mm, light green (ep?) selvage, stockwork 1% q-c veins, 1-3mm, +/- chl/biotite, at 80dca</p> <p>TR py fine-grained blebs TR po fine-grained blebs 1% mt fine-grained disseminated visible</p>
28.23 – 30.00	<p>V3 Massive Possibly 1% white calcite amygdules No carbonate alteration, weak biotite alteration, Mottled texture</p> <p><=1% q-c veins, 1-2mm, deformed</p> <p>TR py fine-grained blebs TR po fine-grained blebs No-weakly magnetic</p>
30.00 – 31.62	<p>V3 Feldspar-phyric Medium green to green-brown, white crystals <<1mm - speckled look Weak biotite alteration in bands</p> <p>TR c veins, <1mm, stockwork 1% q-c veins, 1-3mm, deformed, at 55 and 90dca</p> <p>TR py fine-grained blebs TR po fine-grained blebs near veins No to weakly magnetic</p>

Depth (m)	Description	DDH: 162	CONTINUED	Section: 1104
31.62 – 35.00	V3 Massive Medium green and grey Weak biotite alteration 2% q veins, 3mm-2cm, at 60dca 1% q-c veins, 1mm-1cm, deformed, at ~70dca TR py fine-grained blebs TR po fine-grained blebs Not magnetic			
EOH	31.62-32.00m, 34.50-34.60m: shear at 80-85dca, biotite and chlorite bands			

DDH: 28
 Section: 1111
 Logged by: Jaysen Johnson

August 11/2006

Depth (m)	Description	DDH: 28	Section: 1111
0 – 3.0	V3 Massive Reddish brown to dark grey/green Strong carbonate alteration 10% q veins, 1-5cm, ankerite selvage, 70 and 30 dca: 30° cut and displace 70° veins 10% c veins, 1-3cm, various orientations 2-3% py, ≤1mm Weakly magnetic		
3.0 – 6.0	Shear at 50dca Reddish-brown to dark grey 10% q-a, 1cm, bt and ankerite selvage, 50dca, pinch and swell 2% q veins, 1-2cm, 50dca 1% c veins, 3-4mm, 50dca 2% py, ≤1mm		
6.0 – 7.36	Shear? at 80dca Light brown-orange colour 20-25% q-a veins, 5-10mm, biotite/ankerite selvage, 60dca 1-2% py, ≤1mm 7.2m: strongly sheared, strong biotite and carbonate alteration		
7.36 – 10.1	Shear at 50dca Medium to dark grey colour Strong biotite and carbonate alteration 10% q veins, 7-10mm, mostly parallel to shear at 50dca 1% q veins, 5-7mm, folded 5% py, ≤1-2mm 9.45-9.5m: reddish-brown colour 9.5-9.7m: broken rock – fault?		

Depth (m)	Description	DDH: 28 CONTINUED Section: 1111
10.1 – 13.7	<p>V3 Amygdular Dark grey to green Strong carbonate alteration 10% white (carbonate) amygdules, 5-10mm 5% dark amygdules Foliation at 50dca</p> <p>5% q-a, 1cm, biotite/ankerite selvage, 50dca, light brown alteration around veins</p> <p>2-3% py, ≤1mm</p>	
13.7 – 15.2	<p>V3 Amygdular Light brown to medium green Moderate carbonate alteration 15% white amygdules, 5mm Foliation at 50dca</p> <p>3% q veins, 2cm, chlorite/ankerite selvage, 45dca 7% q-a veins, 1-1.5cm, biotite/ankerite selvage, folded</p> <p>5% py, 1-2mm, locally larger</p>	
15.2 – 20.05	<p>V3 amygdular Medium to dark green Strong carbonate alteration 15% white carbonate amygdules, 10% dark amygdules</p> <p>1% c veins, 5-10mm, irregular 2% q-a veins, 1cm, 50dca and irregular</p> <p>FIRST sign of mt and po in this hole 1-2% py, ≤1mm 3% po, ≤1mm 2-3% mt fine-grained, disseminated</p>	
20.05 – 21.27	<p>Shear at 70dca Strong chlorite, biotite, and carbonate alteration</p> <p>5% q-a, 5-10mm, bt selvage</p> <p>2% py, up to 5mm 1-2% po, ≤1mm</p>	
21.27 – 23.3	<p>V3 Dark green Strong carbonate alteration 1% py / TR po, ≤1mm 23m: 1cm wide ep alteration</p>	

Depth (m)	Description	DDH: 28 CONTINUED Section: 1111
23.3 – 23.95	V3 Amygdular? Dark green Large 'amygdules' maybe veins? TR py, ≤1mm 23.75-23.95m: broken pieces of rock – fault?	
23.95 – 33.4	V3 Dark grey 1-2% q veins, 1cm, 55-60dca 10% c veins, 5-10mm, various orientations 3% py, ≤1mm 5% po, ≤1mm 32.8-33.4m: 5-10mm amygdules	
33.4 – 35.1	QFP 2? Grey colour Medium to coarse grained 5% quartz (5-6mm), 30% plagioclase (3-4mm), 10% euhedral biotite (3-5mm, various orientations), sericite alteration of plagioclase 7% q veins, 1-2cm, 70dca 1% py, ≤1mm 2% po, 1mm+	
35.1 – 39.0	V3 Amygdular Dark green/grey 10-15% calcite amygdules, 2-10mm 5% c veins, 2-5mm, various orientations	
EOH	TR py and po, ≤1mm	

DDH: 140
 Section: 1111
 Logged by: Kathryn Kitney

August 8/2006

Depth (m)	Description	DDH: 140 Section: 1111
0.00 – 0.60	Overburden	
0.60 – 2.31	V3 Massive Medium to dark grey-green Moderate carbonate alteration, moderately rusty 2% q-c veins, 2-7mm, +/- pyrite selvage, at 40-50dca 1% q veins, 2-5mm, +/- pyrite selvage, at 40-50dca 1% py fine-grained to 3mm blebs and cubic Moderately magnetic 0.63-0.75m: strong rusty alteration along veins at 30dca	
2.31 – 8.92	V3 Massive +/- mafic dyke? Medium green Moderate-strong carbonate alteration 1% q-c+/-py veins, 3-5mm, at ~45dca 1% q-c+/-ep veins, 3-5mm, at ~45dca 1% c veins, 1-2mm, stockwork TR py blebs and cubic <=2mm TR mt fine-grained disseminated visible 3.42-3.56m: dark grey/black – possible mafic dyke	
8.92 – 10.98	V3 Altered Medium to light green Weak rusty/brown alteration 8% q-alb-c+/-bt veins, 3mm-2cm, at 40-60dca 1-2% py blebs and cubic <=3mm, in and near veins TR-1% mt fine-grained disseminated visible 9.53-9.58m: rusty alteration along fracture surface	

Depth (m)	Description DDH: 140 CONTINUED Section: 1111
10.98 – 11.44	V3 Massive Medium green-grey Moderate carbonate alteration 1% c veins, 1mm, stockwork Weak to moderately magnetic
11.44 – 12.65	V3 Altered Medium to light green Weak rusty/brown alteration 1% c veins, 1mm, stockwork Thin fracture-fill veins of biotite?
12.65 – 13.00	V3 Altered – Mafic dyke? Dark grey Weak carbonate alteration TR q-c veins, 1-2mm, folded 1% c rusty veins, 1mm, light grey selvage, stockwork TR py fine-grained disseminated TR mt visible
13.00 – 13.25	V3 Altered Medium grey Weak rusty alteration 8% q-alb-c+/-bt veins, 3mm-2cm, at 40-60dca 1-2% py blebs and cubic <=3mm, in and near veins TR-1% mt fine-grained disseminated visible
13.25 – 15.57	V3 Massive +/- breccia Medium green and grey Weak-moderate carbonate alteration 1% q-c veins, 3-7mm, +/- chlorite selvage, at 55-65dca 1% c veins, 1-2mm, deformed TR py <=2mm blebs and cubic 15.34-15.40m: weak rusty band

Depth (m)	Description DDH: 140 CONTINUED Section: 1111
15.57 – 17.48	<p>V3 Altered Medium grey with rusty bands (10-15% rusty, 2-4cm thick) Weak foliation at 70-75dca</p> <p>1% q-c veins, 3-5mm 1% q-alb+/-c veins, 2-5mm, +/- biotite selvage, at 55dca</p> <p>TR-1% py fine-grained disseminated TR-1% mt visible</p>
17.48 – 20.16	<p>V3 Breccia? Medium green and grey, possible fragments Weak-moderate carbonate alteration</p> <p>1% c veins, 1mm, stockwork Not magnetic</p> <p>17.61-17.69m: <1cm broken rock – possible brittle fault? 18.80-19.43m: 1-2% white (quartz?) blebs</p>
20.16 – 23.75	<p>V3 Amygdular Medium green-grey 1-2% calcite, 2-3% quartz amygdules No-weak carbonate alteration</p> <p>1% q-c veins, 5mm-2cm, folded, at 65dca</p> <p>TR py fine-grained in vein</p>
23.75 – 24.61	<p>V3 Massive Medium grey-green Moderate carbonate alteration</p> <p>2% q-c veins, 2mm-1cm, at 45 and 70dca</p> <p>TR py fine-grained TR-1% po replacing py 1% mt disseminated visible</p> <p>23.96-24.25m: “swirls” of carbonate, quartz, chlorite, biotite, cubic po (replacing py cubes)</p>
24.61 – 24.97	<p>V3 Feldspar-phryic / T3 Tuff Feldspar crystals <1mm, possibly graded, no sharp contacts with units above or below, likely feld-phryic</p>

Depth (m)	Description DDH: 140 CONTINUED Section: 1111
24.97 – 26.80	V3 Massive Medium grey-green Moderate carbonate alteration 2% q-c veins, 2mm-1cm, at 45 and 70dca TR py fine-grained TR-1% po replacing py 1% mt disseminated visible
26.80 – 29.48	V3 Amygdular Medium green-grey 10-15% white calcite amygdules 1-2mm, 1% dark amygdules 1mm Weak carbonate and biotite alteration 1% c veins, 2-4mm, +/- biotite selvage, deformed Not magnetic
29.48 – 30.25	V3 Feldspar-phryic / T3 Tuff White crystals fade out to fine-grained aphanitic V3/T3? with depth No sharp contacts with units above/below, likely feld-phryic TR c veins, fracture-fill, stockwork Not magnetic
30.25 – 31.01 EOH	V3 Amygdular +/- breccia Medium green and grey 2-3% white calcite amygdules 1mm, TR dark amygdules <1mm Weak biotite alteration, no-weak carbonate alteration TR-1% c veins, 1mm, stockwork

Murgor Resources

BARRY - MAIN ZONE - Drill Core Logging

Logged by Kathryn Kitney

V3=mafic volcanic
T3=mafic tuff
QFP=quartz-feldspar porphyry

q=quartz
alb=albite
c=carbonate
bt=biotite
ep=epidote
chl=chlorite

VG=visible gold
py=pyrite
po=pyrrhotite
TR=trace
vis=visible
fg=fine grained (<1mm)
diss=disseminated

DDH: 27 Section: 1124

Major Unit		Minor Unit		Rock Name	Colour	Composition	Texture/Primary Structures	Foliation Angle	Alteration	Veins				Mineralization			
From	To	From	To							% , Type	Size	Selvage	Angle to CA	min1	min2	Magnetite	Other
0	13.15			V3 massive	dark green-grey	V3	massive	none	weak-moderate carbonate, mt/bt bands	5% q-c, 1% c, 2% chl (cuts q-c veins)	q-c= 5mm-1cm, c=2mm, chl=3mm	q-c= some chl, chl=brown (bt?) selvages	q-c= 30-60dca, chl=35-55dca	TR fg py diss		TR vis fg diss mt	
		0	0.5	intermittant dark rusty alt				none		1% q, 1% q-c	3-4mm	biotite	q-c=35dca, q=30-55	1% fg cubic py		strongly magnetic in rusty alt	
		3.15	3.64	dark rusty alt				none	carbonate?	10-15% q-alb veins stained pink/red+py	3mm-2cm	bt, py	~35dca	1-3% fg py stringers along/in veins		strongly magnetic	first 5cm very rusty/pitted
		10.11	10.28	dark rusty alt				none	carbonate?	2% q, 4% q-alb	q=3mm, q-alb= 2mm-1,5cm	none	both ~30dca	2% py fg diss, blebs up to 3mm		weakly magnetic	
		10.28	10.79	section of dark green-grey rock with small stockwork veins of calcite (now orange coloured) ~2mm each													
		10.79	11.43	dark rusty alt				none	carbonate?	3% folded q-alb, 1% c, rusty along fractures	q-alb= 3mm, c=2-4mm	q-alb=rusty	q-alb= folded	TR-1% fg py diss		weakly magnetic	

Major Unit		Minor Unit		DDH: 27 Section: 1124 CONTINUED						Veins				Mineralization			
From	To	From	To	Rock Name	Colour	Composition	Texture/Primary Structures	Foliation Angle	Alteration	%, Type	Size	Selvage	Angle to CA	min1	min2	Magnetite	Other
		11.65	11.97	dark rusty alt				none	carbonate?	5% q-alb-py, 2% q-c	q-alb= boudined 2mm- 1.5cm, q-c=2-3mm	q-alb= biotite	q- alb=45dca, q-c=40- 60dca	2% py fg diss, blebs up to 3mm in veins		strongly magnetic	
		12.25	13.03	dark rusty alt				none	carbonate?	5% q-alb-bt-py, 1% q-c, 1% c	q-alb= boudined, 2-7mm, q-c=2mm- 1cm, c=2mm	q-alb= biotite selvage	straight veins at 40- 50dca, c=folded, some q-c=folded	TR-1% fg py diss, 5mm in vein		moderately magnetic	
13.15	20.65			V3 massive +/- breccia?	dark green and grey	V3	massive	none	weak to moderate carbonate	2% c, 1% q-c	1-5mm	chl	stockwork	TR po+ py in q-c veins (<=3mm)		TR vis mt diss, NO MT after 8.3m	
		15.20	15.50	possibly breccia - rounded grey portions are surrounded by chlorite-rich rock													
		16.27	17.08	"swirled" texture, looks mottled in places, possibly breccia - one grey portion (9cm in diameter) surrounded by green													
		17.32	18.61	faint foliation at 65dca, strong foliation at 18.53-18.61, biotite bands at ~80dca													
20.65	22.93			V3 massive/ amygdular	dark green-grey	2-5% amygdules (1-2mm)	massive + amygdules	none	biotite bands	1% q & q-c	2-3mm	white halo and biotite	50dca	TR py diss, blebs up to 2mm		not magnetic	
22.93	23.83			QFP 2	medium-dark grey	50-60% feldspar, 3-5% q, 10% mafics (1-3mm)	porphyry	faint at 40dca, alignment/ elongation of crvstals	none	1% q	1mm	none	stockwork/ fracture fill	1-2% fg py cubic and blebs, locally up to 5%		not magnetic	
		23.75	23.83	fine-grained portion of intrusion - possibly a chilled margin. Not a sharp contact - gradational between coarse and fine-grained portion													

Major Unit		Minor Unit		DDH: 27 Section: 1124 CONTINUED						Veins				Mineralization				
From	To	From	To	Rock Name	Colour	Composition	Texture/Primary Structures	Foliation Angle	Alteration	%, Type	Size	Selvage	Angle to CA	min1	min2	Magnetite	Other	
23.83	30			V3 massive/ amygdular	dark green to medium grey	5% dark amygdules (1-2mm)	massive + amygdules	none	weak biotite in bands	3-5% c, 1% q-c	c=2mm, q-c=2-4mm	none	stockwork or at high angle to CA	TR fg py + po in/near veins			not magnetic	
EOH																		

Murgor Resources

BARRY - MAIN ZONE - Drill Core Logging

Logged by Kathryn Kitney

V3=mafic volcanic
T3=mafic tuff
QFP=quartz-feldspar porphyry

q=quartz
alb=albite
c=carbonate
bt=biotite
ep=epidote
chl=chlorite

VG=visible gold
py=pyrite
po=pyrrhotite
TR=trace
vis=visible
fg=fine grained (<1mm)
diss=disseminated

DDH: 136 Section: 1124

Major Unit		Minor Unit		Veins										Mineralization			
From	To	From	To	Rock Name	Colour	Composition	Texture/Primary Structures	Foliation Angle	Alteration	%, Type	Size	Selvage	Angle to CA	min1	min2	Magnetite	Other
0	2.61			V3 massive +/- breccia?	brown/rusty orange/dark grey to pale green and grey	V3	banded/ "swirled" texture; breccia?	none	moderate carbonate, brown (bt?)	c=1%, q-c=2%, q-alb=3%	c=3-6mm, q-c=2-5mm, q-alb=3mm-1cm often pinch and swell	q-alb has bt	c= deformed; q-c and q-alb=45dca	1% fg py diss		TR vis fg diss mt	
		0	2.74	brown/rusty orange/dark grey													
		1.74	2.07	pale green and grey													
		2.07	2.61	brown/rusty orange/dark grey													
2.61	3			QFP?	grey-beige	grey colour and elongated mafics (0.5x2mm), mafics altered to rusty orange	none	mafics elongated at 60dca	none	5% q with rusty crystals	2-4mm	none	stockwork	TR fg py vis		none	upper contact at 60dca; lower contact in fracture/rust tv zone
3	4.75			V3 massive	ranges brown/rusty orange/dark grey to pale green and grey	V3	massive, locally banded/mottled taxture	none	strong carbonate	q-c=1%, q-alb=3% chl=2%	q-c= 2mm, q-alb=2mm-2cm, chl=1mm	biotite, orange rusty colour near q-alb vns	q-c=40-45dca, q-alb=50-60dca	TR-1% fg py diss		TR vis fg diss mt	
		3	3.9	dark grey with orange rusty colour surrounding/along veins													
		3.9	4.75	green and grey coloured													

Major Unit		Minor Unit		DDH: 136 Section: 1124 CONTINUED						Veins				Mineralization			
From	To	From	To	Rock Name	Colour	Composition	Texture/Primary Structures	Foliation Angle	Alteration	%, Type	Size	Selvage	Angle to CA	min1	min2	Magnetite	Other
4.75	9.7			V3 massive + amygdules	orange rusty and dark grey												
		4.75	6.06	V3 altered	rusty orange-brown and dark and light grey		none	none	none	10% q-alb (white and green-yellow tinged)	2mm-1.5cm	biotite in breaks and boudins of veins	40dca the 60-65dca	1% fg diss py		TR vis fg diss mt	
		6.06	6.25	green-grey colour, no veins, 1% fg vis diss mt, strong carbonate alteration													
		6.25	7.26	V3 altered + amygdular in places	rusty orange-brown and dark and light grey	1-3% white amygdu	none	none	weak-moderate carbonate	q-c=1%, q-alb(with yellow-green tinge)=3%	q-c=3mm, q-alb=2mm-1.5cm pinch and swell	biotite	55-60dca	1-2% fg py diss in bands, (up to 2mm) near veins		TR-1% vis fg diss mt	
		7.26	7.55	grey-green colour (as above: 6.06-6.25m)													
		7.55	9	V3 altered	rusty orange brown and dark grey	quartz amygdules with rusty staining (~8.9-9m; 2mm)	none	none	weak to moderate carbonate, biotite bands	q-alb (with green tinge)=5%, q-alb(white)=5% mostly at 8.34-8.63m	q-alb (green)=3m m-1cm, blocky boudined; q-alb(white)=1-5cm	q-alb (green)= bt in places	q-alb at 55-60dca, q-alb at 75dca	3-4% fg py diss in bands, 3-5mm cubic near veins			
		9	9.7	grey-green colour (as in 6.06-6.25m), but with one white q-alb vn containing cl, and has a thin rusty alt halo around it													
9.7	13			V3 massive + amygdular	green-grey	V3	massive + amygdular	none	moderate to strong carbonate	q-c=3%, q-alb-bt=1%, c=2%	q-c=2mm-4cm, q-alb=1.5cm, c<=1cm	biotite	q-c=70dca, q-alb=60dca, c=folded	TR fg py diss		1% vis fg diss mt	bands of orange alt
		9.7	10	possibly breccia													

Major Unit		Minor Unit		DDH: 136 Section: 1124 CONTINUED						Veins				Mineralization			
From	To	From	To	Rock Name	Colour	Composition	Texture/Primary Structures	Foliation Angle	Alteration	%, Type	Size	Selvage	Angle to CA	min1	min2	Magnetite	Other
		10.17	10.4	amygdular													
		12.44	12.64	possibly breccia													
13	24			V3 massive + amygdular	grey and green to orange and brown rusty alt	V3	massive + amygdular	none	strong carbonate	q=1%, q-alb=5-7%	3mm-2cm	bt on q-alb	60dca	1-3% fg diss py, 4mm near veins		TR-1% vis mt diss	
		13	14	rusty alteration													
		14	14.35	possibly breccia													
		15.75	16	amygdular													
		16.88	17.08	rusty alteration													
		17.08	17.28	amygdular													
		17.68	17.78	amygdular													
		20.65	20.75	amygdular													
		23	23.1	amygdular - 5% white amygdules (2mm)													
24	26.85			V3 breccia? Pillow?	dark grey and rusty orange	V3	breccia? Pillow? Possible elongated clasts with blurred/gradation. l contacts between green and grey - large fragmets (25cm)	none	18.37-22m =moderate carbonate, weak biotite; 22-23m=weak carbonate, 23+=no carbonate	q-alb=1%, q-c=2%, c=3%	q-alb=2cm, q-c=4mm, c=1mm-4mm	biotite	q-alb=40, q-c=55, c=deformed	TR fg py diss	TR po at ~25m and deeper in q-c vns	TR fg vis mt diss	

Major Unit		Minor Unit		DDH: 136 Section: 1124 CONTINUED						Veins				Mineralization			
From	To	From	To	Rock Name	Colour	Composition	Texture/Primary Structures	Foliation Angle	Alteration	%, Type	Size	Selvage	Angle to CA	min1	min2	Magnetite	Other
26.85	29.23			V3 massive	green and grey	V3	massive, locally contains banding	weak to moderate foliation at 55dca	18.37-22m =moderate carbonate, weak biotite; 22-23m=weak carbonate, 23+=no carbonate	q-alb=1%, q-c=2%, c=3%	q-alb=2cm, q-c=4mm, c=1mm-4mm	biotite	q-alb=40, q-c=55, c=deformed	TR fg py diss	TR po at ~25m and deeper in q-c vns	TR fg vis mt diss	
29.23	29.59			QFP 1	medium grey with quartz and feldspar crystals	50% quartz, 10% feldspar, 10% mafics, 30% aphanitic matrix	porphyry	faint at 50-55 dca	none	1% q	2mm	none	stockwork	TR fg py diss		none	upper contact 50-55dca, lower along fracture at 60-70dca?
29.59	30.78			V3 amygdular	pale green-grey	2-5% white amygdules (1-2mm)	amygdules	none	bt and chl bands	c=1%, q-c=1%	c=1mm along fractures, q-c=1-3mm	chl	folded/stockwork	TR py?		TR mt vis fg	
30.78	31.83			V3 altered - pillow? Breccia?	medium grey, dark brown, and green	V3	breccia? Pillow? "swirled" texture	45dca	strong bt and chl	10% c, 1% q-c	c=2mm -1cm, q-c=3mm	none	folded/stockwork	TR py+po in q-c vns		weakly magnetic	
31.83	32.3			V3 amygdular	green and grey	5% white calcite amygdules	amygdules	none	strong bt and chl	2% c, 1% q-c	c=1-2mm, q	chl	folded/stockwork	Tr py+/-po		weakly magnetic	amygs aligned at 55dca near lower contact
32.3	32.91			V3 pillow? Breccia?	green and grey			none	strong bt and chl	2% c, 1% q-c	c=1-2mm, q	chl	folded/stockwork	Tr py+/-po		weakly magnetic	

Major Unit		Minor Unit		DDH: 136 Section: 1124 CONTINUED						Veins				Mineralization			
From	To	From	To	Rock Name	Colour	Composition	Texture/Primary Structures	Foliation Angle	Alteration	%, Type	Size	Selvage	Angle to CA	min1	min2	Magnetite	Other
32.91	35.26			V3 amygdular	green and grey	5% white calcite amygdules	amygdules	none	strong bt and chl	2% c, 1% q-c	c=1-2mm, q chl		folded/stockwork	Tr py+/-po		weakly magnetic	amygs aligned at 55dca near lower contact
35.26	36.15			V3 massive?	beige-brown	V3	massive	60dca	none	2% q	2mm-1cm	none	large vein at 30dca, smaller at 55-60dca	TR fg po?		weakly magnetic	
EOH																	

DDH: 138

Section: 1124

Logged by: Kathryn Kitney

August 4/2006

Depth (m)	Description	DDH: 138	Section: 1124
0.00 – 0.90	Overburden		
0.90 – 3.90	V3 Amygdular Medium green-grey 3% calcite, 2% dark (quartz) amygdules with dark rims (1-2mm) Weak biotite alteration in bands 2% q-c veins, 3-8mm, biotite +/- chlorite selvage, at 55dca 3% c veins, 2-5mm, +/- chlorite selvage, stockwork TR-1% py 1-2mm blebs Not magnetic		
3.90 – 7.47	V3 Amygdular +/- breccia Medium green to grey 2-3% calcite amygdules Moderate to strong carbonate alteration 6% c veins, 2mm-1.5cm, biotite/chlorite selvage, at 60dca 2% q-c veins, 4mm-3cm, biotite selvage, at 60dca 6.10-6.55m, 7.00-7.03m: broken up rock 6.10-6.55m: 90% q-c veins, 2-5% py up to 5mm blebs		
7.47 – 10.62	V3 Amygdular Medium green-grey 1-2% white (calcite), 3-4% dark (quartz) amygdules No carbonate alteration, locally strong biotite alteration around q-c veins 1% q-c veins, 2-4mm, +/- biotite selvage, at 80-90dca 2% c veins, biotite selvage, stockwork TR py 3mm blebs in chlorite-rich bands Weakly magnetic		

Depth (m)	Description DDH: 138 CONTINUED Section: 1124
10.62 – 13.60	<p>V3 Massive +/- breccia Medium green and grey No carbonate alteration</p> <p>3% c veins, 1-5mm, deformed 1% q-c-ep veins, 1.3cm, at 60dca</p> <p>TR-1% py 2mm disseminated blebs Moderately-strongly magnetic</p> <p>11.06-13.60m: mottled texture 12.30m: dark metallic mineral in/along q-c vein</p>
13.60 – 16.70	<p>V3 Amygdular +/- breccia Medium grey and green 1-2% calcite, 2-3% dark amygdules No carbonate alteration except in biotite-rich zones</p> <p>1% q-c veins, 3-7mm, deformed 1% c veins, 1mm, deformed TR py Weakly to moderately magnetic</p> <p>13.60-13.70m: biotite-rich zone, moderate carbonate alteration</p>
16.70 – 17.10	<p>Biotite-carbonate Shear Shear at 50dca Strong biotite and calcite alteration</p> <p>50% q-alb-py veins, 2mm-1.5cm, biotite selvage, at 50dca, boudinaged/ pinch and swell 3% py <=3mm blebs near veins</p>
17.10 – 20.66	<p>V3 Massive +/- breccia Medium green and grey Weak carbonate alteration, weak biotite alteration</p> <p>2% q-c-py veins, <=1cm, biotite selvage, at 30-40dca 1% c veins, 3-5mm, chlorite +/- biotite selvage, stockwork TR-1% py 1-2mm blebs TR white tabular crystals <1mm TR-1% mt fine-grained disseminated visible</p> <p>18.51-18.57m: biotite alteration with q-c-py veins</p>

Depth (m)	Description DDH: 138 CONTINUED Section: 1124
20.66 – 24.07	<p>V3 Massive Medium green-grey No to weak carbonate alteration</p> <p>3% q-alb-bt? veins, 3mm-1.5cm, biotite selvage, at 65-70dca 2% q-c veins, 2-7mm, biotite-chlorite selvage, at 65-70dca 1% c veins, 1mm, stockwork</p> <p>TR-1% py fine-grained 1% mt fine-grained disseminated visible</p> <p>21.33-21.38m, 22.2-22.3m: moderate to strong biotite shears at 65-70dca 22.40-23.25m: contains q-c-py and q-alb veins 23.49-23.75m: broken rock</p>
24.07 – 34.30	<p>V3 Massive +/- breccia Medium green + dark grey/brown No carbonate alteration, locally biotite alteration in bands “Swirled” texture</p> <p>1-2% q-c-ep veins, 2-4mm, deformed <1% q-c veins, 2-5mm, biotite selvage, at ~70dca, in biotite altered zones 1% c veins, 1-4mm, deformed</p> <p>TR py fine-grained blebs TR po fine-grained blebs TR mt visible, no magnetite below a depth of 27m</p> <p>23.59-23.63m: broken rock – brittle fault? 25.30-26.07m, 27.7-28.00m: biotite alteration >27m: not magnetic</p>
34.30 – 35.34	<p>V3 Massive / T3 Tuff? Brown/grey Contains white hard crystals (not calcite) “Swirled” texture</p> <p>1% q-c-ep veins, 2mm-1cm, stockwork 1% c veins, 1-2mm, stockwork</p> <p>TR py fine-grained TR po fine-grained</p>

Depth (m)	Description DDH: 138 CONTINUED Section: 1124
35.34 – 37.30 EOH	V3 Massive +/- breccia Medium green + dark grey/brown No carbonate alteration, locally biotite alteration in bands “Swirled” texture TR py, po fine-grained

DDH: 180

Section: 1124

Logged by: Jaysen Johnson

August 9/2006

Depth (m)	Description	DDH: 180	Section: 1124
0.00 – 0.60	Overburden		
0.60 – 10.60	V3 Amygdular Medium grey with reddish-brown tinge Calcite (70%) and quartz (30%) amygdules Moderate carbonate alteration 5% q-alb veins, 6mm, biotite selvage, at 40dca, boudinaged 5% q veins, 1cm, at 60dca 7% c veins, 1-5cm, stockwork 3% py fine-grained to 3mm 4.30m, 5.76m, 8.14m: 1-2 cm of reddish-brown staining		
10.60 – 15.90	V3 Breccia? Moderate green to grey Strong chlorite alteration, weak to moderate biotite alteration Foliation at 80-90dca Fragments not well defined 3% q veins, 5-7mm, irregular shapes – some pinch and swell at 70dca 10% c veins, 1-2mm 2-3% py fine-grained disseminated 3% po fine-grained 2% mt disseminated visible 12.13-12.36m: moderate to strong shear at 70dca 14.13-14.44m: shear at 65dca, strong biotite, moderate carbonate alteration		
15.90 – 17.40	V3 Breccia? Medium grey with dark green bands Strong chlorite-rich bands 2-15cm wide at 60dca, with py-po-mt 5% c veins, 1-2mm 2% py fine-grained 3% po fine-grained 1% mt disseminated		

Depth (m)	Description	DDH: 180	CONTINUED	Section: 1124
17.40 – 17.82	Mafic dyke? Dark grey Strong carbonate alteration, locally weak biotite (defines foliation) Foliation at 50dca			
17.82 – 19.80	V3 Breccia? Pillow? Medium grey with dark green bands Strong chlorite-rich bands with po-py 3% py fine-grained 1% po fine-grained			
19.80 – 21.30	Biotite-carbonate Shear Shear at 55dca Dark grey 10% q veins, 5mm, biotite/chlorite selvage, at 55dca 5% py fine-grained, as stringers along q veins moderately magnetic 19.90-21.20m: Breccia. 10% angular fragments, fine-grained mafic fragments 5-30mm in size. Appears quartz-rich, 10-15% plagioclase phenocrysts? (anhedral), 3% py fine-grained disseminated			
21.30 – 23.40	V3 Amygdular Dark green 15% dark amygdules (1-2mm) 10% chlorite-rich bands at 70dca 10% c veins, 2-3mm, various directions 2% q veins, biotite/chlorite selvage, at 60dca, slightly folded 1% py fine-grained 1-2% po fine-grained 2-3% mt fine-grained disseminated			

Depth (m)	Description	DDH: 180	CONTINUED	Section: 1124
23.40 – 26.25	<p>Biotite-carbonate Shear Shear at 70-75dca Dark grey</p> <p>10-15% q veins, 1-10cm, biotite/chlorite/light brown selvage, at 70dca</p> <p>5% py fine-grained 5% po fine-grained 2-3% mt fine-grained disseminated</p> <p>25.00-26.25m: amygdular with amygdules elongated at 70dca, pinch and swell and folded/irregular q veins</p>			
26.25 – 30.50	<p>V3 Amygdular Medium to dark grey 30-40% calcite amygdules 26.25-29.20m; 5% amygdules below 29.2m Locally strong chlorite alteration</p> <p>5-10% c veins, 2-10mm, various directions</p> <p>TR po fine-grained</p> <p>26.25-29.2m: 30-40% calcite amygdules 29.20-30.50m: 5% calcite amygdules</p>			
30.50 – 33.00	<p>V3 Massive Dark green, fine-grained</p> <p>3% c veins, 1-2mm, various directions</p>			
33.00 – 34.60	<p>V3 Breccia Fragments ~1cm, angular “Swirled” texture Locally strong chlorite alteration</p> <p>1% py disseminated and stringers 1-2% po</p>			
34.60 – 35.00	<p>V3 Massive Dark green</p>			
EOH	5% c veins, 1-3mm, various directions			

Murgor Resources

BARRY - MAIN ZONE - Drill Core Logging

Logged by Kathryn Kitney

V3=mafic volcanic
T3=mafic tuff
QFP=quartz-feldspar porphyry

q=quartz
alb=albite
c=carbonate
bt=biotite
ep=epidote
chl=chlorite

VG=visible gold
py=pyrite
po=pyrrhotite
TR=trace
vis=visible
fg=fine grained (<1mm)
diss=disseminated

DDH: 101 Section: 1173

Major Unit		Minor Unit												Veins				Mineralization			
From	To	From	To	Rock Name	Colour	Composition	Texture/Primary Structures	Foliation Angle	Alteration	% , Type	Size	Selvage	Angle to CA	min1	min2	Magnetite	Other				
0	0.19			V3 altered	rusty brown	V3	none	none	rusty alteration, carbonate alteration?	q-alb=20%	q-alb=2cm	q-al=py	65dca	2% py, fg and in selvages		weak, not visible					
0.19	0.63			V3 massive +/- amygdular	dark green	V3 <1% calcite amygdules (1mm)	massive +/- amygdular	none	locally 1cm rusty bands	q-c=1%, q=<1%	q-c=1-2mm, q=<1mm	none	various	TR fg py diss		moderate magnetism, no visible magnetite					
0.63	3.86			V3 altered + amygdular	rusty brown	V3	none	faint, locally at 55dca	rusty alteration, carbonate alteration?	q-alb=4%, q=1%, q-c=1%	q-alb=.5-1.5cm, q=1cm, q-c=.5-1.5cm	q-alb=bt/chl dark selavge+py in places	q-alb=65dca, q-c=60dca, q=no direction	1-2%py diss, fg along veins, 1-5mm cubic in/ along veins		weakly magnetic in areas away from veins, no vis mt					
		3.1	3.86	amygdular - 1-2% white (calcite?) amygdules																	
3.86	4.15			V3 breccia?	dark green/grey	V3	breccia? Possible elongated fragments of light grey in dark green/grey	elongated at ~65dca	none?	1% q-c	q-c=1-2mm	rusty carbonate	65dca	none		possibly fg visible mt					

Major Unit		Minor Unit		DDH: 101 Section: 1173 CONTINUED						Veins				Mineralization			
From	To	From	To	Rock Name	Colour	Composition	Texture/Primary Structures	Foliation Angle	Alteration	%, Type	Size	Selvage	Angle to CA	min1	min2	Magnetite	Other
4.15	5.14			V3 altered (massive?)	rusty brown	V3	possibly amygdules near lower contact	weak at 60dca	rusty alteration, carbonate alteration?	2% q-alb, all at 4.57-4.67m	.5cm-1cm	dark - bt/chl + locally py	70dca	1% py with q-alb veins, cubic and blebs <= 1mm		weakly magnetic, but not near the q-alb veins	
5.14	5.74			Mafic dyke?	dark grey and slightly rusty weathering, but not as strong as in V3	fg grey, hard, 8-10% elongated mafics (bt?) .5mmx2mm	none	weak at 55-60 dca elongated mafics	some weak rusty weathering	q-alb=2-3%, q-c=1%	q-alb=.5cm-1cm, q-c=1-2mm	q-alb=dark bt/chl? In places, also rusty crystals	q-alb=30-45dca, q-c=various	none		none	
5.74	6.44			V3 altered	rusty brown	V3	none	none	rusty alteration, carbonate alteration?	q-alb=10-15%, q-c=2%	q-alb=.5cm-3cm, q-c=.5-1cm	q-alb=bt/chl in places +/- py, q-c=none	q-alb=55dca, q-c~55dca, but some are not	1%py fg diss, <= 1mm cubic near q-alb veins		fg diss mt vis cubic near q-c veins	
6.44	7.09			V3 massive? breccia?	dark green/grey some minor rusty bands	V3	breccia? Possible elongated "fragments"	weak, 50dca	minor <1cm rusty bands	1% q-c	q-c=1-2mm	none	40-45dca	none		trace fg diss cubic mt vis	
7.09	7.25			V3 altered	rusty brown	V3	none	none	rusty alteration, carbonate alteration?	q-alb=2%, q-c=1%	q-alb=.5cm, q-c=2-3mm	q-alb=bt/chl dark selvage+py in places	45-50dca	<=1%py fg diss and along selvages		moderately magnetic	
7.25	8.53			V3 massive	medium green with grey and rusty bands	V3	none - banding?	weak to moderate at 50dca	none/ carbonate in places?	q-alb=1%, q-c=<1%	q-alb=1vn 2-3cm, q-c=1-2mm	q-alb=bt/chl +/-py, q-c=none	both=45dca	py fg and blebs along q-alb vn		<=1% cubic mt vis (<1mm)	

Major Unit		Minor Unit		DDH: 101 Section: 1173 CONTINUED						Veins				Mineralization			
From	To	From	To	Rock Name	Colour	Composition	Texture/Primary Structures	Foliation Angle	Alteration	%, Type	Size	Selvage	Angle to CA	min1	min2	Magnetite	Other
8.53	8.85			V3 altered	rusty brown	V3	none	none	rusty alteration, carbonate alteration?	q-alb=5%, c=<1%	q-alb=.5-2.5cm, c=1mm	q-alb=bt/chl+fg py, c=none	q-alb=30 folded?/ boudined?	1% py fg diss cubic		fg diss mt vis, not near q-alb veins	
8.85	14.18			V3 massive	green/grey colour, locally weak rusty weathering	V3	none	none	none/ carbonate?	q-alb=2% locally q-c=1% throughout	q-alb=.5-2cm, q-c=1-2mm	q-alb=bt/chl dark +/-py	q-alb=40-50dca, folded?, q-c= ~45dca	1% py - near/in q-alb vns - fg diss to 5mm cubic		fg diss cubic	
		9.24	9.48	faint rusty alteration in host - q-alb vns here													
		9.38	9.42	strong rusty weathering													
		10.7	11	faint rusty alteration in host - q-alb vns here													
		11	11.27	strong rusty weathering													
14.18	15.36			QFP 2?	dark grey with mafic and felsic crystals	50% fg dark grey matrix, 40% white feld/quartz crystals (2-3mm), 10% mafic (2-3mm)	porphyry, crystal boundaries smeared/blurred	weak at 60dca elongation of crystals	none	q (+/- alb?)=10%	.5cm-3cm	none	stockwork	1-2% cubic py (<1mm) diss and in vns		not magnetic	
		14.18	14.27	fg ,mafic dyke on side of QFP													
		15.17	15.36	fg ,mafic dyke on side of QFP													
15.36	19.71			V3 massive	medium to dark green/grey colour	V3	weak colour banding of green and grey	none-weak?	none/ carbonate	q=<1%; q-c=1%; c=<1%; q-alb=1%	q=2-5cm; q-c=1-2mm; c=1mm; q-alb=2cm	q-alb=bt/chl/py	q=55dca; q-c and c=40dca; q-alb=70dca	py, po - see sub-units below		possible TR mt locally	
		15.36	18.35	1-2% cubic pyrite (~1mm) contained in chlorite-rich bands													
		18.35	19.17	<=1% po blebs <=1mm													

Major Unit		Minor Unit		DDH: 101 Section: 1173 CONTINUED						Veins				Mineralization			
From	To	From	To	Rock Name	Colour	Composition	Texture/Primary Structures	Foliation Angle	Alteration	%, Type	Size	Selvage	Angle to CA	min1	min2	Magnetite	Other
19.17	21.05			V3 amygdular	medium grey and green with weak colour banding	2% calcite, 2% quartz amygdules <1-2mm - quartz and calcite amygdules grouped	weak banding	weak banding at 60dca	none	q-c=<1%; c=<1%	q-c=1-2mm; c=1mm	none	both 60dca	<=1% pyrite fg diss cubic	<=1% po .5-1mm blebs diss	none	
21.05	21.93			V3 massive/feldspar-phyric	medium green with white crystals	<1% white feldspar? crystals <1mm, blurred and irregular crystals	none	none	none	q-c=<1%; c=<1%; chl=<1%	q-c=1-2mm; c=<1mm; chl=1-2mm	none	q-c=various + 45dca; c=various; chl=various + 40dca	tr pyrite fine-grained disseminated		not magnetic	
21.93	25.25			V3 amygdular	medium to dark green/grey colour	<1% quartz, 1% calcite (1mm, elongated to .5x2mm)		faint at 40dca (elongated amvg)	none	q-c=<1%; c=1-2%	q-c=1-2mm; c=1-2mm	none	q-c=50dca; c=various	TR py fg diss	TR po fine-grained disseminated	TR fg diss vis mt - belbs and cubic	
		23.18	23.43	few amygdules here - possibly massive/feldspar-phyric													
25.25	26.06			V3 massive	medium to dark green	V3	none	none	none	q-c=<1%; c=1%; chl=<1%	q-c=2-3mm; c=1mm; chl=1-2mm	none	q-c=30dca; c=55dca; chl=~55	TR py fg diss blebs	TR po fg diss blebs	not magnetic	
26.06	29.6			V3 amygdular	medium to dark green	V3 - 1% quartz, 2-3% calcite		amyg elongated at 40dca	none	q-c=1%; c=1%; chl=1%	q-c=1mm-1cm; c=1-2mm; chl=1-2mm	none	all ~40dca	TR py fg diss	TR po fg diss blebs	not magnetic	
		29.14	29.34	weak to moderate shear at 55dca, q-c vein boudined													
29.6	30.25			V3 massive/feldspar-phyric	medium to dark green/grey	V3 - small white (<1mm) crystals (feld?)	none	none	none	c=1%; chl=<1%	c=1-2mm; chl=1-2mm	none	c=various + 50dca; chl=various	none		not magnetic	

Major Unit		Minor Unit		DDH: 101 Section: 1173 CONTINUED						Veins				Mineralization			
From	To	From	To	Rock Name	Colour	Composition	Texture/Primary Structures	Foliation Angle	Alteration	%, Type	Size	Selvage	Angle to CA	min1	min2	Magnetite	Other
30.25	31.25			V3 amygdular	medium to dark green	V3 - 1% quartz, 1% calcite (1-2mm)	none	none	none	q-c=1%; c=1%; chl=<1%	q-c=3mm-1.5cm; chl=1-3mm	chl=contains mt	q-c=50dca; c=various + 40dca; chl=45dca	none		strong mt in chlorite-rich bands	
EOH																	

Murgor Resources

BARRY - MAIN ZONE - Drill Core Logging

Logged by Kathryn Kitney

V3=mafic volcanic
T3=mafic tuff
QFP=quartz-feldspar porphyry

q=quartz
alb=albite
c=carbonate
bt=biotite
ep=epidote
chl=chlorite

VG=visible gold
py=pyrite
po=pyrrhotite
TR=trace
vis=visible
fg=fine grained (<1mm)
diss=disseminated

DDH: 182 Section: 1158

Major Unit		Minor Unit												Veins			Mineralization			
From	To	From	To	Rock Name	Colour	Composition	Texture/Primary Structures	Foliation Angle	Alteration	% , Type	Size	Selvage	Angle to CA	min1	min2	Magnetite	Other			
0	0.6			overburden																
0.6	3.12			V3 massive	medium green and grey	V3	massive	none	rusty alteration (see below)	q-alb=2%; q-c=1%; c<1%	q-alb=.5-1cm; q-c=3-5mm; c=1mm	q-alb=dark bt/chl +/- py	q-alb=55-60; q-c=75; c=60-75dca	TR-1% py fg diss blebs		TR fg diss mt vis				
		0.6	0.86	faint rusty alteration																
		1.33	1.4	strong, dark rusty alteration																
3.12	3.75			QFP 2? + fine-grained dyke on margins	dark grey fine-grained matix, with white and dark crystals	50% matrix, 5% quartz, 40% feldspar, 3% chlorite, 2% mafics (bt?)	porphyry	none	none/smeared crystal boundaries	q-alb=2%	q-alb=2cm	none	none	TR py fg diss cubic		not magnetic				
		3.12	3.24	fg mafic dyke	dark grey		none	none		none										
		3.56	3.75	fg mafic dyke	dark grey		none	none		none										
3.75	7.87			V3 massive	medium grey to green (closer to 7.87)	V3	faint colour banding of green and grey	weak banding at 64dca	faint rusty alteration (see below)	q-alb=1% (only above 5.25m); q-c=1%; c<1%	q-alb=.5-1cm; q-c=1-3mm; c<1mm	q-alb=bt/chl+py	q-alb=45dca; q-c=55; c=50	TR py diss cubic ~1mm		TR fg diss vis mt				
		5	5.25	faint rusty alteration																
		6.34	VG	visible gold in quartz-carbonate vein with fine-grained pyrite																

Major Unit		Minor Unit		DDH: 182 Section: 1158 CONTINUED						Veins				Mineralization			
From	To	From	To	Rock Name	Colour	Composition	Texture/Primary Structures	Foliation Angle	Alteration	%, Type	Size	Selvage	Angle to CA	min1	min2	Magnetite	Other
7.87	12.11			V3 amygdular	medium grey/green	1-2% calcite (1-4mm), 1% quartz (1-2mm)	elongated amygdules	elongated amygd at 60dca	none	q+/- alb=<1%; q-c=1%, c=<1%	q+/-alb=1-2cm; q-c=1-3mm; c=1mm	none	q+/-alb=30-45dca; q-c and c=40-50dca	TR py fg diss in q+/- alb veins	TR po fg diss especially at (at 9.81 & 10m in chl/carb band)		
12.11	12.66			V3 massive	green/grey	V3	none	faint at 60dca	weak rusty alteration (see below)	q-alb=1%; q-c=2%; c=<1%	q-alb=7mm; q-c=2mm-1cm; c=1mm	q-alb=bt/chl +/- py, po	q-alb=40; q-c=75; c=various	TR py diss in rusty alt & q-alb veins	TR po fg diss blebs in q-alb vein	rusty=strongly magnetic, else weakly magnetic	
		12.11	12.26	weak rusty alteration													
12.66	15.5			V3 amygdular	2% calcite, <1% quartz, all 1-2mm	V3	amydules elongated in places	elongated amygd at 65dca	none	q-c=1%; c=<1%; chl=1%	q-c=2-5mm; c=1mm; chl=1-3mm	chl=TR py	q-c=75 pinch and swell; c=80-90dca/ various; chl= various	TR py diss in q-c veins < 1mm	TR po fg, mostly at 13.9m	TR fg vis cubic mt	
		13.9		local increase in po													
15.5	17.54			V3 massive	green/grey	V3	minor shear (see below), faint colour banding	weak colour banding at 60dca	none	q-alb=1%; q-c=<1%; c=<1%	q-alb=1-2cm; q-c=1mm; c<1mm	q-alb=bt+TR py	q-alb=65; q-c and c=60	TR py near q-alb /q-c veins and shear	TR po near q-alb /q-c veins and shear	TR fg vis diss mt cubic	
		16.32	16.45	amygdular - 2-3% calcite amygdules 1-3mm													
		15.8	15.9	moderate to strong shear at 60dca													

Major Unit		Minor Unit		DDH: 182 Section: 1158 CONTINUED						Veins				Mineralization			
From	To	From	To	Rock Name	Colour	Composition	Texture/Primary Structures	Foliation Angle	Alteration	%, Type	Size	Selvage	Angle to CA	min1	min2	Magnetite	Other
17.54	20			V3 amygdular +/- breccia	green and grey, some chl veins/possible fragments?	V3 - 1-2% calcite (1-4mm), 1% quartz (1-2mm)	possible fragments?	weak colour banding at 50dca	rusty alteration (see minor units below)	q-c=1%; c=<1%; chl=<1%	q-c=2-5mm; c=1mm; chl=1	none	q-c and chl=50dca; c=50dca and various	TR py diss cubic, fg, in host, chl veins		weakly magnetic (po?), local fg vis diss mt	
		17.88	17.94	strong rusty alteration													
		18.8	19	weak rusty /carbonate alteration + q-alb veins, 5mm, bt selvage, 60dca, contains TR py, po													
20	22.88			V3 massive	dark green/grey	V3	faint colour bands of green and grey (bt/chl)	colour bands at 80dca	none	q-c=1%; c=<1%	q-c=1-2mm; c=<1mm	none	q-c=60dca; c=various	TR py fg blebs diss in bt/chl alteration		TR-1% cubic diss fg mt	
		22.21	22.62	TR-1% py													
22.88	23.55			QFP 2?	dark grey matrix + white and mafic crystals	50% matrix, 40% feldspar/quartz, 10% mafic (5% bt, 5% chl)	porphyry	weak at 60dca	none	q=5%	q=3mm-2cm	none	stockwork	TR py fg diss cubic		not magnetic	Mafics elongated at sharp lower contact with V3
		23.34		chl and bt surround quartz vein													
23.55	25.75			V3 massive	medium green to lighter green with depth	V3	none	none	bt alteration (see below)	q-c=<1%; c=TR	q-c=1-2mm; c=<1mm	q-c=bt selvage in places	q-c=65dca; c=various (+folded?)	TR py fg diss blebs <1mm		not magnetic	
		23.55	23.75	strong biotite alteration in shear zones at 40dca													
25.75	27.04			V3 amygdular	medium green	V3 - 1% calcite + quartz (<1mm)	some elongated amygdules	elongated/aligned amyg 50-55dca	locally <1cm wide bt-rich bands	q-c=<1%; c=<1%	q-c=1-2mm; c=<1mm	none	q-c=65dca; c=55dca	TR py fg diss blebs		not magnetic	
27.04	27.65			V3 massive	medium to light green near bottom	V3	none	none	none	c=TR	c=<=1mm	c=bt up to 5mm thick in places	c=55 and 25dca	none		not magnetic	

Major Unit		Minor Unit		DDH: 182 Section: 1158 CONTINUED						Veins				Mineralization			
From	To	From	To	Rock Name	Colour	Composition	Texture/Primary Structures	Foliation Angle	Alteration	%, Type	Size	Selvage	Angle to CA	min1	min2	Magnetite	Other
27.65	32			V3 massive +/- amygdular	light/pale green	V3 +/- amygdules <1% diss amygdules calcite +/- quartz 1-2mm	none	chlorite bands at 70dca	none	q-c=<=1%; c=TR; ch;=TR-1%, blurred vein selvages	q-c=2m-2cm; c=1-2mm; chl=2mm-1cm	q-c=TR bt; chl= locally bt	q-c=55-70; c=55 and various; chl=65	TR py fg blebs with q-c veins, as py-po veinlets	TR po fg blebs with q-c veins, as py-po veinlets		
EOH																	

Appendix G
PETROGRAPHIC DESCRIPTIONS

Petrography was undertaken using transmitted and reflected light microscopy at Queen's University. Samples were chosen to represent the volcanic facies and types, syn-ore alterations (carbonate-quartz-pyrite and biotite-carbonate), and intrusive rocks at Barry. From the petrography a detailed paragenetic sequence has been created for syn-ore carbonate-quartz-pyrite and biotite-carbonate altered mafic volcanics (Fig. 2.7), diorite dikes 1-3 (Fig. 2.12), and QFP and quartz monzonite dikes (Fig. 2.13). Descriptions of the various units at Barry are described below in terms of (G1-6) Mafic volcanics (by facies); (G7) Carbonate-quartz-pyrite altered mafic volcanics; (G8) Biotite-carbonate altered mafic volcanics; (G9) Diorite 1; (G10) Diorite 2; (G11) Diorite 3; (G12) QFP; and (G13) Quartz monzonite.

G1. Mafic Volcanics: Pillowed

59-1113

0.01 g/t

This sample is composed of 5% amygdules (described in more detail below) and 40% carbonate, 27-30% plagioclase, 10% chlorite, 8% muscovite, 5% quartz, trace to 1% pyrrhotite, ilmenite, and magnetite, and trace epidote, magnetite, and chalcopyrite.

Amygdules are approximately 0.9mm x 1.5mm in size, and locally the long axis of the amygdules is aligned with a weak fabric. Amygdules in this sample are generally composed of quartz and/or carbonate and trace chlorite. Quartz crystals range in size from 0.22mm to 0.36mm in diameter, and are locally replaced by chlorite laths.

Carbonate crystals replace quartz and chlorite in amygdules, and locally carbonate is replaced by epidote.

In the host, plagioclase and quartz are present as subhedral crystals in sharp contact and are less than 0.05mm in diameter. Chlorite replaces quartz and plagioclase in the host as laths approximately 0.27mm x 0.04mm in size. Carbonate replaces quartz, plagioclase, and chlorite in the host as crystals 0.03mm x 0.06mm to 0.27mm x 0.55mm in size.

Muscovite replaces plagioclase, quartz, chlorite, and carbonate as crystal laths from <0.03mm to 0.2mm x 0.07mm in size.

Magnetite is present as euhedral cubes that have been fractured. Carbonate fills the fractures in magnetite. Pyrrhotite is present as anhedral crystals, and has sharp contacts with quartz in amygdules and carbonate. Pyrrhotite contains inclusions of ilmenite and appears to be replacing chalcopyrite. Chalcopyrite is present as inclusions and filling fractures in pyrrhotite. Trace pyrite is present as subhedral to anhedral crystals associated with carbonate crystals.

62-1088

0.01 g/t

This sample is composed of 2-5% amygdules in a host composed of 48% plagioclase, 25% carbonate, 10-15% chlorite, 5% muscovite, 2-5% quartz, trace to 1% ilmenite and magnetite, and trace pyrite.

The amygdules in this sample are elongated and are approximately 0.55mm x 1.8mm in size. Amygdules are aligned along their long axis and, along with aligned chlorite laths, they form a moderately strong fabric within this sample. Amygdules are composed mainly of quartz crystals 0.14mm to 2.7mm in diameter that are pseudomorphously replaced and partially replaced by carbonate crystals.

Plagioclase composes most of the host with quartz in elongated crystals approximately 1.4mm x 0.05mm in size. These crystals are aligned along their long axis, and along with chlorite and elongated amygdules these form the foliated fabric of this sample.

Plagioclase and quartz are replaced by chlorite tabular laths as described in sample 59-1113. Chlorite laths in this sample are approximately 0.06mm x 0.04mm in size.

Carbonate and muscovite occurs as described as described in sample 59-1113.

Magnetite occurs as seen in sample 59-1113 – as euhedral cubic crystals that are fractured and fractures are filled with carbonate. Pyrite forms subhedral to anhedral crystals spatially associated with and in sharp contact with carbonate crystals. Ilmenite forms rounded to lamellar crystals and crystal aggregates within and associated with plagioclase, quartz, and chlorite in the host. Ilmenite is present as crystals ranging from 0.01mm in diameter to 0.12mm x 0.04mm in size.

This sample contains veinlets of 0.27mm in width that are aligned with the foliation in the sample. These veinlets are composed of carbonate and trace quartz, with carbonate replacing quartz crystals in the veinlets. Trace ilmenite is present within and between carbonate crystals. There is no visible selvage along the veinlets.

62-1165

0.01 g/t

This sample is composed of 1-2% amygdules and 5% veinlets within a host composed of 52% muscovite, 20% carbonate, 5% plagioclase, 5% quartz, 5% chlorite, 1-2% magnetite, trace to 1% pyrite, and trace biotite, ilmenite, chalcopyrite, and pyrrhotite(?).

Amygdules in this sample are composed of carbonate crystals and trace quartz and chlorite 0.14mm in diameter. Carbonate is pseudomorphously replacing quartz and chlorite crystals. Amygdules are elongated and approximately 1.3mm x 0.55mm in size, and are somewhat aligned with chlorite tabular crystals and elongated carbonate crystals in the foliation fabric of the sample.

Veinlets in this sample are composed of quartz, carbonate, pyrite, and trace chlorite and biotite and are approximately 0.36mm to 1.1mm in width. Quartz, carbonate, pyrite, and chlorite crystals are in sharp contact with each other in the vein and range in size from 0.14mm to 0.4mm in diameter. Finer-grained carbonate crystals also fill corroded zones and partially replace chlorite and quartz crystals.

Plagioclase and quartz form crystals in the host that are almost completely replaced by carbonate and muscovite. Biotite forms dark brown tabular and flaky crystals with low pleochroism that 0.088mm x 0.029mm in size. Biotite fills corroded zones of magnetite

or forms sym-magnetite with sharp, irregular contacts. Chlorite replaces plagioclase, quartz, and biotite as described in sample 59-1113 and 62-1088. Magnetite is lightly fractured (compared to the previous two samples) and fractures appear to be filled with carbonate. Pyrite forms cubic euhedral crystals in sharp contact with quartz and carbonate crystals in the host and vein. Pyrite is also replacing the plagioclase/chlorite in the host. Muscovite fills corroded zones along the rims of pyrite crystals. Ilmenite forms tabular and lamellar crystals disseminated in the host and as inclusions in pyrite. Chalcopyrite forms anhedral crystals along the rims of pyrite and within fractures of magnetite crystals. Pyrrhotite (?) appears to be replacing portions of the chalcopyrite.

G2. Mafic Volcanics: Brecciated

Sample 66-1092

This sample is composed of approximately 20% fragments and 80% host. The fragments in this sample are sub-angular to sub-rounded, and range in size from 1.8 x 4mm in size to 4mm in diameter. Fragments have a different grain size and composition than the host, and have fairly sharp contacts with the host.

The fragments are composed of 88% cryptocrystalline groundmass, 10% epidote (+/- hornblende?), 2% chlorite, and trace biotite, muscovite, carbonate, and magnetite. Biotite and chlorite form 0.01mm laths disseminated in the cryptocrystalline groundmass.

Epidote forms granular aggregates approximately 0.04 to 0.05mm in size that replace crystals in the groundmass. Carbonate is approximately 0.03 to 0.04mm in size and replaces portions of the groundmass and fills corroded zones of epidote. The relationship between epidote and chlorite, epidote and biotite, carbonate and chlorite, carbonate and biotite, and chlorite and biotite is not known. Locally one (possible) fragment contains what appear to be plagioclase laths 0.05 x 0.15mm in size.

The host is composed of 75% chlorite, 10% groundmass (quartz and plagioclase), 8% carbonate, 5% epidote, 2% hornblende, and trace muscovite, rutile, ilmenite, magnetite, pyrite, and chalcopyrite. The groundmass is fine-grained, with crystals of quartz and plagioclase approximately 0.03 to 0.06mm in diameter. Because of their size and the fact that they are altered and replaced by other minerals, the percentages of quartz and plagioclase are unknown. Chlorite replaces the fine-grained groundmass with laths ranging from 0.02 x 0.06mm to 0.03 x 0.08mm in size. Muscovite forms laths approximately 0.03 x 0.06mm in size and replaces chlorite and the fine-grained groundmass. Epidote and hornblende form granular aggregates that replace chlorite, muscovite, and the fine-grained groundmass. Carbonate fills corroded zones of and replaces chlorite, epidote, hornblende, and the groundmass. Rutile forms crystal aggregates that are associated with granular aggregates of epidote. Ilmenite forms clusters of crystals and laths in the host approximately 0.02 x 0.06mm in size. The laths are a possible pseudomorphic replacement of chlorite. Ilmenite, rutile, and epidote form

clusters of crystals that appear to replace skeletal fragments of a crystal. In these cases rutile is associated with regions that are replaced by epidote. Magnetite forms euhedral crystals in the host approximately 0.04mm in diameter. Corroded zones of magnetite are filled with carbonate. Pyrite forms anhedral crystals approximately 0.18mm in size in the host, and contains inclusions of the fine-grained fragments that are being replaced by epidote. Carbonate and epidote fill corroded zones of pyrite. Muscovite forms sharp contacts with pyrite. Chalcopyrite pseudomorphously replaces portions of the larger pyrite crystals, and completely replaces small fragments and crystals of pyrite.

Veins in the sample consist of a quartz-carbonate-epidote vein that cuts both the host and the fine-grained fragments in the sample. The vein ranges in width from 0.18mm wide in the host to two parallel veins each 0.07mm wide within the fine-grained fragment. The vein appears to have been quartz dominated, with possibly some carbonate. The quartz crystals in the vein have been pseudomorphously replaced by carbonate and epidote so that the composition of the vein is now 20% quartz, 60% carbonate, and 20% epidote.

This sample does not exhibit foliation and does not appear to have any other signs of deformation.

Sample 118-1.01

This sample is composed of 55% plagioclase, 20% carbonate, 10-15% muscovite, 3-5% biotite, trace-2% magnetite, trace-2% quartz, trace-2% pyrite, and trace chlorite and ilmenite. There are no fragments visible in this thin section, and the sample appears more massive than it does brecciated.

Plagioclase forms very fine-grained laths (?) or is cryptocrystalline. Plagioclase is heavily replaced by very fine-grained muscovite laths, making it impossible to tell the primary texture of the plagioclase. A dark brown, low birefringence, low pleochroic biotite¹ is present as flakes replacing plagioclase. Magnetite (cubic) and fine-grained rutile (and crystal aggregates) replace plagioclase and biotite¹. Carbonate, quartz, and cubic pyrite replace and fill corroded zones of plagioclase, biotite¹, magnetite, and ilmenite. Biotite² forms laths with sharp contacts with, and filling embayments of, pyrite, carbonate, and quartz. Muscovite replaces plagioclase (described above) and also locally replaces all of the minerals as larger laths.

This sample contains a 2.5mm wide carbonate-albite-quartz vein composed of 55-60% carbonate, 45-50% albite, and trace-5% quartz grains. Albite, quartz, and some carbonate are euhedral 0.78mm, while the remainder of the carbonate is anhedral and filling corroded zones of albite and quartz.

Sample 118-5.16

This sample contains various veins/veinlets including a 1.5cm wide plagioclase-quartz vein (with local carbonate), and several ≤ 1 mm veinlets of carbonate-albite and locally quartz. In the wide vein albite crystals reach the size of 2×2.5 mm. Albite and quartz form these large euhedral crystals and carbonate, biotite, and chlorite fill embayments and fractures in these large grains.

The host of this sample is small and does not appear to contain any breccia fragments (this sample is ~50% vein). It is composed of 90% plagioclase, 1-2% quartz, chlorite, carbonate, biotite, and muscovite, 1% magnetite and pyrite, trace-1% ilmenite, and trace pyrrhotite. Plagioclase, magnetite, ilmenite, pyrite, carbonate, quartz, and muscovite are present as describe in sample 118-1.01. Magnetite locally contains inclusions (?) of pyrite (or pyrite is filling pits/corroded zones in magnetite). Pyrite is cubic to subhedral, is locally zoned, and contains inclusions of magnetite and pyrrhotite. Chlorite and biotite form laths and flakey grains replacing each other and plagioclase and filling embayments in pyrite. Chlorite and biotite are present mainly along the selvage and in close proximity to the large vein.

Foliation is moderate in this sample with what looks like elongated plagioclase laths aligned and stretched (especially near the large vein), and veinlets parallel within the

sample. Foliation is also locally seen in cross-polarized light where fine-grained muscovite laths are aligned.

Sample 118-16.70

This sample is comprised largely of two (1cm wide) carbonate veins. These veins make up >50% of the sample. The remaining portion of the sample does not appear to contain any fragments, but this area is quite small. It is composed of 45% plagioclase, 15% chlorite, 15% epidote, 10% biotite, 10% carbonate, 5% quartz, trace-1% pyrite, and trace magnetite, ilmenite, and pyrrhotite.

Plagioclase, ilmenite, magnetite, carbonate, quartz, and pyrite form as described in sample 118-1.01. Pyrrhotite locally replaces sub-cubic pyrite crystals. The majority of the smaller single grains of pyrite and pyrrhotite are included in carbonate. From this sample it is difficult to tell whether the chlorite and biotite are pre or post carbonate. They locally appear to fill embayments in carbonate and pyrite, but where they contain inclusions of pyrite/pyrrhotite the carbonate appears to replace the chlorite. Epidote replaces and fills corroded zones of all minerals as euhedral crystals.

No fabric is seen in this sample.

Sample 142-1.76

This sample does not appear to contain any fragments and appears to contain several .78-2mm wide quartz (-carbonate) amygdules. This sample is composed of 55% plagioclase, 35% epidote, 5% quartz, 2-5% carbonate, trace-1% chlorite, and trace muscovite, magnetite, ilmenite, and pyrite.

Plagioclase, muscovite, magnetite, ilmenite, pyrite, quartz, and carbonate form as in sample 118-1.01. Chlorite replaces plagioclase and is replaced by magnetite and ilmenite. Locally chlorite alteration is intense and is spatially associated with a region of increased magnetite (up to 5-8% magnetite). Carbonate replaces chlorite. Epidote replaces all minerals as fine-grained crystal aggregates, and locally replaces portions of veinlets and amygdules as large (up to 0.4x0.9mm) euhedral crystals.

Veinlets in this sample are comprised of quartz or carbonate-epidote – with euhedral epidote replacing the carbonate crystals. Epidote locally replaces portions of quartz veins as well. Veinlets range in size from 0.44-0.78mm wide.

Fabric (if any) is weak and possible appears as elongated plagioclase laths that are aligned. Veins are locally parallel to this fabric, although in this sample they appear folded and locally possibly pinch and swell.

G3. Mafic Volcanics: Amygdular

31-25.48

0.03 g/t

This sample is composed of 10% amygdules (of which 5% is quartz and 5% is carbonate), 25% epidote, 10% chlorite, 27% plagioclase, 10% quartz, 5% carbonate, 3% magnetite, 10% biotite, and trace pyrite, chalcopyrite, and pyrrhotite.

The amygdules in this sample range in size from 1.8mm in diameter to 2.2 x 2.9mm. The composition of amygdules ranges from being quartz dominated to carbonate dominated to quartz-carbonate-chlorite. In general quartz, chlorite, and carbonate crystals are approximately 1mm in diameter. Locally quartz-dominated amygdules contain coarse-grained (1mm) crystals in the centre and finer-grained (0.05mm) crystals along the rim, with an incomplete ring of tabular crystals of chlorite and biotite separating the larger and smaller crystals. Within the amygdules quartz is locally replaced by biotite, chlorite, and carbonate. Magnetite and pyrite are locally included in quartz crystals of amygdules.

Plagioclase forms laths approximately 0.13mm in diameter in the host. Chlorite and biotite form flakes and laths in the host ranging in size from 0.04 to 0.1mm in diameter. Chlorite and biotite replace plagioclase, and replace each other in the host. Epidote forms granular aggregates and subhedral crystals 0.05mm in size that replace plagioclase, biotite, and chlorite. Magnetite forms euhedral crystals disseminated in the host. Pits, fractures, and corroded zones in magnetite are filled with carbonate and epidote.

Magnetite locally contains inclusions of pyrite. Pyrite forms cubic euhedral to anhedral crystals disseminated in the groundmass. Pyrite locally contains inclusions of chalcopyrite and partial inclusions of magnetite. Pyrrhotite is present as cubic euhedral to subhedral crystals containing inclusions of magnetite. Pyrrhotite is likely pseudomorphously replacing pyrite in this sample.

Veins in this sample are composed of carbonate and epidote. The largest vein in this sample is 0.5mm wide and is composed of carbonate and magnetite. The carbonate crystals in this vein are approximately 0.06mm in diameter and some crystals are slightly elongated along the strike of the vein. Locally this vein contains laths of biotite and chlorite that appear to be included or partially included in carbonate crystals. Magnetite in this vein is cubic and has sharp contacts with carbonate. This vein appears to cut the tip of at least one amygdule. There is no selvage alteration associated with this vein.

Smaller veins in this sample are composed of epidote +/- carbonate. These veins occur at various angles in the sample, and are not continuous across the sample. These veins do not cut amygdules. These samples are approximately 0.03mm in width and are composed of >90% epidote, and up to 10% carbonate. The epidote vein that comes in contact with the carbonate vein appears to end at the carbonate vein.

This sample does not appear to contain any clear foliation or other deformation fabric.

31-27.03

0.02 g/t

This sample consists of a finer-grained portion and a coarser-grained portion. The finer-grained portion consists of crystals approximately 0.02 to 0.06mm in diameter, and composes approximately 1/3 of the sample, while the coarse-grained portion consists of crystals ranging in size from 0.07 to 0.18mm in diameter, and composes the other 2/3 of the sample.

Finer-grained portion: This portion of the sample is composed of 10% carbonate-quartz amygdules, 50% plagioclase, 15% carbonate, 20% chlorite, 5% epidote, and trace ilmenite, magnetite, pyrite and pyrrhotite.

The amygdules in this portion of the sample are composed of 90% carbonate, 8% quartz, 1% chlorite, 1%, epidote, and trace ilmenite, magnetite, pyrite, and pyrrhotite. Carbonate forms euhedral crystals approximately 0.27 x 0.8mm in size, while quartz forms anhedral crystals approximately 0.14mm in size. Chlorite is present within the amygdules as flakes and laths present at boundaries between carbonate crystals and occasionally as laths included in large carbonate crystals. Epidote is present replacing portions of carbonate crystals in the amygdules. Ilmenite (laths and sub-rounded crystals), magnetite (subhedral), pyrite (subhedral), and pyrrhotite (anhedral) are locally partially included within the carbonate of the amygdules. Carbonate fills corroded zones and fractures of

magnetite and pyrite. Amygdules are elongated and aligned forming a fabric parallel to that found in the coarser-grained portion.

In the host, plagioclase forms laths approximately 0.057mm in size. Chlorite forms tabular crystals and flakes approximately 0.008mm in size that replace the plagioclase. Carbonate forms crystals approximately 0.04mm in size that replace plagioclase and chlorite in the host. Epidote forms laths approximately 0.03mm in size that replace plagioclase and chlorite. Carbonate and epidote have sharp contacts with each other, and locally epidote forms laths that appear to replace (or at least not be replaced by) carbonate. Ilmenite, magnetite, pyrite, and pyrrhotite form as partially included crystals in the amygdules (as described above), and ilmenite is disseminated in the host.

Coarser-grained portion: This portion of the sample is composed of 50% carbonate, 30% chlorite, 15% magnetite, 2% quartz, 2% pyrrhotite, and trace biotite, epidote, quartz and/or plagioclase, pyrite, chalcopyrite, and ilmenite.

Carbonate is present as euhedral crystals ranging in size from 0.03 x 0.12mm to 0.14 x 0.4mm crystals. These crystals are elongated and aligned to form a strong fabric.

Carbonate is also present as smaller crystals that are replacing chlorite in this region.

Chlorite in this portion of the sample forms elongated flakes and laths that have sharp

contacts with the large carbonate crystals. Quartz and/or plagioclase form 0.03mm crystals that are surrounded by chlorite. Epidote forms euhedral crystals replacing the chlorite in this portion. The relationship between carbonate and epidote is not known for this portion of the sample.

Magnetite forms euhedral cubic to subhedral grains within the chlorite, and locally within the carbonate. Magnetite contains inclusions of pyrrhotite and locally a bright white reflective mineral. Pyrrhotite forms anhedral crystals and stringers in this portion of the sample within the chlorite and carbonate portions. Chalcopyrite has sharp contacts with pyrrhotite, and is found in portions of the pyrrhotite stringers. Pyrrhotite contains inclusions of magnetite, and magnetite fills pits in pyrrhotite. Pyrrhotite also locally contains an inclusion of euhedral to subhedral pyrite. Chalcopyrite appears to be altering the pyrrhotite along the contact of pyrite and pyrrhotite. Where chalcopyrite is lacking, the contact between pyrite and pyrrhotite is sharp. Ilmenite forms laths in the chlorite approximately $9\mu\text{m} \times 40\mu\text{m}$ in size.

76-1028

0.04 g/t

This sample is composed of 2-5% amygdules (quartz-carbonate), 62% plagioclase, 30% epidote, 5% chlorite, 2-3% quartz, trace to 1% magnetite, and trace carbonate, pyrite, ilmenite, and chalcopyrite.

Amygdules are a combination of elongated quartz and carbonate crystals, locally with chlorite lath rims. Amygdules themselves are elongated and aligned.

Plagioclase, epidote, chlorite, magnetite, and pyrite occur as described in sample 31-25.48. Quartz and carbonate occur as small (0.07mm) crystals replacing plagioclase and chlorite. Ilmenite is present as small laths and crystal aggregates replacing plagioclase. Chalcopyrite is present in sharp contact with pyrite.

The sinuous/discontinuous vein in this sample is comprised mainly of quartz crystals, is roughly perpendicular (in this section) to the elongated amygdules, and does not have an associated selvage.

88-1093 0.01 g/t

This sample is composed mainly of a 1-2cm wide carbonate vein (composed of 99% carbonate and trace-1% quartz) with crystals 0.5-1.4mm in size.

117-03.48

0 g/t

This sample is composed of 10% amygdules, 55% plagioclase, 15% carbonate, 10% chlorite, 5% quartz, 5% magnetite, and trace muscovite, epidote, ilmenite, and pyrite.

Amygdules occur as described in sample 31-25.48, with 8% of the amygdules composed of carbonate, and 2% composed of a combination of quartz and carbonate. These amygdules are irregularly shaped, and are not elongated/aligned.

Plagioclase, chlorite, magnetite, epidote, and pyrite occur as described in sample 31-25.48. Magnetite in this sample is larger (0.3-0.6mm, with most closer to 0.6mm in size) than in previous samples. Carbonate, quartz, and ilmenite occur as described in sample 76-1028. Muscovite occurs as in sample 91-1119.

118-24.56

0.0025 g/t

This sample is composed of 10% amygdules, 41% plagioclase, 30% epidote, 20% biotite, 2-5% quartz, 2-3% pyrite, 2% carbonate, and trace chlorite, magnetite, and ilmenite.

Amygdules are 4% quartz and 6% carbonate, are slightly elongated, and are somewhat aligned. Amygdules occur as described in sample 31-25.48.

Plagioclase, epidote, biotite, chlorite, pyrite, and magnetite occur as described in sample 31-25.48. Carbonate, quartz, and ilmenite occur as described in sample 76-1028.

143-29.78 0.11 g/t

This sample is composed of 10% amygdules, 60% plagioclase, 15% epidote, 5-8% biotite, 2-5% carbonate, 2% chlorite, 1-2% quartz, 1% pyrrhotite, trace-1% pyrite, and trace ilmenite, and chalcopyrite.

Amygdules in this sample are composed entirely of carbonate with local trace chlorite along the rims. The size of the amygdules is similar to those described in sample 31-25.48.

Plagioclase, chlorite, biotite, epidote, pyrrhotite, and pyrite occur as described in sample 31-25.48. Chalcopyrite, ilmenite, carbonate, and quartz occur as described in sample 76-

1028. Chalcopyrite also locally replaces portions of pyrrhotite crystals (or replaced pyrite which is now replaced by pyrrhotite?)

Veinlets in this sample are composed of epidote-carbonate (0.14mm across) with epidote replacing carbonate as euhedral crystals, and carbonate-chlorite (0.7mm across) with chlorite as elongated sinuous crystals along the rim of the vein.

151-27.33

0.026 g/t

This sample is composed mainly of a 6.9mm wide vein composed of carbonate (70-80%) and quartz (20-30%). Carbonate crystals are 0.3-0.7mm in size, while quartz crystals are generally ≤ 0.3 mm in size. Locally portions of quartz and carbonate crystals are replaced by euhedral epidote.

The remainder of this sample is composed of 1-2% amygdules, 70% plagioclase, 10-15% chlorite, 5-8% carbonate, 5% pyrrhotite, trace-2% biotite, trace-2% quartz, and trace magnetite, pyrite, ilmenite, and chalcopyrite.

Plagioclase laths in this sample are elongated, with approximate dimensions of 4.4mm x 0.55mm. Chlorite has a darker green/rich colour and preferentially replaces minerals between long plagioclase laths (also plag???) as laths, flakes, and locally appears to be granular aggregates. Biotite, pyrrhotite, magnetite, and pyrite occur as described in sample 31-25.48. Carbonate, quartz, and ilmenite occur as described in sample 76-1028. Chalcopyrite occurs as described in sample 143-29.78.

Other veinlets in this sample are composed primarily of carbonate +/- pyrrhotite and pyrite, and 0.55-1.1mm in diameter. These veins are irregular in shape and are discontinuous.

G4. Mafic Volcanics: Massive

31-0.31 Core Sample 0.57 g/t Au

In hand specimen this sample is dark green, fine-grained, and poorly foliated, with approximately 5% rusty veins (possibly carbonate), and visible fine-grained disseminated magnetite. It is composed of plagioclase (46%), chlorite (40%), carbonate (5%), quartz (5%), magnetite (2%), ilmenite (1 to 2%), and traces of epidote, muscovite and pyrite.

Magmatic plagioclase laths are euhedral (~ 0.18 x 0.07 mm), with corroded edges filled by chlorite, carbonate, and epidote. Chlorite forms flaky, lath-like and acicular crystals

(~0.44mm) that are yellow-green coloured, pleochroic, with brown-purple birefringence. Chlorite fills corroded zones of plagioclase, replaces plagioclase, and forms chlorite-rich veinlets in the host. Carbonate is pseudomorphously replacing magmatic plagioclase and/or quartz (~0.03mm). Epidote is pseudomorphously replacing portions of plagioclase and quartz crystals (in veins), as crystals ~0.02mm in size. Muscovite replaces portions in the centre of plagioclase laths.

Magnetite is subhedral, sub-rounded, ~0.14mm and is disseminated throughout the sample. It contains inclusions of ilmenite, and ilmenite fills corroded zones at the edges of magnetite grains. Corroded zones at the edge of magnetite grains are also filled with carbonate, and locally chlorite. Locally magnetite is spatially associated with pyrite, and is found surrounding larger pyrite grains. Pyrite is subhedral with crystals rounded in places, and disseminated in the host. Pyrite crystals are generally ~0.11mm, corroded in the middle and at the edges, and contains inclusions of ilmenite, magnetite, and chalcopyrite. Magnetite and carbonate fill corroded zones of pyrite crystals. Chalcopyrite pseudomorphously replaces portions of pyrite. Ilmenite is also present as inclusions in magnetite, and filling corroded zones of magnetite crystals.

Veins are composed of euhedral quartz and carbonate and range in width from 0.55 to 1mm. Quartz grains (0.60mm) line the edges of the carbonate grains (0.25mm) within the vein, and tabular chlorite replaces portions of both the quartz and carbonate crystals.

These veins do not have any associated selvage. Veinlets of euhedral quartz and flaky chlorite with trace epidote have sharp contacts with the host, and no visible selvage.

Discontinuous bands of flaky chlorite with anhedral quartz cut the quartz-carbonate vein in places, and bands of acicular muscovite replace magmatic plagioclase.

31-2.26 Core Sample 0.08 g/t Au

In hand specimen this sample is dark green-grey with rusty ankerite bands, and contains chlorite-rich bands, quartz-carbonate veins with chlorite-rich selvage, and visible fine-grained disseminated magnetite. It is composed of carbonate (40%), chlorite (25%), plagioclase (15%), biotite (10%), quartz (5%), magnetite (2-3%), pyrite (trace to 1%), ilmenite (trace to 1%), and trace epidote, chalcopyrite, pyrrhotite and rutile.

Plagioclase, carbonate, chlorite and epidote have similar relationships to those described in sample 31-0.31. Plagioclase forms laths ~0.08mm which has been pseudomorphously replaced and corroded by carbonate. Chlorite crystals are flaky (~0.2mm) and form chlorite-rich bands ~1mm wide. Epidote replaces portions of plagioclase laths.

Biotite replaces chlorite in the host and forms flaky crystals (~0.16mm) and biotite-rich bands in places. Quartz forms euhedral crystals (~0.08mm) in the host. Quartz is pseudomorphously replaced by carbonate.

Magnetite is cubic, ~0.12 to 0.55mm, is disseminated throughout the host. Magnetite grains are corroded and pitted and filled with carbonate. Magnetite contains inclusions of pyrite, chalcopyrite, pyrrhotite, and ilmenite. Pyrite is cubic (~0.06 to 0.09mm), in the host and contains inclusions of magnetite and ilmenite. Portions of pyrite grains have been pseudomorphously replaced by chalcopyrite. Corroded zones of pyrite have been filled with carbonate. Ilmenite forms laths (~0.05mm) disseminated in the host, and as inclusions in pyrite and magnetite. Chalcopyrite is present as inclusions in magnetite and pyrite, as a pseudomorphous replacement of pyrite, and as euhedral crystals within the host. Chalcopyrite contains inclusions of ilmenite and pyrite. Pyrrhotite forms inclusions in pyrite and magnetite, sometimes forming with chalcopyrite and pyrite in these inclusions. Sulfides are rimmed with a dark grey mineral that had a white internal reflection in places (possibly rutile).

Veins are composed of quartz (-albite) ~1mm wide. Crystals of quartz and albite are pseudomorphously replaced by carbonate. One quartz (-albite-carbonate) vein has chlorite-rich banding in the selvage and fine-grained carbonate replacing plagioclase and quartz in the host. A second vein of the same composition has a selvage with relict

plagioclase that is being pseudomorphously replaced by carbonate. Veins and chlorite banding are aligned along a fabric in the sample.

31-17.89 Core Sample 0.29 g/t Au

In hand specimen this sample is medium to dark green with visible fine-grained disseminated magnetite. It is composed of chlorite (30%), quartz (20%), carbonate (15%), muscovite (15%), biotite (10%), plagioclase (5%), magnetite (4%), ilmenite (1%), and traces epidote, pyrite and rutile.

Plagioclase, chlorite, carbonate, and epidote have similar modes of occurrence as described in sample 31-0.31. The smaller percentage of plagioclase in this sample is due to the fact that more of the plagioclase laths have been pseudomorphously replaced by carbonate. Plagioclase laths also contain acicular crystals of muscovite replacing plagioclase. Chlorite fills corroded zones of magnetite in places. Quartz in this sample is found as euhedral crystals (~0.04mm) in the host. Quartz is being pseudomorphously replaced by carbonate, chlorite, biotite, and muscovite.

Muscovite is colourless to light yellow-blue, with moderate birefringence. It is found as acicular crystals within plagioclase as a replacement, and as flaky and lath-like crystals

within the host (~0.05-0.08mm). It fills corroded zones of magnetite and pyrite, pseudomorphously replaces quartz and plagioclase, and replaces chlorite crystals. Biotite is colourless to very light brown/orange, with moderate (orange) birefringence and forms sharp contacts with chlorite, muscovite, and carbonate crystals. Epidote pseudomorphously replaces portions of plagioclase laths.

Magnetite is euhedral and cubic (~0.27mm), with fractured/corroded in places filled with carbonate. It contains laths of ilmenite, and is rimmed by a grey mineral (possibly rutile?). Pyrite is light yellow coloured and pitted, containing ilmenite laths (~0.07 x 0.01mm). When in contact in host, ilmenite and pyrite have sharp contacts. Ilmenite in the host is euhedral, lath-shaped or rounded in the host. Rutile pseudomorphously replaces portions of larger, rounded ilmenite grains.

74-1123 Surface Sample 0.01 g/t Au

In hand specimen this sample is dark green-grey with visible fine-grained disseminated magnetite and pyrite. It is composed of carbonate (30%), epidote (23%), plagioclase (15%), quartz (10%), chlorite (10%), muscovite (10%), magnetite (1 to 2%), pyrite (trace to 1%), pyrrhotite (trace to 1%), and traces biotite, ilmenite and chalcopyrite.

Chlorite and carbonate have similar relationships as those described in sample 31-0.31.

Quartz is present as euhedral crystals in the groundmass as in sample 31-2.26.

Plagioclase is present in volcanic laths as seen in sample 31-0.31, with larger relict plagioclase phenocrysts that have been pseudomorphously replaced by fine-grained muscovite.

Muscovite forms fine-grained acicular/lath-like crystals with moderate orange-red to blue birefringence. The crystals are disseminated in the groundmass and fine-grained muscovite pseudomorphously replaces plagioclase phenocrysts. Biotite is present as rusty brown discolouration and partial replacement of crystals along a fracture in the host. In the host biotite pseudomorphously replaces chlorite. Epidote pseudomorphously replaces portions plagioclase and/or quartz grains (~0.04mm) as anhedral crystals and granular aggregates (~0.31mm).

Magnetite is generally euhedral, cubic, and pitted/fractured, containing quartz and carbonate within the fractures. Magnetite crystals are present in the groundmass and within amygdules. Pyrite is euhedral (~0.15mm) and disseminated in the host. It contains inclusions of magnetite, pyrrhotite, and chalcopyrite. Chalcopyrite forms as inclusions in pyrite and as euhedral crystals in the groundmass. Ilmenite forms lath-like crystals (0.02mm) and aggregates of larger, rounded crystals that are disseminated in the host.

Pyrrhotite forms as inclusions within pyrite, and as rounded, euhedral crystals in the host,

replacing plagioclase and quartz (~0.15mm). Larger pyrrhotite crystals exhibit “bubbly” fine-grained re-growth of pyrrhotite along the rims of pyrrhotite grains.

Quartz, carbonate and chlorite grains form amygdules with grains 0.14 to 0.22mm in the amygdules. Amygdules contain pyrrhotite, pyrite, chalcopyrite, magnetite, and sphalerite (?).

Veins are composed of carbonate with trace epidote, or quartz. These veins cut the groundmass, are ~0.10mm wide, and have no associated selvage.

90-1040 Surface Sample 0 g/t Au

In hand specimen this sample is dark green-grey with visible fine-grained disseminated magnetite and pyrite. The sample is weakly foliated, with veinlets aligned sub-parallel to the fabric. It is composed of carbonate (40%), muscovite (30%), chlorite (20%), quartz (7%), magnetite (2%), ilmenite (1%) and trace biotite, pyrite, chalcopyrite, and pyrrhotite.

Carbonate and chlorite have similar relationships as those described in sample 31-0.31. The foliation fabric in this sample is seen most clearly in the elongation and alignment of chlorite crystals. Muscovite has similar relationships as those described in sample 74-1123. Quartz forms euhedral crystals in the host (~0.02mm) that are pseudomorphously replaced by carbonate, chlorite, and muscovite. Biotite pseudomorphously replaces chlorite flakes and laths.

Magnetite is cubic, pitted and approximately ~0.18 to 0.22mm in the host. In places magnetite forms crystal aggregates, and contains inclusions of pyrite. Minor magnetite is disseminated in the host, with the majority of magnetite within quartz-carbonate veins and chlorite-rich bands. Pyrite forms euhedral, cubic crystals ~0.08 to 0.36mm in the host. Smaller pyrite crystals, and crystals within quartz-carbonate veins are pitted. Pyrite contains inclusions of ilmenite, chalcopyrite, and pyrrhotite (~0.007mm). Ilmenite forms laths ~0.02mm disseminated in the host and within pyrite crystals.

Veins cut the host sub-parallel to the fabric in the sample and consist of quartz-carbonate +/- chlorite-magnetite-pyrite, quartz +/- chlorite, and chlorite-magnetite bands. Quartz crystals in the veins are pseudomorphously replaced by carbonate, mostly within thinner portions of the veins. Veins range in width from 0.5 to 0.11mm. One quartz-carbonate (-chlorite) vein is folded into chevron folds ~0.36mm wide, with a 0.07mm quartz-

carbonate vein which is transposed along the fold limb. Veins do not have any associated selvages.

101-21.29

This sample is composed of plagioclase (30-40%), quartz (10%), carbonate (15%), epidote (20%), chlorite (15-20%), muscovite (2-5%), trace-1% biotite, and trace magnetite, ilmenite, and pyrite.

Plagioclase forms laths 0.22mm in length by 0.06 to 0.12mm wide and forms as described in sample 31-0.31. Magnetite is present as anhedral and highly corroded crystals corroded by chlorite, carbonate, and epidote. Quartz replaces portions of plagioclase as anhedral crystals. Chlorite forms as described in sample 31-0.31, replacing plagioclase and quartz, but does not form veinlets. Biotite and chlorite replace each other. Ilmenite is spatially associated with chlorite and forms laths within or partially replacing chlorite crystals. Carbonate replaces plagioclase, quartz, chlorite, and magnetite crystals as euhedral crystals. Pyrite is associated with carbonate and quartz, and forms anhedral crystals. Muscovite forms fine-grained laths and occurs as described in sample 31-0.31. Epidote is present as crystal aggregates and replaces minerals as described in sample 31-0.31 and also replaces chlorite and carbonate crystals.

Veinlets in this sample (trace of entire unit) are composed of euhedral quartz (85%) and carbonate (10%), and fine-grained carbonate (5%) replacing quartz in the veinlets. No fabrics are observed in this sample.

117-22.07

This sample is composed of plagioclase (60%), chlorite (15%), epidote (15%), biotite (5 to 8%), carbonate (3 to 5%), quartz (1 to 2%), and trace ilmenite.

Plagioclase forms as described in samples 101-21.29 and 31-0.31. Quartz, ilmenite, carbonate, and epidote form as described in sample 101-21.29. Chlorite is present as described in sample 31-0.31. Chlorite also forms larger flakey crystals replacing plagioclase, and replaces and is replaced by biotite.

The veinlets (1 to 2%) in this sample are composed of carbonate (95%) and chlorite and biotite (trace to 5%). There does not appear to be any definite fabric in this sample (just aligned chlorite veinlets and carbonate veinlets).

117-26.66

This sample is composed of two portions with very different mineralogy divided by a sinuous flakey chlorite veinlet (1.1mm wide). Locally portions of the chlorite have been replaced by euhedral epidote crystals.

CHLORITE-RICH: One portion of the sample is chlorite-rich and is composed of chlorite (50%), plagioclase (20%), epidote (15%), quartz (5 to 8%), carbonate (5 to 8%), muscovite (trace to 1%), and trace pyrite.

Plagioclase forms as described in sample 31-0.31. Chlorite forms long sinuous flakey crystals that are often elongated and aligned. Chlorite is replaced by fine-grained quartz and larger (0.24mm) carbonate crystals which are associated with anhedral pyrite.

Muscovite replaces chlorite, plagioclase, quartz, portions of carbonate, and fills corroded zones of pyrite. Locally plagioclase replaces chlorite as laths 0.1 by 0.2mm, and does not contain muscovite alteration. Epidote replaces plagioclase, chlorite, quartz, carbonate, muscovite, and fills corroded zones of pyrite as crystal aggregates and euhedral crystals 0.16mm on average.

CARBONATE-RICH: The section is composed of epidote (and hornblende? 40%), carbonate (20%), plagioclase (20%), muscovite (15%), quartz (5%), and trace pyrite.

Plagioclase is present as described in sample 31-0.31. Quartz, carbonate, and pyrite replace plagioclase laths and fill corroded zones of these laths (as described in sample 101-21.29). Muscovite replaces portions of plagioclase laths as fine-grained acicular crystals. Epidote replaces plagioclase, quartz, carbonate, muscovite, and fills corroded zones of pyrite as granular aggregates (low birefringence).

This sample has a moderate to strong fabric which is present in the alignment of elongated chlorite and connected epidote crystal aggregates.

118-03.62

This sample is composed of plagioclase (60%), chlorite (25%), carbonate (5 to 8%), muscovite (5 to 8%), chlorite (3 to 5%), epidote (trace to 1%), magnetite (trace to 1%), ilmenite (trace to 1%), and trace pyrite and rutile.

Plagioclase is present as laths 0.08 by 0.21mm in size. Magnetite (up to 1mm) is present as euhedral cubic to anhedral crystals replacing plagioclase. Ilmenite and chlorite replace plagioclase as described in samples 31-0.31 and 101-21.29. Quartz, carbonate, and pyrite

replace plagioclase laths and chlorite as described in sample 31-0.31 and/or 101-21.29, and fill corroded zones of magnetite. Muscovite replaces plagioclase laths as acicular crystals, and replaces plagioclase, chlorite, carbonate, quartz, and fills corroded zones of pyrite and ilmenite as 0.02 by 0.06mm to 0.6 by 2.4mm laths. Epidote replaces quartz (and others?) as euhedral crystals.

Minor amygdules (trace) are composed of quartz replaced by muscovite laths and euhedral carbonate. A folded quartz vein is composed mainly of quartz which is replaced by carbonate, muscovite, and traces of epidote. A faint fabric may be present in the alignment of fine-grained muscovite laths aligned.

118-05.98

This sample is composed of plagioclase (52%), carbonate (20%), quartz (15%), chlorite (10%), pyrite (3 to 5%), ilmenite (trace to 1%), and biotite (trace to 1%).

Plagioclase laths, carbonate, quartz, chlorite, and biotite form as described in sample 31-0.31 and sample 101-21.29. Ilmenite forms laths as in sample 31-0.31. Pyrite forms euhedral to anhedral pyrite (0.6mm) that contain inclusions of ilmenite. Corroded zones of pyrite are filled with muscovite.

Veinlets are composed of (1) chlorite (locally replaced by carbonate) are 0.3mm wide, and (2) quartz-albite-carbonate with traces biotite 1.8 to 5.5mm wide. Carbonate replaces chlorite as large crystals or elongated crystals in the centre of chlorite veinlets. Carbonate forms euhedral crystals in quartz-albite-carbonate veins and replaces portions of quartz and albite in the veins and filling fractures/between crystals as anhedral crystals. Locally pyrite is present as euhedral crystals in quartz-albite-carbonate veins.

151-04.91

This sample is composed of plagioclase (30%), chlorite (30%), epidote (15 to 25%), muscovite (10%), carbonate (5 to 8%), quartz (5%), pyrite (trace to 1%), and trace magnetite, ilmenite, rutile, and pyrrhotite.

Plagioclase, chlorite, magnetite, ilmenite, carbonate, quartz, pyrite, muscovite, and epidote are present as described in sample 31-0.31, or 101-21.29. Epidote is present as both euhedral crystals and crystal aggregates as in sample 117-26.66 (chlorite-rich). Pyrrhotite is present as cubic 'inclusions' (perhaps a pseudomorphic replacement of an inner zone of pyrite). Rutile is present as crystal aggregates associated with chlorite (replacing chlorite...?).

Veinlets (1.3mm wide) in this sample are composed of quartz (5%) and carbonate (75%) with crystals in the vein replaced by epidote (20%) crystals. Possible amygdules are composed mainly on carbonate crystals (+ minor pyrite) and are locally replaced by epidote. A faint fabric (if present) is formed by somewhat alignment of amygdules.

135-26.96

This sample is composed of chlorite (40% - chlorite 1: 10%, chlorite 2: 30%), epidote (50%), carbonate (10%), trace biotite, pyrrhotite.

Chlorite (1) is present as a lath-like and acicular crystals and crystal aggregates being replaced by carbonate and biotite. Carbonate crystals are also present filling amygdules. Pyrrhotite is present as 0.12mm inclusions in carbonate crystals. Chlorite (2) is replacing portions of carbonate crystals, biotite, and chlorite (1) crystals as laths. Epidote replaces chlorite (1 and 2), carbonate and biotite as euhedral crystals and crystal aggregates.

No fabric is present in this sample.

151-08.02

This sample is composed of plagioclase (65%), carbonate (10 to 15%), muscovite (10%), chlorite (5%), quartz (2 to 5%), magnetite (trace to 1%), ilmenite (trace to 1%), and trace pyrite, chalcopyrite, pyrrhotite, and rutile.

Plagioclase is present as laths as described in sample 31-0.31 replaced by, and corroded zones filled with, chlorite, ilmenite, magnetite, muscovite, quartz, and carbonate. Chlorite forms laths and acicular crystals which are aligned and are locally aggregated. Ilmenite and rutile are spatially associated with chlorite. Magnetite replaces plagioclase.

Muscovite replaces portions of plagioclase as described in sample 31-0.31. Quartz and carbonate replace plagioclase and chlorite and fills corroded zones of magnetite. Quartz crystals are approximately 0.02 to 0.11mm in size and are euhedral. Carbonate crystals are elongated and approximately 0.14 by 0.035mm and have sharp contacts with pyrite and chalcopyrite. Pyrite forms euhedral cubic to subhedral crystals. Chalcopyrite is present along the rims of euhedral pyrite crystals and filling corroded zones of pyrite. Pyrrhotite is replacing pyrite and chalcopyrite.

The fabric in this sample is medium to strong and is defined by the alignment of elongated plagioclase, carbonate crystals and alignment of chlorite laths. Veinlets in this

sample are composed of chlorite, quartz, and carbonate. Crystals in the veinlet are also elongated and aligned with the fabric of the sample.

210-40.69

This sample is composed of a host and epidote-rich bands and carbonate and epidote veinlets. The host is composed of plagioclase (80%), epidote (5%), biotite (4%), chlorite (2%), carbonate (2%), pyrite (2%), magnetite (2%), quartz (2%), muscovite (1%), ilmenite (trace to 1%), and trace pyrrhotite and chalcopyrite.

Plagioclase, biotite, chlorite, quartz, carbonate, magnetite, pyrite, and ilmenite occur as described in sample 101-21.29. Anhedral pyrrhotite and chalcopyrite are present in the host associated with carbonate and quartz crystals and are spatially associated with pyrite crystals. Epidote fills replaces plagioclase, biotite, chlorite, quartz, and carbonate and fills corroded zones of magnetite, ilmenite, pyrite, pyrrhotite, and chalcopyrite as granular aggregates and euhedral crystals.

The epidote-rich bands are composed of epidote (80%), chlorite (10%), biotite (trace to 5% locally), quartz (2%), magnetite (2%), pyrite (2%), carbonate (1 to 2 %), muscovite (1%), ilmenite (tracer to 1%), and trace plagioclase, pyrrhotite, and chalcopyrite.

Chlorite, biotite, quartz, magnetite, pyrite, carbonate, ilmenite and plagioclase are present as in sample 101-21.29. Muscovite forms as lath-like crystals replacing chlorite and biotite. Pyrrhotite and chalcopyrite form as described in the 'host' described above. Epidote forms as described above in 'host' but in larger amounts of granular aggregates and euhedral crystal aggregates.

Veinlets in this sample are composed of carbonate, epidote (with trace quartz and carbonate). Veinlets are generally 1.4mm wide. Pyrite in the carbonate vein is larger (0.69mm) and euhedral to rounded subhedral. The epidote vein is comprised almost entirely of euhedral crystals, with granular crystal aggregates towards the edge/selvage of the veinlets. Locally a carbonate vein appears to cut a through a portion (boudined?) of an epidote veinlet.

There is no general fabric in this sample, and the veins in this sample have a variety of orientations.

210-65.11

This sample mainly composed of a 2.7mm wide vein, the 2.5mm wide altered vein selvage, and the host rock. The vein is composed of carbonate (70%), quartz (20%), albite (10%), and locally epidote (trace).

The vein selvage is composed of plagioclase (30%), chlorite (30%), epidote (25%), hornblende (15%), quartz (1 to 2%), ilmenite (1 to 2%), and trace carbonate, pyrite, chalcopyrite, and pyrrhotite.

Plagioclase, chlorite, epidote (hornblende), carbonate, quartz, ilmenite, and pyrite form laths as described in sample 31-0.31 and appear similar to sample 151-08.02. Pyrrhotite is present in the selvage associated with quartz and with sharp contacts with chalcopyrite. Corroded zones of pyrrhotite and chalcopyrite are filled with epidote.

The host is composed of chlorite (70%), epidote +/- hornblende (20%), quartz (1 to 2%), biotite (trace to 1%), pyrrhotite (trace to 1%), and trace carbonate, pyrite, and ilmenite.

The host of this sample closely resembles sample 135-26.69. Chlorite, epidote, quartz, biotite, pyrrhotite, and carbonate are present as described in sample 135-26.96. The main

difference in this sample is that the chlorite (1) is a dark green-blue in plain light, and has low pleochroism in cross-polarized light, while chlorite (2) is army green to yellow in plain light and highly pleochroic in cross polarized light. Pyrite is present as subhedral and euhedral cubic crystals associated with quartz and carbonate crystals. Ilmenite is very fine-grained and is present as anhedral crystals and euhedral laths associated with chlorite.

210-74.00

This sample is composed of plagioclase (70%), chlorite (15%), epidote (10%), quartz (2 to 5%), carbonate (1 to 2%), biotite (1 to 2%), pyrrhotite (1 to 2%), ilmenite (trace to 1%), and trace muscovite, pyrite, and chalcopyrite.

Plagioclase, chlorite, biotite, ilmenite, quartz, carbonate, pyrite, and epidote form as described in sample 101-21.29. Muscovite forms laths replacing biotite and chlorite. Pyrrhotite and chalcopyrite occur as described in sample 210-40.69.

The veinlet in this sample is boudinaged and is 4mm wide at its widest part, and is composed of quartz (50%), pyrrhotite (30%), carbonate (10%), epidote (5 to 8%), chalcopyrite (2 to 5%), and trace chlorite. Quartz and carbonate form the veins as euhedral crystals. Pyrrhotite form as subhedral crystals in the around the quartz and

carbonate. Fine-grained carbonate replaces portions of quartz crystals as irregular shaped crystals. Chlorite locally replaces portions of quartz crystals as laths. Epidote replaces quartz and carbonate in the veins as euhedral crystals. The selvage of the vein contains increased amounts of chlorite and fine-grained epidote, especially in the cusp where the vein is boudined.

27-02.63

This sample is composed of quartz (30%), carbonate (25%), plagioclase (15%), chlorite (15%), muscovite (15%), magnetite (trace to 1%), pyrite (trace to 1%), and trace ilmenite, chalcopyrite, pyrrhotite, rutile.

Plagioclase, chlorite, magnetite (euhedral, cubic), ilmenite, quartz, carbonate, and pyrite occur as described in sample 101-21.29. Corroded zones of magnetite are filled with carbonate (and epidote). Muscovite, chalcopyrite, and pyrrhotite form as described in sample 210-40.69. Rutile is associated with chlorite.

Veinlets in this sample are composed of quartz (90%), carbonate (10%), and trace chlorite in veinlets approximately 0.37mm wide and the minerals are present as euhedral crystals.

G5. Mafic Volcanics: Feldspar-phyric

31-30.23 Core Sample 0.3 g/t Au

This sample does not appear to contain lath feldspar/plagioclase laths. Instead, approximately 5-10% of the sample is composed of quartz and carbonate amygdules. These amygdules occur mainly in a cluster, and the amygdules are generally 0.55 to 1mm in diameter. The mineralogy and relationships in these amygdules are similar to those described in sample 31-25.48.

This host of this sample is composed of chlorite (30%), plagioclase (25%), quartz (15%), epidote (15%), hornblende (5%), carbonate (5%), biotite (3%), ilmenite (2%), and trace muscovite, pyrite, magnetite and chalcopyrite.

Plagioclase is present as 0.14mm laths, and quartz as 0.36mm crystals in the host. Chlorite is present as flaky (0.12mm) and tabular crystals. Two colours of chlorite are present in plain polarized light: a light green colour with low (brown-purple) birefringence, and a turquoise green-blue colour with slightly higher birefringence (light green to yellow-brown). Chlorite replaces plagioclase and quartz crystals in the host, and fills corroded zone of quartz crystals. Epidote forms as anhedral crystals in veins and granular aggregates that are pseudomorphously replacing plagioclase laths and replacing biotite and chlorite. Hornblende is present as granular aggregates pseudomorphously replacing plagioclase in the host. Carbonate forms 0.16mm crystals in the host that

pseudomorphously replace plagioclase and quartz. Biotite forms lath-like crystals and is pseudomorphously replacing chlorite in the host. Muscovite forms flaky and tabular crystals that replace plagioclase in the host.

Ilmenite is present as crystal aggregates of rounded crystals approximately 0.14mm in diameter, and as tabular crystals approximately 0.01mm in size disseminated in the host.

Pyrite is found as euhedral to subhedral crystals within included in quartz amygdules, and as anhedral crystals in the host, both approximately 0.12mm in size. Chlorite fills corroded zones of pyrite in the host. Locally pyrite is pseudomorphously replaced by chalcopyrite. Magnetite is disseminated in the host and has sharp contacts with muscovite.

Amygdules in this sample are composed of quartz and carbonate. Amygdules range in size from 0.22 to 1.1mm. The majority of the amygdules are composed of fine-grained 0.05mm quartz crystal rims and larger 0.36mm quartz crystals in the centre. Pale green, tabular chlorite crystals 0.03mm in size separate the small and larger quartz crystals in the amygdules. Locally quartz amygdules contain large carbonate crystals in the centre.

Veins in this sample are composed of carbonate, quartz-carbonate, carbonate-chlorite, and epidote. Veins range in size from 0.08mm to 0.4mm in width.

Carbonate (-chlorite, -quartz) veins are approximately 0.5mm wide and contain approximately 85% carbonate, and 0-10% chlorite and 0-5% quartz. Carbonate crystals in these veins are approximately 0.25mm in diameter, and are locally elongated, with their elongated axis at approximately 45° to the strike of the vein. Where present chlorite forms elongated laths 0.08 x 0.27mm in size that form parallel to the elongated carbonate and quartz. Where present quartz forms crystals approximately 0.1mm in diameter, which are also locally elongated parallel to the carbonate crystals. These veins do not appear to have any selvage associated with them. In this sample a sinuous carbonate vein cuts and offsets a quartz-chlorite amygdule.

Epidote forms veins approximately 0.03mm wide composed of euhedral epidote crystals. There is no selvage that appears to be associated with this type of vein.

This sample does not appear to have any form of fabric or deformation other than the angle of crystal growth in the carbonate (-chlorite, -quartz) veins.

31-31.06 Core Sample 0.17 g/t Au

In hand specimen sample 31-31.06 is medium green coloured cut by a quartz veinlet with minor carbonate, and epidote veinlets. The wall rock on either side of the epidote veinlet is a lighter pistachio green colour than the remaining host. The dark host is composed of 45% epidote, 40% chlorite, 5% plagioclase, 5% quartz, 5% carbonate, trace-1% biotite, and trace magnetite, pyrite, ilmenite, chalcopyrite, and pyrrhotite. The lighter green alteration around the epidote vein is composed of 60% epidote, 25% chlorite, 10% quartz, 5% carbonate, and trace magnetite, pyrite, ilmenite, chalcopyrite, pyrrhotite, and plagioclase (?).

DARK: Plagioclase is replaced by ilmenite (described below), magnetite (below), biotite (flakey), and a possible first generation of chlorite (pale light green, flakey, low birefringence, low pleochroism). Carbonate, pyrite and quartz replace these minerals. Pyrite, pyrrhotite, and chalcopyrite form as described below. A possible second generation of chlorite (dark forest green, higher birefringence/pleochroism) replaces and fills corroded zones of the minerals listed above. Epidote forms granular aggregates replacing all previous minerals.

LIGHT: Plagioclase, ilmenite, magnetite, carbonate, pyrite, pyrrhotite, chalcopyrite, and quartz form as described above. Chlorite in this sample occurs as a more pervasive

chlorite¹ as described above. The 'second generation' of chlorite is lacking in this region. Epidote replaces all minerals as crystal aggregates.

BOTH: The following is consistent for both the light and dark coloured alterations:

Magnetite is present as irregular shaped crystals replacing plagioclase in the host, and is mostly present within the light alteration around the epidote vein. Ilmenite forms tabular crystals approximately 0.02mm in size replacing plagioclase and (possibly early?) chlorite, and as inclusions in pyrrhotite and pyrite. Pyrite is cubic near the epidote vein, and contains inclusions of magnetite, ilmenite, and pyrrhotite. Pyrrhotite is present as inclusions in pyrite, and as irregular shaped crystals likely replacing an earlier pyrite (~0.1mm), and contains chalcopyrite.

Amygdules in this sample are composed of quartz and/or carbonate. The amygdules range in size from 0.46-1.37mm with crystals in them generally 0.27mm in size.

Veinlets in this sample are composed of quartz +/-carbonate, or carbonate-epidote. The quartz +/-carbonate vein is approximately 0.69mm wide, with quartz crystals 0.22mm in size. This vein locally contains pyrrhotite and trace chalcopyrite. The carbonate-epidote veinlets cut through the host and are generally 0.18mm wide, with 0.09mm carbonate and epidote crystals. The epidote veinlet with associated with the light pistachio green wall

rock alteration runs parallel to the quartz veinlet in the sample, while several smaller (0.04mm wide) epidote veinlets run at various angles through the sample.

76-1090 Surface Sample 0.87 g/t Au

In hand specimen sample 76-1090 is medium green with a quartz-carbonate vein cutting through the middle of the sample. At a microscopic scale it can be seen that the main alteration in the sample is carbonate. The sample is composed of plagioclase (35%), chlorite (30%), carbonate (20%), quartz (10%), epidote (trace to 1%), magnetite (1%), pyrite (1%), ilmenite (1%), chalcopyrite (trace to 1%), and trace biotite and sphalerite (?).

Plagioclase laths are the main component in the host rock. These laths are approximately 0.11 x 0.3mm in size and have sharp contacts with quartz in the host. Quartz is present in the host as euhedral crystals approximately 0.03mm in size. Chlorite forms tabular and flaky crystals ranging in size from 0.04 to 0.11mm in size. Chlorite replaces plagioclase and quartz in the host, and the large feldspar crystal. Epidote replaces plagioclase, quartz and portions of large chlorite flakes with 0.08mm crystals. Biotite pseudomorphously replaces flaky chlorite, and minor tabular chlorite. Carbonate is present pseudomorphously replacing both plagioclase and quartz crystals in the host.

Replacement of plagioclase and quartz by carbonate is strongest near the quartz-

carbonate vein in the centre of the sample, and weakens as the distance to the vein increases. Also, near the vein the crystal size of the host appears to increase, with plagioclase laths reaching 0.5x0.78mm in size, and the concentration of chlorite decreases.

Magnetite forms cubic to irregular shaped crystals approximately 0.04mm in size in the host. Magnetite is disseminated within the host. Pyrite is disseminated and generally forms cubic crystals 0.8 to 1.5mm in size in the host. Pyrite is a light pale yellow, is pitted/corroded in places, and contains tabular ilmenite crystals and inclusions of chalcopyrite. Sphalerite rims pyrite crystals and fills corroded zones within the crystals. Ilmenite is present as tabular crystals in the host and within pyrite. In the host ilmenite generally forms clusters approximately 0.03mm wide of smaller ilmenite crystals. Sphalerite rims pyrite and magnetite, pseudomorphously replacing the rims of these crystals.

The vein in this sample is composed of quartz and carbonate crystals. The vein is 0.36mm wide, with crystals of both quartz and carbonate averaging 0.11mm in size. The vein is slightly sinuous and is discontinuous throughout the sample. The quartz and carbonate veins in this sample do not occur intermixed, but rather the vein is composed of euhedral-subhedral quartz and then locally changes composition to euhedral-subhedral

carbonate. Carbonate that is present in the quartz portion of the vein is pseudomorphously replacing quartz crystals in the vein.

71-1101

This sample contains several carbonate amygdules approximately 1.37x5.5mm in size, in locally contains the heavily altered remains of larger plagioclase laths (which give feldspar-phyric look?) that are described more fully below.

This sample is composed of 70% plagioclase, 10-15% chlorite, 5-8% carbonate, 5% quartz, 2-5% epidote, and trace magnetite, ilmenite, pyrite, chalcopyrite, pyrrhotite (?), and muscovite.

Plagioclase forms laths up to 0.09x0.22mm in size that are still visible in the sample. Locally these are larger (0.4x1.2mm) and contain intense muscovite alteration. Chlorite forms are fine-grained laths and crystal aggregates replacing plagioclase. Magnetite and ilmenite replace and fill corroded zones of plagioclase and chlorite and laths (ilmenite) and cubic (magnetite) crystals. Carbonate, quartz, and pyrite have sharp contacts with each other and replace and fill corroded zones of the previous minerals. Pyrite forms sub-cubic crystals and parts of pyrite grains are replaced by chalcopyrite. Pyrrhotite locally

pseudomorphously replaces pyrite. Chalcopyrite locally forms grains partially enveloping pyrite. Epidote replaces all minerals as granular aggregates. Muscovite forms laths replacing epidote and other minerals, and locally epidote fills corroded zones in muscovite.

This sample contains a boudinaged carbonate veinlet (or amygdules?) and minor carbonate-epidote veinlets similar to those described in sample 31-31.06.

G6. Mafic Volcanics: Tuffaceous

151-24.32

This sample is composed of 46% epidote, 20% biotite, 10% chlorite, 8% plagioclase, 8% carbonate, and 8% quartz. This sample contains trace to 1% carbonate, chlorite, and epidote veins.

Plagioclase and quartz in this sample are generally 0.09mm in diameter and are replaced by flaky, low birefringence chlorite¹. Chlorite¹, plagioclase, and quartz are replaced by carbonate crystals (in single crystals and crystal aggregates. Chlorite² (high birefringence and very pleochroic) and biotite (high birefringence and very pleochroic) 0.07mm x 0.02mm to 0.16mm x 0.07mm in size replace carbonate, plagioclase, and quartz in flaky

and tabular crystals and crystal aggregates. All minerals in this sample are replaced by epidote in the form of granular aggregates (40%) and tabular crystals (6%).

The veins in this sample are composed mainly of carbonate in elongated crystals 0.27mm x 0.09mm that are interconnected and replaced by elongated tabular chlorite crystals.

Epidote replaces chlorite and carbonate in the veins in prismatic crystals.

151-30.90

This sample is composed of 2-5% veins in the host. The host is composed of 35% epidote, 15% plagioclase +/- quartz, 40% chlorite, 3-5% carbonate, 3-5% biotite, and trace pyrite and chalcopyrite.

Plagioclase, quartz, carbonate, and epidote form as described in sample 151-24.32.

Epidote forms in approximately 60% granular aggregates and 5% euhedral crystals.

Chlorite₁ (low pleochroism, low birefringence) and biotite₁ form flaky crystals approximately 0.18mm x 0.46mm in size, and are replaced by smaller tabular chlorite₂ and biotite₂ crystals (pleochroic and high birefringence), which replace one another.

Chlorite₁ is also present in larger amounts as finer-grained (approximately 0.027mm x 0.009mm) replacing the plagioclase in the host. Chlorite₂ and biotite₂ crystals replacing chlorite₁ and biotite₁ are approximately 0.07mm x 0.024mm in size. Chlorite (except for

fine-grained chlorite¹) and biotite in this sample generally form crystal aggregates that appear to be replacing larger angular to sub-angular fragments in the rock (~0.49mm in diameter). Epidote (in granular aggregates) generally replaces the chlorite² and biotite² in these fragments and locally (in crystals) replaces portions of the carbonate crystals in this sample.

Pyrite forms subhedral crystals between and included within carbonate crystals in the veins and large carbonate crystals adjacent to the veins. Pyrite is generally 0.055mm in diameter. Chalcopyrite is present as inclusions within pyrite, as separate subhedral crystals, and as crystals forming along the rim of the pyrite crystals. Like pyrite, chalcopyrite is present within carbonate crystals within and adjacent to the veins.

The main texture/fabric of this sample is sub-angular to angular fragments in the sample being replaced by biotite² and chlorite², which are then replaced by epidote. There appears to be some alignment of the fine-grained chlorite and chlorite-rich and chlorite-poor zones, which create a faint foliation fabric.

The vein in this sample is 1.1mm in diameter and is composed primarily of carbonate and quartz generally 0.12mm in diameter. Quartz crystals in the veins have a mottled appearance, and are locally replaced by finer-grained carbonate crystals. Trace biotite and chlorite are present in the vein and replace the carbonate and quartz crystals. Epidote

replaces both carbonate and quartz in the vein in both crystal aggregates and epidote crystals.

135-24.35

This sample is composed of chlorite-rich and biotite-rich zones. Overall, this sample is composed of 29% plagioclase, 27% chlorite, 18% epidote, 9% biotite, 8% quartz, and trace carbonate, pyrite, and chalcopyrite. The chlorite-rich zones are composed mainly of 40% chlorite, 40% plagioclase, 15% epidote (and hornblende??), 5% quartz, and trace biotite, pyrite, and chalcopyrite. The biotite-rich zones are composed mainly of 25% fragments (30% epidote, 15-20% hornblende, 30% plagioclase, and trace chlorite and biotite), 26% biotite, 22% epidote, 15% quartz, 7-8% plagioclase, 3-4% chlorite.

At a hand specimen and thin section scale it is possible to observe foliation fabric in this sample defined by chlorite-rich and biotite-rich zones, aligned chlorite veinlets, and alignment of elongated fragments (white).

This sample contains trace to 1% veinlets primarily composed of quartz and containing trace amounts of carbonate and epidote. Carbonate and epidote in the vein is replacing the quartz. The relationship between epidote and carbonate in the vein is not known. The

veinlets cut both chlorite- and biotite-rich zones. Pyrite and chalcopyrite are associated with the quartz in the veins and occur as anhedral crystals in and near the veins. Pyrite and chalcopyrite have sharp contacts with one another.

Plagioclase and quartz in this sample occur as described in sample 151-24.32. In the chlorite-rich portion of the sample fine-grained chlorite occurs as described by fine-grained chlorite¹ in sample 151-30.90. In the biotite-rich portion of the sample chlorite and biotite are replacing plagioclase, quartz, and one another, in tabular laths approximately 0.044mm x 0.014mm in size. Epidote occurs as granular aggregates and crystals replacing all minerals in this sample (as described in sample 151-24.32). The greatest amount of epidote alteration/replacement occurs in portions of the sample that appear to have been sub-angular fragments in the tuff.

Fragments in this sample are mostly replaced by epidote and locally appear to be granular.

G7. Syn-ore Carbonate-quartz-pyrite Alteration of the Mafic Volcanics

31-10.27

4.35-4.66 g/t

This sample is composed of 60-65% plagioclase, 30% carbonate, 6% quartz, 2-3% pyrite, trace to 1% ilmenite and magnetite, and trace muscovite, chlorite, chalcopyrite, and native gold.

Plagioclase in this sample forms laths, which are the main component of the host. The laths are approximately 0.11 x 0.6mm, and appear to be aligned. Quartz is also present in minor amounts in the host, and forms crystals approximately 0.11mm in diameter.

Muscovite and chlorite are associated with pyrite in the host. Muscovite forms laths and chlorite forms flakes adjacent to pyrite, and locally appears to be filling corroded zones in the pyrite. Muscovite appears to be replacing plagioclase in the host. Carbonate replaces plagioclase, quartz, muscovite, and chlorite in the host with crystals 0.07 to 0.1mm in size.

Pyrite is present as euhedral cubic to subhedral crystals in the groundmass. Pyrite crystals range in size from 0.2 to 0.9mm in size, and contain inclusions of chalcopyrite, ilmenite, magnetite, and gold. Corroded zones of pyrite are filled with muscovite and chlorite, and pits in pyrite are filled with magnetite. Gold is also present replacing the host and filling the fractures in two pyrite crystals that are in the host. Ilmenite is also present as 0.01mm sub-rounded and lath-like crystals disseminated in the host. Magnetite is also present

disseminated in the host as euhedral cubic to subhedral crystals 0.02 to 0.05mm in diameter. The size of magnetite decreases as the proximity to the vein increases.

This sample contains several plagioclase-quartz-carbonate veins. These veins range in size from 5mm to 1cm in width. The majority of the veins are composed of plagioclase (90%), quartz (7%), carbonate (3%), and trace chlorite. Plagioclase, quartz, and carbonate form crystals approximately 0.3 to 1mm wide, depending on the width of the vein.

Chlorite is present as flakes, mainly at the contact between carbonate and plagioclase in the vein. Carbonate is also present replacing plagioclase and quartz in the vein, and filling fractures in, and corroded zones between quartz and plagioclase crystals. Pyrite is locally present as cubic crystals included in plagioclase, and along the margin of the vein partially included in plagioclase. The majority of pyrite is not found within the vein.

The main fabric of this sample is a faint foliation indicated by the alignment of the plagioclase laths. The veins in this sample cut this fabric.

31-10.03 4.35 g/t

This sample is composed of 60-65% plagioclase, 25-30% carbonate, 2-3% magnetite, 1-2% pyrite, trace to 1% ilmenite, and trace quartz, muscovite, rutile,

Plagioclase, quartz, and carbonate occur as described in sample 31-10.27. The major difference in this sample is that the carbonate and quartz appear to be finer-grained in this sample (approximately 0.02mm in diameter). Muscovite in this sample does not appear to be associated with pyrite, and instead is replacing the larger plagioclase laths in the host with crystals approximately 7 μ m in diameter.

Pyrite, magnetite, and ilmenite occur disseminated in the groundmass, and pyrite contains inclusions of ilmenite and magnetite as described in sample 310-10.27. As in sample 31-10.27, the size of magnetite crystals decreases as the proximity to the vein increases. Pyrite in this sample also contains inclusions of rutile. The other major difference in this sample is that the pyrite crystals are generally smaller – approximately 0.044 to 0.22mm in diameter.

The veins in this sample are composed of 98% carbonate, 2% quartz, and trace plagioclase. Veins range in width from 0.27 to 5.5mm. Pyrite is locally included within the carbonate of the vein, but is otherwise found within the host rock near the veins. The larger veins in this sample are fairly straight and branch within the host. Some smaller veins are present perpendicular to the larger veins, and appear to fold and become parallel

to the larger veins as they merge together. Host rocks between veins and in branches in veins are largely replaced by carbonate and large quartz crystals (0.1mm in diameter).

The plagioclase laths appear to be somewhat aligned in places in this sample (but not as strongly as in sample 31-10.27). This suggests a weak foliation in the rock.

31-11.10

This sample is comprised of 55% plagioclase, 40% carbonate, 5% pyrite, and trace-1% muscovite, trace ilmenite and magnetite.

The host is comprised mainly of plagioclase (fine-grained and some larger magmatic laths) and possibly quartz. Locally this is replaced by up to 60% fine-grained carbonate. This is cut by veins (>50% of sample) with a variety of compositions including quartz +/- carbonate, carbonate, albite-quartz-carbonate, and albite+/-quartz+/-carbonate.

Muscovite forms laths that have sharp contacts with albite and quartz in veins and are locally included in pyrite. Pyrite is found adjacent to veins (within carbonate altered the host), and within the veins. Pyrite forms euhedral crystals and crystal aggregates and

contains inclusions of ilmenite and locally subhedral magnetite. Ilmenite also forms crystal aggregates adjacent to pyrite crystals.

Locally carbonate replaces portions of albite and quartz in the veins.

Sample 74-1175 10.5 g/t

This sample is composed of 80% plagioclase, 15% carbonate, 2-3% pyrrhotite, 1% pyrite, trace-1% magnetite, trace-1% quartz, and trace chlorite, biotite, ilmenite, and chalcopyrite.

Plagioclase, ilmenite, magnetite, pyrite, chalcopyrite, carbonate, and quartz occur as described in sample 31-10.27. Plagioclase in this sample forms larger laths than those described in sample 31-10.27 and are up to 0.8x0.2mm in size. Chlorite and biotite in this sample are flakey and appear to be replaced by cubic pyrite. Pyrrhotite pseudomorphously replaces cubic pyrite.

This sample contains a folded+pinch and swell vein 2-7mm wide comprised of 90% quartz, 5% albite, 4% carbonate, and 1% pyrite. Quartz and carbonate in this vein have

sharp contacts, but carbonate is filling corroded zones and partially replacing portions of crystals in the vein. Pyrite in the vein is cubic and is up to 1mm in diameter.

Sample 79-1057 5.8 g/t

The sample is composed of 67-83% plagioclase, 8-10% carbonate, 2-5% quartz, trace-10% muscovite, 2-3% pyrite, 2% magnetite, 1% pyrrhotite, trace ilmenite, trace chalcopyrite, trace rutile, trace gold, and 0-trace biotite.

Plagioclase, magnetite, ilmenite, carbonate, pyrite, chalcopyrite, quartz, biotite, and gold form as described in sample 31-10.27. Muscovite is present as inclusions in pyrite as described in sample 31-11.10. Pyrrhotite replaces cubic pyrite as described in sample 74-1175. Plagioclase in this sample is much more fine-grained than that described in sample 31-10.27, and only locally contains laths. Fine-grained rutile is present as inclusions in pyrite and replacing plagioclase in the host. Chalcopyrite locally replaces portions of pyrrhotite crystals.

This sample contains several 1-2mm wide albite-carbonate+/-quartz (2mm wide). Locally these veins contain subhedral pyrite grains and in one location the predominantly carbonate vein contains laths of biotite+/-muscovite that have sharp contacts with carbonate grains. Carbonate in the albite-carbonate-quartz veins is locally euhedral, with

sharp contacts with albite, but is also present as crystals replacing portions of, and filling fractures in, albite grains.

Sample 71-1099 3.2 g/t

This sample is composed of 60% plagioclase, 30% carbonate, 5% quartz, 3% pyrite, 1-2% magnetite, trace-5% muscovite, and trace ilmenite, pyrrhotite, and chalcopyrite.

Plagioclase, magnetite, ilmenite, carbonate, quartz, and pyrite form as described in sample 31-10.27. Plagioclase is locally very fine-grained, with no laths visible. Pyrite forms largely within, or adjacent to, the vein in this sample. Magnetite forms cubic crystals (0.8-0.2mm in size) disseminated in the host, but is not present in this manner within 1mm of veins. Near (and within veins) magnetite forms 0.2-0.3mm euhedral to subhedral crystals containing inclusions of pyrite, chalcopyrite, and pyrrhotite, and locally inter-grown with pyrite. Ilmenite also forms as sub-rounded crystals and crystal aggregates. Muscovite forms very fine-grained crystals, and locally larger laths, replacing plagioclase in the host. Chalcopyrite forms fine-grained anhedral crystals in the carbonate altered host.

The vein in this sample is ~1mm wide and is comprised of albite+carbonate+/-quartz.

This vein contains the large (~1mm wide) cubic pyrite crystals and associated magnetite.

Locally muscovite is present as larger laths associated with pyrite. Carbonate crystals largely replace and fill fractures in albite grains.

Sample 81-1119 0.1 g/t

This sample is composed of 90% plagioclase, 8-10% carbonate, trace-1% quartz, trace-1% magnetite, and trace chlorite, biotite, muscovite, pyrite, and ilmenite.

This sample is very similar looking to sample 79-1057, as the plagioclase is fairly fine-grained and it contains similar proportions and modes of occurrence of plagioclase, carbonate, magnetite, ilmenite, and pyrite. Muscovite is fine-grained and replacing plagioclase, as well as larger laths, as described in sample 71-1099.

Veins in this sample occur as described in sample 79-1057 with the exception that they contain local chlorite. Chlorite, muscovite, and biotite form laths in one vein and replace carbonate in the veinlet.

Sample 27-03.24

This sample is composed of 82% plagioclase, 8-10% carbonate, 8% pyrite, trace-1% quartz, trace-1% biotite, trace-1% magnetite, and trace chlorite, muscovite, ilmenite, and gold.

Plagioclase, carbonate, quartz, magnetite, chlorite, ilmenite, and gold form as described in sample 31-10.27, although they are generally finer-grained as described in sample 79-1057. Pyrite is present as crystal aggregates largely along the selvage of the veins or within the vein. Minor pyrite is present as cubic crystals in the altered host, although these crystals have corroded rims filled with carbonate and quartz. Biotite, chlorite, and muscovite are largely associated with the pyrite along the vein selvage, although biotite and chlorite appear to be replaced by the pyrite, while muscovite forms laths and has sharp contacts with pyrite. Biotite and chlorite locally occur as smaller laths further from the vein. Two generations of biotite appear to be present in this region, with the later generation replacing the earlier biotite and chlorite.

The veinlets in this sample are up to 2mm wide and are comprised of albite+carbonate+/- quartz. Carbonate is present as grains with sharp contacts with albite +/- quartz, and locally as fine-grained carbonate replacing portions of, and filling fractures in, crystals in veins.

Sample 31-12.00

10.5 g/t

The majority of this sample is comprised of pervasively carbonate altered rock. Small regions (eg. several ~1mm wide strips of rock adjacent to veins is largely 'unaltered' [or pervasively plagioclase altered?]): 97% plagioclase, 5% magnetite, 1-2% muscovite, trace-1% pyrite, and trace carbonate and ilmenite.

This carbonate altered portion of this sample is composed of 70% carbonate, 15% quartz, up to 8% pyrrhotite, 2-5% plagioclase, 2% pyrite, and trace chlorite, muscovite, magnetite, ilmenite, chalcopyrite, rutile, and gold. Plagioclase, chlorite, muscovite, magnetite, ilmenite, chalcopyrite, pyrite, gold, quartz, and carbonate form as described in sample 31-10.27. Rutile and pyrrhotite form as described in sample 79-1057. Carbonate alteration in this sample is much more pervasive than observed in the previous samples.

Veinlets in this sample range from <1mm wide to ~4mm wide. Three types of veins are present: (1) a predominantly quartz vein (4mm wide) with trace carbonate replacing and filling fractures in quartz grains, (2) a predominantly carbonate+/-quartz vein, with large carbonate crystals locally replaced by fine-grained carbonate and local muscovite laths, and (3) albite+carbonate+/-quartz veins containing large albite laths and fine-grained carbonate locally replacing these laths.

For timing of the veins, the quartz vein contains only minimal carbonate alteration, and appears to cut the heavily carbonate altered carbonate vein. Relative timing of the albite+carbonate+/-quartz vein is unknown.

Sample 135-10.80

This sample is composed of 55-85% plagioclase, 10% pyrrhotite, 3-20% carbonate, 5-20% biotite, 3-5% quartz, 0-3% magnetite, and trace pyrite (? all altered to po?), ilmenite, chalcopyrite, and gold.

Plagioclase, quartz, carbonate, magnetite, pyrite(?), ilmenite, chalcopyrite, and gold form as described in sample 31-10.27. Pyrrhotite pseudomorphously replaces crystals and crystal aggregates of cubic pyrite. Pyrrhotite is found largely adjacent to, or within, veins.

This sample contains very large amounts of biotite. Biotite is present as fine-grained laths throughout the altered host rock, but locally larger biotite flakes (1) and laths (2) are present in the selvages and adjacent to large pyrrhotite crystals. Biotite 1 flakes generally appear to be replaced by cubic pyrrhotite (replacing pyrite), while biotite 2 laths has sharp contacts with pyrite or are included in pyrite.

Veins in this sample comprise various ~1mm wide euhedral carbonate+quartz veins. The main vein in this sample is up to 5mm (or more?) wide and is comprised of 40% carbonate, 40% cubic pyrrhotite, 15% biotite (1&2) and 5% quartz. Carbonate, pyrite, biotite 2 and quartz have sharp contacts with one another.

Sample 136-16.26 100 g/t Au

This sample is composed of 65% carbonate, 15-20% pyrrhotite, 10% quartz, <5% pyrite, 2-5% plagioclase, trace-1% biotite, and trace magnetite, ilmenite, and chalcopyrite.

This sample is very intriguing as it has a very high gold grade, but no gold has been identified in this section. Normally at Barry samples with high gold grade (>10 g/t) contain microscopic gold grains. Microprobe analysis of this sample showed that gold is present as sub-microscopic inclusion in pyrite, although the pyrite itself had low concentrations of gold.

Plagioclase, quartz, pyrite, carbonate, magnetite, ilmenite, and chalcopyrite form as described in sample 31-10.27. As in sample 31-12.00, this sample contains much more

carbonate alteration then that seen in previous samples. Pyrrhotite forms as subhedral crystals in the altered sample, and replaces the majority of the cubic pyrite. Biotite forms flakes (like biotite 1?) spatially associated with the pyrite and pyrrhotite crystals, but appear to be replaced by the sulfides.

Two 3+mm veins are present on the two edges of this sample and albite+carbonate+quartz. Carbonate in these veins is euhedral and has sharp contacts with albite and quartz. Locally these veins contain cubic pyrrhotite and/or pyrite.

143-00.64 5 g/t

The sample is composed of 30% plagioclase, 30% chlorite, 25-30% muscovite, 10% quartz, 2% carbonate, 1% pyrite, trace-1% magnetite, and trace ilmenite, biotite, and chlorite.

Plagioclase, quartz, carbonate, pyrite, magnetite, and ilmenite form as described in sample 31-10.27. Locally magnetite contains inclusions of pyrite. Muscovite is mainly present as very fine-grained laths replacing portions of plagioclase laths. Chlorite is present as sinuous and elongated laths replacing plagioclase, replacing all phases (except muscovite) in the sample.

Veins in this sample are composed mainly of carbonate + minor quartz, and are locally pervasively replaced by fine-grained muscovite and local chlorite. One vein in this sample is mainly quartz, and is replaced by laths of biotite and chlorite.

This sample has a strong fabric seen in the elongation of chlorite laths and the sinuous, elongated chlorite crystals. It runs roughly parallel to the carbonate and quartz veins.

210-42.75

This sample is composed of 60% plagioclase, 25-30% biotite, 5-8% carbonate, 3-5% pyrite, 2% quartz, and trace magnetite, ilmenite, and gold.

Plagioclase, magnetite, ilmenite, carbonate, pyrite and quartz form as described in sample 31-10.27. This sample contains a high proportion of biotite, similar to that in sample 135-10.80, but in this sample all biotite forms large laths. Biotite is disseminated throughout the sample replacing plagioclase and has sharp contacts with carbonate and pyrite. Gold is present as inclusions in, filling micro-fractures in, and adjacent to pyrite in the altered

host. This sample contains a large amount of gold that is visible when using a microscope.

Veins in this sample are deformed, discontinuous, and are composed of carbonate+quartz.

One corner of this sample appears to be a contact with a QFP(?) dike. In this location biotite alteration is minimal, and the grain size changes: large phenocrysts of plagioclase in a fine-grained groundmass. Carbonate alteration and minimal biotite is present replacing portions of the groundmass.

G8. Syn-ore Biotite-carbonate Alteration of the Mafic Volcanics

31-27.20 65.5 g/t

This sample is composed of 55% biotite, 30% carbonate, 10% plagioclase, 3-5% pyrrhotite, 2% quartz, and trace chlorite, pyrite, ilmenite, chalcopyrite, and rutile.

Plagioclase forms small laths (0.14x0.24mm) and very fine-grained crystal (perhaps recrystallized??). Local flakey chlorite is replaced and replaces flakey biotite 1 (15-20% of the biotite). Ilmenite laths and rutile crystal aggregates fill corroded zones of biotite1

and chlorite as laths. Carbonate and quartz replace plagioclase, chlorite, and biotite1 as euhedral crystals. Pyrite has sharp contacts with carbonate and quartz, is euhedral to slightly rounded, and is locally mantled and pseudomorphously replaced by anhedral pyrrhotite. Chalcopyrite has sharp contacts with pyrrhotite. Biotite2 (35-40% of the biotite) forms laths and fills corroded zones of pyrrhotite, carbonate, quartz, biotite1, and chlorite.

A veinlet of carbonate and pyrrhotite (3-4mm wide) cuts this sample and has a 1-2 mm selvage of very intense biotite2 alteration (almost completely biotite 2).

31-16.28

4.5 g/t

This sample is composed of 50% plagioclase, 25% carbonate, 15% biotite, 8% muscovite, 2% quartz, trace-1% pyrite, and trace chlorite and magnetite.

Plagioclase, chlorite, biotite1 (~6%), carbonate, quartz, and biotite2 (~9%) form as described in sample 31-27.20. Magnetite is present as euhedral cubic to sub-rounded crystals (0.027mm in size) filling corroded zones of plagioclase, chlorite, and biotite1. Carbonate, quartz, and biotite2 fill corroded zones of and fractures in magnetite. Muscovite forms very fine-grained laths (0.03x0.008mm) replacing portions of

plagioclase. In this sample it is not clear the relationship between muscovite and carbonate, quartz, pyrite, and biotite2.

An undulating and pinch and swell veinlet in this sample is 0.3-5.5mm wide and is composed primarily of quartz crystals. Locally carbonate (possibly carbonate 2) replaces portions of quartz crystals and fills corroded zones between crystals.

151-19.34 5.5 g/t

This sample is composed of 60% plagioclase, 20% biotite, 10% quartz, 7% pyrite, 5% carbonate, and trace ilmenite.

Plagioclase, biotite1 (5-8%), ilmenite, quartz, carbonate, pyrite, and biotite2 (12-15%) form as described in sample 31-27.20.

This sample contains a quartz-albite vein (1.5cm+ it goes off of the thin section) composed of 80-90% quartz and 10-20% albite in euhedral crystals (0.39-0.78mm in size). Corroded zones of crystals and between crystals in the vein are filled with carbonate2 (anhedral) and euhedral biotite2.

117-25.95

5.3 g/t

This sample is composed of 40% plagioclase, 30% biotite (all biotite₂), 25% carbonate, 3% quartz, 2-3% pyrite, and trace magnetite, ilmenite, chalcopyrite, and pyrrhotite.

Plagioclase, ilmenite, carbonate, quartz, pyrite, pyrrhotite, chalcopyrite, and biotite₂ form as described in sample 31-27.20. Chalcopyrite in this sample also pseudomorphously replaces portions of pyrite crystals, and is locally found as inclusions in pyrite. Ilmenite likely replaced portions of biotite₁ (???) and then was replaced by 2. Magnetite occurs as described in sample 31-16.28. Locally it appears as if quartz (or plag?) crystals replace biotite₂ as euhedral crystals, but other places biotite₂ clearly replaces portions of carbonate crystals.

Biotite₂ in this sample is elongated laths which are connected to form biotite-rich zones in the sample. The elongated laths form sinuous biotite alteration “veinlets”(?) that are parallel to one another throughout the sample, creating a strong fabric. Locally carbonate crystals in the sample appear larger and perhaps form veinlets that ‘pinch out’ between the biotite-rich zones (Are these veinlets or just a part of the alteration???)

This sample contains a portion of a veinlet (boudined? up to 4.2mm wide) composed of albite (90%), quartz (5%), locally carbonate (2%), and flakey chlorite (3%). Corroded

zones of crystals and crystal boundaries are filled with carbonate (2?) and biotite² replaces portions of crystals as laths. A more intense biotite alteration is present along the selvage of this veinlet.

31-20.02

This sample is composed of 45% plagioclase, 12% chlorite (vein), 12% biotite, 10% carbonate, 4% quartz, 1-2% magnetite, 1% pyrite, and trace ilmenite, and chalcopyrite.

Chlorite is found within the carbonate veinlets of this sample. Veinlets are approximately 1.8-2.5mm wide, and also locally contain euhedral magnetite and pyrite. As in sample 117-25.95, this sample contains carbonate crystals together that may be considered veinlets that pinch out in the sample.

The fabric of this sample is not defined by the elongation and 'veinlet'-like style of biotite alteration as in sample 177-25.95, but instead appears to be defined by the elongation and alignment of plagioclase laths. Zones of biotite alteration (without elongated laths) are present and define a sinuous fabric parallel to the plagioclase crystals. Veinlets in this sample run parallel to this fabric.

Plagioclase, biotite1 (~6%), ilmenite, carbonate, quartz, pyrite, biotite2 (~6%) form as described in sample 31-27.20. Chalcopyrite forms as in 117-25.95. Magnetite forms as in sample 31-16.28. Pyrite locally mantles magnetite.

G9. Diorite 1

69-1164

This sample is composed of 33% plagioclase, 30% chlorite, 30% carbonate, 3% quartz, 2 to 3% epidote, 1% pyrite, trace to 1% rutile and ilmenite, and trace biotite, muscovite, magnetite, and sphalerite.

Plagioclase in this sample is present as laths 0.1mm x 0.05mm in size. These laths have a mottled look and are locally replaced by fine-grained muscovite approximately 9µm in diameter. Plagioclase is replaced by chlorite and biotite tabular crystals with low birefringence and low pleochroism. Chlorite crystals generally form sinuous crystal aggregates. Plagioclase, chlorite, biotite, and muscovite are replaced by carbonate crystals 0.1mm or less in diameter that have a mottled appearance. Quartz is also replacing these minerals, but the relationship between quartz and carbonate is unknown (coeval?). Epidote replaces all minerals, and forms granular aggregates when replacing chlorite (and/or biotite) and forms crystals when replacing carbonate (and/or plagioclase).

Ilmenite forms laths in the host that are generally 0.059mm x 0.007mm in size. Magnetite forms euhedral cubic crystals 0.04mm in diameter. Both magnetite and ilmenite are associated with chlorite, and have sharp contacts with chlorite. Locally it appears that chlorite is filling corroded zones of magnetite and ilmenite. Pyrite is present as cubic euhedral to anhedral crystals replacing plagioclase, chlorite, and biotite in the sample. Pyrite contains inclusions of ilmenite and rutile and sphalerite are replacing pyrite along the rims and filling corroded zones in pyrite crystals.

The foliation fabric of this sample is weak and is defined by the elongation and alignment of chlorite (and/or biotite) crystals. These crystals form aggregates that are linear and sinuous in nature.

70-1167

This sample is composed of 60% plagioclase, 25% carbonate, 8% biotite, 3% chlorite, 3% pyrite, 1% magnetite, and trace muscovite and ilmenite.

Plagioclase is present as crystals 0.03mm to 0.15mm in diameter that have sharp, irregular shaped contacts. Locally muscovite replaces portions of plagioclase crystals with crystals 2µm in diameter. Chlorite and biotite replace plagioclase as flaky and

occasionally tabular crystals from 0.03mm x 0.07mm to 0.11mm in diameter. Chlorite₁ and biotite₁ also replace each other. Chlorite and biotite₁ are not very pleochroic and have a low birefringence. Carbonate replaces and fills corroded zones of plagioclase, chlorite₁, and biotite₁ in irregular shaped crystals approximately 0.03mm to 0.15mm in size. Carbonate is replaced by tabular crystals of biotite₂ and trace (?) amounts of tabular chlorite₂. Chlorite₂ and biotite₂ are more pleochroic than chlorite₁ and biotite₁, and have a higher birefringence. It appears that chlorite₂ and biotite₂ replace each other. In general, biotite and chlorite are not disseminated throughout the sample, and instead are concentrated together in biotite (-chlorite)-rich bands which are generally 1mm wide by 5-10mm in length.

Magnetite is present as subhedral crystals when in contact with plagioclase and carbonate, and as euhedral cubic crystals when associated with chlorite₂ and biotite₂. Magnetite crystals are generally 0.03mm to 0.055mm in diameter. Pyrite is present as euhedral cubic to subhedral crystals 0.026mm to 0.22mm in diameter. Ilmenite is present as inclusions and filling fractures in pyrite as 0.018mm crystals. Locally chlorite₂ and biotite₂ fills corroded zones of pyrite. Pyrite has irregular (but still cubic) contacts with carbonate (possibly coeval?).

Veinlets in this sample are 0.07mm in width and are composed of very fine-grained (granular-looking) biotite that appear to be cutting all minerals including carbonate. Locally it appears that the biotite is replaced by carbonate.

The fabric in this sample is weak and is formed by the slight elongation and alignment of all crystals (including plagioclase and carbonate), and the alignment of biotite laths in biotite-rich zones. Biotite-rich zones are also aligned in the sample, and are visible in hand specimen.

G10. Diorite 2

71-1159 Surface Sample 0.5 g/t Au

This sample is fine-grained, brown-grey in colour, and contains approximately 1% cubic disseminated pyrite crystals approximately 0.5mm in size. The sample contains several white to rusty-coloured quartz-carbonate veins, with minor black biotite near the veins and within the host. The sample is composed of plagioclase (75%), quartz (5%), carbonate (10%), chlorite (3%), biotite (3%), muscovite (2%), pyrite (1 to 2%), ilmenite (trace to 1%) and trace magnetite, chalcopyrite and sphalerite(?).

Plagioclase forms euhedral laths in the host approximately 0.2mm in size, with corroded zones filled with fine-grained muscovite laths, flaky chlorite (0.46mm), biotite, and carbonate. Quartz in the host is euhedral, 0.03mm in size, with crystals being pseudomorphously replaced by carbonate and corroded zones filled with flaky chlorite and biotite. Biotite also pseudomorphously replaces flaky and tabular chlorite crystals. Muscovite is fine-grained, acicular, fills corroded zones of plagioclase crystals (0.02 x 0.008mm), and pseudomorphously replaces portions of plagioclase as tabular crystals (~0.88mm).

Pyrite is generally cubic, 0.27mm in size, contains inclusions of ilmenite, magnetite and chalcopyrite, and locally sphalerite(?) and ilmenite fill corroded zones along the rims and fractures in the pyrite. Muscovite, biotite, and chlorite laths fill corroded zones of pyrite and locally the sphalerite rim. Ilmenite is also found as rounded aggregates of crystals (~0.02mm), and laths (~0.02 x 0.01mm) disseminated in the host. Magnetite is present as rounded crystals disseminated in the host.

Veins are 0.18 to 2.75mm in size, and are composed of quartz-albite-carbonate or tabular biotite (0.22 x 0.044mm) veinlets. Albite (1.8 x 0.6mm) and quartz crystals (0.14 to 1mm) in the vein and wall rock are pseudomorphously replaced by carbonate with dark rims around the crystals, and large quartz and plagioclase crystals are fractured, with

fractures locally filled with biotite. Minor carbonate is present as euhedral crystals (~0.55mm) in the veins.

69-1170

This sample is composed of 65% plagioclase, 17% biotite, 15% carbonate, 3% chlorite, trace to 1% pyrite and ilmenite, and magnetite. This sample contains trace to 1% veinlets.

Veinlets in this sample are approximately 0.73mm wide and are composed of 39-40% plagioclase, 60% carbonate, and 1 to 2 % quartz in 0.18mm crystals. Carbonate crystals in the vein generally have sharp contacts with plagioclase and quartz, and locally carbonate is pseudomorphously replacing quartz and plagioclase.

Plagioclase forms laths approximately 0.27mm x 0.14mm in size. Chlorite₁ and biotite₁ (low birefringence and weakly pleochroic tabular crystals) replace each other and replace and fill the corroded zones of plagioclase crystals as crystal laths and flakes approximately 0.1mm in diameter. Carbonate pseudomorphously replaces and fills corroded zones of plagioclase, chlorite₁, and biotite₁. The plagioclase-carbonate-quartz vein cuts plagioclase, chlorite₁, and biotite₁ in the host. Biotite₂ and chlorite₂ form laths

0.27mm x 0.08mm in size and replace the chlorite1, biotite1, and carbonate in the host. Chlorite2 and biotite2 also replace one another.

Pyrite forms euhedral to subhedral cubic crystals that are replacing plagioclase, biotite1, and chlorite1 in the host. Corroded zones of pyrite are filled with biotite2. Ilmenite is present as inclusions in pyrite and in the host associated with flaky biotite1. Magnetite (if any) is associated with biotite1 and forms subhedral, sub-rounded crystals.

71-1144

This sample is composed of 73% plagioclase, 25% carbonate, 1 to 2% pyrite, and trace biotite, muscovite, ilmenite, and magnetite. This sample contains 1 to 2% veinlets that are composed of 90% plagioclase, 5 to 8% carbonate, and 1 to 3% quartz.

The veinlets are generally 0.22 to 1mm wide, with plagioclase and quartz crystals that are generally 0.11mm to 0.27mm in diameter. Carbonate appears to be later than the vein as it is pseudomorphously replacing and filling corroded zones in plagioclase and quartz crystals within the veinlets.

In the sample, plagioclase is present as laths and fine-grained crystal aggregates that range in size from 0.24mm (laths) to less than 0.02mm in diameter (crystal aggregates). Plagioclase has been replaced by flaky biotite (now just a rusty colour in most places). Carbonate pseudomorphously replaces and fills corroded zones of biotite and plagioclase in crystals generally 0.01mm to 0.02mm in size. Locally carbonate crystals have a brown mottled 'dirty' look to them. Pyrite is present as euhedral to subhedral cubic crystals disseminated in the host and within the plagioclase-quartz-carbonate veinlets. Pyrite crystals are generally 0.1mm to 0.37mm in diameter, and contain inclusions of ilmenite. Ilmenite and magnetite are also present in fractures and with sharp contacts along the rim pyrite crystals. Pyrite replaces plagioclase in the host and veinlets, and is associated with the finer-grained 'dirty' looking carbonate crystals. Ilmenite and magnetite are associated with the finer-grained 'dirty' carbonate as well, and are present as inclusions in and between carbonate crystals. Muscovite fills corroded zones of pyrite crystals and replaces portions of carbonate crystals.

G11. Diorite 3

101-15.71

This sample is composed of plagioclase (55 to 65%), carbonate (10 to 20%), chlorite (10%), biotite (5%), quartz (up to 2% if present?), pyrite (1 to 2%), magnetite (1%), and trace ilmenite, chalcopyrite, and pyrrhotite.

Plagioclase, chlorite1, biotite1, carbonate, pyrite, magnetite, and ilmenite are present as described in sample 59-1164. Quartz occurs with sharp contacts with pyrite and carbonate. Ilmenite, chalcopyrite, and pyrrhotite form as inclusions in pyrite. Pyrite fills corroded zones and fills fractures in magnetite. Chlorite2 forms as described in sample 59-1164, and biotite2 (?) and chlorite2 replaces each other.

This sample contains a plagioclase-carbonate-quartz vein that is 0.44mm wide, and locally contains biotite2 and chlorite2 replacing plagioclase. Crystals in the veins are approximately 0.27mm wide on average.

182-03.71

Fine-grained side: This portion of the sample is composed of plagioclase (90 to 95%), biotite (2 to 5%), chlorite (1 to 2%), carbonate (1%), pyrite (1%), and trace ilmenite.

Plagioclase forms as very fine-grained crystals and as laths. Chlorite1&2 and biotite1&2 forms as described in sample 101-15.71, as laths and flakey crystals 0.12mm in size.

Carbonate and pyrite form as described in sample 59-11164, and biotite² fills corroded zones of pyrite. Ilmenite forms as described in sample 101-15.71.

Coarse-grained side: This portion of the sample is composed of plagioclase (50 to 55%), carbonate (30 to 35%), biotite (10%), chlorite (2 to 3%), pyrite (2 to 3%), and trace ilmenite.

Plagioclase forms very fine-grained crystals (w quartz?) replaced by chlorite and biotite as described in sample 101-15.71. Carbonate and pyrite form as described in sample 59-1164. Ilmenite forms as described in sample 59-1164 and as inclusions in pyrite.

This sample contains a folded (appears to be isoclinal and possibly transposed???) albite-carbonate-quartz vein containing 50 to 60% albite, 30% carbonate, and 10 to 20% quartz. Carbonate in this vein generally does not form euhedral crystals, but instead replaces portions of and fills fractures in and between plagioclase and quartz crystals.

59-1164

This sample is composed of 75% plagioclase, 10% chlorite, 5% muscovite, 3-5% carbonate, 1-2% pyrite, trace to 1% epidote and magnetite, and trace biotite, ilmenite, and rutile.

Plagioclase forms laths 0.22mm x 0.33mm in size. Plagioclase is replaced by chlorite¹ and biotite that form as 0.27mm flakes that are locally elongated in the sample and replace one another. Carbonate replaces plagioclase, chlorite, and biotite in the sample similarly to that described in sample 71-1159 (20-30cm dacite dyke). Chlorite² forms as described in 71-1159. Muscovite replaces portions of plagioclase crystals as laths 0.07mm x 0.018mm in size, and replaces larger portions of plagioclase, carbonate, chlorite, and biotite as larger laths 0.22mm x 0.055mm. Epidote replaces chlorite and muscovite in the sample as crystals 0.07mm, crystal aggregates of large crystals, and to a lesser extent in granular aggregates.

Pyrite forms sub-rounded and locally cubic crystals approximately 0.11mm to 0.44mm in diameter. Chlorite² has sharp contacts with pyrite (appears to be post-pyrite?). Pyrite has sharp contacts with carbonate. Magnetite is present as cubic to sub-rounded crystals in the groundmass and as inclusions in pyrite. Magnetite crystals are generally 0.088mm in diameter, and when in the host corroded zones of magnetite are filled with biotite and

chlorite₂. Ilmenite is present as laths disseminated in the groundmass and as coarser crystal aggregates. Rutile replaces crystal aggregates and fills corroded zones in larger crystals and crystal aggregates of ilmenite.

85-1058

This sample is composed of plagioclase (85%), biotite (5 to 8%), muscovite (5 to 8%?), carbonate (3%), chlorite (trace to 1%), pyrite (trace to 1%), and trace quartz, epidote, ilmenite, and rutile.

Plagioclase, chlorite, biotite, muscovite, carbonate, pyrite, ilmenite, and rutile form as described in sample 59-1164. Quartz forms as described in sample 101-15.71 (associated with carbonate). Flakey chlorite₁ is not present, but biotite_{1&2} and chlorite₂ are present as described in sample 101-15.71. Muscovite is present as in sample 59-1164, but is much more pervasive and is replacing the core of plagioclase laths. Epidote is replacing chlorite₂ and biotite₂ as euhedral crystals. Rutile forms as in 59-1164 and is replacing portions of flakey biotite₁.

No fabric is present in this sample.

G12. Quartz-feldspar Porphyry (QFP)

118-22.78 Core Sample 0.03 g/t Au

Sample 118-22.78 is composed of cryptocrystalline groundmass (50%), plagioclase phenocrysts (approximately 5%), potassium feldspar phenocrysts (approximately 25%), quartz (5%), chlorite (5%), carbonate (5%), muscovite (3%), apatite (2%), and trace biotite, zircon, ilmenite, rutile (+titanium mineral – titanite?), pyrite, chalcopyrite, and pyrrhotite.

The groundmass of this sample is cryptocrystalline. Plagioclase and potassium feldspar form phenocrysts in the groundmass ranging in size from 1mm to 1.5 x 2.4mm.

Plagioclase crystals generally exhibit oscillatory zoning, melt inclusion zoning, and/or Carlsbad / multiple lamellar twinning. Potassium feldspar crystals exhibit no twinning or simple twinning. Locally feldspar phenocrysts have thin rims of feldspar overgrowth around the crystals. Both plagioclase and potassium feldspar crystals are replaced by acicular, radiating, and flaky muscovite. The muscovite is present throughout the phenocrysts, but preferentially replaces the phenocrysts along oscillatory and melt inclusion zones. Flaky and tabular muscovite crystals approximately 0.08mm in size replace carbonate, quartz, and feldspar in the groundmass. A later phase of quartz is present as phenocrysts 0.55mm in size in the groundmass, and as 0.04mm crystals with chlorite in relict mafic phenocrysts. Chlorite is present as tabular and flaky crystals pseudomorphously replacing minerals in the groundmass, and as coarse grains showing

crenulations that are pseudomorphously replacing the mafic phenocrysts. These crystals are approximately 1.4 x 0.9mm in size, and vary in shape from triangular to sub-rounded. Chlorite contains inclusions of quartz, and corroded zones of chlorite are filled with quartz and feldspar. Chlorite has a pale brown-green colour in plane light and a dark grey-brown to purple colour in cross-polarized light. Carbonate is pseudomorphously replacing portions of the cryptocrystalline groundmass (clusters ~0.36mm in size). Apatite is present as long prismatic crystals (~0.5mm long) and as six-sided cross-sections (~0.18mm) in the groundmass, and locally included in feldspar and plagioclase phenocrysts. Biotite pseudomorphously replaces portions of flaky and tabular chlorite crystals. Zircon is present as doubly terminating crystals and cubic crystal cross-sections as inclusions within feldspar phenocrysts. At least 4 zircons have been identified in this sample to date, with an average cross-section width of 0.1mm.

Ilmenite is present as tabular crystals approximately 0.03mm in size altering mafic phenocrysts that have been pseudomorphously replaced by chlorite. Rutile is present with a titanium mineral (titanite?) crown as acicular crystals and clusters of crystals (≤ 0.04 mm) altering chlorite and within the groundmass. Pyrite forms irregular shaped crystals in the groundmass that range in size from 0.05 to 0.36mm. Pyrite occurs with sharp contacts with rutile, and contains inclusions of chalcopyrite and pyrrhotite.

Locally carbonate alteration of the cryptocrystalline groundmass, feldspar phenocrysts, and plagioclase phenocrysts is intense. In this region carbonate composes up to 40% of the rock.

The vein in this sample is approximately 1.6mm wide and is composed of carbonate and minor quartz. Carbonate crystals are euhedral and up to 1 x 3mm in size. The selvage of this vein is fine-grained carbonate crystals that have pseudomorphously replaced the groundmass adjacent to the vein.

There is a possible weak foliation in this sample, as some phenocrysts (particularly those replaced by chlorite) appear to be elongated and aligned with a fabric. Deformation is also apparent in the crenulated chlorite.

210-48.38 Core Sample 0.02 g/t Au

Sample 210-48.38 is composed of groundmass (50%), plagioclase phenocrysts (12%), feldspar phenocrysts (8%), quartz phenocrysts (10%), carbonate (8%), muscovite (5%), biotite (4%), chlorite (2%), magnetite (1%), and trace apatite, zircon, pyrite, and rutile.

The groundmass in this sample is coarser-grained than in sample 118-22.78, with crystals ranging in diameter from 30 to 70 μm , but the mineralogy of the groundmass is still undeterminable. The feldspar and plagioclase phenocrysts occur as described in sample 118-22.78, however these phenocrysts are more strongly altered by acicular and tabular muscovite. Biotite forms phenocrysts that contain acicular rutile and are altered by chlorite, biotite₂, and muscovite. Quartz phenocrysts contain sub-grains of quartz, some of which are polygonal. Zircon is present at doubly terminating crystals and cubic crystal sections. At least one zircon (cubic cross-section approximately 0.1mm wide) has been identified in this section between quartz, chlorite, and biotite crystals within the groundmass. Apatite is present as described in sample 118-22.78.

Chlorite is present as large flakes (low birefringence – dark grey colour), which replace biotite phenocrysts. Chlorite is being replaced by biotite₂ (flaky, higher birefringence, more anisotropic) and muscovite. Carbonate replaces sub-grains of quartz in quartz phenocrysts, fills corroded zones of plagioclase and feldspar phenocrysts, and locally replaces crystals in the groundmass.

Magnetite forms anhedral and euhedral cubic crystals disseminated in the groundmass, and locally associate with biotite. Cubic crystals of magnetite are corroded zones filled with ilmenite and biotite. Rutile forms acicular crystals in biotite, and clusters of crystals

with titanium crowns that are spatially associated with biotite. Pyrite forms cubic crystals within the groundmass.

The veins in this sample are composed of carbonate and albite (-quartz). Carbonate forms thin (0.2mm wide) sinuous veinlets that cut plagioclase phenocrysts, feldspar phenocrysts, and the groundmass. Plagioclase and feldspar phenocrysts close to and cut by these veins appear elongated along the length of the veins. The albite (-quartz) vein is approximately 2.7 to 3.5mm wide, and cuts plagioclase phenocrysts and the groundmass. The vein is composed mostly of anhedral plagioclase (>95%) and quartz (<5%) crystals ranging in diameter from 0.2 to 1.3mm. Carbonate pseudomorphously replaces crystals in the albite (-quartz) vein, and fills corroded zones between albite and quartz crystals in the vein. Chlorite and biotite fill corroded zones of the albite crystals along the margins of the veins.

There does not appear to be a foliation in this sample. Sinuous veins of carbonate appear to be generally aligned in this sample. Near carbonate veins chlorite and biotite appear to be aligned parallel to the veins along fractures/veinlets.

210-55.21 Core Sample 0.01 g/t Au

Sample 210-55.21 is composed of cryptocrystalline groundmass (50%), potassium feldspar phenocrysts (24%), plagioclase phenocrysts (6%), quartz phenocrysts (5%), biotite phenocrysts (3%), biotite (5%), epidote (3%), muscovite 1 (3%), muscovite 2 (2%), apatite (trace to 1%), pyrite 1 and 2 (trace to 1%), and trace zircon, and ilmenite, rutile.

The cryptocrystalline groundmass composes the largest amount of this sample, and is similar to the groundmass in 118-22.78. The crystals of the groundmass in this sample are larger than those in 118-22.78, however they are too small to determine their mineralogy. Potassium feldspar and plagioclase phenocrysts are similar in their crystal size, zoning, and the fact that muscovite (as sericite) has locally replaced portions of the phenocrysts, to those found in sample 118-22.78. The difference between the phenocrysts in this sample and those of 118-22.78 is that biotite is present in this sample as phenocrysts (with low birefringence). A tabular/flaky biotite (higher birefringence) replaces portions of the plagioclase and feldspar phenocrysts. Feldspar/albite overgrowth is present along the margins of many of the feldspar phenocrysts, and alters the biotite phenocrysts. Quartz forms similar phenocrysts as those described in 118-22.78, however the rims of the quartz phenocrysts in this sample contain irregularly shaped sub-grains of quartz. Large quartz crystals are fractured. Muscovite (1) in this sample is present as described in sample 118-22.78 as acicular crystals altering plagioclase and feldspar phenocrysts.

Apatite is present as described in 118-22.78, but in this sample crystals are smaller: approximately 0.25cm in length for the long, prismatic crystals, and 0.1mm in width for the six-sided cross-sections. Zircon forms doubly terminating crystals approximately 0.07 x 0.21mm in size and cubic crystal sections included in plagioclase and quartz phenocrysts and in the groundmass. Three zircon crystals have been identified in this thin section to date. Several of the zircons appear to be zoned.

Tabular and flaky crystals of biotite (higher birefringence) replace crystals in the groundmass (with higher birefringence). In places biotite forms sinuous veinlets that are spatially associated with epidote. Epidote replaces plagioclase, is sub-rounded crystals, and is spatially associated with biotite. Corroded zones of epidote are filled with biotite. Muscovite (2) forms larger tabular and flaky crystals that are associated with the tabular/flaky biotite. Chlorite in this sample is brown coloured with a low (brown) birefringence. Chlorite is present as inclusions within feldspar and quartz phenocrysts.

Pyrite forms as cubic crystals 0.03 to 0.16mm in size in the groundmass, contains inclusions of ilmenite, and is spatially associated with biotite 2. Locally cubic pyrite is present as inclusions in unaltered biotite phenocrysts. Ilmenite is present as inclusions in pyrite, and is not disseminated in the groundmass. Rutile is present as inclusions in mafic phenocrysts and disseminated in the groundmass. Needles of rutile are also present in unaltered portions of biotite phenocrysts. When disseminated in the groundmass, rutile

has a titanium crown surrounding it. This titanium alteration is also present in the groundmass without titanium, and is locally spatially associated with the flaky/tabular biotite. .

There does not appear to be a foliation in this sample, and deformation is apparent only in sub-grains of quartz.

60-1160 Surface Sample 0.04 g/t Au

This sample is composed of fine-grained groundmass (35%), feldspar phenocrysts (20%), plagioclase phenocrysts (20%), quartz phenocrysts (trace to 1%), biotite phenocrysts (2%), carbonate (5%), biotite 2 (5%), muscovite (5%), feldspar overgrowth (2%), quartz (2%), chlorite 1 (1-2%), chlorite 2 (trace to 1%), pyrite (trace to 1%), and trace apatite, zircon, rutile, and ilmenite.

The groundmass of this sample is similar in size to that of sample 210-48.38. The mineralogy of the groundmass in this sample is not known. Feldspar and plagioclase phenocrysts are larger than those in sample 210-48.38 – phenocrysts are on average 2 x 2mm, but are locally up to 3.6 x 5.5mm in size. Feldspar and plagioclase phenocrysts exhibit the same zoning (concentric), twinning (albite twins, simple twins), and intense

muscovite alteration as seen in 210-48.38. Locally feldspar and plagioclase phenocrysts are rimmed by feldspar overgrowth. Quartz phenocrysts locally contain sub-grains of quartz. Biotite phenocrysts are dark brown in colour, with low (brown-green) birefringence, are not very pleochroic, and occur as described in sample 210-48.38. Locally the biotite phenocrysts are coarse-grained and crenulated, and contain inclusions of feldspar phenocrysts and apatite. Corroded zones of biotite phenocrysts are filled with quartz. Portions of biotite 1 are included in feldspar and plagioclase phenocrysts. Apatite is present as described in sample 118-22.78. At least four possible zircons have been identified in this sample. The zircons are present as cubic cross-sections, one within the groundmass, and one included in the feldspar overgrowth of a concentrically zoned feldspar phenocryst, and two included in a carbonate crystal of a carbonate veinlet adjacent to the zircon in the feldspar overgrowth.

Chlorite 1 has a dark green colour, low (dark grey) birefringence, and is not very pleochroic. It replaces biotite phenocrysts and replaces crystals of the groundmass.

Chlorite 2 is lighter coloured, strongly pleochroic (from light/clear to green), has a higher birefringence (brown-purple), and replaces biotite 1 and chlorite 1. Biotite 2 is lighter coloured, strongly pleochroic (from light/clear to brown), and has a higher (orange-red to pink-blue) birefringence. Biotite 2 replaces biotite phenocrysts, and chlorite 2. The relationship between chlorite 2 and biotite 2 is unknown. Tabular muscovite replaces portions of both biotites and both chlorites. Fine-grained muscovite alters plagioclase and

feldspar phenocrysts. Flaky and tabular biotite 2 and chlorite 2 also replace portions of muscovite altered plagioclase and feldspar phenocrysts.

Rutile and ilmenite are spatially associated with biotite 1, biotite 2, and both chlorites. Rutile forms acicular crystals in biotite 1, and ilmenite and rutile form anhedral crystals filling corroded zones around biotite 1. Ilmenite and rutile form inclusions within biotite 2 and both chlorites, and rutile forms anhedral crystals around biotite 2 and both chlorites. Pyrite forms euhedral cubic to anhedral crystals. Cubic crystals are found disseminated in the groundmass and included in feldspar and plagioclase phenocrysts. Anhedral crystals are locally associated with carbonate and quartz alteration of the groundmass, and in places fill corroded zones of plagioclase and feldspar phenocrysts.

There does not appear to be a foliation in this sample, and deformation is apparent only in sub-grains of quartz and crenulated biotite.

62-1119 Surface Sample 0.18 g/t Au

This sample is composed of groundmass (50%), plagioclase phenocrysts (25%), feldspar phenocrysts (10%), quartz phenocrysts (5%), biotite phenocrysts (2%), chlorite (3%), muscovite (3%), carbonate (2-3%), biotite 2 (trace to 1%), apatite (trace to 1%), feldspar

overgrowth (trace to 1%), quartz (coarser-grained in the groundmass – magmatic??? trace to 1%), pyrite (trace to 1%), and trace zircon, rutile, and ilmenite.

The groundmass in this sample ranges from cryptocrystalline to fine-grained anhedral quartz and laths of plagioclase up to 2 or 3mm in diameter. Feldspar and plagioclase phenocrysts occur as described in sample 60-1160, but are more intensely altered by muscovite throughout. Feldspar overgrowth occurs on plagioclase and feldspar phenocrysts as described in sample 60-1160. Locally feldspar and plagioclase contain remnants of included biotite phenocrysts. Muscovite alteration is pervasive in the feldspar and plagioclase phenocrysts, with flakes and laths of muscovite up to 0.15 x 0.36mm in size. Muscovite in the phenocrysts locally replaces portions of the included biotite phenocrysts. Quartz phenocrysts range in size from 1.3mm in diameter to 1.8 x 4.4mm in size. Quartz phenocrysts and large quartz crystals in the groundmass are fractured, and locally contain sub-grains of quartz and/or zoned extinction. Biotite phenocrysts occur as described in sample 60-1160. Apatite occurs as described in sample 118-22.78. One possible zircon has been identified in this sample to date. The zircon occurs as a doubly terminating crystal 55µm x 122 µm within a corrode zone of a quartz phenocryst which is filled with carbonate, muscovite, quartz, and possibly fine-grained plagioclase.

Carbonate occurs as anhedral crystals generally 0.18mm in diameter that replace the cryptocrystalline groundmass, pseudomorphously replace the coarser plagioclase and

quartz in the groundmass, and fills corroded zones and fractures of plagioclase, feldspar, and quartz phenocrysts. Chlorite is light coloured, strongly pleochroic (from light/clear to green), has a higher birefringence (brown-purple), and replaces biotite phenocrysts and crystals in the groundmass. Biotite 2 is lighter coloured, strongly pleochroic (from light/clear to brown), and has a higher (orange-red to pink-blue) birefringence. Biotite 2 replaces biotite phenocrysts, and biotite 2 and chlorite replace each other. Tabular muscovite replaces portions of both biotites and chlorite as described in sample 60-1160.

Rutile and ilmenite are present as described in sample 60-1160. Pyrite is present as subhedral crystals in the groundmass and as cubic crystals included in plagioclase and feldspar phenocrysts. Corroded zones of pyrite are filled with chlorite and pits are filled with fine-grained plagioclase or quartz. Pyrite contains inclusions of rutile, and has a replacement by ilmenite around the rims, pits, and along fractures in the pyrite.

There does not appear to be a foliation in this sample, and deformation is apparent only in fractured quartz and crenulated chlorite.

83-1038 Surface Sample 0.03 g/t Au

This sample is composed of groundmass (37%), plagioclase phenocrysts (28%), feldspar phenocrysts (7%), quartz phenocrysts (15%), chlorite 2 (5%), carbonate (5%), muscovite (3%), feldspar overgrowth (trace to 1%), and trace apatite, zircon, chlorite 2, pyrite, rutile, and magnetite.

The groundmass in this sample is similar to that of sample 210-48.38, and locally up to 3% of the groundmass is composed of coarser quartz grains approximately 0.07 to 0.09mm in diameter. Feldspar and plagioclase phenocrysts occur as described in sample 60-11160. Locally muscovite flakes and laths up to 0.14 x 0.4mm in size pseudomorphously replace portions of plagioclase phenocrysts. Feldspar overgrowth occurs as described in sample 60-1160. Quartz phenocrysts range in size from 0.55mm in diameter to 5.5 x 8mm in size. Quartz phenocrysts are fractured, and locally contain sub-grains of quartz and/or zoned extinction. Fractures in the quartz are locally open and contain fine-grained groundmass, carbonate, and muscovite. The largest quartz phenocrysts contain inclusions of groundmass. Apatite occurs as described in sample 118-22.78. One zircon has been identified in this sample to date. Zircon occurs as a cubic crystal sections included in a quartz phenocryst.

Chlorite 1 (dark green, not pleochroic, low grey birefringence) forms coarse-grained and crenulated crystals pseudomorphously replacing mafic phenocrysts. Locally the phenocrysts replaced by chlorite contain acicular needles that appear to be remnant rutile.

Chlorite 1 also replaces portions of the groundmass. Chlorite 2 (light green, pleochroic, low brown birefringence) replaces chlorite 1 and portions of the groundmass. Carbonate fills corroded zones of plagioclase, feldspar, and quartz phenocrysts, replaces chlorite 1, and replaces quartz and fine-grained portions of the groundmass. Muscovite replaces both chlorites, the feldspar and plagioclase phenocrysts, and portions of the groundmass.

Pyrite forms cubic euhedral crystals included in quartz phenocrysts, and within the groundmass. One cubic pyrite crystal appears to have been split open. Chlorite 1 and carbonate fill the fracture. Magnetite forms subhedral crystals in the groundmass. Rutile is associated with chlorite 1 where it is replacing a mafic phenocryst. Clusters of rutile are disseminated in the groundmass and replacing crystals in the groundmass.

Red colouration: stains edges of some phenocrysts, and carbonate crystals (along the fractures in them).

The vein in this sample extends throughout the width of the section, and is approximately 5.5mm wide. The vein is composed of >99% quartz crystals ranging in size from 0.5mm to 1mm in diameter, and <1% plagioclase approximately 0.5mm in diameter. Quartz crystals are corroded between crystals, along fractures, and along the edge of the vein by carbonate. Fractures in quartz in the vein are also locally filled with muscovite.

There does not appear to be a foliation in this sample, and deformation is apparent only in fractured quartz and crenulated chlorite.

58-1165

This sample is composed of 35% plagioclase phenocrysts, 5% feldspar phenocrysts, and 1-2% chlorite and biotite phenocrysts, and 48% aphanitic groundmass. The groundmass is composed of 3-5% carbonate, 3% muscovite, trace to 1% chlorite and biotite, and trace feldspar overgrowth, apatite, magnetite, ilmenite, and rutile, and zircon.

This sample (groundmass, plagioclase, feldspar, muscovite, apatite) is similar to sample 62-1119, but does not contain quartz phenocrysts. Zircon is present as cubic crystal sections and doubly terminating crystals included in plagioclase and feldspar phenocrysts. Mafic phenocrysts are composed of biotite₁ (flaky) replaced by chlorite. Chlorite and biotite₁ are replaced by biotite₂, which is in turn replaced by muscovite. Locally chlorite-biotite phenocrysts are coarse-grained and crenulated, and contain inclusions of feldspar phenocrysts and apatite. Zircon is present as cubic crystal sections and doubly terminating crystals included in feldspar and plagioclase phenocrysts. Carbonate, chlorite, and biotite₂ occurs as described in sample 62-1119.

Rutile and ilmenite are spatially associated with biotite 1, biotite 2, and chlorite. Rutile and ilmenite form as described in sample 62-1119, but rutile does not form acicular crystals in biotite in this sample. Pyrite forms as described in sample 62-1119, and locally subhedral to anhedral pyrite contains inclusions of/has corroded zones filled with quartz and muscovite.

84-1059

The sample is composed of 30% plagioclase phenocrysts, 10% feldspar, 1 to 2% chlorite phenocrysts, trace to 1% quartz phenocrysts and 40% aphanitic groundmass. The groundmass also contains 3 to 5% quartz, carbonate, and muscovite, 3% chlorite, 1-2% biotite, trace to 1% pyrite, and trace apatite, ilmenite, rutile, and zircon.

This sample is similar to sample 62-1119 (groundmass, plagioclase and feldspar phenocrysts, muscovite, apatite, carbonate, and quartz). Chlorite, biotite1, biotite2, and zircon occur as described in sample 58-1165. Chlorite and biotite in this sample also occur as disseminate flakes in the sample, and as laths replacing these flaky crystals 0.1mm in size. These minerals are replacing portions of the groundmass, filling fractures in plagioclase and feldspar phenocrysts, and locally filling corroded zones and replacing within phenocrysts.

Rutile, ilmenite, and pyrite form as described in sample 58-1165. Pyrite in this sample is replaced along the rim and fractures of crystals by a grey mineral.

Sample 80-1025 0.1 g/t

The sample is composed of 30% plagioclase phenocrysts, 10% feldspar phenocrysts, 10% quartz phenocrysts, and 50% aphanitic groundmass. The groundmass also contains 8% muscovite, 2% chlorite, trace-1% carbonate, and trace magnetite, pyrite, and rutile.

The minerals (phenocrysts, groundmass etc) in this sample formed similarly to sample 210-48.38. Plagioclase phenocrysts locally have plagioclase (albite?) overgrowth. Quartz phenocrysts in this sample are quite large – up to 5mm in diameter in some cases – and contain fractures which are more or less aligned in the quartz crystals and among quartz crystals. Chlorite forms flakes that are replaced by acicular rutile and locally magnetite. Carbonate forms fine-grained crystals replacing and filling cracks in phenocrysts, vein minerals, and the groundmass.

The vein in this sample is comprised mainly of quartz, with minor albite. It is 2-3 mm wide, cuts phenocrysts, and locally contains carbonate alteration.

Sample 94-1015

0.01 g/t

This sample is composed of 25% plagioclase phenocrysts 5%(?) feldspar phenocrysts, 10% quartz phenocrysts, and 60% aphanitic groundmass. The groundmass also contains 10% muscovite, 5-10% carbonate, and trace biotite, chlorite, apatite, zircon, magnetite, pyrite, ilmenite, and rutile.

Plagioclase, feldspar, quartz, chlorite, biotite, muscovite, apatite, zircon, rutile, pyrite, magnetite, and groundmass (phenocrysts, groundmass, etc) are similar to those in sample 210-48-38. The main difference in this sample is that the boundaries between phenocrysts and the groundmass are not sharp/well defined as in other samples. This gives the sample a 'smeared' look in both hand sample and this section.

Phenocrysts in this sample are elongated and roughly aligned within the sample, forming a weak fabric. Phenocrysts appear to be stretched to ~ 2x's their normal length and ½ their normal length (ex. one muscovite altered feldspar phenocryst is 3.3x0.5mm in size). Locally muscovite forms larger laths replacing portions of biotite, chlorite, and phenocrysts.

Sample 127-21.35

0.3 g/t

This sample is composed of 30% plagioclase phenocrysts, 10% feldspar phenocrysts, 10% quartz phenocrysts, 3% chlorite phenocrysts (after another mafic mineral) and 50% fine-grained groundmass. More than half of the 'groundmass' is coarser-grained and appears to be quartz. Other minerals present in the groundmass include 2-3% carbonate, 8% muscovite, and trace magnetite, pyrite, and rutile. A brown-coloured, mottled mineral is present as phenocrysts as well – possibly a remnant mafic phenocryst?

This sample is similar to sample 210-48.38. The groundmass in this sample is locally coarser-grained, allowing for the identification of quartz. Chlorite forms sinuous crystals replacing mafic phenocrysts. Rutile forms acicular crystals in the chlorite. Muscovite forms fine-grained laths and acicular crystals, as well as larger crystal 'fans' replacing plagioclase and feldspar phenocrysts.

Sample 151-11.41

0.2 g/t

This sample is composed of 38% plagioclase phenocrysts, 10% feldspar phenocrysts, 2% quartz phenocrysts, and 40-45% groundmass. Other minerals in the groundmass are: 5% carbonate, 3-5% muscovite, trace-1% chlorite, and trace pyrite and rutile.

Minerals in this sample are similar to those described in sample 118-22.78. Carbonate in this sample locally replaces a whole phenocryst – it is not known what the previous mineral was. Chlorite forms tabular crystals locally replacing carbonate in the groundmass, and is seen proximal to veins. Muscovite alteration is pervasive in some plagioclase and feldspar phenocrysts, and is weak to moderate in others.

The vein in this sample is ~4mm wide and is composed mainly of quartz. Locally fine-grained carbonate and muscovite replace portions of quartz crystals and carbonate fills fractures in the vein. Pyrite is found mostly proximal to veins, and locally appears to be in a pyrite stringer (+/- albite vein?).

Sample 58-1165

0.4 g/t

This sample is composed of 35% plagioclase phenocrysts, 5% feldspar phenocrysts, 1-2% chlorite phenocrysts, and 48% groundmass. The groundmass also contains 3-5%

carbonate, 3% muscovite, trace-1% biotite, trace-1% chlorite, trace-1% pyrite, and trace apatite, magnetite, ilmenite, and rutile.

The minerals in this sample resemble those of sample 210-48.38. Chlorite locally replaces mafic phenocrysts as sinuous grains. These are locally replaced by magnetite, ilmenite, and acicular rutile. Chlorite 2 and biotite 2 locally replace plagioclase phenocrysts, the groundmass, and one another as laths. Carbonate crystals replacing the groundmass in this sample are in turn replaced by biotite2.

Sample 84-1059

0.03 g/t

This sample is composed of 30% plagioclase phenocrysts, 10% feldspar phenocrysts, trace-2% biotite phenocrysts, trace-1% chlorite phenocrysts, and 40% aphanitic groundmass. The groundmass also includes 3-5% quartz, 3-5% carbonate, 3-5% muscovite, 3% chlorite, 1-2% biotite, trace-1% pyrite, and trace apatite, ilmenite, and rutile.

This sample is similar to 118-22.78. In this sample the biotite and chlorite 'phenocrysts' refer to mafic phenocrysts being pseudomorphously replaced by sinuous biotite or

Sample 117-11.95

0.2 g/t

This sample is composed of 10% plagioclase phenocrysts, 3% feldspar phenocrysts, trace-1% quartz phenocrysts, and 70% aphanitic groundmass. The groundmass also includes 15% carbonate, 2-5% quartz, trace-1% muscovite, and trace chlorite, biotite, apatite, magnetite, pyrite, and ilmenite.

Minerals in this sample formed as described in sample 118-22.78. As in sample 97-1158, this sample contains more carbonate than is normally seen in QFP.

This sample contains a fairly strong fabric evident in the elongation (ex. one crystal is 5.5x0.7mm – and aspect ratio of almost 8-1, when normal aspect ratios are closer to 2:1) and alignment of the long axes of phenocrysts.

This sample contains the contact of the QFP with a carbonate altered mafic volcanic rock. The contact in this sample is not very sharp. This rock is comprised of 40% plagioclase, 50% carbonate, 10% pyrite, and trace ilmenite and muscovite. The carbonate alteration in this sample is consistent with that seen in other pervasively carbonate altered samples.

Sample 143-27.82

0.1 g/t

This sample is composed of 20% plagioclase phenocrysts, 15% feldspar phenocrysts, 2% quartz phenocrysts, 2-5% biotite phenocrysts, and 50% aphanitic groundmass. The groundmass also includes 2-5% carbonate, 3% biotite, trace-1% muscovite, trace-1% quartz, and trace apatite, magnetite, and pyrite.

Minerals in this sample are similar to those described in sample 118-22.78. The groundmass in this sample is cryptocrystalline. Biotite 'phenocrysts' take on two forms: (1) solid biotite crystal, likely magmatic(?), and (2) sinuous biotite crystals replacing the mafic phenocryst. Locally portions of replaced phenocrysts contain quartz between sinuous biotite. Rutile forms acicular crystals replacing both. Plagioclase and feldspar phenocrysts have concentric zoning or albite twins.

This sample contains a contact between QFP and biotite-epidote altered mafic volcanic rock. The contact in this sample is very sharp. The mafic volcanic rock is comprised of 65% plagioclase, 20% epidote, 10-15% biotite (locally near intrusion this rises to 20-30%), 3% carbonate, and trace muscovite. A carbonate veinlet in this section of the rock is heavily replaced by fine-grained muscovite along the selvage and carbonate crystals in the vein have sharp contacts with biotite in the vein selvage.

Sample 182-03.42

0.3 g/t

This sample is composed of 30% plagioclase phenocrysts, 15% feldspar phenocrysts, 1% quartz phenocrysts, and 35-40% aphanitic groundmass. The groundmass also contains 10% carbonate, 5% quartz, trace-2% chlorite, trace-1% muscovite, trace-1% pyrite, and trace biotite, epidote, apatite, magnetite, and ilmenite.

This sample has a fairly coarse-grained groundmass, most similar to 210-48.38.

Carbonate alteration is quite string in this sample, with carbonate seen as euhedral crystals in veins, and as irregular crystals replacing the groundmass and filling fractures and corroded zones in phenocrysts. Locally carbonate is present altering the centre of plagioclase phenocrysts (as muscovite is normally seen doing). Chlorite and biotite replace carbonate.

Sample 182-23.00

0.3 g/t

This sample is composed of 35% plagioclase phenocrysts, 15% feldspar phenocrysts, 1% quartz phenocrysts, and 40% aphanitic groundmass. The groundmass also contains 5-8% muscovite, 2-5% biotite, 2-3% quartz, 2-3% carbonate, and trace chlorite, apatite, pyrite, ilmenite, and rutile.

The size of the crystals in the groundmass, and the other minerals, are similar to those seen in sample 210-48.38. In this sample biotite forms flakey laths (1) replacing the groundmass, which are replaced by tabular crystals. Chlorite also locally replace biotite 1 as laths. Pyrite appears to replace biotite 1, but has sharp contacts with biotite 2.

G13. Quartz Monzonite

210-4.33

This sample is composed of 36-42% plagioclase, 23-25% feldspar, 15% quartz, 10% muscovite, 8% chlorite, 5% carbonate, and trace apatite, zircon, rutile, and pyrite.

Quartz, plagioclase, feldspar, and mafic minerals (replaced by chlorite) are commonly equigranular and coarse grained ($\geq 3\text{mm}$), with crystals in direct contact with each other (no groundmass in between). Quartz crystals locally contain minor fractures. Plagioclase and feldspar crystals are locally overgrown by feldspar/albite. Chlorite pseudomorphously replaces large (3mm) mafic minerals with coarse grains of chlorite showing crenulations. Chlorite contains inclusions of quartz, feldspar in flaky and elongated, sinuous growths. Corroded zones of chlorite are filled with carbonate. Zircon forms doubly terminating crystals and cubic crystal sections included in feldspar phenocrysts and associated with quartz-feldspar alteration of feldspar and chlorite.

Apatite forms rectangular crystals and hexagonal crystal sections both within the coarse-grained plagioclase and feldspars, and between the finer-grained quartz, plagioclase, feldspar, and chlorite crystals. At least one zircon has been identified in each crowded QFP thin section. Carbonate crystals are generally finer-grained. Carbonate replaces and fills corroded zones of plagioclase, feldspar, quartz, and chlorite. A possible second generation of chlorite forms flaky crystals replacing the finer-grained plagioclase, quartz, feldspar, carbonate, and chlorite (1) crystals. Muscovite replaces plagioclase and feldspar as flaky and acicular, radiating crystals, and replaces coarse-grained chlorite (which is replacing mafic minerals) and finer-grained flaky chlorite as laths.

Rutile fills corroded zones of mafic crystals replaced by chlorite. Pyrite forms euhedral to subhedral crystals between coarse-grained plagioclase, feldspar, and quartz and filling embayments in plagioclase and feldspar crystals.

This sample does not exhibit foliation, but deformation is apparent in the crenulated chlorite and fractured quartz crystals.

210-5.97

This sample is composed of 37% feldspar, 29% plagioclase, 13% quartz, 9% chlorite, 5% muscovite, 4% epidote, 3% carbonate, 2% biotite, trace to 1% pyrite, and trace apatite, zircon, rutile.

Plagioclase, feldspar, apatite, zircon, carbonate, pyrite, rutile, and chlorite occur as described in 210-4.33. Quartz in this sample does not appear to be fractured, but instead contains sub-grains of quartz. In this sample, a portion of the quartz is present as smaller (0.2 to 0.4mm – possibly magmatic) grains between the larger quartz, feldspar, and plagioclase grains. As in sample 210-4.33, there appear to be two generations of chlorite.

Biotite is present within the coarser-grained mafic minerals, and is being pseudomorphously replaced by chlorite. Muscovite replaces plagioclase and feldspar as laths and acicular crystals, and replaces coarse-grained chlorite (which is replacing mafic minerals) and finer-grained flaky chlorite as laths. Epidote replaces portions of coarse-grained biotite crystals that have been replaced by chlorite. Epidote also fills embayments and corroded zones of pyrite, and replaces finer-grained carbonate and plagioclase (?).

There does not appear to be a foliation in this sample, and deformation is apparent only in sub-grains of quartz and crenulated chlorite.

210-14.00

This sample is composed of 60% vein and 40% quartz monzonite. The vein in this sample is approximately 14mm wide and is composed of >99% quartz and <1% plagioclase. Quartz in the vein has irregular shapes and ranges in size from 0.2 to 0.9mm in diameter. Many quartz crystals show a slight elongation along the axis of the crystal parallel to the strike of the vein. Plagioclase in the vein is generally about 8mm in diameter, and is not altered by muscovite. A veinlet of muscovite cuts the quartz crystals of the vein at an angle oblique to the vein. The muscovite veinlet is sinuous and approximately 0.5mm in diameter. Carbonate replaces small portions of quartz crystals and fills corroded zones between quartz crystals in the vein, and form larger crystals near the contact between the vein and the host.

The quartz monzonite in this sample is composed of 6% quartz, 57% plagioclase, 25% feldspar, 5% carbonate, 3 to 5% muscovite, 2-3% pyrite, and trace chlorite, apatite, magnetite, ilmenite, chalcopyrite, and rutile.

Plagioclase, feldspar, quartz, and chlorite form as described in sample 210-4.33. Chlorite in this sample is also replaced by tabular muscovite. Apatite is present as hexagonal

crystal sections included in quartz and plagioclase. This sample does not contain feldspar overgrowth. No zircon has been identified in this sample.

Pyrite forms both euhedral cubic crystals that have sharp contacts with plagioclase, feldspar, and quartz, anhedral irregular-shaped crystals that fill corroded zones and fractures in plagioclase, feldspar, and quartz. The euhedral and anhedral pyrite do not appear to tarnish in the same way (euhedral=even tarnish; anhedral=mottled/speckled tarnish), which suggests (along with their shape and mode of occurrence) that there are two generations of pyrite. Both pyrites contain miniscule inclusions of chalcopyrite, and pits in the pyrite are filled with magnetite. The euhedral pyrite locally contains inclusions of ilmenite. Rutile fills embayments in the euhedral pyrite. Rutile is also present as crystal aggregates and forming lattice-like crystal forms (Brown under plain light, like many tiny speckles).

This sample does not exhibit foliation, but deformation is apparent in the fractured quartz crystals.

443846

This sample is composed of 32% feldspar, 33% plagioclase, 10% carbonate, 10% muscovite, 7% quartz, 7% chlorite, trace to 1% ilmenite, and trace apatite, rutile, pyrite, magnetite, and zircon.

Plagioclase, feldspar, apatite, carbonate, pyrite, and chlorite occur as described in 210-4.33. Quartz occurs as described in sample 210-5.97. Ilmenite occurs as crystals which are replacing magnetite crystals. This sample does not contain feldspar overgrowth on the plagioclase and feldspar crystals. As is sample 210-4.33, there appear to be two generations of chlorite. Muscovite occurs as described in sample 210-5.97. Magnetite forms subhedral grains in sharp contact with quartz and carbonate crystals between coarse-grained plagioclase, feldspar, and quartz. Rutile forms crystal aggregates replacing finer-grained quartz crystals, and contain inclusions of magnetite(?).

The major difference in this sample is that it contains more carbonate and muscovite replacing the plagioclase, feldspar, and/or quartz in the sample. No zircon has been identified in this sample.

As in sample 210-5.97, there does not appear to be a foliation in this sample.

Deformation is apparent in sub-grains of quartz and crenulated chlorite.

443945

This sample is composed of 43% plagioclase, 20% feldspar, 14% quartz, 8% carbonate, 8% chlorite, 5% muscovite, 1% biotite, 1% pyrrhotite, trace to 1% pyrite, and trace apatite, zircon, rutile, ilmenite, magnetite, and chalcopyrite.

This sample is not equigranular as described in sample 210-4.33. In this sample plagioclase and feldspar are generally 1 to 2mm in diameter, and are surrounded by finer-grained quartz and plagioclase ranging in size from 0.05 to 0.25mm in diameter (may be magmatic? – fill corroded zones of larger crystals). The finer-grained quartz and plagioclase fill corroded zones of the larger plagioclase and feldspar. Larger plagioclase and feldspar are locally altered with fine-grained muscovite laths. Locally (crystal scale) the alteration by muscovite is intense, and in places nearly complete. Apatite is present as rectangular crystals and hexagonal crystal sections included in plagioclase and feldspar, and between the large plagioclase and feldspar crystals. When it is not included in the plagioclase and feldspar, apatite contains corroded zones that are filled with the finer-grained quartz and plagioclase. To date three zircons have been identified in this sample. All three zircons are present as doubly terminating crystals approximately 0.1mm in length. Two of zircons are included in the larger plagioclase, while the third is present between a chlorite flake and apatite hexagonal section in the finer-grained quartz and plagioclase.

Biotite appears to have two generations: a dark brown, low birefringence, non-pleochroic generation (biotite 1), and a light brown, higher birefringence, pleochroic generation (biotite 2). Chlorite also appears to have two generations: a dark green, low birefringence, non-pleochroic generation (chlorite 1), and a light green, higher birefringence, pleochroic generation (chlorite 2). In this sample chlorite 1 pseudomorphously replaces biotite 1, and biotite and chlorite 2 replace both chlorite and biotite 1 as tabular and lath-like crystals. Chlorite and biotite 2 replace each other in the sample. Muscovite replaces both types of chlorite and biotite. Carbonate replaces and fills corroded zones of both types of chlorite and biotite, the larger feldspar and plagioclase crystals, the finer-grained quartz and plagioclase, and muscovite.

Pyrite forms euhedral cubic crystals to subhedral crystals disseminated in the finer-grained quartz and plagioclase. There appear to be two generations of pyrite because of different amounts of tarnishing. In one location this is especially prevalent, as tarnished cubic pyrite is partially enveloped by subhedral non-tarnished pyrite. Ilmenite, rutile, and magnetite are locally found as inclusions in pyrite. Chalcopyrite pseudomorphously replaces portions of pyrite, and pyrrhotite pseudomorphously replaces chalcopyrite and pyrite. Rutile is also found included in biotite 1 as acicular crystals, and as crystal aggregates spatially associated with both chlorites, biotites, and with pyrite and pyrrhotite.

Locally microfractures cut the rock and are parallel to one another. The fractures are generally 0.09 to 0.2mm wide and are filled with muscovite and carbonate.

This sample does not exhibit foliation, and the only sign of deformation is possibly the microfractures.

Appendix H
XRD ANALYSES

H1. Purpose of XRD Analyses

XRD analyses were conducted on seventeen samples in order to determine the primary mineral phase present in mineralized (and carbonate-quartz-pyrite altered) and un-mineralized (ie. un-mineralized pillow) mafic volcanic rocks. Various intrusive rocks at Barry were also analyzed to determine the primary minerals present. The samples that were analyzed are summarized in Table H1.

Table H1: Samples chosen for XRD analyses

Sample ID	Volcanic Type	Description	Au Grade (g/t)
118-16.70	A	Less altered sample	0.00
91-1119	B	Least altered sample	0.01
81-1119	B	Low gold grade, carbonate altered	0.10
59-1113	A	Pillow: low gold grade, carbonate altered	0.01
62-1088	A	Pillow: low gold grade, carbonate altered	0.01
31-12.00	B	High gold grade, carbonate altered	10.54
71-1099	B	High gold grade, carbonate altered	3.24
69-1164		Diorite 1	0.00
70-1167		Diorite 1	0.15
69-1170		Diorite 2	0.20
71-1159		Diorite 2	0.47
59-1164		Diorite 3	0.01
85-1058		Diorite 3	0.01
58-1165		QFP	0.41
83-1038		QFP	0.02
210-4.33		Quartz Monzonite	0.37
443945		Quartz Monzonite	0.36

The main results of XRD analysis are:

- A) Carbonate is generally calcite in un-mineralized rocks, while the carbonate tends from Fe-dolomite to ankerite in mineralized rocks
- B) Chlorite present is largely clinocllore

The analytical methods for microprobe analysis is summarized in Chapter 2, section 2.4, titled 'Analytical Methods'.

Results are summarized in Figures H1-H17.

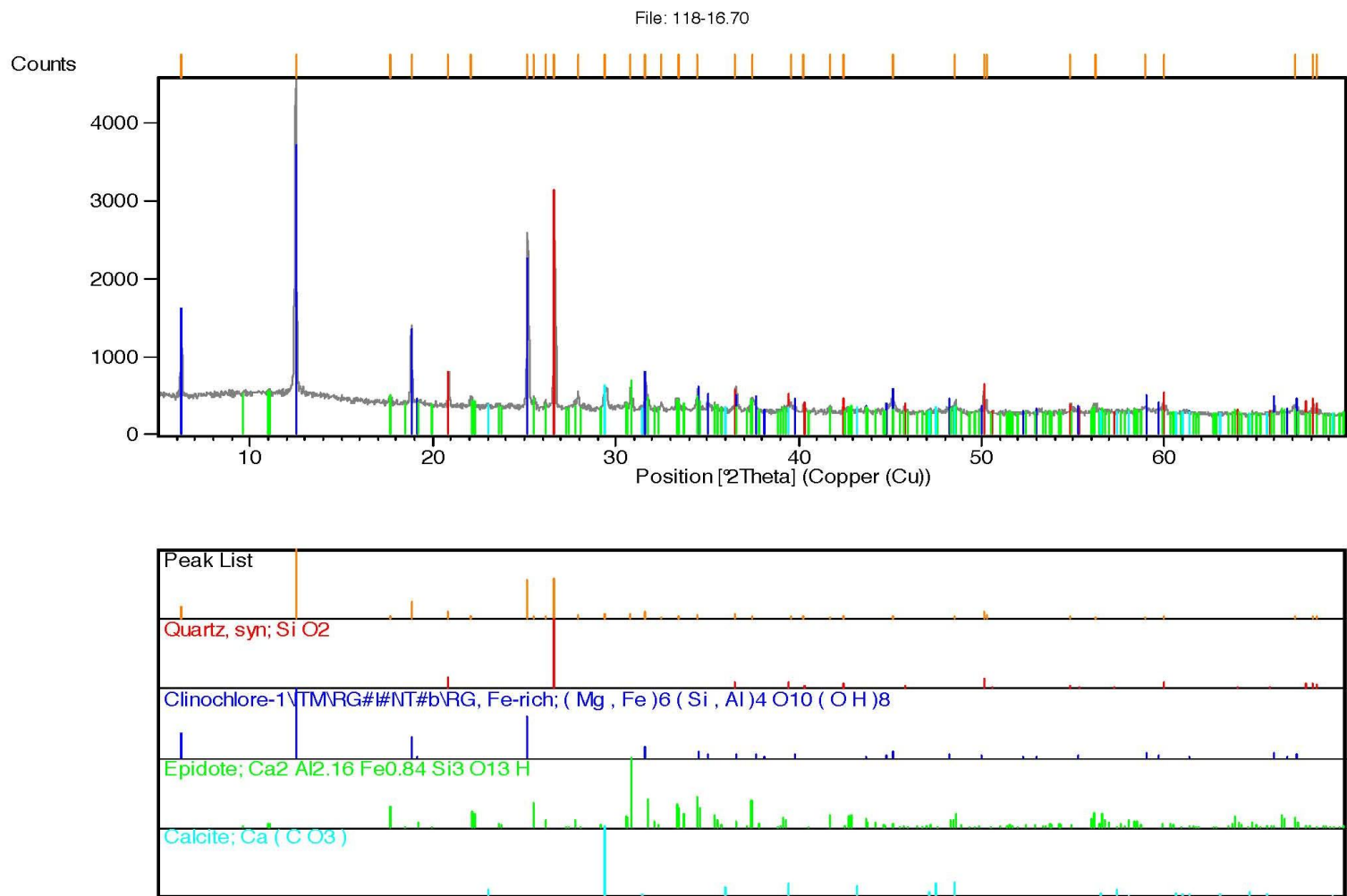


Fig. H1: Sample 118-16.70 - less altered Type A mafic volcanic

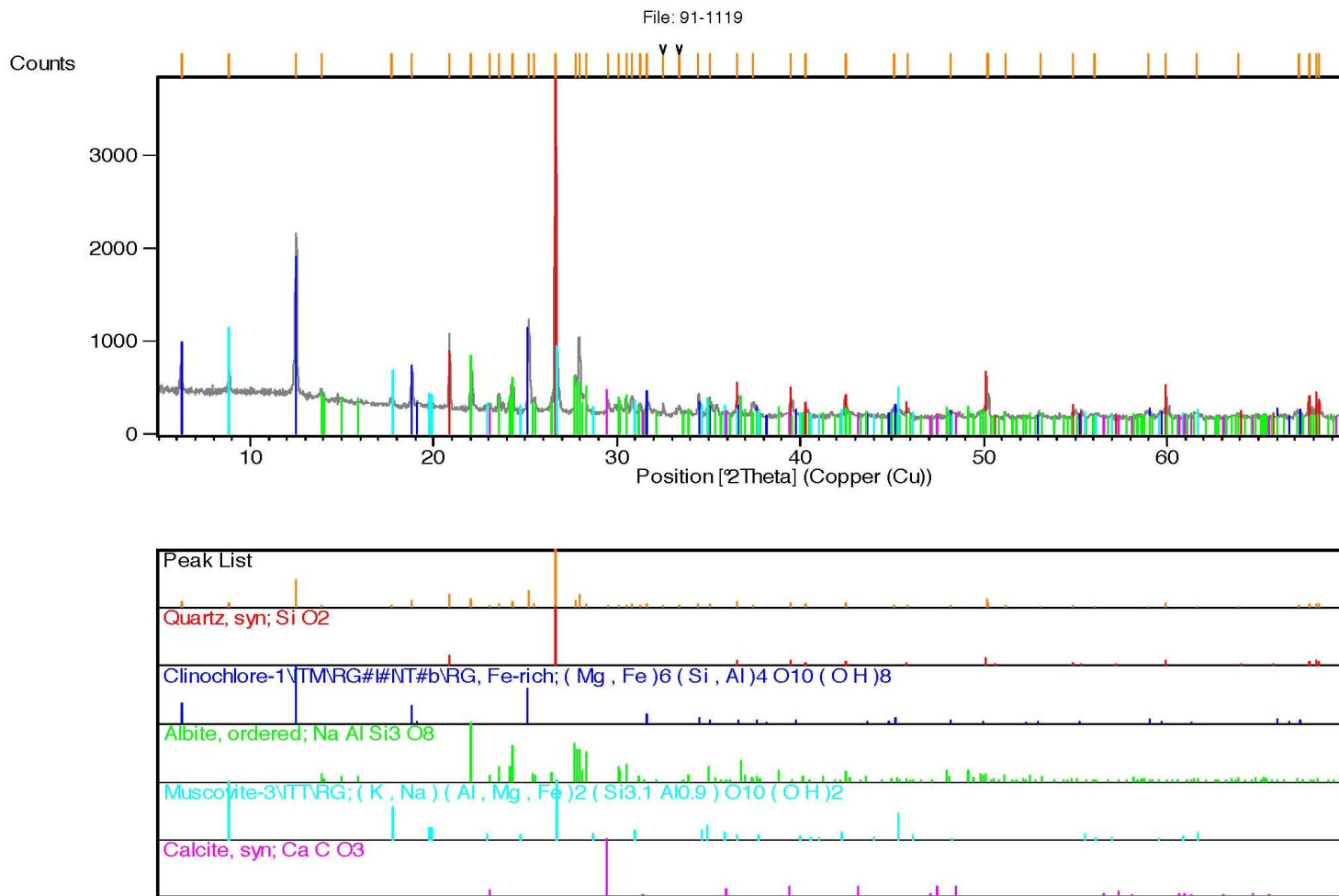


Fig. H2: Sample 91-1119 - least altered Type B mafic volcanics

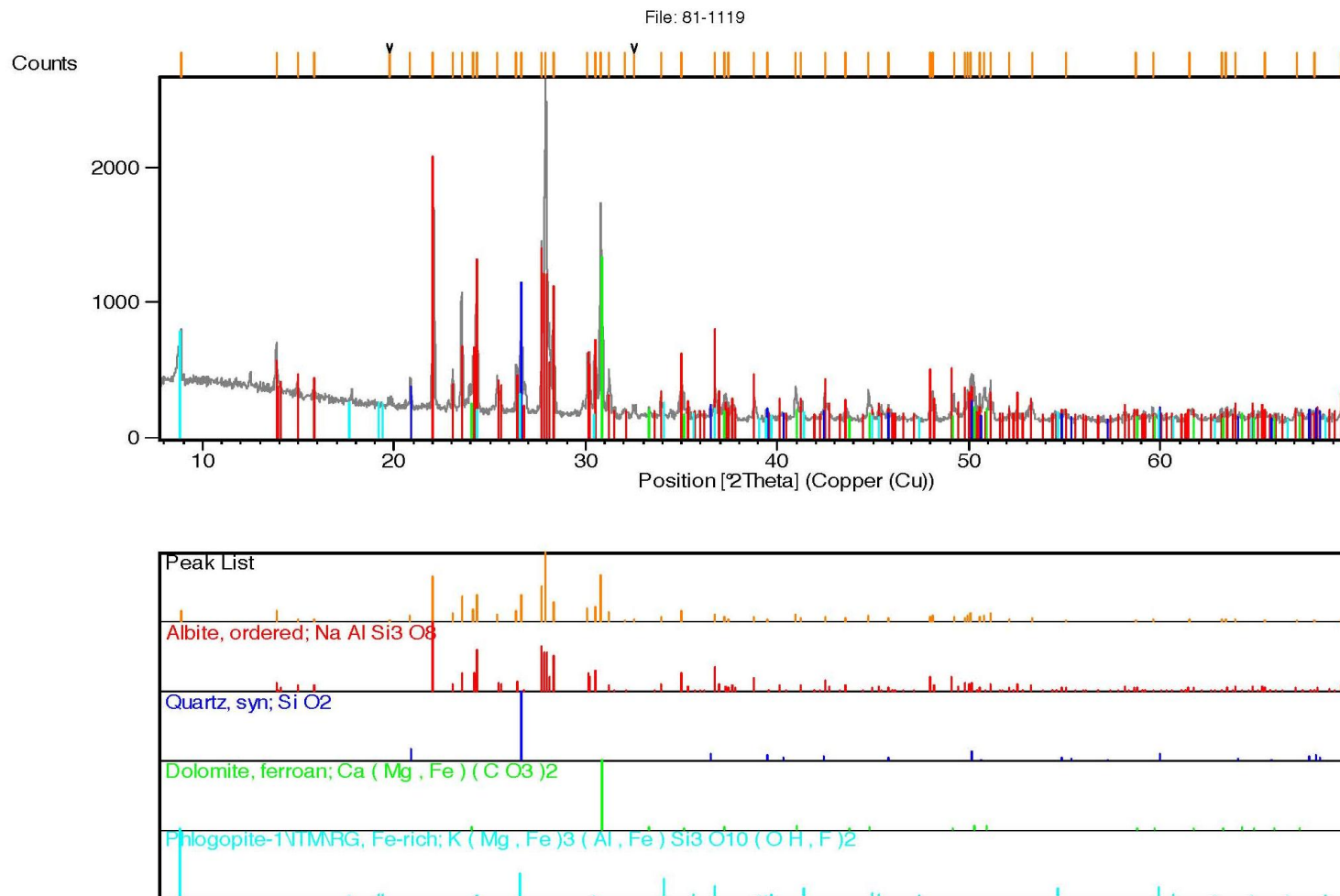


Fig. H3: Sample 81-1119 - low gold grade carbonate alteration in Type B mafic volcanics

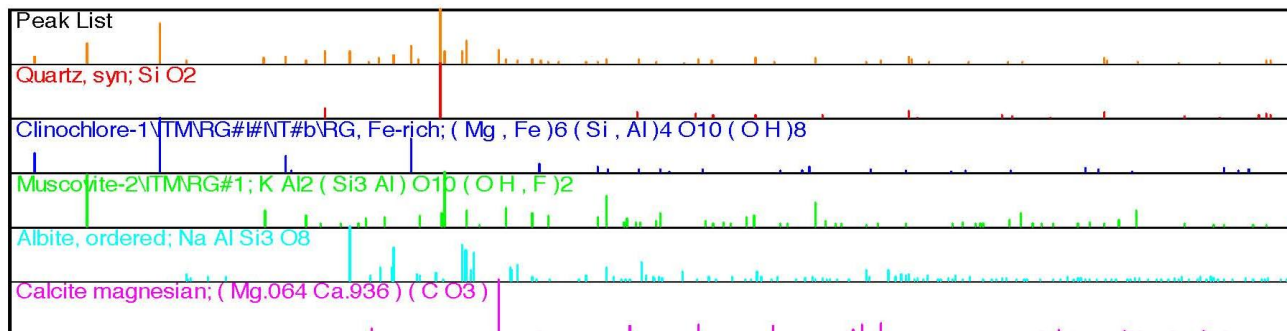
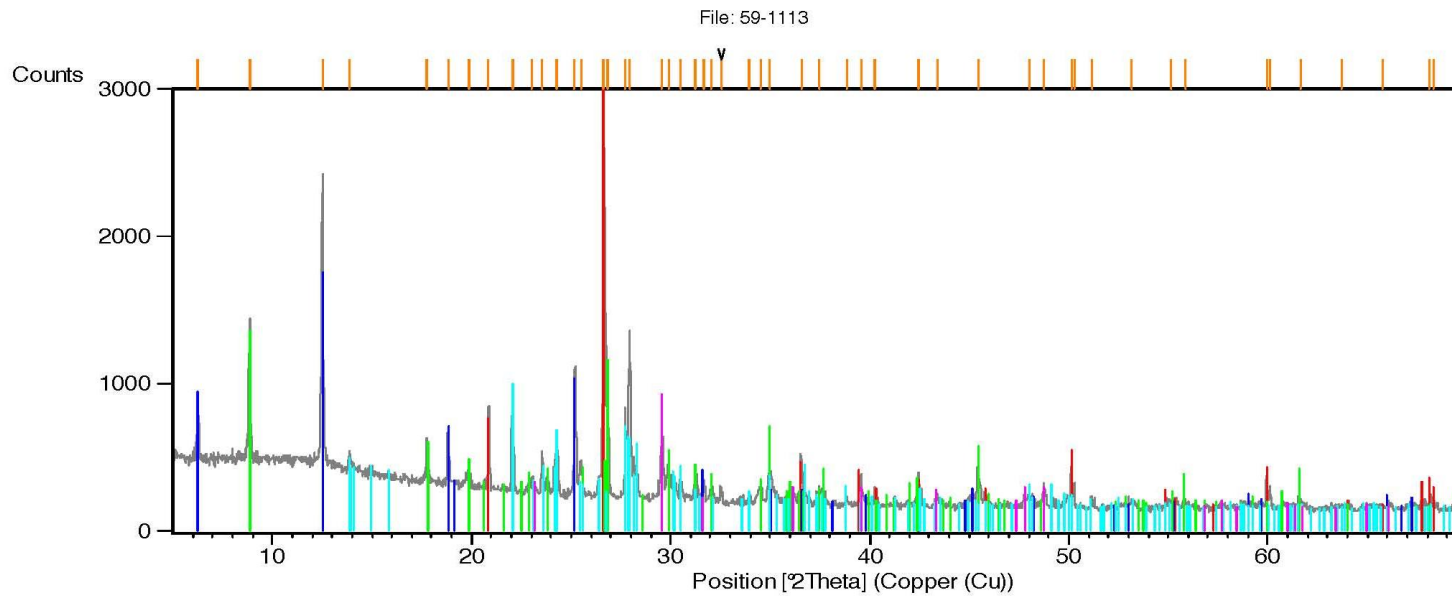


Fig. H4: Sample 59-1113 - pillow, low gold grade carbonate alteration in Type A mafic volcanics

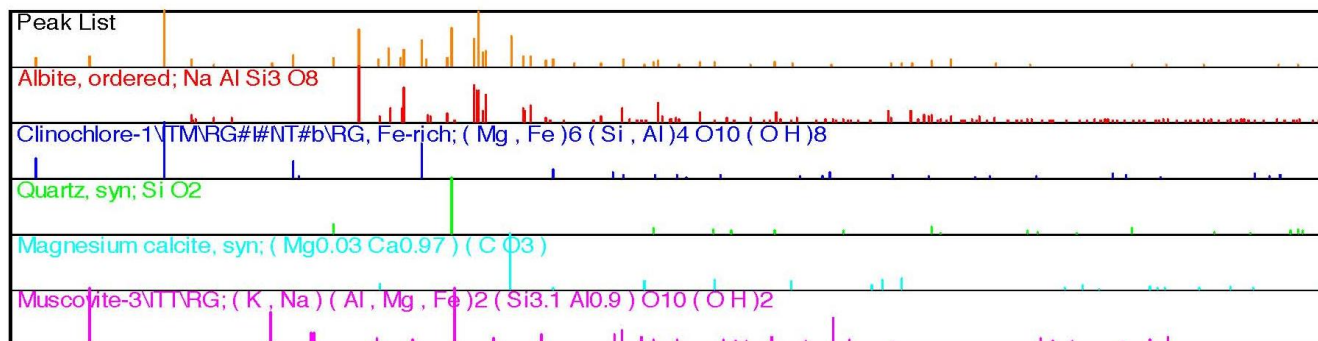
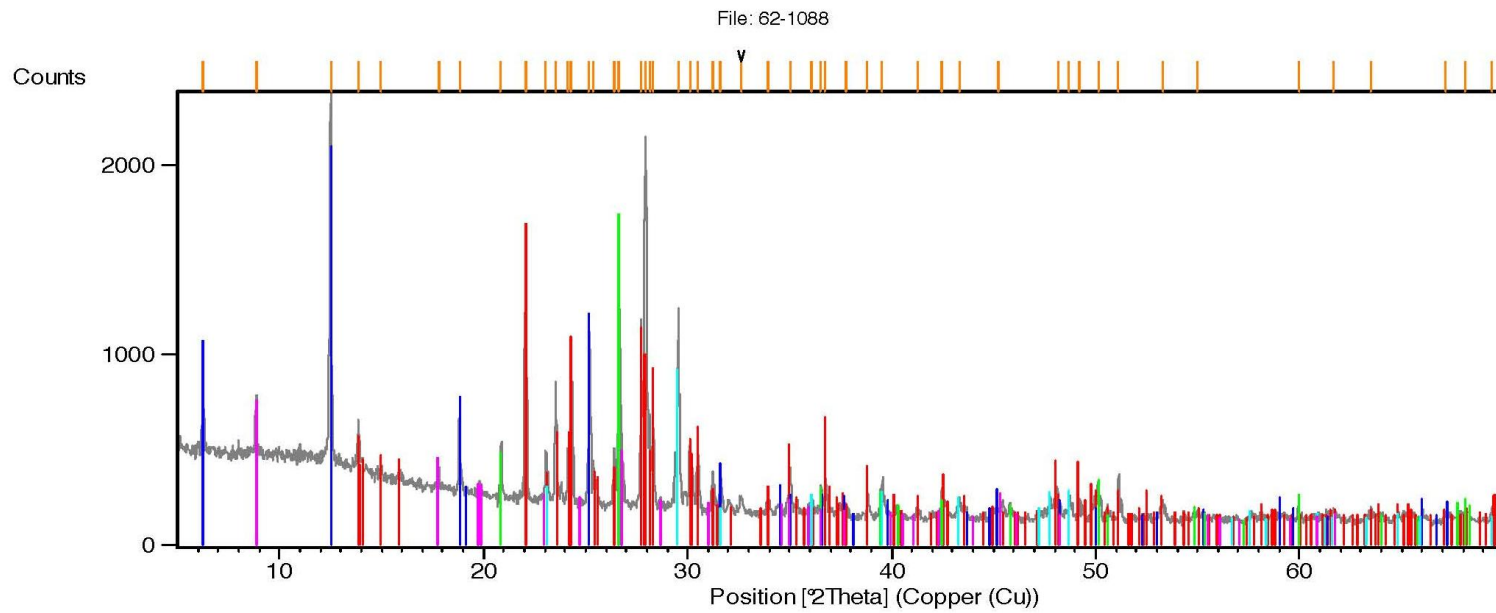


Fig. H5: Sample 62-1088 - pillow, low gold grade carbonate alteration in Type A mafic volcanics

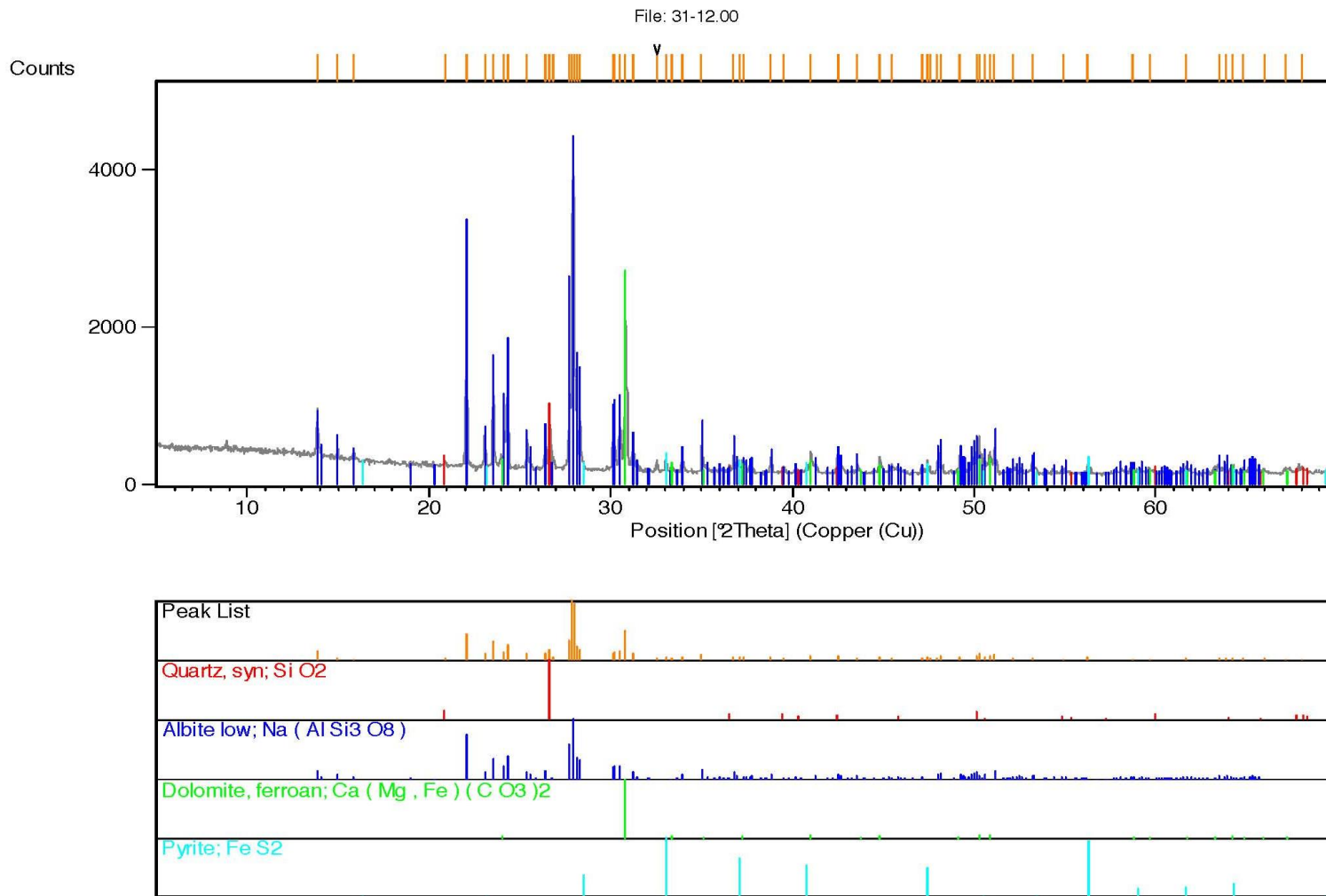


Fig. H6: Sample 31-12.00 - high gold grade carbonate alteration in Type B mafic volcanics

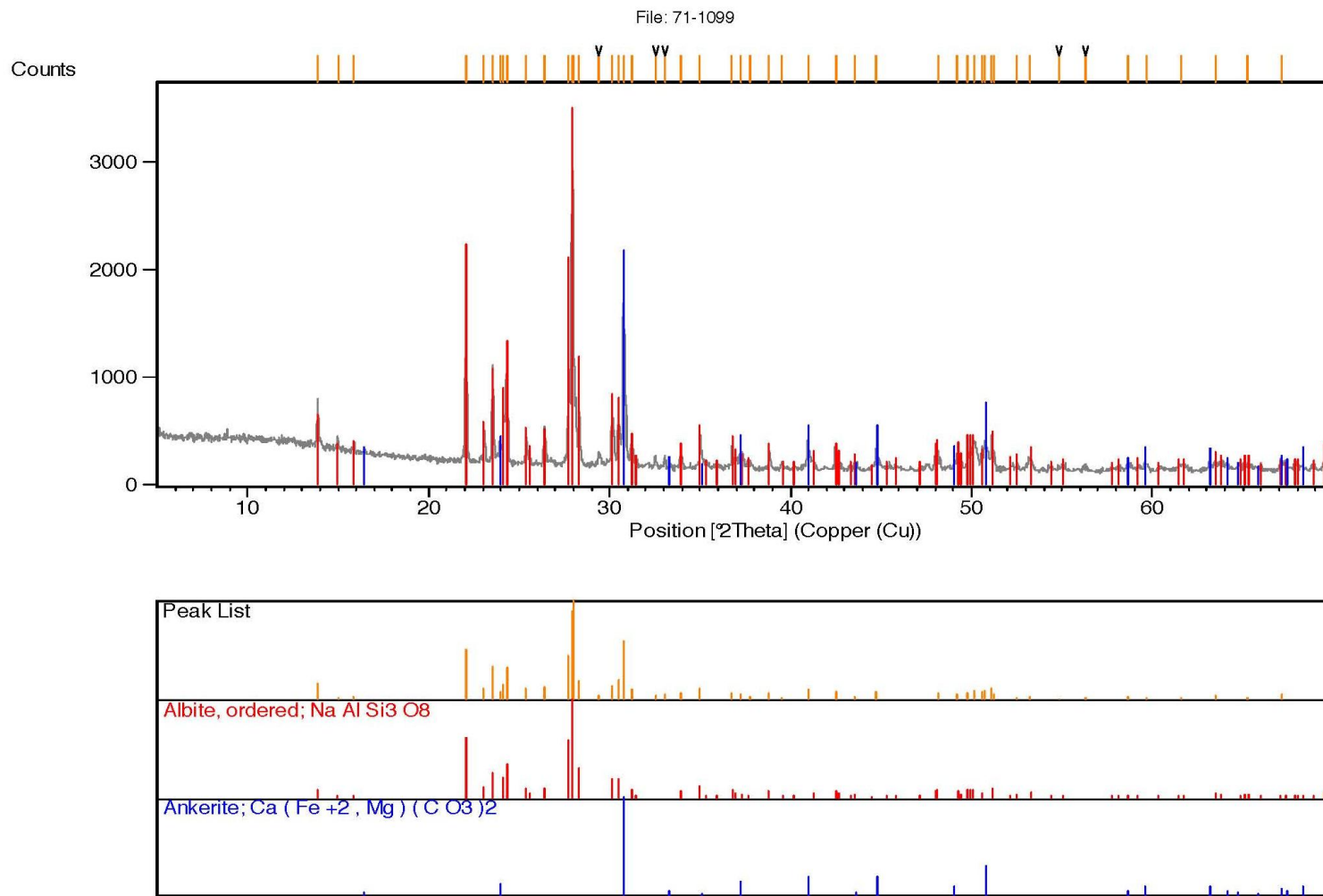


Fig. H7: Sample 71-1099 - high gold grade carbonate alteration in Type B mafic volcanics

File: 69-1164

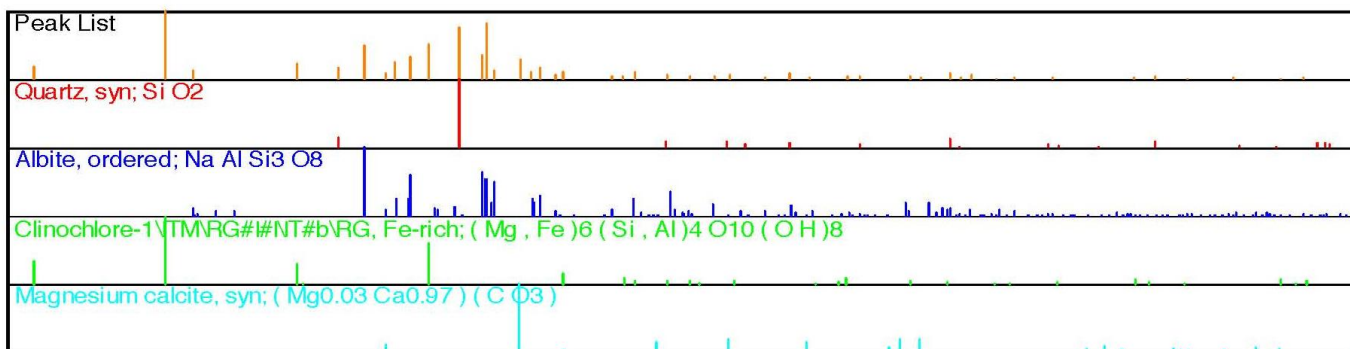
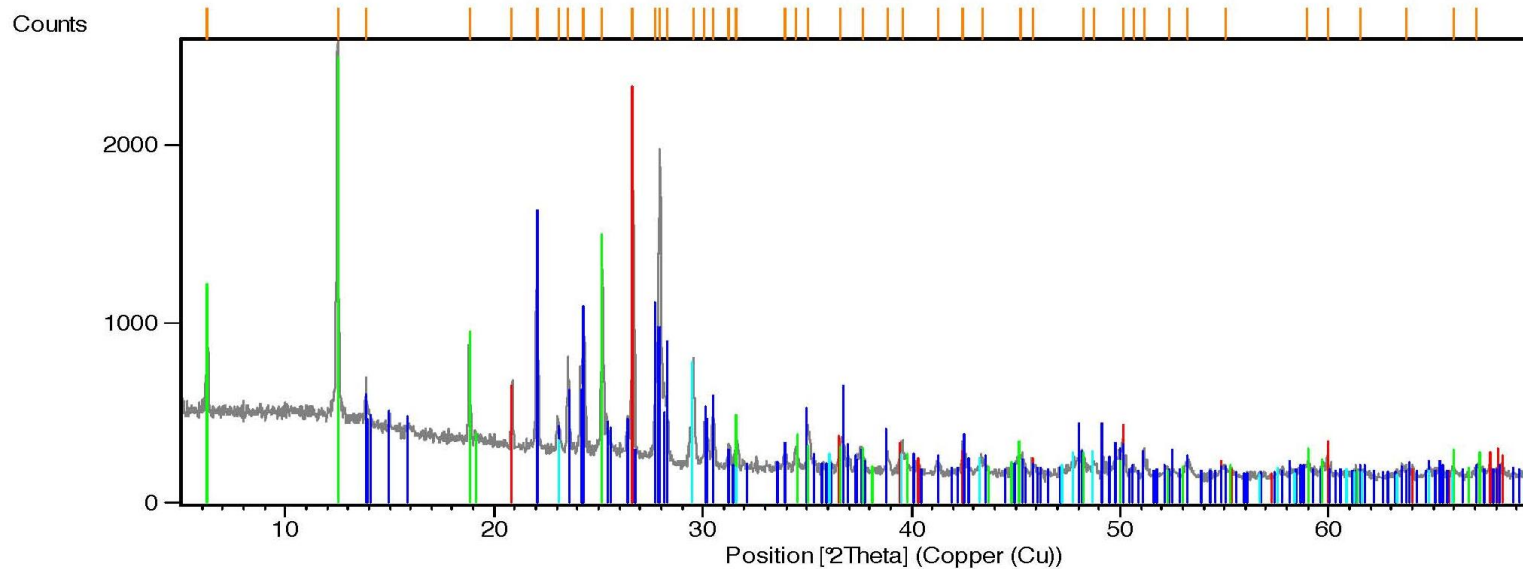


Fig. H8: Sample 69-1164 - Diorite 1

File: 70-1167

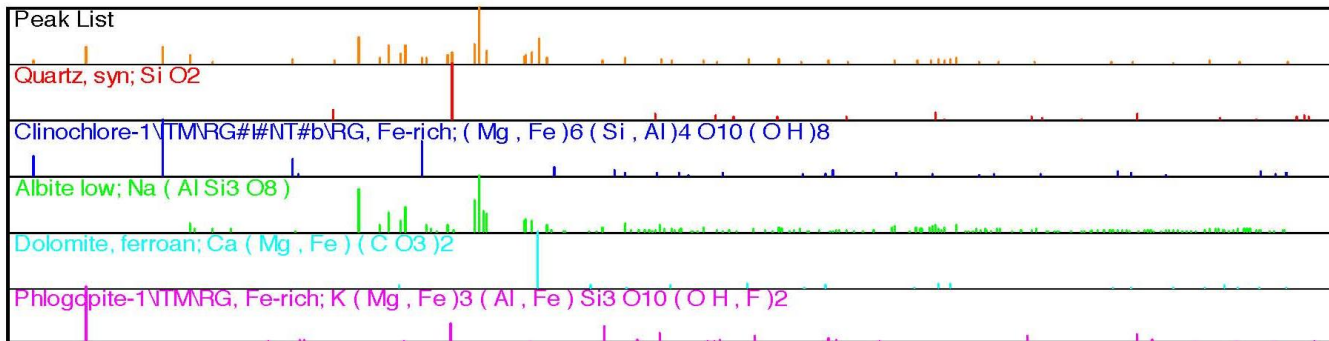
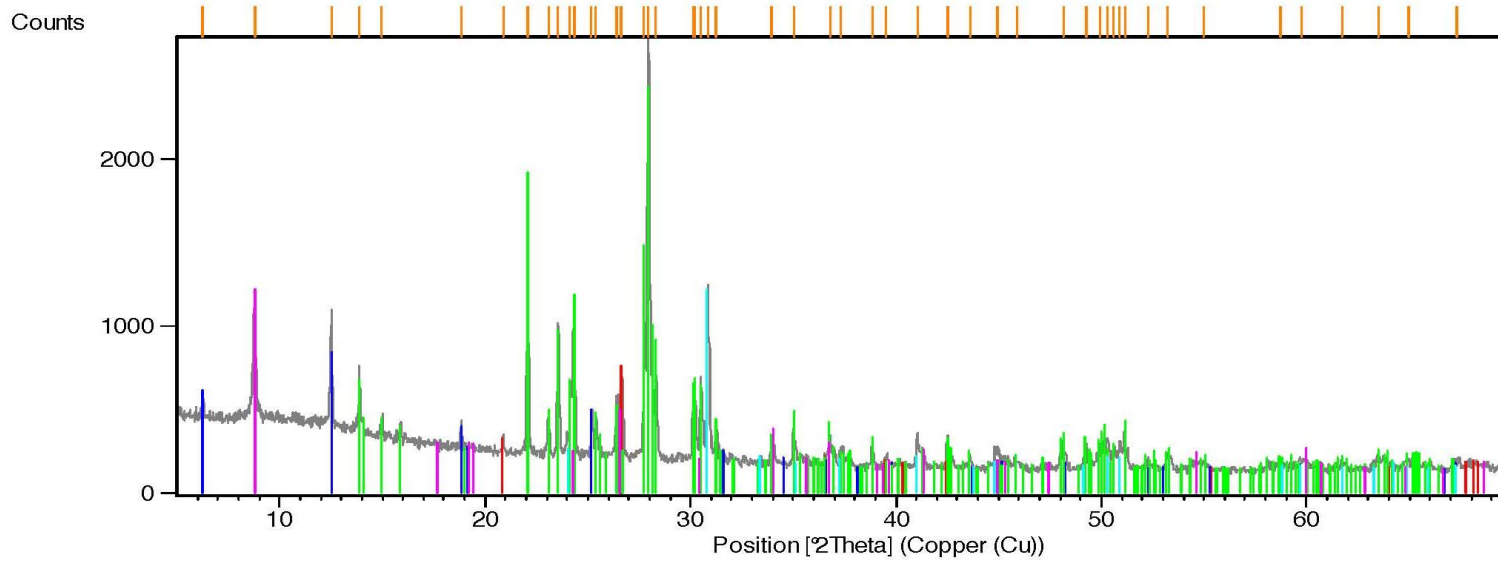


Fig. H9: Sample 70-1167 - Diorite 1

File: 69-1170

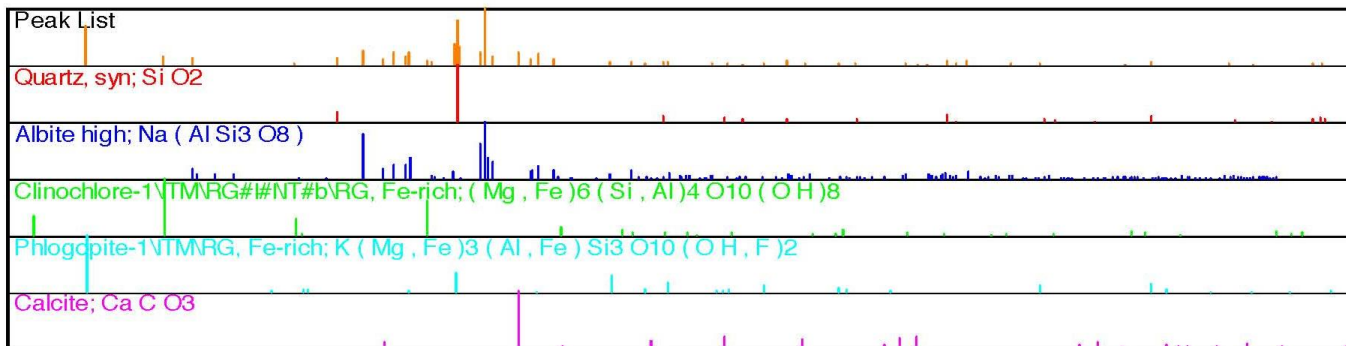
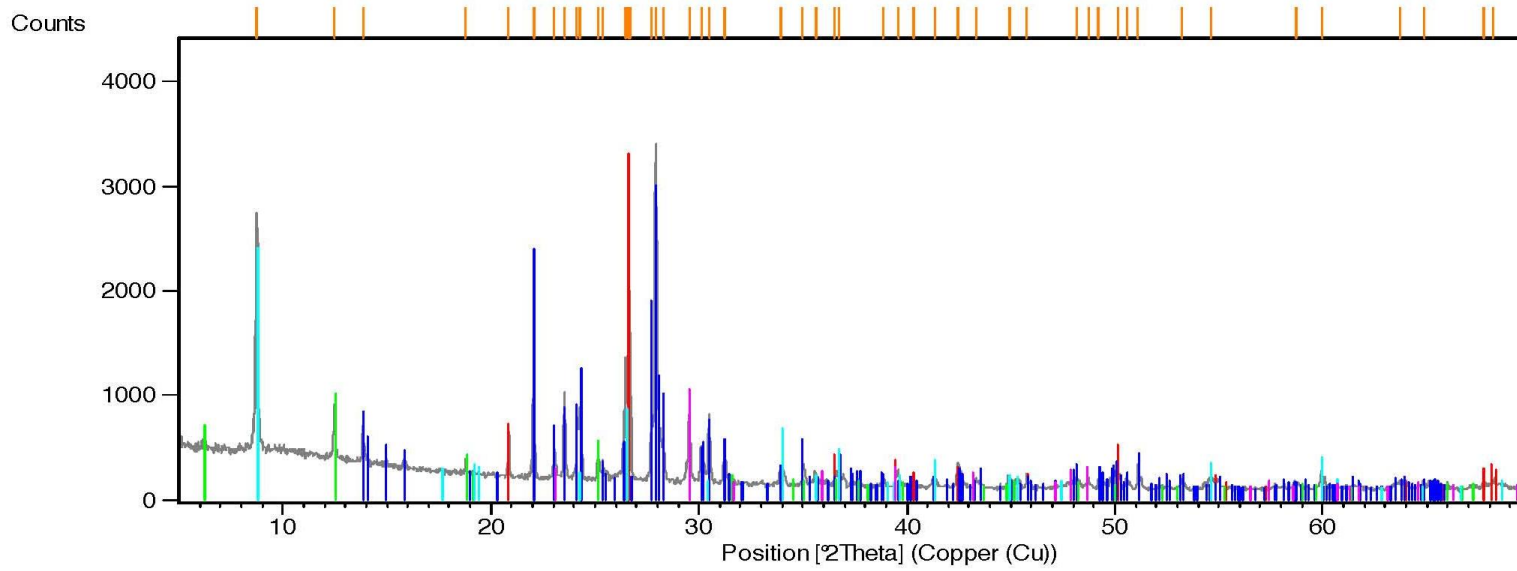


Fig. H10: Sample 69-1170 - Diorite 2

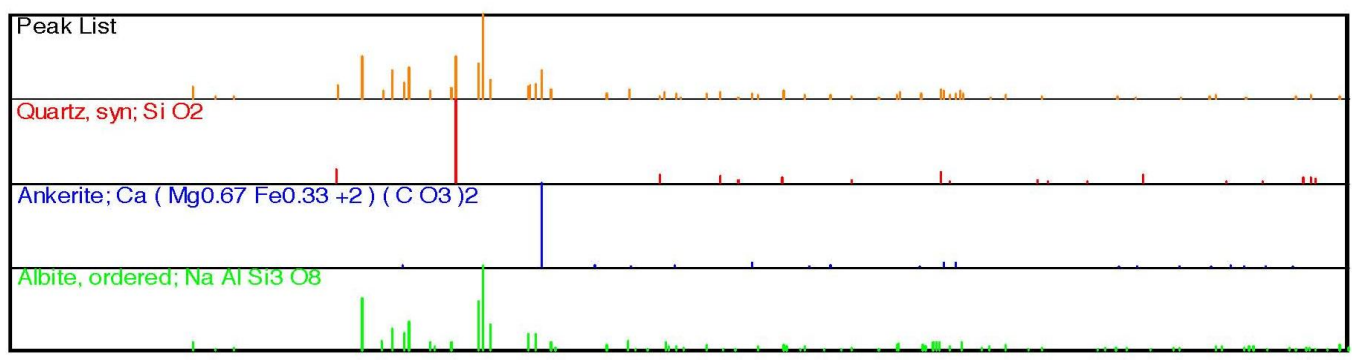
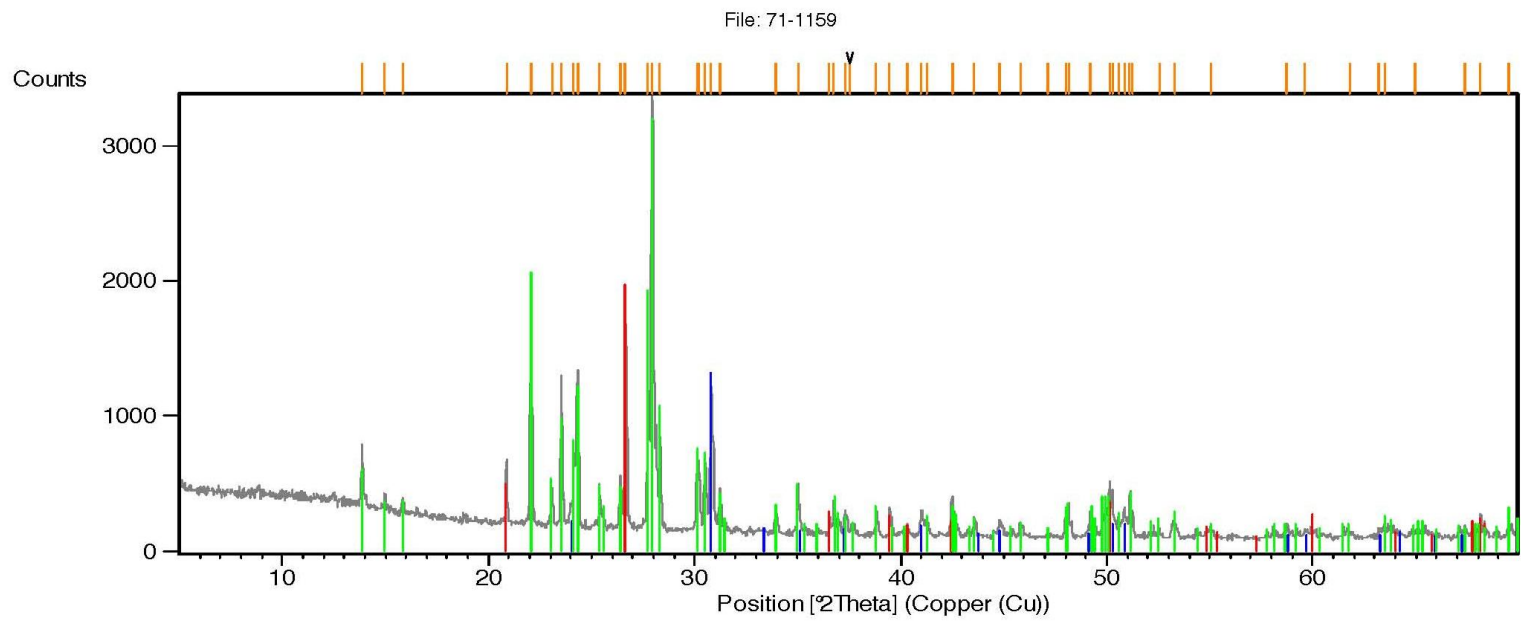


Fig. H11: Sample 17-1159 - Diorite 2

File: 59-1164

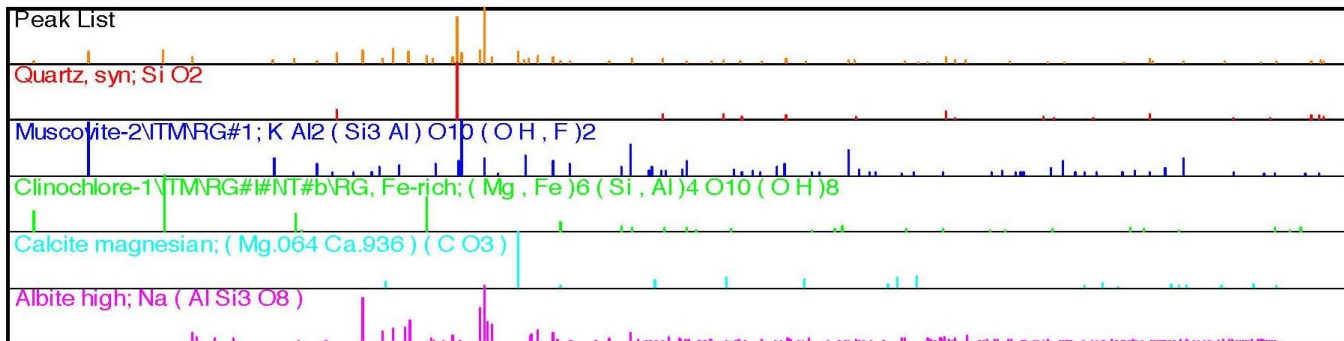
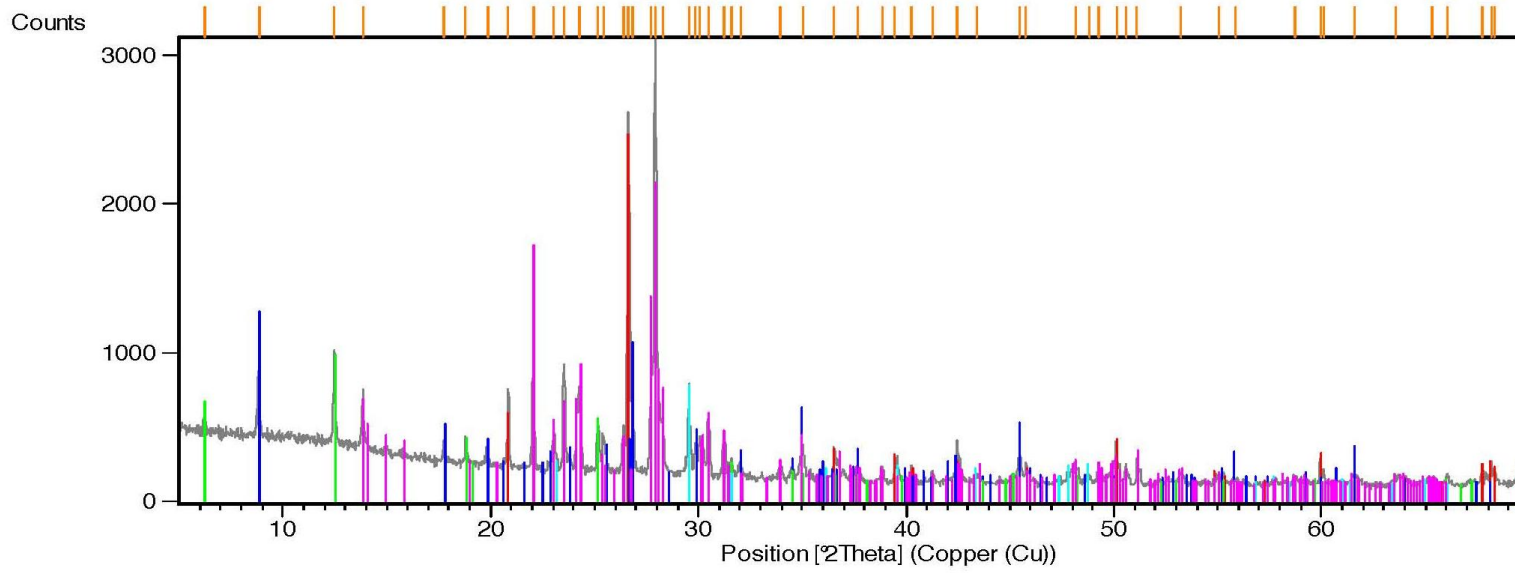


Fig. H12: Sample 59-1164 - Diorite 3

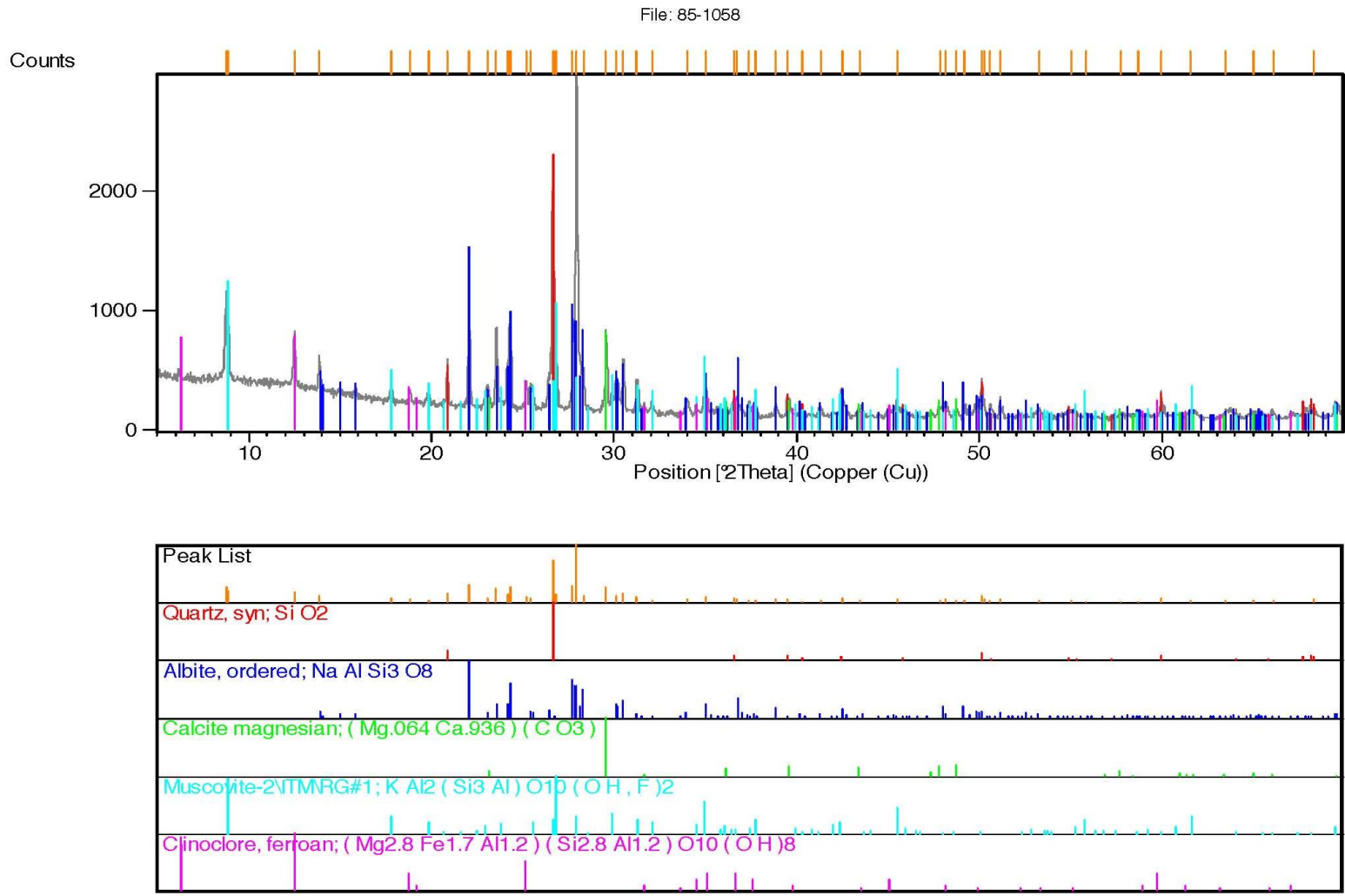


Fig. H13: Sample 85-1058 - Diorite 3

File: 58-1165

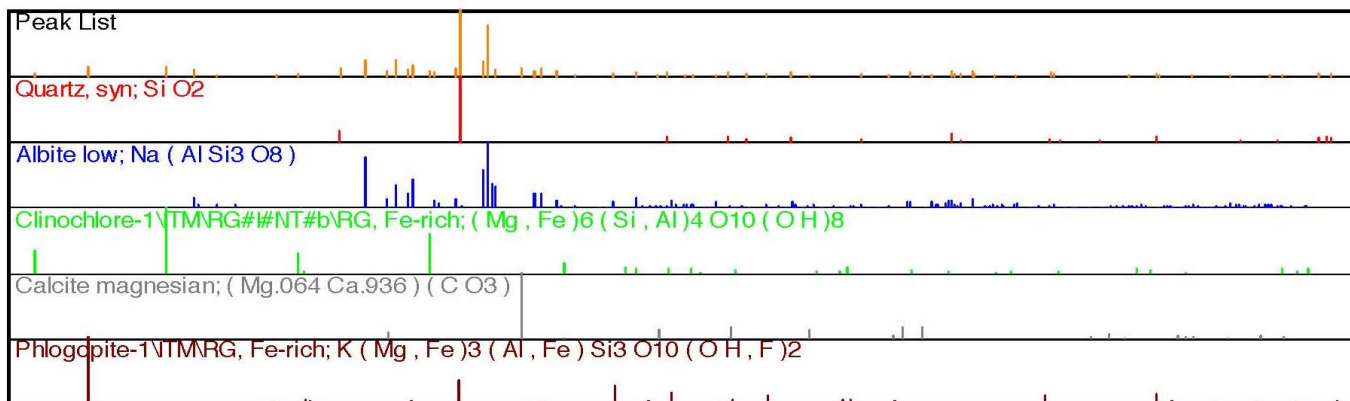
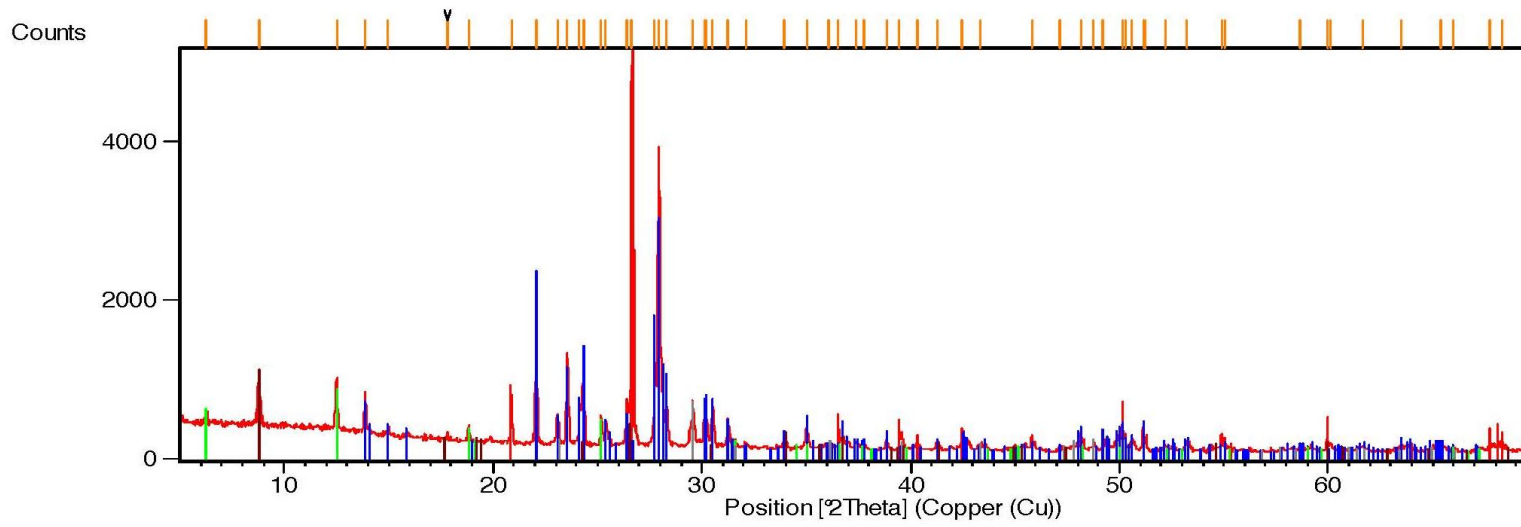


Fig. H14: Sample 58-1165 – QFP

File: 83-1038

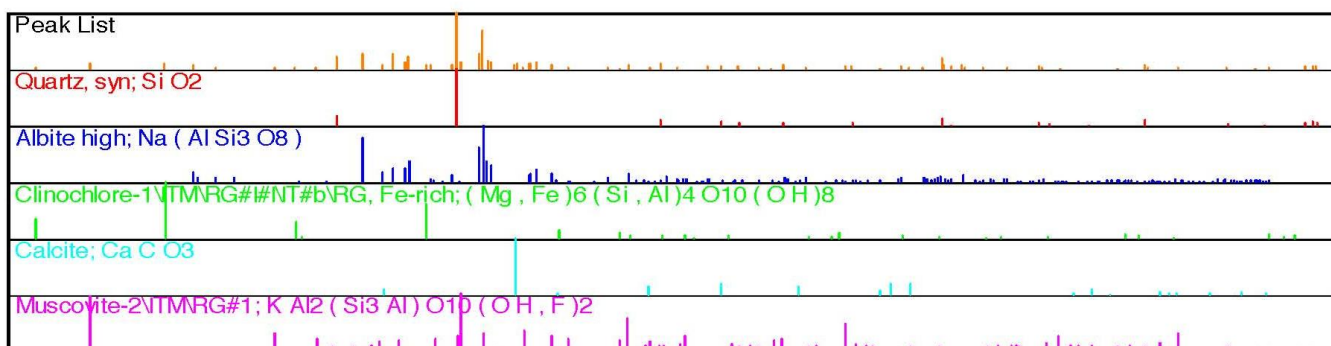
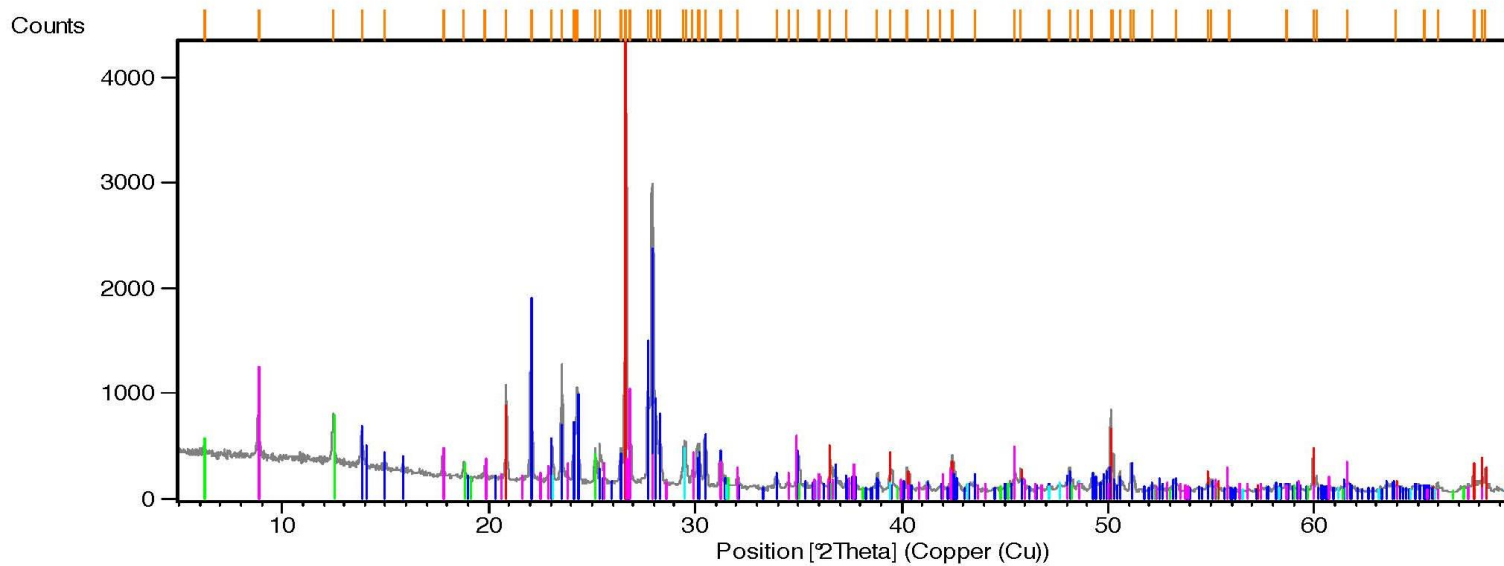


Fig. H15: Sample 83-1038 - QFP

File: 210-4.33

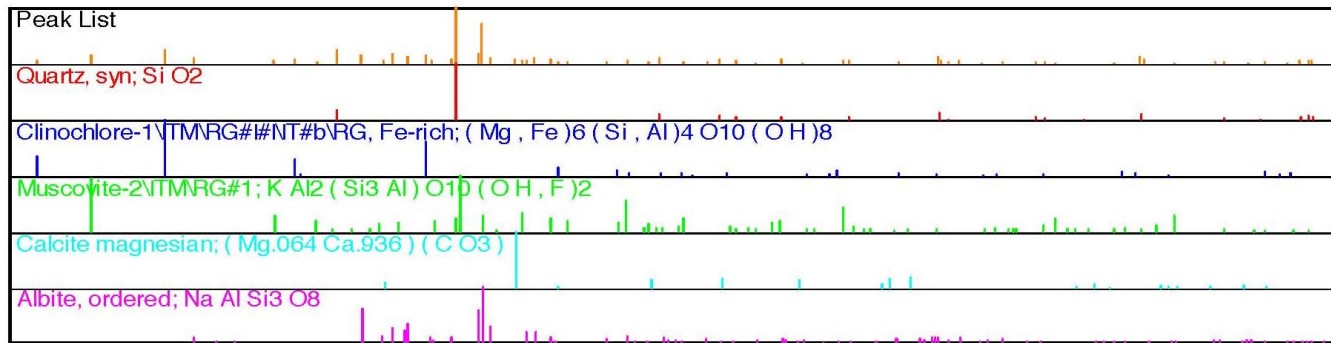
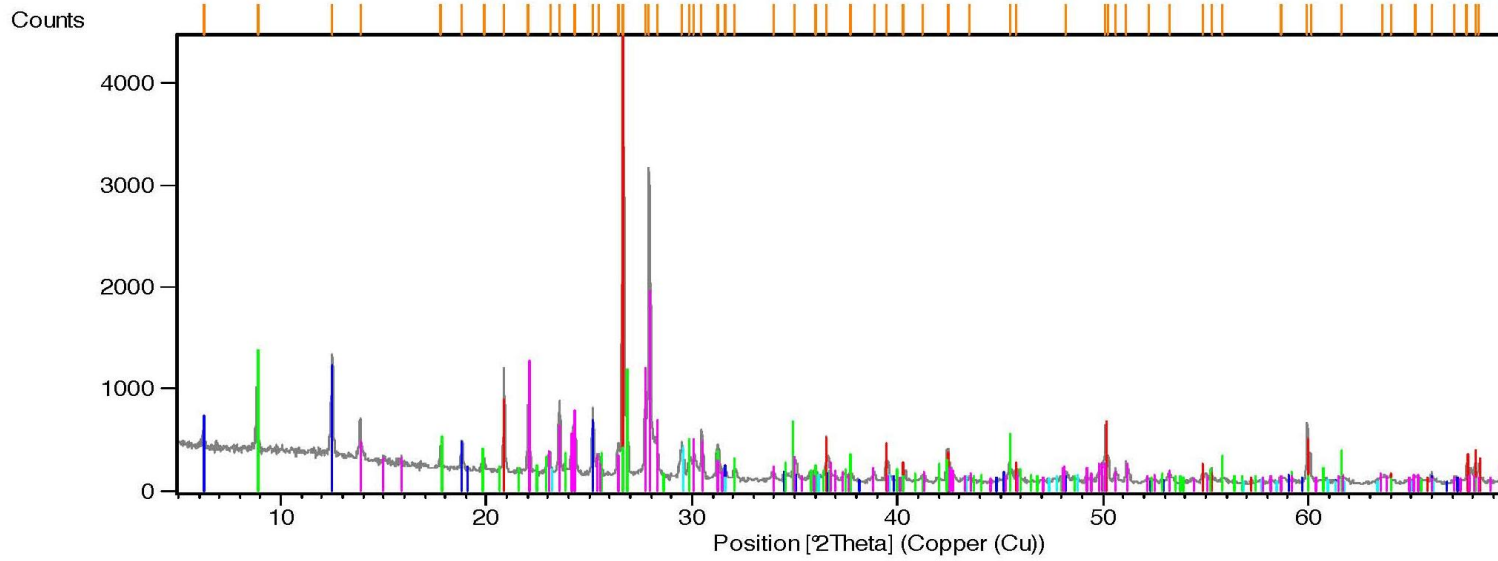


Fig. H16: Sample 210-4.33 - Quartz Monzonite

File: 443945

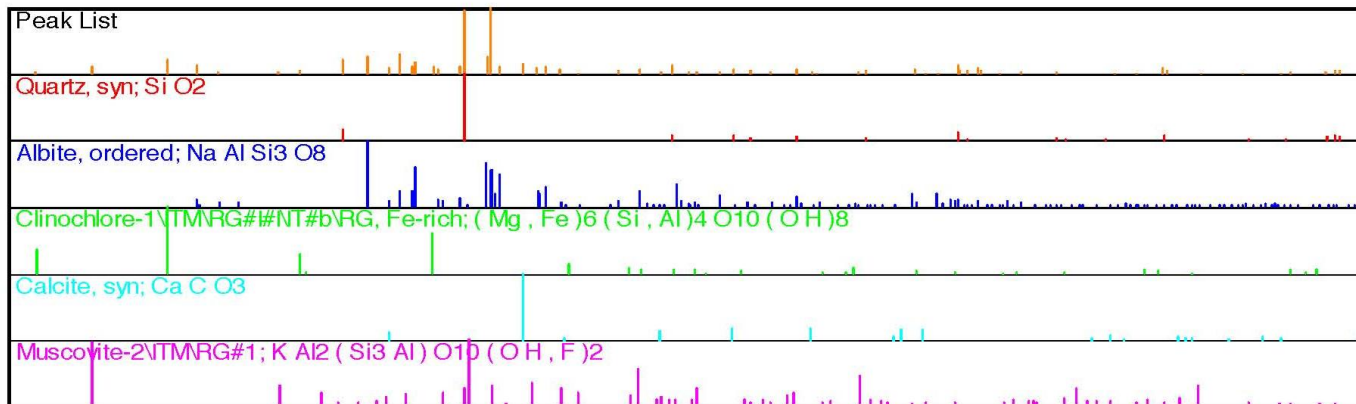
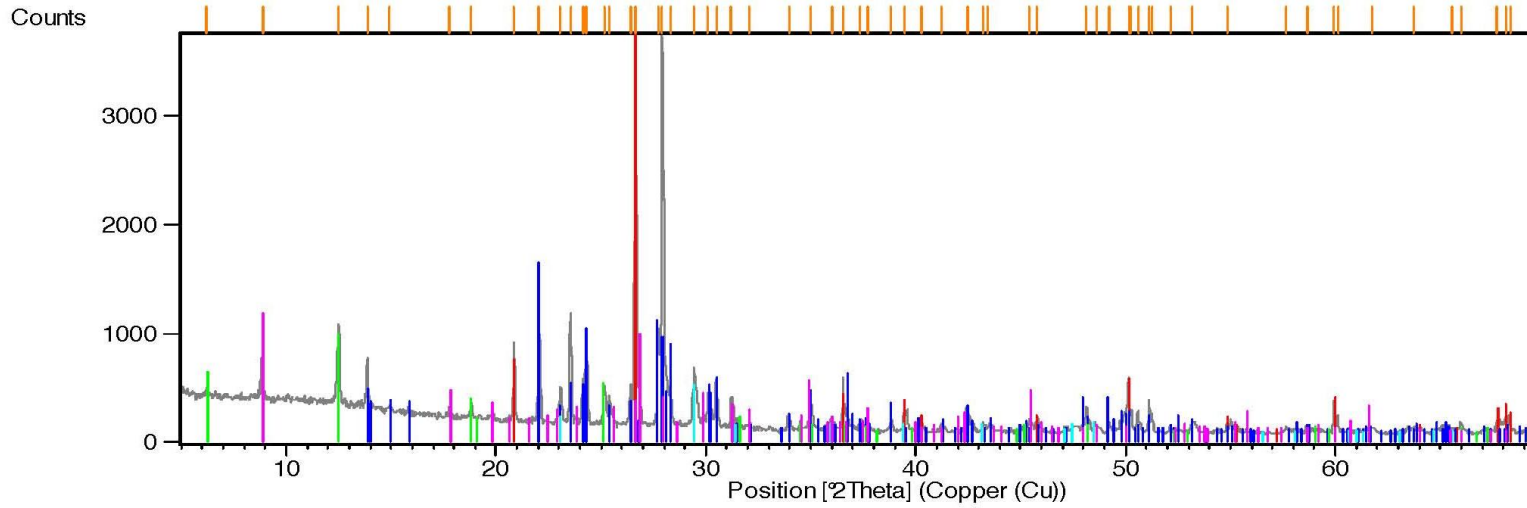


Fig. H17: Sample 443945 - Quartz Monzonite